THESE TURBULENT TIMES: INTERACTIONS BETWEEN FISH AND TURBULENCE-GENERATING SIMULATED INSTREAM RESTORATION STRUCTURES AND THEIR INFLUENCE ON FISH ENERGY USE AND HABITAT SELECTION

BY

KATHERINE KEALOHA STRAILEY

DISSERTATION

Submitted in partial fulfillment of the requirements
for the degree of Doctor of Philosophy in Ecology, Evolution and Conservation Biology
in the Graduate College of the
University of Illinois Urbana-Champaign, 2022

Urbana, Illinois

Doctoral Committee:

Professor Cory Suski, Co-Chair and Co-Director of Research
Assistant Professor Piotr Cienciala, Co-Chair and Co-Director of Research
Assistant Professor Rafael Tinoco
Professor Bruce Rhoads
Professor Michael Ward
Dr. Eva Enders, Institute national de la recherche scientifique

ABSTRACT

Due to extensive human modification, streams and rivers are among the most degraded ecosystem types on the planet. Habitat degradation and loss are among the factors leading to widespread declines in the abundance of freshwater fish, and thus riverine fish have borne the brunt of the damage. In recent decades, river restoration has emerged as a tool aimed at reversing the degradation of rivers. River restoration commonly utilizes instream restoration structures to create and improve fish habitat in an effort to reverse population declines. Such structures alter the natural flow of a river and generate additional turbulence. Turbulence has major impacts on fish energetics, swimming performance, and behavior. However, the effects of turbulence on fish have largely been ignored in the implementation and design of instream restoration structures. Therefore, the goal of my research was to investigate the interplay between fish energetics, habitat selection, and turbulence generated by structures. In my first study, I utilized a small-scale laboratory experiment to examine how close-range interactions between fish and turbulence-generating structures at the microhabitat scale impacted fish swimming stability and energetics. For my second and third studies, I utilized large-scale laboratory experiments. In my second study, I identified the specific aspects of turbulent flow that most influence fish energetic costs, and yielded bioenergetics models that can be employed to predict fish energy use in turbulence. Finally, in my third study, I quantified how energetics and turbulent flow jointly mediate fish habitat selection. Together, these three studies provide novel insight into fish usage of and responses to the turbulence generated by structures and, in turn, serves to increase the success of restoration activities by identifying a range of flow characteristics that are attractive to and can provide energetic benefits for fish.

ACKNOWLEDGMENTS

I have been so incredibly fortunate to be helped, guided, and supported by so many people as I have found my way through graduate school. I first want to thank the core group that have mentored me: Dr. Bruce Rhoads, Dr. Piotr Cienciala, Dr. Rafael Tinoco, and Dr. Cory Suski. Thanks to my mentors, I have learned so much more and done so much than I could have ever imagined myself doing on my own. Few people ever get to cross boundaries and delve into the interdisciplinary in the way that I have been able to, thanks to this group. I am appreciative of all the help they have given me, and all the support that their lab groups have given me as well. In particular, I am grateful for Dr. Suski's unwavering support and understanding. I had no intention of pursuing a PhD until he suggested it, and entered my PhD program with no more than a couple weeks' research experience. Without Dr. Suski, I could have never gotten where I am today. I also want to thank the other members of my committee, Dr. Michael Ward and Dr. Eva Enders, for bringing additional perspective to my research.

I would also like to thank the institutions that helped me with my logistics along the way: Illinois-Indiana Sea Grant, for funding all of my research and half of my time in graduate school, and Jake Wolf Memorial Fish Hatchery (along with everyone that works there) for providing me and the other fish folk of UIUC with healthy, happy fish for our research.

Outside of the senior scientists that have mentored me, there are so many other people that have helped both myself and my research along the way. Various people from the Tinoco, Rhoads, and Cienciala lab groups have all assisted me throughout my time. My labmates in the Suski group, past and present, Amy Schneider, Emi Tucker, John Bieber, Qihong Dai, and Toniann Keiling, other lab- and fish-adjacent folks Emily Allen, Kayleigh Smith, Kealie Vogel. Some of you have often (almost literally) been down in the trenches with me, and most of you

have played fish anesthesiologist (only for those of you with IACUC approval on the appropriate protocol) or fish nurse (no fish-touching, data recording only) for me at some point. All of you have supported me with your friendship.

Lastly, I want to thank my family and loved ones. Kathi and Rick, who have always encouraged me to keep going and pursuing the things I love. Thank you for being my PhD fairy godfather, Rick. Nick O'Donnell, for telling me he could listen to me talk about fish all day. Most importantly, I want to thank my parents, who have always been on my side, encouraging me from the time that I was little. Getting to this point would have been impossible without their love, patience, and support.

Dedicated to my dad. You always knew where I was headed. This one's for you.

TABLE OF CONTENTS

CHAPTER ONE: GENERAL INTRODUCTION

Freshwater ecosystems worldwide are currently at risk due to anthropogenic degradation that imperils water quality, connectivity, and biodiversity (Gleick 2003; Dudgeon 2010; Vörösmarty et al. 2010). The Environmental Protection Agency (EPA) estimates that, of 750,000 sampled river kilometers in the United States, half were considered impaired, and nearly half (46%) were in poor biological condition (EPA 2000). In addition, between 10,000 to 20,000 freshwater species are at risk of extinction, and, in North America, it is estimated that 39% of freshwater and diadromous fish species are imperiled (Jelks et al. 2008). Overall, freshwater systems are highly degraded, and the consequences of human impact are widespread.

Restoration is one way to counteract and mitigate the deterioration of freshwater habitats while complementing other conservation and management actions (Wohl et al. 2005, 2015; Bernhardt and Palmer 2007; Beechie et al. 2010). In the United States, tens of thousands of stream restoration projects have been undertaken over the past several decades, and this approach to management is now a multibillion dollar industry (Bernhardt et al. 2005). The goals of river restoration vary widely, but enhancing the environmental quality of human-impacted streams and improving fish populations are among the most common (Bernhardt et al. 2005). From an ecological perspective, restoration, and the related activity of stream naturalization (Wade et al. 2002; Rhoads et al. 2011), often seek to counteract adverse impacts on aquatic communities through improvement of instream habitat (Bernhardt et al. 2005).

Many restoration efforts aimed at reversing declines in fish populations involve placement of artificial structures in streams, or the adoption of management approaches that encourage the development of natural structures in streams, to improve physical habitat (Thompson 2006; Palmer et al. 2014). Artificial structures can be large and highly complex, such

as engineered log jams and woody debris (Abbe and Brooks 2011) or small and simple, such as sunken root wads and lunkers (crib-like structures supported by vertical piles and sunken into banks to provide cover for fish) (Radspinner et al. 2010). Besides providing habitat for fish, natural and artificial structures can also contribute to erosion control and flood protection (Gilvear et al. 2013). Structures can positively impact individual fish, as well as fish populations and communities, by increasing habitat heterogeneity (Tews et al. 2004), providing cover from predators (Fausch 1993), and generating regions of low-velocity flow that may benefit fish energetically (McMahon and Hartman 1989; Shuler et al. 2004; Boavida et al. 2011; Jähnig et al. 2011). As such, artificial instream structures, as well as management approaches aimed at developing and preserving natural structures, have been implemented widely to address a variety of issues related to degradation of the environmental quality of rivers (Nagayama and Nakamura 2010).

Despite the widespread adoption of restoration strategies based on the enhancement of instream structure through augmentation with artificial structures or promotion of natural structure development, mixed outcomes have been reported following restoration activities, with not all projects resulting in improvements to fish populations (Kail et al. 2015). In fact, many restoration projects intended to increase fish population size and biodiversity through improved habitat heterogeneity have been ineffective (Stewart et al. 2009; Palmer et al. 2010; Lepori et al. 2017). Long-term impacts of instream structures on population changes often are difficult to assess because few projects include pre- and post-project monitoring (Downs and Kondolf 2002; Bernhardt and Palmer 2007). Fish response times to changes in habitat remain relatively unknown and many years of monitoring may be required to determine whether instream habitat structures actually benefit fish populations (Louhi et al. 2016). Moreover, any favorable

biological responses that are documented, such as increases in fish abundance or biomass, typically are assumed to result from restoration, but such changes are often unable to be clearly attributed to habitat enhancement. Physiological metrics provide a promising alternative to quantify the effectiveness of a restoration project that can be used in conjunction with, or in place of, traditional population monitoring. Physiological metrics, such as metabolism, thermal tolerance, and activity rate, can influence life-history (Ricklefs and Wikelski 2002), community composition (Start et al. 2018), and species resilience (Hofmann and Todgham 2010), and also respond quickly to changes in the environment. Thus, quantifying the physiological responses of fishes to restoration activities may contribute to a more holistic, mechanistic understanding of how habitat alterations impact both individual fish, as well as fish populations. This novel tool offers new opportunities in the face of the alarming decline in freshwater fish biodiversity, especially considering the general failure of restoration efforts to reverse such declines.

One of the challenges with current approaches to restoration is that they fail to recognize and incorporate aspects of flow and turbulence when structures are placed into rivers during restoration. Both natural obstructions and instream structures alter flow characteristics (Daniels and Rhoads 2013; Bennett et al. 2015), largely by generating increased levels of turbulence. Turbulence in rivers is characterized by chaotic, irregular fluctuations in velocity imposed onto the mean flow, manifesting as vortices and eddies of various sizes and strengths (Warhaft 2002). More importantly, turbulence can affect fish swimming behavior and kinematics, and also increase energy consumption (Tritico and Cotel 2010; Tullos and Walter 2014; Maia et al. 2015). The size, orientation, and intensity of such turbulence features are dependent on mean water velocity, depth of flow, and characteristics of instream structures (Williamson 1996; Beal et al. 2006), while the intensity, periodicity, orientation, and scale of turbulent eddies, along with fish

size and shape (Lupandin 2005; Tritico and Cotel 2010) determine interactions between fish and turbulence (Lacey et al. 2012).

Unfortunately, interactions between fish and structure-induced flow characteristics are rarely emphasized in either instream structure design or project monitoring; instead, the research, design, and evaluation of instream restoration structures largely focuses on geomorphic effects, such as increased scour and pool formation and erosion-control benefits that contribute to channel stability (Thompson 2002; Miller and Kochel 2010; Radspinner et al. 2010; Bennett et al. 2015). High levels of turbulence generated by structures introduced into rivers as part of restoration activities may place a large energetic burden on fish, affecting energetics, position and habitat selection (Wilkes et al. 2017). The added energetic burden can lead to a failure of restoration activities to enhance populations, and may actually lead fish to vacate an area if habitat parameters exceed preferred ranges. On the other hand, certain patterns of coherent fluid motion may correspond to patterns of swimming mechanics by fish, thereby reducing energetic costs (Liao 2003; Liao et al. 2003; Taguchi and Liao 2011), allowing restoration projects to benefit fish populations. However, the interactions between fish and turbulence are highly understudied outside of a handful of species, and studies emphasizing the specific impacts of turbulence generated by restoration structures are rare, precluding our ability to make specific recommendations to help restore declining fish populations.

The overall aim of my research was to investigate the interplay between fish energetics, habitat selection, and turbulence generated by structures. I explored this across a range of spatial scales, differing levels of structural size, orientation, and complexity, and environmental contexts to potentially provide new explanatory mechanisms for fish-instream structure interactions. To achieve this aim, I completed this research in three parts. In Chapter Two, I describe small-scale

laboratory experiments conducted to provide new insights regarding the close-range, local interactions between fish and turbulent flow generated by simulated instream restoration structures. In Chapter Three, I describe large-scale laboratory experiments that allowed for a detailed, mechanistic evaluation of the impact of turbulence generated by structures on fish energy use, and resulted in the development of bioenergetics models linking specific characteristics of turbulent flow with fish energy use. Finally, in Chapter Four, I describe large-scale laboratory experiments conducted to quantify how energetics and turbulent flow jointly mediate fish habitat selection. Together, these three chapters provide novel insights into the use of energy use as a means to assess the effectiveness of instream restoration structures, and also serve to increase the success of restoration activities by identifying the characteristics of instream restoration structures that lead to flow conditions that are energetically beneficial for fish and that encourage fish to select habitat within and near restoration structures.

CHAPTER TWO: SIMULATED INSTREAM RESTORATION STRUCTURES OFFER SMALLMOUTH BASS (*MICROPTERUS DOLOMIEU*) SWIMMING AND ENERGETIC ADVANTAGES AT HIGH FLOW VELOCITIES[1]

Abstract

Restoration practices aimed at fish habitat enhancement often include installation of instream structures. However, mixed outcomes have been reported regarding structure effectiveness, while mechanisms underlying success remain unknown. The interactions between fish and flow conditions generated by instream structures and their subsequent impact on fish energetics, may provide some insight. This study seeks to quantify how restoration structures, simulated by cylinders in three orientations, alter the energetics and swimming stability of smallmouth bass (*Micropterus dolomieu*). Accelerometers measured swimming stability, while a respirometer measured energy expenditure at multiple velocities. Particle image velocimetry was used to characterize flow fields behind structures. Structures generated flow conditions that benefited fish energetically. Fish had a smoother gait and expended less energy when swimming near a structure, regardless of its orientation. Benefits varied with flow conditions; reductions in energy expenditure were especially apparent at high flow velocities. Results suggest that restoration structures may be most energetically beneficial in stream systems with consistently high velocities and inform restoration by indicating flow conditions in which structures provide the greatest energetic benefits for fish.

[1] This work was published in the journal *Canadian Journal of Fisheries and Aquatic Sciences.*

Full citation: Strailey, K.K. Osborn, R.T., Tinoco, R.O., Cienciala, P., Rhoads, B.L., and C.D. Suski. 2021. Simulated instream restoration structures offer smallmouth bass (*Micropterus dolomieu*) swimming and energetic advantages at high flow velocities. Canadian Journal of Fisheries and Aquatic Sciences 78: 40-56.

Introduction

Freshwater ecosystems worldwide are currently at risk due to anthropogenic degradation that imperils water quality, connectivity, and biodiversity (Gleick 2003; Dudgeon et al. 2006; Vörösmarty et al. 2010). The Environmental Protection Agency (EPA) estimates that, of 750,000 sampled river kilometers in the United States, half were considered impaired, and nearly half (46%) were in poor biological condition. In addition, between 10,000 to 20,000 freshwater species are at risk of extinction, and, in North America, it is estimated that 39% of freshwater and diadromous fish species are imperiled (Jelks et al. 2008). Overall, freshwater systems are highly degraded, and the consequences of human impact are widespread.

Restoration is one way to counteract and mitigate the deterioration of freshwaters while complementing other conservation and management actions, such as erosion control, stormwater management, and riparian re-vegetation (Wohl et al. 2005, 2015; Bernhardt and Palmer 2007; Beechie et al. 2010). In the United States, tens of thousands of restoration projects have been undertaken over the past several decades and this approach to stream management is now a multibillion dollar industry (Bernhardt et al. 2005). The goals of river restoration vary widely, but generally focus on enhancing the environmental quality of human-impacted streams (Bernhardt et al. 2005). From an ecological perspective, restoration and the related activity of stream naturalization (Wade et al. 2002; Rhoads et al. 2011), often seek to counteract adverse impacts on aquatic communities through improvement of instream habitat (Bernhardt et al. 2005).

Many restoration efforts aimed at reversing declines in fish populations involve placement of artificial structures in streams or adoption of management approaches that encourage the development of natural structures in streams to improve physical habitat

(Thompson 2006; Palmer et al. 2014). Artificial structures can be large and highly complex, such as engineered log jams and woody debris (Abbe and Brooks 2011), or small and simple, such as sunken root wads and lunkers (crib-like structures supported by vertical piles and sunken into banks to provide cover for fish) (Radspinner et al. 2010). Besides providing habitat for fish, natural and artificial structures can also contribute to erosion control and flood protection (Gilvear et al. 2013). Structures can positively impact individual fish as well as fish populations and communities by increasing habitat heterogeneity (Tews et al. 2004), providing cover from predators (Fausch 1993), and generating regions of low-velocity flow that may benefit fish energetically (McMahon and Hartman 1989; Shuler et al. 2004; Antón et al. 2011; Boavida et al. 2011). As such, artificial instream structures as well as management approaches aimed at developing and preserving natural structures have been implemented widely to address a variety of issues related to degradation of the environmental quality of rivers (Nagayama and Nakamura 2010).

Despite widespread adoption of restoration strategies based on enhancement of instream structure through augmentation with artificial structures or promotion of natural structure development, mixed outcomes have been reported, with not all projects resulting in enhancements to fish populations (Kail et al. 2015). In fact, many restoration projects intended to increase fish population size and biodiversity through improved habitat heterogeneity have been ineffective (Stewart et al. 2009; Palmer et al. 2010; Lepori et al. 2017). Long-term impacts of instream structures on population changes often are difficult to assess because few projects include pre- and post-project monitoring (Downs and Kondolf 2002; Bernhardt et al. 2007). The response time to changes in habitat remains poorly constrained and many years of monitoring may be required to determine whether instream habitat structures actually benefit fish

populations (Louhi et al. 2016). Moreover, any favorable biological responses that are documented, such as increases in fish abundance or biomass, typically are assumed to result from restoration, yet detailed mechanism(s) underlying these changes remain unknown.

Stream restoration may yield inconsistent results, in part, due to a lack of understanding of the mechanisms that guide fish interactions with natural or artificial structures. The majority of studies examining restoration success have focused primarily on ecological metrics, such as changes in population size or community dynamics, that may be unable to clearly attribute responses to habitat enhancement. In contrast, physiological metrics, which can influence life-history (Ricklefs and Wikelski 2002b), community composition (Start et al. 2018), and species resilience (Hofmann and Todgham 2010), have largely been ignored. Individual physiology responds swiftly to changes in the environment, and as such may contribute to a more holistic, mechanistic understanding of how restoration impacts fish view of the results of restoration on fish.

The small-scale interactions between fish and structure-induced flow characteristics are rarely emphasized in either instream structure design or project monitoring; instead, the research, design, and evaluation of instream restoration structures largely focuses on geomorphic effects, such as increased scour and pool formation and erosion-control benefits that contribute to channel stability (Thompson 2002; Miller and Kochel 2010; Radspinner et al. 2010; Bennett et al. 2015). This is a concern because both natural obstructions and instream structures alter flow characteristics (Daniels and Rhoads 2013; Bennett et al. 2015), largely by generating coherent turbulent structures that increase levels of turbulence. Instream structure provides cover from predators and increases food availability (Angermeier and Karr 1984; Schneider and Winemiller 2008), but also generates turbulence that affects fish swimming behavior, kinematics, and energy

consumption (Tritico and Cotel 2010; Tullos and Walter 2014; Maia et al. 2015). Turbulence in rivers is characterized by chaotic, irregular fluctuations in velocity imposed onto mean flow, manifesting as vortices and eddies of various sizes and strengths (Warhaft 2002). The size, orientation, and intensity of such turbulence features are dependent on the mean water velocity, the depth of flow, and the characteristics of instream structures (Williamson 1996; Beal et al. 2006), while the intensity, periodicity, orientation, and scale of turbulent eddies, along with fish size and shape (Lupandin 2005; Tritico and Cotel 2010), determine interactions between fish and turbulence (Lacey et al. 2012). High levels of turbulence may place a large energetic burden on fish, in turn affecting fish position choice and habitat selection (Wilkes et al. 2017). On the other hand, certain patterns of coherent fluid motion may correspond to patterns of swimming mechanics by fish, thereby conferring reducing energetic costs (Liao 2003; Taguchi and Liao 2011). The possible energetic benefits of instream structure may be increased if structures are able to generate such flow conditions. However, the interactions between fish and turbulence are highly understudied outside of a handful of species, and studies emphasizing turbulence generated by instream structures largely focus on large-scale turbulence (Tullos and Walter 2014; Tullos et al. 2015).

The goal of this study is to quantify the small-scale interactions between a riverine fish and simulated instream structures at short range using an experimental, laboratory-based approach. We investigated the influence of structures on swimming performance and energetics, and chose to utilize energetics because energy expenditure is a metric firmly based on well-understood physiological mechanisms, as well as being particularly sensitive to environmental conditions and can be immediately responsive to changes in the environment (Enders and Boisclair 2016), such as the altered flows and turbulence generated by instream structures. Fish

were placed in a swimming respirometer outfitted with several different structures to vary flow conditions and explore potential influences of orientation or design elements of artificial structures. Rate-of-change accelerometers were implanted in fish to quantify position stability, concurrent with measurements of oxygen consumption; position stability was expected to decrease as water velocity increased and fish increasingly became unstable within the swim tunnel. Flow in the respirometer was characterized through the use of particle image velocimetry (PIV), with a particular emphasis on the intensity and orientation of turbulent vortices in addition to mean flow characteristics. The Centrarchid smallmouth bass (*Micropterus dolomieu*) was selected as the model species for this study as these river-dwelling fish often are a target species for instream restoration efforts in the United States (Moerke and Lamberti 2003; Hrodey and Sutton 2008). Results contribute to the understanding of fish energetics and provide insight into the physical characteristics of stream restoration structures that maximize energetic benefits for fish.

Methods

Fish collection and care

Smallmouth bass (n = 48) were delivered from Jake Wolf Memorial Fish Hatchery (Topeka, IL) to the Illinois Natural History Survey Aquatic Research Facility (Champaign, IL) on September 21, 2018. Upon arrival at the aquatic facility, smallmouth bass were held overnight in outdoor, 1135 L circular tanks to recover from hauling; tanks were connected to an earthen-bottom pond, and water temperature was 22 °C. The following day, each fish was weighed to the nearest gram (overall mean = 296.9 g ± 11.3 standard error, SE) and its length (total length, TL) measured to the nearest centimeter (mean = 27.5 cm ± 0.4 SE), before being divided among three indoor 567 L tanks at an initial temperature of 22° C. Water temperature in these indoor

tanks was then adjusted by 1 °C every day using heater-chiller units (TK 500, TECO, Ravenna, Italy) until treatment temperatures of 15 °C, 18 °C, and 21 °C were reached (Peake et al. 1997; Webb 1998); these temperatures reflect a range of ecologically relevant temperatures commonly encountered by stream-dwelling smallmouth bass (McClendon and Rabeni 1987; Wehrly et al. 2003). Multiple acclimation temperatures were utilized because swimming performance can vary across temperatures (Hocutt 1973; Kolok 1991), oxygen consumption ($\dot{M}O_2$) correlates positively with temperature (Enders et al. 2003), and the use of multiple temperatures increases the range of temperatures at which conclusions could be drawn for wild, free-swimming smallmouth bass. Once target temperatures were reached, an acclimation period began, and fish remained at target temperatures for between 65 and 70 days to ensure thermal acclimation (Johnston and Dunn 1987; Currie et al. 1998; Sandblom et al. 2014). Throughout the acclimation period, water quality (levels of dissolved oxygen and ammonia) was measured regularly (YSI Inc. Professional Plus; API Ammonia Test Kit) (Table 2.1). Smallmouth bass were fed live minnows (e.g., fathead minnows *Pimephales promelas*) once a week at a rate of 2% of their body mass.

Tagging procedure

Following the end of the acclimation period, each smallmouth bass was surgically implanted with an accelerometer tag (model MCFT3-SO, 6.8 g in air, 12.5 Hz recording frequency; Lotek Wireless, Newmarket, Ontario, Canada) to quantify position stability during swim trials. These tags measured jerk acceleration (i.e., the rate of change of acceleration), which has previously been used to quantify position changes in other aquatic organisms including Chinook salmon *(Oncorhynchus tshawytscha)* passing through dams and feeding harbor seal (*Phoca vitulina*) (Deng et al. 2005; Ydesen et al. 2014); jerk acceleration was utilized

as fish become increasingly unstable as water velocity increases and they approach the point of fatigue (Beamish 1970; Webb 1971). On average, tag burden was 2.17% of body mass, and, for the smallest individuals, the mass of the accelerometer tag in air did not exceed 4% body mass (Cooke et al. 2011). Visual inspections ensured that the volume of the tag was appropriate for the body cavity of the fish. Surgeries followed methods outlined in Wagner et al. (2011) and Harms (2005), and all fish were fasted for a minimum of 48 h before surgeries took place to allow sufficient time for digestion (Adams et al. 1998).

Fish were anesthetized with AQUI-S 10E (AQUI-S New Zealand LTE, Lower Hutt, New Zealand) at a concentration of 50 mg L^{-1} at a temperature identical to their acclimation temperature, until they lost equilibrium and were unresponsive to tail pinches. Each individual was then weighed, measured, and transferred to a wet surgical tray for tagging; no significant loss of mass was observed for the group as a whole between fish arrival at the facility and tagging (Welch two-sample t-test, $t_{83.9} = -0.97$, $p = 0.34$). A tube was placed into the fish's mouth to provide a constant flow of AQUI-S 10E-dosed water over the gills and maintain anesthetization. A 15-mm-long incision parallel to the ventral midline was made 2 mm anterior to the terminus of the pelvic fins and 1 mm off of the ventral midline. The accelerometer was gently inserted into the peritoneal cavity, while the antenna exited through the incision and was allowed to trail freely. The incision was then closed with a single absorbable suture (M452, size 3/0, NFS-2 needle; SouthPointe Surgical, Coral Springs, FL) and fish were immediately placed in a container of aerated water, matched to their acclimation temperature, to facilitate recovery. Once equilibrium was regained and normal swimming behavior resumed, fish were transferred to isolation totes and returned to their original acclimation tank. Isolation totes were clear and allowed for water flow and visual contact with other fish but prevented physical interaction or

tangling of antennas. Each fish was allowed to recover overnight for a minimum of 16 hours after tagging before participating in respirometer swim trials (Wilson et al. 2013), and no more than 7 days passed between a fish's tagging event and its inclusion in swim trials (Rodgers et al. 2016; Svendsen et al. 2016b). All surgeries were performed by the same individual, and average surgery time was 3:53 min (± 6.8 s SE).

Respirometer swim trials

Quantification of $\dot{M}O_2$ (energy use) when interacting with simulated instream structures was performed with tagged fish in a 30 L Steffensen-type swimming respirometer (#SW10150; Loligo Systems, Viborg, Denmark; Figure 2.1, panel a) using intermittent-flow respirometry (Steffensen et al. 1984; Nelson 2016; Svendsen et al. 2016b). The manufacturer indicates that this swimming respirometer is ideally suited for fish weighing between 175 and 500 g (https://www.loligosystems.com/secwim-tunnel-respirometer-3). Experimental treatments with turbulent flow consisted of the addition of a single 2.54-cm-diameter clear acrylic cylinder (hereafter referred to as a structure) securely mounted in the swimming chamber in one of three orientations (Taguchi and Liao 2011). In addition, control trials were conducted with no structures (NS). The reference frame is defined such that X is the longitudinal coordinate in the direction of the mean flow, Y is the horizontal transverse coordinate perpendicular to the mean flow, and Z is vertical (Figure 2.1, panels b-f). The structure was thus aligned with the Y-axis (horizontal structure - HS), Z-axis (vertical structure - VS), and diagonally within the YZ plane (diagonal structure - DS). VS was placed on the centerline of the chamber, HS was centered at half depth, and DS was placed with the high end of the structure against the swim chamber's inner wall oriented at a 45° angle. Structures were always placed in the swim chamber prior to introducing fish into the respirometer. The cylinders represented simplified versions of common

flow restoration structures, such as lunkers and root wads. The vertical support posts of a lunker are emulated by the vertical cylinder (Thompson 2005; Rosi-Marshall et al. 2006), whereas the complex structure of a root wad extending horizontally and diagonally into flow are represented by the horizontal and diagonal cylinders (Figure 2.1, panels b-f) (Shirvell 1990; Manners and Doyle 2008).

Swimming trials were conducted between December 3 and December 23, 2018. Tagged smallmouth bass, hereafter referred to by structure treatment (HS, VS, DS, or NS) were randomly assigned to one of the four treatments. Each fish was only assigned to a single treatment in the study, and fish size did not differ across treatments (one-way analysis of variance on body length, BL, $F_{1,40} = 1.4$, $P = 0.3$). The order that the study progressed was randomized in a three-tiered fashion intended to minimize the potential of temporal bias. First, tagged fish used in a trial were randomly chosen from the pool of all tagged individuals available on a given day. Second, for days in which fish from multiple acclimation temperatures were scheduled to swim, the order in which temperature treatments occurred was randomized, and the water within the respirometer was drained and re-filled as needed. Finally, the order that structures were added to the swimming respirometer at a given temperature was also randomized. Following introduction into the swimming respirometer, smallmouth bass were acclimated at 0.5 body lengths (BL)/sec for 30 min until normal behavior resumed (Peake et al. 1997; Cooke et al. 2001), indicated by the fish facing upstream and maintaining position within the swim chamber (Kern et al. 2018).

Following the acclimation period, water velocity in the respirometer was increased to 1.0, 1.5, 2.0, 2.5, and 3.0 BL/sec (where 1.0 BL/sec approximates 0.30 m/sec); approximate water velocity was determined via a pre-existing conversion relating tunnel motor revolutions per

minute (rpm) to water velocity (m/sec), initially generated with a flow meter (HFA, Höntzsch GmbH,Waiblingen, Germany). Water velocities were chosen based on previous measurements of critical swimming speed in similarly-sized smallmouth bass (Peake 2004) One measurement of $\dot{M}O_2$ was obtained at each of the six water velocities (Bouyoucos et al. 2017). During the swimming trial, the program AutoResp v.1 (Loligo Systems, Viborg, Denmark) was used to quantify $\dot{M}O_2$. For all trials, the length of the mix phase of each measurement cycle was held constant at 1 min; the length of each flush phase was set at 3 or 4 min, depending on the flush pump in use. To obtain a high coefficient of determination (r^2 value) across different flow velocities, the time of the measurement period (closed phase) varied from 4 to 15 minutes. Only $\dot{M}O_2$ values with an r^2 value above 0.9 were included in this study (Svendsen et al. 2016b). Trials ended either when a fish had successfully completed swimming at all five velocities, if a fish fell to the grate at the rear of the swimming chamber and refused to swim, or if a measurement period exceeded 15 minutes, a commonly used measurement period in similar studies (Bouyoucos et al. 2017; Brownscombe et al. 2018). Upon completion, each fish was removed from the respirometer and euthanized via an overdose of tricaine methanesulfonate (MS-222). The entire respirometer was cleaned with a bleach solution prior to trials beginning and regularly until all trials were completed. $\dot{M}O_2$ measurements of the empty respirometer were obtained regularly to assess any background microbial respiration, which was found to be negligible (Rodgers et al. 2016).

Flow measurements

Particle image velocimetry (PIV) was used to measure the velocity field within the respirometer on two two-dimensional (2D) planes within the test section: first, a vertical plane oriented along the direction of the flow (XZ plane) at the tank centerline, and second, a

horizontal plane oriented along the direction of the flow (XY plane) at mid depth. According to our reference frame, we define the components of the velocity as *u* in the longitudinal direction (X), *v* in the transverse direction (Y), and *w* in the vertical direction (Z). We use lower case symbols (*u, v, w*) to indicate instantaneous values, and upper case for time averages (*U, V, W*). (Figure 2.1). A 5W, 532nm, continuous-wave laser (PIV-01251 DPSS, OptoEngine LLC, Midvale, UT) coupled with a 45^{o} cylindrical lens was used to generate a vertical or horizontal light-sheet (with a thickness < 1 mm) for illuminating particles traveling within the illuminated plane (11-18 microns diameter spherical glass particles) (Figure 2.1, panels d-f). A monochromatic camera (JAI GO-5000M-USB; JAI Inc., San Jose, CA) captured 12-bit images with a 2560 × 2048 pixel resolution at frequencies from 30 to 60 frames per second (fps). Trials with the investigated scenarios, NS, VS, HS, and DS, were run at respirometer motor frequencies of 108, 161, and 200 Hz, equivalent to mean longitudinal velocities of U1=0.09, U2=0.18, and U3=0.24 m/sec, respectively.

Jerk acceleration data processing and statistical analysis

The accelerometer tags used in this study yielded data in the form of jerk acceleration (i.e., change in acceleration between two successive times of measurement), summed in all three axes of movement (X, Y and Z). For a given data point at time t_x, a jerk acceleration value greater than zero corresponds to a change in acceleration relative to acceleration at time t_{x-1} (i.e., a 'jerk' or change in swimming acceleration); a jerk acceleration value equal to zero at t_x indicates an unchanged acceleration relative to acceleration at time t_{x-1}. Thus, when quantified over longer sampling intervals, periods of zero jerk acceleration indicate a consistent, smooth swimming gait, while non-zero values of jerk acceleration indicate that fish are changing gait, and not swimming in a consistent fashion. Because the quantity of jerk acceleration data

generated varied across fish and across trials (i.e., different oxygen measurement durations occurred at different water velocities), the total number of data points greater than zero, and the number of data points equaling zero (referred to here as jerk and zero measurements, respectively) were first counted for each individual fish at a given swimming velocity. These counts were then used to create a response variable that consisted of the proportion of jerk accelerations relative to jerk-acceleration values of zero for a fish at that swim velocity, as shown below:

$$Jerk\ proportion = \frac{\#\ of\ jerk\ measurements}{Total\ measurements} \quad (2.1)$$

With this proportion as the response variable, data were modeled with a generalized linear mixed model that included structure treatment, water velocity, and temperature as fixed effects, structure treatment and water velocity as an interactive effect, and fish ID as a random effect (Bolker et al. 2008); structure and water velocity were interacted in all models due to this study emphasis on the role of environmental conditions in affecting swimming stability and oxygen consumption. A linear mixed effects model was appropriate because multiple fixed effects, including water velocity, structure type, and temperature, and their interactions were of interest, and because the inclusion of individual fish across multiple swimming velocities involved repeated measures (Zuur et al. 2009). A beta-binomial distribution was used in the model not only to account for the fact that the jerk acceleration data are proportions (zero or non-zero) (Crowder 1978; Bolker et al. 2008), but also because of overdispersion of the data as indicated by residual deviance greater than the residual degrees of freedom (Ennis and Bi 1998; Crawley 2013). Model selection was based on fixed effects that best fit the data with the best fit defined by the model with the lowest AIC value (Table 2.2) (Zuur et al. 2009; Crawley 2013). Due to the large number of zero values in the data, a number of candidate zero-inflation models

were also tested (Zuur et al. 2009); ultimately, the best-fitting model specified no zero inflation. While it ultimately was not included in the best-fitting model, fish length was tested as a possible fixed effect because the effect of turbulence is related to how an eddy's diameter corresponds to a fish's length, whereby a fish is more likely to be affected when its length is similar to the diameter of the eddy (Lacey et al. 2012). Model fit was assessed through examination of predicted and observed quantile residuals for the overall model (i.e., quantile-quantile plots and examination of distribution of residuals), as well as for the structure and water velocity predictors (Pereira 2019). Possible effects of outliers or influential data points were considered to ensure that these effects were not present and did not influence model fitting (Zuur et al. 2009). Estimated marginal means were used to make *post-hoc* pairwise comparisons between fixed effects (West et al. 2007).

Oxygen consumption statistical analysis

Because fish mass does not scale linearly with metabolic costs (Clarke and Johnston 1999), raw $\dot{M}O2$ data were transformed from mg O_2 kg^{-1} hr^{-1} to mass-independent mg O_2 hr^{-1}. As with the jerk acceleration data, a linear mixed effects model was used to define the impacts of various fixed effects on $\dot{M}O2$. Water velocity, structure type, and temperature, interactions among these variables, and fish mass, were included as fixed effects in models with $\dot{M}O2$ treated as the dependent variable. Fish ID was specified as a random effect to account for the repeated sampling of the same individual across multiple swimming velocities (Crawley 2013). Additional models including respirometer swim trial date and days between surgical tagging and trial date as random effects were also tested. Model selection was based on the model that best fit the data where the best fit corresponded to the model with the lowest AIC score (Table 2.3) (Crawley 2013). Both $\dot{M}O2$ and fish mass (g) were scaled logarithmically because the

relationship between $\dot{M}O_2$ and mass is not linear (Clarke and Johnston 1999; Killen et al. 2012). Interestingly, although temperature was included in the best-fitting model for jerk acceleration, the variable was not included in the best-fitting model for $\dot{M}O_2$ data; the fixed effect factors ultimately included in the best-fitting $\dot{M}O_2$ model were water velocity, structure treatment, the interaction between these two variables, and logarithmically-scaled fish mass. The model fit for $\dot{M}O_2$ data was assessed through a visual assessment of fitted residual and quantile-quantile plots (Zuur et al. 2009). Outlier tests were used to ensure that model fitting was not affected by influential data points (Zuur et al. 2009). Estimated marginal means were used to make *post-hoc* pairwise comparisons between fixed effects terms (West et al. 2007).

All data derived from swim trials were processed and analyzed in R (v3.6.0 R Foundation for Statistical Computing, Vienna, Austria). The package 'lme4' v. 1.1-21 (Bates et al. 2015) was used to estimate mixed effects models for $\dot{M}O_2$ data, while 'glmmTMB' v. 0.2.3 (Brooks et al. 2017) was used to analyze jerk acceleration proportion data. Packages used for model selection include 'car' v.3.0-3 (Fox and Weisberg 2019), 'sjstats' v. 0.15.5 (Lüdecke 2019), 'rsq' v. 1.1 (Zhang 2018), and 'DHARMa' v.0.2.4 (Hartig 2019); 'car' was utilized to generate outlier and influential data plots, while 'sjstats' and 'rsq' were used to generate marginal and conditional r^2 values for each model, and 'dHARMA' was used to generate quantile residuals for the best-fitting jerk acceleration model. Post-hoc pairwise comparisons were made with 'emmeans' v. 1.3.4 (Lenth 2019). Figures were generated and arranged with 'ggplot2' v. 3.1.1 (Wickham 2016) and 'cowplot' v. 0.9.4 (Wilke 2019). The level of significance (α) for all tests was set at 0.05, and all reported are shown as ± SE where appropriate.

Analysis of velocity statistics

PIV images were analyzed using Matlab-based (MathWorks R2017a) open source software PIVlab (v2.02) (Thielicke and Stamhuis, 2014). Data analysis through PIVlab yielded 2D fields of instantaneous velocities *u* and *v* for horizontal XY planes, and of *u* and *z* for vertical XZ planes, with a spatial resolution of 3.2 mm. Plots of 2D time-averaged velocities in the longitudinal (*U*), transverse (*V*), and vertical direction (*W*) were obtained from the full time series of velocity data at each measurement location for all tested cases. Three turbulence metrics with potential effects on fish swimming capabilities were calculated (Lacey et al. 2012): Reynolds stresses, turbulent kinetic energy (TKE), and vorticity. Reynolds decomposition was used to calculate instantaneous velocity fluctuations, *u', v', w'*, as:

$$u' = u - U \tag{2.2}$$

$$v' = v - V \tag{2.3}$$

$$w' = w - W \tag{2.4}$$

Turbulent kinetic energy, TKE, is calculated in XZ and XY planes, respectively, as:

$$TKE_{XZ} = \frac{1}{2}\left(2\overline{u'^2} + \overline{w'^2}\right) \tag{2.5}$$

$$TKE_{XY} = \frac{1}{2}\left(2\overline{u'^2} + \overline{v'^2}\right) \tag{2.6}$$

Instantaneous fluctuations are used to calculate time-averaged (indicated by overbars) Reynolds stresses, $\overline{u'v'}$ *and* $\overline{u'w}$. Components of vorticity, ω_y and ω_z, were calculated as the curl of the velocity vector, $\vec{\omega} = \nabla \times \vec{v}$, where $\vec{v} = (u, v, w)$. Reynolds stresses, TKE, and vorticity are all measures of the strength of turbulence that may affect fish swimming capabilities (Lacey et al. 2012).

To ensure all cases were within the fully turbulent wake regime (Williamson 1996), the Reynolds number (*Re*) based on cylinder diameter (*d*) was calculated for each case, yielding values of $Re = Ud/\nu$ = {1200, 5200, 6800}, where ν is the kinematic viscosity of water. To estimate the spatial effect of the structures, we calculate the cylinder wake wavelength, λ, the characteristic eddy frequency, f_p, and associated length scale, L_T. λ was calculated based on the shedding frequency, *f*, Strouhal number, *St*, and the mean velocity (*U*) as $\lambda = U/f$. Shedding frequency was estimated through $St = fd/U$, using the expected value of *St* =0.21 for the range of *Re* investigated (e.g., Liao, 2003). Characteristic eddy frequency was obtained by computing the frequency spectra at each PIV subwindow, and identifying the frequency f_p of the largest peak on the spectrum. The associated eddy length scales were computed using the corresponding time scale, $T_T=1/f_p$, and mean velocity magnitude (i.e., $L_T=T_TU$)

For a consistent comparison across all treatments, TKE, vorticity, and Reynolds stresses were converted to non-dimensional form based on the undisturbed velocity U_∞ obtained from the temporal and spatial average of the case with no structure at each flow rate, and the diameter of the obstruction (i.e., TKE/U_∞^2, $\overline{u'w'}/U_\infty^2$, $\omega_y d/U_\infty$ $\omega_y d/U_\infty$). Values of nondimensional turbulence metrics were extracted and plotted for the vertical (XZ), and horizontal (XY) planes.

Results

Jerk acceleration

The model that best fit the jerk acceleration data, indicated by the lowest AIC score amongst the candidate models compared, included simulated structure, water velocity, and temperature as fixed effects as well as the interactive effect of simulated structure and velocity. Although the inclusion of temperature improved the fit of the jerk acceleration model based on

AIC score, it did not significantly impact proportion of jerk acceleration measurements (Table 2.2). All results are derived from post-hoc pairwise comparisons.

Smallmouth bass swimming in the respirometer with no flow-modifying structures (NS treatment) did not differ significantly in proportion of jerk measurements when water velocity increased from 1.0 BL/sec to 1.5 BL/sec (Table 2.3; Figure 2.2, panel A). As water velocity further increased beyond 1.5 BL/sec to 2.0, 2.5, and 3.0 BL/sec, the proportion of jerk acceleration movement in the NS treatment increased significantly with each increase in flow rate. At the highest flow rates of 2.5 and 3 BL/sec, the proportion of jerk acceleration measurements observed in the NS treatment was over 400 times greater than the proportion when fish were swimming at 1.0 BL/sec. In contrast, at 2.0, 2.5, and 3.0 BL/sec, the proportion of jerk measurements for fish swimming with any type of structure was significantly less than fish in the no structure treatment swimming at that same velocity (Table 2.3; Figure 2.2, panel A). The proportions of jerk measurements generated by smallmouth bass swimming in the respirometer with a diagonal structure, DS, at velocities greater than 1.0 BL/sec did not differ significantly from the proportion at 1.0 BL/sec suggesting that the fish in this treatment maintain a smooth swimming gait across all velocities (Table 2.3; Figure 2.2, panel A). In fact, the proportion of jerk measurements generated by smallmouth bass swimming with a DS at velocities of 2.0 BL/sec and 2.5 BL/sec was significantly less than the proportions of NS fish swimming at 1.5 BL/sec. Smallmouth bass in the HS treatment showed a 12-fold increase in the proportion of jerk measurements at 2.5 and 3.0 BL/sec relative to proportions at 1.0 BL/sec. Fish in the VS treatment also displayed significantly higher proportion of jerk measurements relative to 1.0 BL/sec, but only when swimming velocity increased to 3.0 BL/sec. While differences between

different structures at a given velocity were not significant, DS fish consistently had the lowest proportion of jerk measurements at high velocities, followed by VS fish and then HS fish.

Oxygen consumption

For $\dot{M}O_2$ data, the best fitting model included the interaction between simulated structure and velocity as well as the log of fish mass (g); temperature was not included as a parameter in the best-fitting model. The $\dot{M}O_2$ of smallmouth bass swimming with structures did not differ across water velocities; even at the highest velocities of 2.5 and 3.0 BL/sec, $\dot{M}O_2$ did not differ significantly from $\dot{M}O_2$ at 1.0 BL/sec (Figure 2.2, panel B). In contrast, fish swimming without a structure experienced an increase in $\dot{M}O_2$ of about 20%, relative to $\dot{M}O_2$ at 1.0 BL/sec, at 2.5 and 3.0 BL/sec (Figure 2.2, panel B). However, at a given water velocity $\dot{M}O_2$ did not differ significantly for fish swimming with or without a structure (Table 2.5).

Flow characteristics

Water velocity was highest overall throughout the test section for tests without a simulated structure (Figure 2.3). Alternating bands of high and low velocity along the Y axis highlighted the effect of the flow-redirecting vanes at the end of the tunnel (Figure 2.4). Although this banding was evident to some extent in the tests with structures, it was clearly overwhelmed by the effect of the structures on the flow.

As expected, the added resistance from the obstructions reduced overall water velocity throughout the test section of the respirometer. Moreover, pockets of reduced velocity developed in the lee of all structures, which produced a wake effect in the corresponding plane of orientation (Williamson 1996): the XZ (vertical) plane for the HS (Figure 2.3) and the XY (horizontal) plane for the VS (Figure 2.4). The DS produced a diagonal wake in both the XZ and

XY planes (Figure 2.3; Figure 2.4). A clear zone of recirculating fluid existed behind all structures (Figure 2.3 - VS, HS, DS; Figure 2.4 - VS, HS, DS). Since only one diameter was tested, wake wavelength remained similar across all cases, at $\lambda \approx 0.12\ m$, with shedding frequencies f = [0.7, 1.5, and 2.0] Hz corresponding to bulk velocities U = [0.09, 0.18, 0.24] m/sec.

Patterns of TKE, vorticity and Reynolds stresses (Figures 2.5 to 2.9) clearly illustrated the influence of the simulated structures on turbulence. For the NS case, TKE, vorticity, and Reynolds stresses were relatively uniform in the XZ plane (Figure 2.5). However, as seen in the mean velocities in Figure 2.4, the deflecting vanes have an effect on mean velocity and vorticity in the XY plane (Figure 2.6). Nondimensional profiles of TKE, vorticity, and Reynolds stresses in the X-Z (Figure 2.7) and X-Y (Figure 2.8) planes confirm that, even in the horizontal plane, the flow is dominated by the cylindrical structures. The biggest impact of the vanes is noticed in the vertical component of vorticity (Figure 2.8), but is not translated to the TKE and Reynolds stress, for which magnitudes for the NS case are an order of magnitude lower than the VS, HS, and DS (Figure 2.7; Figure 2.8). A 2D analysis of eddy frequency, fp, and eddy length scale, LT (Figures 5(j-o), 6(j-o)) shows that even if the vorticity magnitude is of similar order for NS and VS, this is the result from faster, smaller eddies with length scales smaller than fish size.

High TKE values were present downstream of the structures, with a wake in the vertical plane formed in the lee of the HS (Figure 2.5, panel b), a wake in the horizontal plane generated behind the VS (Figure 2.6, panel b), and a diagonal wake formed behind the DS (Figure 2.5, panel c; Figure 2.6, panel c). Positive and negative patterns of vorticity (Figure 2.5, panels d-f; Figure 2.6, panels d-f) and Reynolds stress (Figure 2.5, panels g-i; Figure 2.6, panels g-i) on each side of the wake clearly show that opposing patterns of fluid rotation occurred in shear layers

bounding the wakes and that vortex shedding produced a Karman vortex street downstream of the structures. The DS produced a noticeably wider spread of vortex shedding compared to the VS and HS. Non-dimensional transects of TKE, vorticity, and Reynolds stresses show that enhanced turbulent conditions were present for all structures for the full range of velocities investigated in this study (Figure 2.7; Figure 2.8). The DS enhanced TKE, vorticity, and Reynolds stresses both in the horizontal and vertical planes, while the VS and HS enhanced these parameters only in the X-Y and X-Z planes, respectively.

Discussion

The results of this study show that the presence of structures in the respirometer alters characteristics of the mean flow and turbulence, which in turn alters fish swimming behavior, and fish energy expenditure.

Jerk acceleration

The presence of simulated structures in the respirometer resulted in a smoother swimming (i.e., less 'jerky') gait for smallmouth bass. Fish swimming with structures experienced a significantly lower proportion of non-zero jerk measurements relative to fish in the control treatment, likely due to altered flow characteristics. Unobstructed flow is naturally turbulent, but does not develop coherent turbulent structures to the degree that flow does when physical structures are present (Robinson 1991). Immersed structures generate wakes, or zones of reduced velocity, downstream of the structures, and both the shear layers bounding the wakes as well as vortices shed from the wakes produce high levels of vorticity and TKE (Williamson 1996). Generally, the results indicate that structures confer benefits when fish are interacting with them at short range by improving swimming stability, especially for flows with high mean velocities within the ranges used in this study, as shown in Figures 2.5 and 2.6.

Smallmouth bass swimming with structures experienced a lower proportion of jerk acceleration measurements and were able to maintain a more stable swimming position (i.e., lower proportion of jerk measurements), particularly at swimming speeds above 2 BL/secec, likely due to their utilization of the flow conditions generated by the structures. These fish were likely able to exploit pockets of reduced velocity as refugia from the relatively high velocity in other areas of the flow (identified as low-velocity areas in Figures 2.3 and 2.4, corresponding to high vorticity as shown in Figures 2.5 and 2.6), thereby resulting in a smooth swimming gait and a reduced proportion of jerk measurements at a given swimming speed compared to NS fish. Alternatively, smallmouth bass may also have coordinated their swimming mechanics with characteristics of coherent turbulent structures generated by simulated structures. The ability of certain fish species to exploit turbulence has been well-documented (Liao 2007). Previous laboratory studies have shown that rainbow trout reduce muscle activity when swimming in turbulent eddies shed by cylinders by utilizing a unique swimming gait known as the Kármán gait (Liao et al. 2003; Liao 2004); this gait allows trout to essentially slalom between eddies and reduce their need for powered swimming. Others have shown that when fish swim in the turbulent flows generated within a school, they have lower tail-beat frequencies than fish swimming alone, likely due to interactions with vortices shed by other members of the school (Svendsen et al. 2003). Smallmouth bass may potentially be capable of exploiting turbulent vortices as well, and may have utilized such a swimming strategy in this study.

While the zones of reduced velocity behind each structure can be beneficial regardless of orientation, the orientation of a vortex affects whether it can be exploited by fish. Flow analyses characterizing flow on vertical and horizontal planes for three structure orientations (HS, VS, and DS) demonstrated the similarities of generated wakes in their respective planes (Figure 2.7;

Figure 2.8), allowing for the assessment of a broad range of *Re* and TKE levels. Direct comparison across treatments (Figure 2.9) displayed the various patterns generated by the 3 orientations, allowing for the identification of specific zones that may work as attractors or distractors for fish swimming behind such structures based not only on bulk velocity, but also on turbulence and vorticity metrics. Typically, horizontally-oriented vortices, such as those generated by the VS, can be exploited by fish (Liao et al. 2003; Taguchi and Liao 2011), reducing their need for powered swimming, while vertically-oriented vortices, such as those generated by the HS, may destabilize fish (Tritico and Cotel 2010; Maia et al. 2015). These documented relations may explain why smallmouth bass in the DS treatment, which included both the development of a zone of low-velocity behind the structure and horizontally-oriented vortices, experienced no increases in jerk acceleration across water velocities. On the other hand, HS fish, which were exposed to potentially destabilizing vertically-oriented vortices, experienced a higher number of jerk accelerations at high velocities than either DS or VS fish.

Oxygen consumption

The presence of simulated structures provided an energetic advantage for smallmouth bass relative to fish in the control (NS treatment), particularly when water velocities reached 2.5 BL/secec. More specifically, the $\dot{M}O2$ of smallmouth bass swimming with structures did not differ across water velocities, whereas smallmouth bass swimming with no structure in the respirometer had higher $\dot{M}O2$ at 2.5 and 3.0 BL/sec relative to $\dot{M}O2$ at the lowest velocity. Energetic demand correlates positively with swim velocity for fish due to the increased recruitment of aerobic red muscle fiber necessary to power swimming (Coughlin 2002), which, in turn, results in an increase in $\dot{M}O2$ across swim speeds until anaerobic (burst) swimming occurs (Beamish 1970; Webb 1971). Certain fish species have previously been shown to reduce

$\dot{M}O_2$ when swimming with structures or swimming in enhanced turbulent conditions (Liao 2007). Rainbow trout, for example, are able to employ specific swimming gaits, including the Kármán gait, and may preferentially position themselves in turbulent flow generated by cylinders to consume less oxygen when swimming (Cook and Coughlin 2010; Przybilla et al. 2010), and, at times, can decrease their $\dot{M}O_2$ even when water velocity increases (Taguchi and Liao 2011). Shiner perch (*Cymatogaster aggregata*) are also able to reduce $\dot{M}O_2$ in turbulent flow, even when such flow is lacking in coherent vortical structures (van der Hoop et al. 2018). While no studies to date have demonstrated a similar gait in smallmouth bass, as a riverine species, this species may have some ability to exploit turbulent flow, similar to rainbow trout. Such behavior may account for the lack of an increase in $\dot{M}O_2$ values, despite an increase in water velocity. Alternatively, smallmouth bass in the structure treatments may have simply positioned themselves in the low-velocity pockets behind each simulated structure (Figure 2.9), thereby reducing swimming oxygen costs. Further work that examines in detail the swimming gait and position of fish in relation to structures is needed to determine which of these strategies was potentially at play. What the results do confirm is that smallmouth bass swimming in the presence of simulated structures maintained a consistent $\dot{M}O_2$ across water velocities compared to fish swimming without simulated structures, which experienced pronounced increases in $\dot{M}O_2$ at high velocities.

Interestingly, temperature was not a significant predictor in the best-fitting model for $\dot{M}O_2$, indicating that the oxygen consumed by smallmouth in the swimming respirometer did not vary with temperature. $\dot{M}O_2$ in fish normally correlates positively with temperature, with fish consuming greater amounts of oxygen at higher temperatures (Enders and Boisclair 2016). Three explanations are possible as to why temperature did not significantly relate to $\dot{M}O_2$ in the current

study. First, the range of temperatures may not have been sufficiently broad to result in a significant temperature relationship for smallmouth bass, which have a wide thermal range and high thermal tolerance. These fish commonly occur in environments where water temperatures may drop to near 0 °C in the winter and rise to well over 20 °C in the summer (Eaton and Scheller 1996; Suski and Ridgway 2009). As such, varying temperature by 6 °C, from 15-21 °C, may not have been sufficient to produce differences in $\dot{M}O_2$ over this range for such a eurythermal fish, which has evolved to tolerate a wide range of temperatures. Second, the temperatures used in the current study may not have been sufficiently distinct to generate significant differences in statistical models. Notably, when the impact of temperature on $\dot{M}O_2$ was plotted across structure types (Figure A.1), the 15 °C and 21 °C treatments appeared to differ, whereas the 18 °C treatment had a wide range of $\dot{M}O_2$ values across all structure types. Indeed, if a simple analysis of variance is performed with temperature included as the sole fixed effect and $\dot{M}O_2$ as the response variable, $\dot{M}O_2$ differs for fish swimming at 15 °C and 21 °C, but fish swimming at 18 °C do not differ significantly from the other two temperature treatments (Table A.1). This analysis suggests that temperature may have an effect on $\dot{M}O_2$, with higher amounts of oxygen consumed at the warmest treatment relative to the other treatments, but that the temperature effect was masked by strong effects from other factors. Lastly, the lack of a relation between temperature and $\dot{M}O_2$ may be the result of reduced statistical power due to relatively small sample sizes and complex modeling procedures. To better account for thermal impacts on both swimming ability and $\dot{M}O_2$, future studies should utilize a wider range of acclimation temperatures that more thoroughly represent the conditions commonly experienced by the study species in the wild.

Results from this study have three main implications for the use and design of instream restoration structures in relation to their physiological influence on stream-dwelling smallmouth bass. First, regardless of the orientation of a structure, its components, or the water temperature, restoration structures can confer energetic benefits for smallmouth bass when they are interacting with structures at short range. The addition of simulated structures, regardless of their orientation, produced pockets of reduced velocities and coherent turbulent structures that provide energetic advantages for fish. Second, energetic expenses (such as $\dot{M}O_2$ rates) serve as an important physiologic metric for documenting short-term responses of fish to altered flow generated by instream structures. As such, energy expense may be a useful tool to supplement existing *in situ* monitoring for evaluating and monitoring the effectiveness of restoration projects. Such a tool can complement measures of population- and community-level changes following restoration, some of which may change only slowly over several years (Jeffrey et al. 2015). By providing insight into fish interactions with turbulent flow, an aspect of the environment known to strongly influence swimming performance, energetics may contribute, in conjunction with other metrics, to a more holistic understanding of population-level responses to instream structures and stream restoration. Finally, at low velocities, structures conferred no apparent benefit for either energetic expense or position stability, but at high velocities, the value of structures became more pronounced, suggesting that the benefits of instream structures change across hydraulic contexts. While this potential threshold effect requires future study to relate precisely to fish response, these results suggest that the energetic benefits of structures may be most pronounced in fast-flowing rivers or during high-flow events when fully turbulent coherent flow structures are developed. On the other hand, structures may not provide energetic advantages in streams with consistently low flow velocities.

Caveats and future directions

Not all aspects of the relation between swimming energetics and flow characteristics could be explored in this laboratory investigation using a respirometer. Several caveats are identified that should be addressed in future work. First, although non-dimensional turbulence statistics allow extrapolation of results of measured cases to those of unmeasured cases within the range of *Re* investigated (as shown in Figures 2.7 and 2.8), turbulence statistics did not directly correspond to all mean flow velocities tested in swimming trials, limiting direct quantification of fish-flow interactions in this study. Second, conclusions from this study may be somewhat limited due to the physical constraints of the swimming respirometer, and results apply to short-range interactions between smallmouth and instream structures. Swimming respirometers have a defined swimming chamber to keep fish in a consistent location, and the size of the chamber and volume of water in the tunnel dictate the size of the fish that can be used. If fish are too small, $\dot{M}O_2$ data are unreliable, and, in contrast, fish that are too large cannot move freely (Svendsen et al. 2016b). In the current study, the fish were adequately sized for the tunnel and for the size of the accelerometer tags (Brown et al. 2004; Cooke et al. 2011), but were somewhat restricted in motion with little 'choice' in which portion of the swim chamber they could occupy, in part due to the presence of structures. As such, some uncertainty exists as to whether smallmouth bass were purposefully utilizing low velocity pockets behind simulated structures and/or coherent turbulent vortices generated by these structures. A critical need exists to utilize large flumes, or field deployments in future work that allow fish unrestricted choice in position and enable tracking of fish positions, which in turn will allow for the precise evaluation of potential swimming strategies at play. Through such studies instantaneous swimming responses can be linked to local characteristics of the flow to provide improved insight into how

much fish benefit from turbulent structures, low-velocity zones, or both. Larger test environments will additionally allow for the investigation of interactions between fish and structure-generated turbulence on a longer range. Third, only a single structure diameter was investigated due to the size of the respirometer test section, limiting the size of eddies that could be generated. The influence of an eddy on a fish's swimming behavior depends in part on elements of scale, with eddies much smaller or larger than a fish having little effect on swimming, but eddies of diameters near the length of a fish being more likely to alter swimming kinematics and behavior (Lacey et al. 2012). Depending on the species, this may result in improved or reduced swimming performance (Lacey et al. 2012). Future studies with multiple combinations of BL:structure diameter ratio will allow detailed characterization of eddy size and eddy orientation. Despite these caveats, this study shows that structures do provide benefits to smallmouth bass both in terms of energetic expenses and position stability, particularly when smallmouth bass are interacting with structures at short range.

Conclusion

Although instream structures are a common tool for restoration of fish habitat in freshwater systems, the independent effects of these structures on fish energetics are poorly understood. This study utilized a laboratory approach to isolate how altered flows generated by simple simulated instream structures impact the energetic expense and swimming stability of smallmouth bass when smallmouth are interacting with structures at close range. Results showed that smallmouth bass swimming with structures were able to utilize altered flow conditions both to maintain a stable swimming position and to reduce energy expenditure compared to unaltered flow conditions in the absence of simulated structures. Interestingly, benefits of structures were most evident at high mean water velocities but were not statistically significant at low velocities.

These findings provide direction for future laboratory or mesocosm studies investigating the interactions between smallmouth bass and restoration structures, and additionally inform management aimed at the design, implementation, and augmentation of natural and artificial instream restoration structures by illustrating the hydraulic conditions in which instream structures may be most energetically beneficial for smallmouth bass. However, further work is needed to identify precisely the threshold velocities in natural streams that lead to energetic benefits by structures. Future investigations should move into larger laboratory spaces or beyond the lab, into the field, to directly estimate the energetic consequences of natural turbulent flows for fish, which is now possible due to recent advances in telemetry methods (Metcalfe et al. 2016) that allow indirect measurement of energetic expenses of free-swimming fish. The findings of this study may additionally illuminate particular flow conditions of interest in future field-based investigations. Subsequent studies as well as restoration monitoring efforts should continue to include physiological metrics to improve fish management and conservation (Young et al. 2006); while many factors impact the interactions between fish and instream structures, and the responses of fish communities to such restoration are complex, energetics, in particular, can clearly demonstrate the direct physiological responses of individual fish to altered flow conditions. By combining estimates of $\dot{M}O_2$ with direct measurements of the flow field in spaces much larger than the typical respirometer, the effect of instream structures of increased size and complexity, as well as arrangements of multiple structures, on fish energetics can be tested. Developing a more complete understanding of the role of energetics within the context of the many other ecological aspects of structures is a complex endeavor that will require multifactor field and experimental investigations in the future.

Figures

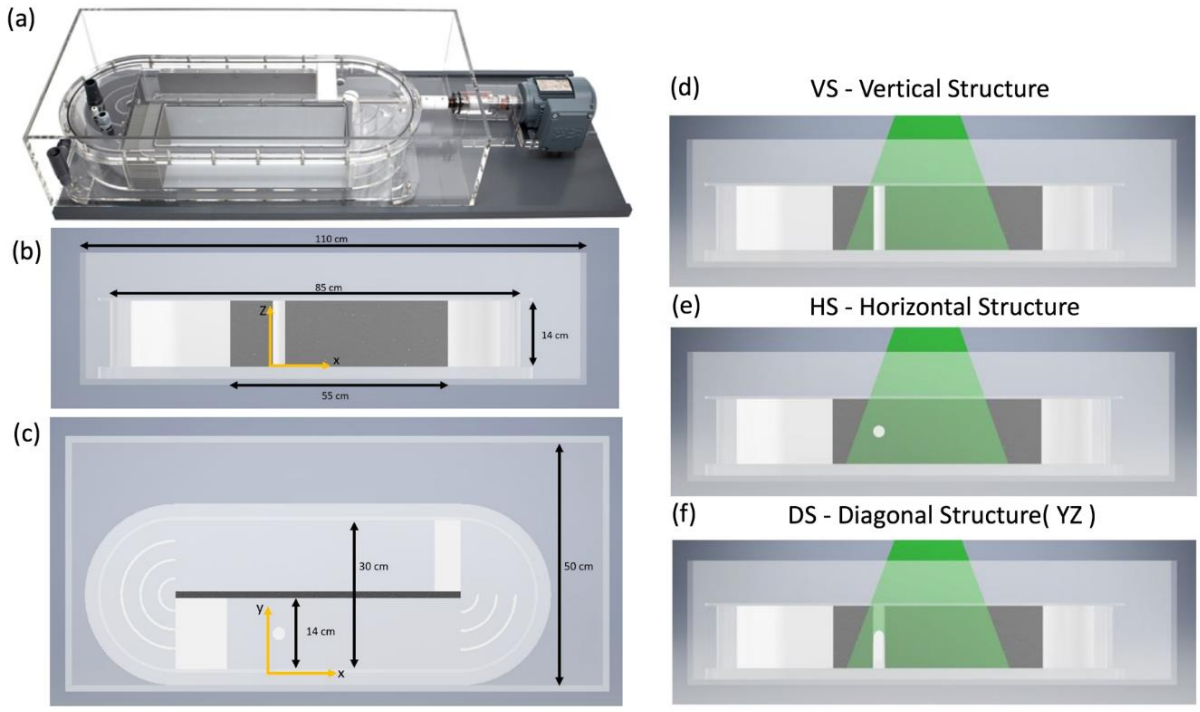

Figure 2.1. Photo of a 30 L swimming respirometer (a) utilized for accelerometer-tagged smallmouth bass swim trials and flow measurements, depicting the side (b) and top (c) views of the respirometer with relevant dimensions. The location of each tested structure, including the vertical structure (VS, d), the horizontal structure (HS, e), and the diagonal structure (DS, f) are depicted during vertical XZ plane tests.

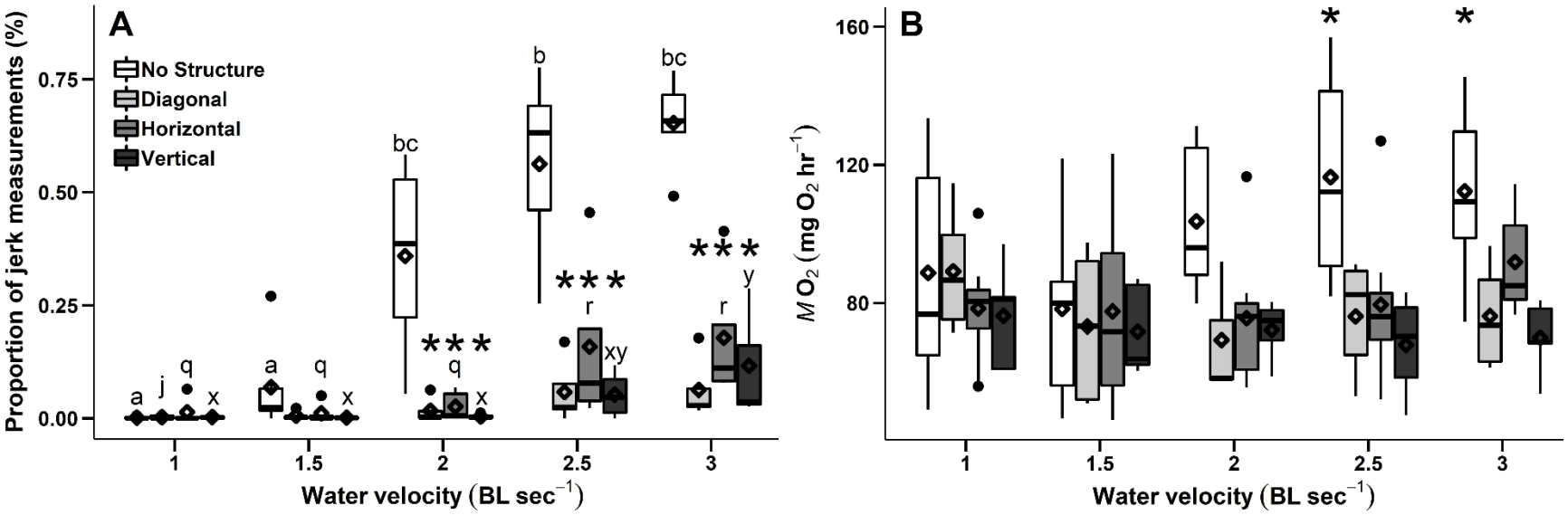

Figure 2.2. The proportion of jerk measurements (Panel A) and oxygen consumption (in mg O_2 hr^{-1}; Panel B) by structure treatment and swimming velocity (BL/s) for smallmouth bass acclimated to one of 3 different temperatures. For jerk acceleration sample sizes varied from 3 to 6 fish per structure per swimming velocity. Letter assignments indicate a significant difference across velocities within a given structure treatment, either no structure (abc), diagonal, horizontal (qr), or vertical (xy). Stars indicate a significant difference for a particular structure in comparison to the control treatment at that given swimming velocity. For oxygen consumption, sample size varied from 2 to 9 fish per structure per swimming velocity, and stars indicate a significant difference between MO_2 at the given velocity and MO_2 for that same structure at 1.0 BL/s.

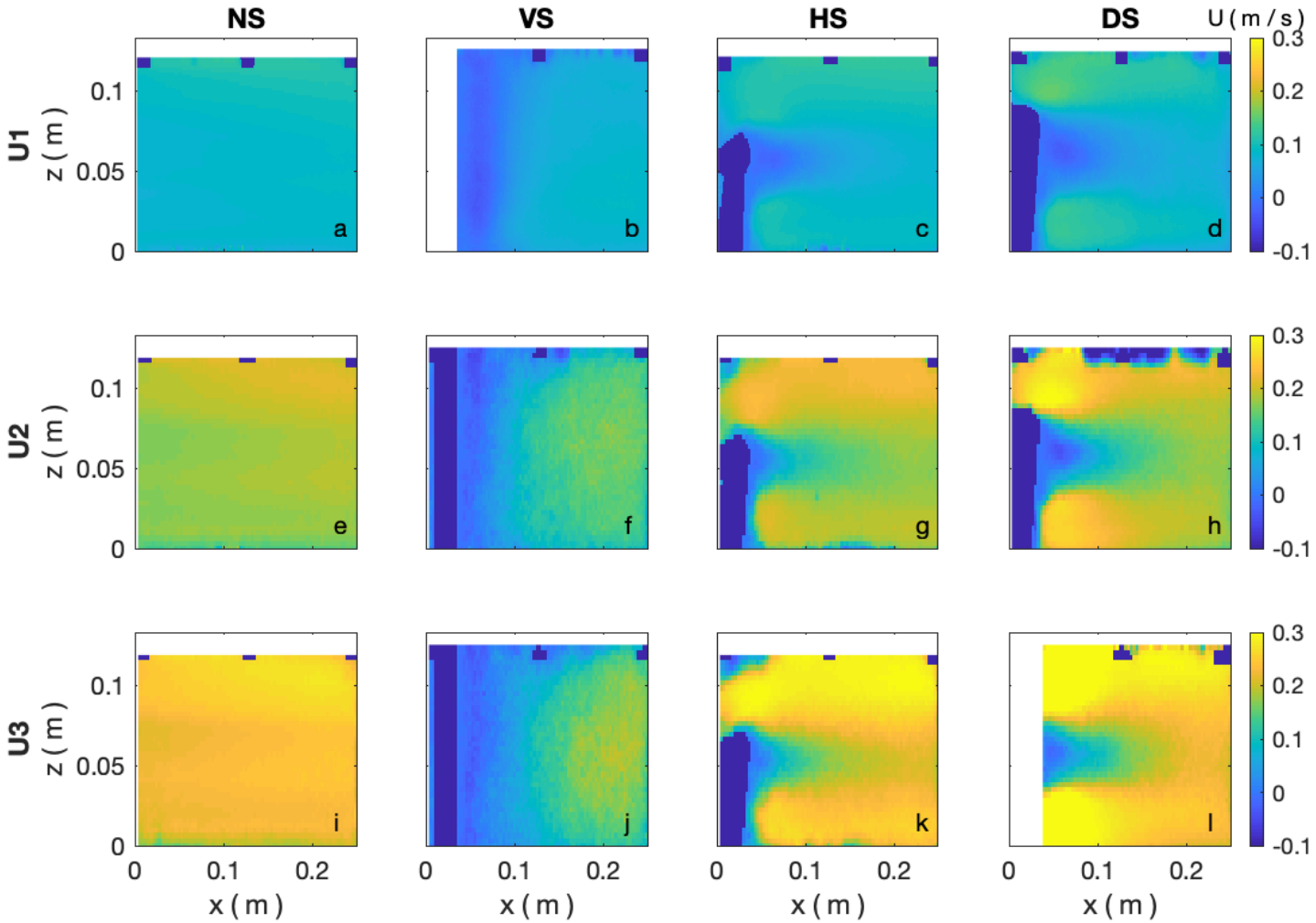

Figure 2.3. Time averaged longitudinal velocity field *U* (m/s) on the vertical XZ plane tested within a 30L swimming respirometer. Velocity fields are visualized for all four structure treatments (no structure [NS], vertical structure [VS], horizontal structure [HS], and diagonal structure [DS]) at each of the three velocities (U1, U2, U3) investigated.

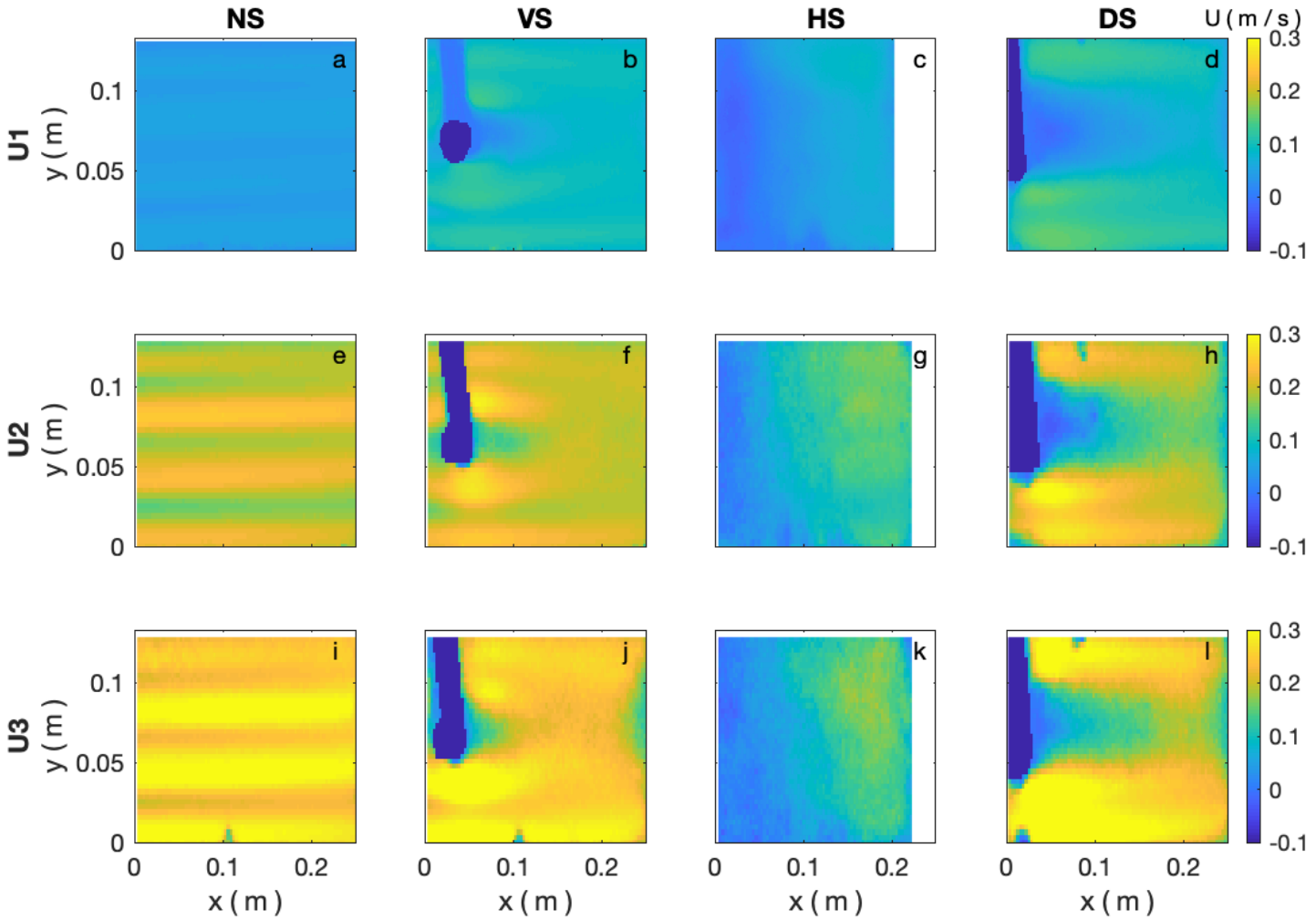

Figure 2.4. Time averaged longitudinal velocity field *U* (m/s) on the horizontal XY plane tested within a 30L swimming respirometer. Velocity fields are visualized for all four structure treatments (no structure [NS], vertical structure [VS], horizontal structure [HS], and diagonal structure [DS]) at each of the three velocities (U1, U2, U3) investigated.

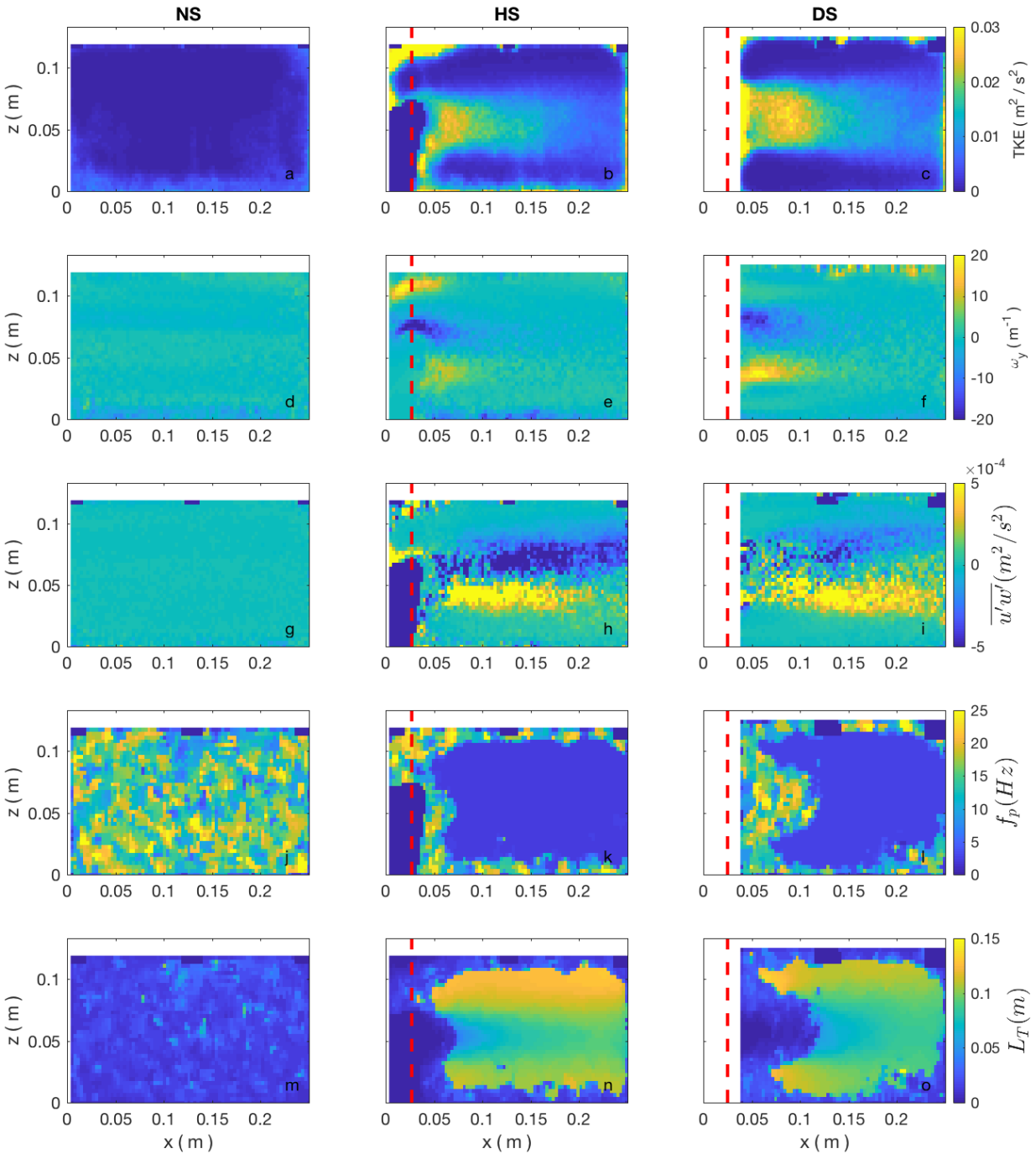

Figure 2.5. Time averaged turbulent kinetic energy, TKE field (m^2/s^2) [a-c], vorticity ω_y (s^{-1}) [d-f], Reynolds stresses $\overline{u'w'}$ (m^2/s^2) [g-i], eddy frequency f_p [j-l], and eddy length scale L_T [m-o] on the XZ plane for no structure [NS], horizontal structure [HS], and diagonal structure [DS], respectively, at the highest velocity, U3 (0.24 m/s).

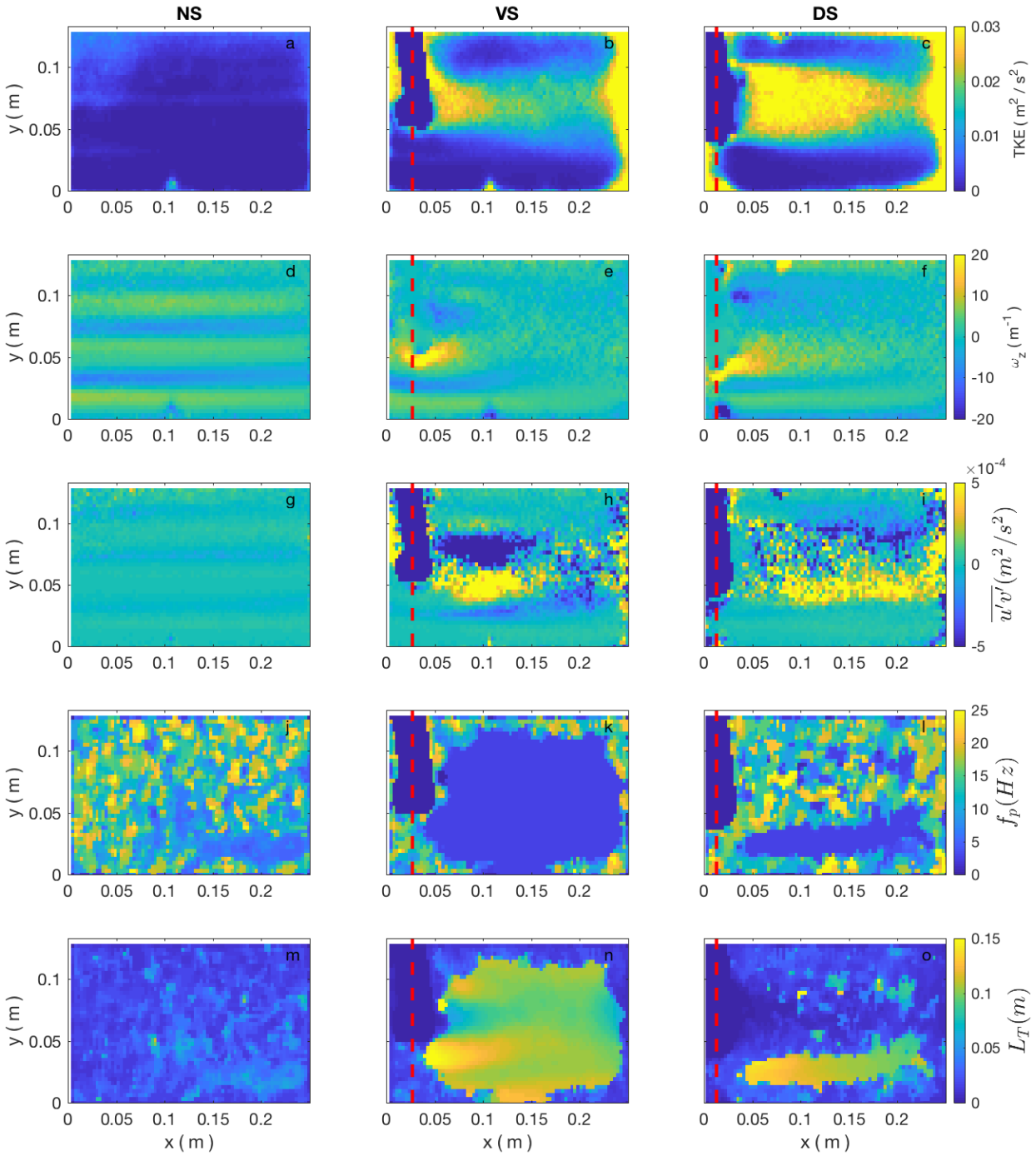

Figure 2.6. Time averaged turbulent kinetic energy, TKE field (m^2/s^2) [a-c], vorticity ω_z (s^{-1}) [d-f], Reynolds stresses $\overline{u'v'}$ (m^2/s^2) [g-i], eddy frequency f_p (Hz) [j-l], and eddy length scale L_T (m) [m-o] on the XY plane for no structure [NS], vertical structure [VS], and diagonal structure [DS], respectively, at the highest velocity, U3 (0.24 m/s).

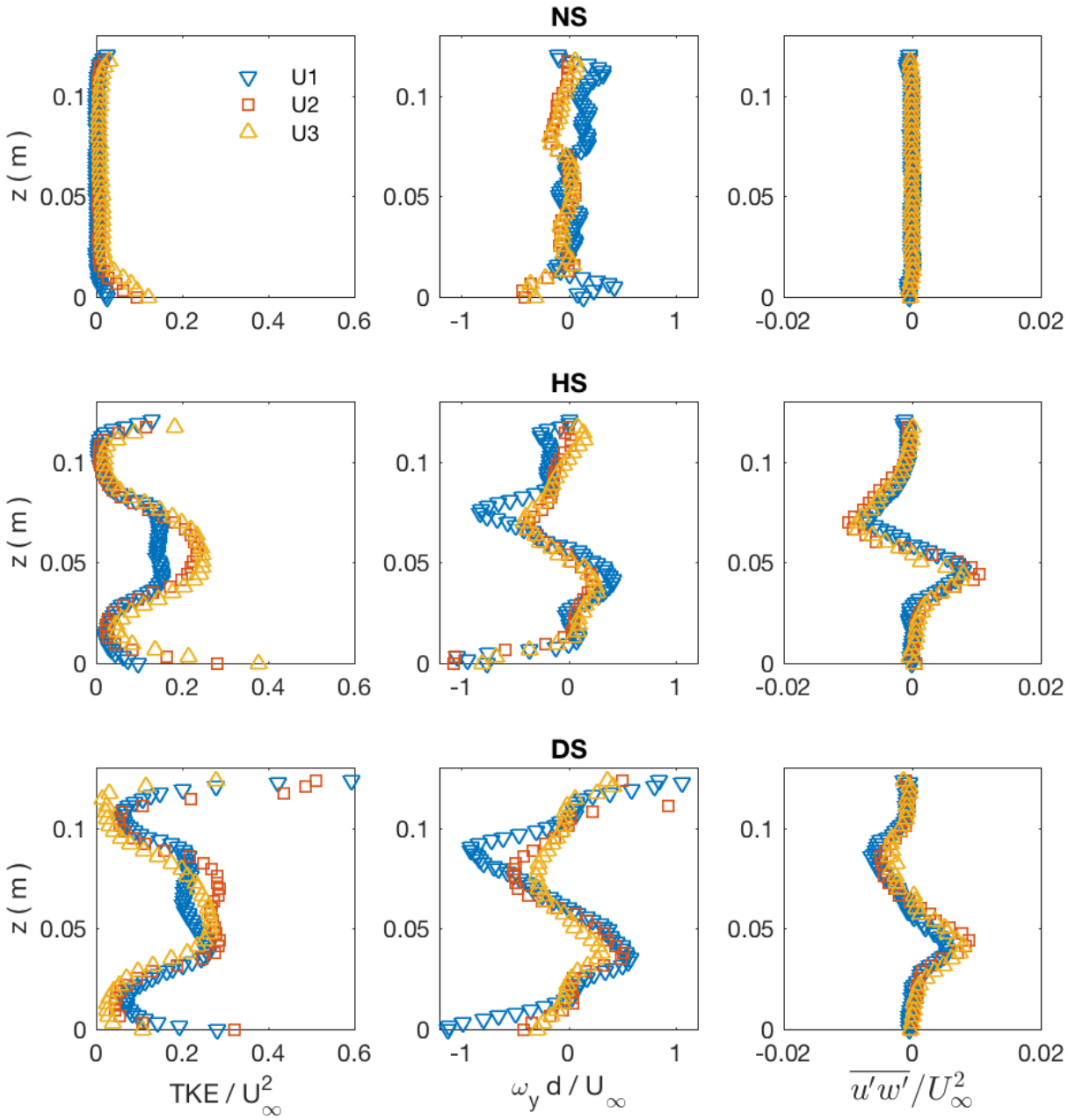

Figure 2.7. Non-dimensional temporally and spatially averaged (over the *x*-direction) vertical profiles of turbulent kinetic energy TKE (top row), vorticity ω_y (middle row), and Reynolds stresses $\overline{u'w'}$ (bottom row), measured at the highest velocity (U3, 0.24 m/s) on a vertical XZ plane, for the cases with no structure (NS-left), horizontal structure (HS-center) and diagonal structure (DS-right). Values are made non-dimensional using the undisturbed velocity U_∞.

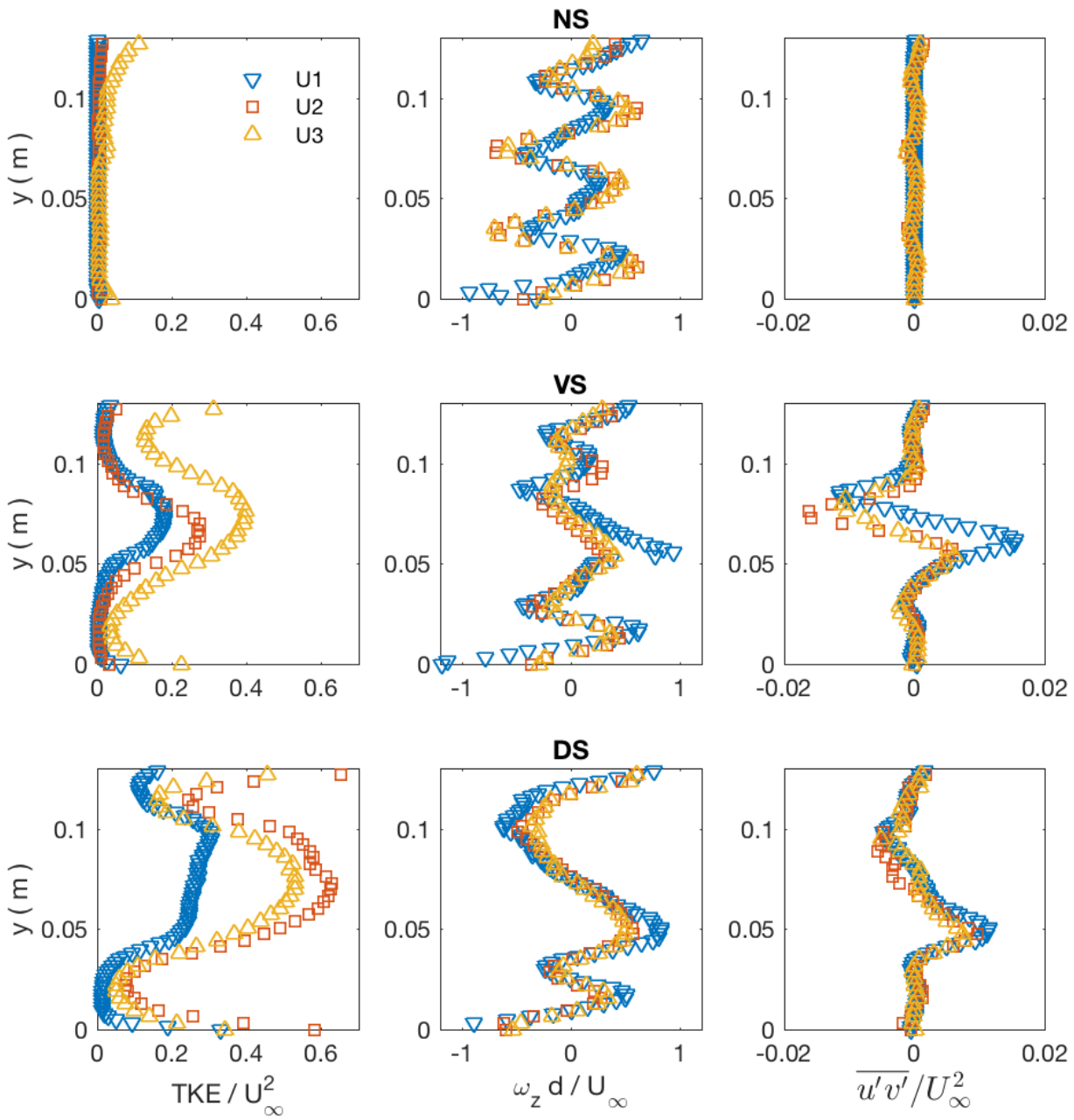

Figure 2.8. Non-dimensional temporally and spatially averaged (over the *x*-direction) transects of turbulent kinetic energy TKE (top row), vorticity ω_z, (middle row), and Reynolds stresses $\overline{u'v'}$ (bottom row), measured at the highest velocity (U3, 0.24 m/s) on a horizontal XY plane, for the cases with no structure (NS-left), horizontal structure (HS-center) and diagonal structure (DS-right). Values are made non-dimensional using the undisturbed velocity U_∞.

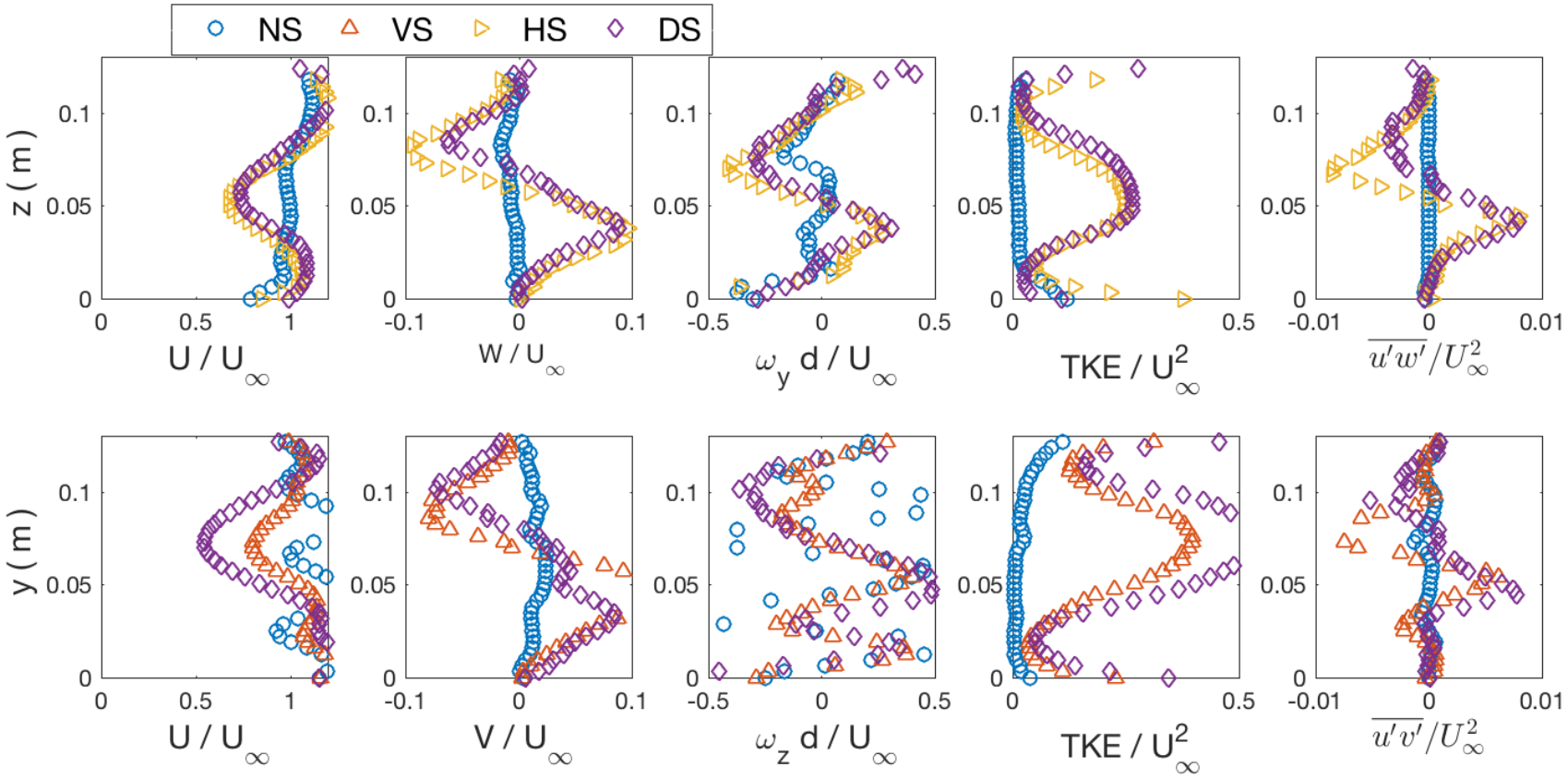

Figure 2.9. Temporally and spatially averaged (over the *x*-direction) non-dimensional profiles of velocity (U & W), vorticity, turbulent kinetic energy, and Reynolds stresses, for all simulated structure cases (no structure NS, vertical structure VS, horizontal structure HS, diagonal structure DS) at the fastest flow (U3, 0.24 m/s).

Tables

Table 2.1. Average size of smallmouth bass, along with metrics of water quality data, across the 60-day acclimation period at one of 3 different temperature treatments. Smallmouth bass were measured following the end of the acclimation period, while water quality metrics were measured either daily (temperature and dissolved oxygen saturation) or every several days (ammonia). Length and mass data are shown with standard error and did not vary across temperature treatments ($P > 0.05$).

Treatment Temperature (°C)	Average Temperature (°C)	Total Length (cm)	Mass (g)	Dissolved Oxygen Saturation (%)	Ammonia (ppm)
15 °C	15.6 (± 0.16)	29.7 (± 0.5)	303.5 (± 13.1)	93.2	< 1.0
18 °C	18.3 (± 0.08)	29.5 (± 0.6)	309 (± 16.7)	94.3	< 1.0
21 °C	20.8 (± 0.04)	30.1 (± 0.3)	325 (± 6.9)	91.9	< 1 .0

Table 2.2. Model selection process to identify the top model to explain jerk data derived from accelerometer-tagged smallmouth bass swimming in respirometer trials. Parameters tested include structure (horizontal, diagonal, vertical, or no structure), water velocity (1.0, 1.5, 2.0, 2.5, 3.0BL s^{-1}), temperature ("temp"; 15, 18, 21 °C), and fish mass (g) as fixed effects, and fish ID as a random effect. Models are ranked by lowest AIC score, indicating best fit; the best fitting model is indicated in bold.

Model formula	AIC score	Likelihood ratio	Marginal r^2	Conditional r^2
~ Structure × Velocity + Temp + (1|ID)	**709.51**	**-330.76**	**0.50**	**0.57**
~ Structure × Velocity + (1|ID)	709.72	-332.86	0.48	0.57
~ Structure × Velocity + Temp + Length + (1|ID)	711.50	-330.75	0.50	0.57
~ Structure × Velocity + Temp + (1|ID)	711.51	-330.76	0.50	0.57
~ Structure × Velocity + Length + (1|ID)	711.72	-332.86	0.48	0.57
~ Structure × Velocity + Temp + (1|ID)	715.51	-330.76	0.50	0.57
~ Structure × Velocity + Temp + (1|ID)	717.02	-329.01	0.45	0.53
~ Structure × Velocity + Temp + (1|ID)	717.51	-330.76	0.50	0.57
~ Structure × Velocity + Temp + (1|ID)	744.60	-328.30	0.50	0.56

Table 2.3. Model selection process for oxygen consumption ($\dot{M}O_2$, mg O_2/hr) data derived from respirometer trials with smallmouth bass. Smallmouth bass were acclimated to one of 3 different temperatures ("temp"; 15, 18 or 21° C), and then added to a swimming respirometer outfitted with one of 3 different flow-modifying structures (horizontal, diagonal, or vertical) along with a control treatment with no structure. Water velocity varied from 1.0, 1.5, 2.0, 2.5, and 3.0 body lengths per second, and one $\dot{M}O_2$ measurement was collected for each fish at each swimming velocity. In all models, $\dot{M}O_2$ has been log-transformed. Fixed effects tested include structure, flow velocity, temperature, and log-transformed fish mass, fish ID was considered a random effect in all models, though additional models including swim trial date ("date") and days between surgical tagging and swim trial ("days") as random effects were tested as well. The model that best fits the data based on the lowest AIC score (i.e., the top model) is shown in bold text.

Model formula	AIC score	Likelihood ratio	Marginal r^2	Conditional r^2
~ Structure × Velocity + log (Mass) + (1|ID)	**51.25**	**-2.62**	**0.39**	**0.69**
~ Structure × Velocity + log (Mass) + (1|ID) + (1|Days)	52.35	**-2.17**	**0.31**	**0.70**
~ Structure × Velocity + log (Mass) + (1|ID) + (1|Date)	52.82	**-2.41**	**0.30**	**0.69**
~ Structure × Velocity + log (Mass) + (1|ID) + (1|Date) + (1|Days)	54.04	**-2.02**	**0.30**	**0.70**
~ Structure × Velocity + Temp + log (Mass) + (1|ID)	55.80	-2.90	0.38	0.69
~ (Structure + Velocity + Temp)^2 + log (Mass) + (1|ID)	106.37	-14.18	0.37	0.71
~ Structure × Velocity × Temp + log (Mass) + (1|ID)	148.10	-12.05	0.39	0.75

Table 2.4. Summary of the model relating structure treatment (diagonal, horizontal, vertical or control), swimming velocity (1.0, 1.5, 2.0, 2.5 and 3.0 BL/s), water temperature (15, 18 or 21° C) and their interaction to the proportion of jerk measurements generated at a swimming velocity for smallmouth bass in a swimming respirometer. Data are visualized in Figure 2.2, panel A.

	Estimate	Standard Error	z value	Pr(>|z|)
(Intercept)	-5.73	0.86	-6.61	<0.001
Diagonal	0.48	1.10	0.44	0.66
Horizontal	0.59	1.06	0.55	0.57
Vertical	0.12	1.15	0.10	0.92
1.5 BL/s	2.76	0.79	3.51	<0.001
2.0 BL/s	5.13	0.75	6.84	<0.001
2.5 BL/s	5.81	0.75	7.74	<0.001
3.0 BL/s	6.21	0.76	8.22	<0.001
18 °C	-0.36	0.48	-0.75	0.43
21 °C	0.82	0.52	1.59	0.11
Diagonal:1.5 BL/s	-2.15	1.19	-1.81	0.07
Horizontal:1.5 BL/s	-2.76	1.16	-2.38	0.02
Vertical:1.5 BL/s	-2.84	1.28	-2.23	0.03
Diagonal:2.0 BL/s	-4.13	1.14	-3.63	<0.001
Horizontal:2.0 BL/s	-4.17	1.06	-3.95	<0.001
Vertical:2.0 BL/s	-4.44	1.16	-3.82	<0.001
Diagonal:2.5 BL/s	-3.52	1.08	-3.25	<0.01
Horizontal:2.5 BL/s	-2.83	1.01	-2.80	<0.01

Table 2.4 (cont.)

Vertical:2.5 BL/s	-3.64	1.10	-3.32	<0.001
Diagonal:3.0 BL/s	-3.48	1.08	-3.23	0.00
Horizontal:3.0 BL/s	-3.06	1.01	-3.0	<0.01
Vertical:3.0 BL/s	-3.14	1.08	-2.90	<0.01

Table 2.5. Summary of model relating structure treatment (diagonal, horizontal, vertical or control), swimming velocity (1.0, 1.5, 2.0, 2.5 and 3.0 BL/s), fish mass, and the interaction of structure and velocity to oxygen consumption ($\dot{M}O2$, mg O_2/hr) at a swimming velocity for smallmouth bass acclimated to one of 3 different water temperatures (15, 18 or 21° C). Both $\dot{M}O2$ and fish mass were log-transformed. Data are visualized in Figure 2.2, panel B.

	Estimate	Standard error	df	t value	Pr(>|t|)
(Intercept)	-1.75	1.82	27.90	-0.96	0.34
Diagonal	0.17	0.15	52.89	1.15	0.25
Horizontal	-0.001	0.13	52.52	-0.05	0.96
Vertical	0.03	0.15	51.45	0.20	0.84
1.5 BL/s	-0.05	0.08	96.25	-0.63	0.53
2.0 BL/s	0.23	0.09	96.63	2.70	0.01
2.5 BL/s	0.34	0.09	97.26	3.84	<0.001
3.0 BL/s	0.36	0.09	97.29	4.04	<0.001
log (Mass)	1.05	0.31	27.86	3.33	<0.01
Diagonal:1.5 BL/s	-0.16	0.14	96.64	-1.16	0.25
Horizontal:1.5 BL/s	0.02	0.12	96.43	0.15	0.88
Vertical:1.5 BL/s	-0.01	0.13	96.04	-0.08	0.94
Diagonal:2.0 BL/s	-0.47	0.14	96.56	-3.43	<0.001
Horizontal:2.0 BL/s	-0.28	0.12	96.29	-2.39	0.02
Vertical:2.0 BL/s	-0.34	0.14	96.49.	-2.43	0.02
Diagonal:2.5 BL/s	-0.58	0.14	96.83	-4.14	<0.001
Horizontal:2.5 BL/s	-0.30	0.12	96.90	-2.46	0.01

Table 2.5 (cont.)

Vertical:2.5 BL/s	-0.37	0.14	96.49	-2.74	0.01
Diagonal:3.0 BL/s	-0.65	0.14	97.04	-4.64	<0.001
Horizontal:3.0 BL/s	-0.18	0.12	96.82	-1.46	0.14
Vertical:3.0 BL/s	-0.43	0.14	96.50	-3.17	<0.01

CHAPTER THREE: REVISITING THE IPOS FRAMEWORK TO DETERMINE THE IMPACT OF TURBULENCE ON FISH ENERGETICS

Abstract

The complex interactions between fish and turbulent flow have been the subject of interdisciplinary research for several decades. These interactions are often quantified within the context of the IPOS framework, which proposes that fish-turbulence interactions are regulated by aspects of turbulence that fall into the categories of intensity, periodicity, orientation, and scale (IPOS). Fish-turbulence interactions have been examined extensively, but studies often yield conflicting results regarding the impact of turbulence on fish energy usage. This is likely due to several reasons: (1) studies often do not characterize turbulence, (2) studies often do not make quantitative links between turbulence and fish responses, and (3) studies often only examine one or two categories of the IPOS framework. Therefore, this study sought to quantify the impact of multiple metrics of turbulence, from different categories of the IPOS framework, on fish energetics across a range of turbulent flow conditions. To accomplish this goal, I first swam accelerometer-tagged rainbow trout (*Oncorhynchus mykiss*) and smallmouth bass (*Micropterus dolomieu*) within an intermittent-flow respirometer to link oxygen consumption ($\dot{M}O_2$, energy use) with swimming acceleration, allowing for the estimation of $\dot{M}O_2$ in different flow environments. Accelerometer-tagged fish were swam in a large racetrack flume with turbulence-generating structures in three orientations and three diameters across a range of flow velocities. Flow characteristics downstream of each structure were characterized with particle image velocimetry. These two components allowed me to directly and quantitatively link specific components of turbulence, from multiple categories of the IPOS framework, with fish energetics. Results revealed that turbulence scale and mean flow velocity interacted to impact fish energy

use, and that energy usage was driven by a different measure of turbulence intensity for each species. Overall, this study provides a new approach to evaluate how fish interact with turbulent flow and demonstrates the value of making clear, mechanistic links between fish energetics and the flow conditions they occupy.

Introduction

Turbulence is an inherent feature of flowing water environments with which fish must constantly contend. Turbulence is characterized by chaotic, irregular fluctuations in velocity imposed onto mean velocity. At its simplest, turbulence can be thought of as "everything besides the mean" flow (Warhaft 2002). Turbulence results in the manifestation of eddies, discrete parcels of swirling water, of various sizes and strengths (Lacey et al. 2012). Flowing water environments, such as rivers, are virtually always turbulent, but additional turbulence can be generated when physical structures is placed within flow (Daniels and Rhoads 2013; Bennett et al. 2015; Rhoads 2020).

Laboratory experiments have demonstrated that turbulence can influence fish energetics, swimming performance, and behavior in a variety of ways and can be quantified within the context of the IPOS framework (Lacey et al. 2012). The IPOS framework proposes that fish-turbulence interactions are regulated by aspects of turbulence that fall into the categories of intensity, periodicity, orientation, and scale (IPOS). These aspects, along with characteristics of fish themselves such as body length and swimming kinetics, determine whether turbulence has a positive, negative, or neutral impact on fish (Lupandin 2005, Tritico and Cotel 2010, Lacey et al. 2012). Eddies that possess high intensity, for example, may be expected to interfere with swimming or increase energy use (Lacey et al. 2012). However, if the diameter of such eddies are small relative to the fish, they may have little or even no impact (Cotel and Webb 2015).

Understanding how turbulence affects fish swimming is important because swimming performance has major implications for Darwinian fitness in fish because it impacts the ability of individuals to escape predators, obtain food, and find mates (Webb 1994; Plaut 2001; Brownscombe et al. 2017). Additionally, swimming accounts for a major proportion of energy use in fish (Webb 1971, 1994; Beamish 1978), and elevated swimming costs can result in less energy available for gonadal development and reproduction that can have population-level consequences (Minke-Martin et al. 2018). Therefore, results of investigations of the interactions between swimming fish and turbulent flow can have broad implications that extend beyond the laboratory environment and impact populations.

Though a number of studies have examined how fish interact with turbulent flow across different contexts, they have often yielded conflicting result such that the impact of turbulence on fish energy usage is largely unclear. Some studies report that turbulent flow may destabilize fish and increase the cost of swimming, thus requiring fish to use more energy when swimming in turbulent flows (Enders et al. 2003; Tritico and Cotel 2010; Maia et al. 2015). Others have found the opposite and reported that fish can exploit turbulence and use it to reduce energy expenditure (Taguchi and Liao 2011; van der Hoop et al. 2018). One potential explanation for this discrepancy is that different studies are utilizing different flow conditions and/or different species of fish (Liao 2007; Lacey et al. 2012; Cotel and Webb 2015). However, contrasting results have been found for even closely related or morphologically-similar species of fish. For example, while rainbow trout (*Oncorhynchus mykiss*) are able to exploit certain types of turbulence to decrease muscle usage and reduce energy usage (Liao et al. 2003; Liao 2004; Taguchi and Liao 2011), tturbulent flow appears to increase swimming costs for Atlantic salmon (*Salmo salar*), a related species (Enders et al. 2003). Overall, investigations of fish-turbulent

flow interactions have often produced conflicting results, and the reasons for this are largely unknown.

While it is likely that some of these discrepancies in findings across studies are due to the use of different species of fish and different flow conditions, this is difficult to quantify for four reasons. First, some studies have neglected to characterize flow conditions used, beyond labeling them as "turbulent" (Taguchi and Liao 2011). Such studies often use physical structures, such as cylinders, to generate turbulent eddies. The overall effects of such structures on flow characteristics are generally well-understood; cylinders, for example, will generate pockets of reduced flow velocity, increase levels of turbulence intensity, and shed eddies in their lee (Williamson 1996). Despite this understanding, it is not possible to make quantitative links between turbulent flow conditions and fish responses without quantifying the flow conditions generated (e.g., turbulence intensity, turbulence scale). Furthermore, without specific, quantitative assessments of all aspects of IPOS, direct comparisons of how turbulence influences fish across studies are challenging, as are comparisons between laboratory and *in-situ* flow conditions (Lacey et al. 2012). Second, in studies where turbulent flow metrics are characterized, quantitative links are often not made between fish responses and specific measures of turbulence (Taguchi and Liao 2011). Instead, turbulence may be treated as a categorical variable (i.e., low versus high turbulence, turbulence generated by a structure, etc.) or flow data may be presented separately, with no integration into analyses of data derived from fish (Tritico and Cotel 2010; van der Hoop et al. 2018; Strailey et al. 2021). Third, even when data derived from fish and flow measurements are integrated, the flow measurements utilized are typically those that are representative of a treatment as a whole or representative of a broader region in which fish spend time, and thus may not accurately reflect the conditions actually selected by fish (Lupandin

2005). Finally, studies commonly focus on turbulence metrics from one or two categories of the IPOS framework, or utilize a single metric within a category (Liao et al. 2003; Lupandin 2005; Maia et al. 2015; Strailey et al. 2021). This is particularly true for studies linking turbulence with energetics, in which measures of turbulence intensity are those most commonly used to predict fish energy use (Enders et al. 2003, 2005b; Trinci et al. 2020; Strailey et al. 2021). Ultimately, without making quantitative links between fish responses to turbulent flow and the turbulent flow conditions selected by fish themselves, it is impossible to know for certain why fish responses appear to vary so widely.

To address this gap and define how aspects of turbulence within the IPOS framework impact fish swimming, this study sought to quantify the impact of multiple metrics of turbulence, from different categories of the IPOS framework, on fish energetics across a range of turbulent flow conditions. For this, accelerometers were implanted into two species of fish, rainbow trout (*Oncorhynchus mykiss*) and smallmouth bass (*Micropterus dolomieu*), and accelerometer-tagged fish were swam in an intermittent-flow respirometer to generate a relationship linking fish $\dot{M}O_2$ with acceleration. Fish tagged with accelerometers were then swam in a large racetrack flume with several different structures across a range of velocities to generate a variety of different flow conditions. Particle image velocimetry (PIV) was used to characterize the flow conditions downstream of structures, and video recorded during fish swim trials was used to track the locations occupied by fish, allowing me to link fish $\dot{M}O_2$ with specific aspects of turbulence in locations selected by fish. Results will detail not just how turbulence impacts fish swimming energetics, but also what specific elements of turbulent flow have the greatest impact. This in turn in turn will help guide fish conservation by suggesting the types of flow that conservationists should most aim to protect.

Methods

Fish care for respirometry experiments

Respirometry data were collected at the Illinois Natural History Survey (INHS) Aquatic Research Facility (Urbana, IL). Smallmouth bass (SMB) arrived on August 27, 2019, while rainbow trout (RBT) were delivered on October 5, 2019; all fish were obtained from Jake Wolf Memorial Fish Hatchery (Topeka, IL). Upon arrival, fish were held overnight in outdoor, 1135 L circular tanks to recover from transport. After 24 hours, smallmouth bass were divided across two indoor 567 L tanks at an initial temperature of 22.2 °C, while rainbow trout were divided between indoor 121 L aquaria, with an initial temperature of 14.4 °C; three fish were placed in each aquarium. These aquaria were connected through a flow-through filtration system, and thus maintained similar temperature and water quality parameters. Rainbow trout were held in aquaria until October 28, 2019. During this pre-acclimation holding period for rainbow trout, average water temperature was 14.6 °C (±0.4 SE), average dissolved oxygen (DO) was 8.59 mg O_2/L (YSI Professional Plus, YSI Inc, Yellow Springs, OH, USA), and average ammonia levels were below 0.5 ppm (API Ammonia Test Kit, API Fish Care, Chalfont, PA, USA). For both species, fish were held for another 24 hr to acclimate after being moved to indoor 567 L tanks, and then heater-chiller units (TK 500, TECO, Ravenna, Italy) were used to adjust water temperature in each tank by 1 °C per day (Peake et al. 1997; Webb 1998) until treatment temperatures were attained. Two temperature treatments were used for each species because swimming performance can vary across temperatures and oxygen consumption ($\dot{M}O_2$) has a positive correlation with temperature (Hocutt 1973; Kolok 1991). Treatment temperatures were 12°C and 18°C for rainbow trout and 15 °C and 25 °C for smallmouth bass, and. These temperatures reflect a range of ecologically relevant temperatures for stream-dwelling smallmouth bass

(McClendon and Rabeni 1987; Wehrly et al. 2003) and rainbow trout (Matthews and Berg 1997; Weigel and Sorensen 2001). Once reached, treatment temperatures were maintained for a minimum of 30 days to ensure thermal acclimation (Currie et al. 1998; Beitinger and Lutterschmidt 2011). The acclimation period for smallmouth bass was 33 days, while the acclimation period for rainbow trout was 30 days. Water quality was measured regularly throughout the fish holding period; dissolved oxygen and temperature were measured daily, while ammonia was measured daily until ammonia levels remained consistently low (below 0.25 ppm), after which point ammonia was measured once a week (Table 3.1). Smallmouth bass were fed fathead minnows *Pimephales promelas* once a week to satiation. Rainbow trout were fed Skretting high protein pellets (Tooele, Utah) daily to satiation; any uneaten pellets were removed after 30 minutes.

Accelerometer tags and surgical procedure for respirometry experiments

Following the acclimation period, fish were surgically implanted with an accelerometer (model V13A, 6.2 g in water, 10 Hz recording frequency; Vemco, Bedford, Nova Scotia, Canada). These are triaxial tags, meaning that acceleration is measured in three axes: the lateral X axis, the longitudinal Y axis, and the vertical Z axis. These definitions, as given here, apply solely for measurement by accelerometer tags- elsewhere in this text, they are defined in other manners. Measurements are taken on each of these axes at a frequency of 10 Hz over a period of 10 sec, after which point the tags calculate and report the root mean square (RMS) acceleration of those three axes:

$$m\,s^{-2} = \sqrt{X^2 + Y^2 + Z^2} \tag{3.1}$$

Accelerometers were programmed to report data in this manner once every 20 sec. Root mean square acceleration has previously been used to quantify acceleration in a number of fish

species, including Pacific salmon (genus *Oncorhynchus*) (Wilson et al. 2013), bonefish (*Albula vulpes*) (Murchie et al. 2011), and lake trout (*Salvelinus namaycush*) (Cruz-Font et al. 2016).

Before surgical procedures began, fish were visually inspected to confirm they were adequately sized for the accelerometers (Brown et al. 2004). Tag burden averaged 2.8 % of body weight for smallmouth bass and 1.9 % for rainbow trout, and the mass of the accelerometer tag in air did not exceed 3.8% of body mass even in the smallest individuals of either species. Prior to surgeries, all fished were fasted for a minimum of 48 h to ensure that they were in a post-absorptive state (Adams et al. 1998). Surgical procedures were identical for smallmouth bass and rainbow trout, occurred at a temperature identical to each individual's acclimation temperature, and followed methods recommended by Wagner et al. (2011) and Harms (2005). Briefly, fish were anesthetized using AQUI-S 10E (AQUI-S New Zealand LTE, Lower Hutt, New Zealand) at a concentration of 50 mg L^{-1}. Fish were considered to be fully anesthetized once they lost equilibrium and were unresponsive to tail pinches. Each individual was then weighed, measured, and transferred to a wet surgical tray for tagging; rainbow trout were measured for fork length (FL) and smallmouth bass were measured for total length (TL). For each species, respectively, this was considered one body length (BL). To maintain anesthetization, a tube was placed into the fish's mouth to provide a constant flow of a maintenance dose of AQUI-S 10E over the gills. A 15 to 20-mm-long incision parallel to the ventral midline was made 2 mm anterior to the terminus of the pelvic fins and 1 mm off of the ventral midline; incision length was dependent on the surgeon's visual assessment of each fish's general size. The accelerometer was gently inserted into the peritoneal cavity, and the incision was closed with one or two absorbable sutures (M452, size 3/0, NFS-2 needle; SouthPointe Surgical, Coral Springs, FL, USA) dependent on the length of the incision. Fish were immediately moved to a container of aerated

fresh water to recover from surgery. Once equilibrium was regained and normal swimming behavior resumed, fish were transferred to isolation totes and returned to their original acclimation tank. Isolation totes were clear and allowed for water flow and visual contact with other fish but prevented physical interaction. A minimum of 16 hours passed before fish participated in respirometer swim trials (Wilson et al. 2013; Strailey et al. 2021). All surgeries were performed by the same individual, and average surgery time, from the moment when fish were first placed on the surgical station to when they were transferred to the recovery container, was 3:11 min (±13.2 s SE) for smallmouth bass and 4:43 min (±11.8 SE) for rainbow trout.

Respirometry swim trials

Swimming acceleration and $\dot{M}O_2$ were measured simultaneously by transferring tagged fish to a 30 L Steffensen-type swimming respirometer (#SW10150; Loligo Systems, Viborg, Denmark) (Steffensen et al. 1984). In this respirometer, a motor-driven propeller generated a constant flow for fish to swim against, allowing fish to swim freely within a bounded, rectangular swimming chamber (55 cm long, 14 cm wide, 14 cm tall), with a total water volume that is small enough to allow for reliable oxygen consumption measurements. The manufacturer indicates that this swimming respirometer is best suited for testing fish weighing between 175 and 500 g.

$\dot{M}O_2$ was quantified using intermittent-flow respirometry (Svendsen et al. 2016b). Briefly, measurements of dissolved oxygen were taken within the chamber during a closed "measurement" period, in which no fresh water entered the respirometer. Following the end of this period, the respirometer switched to an open "flush" period, in which freshly aerated water was pumped into the respirometer from the surrounding water bath, during which time no oxygen measurements are taken. During the final "mixing" period, the respirometer was again

closed, and the respirometer's propeller mixed the water to ensure that all water within the respirometer is evenly saturated with oxygen; no oxygen measurements were taken during this time. By taking oxygen measurements only during the closed "measurement" period, any decreases in the dissolved oxygen content of the water can be attributed to the fish consuming it during swimming, while the pumping of freshly aerated water into the respirometer during the open "flush" period prevents the dissolved oxygen content of the water from dropping to hypoxic levels (Svendsen et al. 2016b).

Smallmouth bass swim trials were conducted between October 19 and October 22, 2019, and rainbow trout swim trials were conducted between December 16 and December 19, 2019. Procedures for swim trials were identical for both species. The order in which fish were tested was randomized in a three-step process using a random number selector. First, for each day of testing, one treatment temperature for each species was randomly selected. Second, 3 to 4 tagged fish from that temperature group were randomly selected for inclusion in the day's swim trials. Finally, the swimming order of fish selected for a given day was randomized. Water temperature in the swimming respirometer matched the acclimation temperature for each fish.

At the beginning of each trial, fish were placed into the respirometer and acclimated at 0.5 body lengths (BL)/s for 45 min (Peake et al. 1997; Cooke et al. 2001) until normal swimming behavior occurred, with the fish facing upstream and maintaining its position within the swim chamber (Kern et al. 2018). After this acclimation period, water velocity in the respirometer was increased in 0.5 BL/s steps to 1.0, 1.5, 2.0, 2.5, and 3.0 BL/s; hereafter, these will be referred to as body-length (BL) velocities. A conversion relating the tunnel motor's revolutions per minute (rpm) to water velocity (m/s), generated with a flow meter (HFA, Höntzsch GmbH,Waiblingen, Germany), was used to determine these BL velocities. $\dot{M}O_2$ was quantified by the program

AutoResp v.1 (Loligo Systems, Viborg, Denamrk), and a single $\dot{M}O_2$ measurement was made for each fish at each BL velocity. The length of each flush phase and mixing phase was held constant at 4 min and 1 min, respectively, while the length of the closed measurement period varied from 6 to 20 minutes as necessary to obtain a high coefficient of determination (r^2 value) (Svendsen et al. 2016a). Only r^2 values of 0.85 or above were included in this study, and less than 10% of measurements were below an r^2 of 0.9. An omnidirectional hydrophone (VH165; Vemco, Bedford, Nova Scotia, Canada) connected to an acoustic receiver (VR100; Vemco, Bedford, Nova Scotia, Canada) was inserted into the outflow of the swimming respirometer to record acceleration data generated during swim trials.

Trials ended either when a fish successfully completed swimming at all five BL velocities, or if a fish fell to the grate at the rear of the test section and refused to swim. Following trial completion, each fish was removed from the respirometer and euthanized via an overdose of tricaine methanesulfonate (MS-222). Prior to trials beginning, the entire respirometer was cleaned with a bleach solution and additional $\dot{M}O_2$ measurements were then taken with the respirometer empty. $\dot{M}O_2$ measurements of the empty respirometer were taken again following the last trial. These pre- and post-trial measurements were used to quantify any background microbial respiration; background respiration was found to be negligible (Rodgers et al. 2016).

Acceleration data processing for respirometry experiments

Before analyses were conducted, it was first necessary to process acceleration data to reconcile differences in the number of $\dot{M}O_2$ measurements and acceleration measurements. A single measurement of $\dot{M}O_2$ was captured for each fish at each BL velocity over the 6 to 20 minute measurement period (a technique common in these kinds of studies (Wilson et al. 2013;

Strailey et al. 2021). In contrast, acceleration data during the measurement period were generated every 10 seconds, but also varied across fish and velocities due to the variable length of $\dot{M}O_2$ measurement periods and occasional missed detections by the receiver. Several methods of processing acceleration data were compared to identify a "characteristic acceleration" that would represent steady-state swimming for each fish at each velocity: (1) filtering to remove moments of low swimming intensity (i.e., 'coasting') (defined as accelerations below the 25th percentile at a water velocity) and moments of burst swimming (defined as accelerations above the 75th percentile), then averaging the remaining measurements, (2) averaging all acceleration data points generated for each fish at each BL velocity, and (3) removing bursting and coasting acceleration points for each fish at each BL velocity through a combination of visual inspection of acceleration histograms and use of Rosner's outlier test (Rosner 1975; Meuser et al. 2022), then averaging the remaining measurements. A linear model relating $\dot{M}O_2$ to acceleration was produced for each processing method and the resulting models were compared via Akaike information criterion (AIC), where the best fitting model was indicated through a combination of the lowest AIC score and highest model r^2 (Wagenmakers and Farrell 2004). The tables showing the results of this model selection process are shown in the supplemental materials (Tables B.1 and B.2). For both smallmouth bass and rainbow trout, the third processing method described above (removal of extreme acceleration points due to bursting/coasting identified through a combination of visual inspection and Rosner's outlier test) yielded the best fitting model, and data were processed using this method in subsequent analyses.

Analysis of oxygen consumption and acceleration data from respirometry experiments

Linear mixed effects models were used to relate acceleration with fish $\dot{M}O_2$; other fixed factors in models were fish mass and water temperature (Figure 3.1). Because fish metabolic

costs do not scale linearly with mass, both $\dot{M}O_2$ and mass were log-transformed (Clarke and Johnston 1999). Fish ID was added as a random effect to account for the repeated sampling of individual fish across multiple velocities. A null model, including only this random effect, was also included for each species. All models were assessed for fit by a comparison of AIC scores, whereby the best-fitting model would be expected to have the lowest AIC score (Zuur et al. 2009; Crawley 2013). For both rainbow trout (Table 3.2) and smallmouth bass (Table 3.3), this model included acceleration as the only fixed effect, likely because the AIC analysis rewarded models with a small number of parameters (Zuur et al. 2009). However, for subsequent analyses, I chose to use the models that included acceleration, mass, and temperature to relate $\dot{M}O_2$ to acceleration. These models were selected for use for three reasons. First, while models including mass and temperature in addition to acceleration did not have the lowest AIC scores, they had the highest conditional r^2 and highest marginal r^2 of all models tested, indicating that these models and this combination of fixed effects explained the greatest amount of variance within the data (Zuur et al. 2009). Second, the AIC score differences between tested models were minimal, with a ΔAIC of 3.5 between the "top" model and selected model for rainbow trout, and a ΔAIC of 2.5 between the "top" model and selected model for smallmouth bass indicating that there is some support for the inclusion of these models and some strength-of-evidence for their use (Burnham and Anderson 2004). Finally, and most importantly, a model that included mass, temperature, and acceleration to predict $\dot{M}O_2$ makes the most "biological sense". A number of authors have stressed the importance of using models supported by 'biological evidence' during the selection process (Zuur et al. 2010; Burnham et al. 2011). Both temperature and fish mass are known to have a strong impact on $\dot{M}O_2$, and, furthermore, excluding mass and temperature would have greatly reduced the applicability of our $\dot{M}O_2$-acceleration models for use in future studies

where average temperatures or fish size may not exactly match the ones as in this study. Therefore, the models used to relate acceleration with $\dot{M}O_2$ included acceleration, water temperature, and logarithmically-transformed fish mass as fixed effects (Tables 3.4 and 3.5).

Model fit was visually assessed through assessment of fitted residuals and quantile-quantile plots. To further confirm model fit, a cross-validation approach was taken in which 25% of the data for each species was randomly selected for removal, and the selected models were built again using the remaining 75% of data (Morin and Davis 2017; Yates et al. 2022). These models were then used to calculate estimated $\dot{M}O_2$ values for the removed 25%. The estimated $\dot{M}O_2$ values for the 25% subset were compared with the actual $\dot{M}O_2$ values for the subset using a Welch two sample t-test (Rainbow trout: t = 0.31, df = 27.1, p = 0.76; Smallmouth bass: t = 0.07, df = 25.9, p = 0.94); the estimated values did not differ from the actual values, indicating that the model fit the data well.

Fish care for flume experiments

Large-scale laboratory trials were conducted at the Ecohydraulics and Ecomorphodynamics Laboratory (EEL) in Rantoul, IL. Holding procedures varied slightly for the two species, and differed slightly from the holding setup utilized for respirometry experiments. Both species were maintained at ambient temperature. This was done because the flume in which swim trials took place lacked temperature control, thus the use of ambient temperatures for fish holding ensured that temperatures were similar between holding aquaria and the flume. Rainbow trout (n = 13) were sourced from Keystone Fish Hatchery (Richmond, IL) and delivered to the EEL on April 3, 2019. Fish were held for 12 days in an indoor 379 L tank at ambient room temperature; otherwise, the holding setup was the same as described for respirometry acclimation procedures. During this period, average water temperature was 16.3 °C

(± 0.5), average DO was 9.22 mg O_2/L, and average ammonia remained below 0.5 ppm. After the initial holding period, 6 individuals were randomly selected and surgically implanted with accelerometer tags as described above; average surgery time for rainbow trout was 6:10 min (±16.4 s SE) and tag burden was no greater than 3.4% body mass. Following surgeries, fish were moved to 208 L aquaria and allowed to recover overnight before trials began. Two fish were held in each aquarium and separation was maintained by a clear screen. Each aquarium was outfitted with an aerator, water quality was measured daily, and water changes were performed as needed to maintain quality. Smallmouth bass (n = 6) were randomly selected from the larger group of individuals from Jake Wolf Memorial Fish Hatchery held at the INHS Aquatic Research Facility, and transported to the EEL on September 22, 2019. Two smallmouth bass were placed in each of three 208 L aquaria with a clear screen separating individuals to minimize interactions. After a two-day acclimation, smallmouth were implanted with accelerometers as described above and allowed to recover overnight before usage in large-scale laboratory trials. Average surgery time for smallmouth bass was 4:05 min (±34.6 s SE) and tag burden was no greater than 3% body mass. Water quality metrics for the duration of fish holding within aquaria are shown in Table 3.6 for both rainbow trout and smallmouth bass.

Experimental setup for flume swim trials

Large-scale laboratory swim trials took place in a racetrack flume in which flow was generated by a large paddle wheel (Leman et al. 2018). A pre-existing calibration allowed for estimation of flow velocity based on the frequency of the paddle wheel's rotation. To allow for multiple fish to be tested concurrently, three separate 1.0 m long test sections were established on the side of the flume opposite the paddle wheel. Each section was preceded by a 25.4 cm long flow straightener composed of 7.62 cm-diameter PVC pipe, used to minimize flow perturbations

and ensure that each test section experienced similar flow conditions regardless of location. A screen barrier was placed at the terminus of each test section to ensure fish remained in place, and sections were additionally spaced to avoid visual contact between individual fish. Experimental treatments to quantify the impact of turbulence generated by simulated structures on fish consisted of a single PVC pipe of one of three diameters (2.54 cm, 5.08 cm, 7.62 cm) secured within a test section in one of three orientations (vertical, horizontal, diagonal). Structures were placed such that their midpoint was 33 cm downstream from the flow straightener, one-third of the way through the test section.

The reference frame for this study is defined such that X represents the longitudinal coordinate in the direction of mean flow, Y represents the horizontal transverse coordinate perpendicular to mean flow, and Z represents the vertical dimension (depth). Vertical structures were aligned with the Z-axis and were placed on the centerline of the flume. Horizontal structures were aligned with the Y-axis and were centered at mid-depth within the flume. Diagonal structures were placed at a 45° angle within the YZ plane, with the high end of the structure placed against the flume's inner wall. A case in which no structures were present was used as a control. Hereafter, each flow condition is referred to by the combination of the orientation (vertical – V; horizontal – HS; diagonal – D) and diameter (2.54 cm – 1; 5.08 cm – 2; 7.62 cm – 3) of a structure present, or simply by its orientation (vertical structure– VS; horizontal structure – HS; diagonal structure – DS); the control condition is referred to as NS (no structure).

Flume swim trials

Trials followed a crossover experimental design in which each fish experienced all possible flow and structure conditions, applied in a random order. To minimize the risk of fish becoming over-exercised, a schedule was followed in which a single group of three fish swam

each day. Fish were randomly assigned to their swim group, and the order in which each fish underwent each flow treatment was similarly randomized. Each morning, flow was set at a low BL velocity (approximately 0.5 BL/sec), and one fish was placed within each test section. Structures were secured as needed within the test section and fish were allowed to acclimate to their surroundings for one hour. After this initial acclimation, swim trials began. Each individual swim trial was 45 minutes long, and consisted of three 15 minute sub-trials in which BL velocity was set to approximately 1.0 BL/sec, 1.5 BL/sec, and 2.0 BL/sec, respectively.

Testing velocities were determined based on the average body length of all rainbow trout used in flume trials (Table 3.7); rainbow trout did not vary significantly in length between the two swim groups (Welch two-sample T-test: $t = 0.92$, $df = 3.89$, $p = 0.41$). Smallmouth bass did not vary significantly in length between groups (Welch two-sample T-test: $t = 0.33$, $df = 2.31$, $p = 0.77$), nor did they vary significantly in length from rainbow trout (Welch two-sample T-test: $t = 1.12$, $df = 9.98$, $p = 0.29$), and thus the same velocities were used during smallmouth bass trials. Specific velocities were chosen to prevent exhaustive exercise, as they were unlikely to induce excessive burst swimming or exhaustion in either smallmouth bass (Peake and Farrell 2006), or in rainbow trout (Farrell et al. 1991; Milligan 1996). Upon completion of a swim trial, structures were changed as necessary, and fish were allowed to rest for an hour until the next trial began. Up to four trials were conducted in a day, and fish remained in their designated test section until the day's trials were complete. When trials were completed for the day, fish were returned to their original aquarium and allowed to rest at least 16 hours before inclusion in further trials. Each fish participated in ten total trials across 5 days; after the third day of trials, fish were fed and rested for two days to allow for complete digestion of food.

To record acceleration during swim trials, an acoustic receiver (VR2W VH165; Vemco, Bedford, Nova Scotia, Canada),) was secured to one of the barrier screens within the flume. An additional omni-directional hydrophone (VH165; Vemco, Bedford, Nova Scotia, Canada), connected to an acoustic receiver (VR100; Vemco, Bedford, Nova Scotia, Canada), was also placed within the flume, and secured to a barrier screen to prevent excessive movement from interfering with tag detection. Vemco V13A tags (6.2 g in water, 10 Hz recording frequency; Bedford, Nova Scotia, Canada) were again utilized for flume swim trials, but programming for these tags differed slightly from that used for respirometry experiments. To avoid signal collisions, tags reported data every 80 to 160 sec, at random intervals. As with respirometry experiments, tags recorded acceleration data at a frequency of 10 Hz, and the acceleration value reported was the RMS of all data collected for the previous 10 sec before a tag pinged.

Fish locations during swim trials were recorded via video cameras. As structures of different orientation do not necessarily alter flow characteristics on multiple planes, cameras were placed to capture video in the plane (or planes) expected to be most affected by a particular structure. For example, when fish swam with a VS or HS, video was recorded from a single angle. For VS, which alter flow characteristics on the horizontal XY plane, cameras were placed to capture an overhead view and were secured above where structures were placed; thus, video was only captured for the portion of the test section that was downstream of a structure. For HS, which alter flow characteristics on the vertical XZ plane, cameras were placed to capture a side view, and were able to capture video for the entirety of the test section. DS alter flow on both the XY and XZ planes, and so two cameras were used when a DS was present and were placed to capture the two views described above for the HS and VS. For the NS condition, video was captured from the side.

Flow measurements

The velocity field within the racetrack flume was measured on two two-dimensional (2D) planes using particle image velocimetry (PIV). A vertical plane oriented along the direction of the flow (XZ plane) was measured at the flume's centerline, while a horizontal plane oriented along the direction of the flow (XY plane) was measured at mid depth. A 5W-532nm laser (PIV-01251 DPSS, OptoEngine LLC, Midvale, UT) equipped with a cylindrical lens was used to generate a light-sheet to illuminate particles traveling within either the XZ or XY plane. A monochromatic camera (JAI GO-5000M-USB; JAI Inc., San Jose, CA) recorded 12-bit images with a 2560 × 2058 pixel resolution, with the same paddle wheel frequencies and flow conditions tested in fish trials. For paddle wheel frequencies equivalent to 1.0 BL/sec and 1.5 BL/sec, images were recorded at a frequency of 50 frames per second (fps) and a frequency of 60 fps for 2.0 BL/sec.

Acceleration and location data processing for flume experiments

As with acceleration data derived from respirometry experiments, the quantity of acceleration data available for each fish under each flow condition varied, likely due to signal collisions, thus interfering with detection by the receiver. To account for differing quantities of acceleration data across individuals, data were processed to identify a "characteristic acceleration" value for each individual fish was generated, with each combination of structure and BL velocity. For this, Rosner's outlier test was again used to identify and remove extreme values due to bursting and coasting and identify steady-state swimming at each velocity (Rosner 1975). The remaining acceleration data, considered to be representative of swimming behavior for a fish during a sub-trial, were then averaged. Models developed from small-scale

respirometer experiments described above were then used to estimate $\dot{M}O_2$ from the characteristic acceleration values calculated for each separate swim trial in the racetrack flume.

Video recorded during swim trials were processed using the software Matlab (MathWorks R2021A) to determine the locations occupied by fish in downstream portion of the flume downstream of structures where altered turbulence is to be expected. The position of each fish was manually tracked every five seconds for the duration of each video, and then converted to X and Y coordinates that could be overlaid on a grid. Only fish that spent 50% or more of their time downstream (i.e., interacting with the wake produced by the structure) during a given sub-trial were included for analysis. This was done for two reasons. First, I was interested in the effects of turbulence generated downstream of structures on fish energetics. Second, all flow measurements were conducted downstream of structures, and flow data were unavailable for any time fish spent upstream. Therefore, fish that spent more than 50 % of their time upstream of a structure spent the majority of the time experiencing unknown flow conditions that likely influenced $\dot{M}O_2$. Most datapoints excluded through this method were derived from sub-trials in which fish spent more than 75% of their time upstream. For rainbow trout, only 3 such datapoints were excluded from fish spending more than 50% but less than 75% of their time upstream, and for smallmouth bass, 5 such datapoints were excluded. Due to this exclusion, the ultimate sample sizes for species and each combination of structure and BL velocity were variable (n = 0-5) ; rainbow trout, for example, spent the majority of their time upstream when NS was present, and at 2.0 BL/s with NS, all rainbow trout spent the majority of their time upstream.

Analysis of velocity statistics

Images captured through PIV were analyzed using the open source, Matlab-based software PIVlab (version 2.5; Thielicke and Stamhuis 2014). Utilizing this study's reference frame, the velocity components analyzed through PIVlab are defined as such: *u* in the longitudinal direction (X), *V*in the transverse direction (Y), and *w* in the vertical direction (Z). Lower case symbols (*u*, *v*, *w*) are used to indicate instantaneous velocity values, while upper case symbols (*U, V, W*) are used to indicate time averaged velocity values. Analyses yielded 2D fields of instantaneous velocities *U* and *V* for PIV conducted on the horizontal XY plane and velocities *U* and *w* for PIV conducted on the vertical YZ plane; the spatial resolution of PIV data was 5.7 mm. Reynolds decomposition was used to calculate instantaneous velocity fluctuations, *u'*, *v'*, and *w'* as:

$$u' = u - U \tag{3.2}$$

$$v' = v - V \tag{3.3}$$

$$w' = w - W \tag{3.4}$$

This allowed for the calculation of turbulence metrics with the potential to impact fish swimming. Seven measures associated with turbulence intensity were calculated (Lacey et al. 2012): turbulent kinetic energy (TKE), U_{rms}, V_{rms}, W_{rms}, Reynolds stresses, turbulence intensity (TI_u), and vorticity. TKE was calculated on the XZ and XY planes, respectively, as:

$$TKE_{xz} = \frac{1}{2}\left(2\overline{u'^2} + \overline{w'^2}\right) \tag{3.5}$$

$$TKE_{xy} = \frac{1}{2}\left(2\overline{u'^2} + \overline{v'^2}\right) \tag{3.6}$$

U_{rms}, V_{rms}, and W_{rms} were calculated as the root mean square of the instantaneous velocity fluctuations u', v', and w':

$$U_{rms} = \sqrt{\overline{u'^2}} \tag{3.7}$$

$$V_{rms} = \sqrt{\overline{v'^2}} \tag{3.8}$$

$$W_{rms} = \sqrt{\overline{w'^2}} \tag{3.9}$$

While TKE is an overall measure of the mean kinetic energy per unit mass associated with eddies, U_{rms}, V_{rms}, and W_{rms} are directional, and represent turbulence intensity in the longitudinal, lateral, and vertical directions respectively. Time-averaged (indicated by overbars) Reynolds stresses were calculated as $\overline{u'v'}$ and $\overline{u'w'}$. Turbulence intensity in the longitudinal direction was calculated as:

$$TI_u = \frac{standard\ deviation\ (u)}{U} \tag{3.10}$$

Two components of vorticity, ω_y and ω_z, were calculated as the curl of the velocity vector, $\vec{\omega} = \nabla \times \vec{v}$, where $\vec{v} = (u, v, w)$; vorticity describes how fast an eddy is spinning (Lacey et al. 2012). A measure of periodicity, turbulent integral time scale, $T = \int_0^\infty \rho_{uu}(\tau)d\tau$, was calculated using the autocorrelation function $\rho_{uu}(\tau) = \langle u'(t)u'(t+\tau)\rangle / \langle u'(t)^2\rangle$, where τ stands for a lag between measurements. The integral time scale, *T*, reflects the time scale of the larger, predominant eddies in the flow and indicates how long it takes for such an eddy to complete one full revolution (Pope 2000). *T* was then used to estimate a measure of scale, turbulent integral length scale, *L*, the length scale associated with these predominant eddies. Following Taylor's frozen-turbulence hypothesis, *L* was calculated by multiplying *T* at a given

location within the test section by a representative velocity, taken as the time-averaged velocity *U* at that location (Taylor 1938).

Reynolds number (Re), based on cylinder diameter (*d*), was calculated for each PIV case as Ud/ν, where ν is the kinematic viscosity of water. Values of Re calculated ranged from approximately 7500 up to over 40,000, indicating that all cases were fully turbulent (Williamson 1996). The Froude number for each case was calculated as $Fr = U / \sqrt{g \times H}$, where H is the water depth in m and g is the gravitational constant. The Froude number was less than 1 for all cases, indicating subcritical flow (Rhoads 2020). To further estimate the spatial effect of structures, cylinder wake wavelength, λ, was calculated based on the shedding frequency, *f*, Strouhal number, *St*, and the mean velocity (*U*) as $\lambda = U / f$. Using the expected value of $St = 0.21$ for the range of *Re* investigated (e.g., Liao 2003, Strailey et al. 2021), shedding frequency was estimated using $St = fd / U$.

Lacey et al. (2012) suggested that flow metrics should be reported with their units, as this allows comparisons to be made between different experimental setups and between laboratory and field environments. As such, all flow metrics are presented with their units with the exception of turbulence intensity $TI_{u,}$ which is unitless (Enders et al. 2005a).

Flow data extraction and selection for bioenergetics modeling

Because PIV requires the use of a laser to illuminate particles moving through water, it was not possible to collect PIV data at the same time that fish were participating in swimming trials as this would have disturbed fish and altered behavior. However, PIV analyses yielded 2D time-averaged plot of the turbulence metrics described above that could be related to the conditions experienced by fish during swimming trials. Location coordinates obtained from

swim trial videos were overlaid onto the 2D time-averaged plots for all calculated velocity statistics and the value for each statistic at each location occupied by a fish was then extracted (Fig. 3.2). This yielded a large compilation of all the flow conditions selected by fish downstream of structures.

For certain PIV cases, reflections and differences in illumination lead to aberrations of PIV data, particularly near the boundaries of the flume (i.e., the walls and floor of the flume). When PIV heat maps were plotted, this manifested in small regions in which flow characteristic values appeared to be inflated or deflated in comparison to surrounding values. An example heat map, in which such areas are indicated in red, is shown Figure 3.3. Because these inflated and deflated values did not have a physical basis, any fish location coordinates that fell within these areas were filtered out to prevent these measurements from biasing the overall dataset. These removed data points accounted for just over 1% of all location data points for rainbow trout and less than 1% of all location data points for smallmouth bass.

To integrate flow data with estimated $\dot{M}O_2$ data, it was necessary to pare each metric down to a single value for each sub-trial, and so I calculated and tested the mean, median, maximum, and minimum values for each metric during sub-each trial. A linear regression relating each with $\dot{M}O_2$ data was generated and plotted to determine which descriptive statistic best fit the data, assessed via the r^2 and p values for each model. Ultimately, models were similar with no clear best-fitting statistic. Examples of the plots use to determine descriptive statistic are shown in Figures 3.4 and 3.5; plots for each species and each metric are available in the supplemental materials (Figures B.1 to B.18). Therefore, because acceleration data were averaged to produce estimated $\dot{M}O_2$, mean values for each turbulence metric were chosen for integration with $\dot{M}O_2$ data. Because all data presented were extracted from a single plane, V_{rms}

and W_{rms} were not available for all structures. However, these represent turbulence intensity in the perpendicular direction to VS and HS, respectively, and could be pooled together as U_{Trms}. Therefore, for VS, U_{Trms} represented V_{rms}, measured on the horizontal XY plane, and for HS and DS, U_{Trms} represented W_{rms}, measured on the vertical XZ plane.

Bioenergetics model development and statistical analysis

Previous bioenergetics models with turbulence metrics as a predictor of fish $\dot{M}O_2$ have largely focused on intensity and overlooked other components of turbulence. Therefore, one of my goals was to define the potential effect of metrics from other categories of the IPOS framework on energetics and to examine a wider range of metrics beyond just turbulence intensity, which has been the focus of most work to date. To define which metrics to include during bioenergetics model development, and to identify potential interactions, scatter plots of the flow conditions selected by fish, relating mean U to various turbulence metrics, were generated for each species at each structure orientation and visually inspected to identify potential relationships between them. If the levels of a turbulence metric of interest clearly varied across differing levels of mean U, this indicated such a relationship, and thus the metric was included for further analyses. Based on these plots, U, TKE, TI_u, U_{rms}, U_{Trms}, T and L were chosen to test for inclusion within bioenergetics models. These plots can be found in the supplemental materials (Figures B.19 to B.24).

Selected flow conditions were available on one plane for VS, HS, and NS, but on two for DS. To determine which plane to use in bioenergetics modeling, two linear mixed-effects models were generated for each of the selected flow metrics, one developed using data for DS from the XZ plane and one developed using data for DS from the XY plane. These followed the structure of a bioenergetics model, and each included log-transformed fish mass, water temperature, the

flow metric of interest, and fish ID as a random effect, with log-transformed $\dot{M}O_2$ as the response variable. The two models developed for each metric were compared via model selection, and the model with the lower AIC score was considered to provide the better fit for the $\dot{M}O_2$ data. For all metrics, the best fit was provided when DS data from the XZ plane was used.

Linear mixed-effects models were employed to define the impact of turbulence on estimated $\dot{M}O_2$ for each species. Following the framework of a bioenergetics model, log-transformed fish mass and water temperature were included in all models. Time-averaged velocity U was also included in all models, as multiple studies have found that the impact of turbulence can vary across velocity, with its impact largely being small or non-existent at low flow velocities (Strailey et al. 2021, van der Hoop et al. 2018). As each fish was used in multiple trials, fish ID was included as a random effect to account for repeated measures (Laird and Ware 1982; Lindstrom and Bates 1990). inflation factor (VIF) used to assess turbulence metrics for collinearity (Tables B.3 and B.4). Increasing values of VIF indicated higher correlation between variables, with values between 1 and 5 indicating moderate levels of correlation, and values over 5 indicating high levels of correlation between variables. If turbulence metrics were found to have a VIF greater than 2.5, further models were tested to identify which specific variables were correlated (Zuur et al. 2010).

Structure was not included as a possible predictor in any models tested for three reasons. First, with a total of nine different structures plus a structureless control, the inclusion of structure within models would have negatively impacted the statistical power possible for a tested model (Baguley 2004; Akobeng 2016). Second, as candidate models followed the framework of a bioenergetics model, the inclusion of a categorical variable would have reduced the models' applicability for future usage (Kitchell et al. 1977; Hansen et al. 1993; Bureau et al.

2002). Finally, and most importantly, the goal of this study was to make direct, quantitative links between specific characteristics of turbulence and fish energetics; including structure as a categorical variable was not necessary because their effects were accounted for by including the hydrodynamic metrics created by structures, which can only be seen by coupling the actual location of the fish with the hydrodynamics of those locations, rather than using average statistics without consideration for fish choice of location.

Ultimately, I developed models that included various measures of turbulence, moving beyond simply testing measures of intensity such as TKE (e.g., TKE). Each model included a measure of turbulence intensity (i.e.,TKE, $TI_{u,}$ U_{rms}, U_{Trms}) and either integral time scale T as a measure of periodicity or turbulent integral length scale L as a measure of scale. T And L were not included concurrently in individual models due to a high level of correlation between them, revealed by VIF assessment. Because the categories of turbulence metrics tested (intensity, periodicity, and scale) are all known to have an impact on fish $\dot{M}O_2$, all models were supported by their known biological relevance (Burnham and Anderson 2002). Thus, a statistical approach was taken in which the best-fitting model was determined to be that which had the lowest AIC score (Tables 3.8 and 3.9). The top bioenergetics models for both species included an interaction between U and L. Because L is calculated as U this interaction can also be viewed as $U^2 \times T$. The square of the velocity, U^2, can be seen as a proxy for drag force, and therefore additional models including a $U^2 \times T$ interaction were developed for both species and compared with all other models through model selection. Hereafter, models incorporating a $U^2 \times T$ interaction are referred to as drag models.

Ideally, the top model selected via AIC should be lower than all other tested models by a ΔAIC of 2 (Burnham and Anderson 2002). For rainbow trout, three of the top models were

within 2 AIC points, and it is often recommended in such situations to average models or include the fixed effects from these top models (Burnham and Anderson 2002; Richards et al. 2010). Taking this approach was not possible for two primary reasons. First, the use of model averaging would not have suited the format of a bioenergetics model, which is meant to predict fish energy usage based on environmental conditions (Brandt and Hartman 1993; Hansen and Budy 2011). Second, the three models within 2 ΔAIC points contained all the same fixed effects, with the exception of their measure of turbulence intensity; in the model with the lowest AIC score, this was TKE, and in the other two models were TI_U and U_{rms}. These metrics are ultimately all derived from the same underlying data, with TI_U representing a dimensionless measure of turbulence intensity, and U_{rms} representing a component of turbulence intensity that is accounted for in the calculation of TKE. Therefore, it was not possible to separately include or average fixed effects from all top models. Thus, the rainbow trout bioenergetics model with the lowest AIC score was selected as the top model.

Model fit was assessed through a comparison of model r^2 values and visual inspection of fitted residual and quantile-quantile plots, while estimated marginal means were utilized as *post hoc* test to define the specific impact of fixed effects on $\dot{M}O_2$ (West et al. 2007; Zuur et al. 2009). The variance explained by each fixed effect in the top bioenergetics models was partitioned to quantify the relative influence of the fixed effects included on $\dot{M}O_2$ (Nakagawa and Schielzeth 2013). The r package "emmeans" version 1.7.3 (Lenth 2022) was used to quantify and visualize the interaction between U and *L* for each top model, while "r2glmm" version 0.1.2 (Jaeger 2017) was used to partition the variance explained by each fixed effect in the top bioenergetics models.

Results

Flow characteristics

Due to the large number of cases measured, data are only presented for all structures at all BL velocities for time-averaged velocity U. TKE is shown for the mid-size structure diameter (5.08-cm) for all structures at the mid-range BL velocity (1.5 BL/sec) to illustrate the effect of increasing structure diameter on the spread of turbulence within the test section. TKE, Reynolds stresses, vorticity, U_{rms}, U_{Trms}, *L*, and *T* are shown for the mid-size structure diameter at the mid-range BL velocity for all structure orientations. The full suite of plots for each metric, structure diameter, and BL velocity are available within the supplemental materials for this chapter (Figures B.25 to B.69).

At the lowest velocity of 1.0 BL /sec, temporally- and spatially-averaged longitudinal velocity, U, was similar for most cases, with flow rates ranging from 0.28 to 0.32 m /sec. Only H3 and D2 deviated strongly from this, with U of 0.24 and 0.38 m /sec, respectively (Figure 3.6; Figure 3.7). At the mid-range velocity of 1.5 BL /s^{-1}, temporally- and spatially-averaged U was similar for the case with NS and cases with all diameters of VS, around 0.45 m /sec, while U was lowest for H3 and D3, around 0.27 m/sec. At the highest velocity of 2.0 BL /sec, U was higher for the NS case than for cases with any structure.

All structures, regardless of orientation, formed a recirculating zone on the wake behind them, creating a region of reduced longitudinal time-averaged velocities. Longitudinal velocities were elevated at the margins of these wakes, likely due to continuity as the flow was constricted to a smaller space when structures were present. For VS, a wake was formed on the horizontal XY plane, and for HS, a wake was formed on the vertical XZ plane. DS generated a wake on both the XY and XZ planes. For the two orientations that influenced flow on a single plane, VS

and HS, this wake tended to be narrower in size and lower in mean velocity as compared to the DS. DS generated pockets that were larger in size and impacted more of the test section, but had typically higher velocities relative to the VS and HS at a given structure diameter and test velocity. DS generated a pattern of flow in which the time-averaged longitudinal velocity was reduced downstream of the center point of a structure in both the XY and XZ planes, but time-averaged longitudinal flow velocity surrounding this area was elevated compared to VS or HS (Figure 3.6, panels M-U; Figure 3.7, panels M-U). This was most pronounced on the XZ plane for the structures with the two larger diameters, where velocities near the margins of the test section were approximately 50-60% higher than those immediately downstream of the structures' center points (Figure 3.7, panels P-U). The VS and HS, in contrast, did not have such a large difference in time-averaged longitudinal velocity. In addition to structure orientation, structure diameter also influenced these low velocity zones. Structures of a smaller diameter blocked flow in a smaller portion of the test section, and thus the diameters of the pockets in their lee were smaller as well. At the highest BL velocity of 2.0 BL/sec, there did not appear to be a clear wake downstream of H2 and H3; this was likely due to a flow regime change, as flow above the thicker horizontal cylinders reached critical flow (i.e., Fr = 1), approaching the formation of a drowned hydraulic jump past the cylinder (Figure 3.7, panels I and L).

All cases tested were fully turbulent, Re > 2000, including the control case with NS. However, the level of turbulence that was generated when structures were present was much higher than for NS. Turbulence intensity was highest in the immediate lee of structures, yielding increased levels of turbulence intensity metrics TI_U, TKE, and its components U_{rms} and U_{Trms} (Figure 3.8; Figure 3.9). This occurred for VS and HS, on the XY and XZ planes respectively, in the same areas that experienced reduced flow velocity due to the structures' presence. Among

the structures tested, TKE and its components U_{rms} and U_{Trms} were lowest for all VS cases (Figure 3.8) compared to the HS and DS cases (Figure 3.8; Figure 3.9). While turbulence intensity varied with structure orientation and diameter and flow velocity, it was typically highest for DS. TKE could be over two times greater for DS than HS, and over three times greater for DS than VS under the same mean flow conditions, especially at 1.5 and 2.0 BL/sec (Figure 3.8, panel C; Figure 3.9, panel C).

The portion of the test section affected by a structure's presence was also variable. For a given diameter, DS tended to have the widest ranging impact, generating turbulence that occupied most of the downstream portion of the test section. D3, in particular, affected the largest area downstream of the structure. Turbulence shed by D3, in particular, occupied nearly the entirety of the downstream portion of the test section (Figure 3.10, panel F; Figure 3.11, panel F). Turbulence generated by VS, in contrast, tended to be restricted to the longitudinal portion of the test section immediately downstream of a structure (Figure 3.10, panels A-B). However, the cylinder wake wavelength, λ, was the same for structures of the same diameter, with λ = [0.12, 0.24, and 0.36] m for 2.54, 5.08, and 7.62-cm diameters, respectively. Shedding frequency, *f*, varied between structures, but was generally similar for structures of the same diameter at a given velocity. Shedding frequency ranged between 2.4 and 5.2 Hz for 2.54-cm diameter structures, between 1.2 and 2.5 Hz for 5.08-cm diameter structures, and between 0.7 and 1.7 Hz for 7.62-cm diameter structures.

The effect of HS fell somewhere between that of DS and VS. The impacts of H1 and H2, the two smaller diameters of HS, tended to be limited to the region directly downstream of the structures (Figure 3.11), like with VS, but the turbulence generated by H3 began to fill a larger portion of the test section. The area effects of each structure were clearly visible in plots of time-

averaged Reynolds stresses $\overline{u'v'}$ and $\overline{u'w'}$ (Figure 3.8, panels D-F; Figure 3.9, panels D-F) in which Reynolds stress levels tended to be elevated immediately downstream from VS, but filled a greater portion of the test section for HS and DS. Much of the wide-ranging impact of DS was likely because DS altered flow characteristics in both the XY and XZ planes. However, both DS and the larger HS may have also caused surface effects, noticeable in Figure 3.7.

Alternating bands of vorticity were visible for VS, DS, and NS on the XY plane (Figure 3.8; Figure 3.9); these bands likely reflected the effects of small eddies generated as water passed through the flow straightener upstream of the test section. Despite the presence of these eddies, plots of vorticity and Reynolds stresses still clearly showed the development of eddies of opposing rotation on each side of the wakes of VS and DS in the XY plane (Figure 3.8, panels H and I); these were also seen for HS on the XZ plane (Figure 3.9, panels H and I), indicating the likely presence of a Karman vortex street.

The largest, slowest-rotating eddies were produced by VS (identified by largest values of L and highest values of T in Figures 3.12 and 3.13, respectively). At a given BL velocity, *L* and *T* for VS of a given diameter was higher than *T* or *L* for a DS or HS of the same diameter. For example, at the mid-range velocity, the spatially-averaged *L* for V2 was 0.036 m, three times greater than the spatial average for D2 on the XY plane (0.014 m), and approximately two times greater than the spatial average for D2 on the XZ plane (0.020 m) and the spatial average for H2 (0.018 m). At this velocity, the spatially-averaged *T* for V2 was 0.081 s, approximately two times greater than the spatial average for D2 on the XY plane (0.039 s), D2 on the XZ plane (0.043 s), and H2 (0.043 s). Which structure had the lowest *L* and *T* was not consistent across velocities and diameters, but generally HS had the lowest *L* and *T*, indicating that HS produced the fastest-rotating eddies. The differences in *L* and *T* may have been due to depth and the space obstructed

by cylinders on each orientation; the flume was filled to a depth of 0.25 m, which may have potentially prevented the vertically-oriented eddies generated by HS and DS from developing fully.

Bioenergetics models

A description of how the developed bioenergetics models can be utilized to estimate rainbow trout or smallmouth bass $\dot{M}O_2$ is provided in Figure B.70. For both rainbow trout and smallmouth bass, the best-fitting model relating flow metrics to $\dot{M}O_2$ included an interaction between time-averaged velocity U and *L* (a measure of turbulence scale) as a fixed effect. This interaction between U and *L* explained 29% of the fixed-effect variance for rainbow trout (Table 3.10) and 19% of such variance for smallmouth bass (Table 3.11). The drag model, in which the interaction between U and *L* was swapped for an interaction between U^2 and *T*, provided an equally good fit for data derived from smallmouth bass, but did not provide a good fit for data derived from rainbow trout. As it was not possible to disentangle the potential effects of the interaction between U and *L* from the potential effects of the interaction between U^2 and *T*, both are discussed for smallmouth bass. However, as I was interested in the effects of turbulence on fish energetics, I focused primarily on the interaction between U and *L*.

At low U, rainbow trout and smallmouth bass $\dot{M}O_2$ was lowest when fish occupied eddies with high *L* (i.e., large eddies) and highest when fish occupied eddies with low *L* (i.e., small eddies) (Figure 3.14). A reversal of this relationship occurred at high U, where fish had the lowest $\dot{M}O_2$ when occupying small eddies with low *L* and the highest $\dot{M}O_2$ when occupying large eddies with high *L*. The $\dot{M}O_2$ of fish that selected eddies of a size near mean *L*, however, did not differ from that of fish selecting high *L* or low *L* at any U (Figure 3.15).

The impact of the U × *L* interaction differed between the two species. At U below approximately 0.5 m/s, rainbow trout used the least amount of oxygen when swimming near eddies that with large *L*, as compared to when they swam near eddies with low *L* (Figure 3.14, panel A). At 0.5 m/s, rainbow trout had approximately the same $\dot{M}O_2$ regardless of what *L* they selected, but, above this velocity, the relationship that existed at lower U reversed, with fish having lower $\dot{M}O_2$ when selecting eddies with small *L*, and higher $\dot{M}O_2$ when selecting eddies with large *L*. Interestingly, when rainbow trout occupied areas of low *L* at high U (around 0.75 m/s), their $\dot{M}O_2$ was lower than when occupying eddies with any *L* at the lowest U.

As with rainbow trout, smallmouth bass $\dot{M}O_2$ was lowest at low U when fish swam with eddies with large *L*, but lowest at high U when fish occupied eddies with small *L* (Figure 3.14, panel B). However, the U at which this inversion occurred at a lower U for smallmouth bass, around 0.3 m/s, at which U smallmouth bass $\dot{M}O_2$ was essentially the same regardless of the *L* they occupied. At velocities above 0.3 m/s, smallmouth bass $\dot{M}O_2$ increased with increasing U and *L*. Unlike rainbow trout, smallmouth bass $\dot{M}O_2$ increased consistently with increasing U, regardless of the *L* of the eddies they selected. However, the degree to which $\dot{M}O_2$ increased was dependent on the *L* of the eddies smallmouth bass occupied, with eddies of larger *L* yielding a greater rate of increasing $\dot{M}O_2$. A largely similar pattern was observed for the smallmouth bass drag model (Table B.5). When occupying quickly-rotating eddies with very low *T* (around 0.0005 sec), smallmouth bass $\dot{M}O_2$ was largely stable, regardless of the level of U^2 that fish were experiencing (Figure B.71). When fish occupied more slowly-rotating eddies, with increasing rates of *T*, however, $\dot{M}O_2$ increased as fish experienced increasing levels of U^2.

Fish of both species swam within eddies that varied greatly in size, but ultimately the average size of eddy occupied by fish was small (Figure 3.16). At times, rainbow trout occupied

eddies with *L* of nearly 20 cm (Figure 3.4). However, the average size *L* of eddies occupied by all rainbow trout was 2 cm, and the bulk of eddies in which rainbow trout swam had a narrow range of *L*, and the average *L* selected by any single fish under any flow condition was less than 7 cm. The range of eddy sizes encountered by smallmouth bass at any point were higher than for rainbow trout, as smallmouth bass occasionally occupied eddies with *L* in excess of 25 cm (Figure 3.5). Like rainbow trout, however, most eddies occupied by smallmouth bass were much smaller. The highest average *L* experienced by an individual fish was 13 cm, and the average *L* selected by smallmouth bass overall was 5 cm (Figure 3.5).

The best-fitting model relating flow metrics to $\dot{M}O_2$ for rainbow trout and smallmouth bass also included a measure of turbulence intensity. The impact of turbulence intensity on fish $\dot{M}O2$ was independent of U, and the most influential metric of intensity was different for each species. Rainbow trout were mostly strongly impacted by TKE, which reflects the total level of turbulence intensity occurring on all three axes of movement. This metric accounted for 14% of variance explained by fixed effects within the top bioenergetics model. Smallmouth bass were most impacted by U_{Trms} which reflects turbulence intensity occurring transverse to the longitudinal flow; this accounted for 29% of the proportion of variance explained by fixed effects in the top smallmouth bass bioenergetics model. For both species, increasing turbulence intensity resulted in higher levels of $\dot{M}O_2$. Rainbow trout showed higher $\dot{M}O_2$ as TKE increased (Figure 3.17, panel A), while smallmouth bass experienced elevated $\dot{M}O_2$ as U_{Trms} increased (Figure 3.17, panel B). This did not appear to be influenced by any particular structure, with no apparent clustering by structure of particular levels of turbulence intensity experienced by fish (Figure B.72, panels A and B).

Log-transformed mass and water temperature were additionally included as fixed effects for both species, however mass was not significant for either species and water temperature only impacted the $\dot{M}O_2$ of rainbow trout (Tables 3.10 and 3.11).

Discussion

The most important environmental factor affecting oxygen consumption in both rainbow trout and smallmouth bass was turbulence, with oxygen consumption was impacted by multiple aspects of turbulence simultaneously. More specifically, both turbulence intensity and scale, rather than just turbulence intensity alone, were important drivers of oxygen consumption for both rainbow trout and smallmouth bass, and the impact of turbulence scale varied across water velocities.

Turbulence scale and velocity

The impact of an eddy size on fish energy use was influenced by mean velocity. At low water velocities, both rainbow trout and smallmouth bass used the most energy when swimming in eddies with a small *L*, and used the least energy when swimming in eddies with a large *L*. In contrast, at high water velocities, this relationship was reversed, whereby fish used more energy when selecting eddies with a large *L*, and used the least energy when selecting eddies with a small *L*. One potential explanation for this relates to both eddy size (turbulence scale) and rotation speed. A number of studies, conducted with multiple fish species, have found that turbulence scale has the potential to impact swimming performance and swimming stability, with the ability of an eddy to impact a fish dependent on the size of the eddy in relation to the size of the fish (Pavlov et al. 2000; Tritico and Cotel 2010; Webb and Cotel 2010; Lacey et al. 2012; Smith et al. 2014). More specifically, eddies smaller than a fish lack the momentum needed to influence swimming, while eddies larger than a fish will pass around it and not exert any

influence. In contrast, eddies with a length scale matched to the size of a fish will increase contact time and energy transfer, and will reduce swimming stability (Pavlov et al. 2000; Smith et al. 2014). When fish encounter such destabilizing flows, remaining in place requires frequent adjustments of body and fins, and, at times, fish may be pushed downstream requiring additional bursts to remain in place (Tritico and Cotel 2010; Maia et al. 2015). Control and maintenance of a stable swimming posture accounts for a substantial portion of energetic expenditure in fish, even outside of turbulent flows (Webb 2002), and swimming in a destabilizing flow requires fish to exert more energy to maintain their position, resulting in increased levels of oxygen consumption (Cotel and Webb 2015; Strailey et al. 2021). The length scale and time scale of eddies are closely related, with larger eddies tending to rotate more slowly, and smaller eddies tending to rotate more quickly (Rhoads 2020). At low water velocities, fish likely had time to navigate large, slowly-rotating eddies, and thus may have been able to reduce potential destabilization. In contrast, a small, quickly-rotating eddy would be more difficult to avoid, thereby increasing energy use even at low water velocity. As mean water velocity increased, however, fish occupying larger eddies had higher $\dot{M}O_2$, while fish occupying smaller eddies instead had lower $\dot{M}O_2$. Another possible explanation for the effect of the interaction between velocity and L on $\dot{M}O_2$ is that, at low velocities, eddies with a large L may simply lack the momentum needed to affect fish swimming stability (Tritico and Cotel 2010). In this study, large L eddies at low velocities may not have had the momentum required to present a stability challenge for fish, and thus would not have required position correction that in turn increases energy usage. Overall, the combined impact of flow velocity and eddy size on fish oxygen consumption seen in this study likely relates to the role these play in affecting fish swimming stability.

Interestingly, eddy size (in conjunction with flow velocity) still appeared to be a driver of fish energy use even though the majority of the eddies occupied within this study were small in comparison to the fish. Conventional wisdom regarding the interplay between turbulence scale and fish size is that eddies smaller in size than a fish are not expected to affect swimming. Tritico and Cotel (2010), for example, found that creek chub (*Semotilus atromaculatus*) only began to lose control of their posture when turbulence eddy diameter approached 75% of their body length, while Nikora et al. (2003) found that neither the swimming ability nor energy usage of inanga (*Galaxias maculatus*) was affected by turbulent eddies that were small in comparison to fish. In this study, the average length of fish was 27 cm, and the majority of locations occupied by fish had eddies with *L* of <less than 10 cm, though larger eddies were available. Thus, fish primarily occupied eddies with *L* approximately one-third of their length (or smaller). This may be due in part to the interaction between eddy size and mean velocity experienced by fish. The effects of turbulence intensity on fish, for example, are known to vary across different velocities (Lacey et al. 2012; Strailey et al. 2021). Similarly, there is evidence that eddies similar in scale to the size of a fish have reduced impacts at low velocities (Tritico and Cotel 2010). However, this study appears to be the first to discover the potential for even small eddies to affect fish when considered in conjunction with flow velocity, which can be only seen by coupling the actual location of the fish with the hydrodynamics of those locations, rather than using average statistics without consideration for fish choice of location.

The interaction between eddy size and velocity impacted the oxygen consumption of rainbow trout and smallmouth bass in different ways, and one possible explanation relates to swimming gait and pattern. The terms “swimming gait” and “swimming pattern” refers to the combination of locomotor behavior (i.e., continuous swimming, burst-and-glide swimming), and

propulsor kinematics (i.e., steady swimming, station-holding, hovering) (Webb 1994). When exposed to turbulent flow, particularly that generated by a cylindrical structure, fish may be able to employ a number of swimming patterns that allow them to exploit turbulent eddies to hold station or reduce swimming costs, including entraining and bow waking (Liao et al. 2003; Webb 1998; Przybilla et al. 2010; Wang and Chanson 2018). In particular, a number of fish species are able to employ a specific gait known as the Kármán gait to exploit the energy contained within eddies shed by cylinders (Liao et al. 2003; Liao et al. 2004; Ke et al. 2021). In the Kármán gait, fish slalom between eddies, reducing their need for powered swimming in turn. Rainbow trout specifically have the demonstrated ability to use the Kármán gait to decrease their energy use in turbulent flow even as water velocity increases (Liao et al. 2003; Liao 2004; Cook and Coughlin 2010; Taguchi and Liao 2011). In this study, rainbow trout $\dot{M}O_2$ decreased as water velocity increased when fish occupied the smallest eddies (2 cm or smaller, relative to approximately 27 cm long fish). Eddies of these sizes may potentially encourage Kármán gaiting in rainbow trout, therefore resulting in fish using less oxygen. Strong evidence for smallmouth bass using exploitative swimming gaits or patterns, however, has not been found. Web (1998), for example, determined that smallmouth bass would entrain on cylindrical structures of a narrow range of sizes and under a narrow range of environmental conditions. In contrast to rainbow trout, smallmouth bass have also never been formally documented to exhibit the Kármán gait. This could explain why smallmouth bass experienced consistently higher $\dot{M}O_2$ water velocity increased, with eddy L controlling the rate at which $\dot{M}O_2$ increased. Without the usage of turbulence-exploiting swimming patterns and gaits, turbulence is more likely to have a deleterious effect on fish where fish expend more energy during swimming (Pavlov et al. 2000; Enders et al. 2003). Therefore, the effect of the interaction between eddy size and velocity on

fish oxygen consumption may have differed between species because rainbow trout were able to take advantage of a "boost" that was simply not available for smallmouth bass.

Differences in swimming style and morphology may also be responsible for the differing impact of eddy size and flow velocity on the energetic expenditures of rainbow trout and smallmouth bass. As opposed to swimming gait or swimming pattern, the term "swimming style" refers to the manner in which fish employ different fins and regions of the body to swim, and is more closely tied with morphology (Webb 1984; Webb 1994; Blake 2004). Rainbow trout are primarily body-caudal fin (BCF) swimmers, relying most heavily on their body and caudal fin for propulsion, while smallmouth bass are primarily median-paired fin (MPF) swimmers, using the dorsal and paired fins to provide the primary propulsive force for most swimming (Webb 1984). MPF swimmers typically possess large, flexible median and paired fins that increase maneuverability and reduce time it takes fish to turn as compared to BCF swimmers (Gosline 1971; Alexander 1967; Webb 1984; Webb 2004). At low water velocities, MPF swimming is more energetically economical than BCF swimming, but at high water velocities, the swimming performance of primary MPF swimmers is impaired (Blake 2004; Webb and Cotel 2010). At lower water velocities, the smallmouth bass in this study were likely able to maneuver easily around both small and large eddies. As water velocity increased, the ability of smallmouth bass to effectively maneuver around turbulent eddies likely diminished, requiring fish to adjust their position more frequently therefore increasing $\dot{M}O_2$. Though not as maneuverable at low velocities as MPF swimmers, primary BCF swimmers have superior swimming performance and can attain higher water velocities without exerting as much energy as a primary MPF swimmer would at the same velocity (Webb 1971; Blake 2004; Webb and Cotel 2010). Therefore, rainbow trout may not have experienced a consistent increase in $\dot{M}O2$ as

velocity and eddy size changed largely due to their ability to perform well at high velocities. Ultimately, it is likely that multiple factors contributed to the difference in the interaction between eddy size and velocity for rainbow trout and smallmouth bass.

The apparent interactive effect of U and *L* on fish energy use may potentially relate instead to drag force. In this study, *L* was calculated by multiplying integral time scale *T* by a representative velocity U, following Taylor's frozen turbulence hypothesis (Taylor 1938). As a result, this interaction essentially approximated $U^2 \times T$; indicating a relevant role of U^2, which relates directly to drag force. Drag forces act against fish as they swim, requiring fish to generate sufficient thrust in order to overcome drag (Vogel 1994; Drucker and Lauder 2000). When water velocity and swimming speed increase, the drag forces acting upon a fish similarly increase, and fish must provide more propulsive power to overcome this (Drucker and Lauder 1999; Webb 2002). This requires the activation of muscle fibers that are more metabolically costly (Webb 1971; Kendall et al. 2007). In this study, as water velocity increased, the drag forces acting against fish likely increased as well. However, it appeared that only smallmouth bass may have used more energy to overcome these increasing drag forces. When a model containing this interaction was compared with a model containing a $U \times L$ interaction, both models performed equally as well for smallmouth bass, indicating that drag may have impacted their energy use. However, this was not the case for rainbow trout, for which the model with a $U^2 \times T$ had less support than the model with a $U \times L$ interaction, indicating that, in this situation, drag may not be as strongly predictive of rainbow trout energy use. Given that a model with a $U \times L$ interaction inherently includes a $U^2 \times T$ interaction, it is unclear as to why the model directly including U^2 did not perform well for rainbow trout. Further study will be needed to tease out the potential impacts of drag on energy use in these species.

Turbulence intensity

Increasing levels of turbulence intensity manifested in greater energetic expenditures for both rainbow trout and smallmouth bass, but energy use in rainbow trout was driven by TKE, while energy use in smallmouth bass was most strongly affected by $U_{T rms}$. TKE measures turbulence occurring in the X, Y, and Z directions, and so reflects the overall level of intensity occurring (Rhoads 2020). The inclusion of TKE within the top model for rainbow trout indicates that there is no single direction of flow that has the greatest impact on how rainbow trout respond to increasing levels of turbulence intensity. $U_{T rms}$ combines turbulence intensities V_{rms} and W_{rms}, both of which reflect turbulence occurring in directions transverse to the longitudinal X direction. Therefore, the inclusion of $U_{T rms}$ in the top bioenergetics model for smallmouth bass indicates that turbulence in the lateral Y and vertical Z directions had the strongest impact on smallmouth bass energy use, and that turbulence occurring in the longitudinal X direction is not as important for these fish. As with the interactive effect of water velocity and eddy size on $\dot{M}O_2$, morphology may explain why the energy use of rainbow trout was equally impacted by turbulence intensity in all directions, while smallmouth bass were impacted by turbulence intensity occurring in the transverse directions to the longitudinal flow. Rainbow trout possess a highly streamlined, fusiform body shape (Webb 1984). This type of body shape reduces drag, increases swimming efficiency, and reduces the energetic costs of swimming (Ohlberger et al. 2006; Webb and Cotel 2010). Because of this streamlined body shape, rainbow trout essentially exist in each plane equally, and as flow moves downstream toward a swimming rainbow trout, the momentum of the flow is distributed evenly. In comparison to rainbow trout, smallmouth bass are laterally-compressed, with deep bodies, and, as a result, turbulence generated in differing directions will not all be encountered equally by a smallmouth bass (Lauder and

Drucker 2002). This means that smallmouth bass are, therefore, unlikely to be impacted equally by turbulence generated in differing directions. Overall, each species was more strongly impacted by a different measure of turbulence intensity, which may relate to morphology.

Implications and future directions

Results from this study have three major implications, not only for future laboratory-based investigations on the interactions between fish and turbulent flow, but also for the "real world" application of the information resulting from such studies. First, results highlight the value of conducting investigations with different species across a range of turbulent flow conditions. Some of the contrasting results regarding how fish interact with turbulence and how that, in turn, affects fish potentially originates from the lack of consistency and standardization within this area of research. Testing two species of fish, one of which is understudied in the context of fish-turbulence interactions, within the same flow conditions allows us to quantitatively relate differences in fish responses to specific flow characteristics. Currently, the bulk of information regarding these interactions comes from a small handful of species, tested within a limited range of flow characteristics. For example, the Kármán gait has been studied extensively (Liao et al. 2003; Liao 2004; Chagnaud et al. 2007; Liao and Akanyeti 2017; Harvey et al. 2022), but almost entirely for rainbow trout. This makes it difficult to assess whether this or a similar gait plays a role in driving energy use in turbulence for other species of fish. Future studies, whether their focus be on fish energy use or another response to turbulence, should aim to utilize a broader range of fish species and turbulent flow conditions to maximize the conclusions that can be drawn from them.

Second, results show the utility of making specific, quantitative links between the turbulent flow characteristics of location occupied by fish and the responses of fish to these

characteristics. In this study, fish often occupied a narrow range of the flow conditions available to them; this was clearly seen for integral length scale, for which fish most frequently occupied locations with small eddy size relative to the range of eddy sizes available. Had this study simply examined temporally- and spatially-averaged values for flow metrics, or treated each treatment as a categorical variable, results may have changed partially or entirely, and a large part of the "story" would likely have been missed. Therefore, future work should seek to track fish movement as much as possible in order to identify the specific locations and thus flow conditions selected by fish.

Third, results demonstrate the importance of expanding the range of flow metrics investigated and integrating flow metrics from multiple categories of the IPOS framework into fish-turbulence studies, particularly in regards to those examining fish energetics. TKE, for example, has been the most commonly used metric of turbulence intensity used to relate fish energetics with turbulence, but U_{Trms} was the intensity metric that was most impactful for smallmouth bass in this study, and has been largely overlooked to date. Similarly, analyses revealed that turbulence intensity is not the sole aspect of turbulence influencing fish energy usage, but that turbulence scale is important as well. Therefore, the expansion of flow metrics examined in studies of fish-turbulence interactions will serve to broaden the potential conclusions that can be made regarding these interactions.

Although missing such details may not be greatly impactful within the scope of laboratory-based investigations focused on basic science, there has been an increasing trend towards the integration of flow characteristics into the design of fish passageways and instream restoration structures (Tullos et al. 2015; Wang and Chanson 2018; Strailey et al. 2021). If studies do not adequately relate flow characteristics with fish responses, this may lead to the

design and implementation of passageways and structures that are poorly suited for fish use. To prevent this potential from happening, future fish-turbulence studies should aim to (1) test a greater number and variety of fish species across a greater range of standardized flow conditions, (2) track specific locations of fish to directly link location with the flow conditions that fish experience, and (3) measure a greater range of turbulence metrics from multiple categories of the IPOS framework.

Conclusion

Turbulent flow, characterized by fluctuating velocity manifesting in swirling eddies, is a ubiquitous feature of flowing-water environments. The complex interactions between fish and turbulent flow have been the subject of interdisciplinary research for several decades. Considerable knowledge has been gleaned, in particular, from laboratory studies, that allow for precise control of flow conditions and high-resolution characterization of turbulence, while simultaneously ensuring that fish responses to this turbulence can be closely monitored. Although laboratory-based studies offer many advantages, studies have often differed dramatically in their results, due potentially in part to differences in species tested, turbulent flow conditions and metrics investigated, and differing levels of integration between data derived from fish with data derived from flow. Due to this lack of standardization between studies, it is difficult to determine why results differ, or to draw firm conclusions moving forward. To address this, the current study utilized a laboratory-based approach in which two different species of fish were tested with the same set of turbulence-generating structures and fish were tracked to directly link flow metrics from multiple categories of the IPOS framework with fish energetics. Results revealed that turbulence scale and mean flow velocity combined to impact fish energy use, and showed that fish were affected by small eddies conventionally considered to have little

impact on energetics, particularly at low velocities. Furthermore, energy usage was driven by a different measure of turbulence intensity for each species, with rainbow trout being most affected by TKE, demonstrating that turbulence intensity in all directions impacted rainbow trout equally, while smallmouth bass were most affected by $U_{Trms,}$ showing that energy usage for this species was most impacted by turbulence intensity occurring in the transverse directions to the longitudinal velocity. Overall, this study provides a new approach to evaluate how fish interact with turbulent flow and demonstrates the value of making clear, mechanistic links between fish energetics and the flow conditions they occupy.

Figures

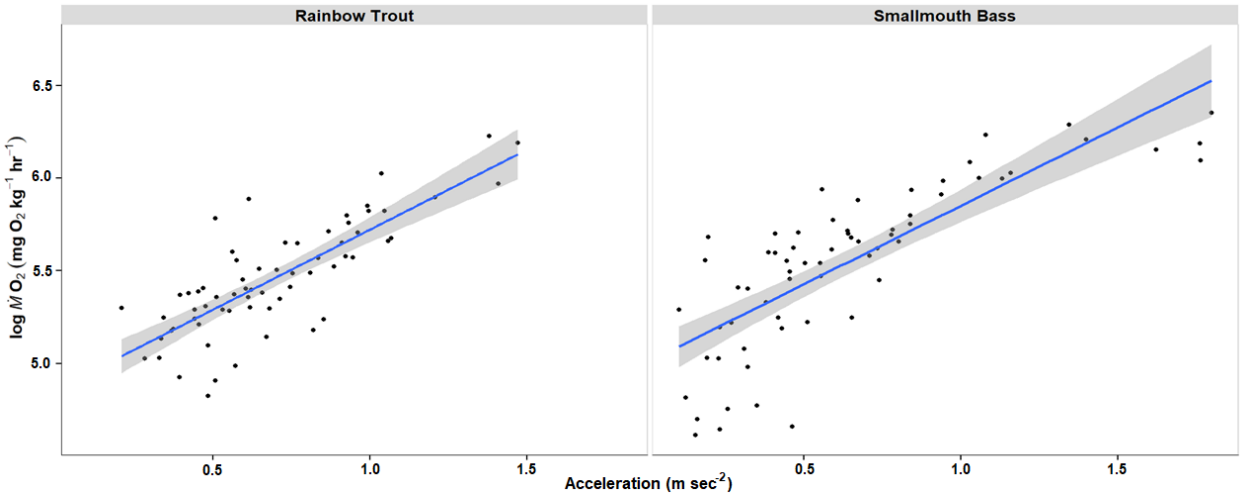

Figure 3.1. The oxygen consumption, $\dot{M}O_2$ (in mg O_2 kg^{-1} fish hr^{-1}) and swimming acceleration (in m sec^{-2}) of rainbow trout (left panel) and smallmouth bass (right panel) participating in respirometry experiments. Fish were acclimated to one of two different temperatures (10 and 18 °C for rainbow trout; 15 and 25 °C for smallmouth bass) and then swam in a respirometer across five body length (BL) velocities from 1.0 to 3.0 BL $/s^{-1}$. Resulting data were used to generate a model linking fish $\dot{M}O_2$ and acceleration.

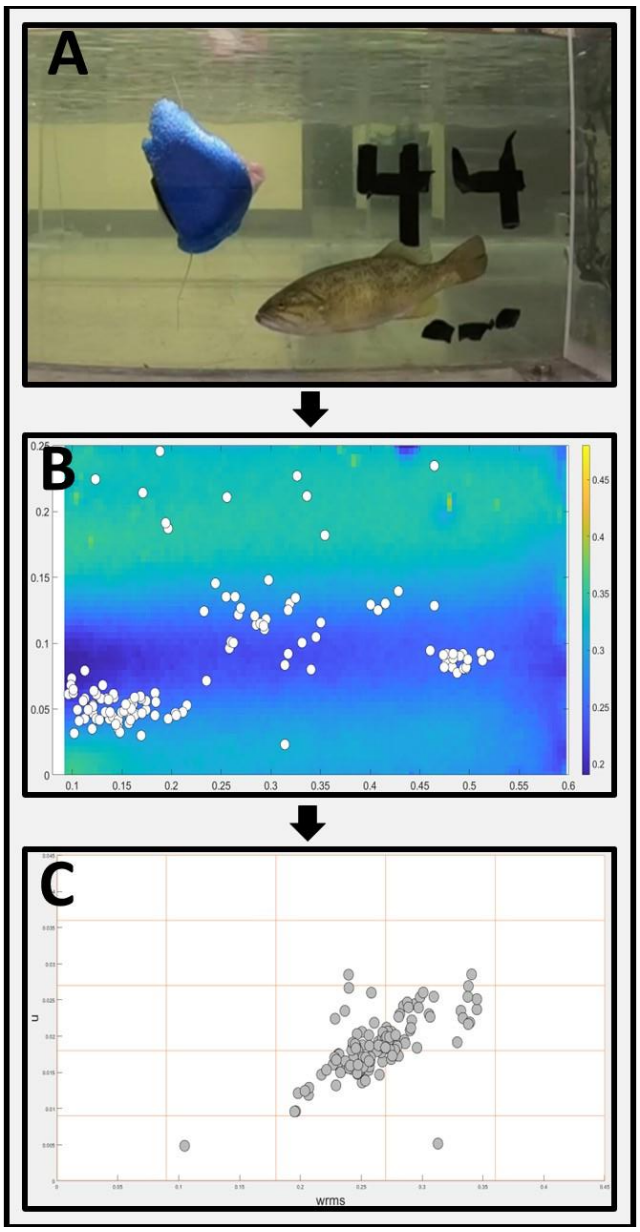

Figure 3.2. Flowchart visualizing the process of identifying the flow data used for bioenergetics modeling. Videos from swim trials were manually processed to track fish locations every 5 s for the duration of each trial (Panel A). The resulting coordinates were scaled and then overlaid onto 2D time-averaged plots of measured flow metrics (Panel B). The values for each metric at each coordinate were extracted, allowing flow data to be integrated directly with fish-derived data.

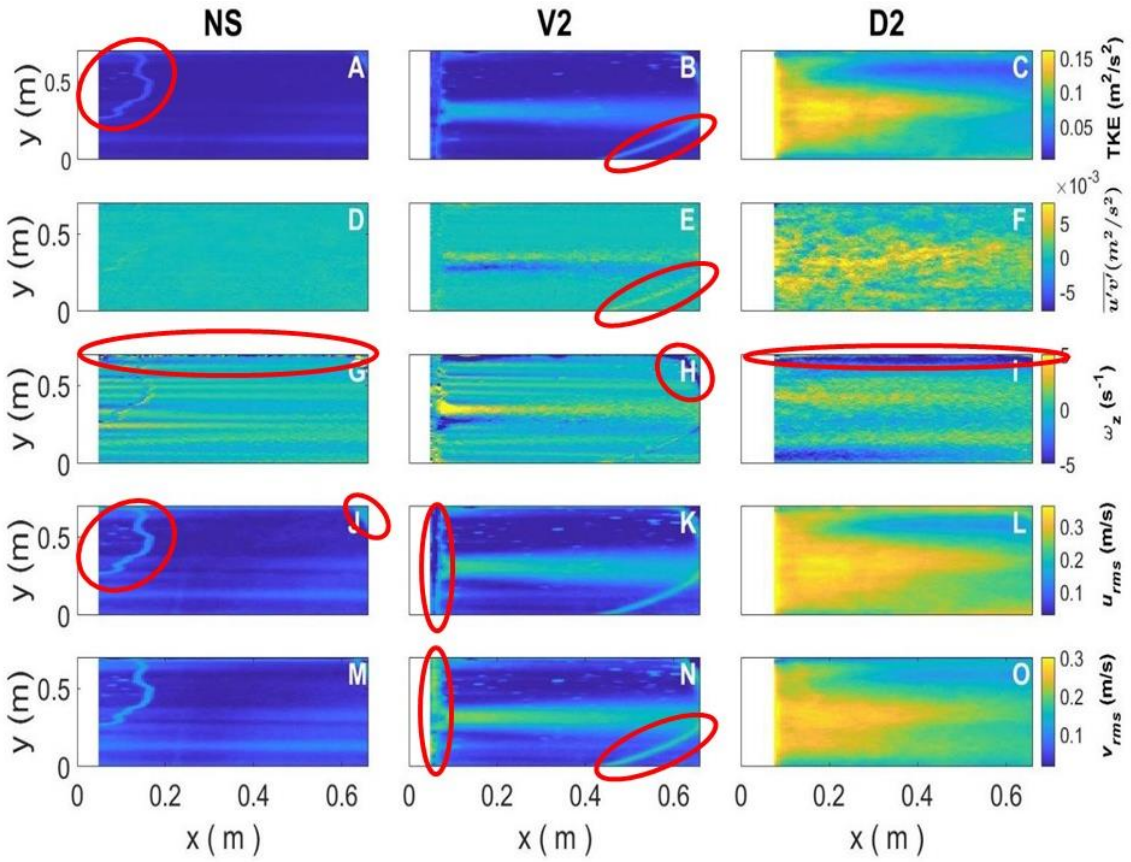

Figure 3.3. Heat map derived from PIV analyses. Issues with reflection and illumination sometimes caused the appearance of non-physically based aberrations within the PIV data, in which certain areas had higher or lower values than would be expected relative to other values for the given case; this commonly occurred near the test section boundaries. Examples of these areas are circled in red. During analyses of fish-derived data from flume experiments, fish location points from such areas were removed.

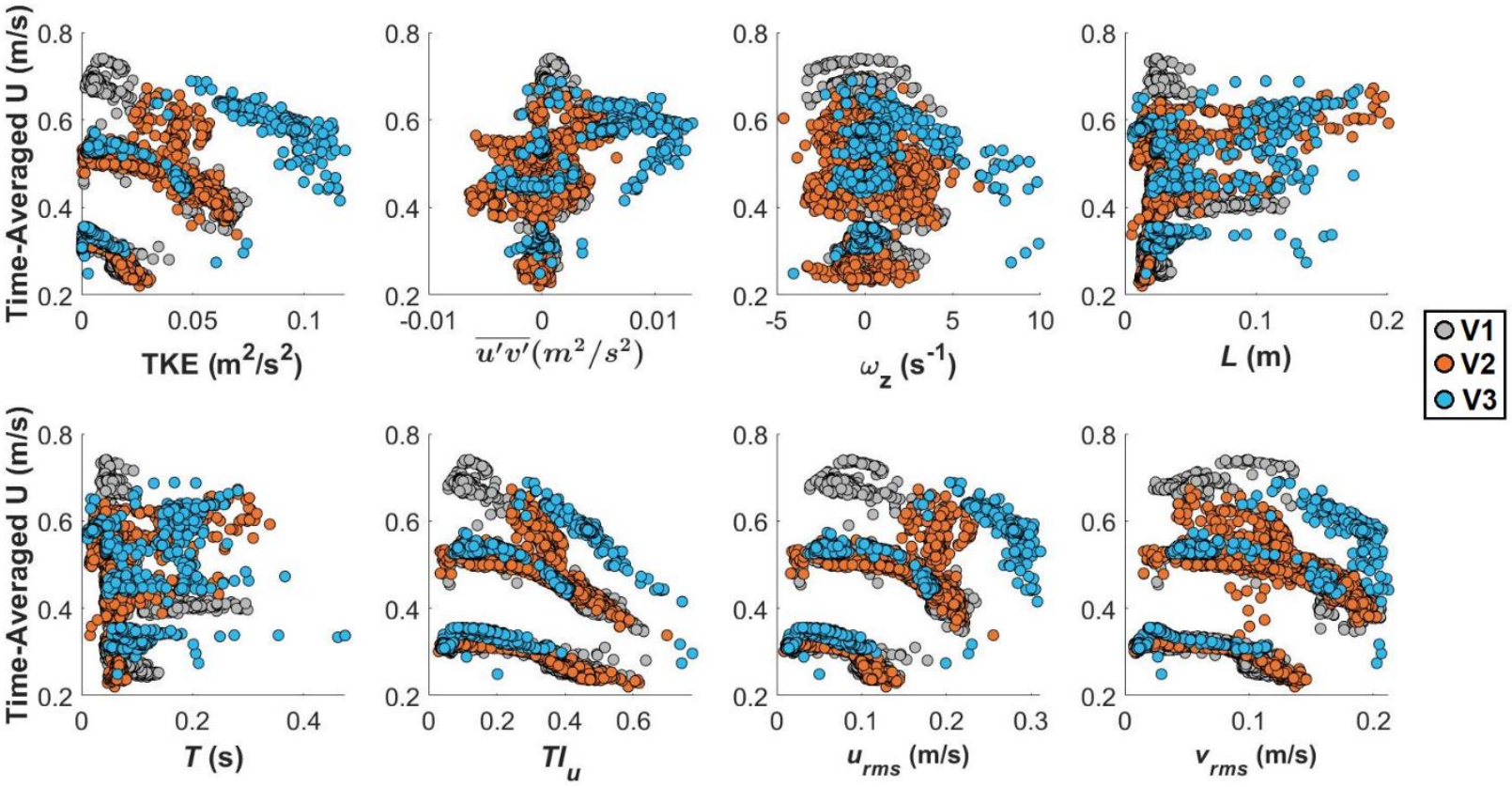

Figure 3.4. Time-averaged longitudinal velocity U extracted from locations occupied by rainbow trout swimming with diagonal structures (VS) compared with the turbulent flow conditions for each location. Turbulence metrics depicted include turbulent kinetic energy (TKE), Reynolds stress ($\overline{u'v'}$), vorticity (ω_z), turbulent integral length scale (L), turbulent integral time scale (T), turbulence intensity (TI_U), U_{rms}, and V_{rms}. Scatter plots were generated to identify potential relationship between U and the turbulence metrics examined. Different colors indicate the diameter of the VS, V1 [2.54-cm], V2 [5.08-cm], V3 [7.62-cm].

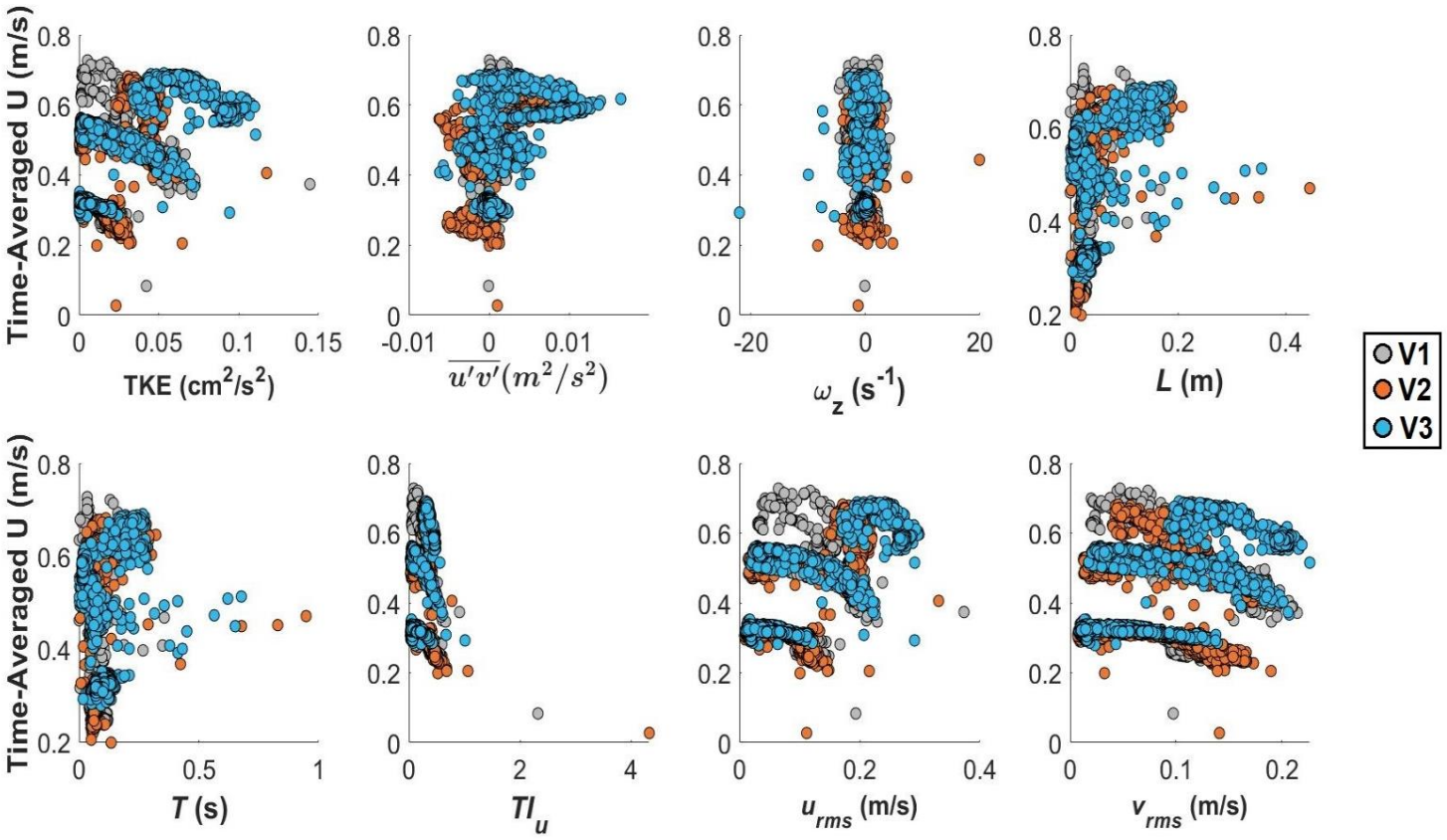

Figure 3.5. Time-averaged longitudinal velocity U extracted from locations occupied by smallmouth bass swimming with diagonal structures (VS) compared with the turbulent flow conditions for each location. Turbulence metrics depicted include turbulent kinetic energy (TKE), Reynolds stress ($\overline{u'v'}$), vorticity (ω_z), turbulent integral length scale (L), turbulent integral time scale (T), turbulence intensity (TI_U), U_{rms}, and V_{rms}. Scatter plots were generated to identify potential relationship between U and the turbulence metrics examined. Different colors indicate the diameter of the VS, V1 [2.54-cm], V2 [5.08-cm], V3 [7.62-cm].

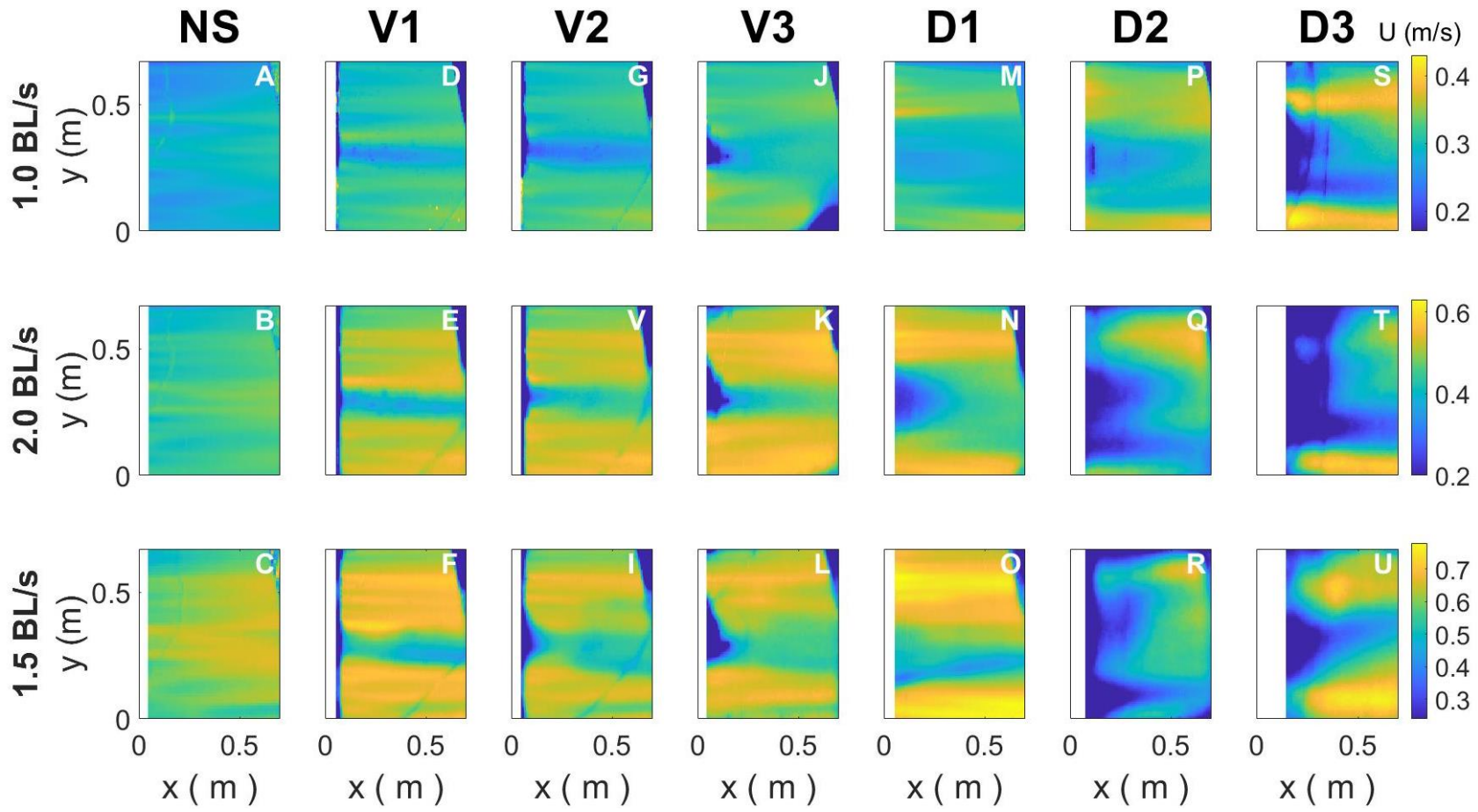

Figure 3.6. Time-averaged longitudinal velocity field (U; m/s) on the horizontal XY plane tested within a 1.0 m long test section established in a large racetrack flume. Velocity fields are visualized for vertical structures (VS) and diagonal structures (DS) of all diameters tested (V1, D1 – 2.54-cm; V2, D2 – 5.08-cm; V3, D3 – 7.62-cm), across all body-length velocities at which fish were tested (1.0, 1.5, and 2.0 BL/s). The control case with no structure (NS) is also shown.

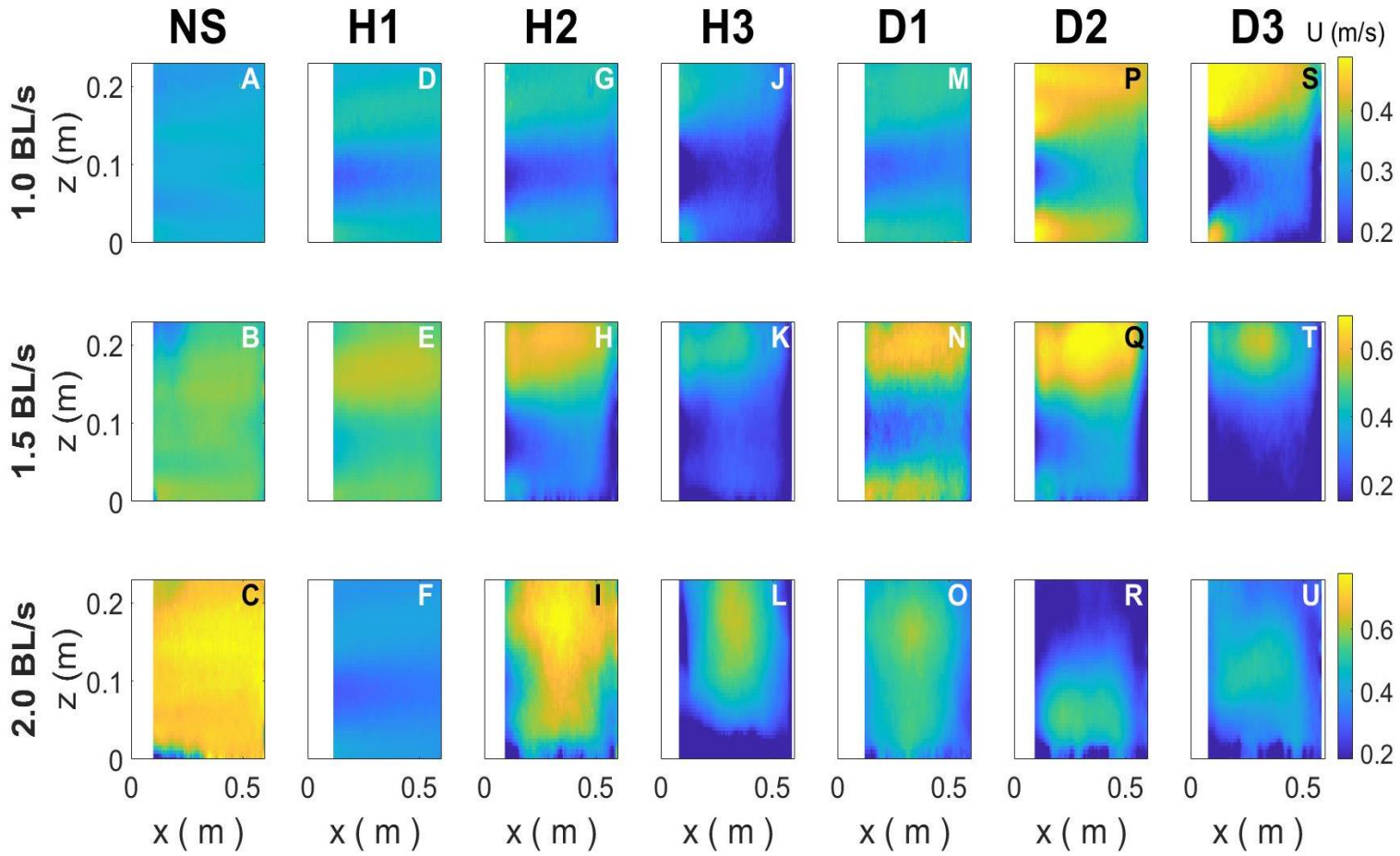

Figure 3.7. Time-averaged longitudinal velocity field (U; m/s) on the vertical XZ plane tested within a 1.0 m long test section established in a large racetrack flume. Velocity fields are visualized for vertical structures (HS) and diagonal structures (DS) of all diameters tested (H1, D1 – 2.54-cm; H2, D2 – 5.08-cm; H3, D3 – 7.62-cm), across all body-length velocities at which fish were tested (1.0, 1.5, and 2.0 BL/s). The control case with no structure (NS) is also shown.

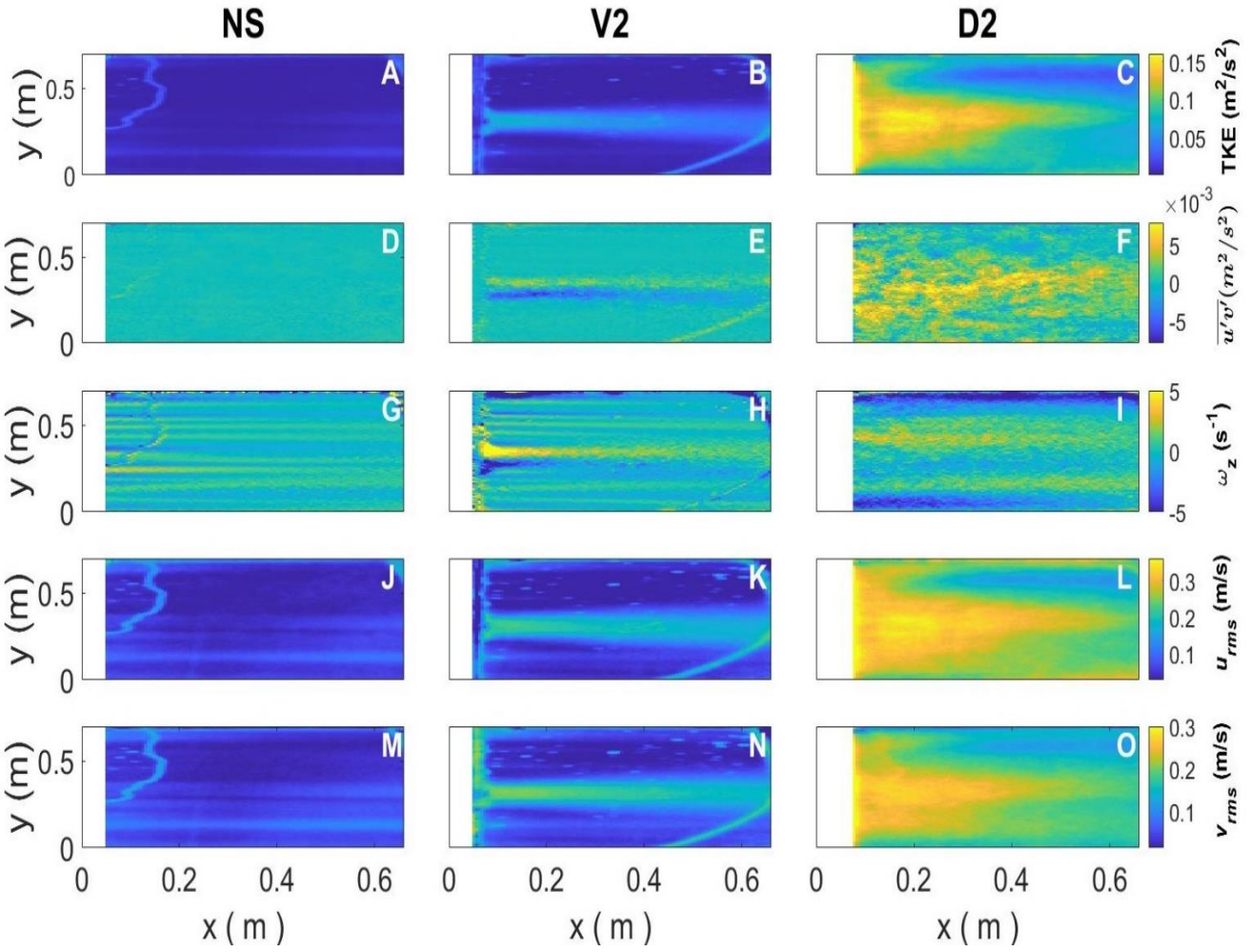

Figure 3.8. Time-averaged turbulent kinetic energy field (TKE; m^2/s^2)(A-B), Reynolds stresses ($\overline{u'v'}$;m^2/s^2) (D-F), vorticity (ω_z; s^{-1}) (G-I), U_{rms} (m/s) (J-L), and V_{rms} (m/s) (M-O) on the horizontal XY plane for no structure (NS), 5.08-cm diameter vertical structure (V2), and 5.08-cm diameter diagonal structure (D2), respectively, at the mid-range body-length velocity tested, 1.5 BL/S.

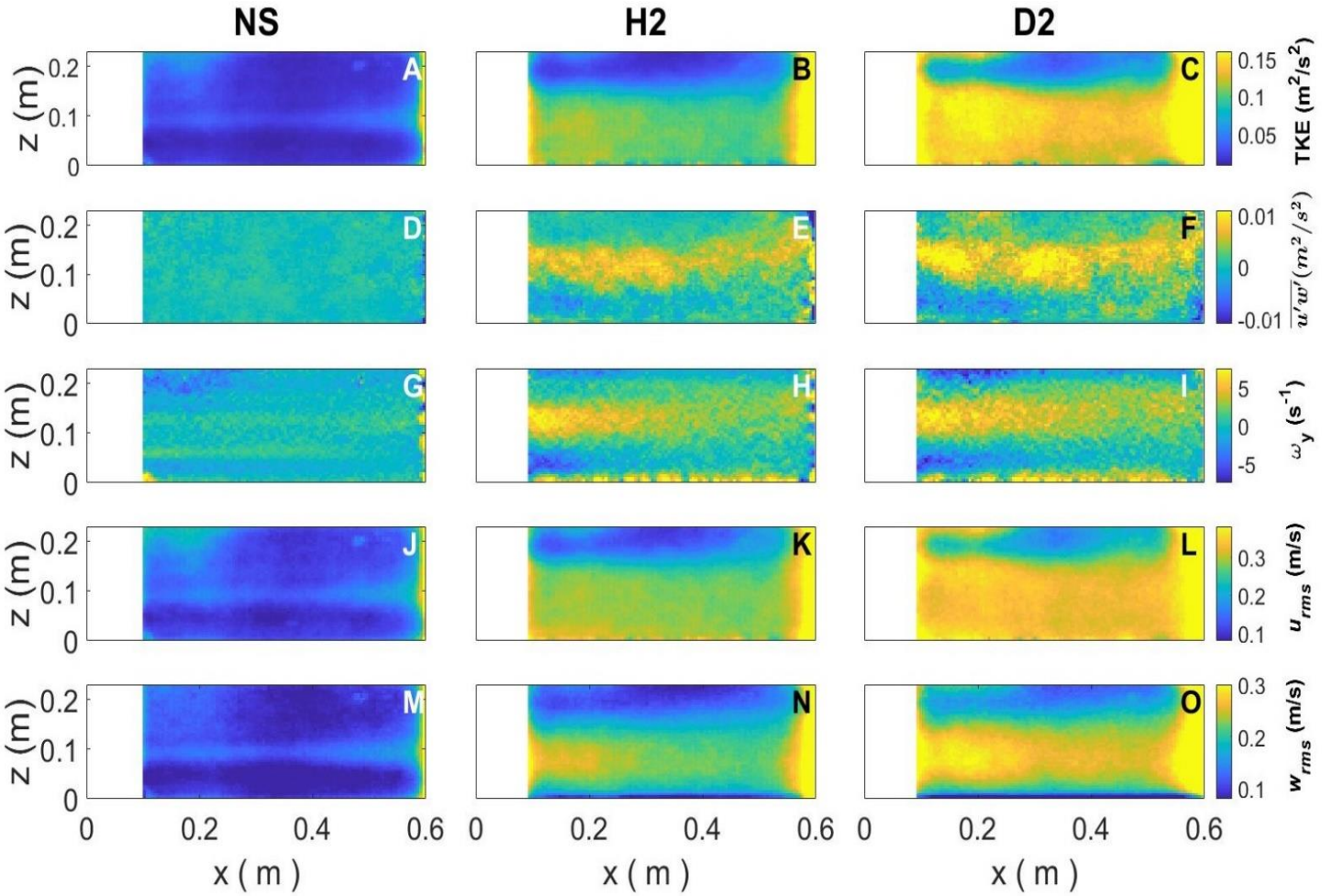

Figure 3.9. Time-averaged turbulent kinetic energy field (TKE; m^2/s^2)(A-B), Reynolds stresses ($\overline{u'w'}$;m^2/s^2) (D-F), vorticity (ω_y; s^{-1}) (G-I), U_{rms} (m/s) (J-L), and W_{rms} (m/s) (M-O) on the vertical XZ plane for no structure (NS), 5.08-cm diameter horizontal structure (H2), and 5.08-cm diameter diagonal structure (D2), respectively, at the mid-range body-length velocity tested, 1.5 BL/S.

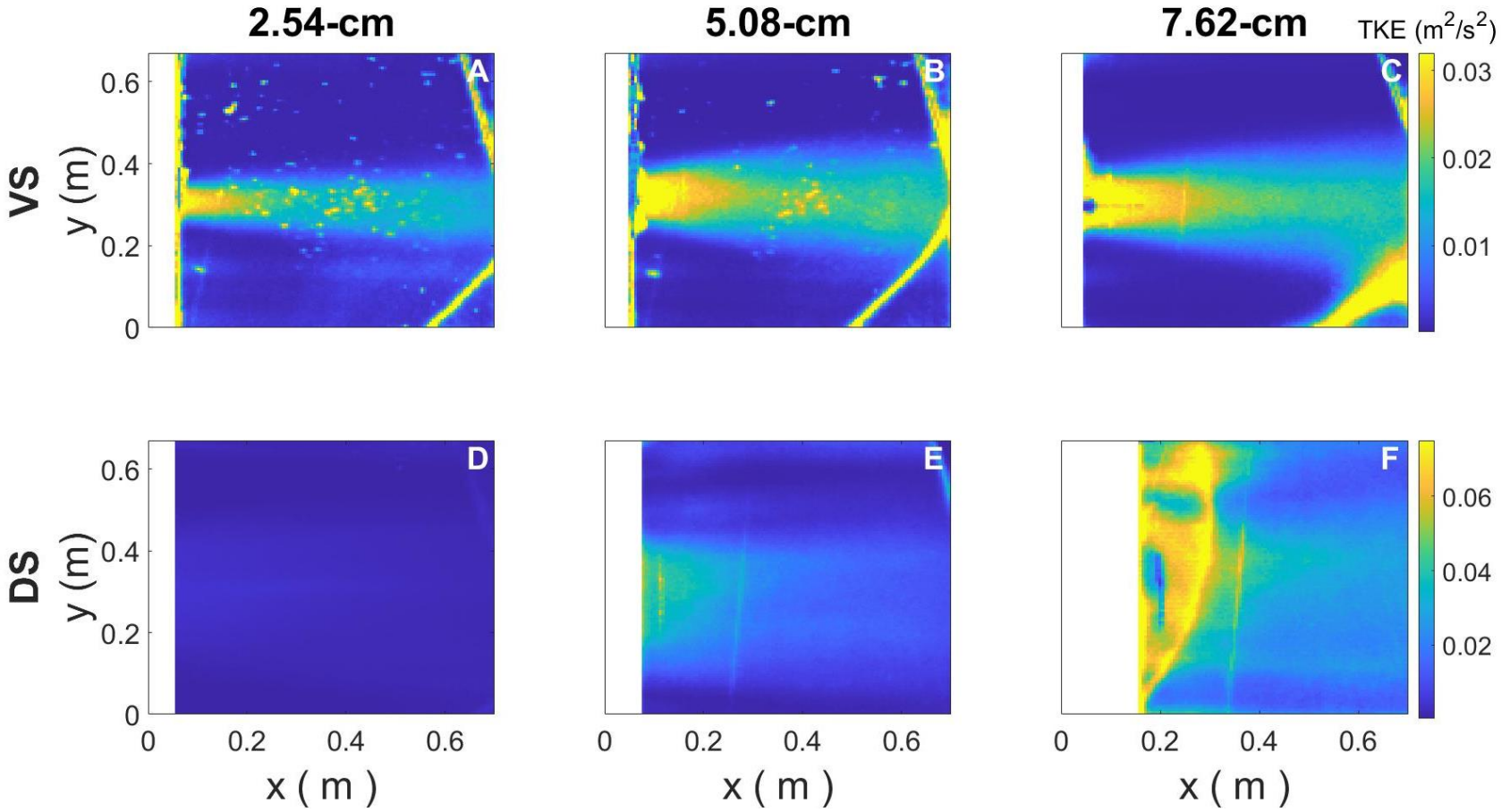

Figure 3.10. Time-averaged longitudinal turbulent kinetic energy field (TKE; m^2/s^2) on the horizontal XY plane tested within a 1.0 m long test section established in a large racetrack flume. TKE fields are visualized for vertical structures (VS) and diagonal structures (DS) of all diameters tested (2.54-cm – V1, D1; 5.08-cm - V2, D2; 7.62-cm – V3, D3). The measurements for all plots are shown at the same body-length velocity (1.5 BL/s) to highlight the effect of structure orientation and diameter turbulence intensity.

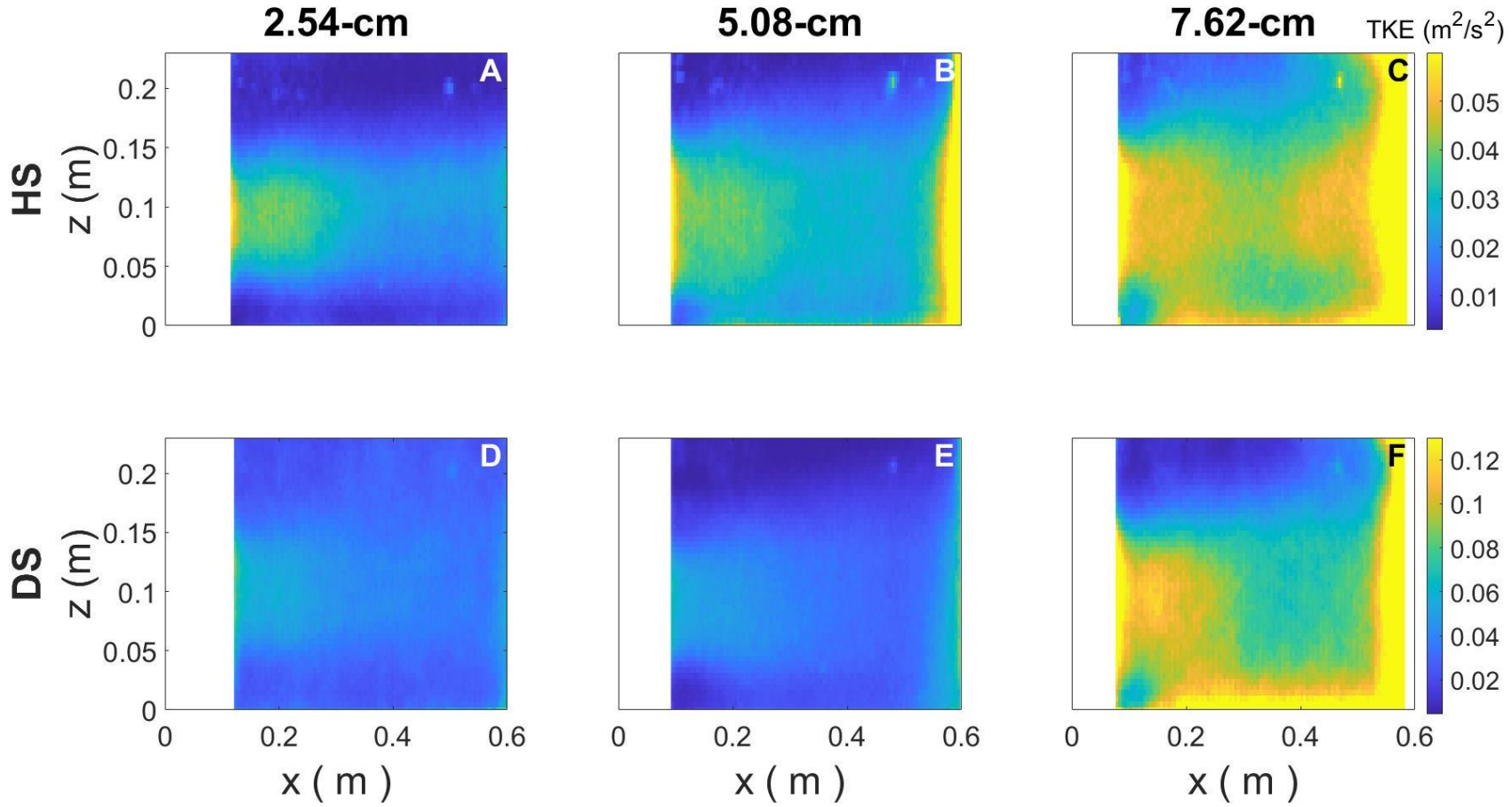

Figure 3.11. Time-averaged longitudinal turbulent kinetic energy field (TKE; m^2/s^2) on the vertical XZ plane tested within a 1.0 m long test section established in a large racetrack flume. TKE fields are visualized for vertical structures (VS) and diagonal structures (DS) of all diameters tested (2.54-cm – V1, D1; 5.08-cm - V2, D2; 7.62-cm – V3, D3). The measurements for all plots are shown at the same body-length velocity (1.5 BL/s) to highlight the effect of structure orientation and diameter turbulence intensity.

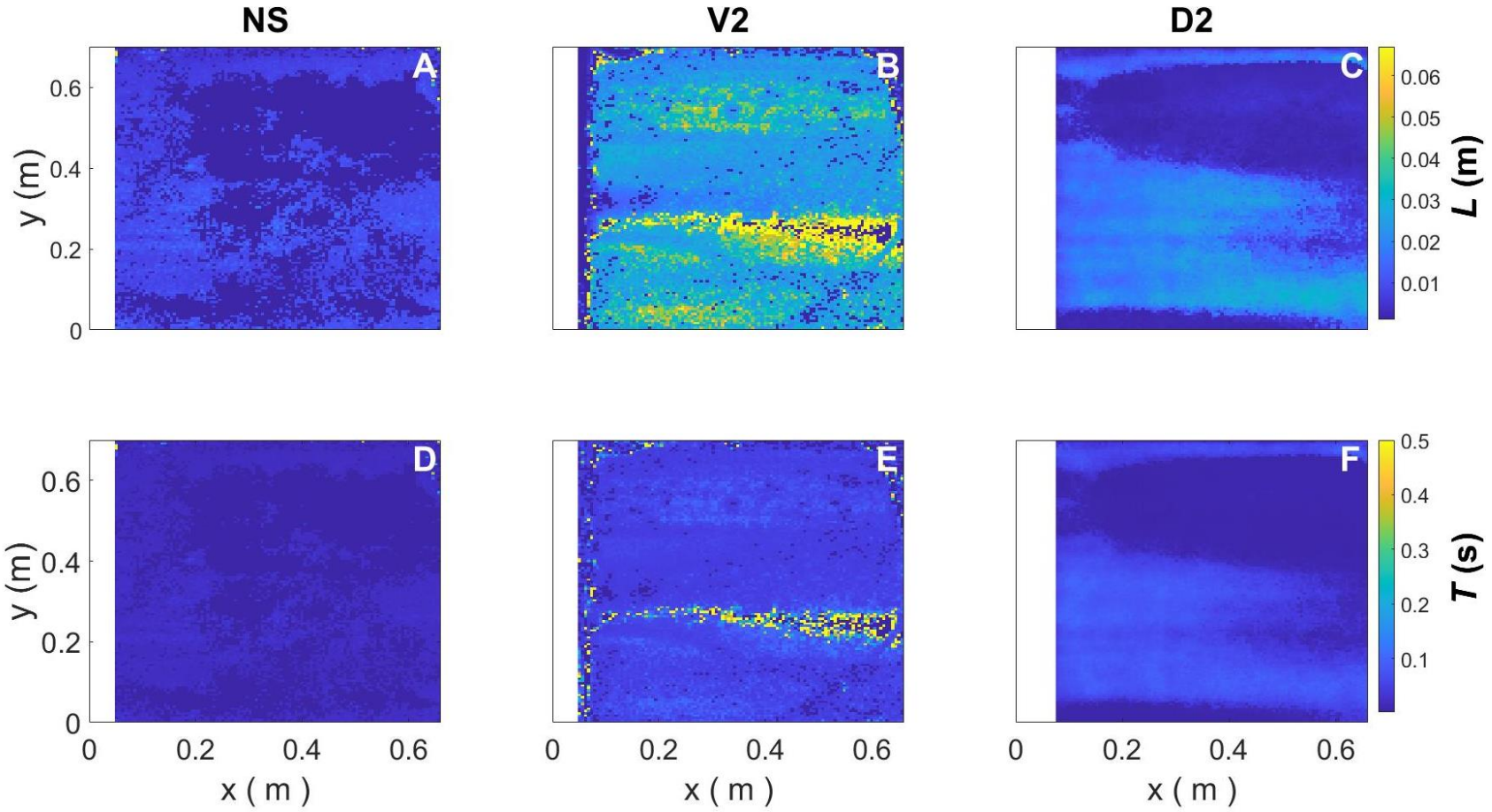

Figure 3.12. Time-averaged turbulent integral length scale (*L*; m) and turbulent integral time scale (*T*; s) on the horizontal XY plane for no structure (NS), 5.08-cm diameter vertical structure (V2), and 5.08-cm diameter diagonal structure (D2), respectively, at the mid-range body-length velocity tested, 1.5 BL/S.

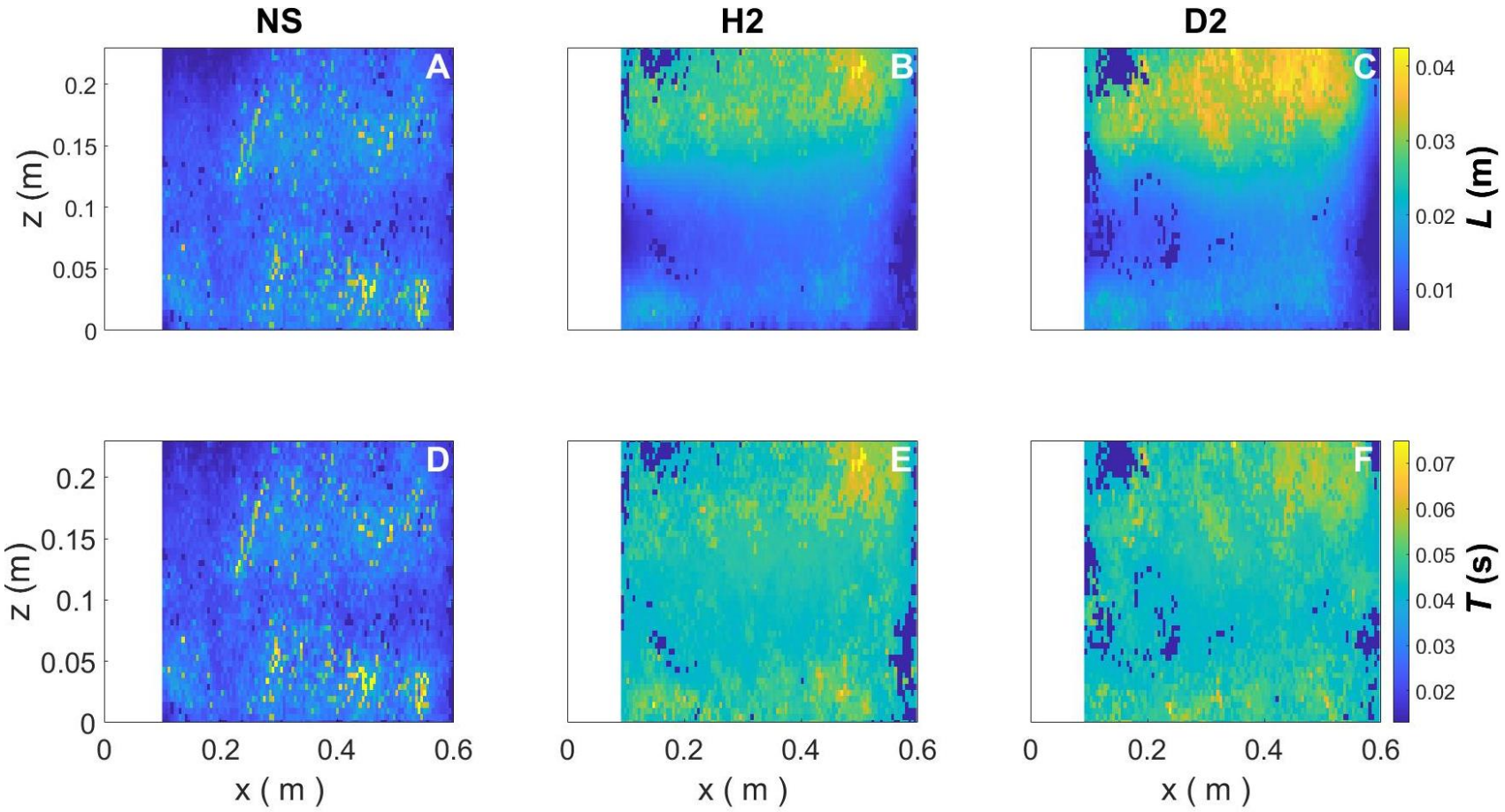

Figure 3.13. Time-averaged turbulent integral length scale (*L*; m) and turbulent integral time scale (*T*; s) on the vertical XZ plane for no structure (NS), 5.08-cm diameter vertical structure (H2), and 5.08-cm diameter diagonal structure (D2), respectively, at the mid-range body-length velocity tested, 1.5 BL/S.

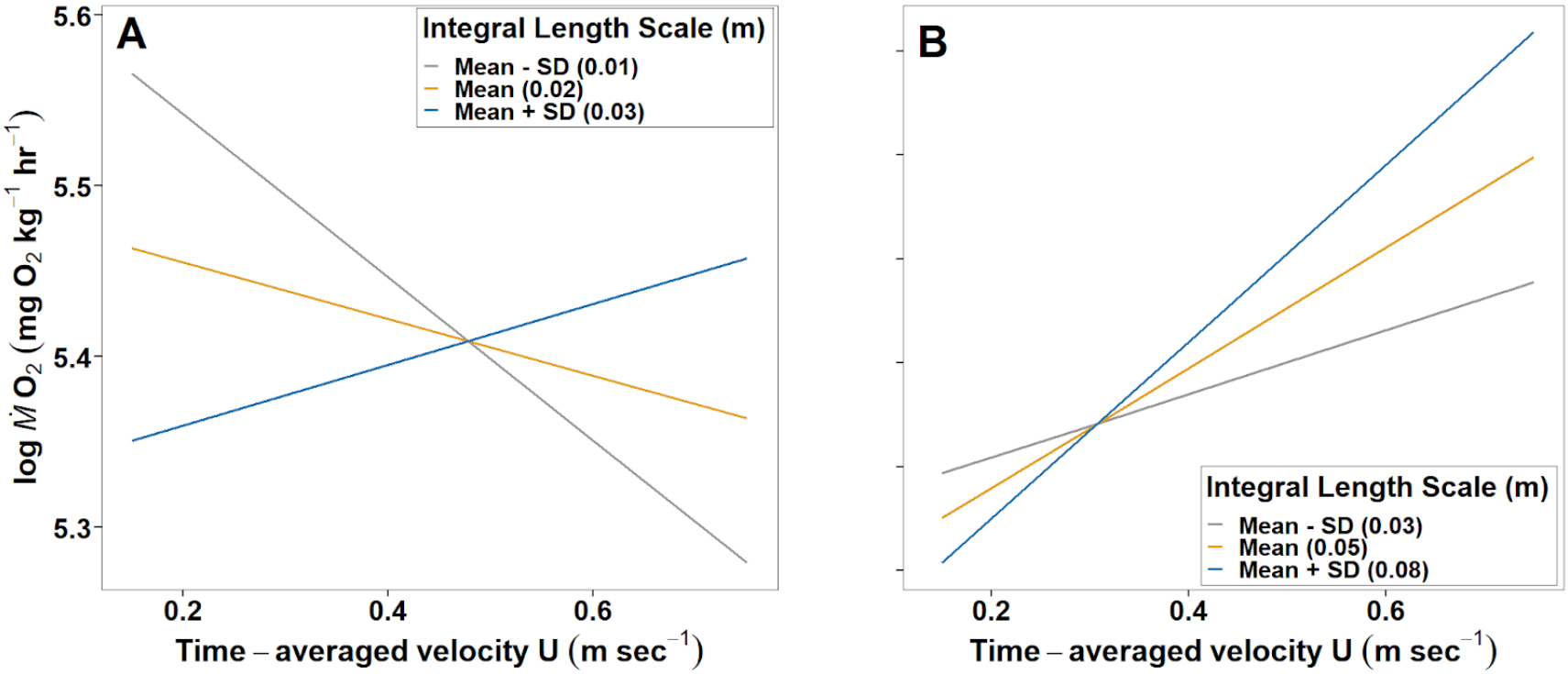

Figure 3.14. Plot showing how the influence of time-averaged longitudinal water velocity (U) on fish oxygen consumption ($\dot{M}O_2$) changes with different integral length scales (L) for rainbow trout (panel A) and smallmouth bass (panel B). The average values of L selected for each fish during each sub-trial were pooled, and the levels of L shown calculated from the overall pool of values for each species.

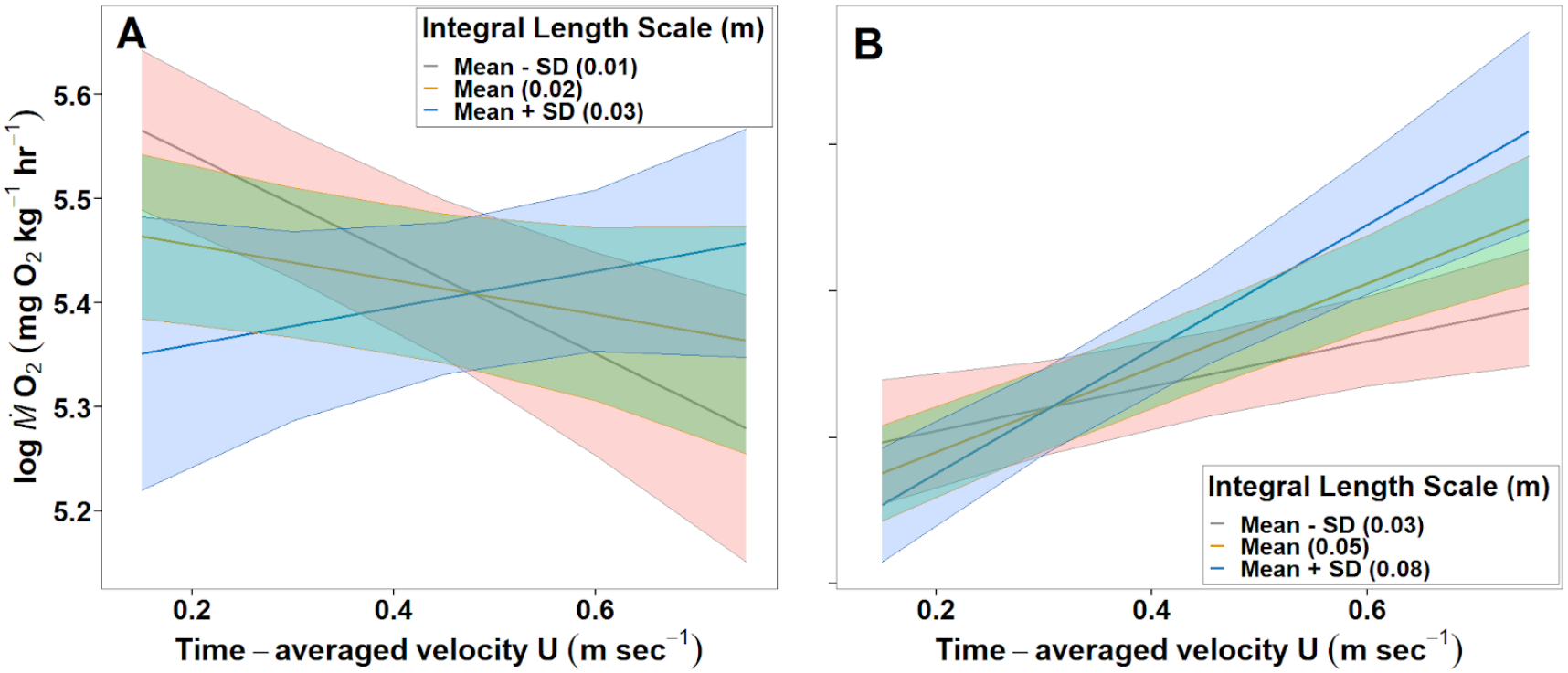

Figure 3.15. Plot showing how time-averaged longitudinal water velocity (U) and different integral length scales (*L*) influence fish oxygen consumption ($\dot{M}O2$) for rainbow trout (panel A) and smallmouth bass (panel B). Confidence intervals are shown for each level of *L*, demonstrating the overlap between $\dot{M}O2$ at mean *L* with $\dot{M}O2$ at mean + SD and mean – SD *L*. Fish $\dot{M}O2$ at the highest and lowest levels of *L* are significantly different from each other, while the mean is not different from either.

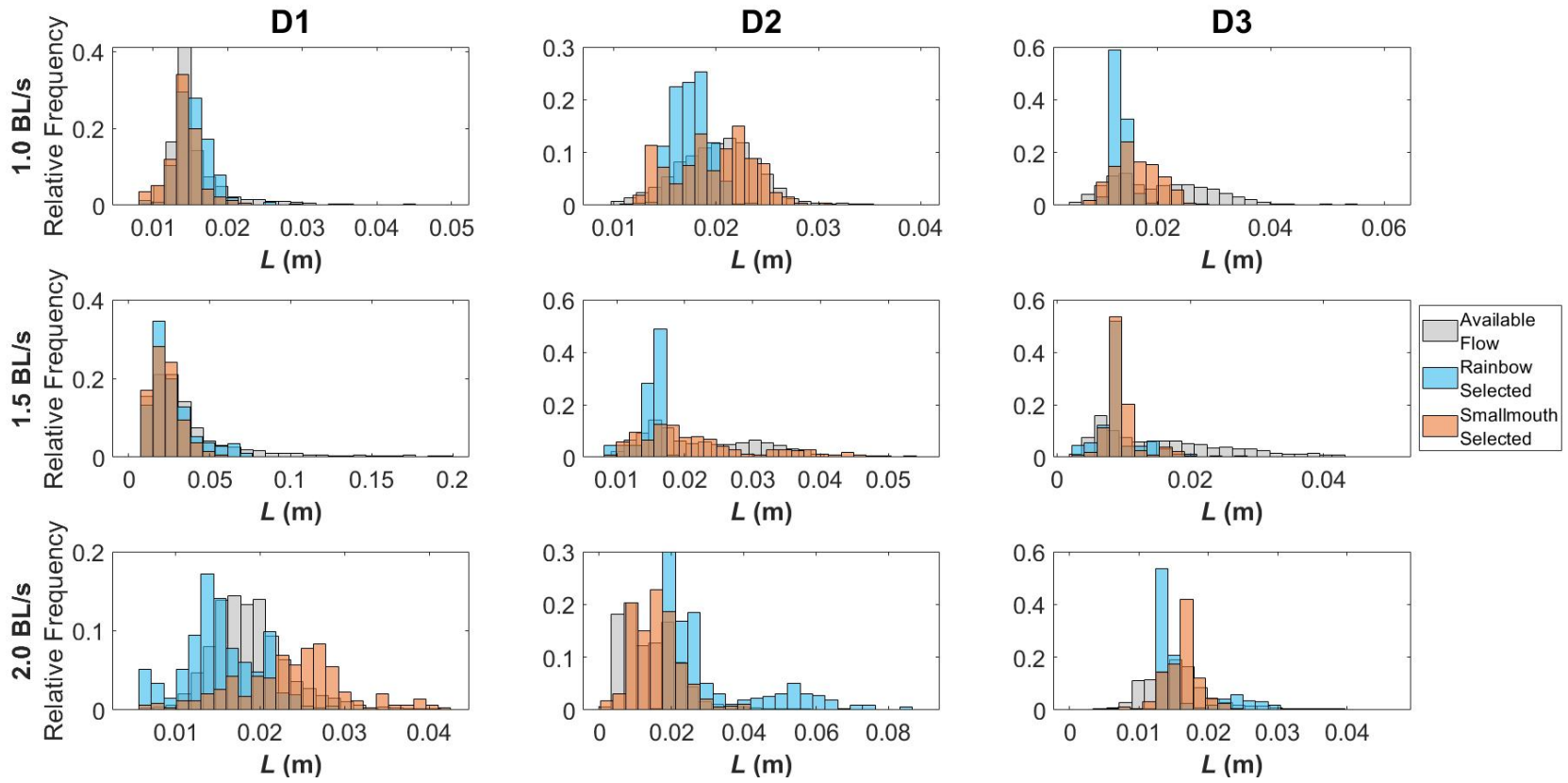

Figure 3.16. Relative frequency distribution of all levels of turbulent integral length scale (*T*; m) generated downstream of structures and thus available to fish, shown with the distribution of flow conditions selected by rainbow trout and by smallmouth bass. Distributions are shown for diagonal structures of all diameters (D1 – 2.54 cm; D2 – 5.08-cm; D3 – 7.62-cm) at all body-length velocities tested (1.0 BL/s, 1.5 BL/s, 2.0 BL/s). Data shown are derived from the XZ plane.

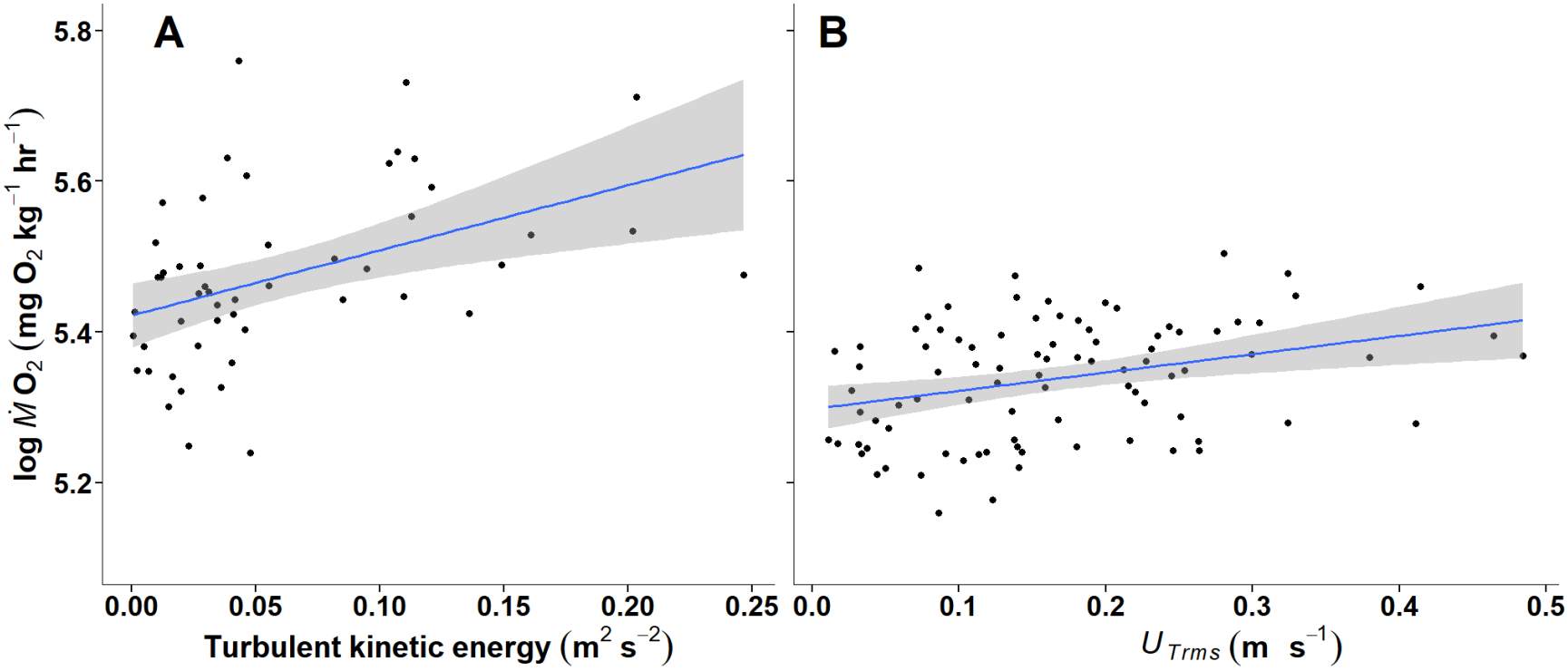

Figure 3.17. Relationship between oxygen consumption (ṀO2) and the measure of turbulence intensity included in the top bioenergetics model for rainbow trout (Table 10) and smallmouth bass (Table 11). Turbulent kinetic energy was the most impactful measure of turbulence intensity for rainbow trout (panel A), while U_{Trms} was the most impactful measure of turbulence intensity for smallmouth bass (panel B). For both species, fish ṀO2 increased as fish experienced higher levels of turbulence intensity.

Tables

Table 3.1. Average size of rainbow trout and smallmouth bass used for respirometry experiments (± standard error, SE), along with the metrics of water quality data across a 30-day acclimation period at one of two different temperature treatments.

Species	Treatment Temperature (°C)	Average Temperature (°C)	Fork Length (cm)	Mass (g)	Dissolved Oxygen Concentration (mg O_2/L)	Ammonia (ppm)
Rainbow Trout	12 °C	11.7 (± 1.24)	32.0 (± 2.2)	366 (± 66)	10.10	< 0.25
	18 °C	17.6 (± 1.46)	29.8 (± 2.2)	325 (± 99)	8.83	< 0.3
Smallmouth Bass	15 °C	16.6 (± 1.45)	26.5 (± 2.0)	243 (± 63)	9.11	< 0.25
	25 °C	24.5 (± 1.41)	25.2 (± 1.1)	193 (± 24)	7.68	< 0.25

Table 3.2. Model selection process to identify the top model relating oxygen consumption ($\dot{M}O_2$) to acceleration for rainbow trout participating in respirometry experiments. Accelerometer-tagged rainbow trout were acclimated to one of two different temperatures ("temp"; 12 or 18° C), and then placed in a swimming respirometer. Water velocity varied from 1.0, 1.5, 2.0, 2.5, and 3.0 body lengths per second, and one $\dot{M}O_2$ measurement was collected for each fish at each swimming velocity. In all models, $\dot{M}O_2$ has been log-transformed. The selected model is presented in the top row in bold; all models below the top model are ranked by AIC score from lowest to highest.

Model formula	AIC score	ΔAIC	Log likelihood	Marginal r^2	Conditional r^2
~ Acceleration + Temp + log (Mass) + (1|ID)	**-48.3**	**3.5**	**29.80**	**0.770**	**0.862**
~ Acceleration + (1|ID)	-51.8	0	29.24	0.625	0.856
~ Acceleration + Temp + (1|ID)	-51.3	0.5	29.57	0.760	0.860
~ Acceleration + log (Mass) + (1|ID)	-50.1	1.7	30.08	0.659	0.858
~ 1 + (1|ID)	26.9	78.7	-10.26	0	0.418

Table 3.3. Model selection process to identify the top model relating oxygen consumption ($\dot{M}O_2$) to acceleration for smallmouth participating in respirometry experiments. Accelerometer-tagged smallmouth bass were acclimated to one of 2 different temperatures ("temp"; 15 or 25 °C), and then placed in a swimming respirometer. Water velocity varied from 1.0, 1.5, 2.0, 2.5, and 3.0 body lengths per second, and one $\dot{M}O_2$ measurement was collected for each fish at each swimming velocity. In all models, $\dot{M}O_2$ has been log-transformed. The selected model is presented in the top row in bold; all models below the top model are ranked by AIC score from lowest to highest.

Model formula	AIC score	ΔAIC	Log likelihood	Marginal r^2	Conditional r^2
~ Acceleration + Temp + log (Mass) + (1|ID)	**0.3**	**2.5**	**6.61**	**0.741**	**0.857**
~ Acceleration + (1|ID)	-2.2	0	5.45	0.528	0.830
~ Acceleration + Temp + (1|ID)	-1.2	1	6.11	0.726	0.855
~ Acceleration + log (Mass) + (1|ID)	0.5	2.7	5.26	0.520	0.836
~ 1 + (1|ID)	71.3	73.5	-32.47	0	0.434

Table 3.4. Summary of model relating acceleration, water temperature, and fish mass to oxygen consumption ($\dot{M}O_2$) for rainbow trout participating in respirometry experiments. Rainbow trout were acclimated to one of two water temperatures (12 or 18 °C), and tested in a swimming respirometer across five swimming velocities (1.0, 1.5, 2.0, 2.5, and 3.0 BL/s).

	Estimate	Standard error	df	t value	Pr(>|t|)
(Intercept)	5.55	0.81	11.75	6.81	<0.01
Acceleration	0.80	0.06	55.47	13.44	<0.01
Temperature	0.03	0.00	11.16	3.30	<0.01
log (Mass)	-0.17	0.14	12.00	-1.27	0.23

Table 3.5. Summary of the model relating acceleration, water temperature, and fish mass to oxygen consumption ($\dot{M}O_2$) for smallmouth bass participating in respirometry experiments. Smallmouth bass were acclimated to one of two water temperatures (15 or 25° C), and tested in a swimming respirometer across five swimming velocities (1.0, 1.5, 2.0, 2.5, and 3.0 BL/s).

	Estimate	Standard Error	df	t value	Pr(>|t|)
(Intercept)	2.39	1.48	12.58	1.613	0.13
Acceleration	0.69	0.06	50.63	12.44	<0.01
Temperature	0.04	0.01	12.34	3.71	<0.01
log (Mass)	0.35	0.25	12.41	1.40	0.19

Table 3.6. Average water quality parameters for fish holding setup during large-scale flume experiments, shown for each aquarium for rainbow trout (RBT) and for smallmouth bass (SMB). Two fish were held in each aquarium, and all aquaria were maintained at ambient temperature.

Species	Aquarium	Average Temperature (°C)	Dissolved Oxygen Concentration (mg O_2/L)	Ammonia (ppm)
RBT	T1	17.2 (± 0.05)	9.36	< 0.25
	T2	17.4 (± 0.08)	9.15	< 0.25
	T3	17.2 (± 0.04)	9.46	< 0.25
SMB	T1	21.1 (± 0.35)	7.23	< 0.25
	T2	21.1 (± 0.11)	7.32	< 0.25
	T3	21.9 (± 0.04)	7.12	< 0.25

Table 3.7. Average size of rainbow trout (RBT) and smallmouth bass (SMB) used for large-scale flume experiments. Fish were divided into one of two groups, which participated in swimming trials on alternating days. Rainbow trout were measured to fork length, while smallmouth bass were measured to total length.

Species	Group	Length (cm)	Mass (g)
RBT	A	28.5 (± 1.04)	236.3 (± 15.01)
	B	27.3 (± 0.88)	207.3 (± 16.83)
SMB	A	27.1 (± 1.36)	270.0 (± 39.31)
	B	26.6 (± 0.38)	258.0 (± 4.51)

Table 3.8. Model selection process to identify the top bioenergetics model relating oxygen consumption ($\dot{M}O_2$) to the log of fish body mass, water temperature ("temp"), and flow metrics for rainbow trout participating in flume experiments. Fish were tested with structures in one of three orientations (vertical, horizontal, diagonal) and one of three diameters (2.54-cm, 5.08-cm, 7.62-cm), across three body-length (BL) velocities (1.0, 1.5, and 2.0 BL/sec). Models are ranked by AIC score from lowest to highest.

Model formula	AIC score	ΔAIC	Log likelihood	Marginal r^2	Conditional r^2
~ log (Mass) + Temp + U × *L* + TKE + (1|ID)	**-104.1**	**0**	**63.23**	**0.538**	**0.726**
~ log (Mass) + Temp + U × *L* + TI_U + (1|ID)	-102.6	1.5	62.52	0.537	0.740
~ log (Mass) + Temp + U × *L* + U_{rms} + (1|ID)	-102.2	1.9	62.30	0.526	0.719
~ log (Mass) + Temp + U × *L* + U_{Trms} + (1|ID)	-100.3	3.8	61.36	0.498	0.701
~ log (Mass) + Temp + U × TKE + *T* + (1|ID)	-97.3	6.8	59.87	0.506	0.717
~ log (Mass) + Temp + U * *T* + TI_U + (1|ID)	-97.3	6.8	59.83	0.526	0.729
~ log (Mass) + Temp + U * *T* + TKE + (1|ID)	-95.8	8.3	59.12	0.507	0.692
~ log (Mass) + Temp + U + TI_U + *T* + (1|ID)	-95.6	8.5	57.50	0.511	0.728
~ log (Mass) + Temp + U * *T* + U_{rms} + (1|ID)	-94.6	9.5	58.50	0.499	0.689
~ log (Mass) + Temp + U * U_{rms} + *T* + (1|ID)	-94.3	9.8	58.36	0.488	0.709
~ log (Mass) + Temp + U * TKE + *T* + (1|ID)	-94.2	9.9	58.29	0.502	0.706
~ log (Mass) + Temp + U * TI_U + *L* + (1|ID)	-94.0	10.1	58.20	0.507	0.738

Table 3.8 (cont.)

~ log (Mass) + Temp + U * *T* + $U_{T rms}$ + (1|ID)	-93.8	10.3	58.10	0.484	0.679
~ log (Mass) + Temp + U^2 * *T* + TKE + (1|ID)	-94.3	9.8	58.33	0.490	0.674
~ log (Mass) + Temp + U^2 + *T* + (1|ID)	-94.0	10.1	56.74	0.426	0.639
~ log (Mass) + Temp + U + TI_U + *T* + (1|ID)	-93.2	10.9	56.29	0.511	0.723
~ log (Mass) + Temp + U * TI_U + *T* + (1|ID)	-91.7	12.4	57.03	0.506	0.734
~ log (Mass) + Temp + U * U_{rms} + *T* + (1|ID)	-91.4	12.7	56.88	0.486	0.699
~ log (Mass) + Temp + U * $U_{T rms}$ + *L* + (1|ID)	-90.2	13.9	56.29	0.436	0.666
~ log (Mass) + Temp + U + U_{rms} + *L* + (1|ID)	-89.9	14.2	54.64	0.462	0.666
~ log (Mass) + Temp + *L* + TKE + (1|ID)	-89.7	14.4	53.15	0.430	0.623
~ log (Mass) + Temp + TKE + (1|ID)	-89.7	14.4	51.82	0.411	0.625
~ log (Mass) + Temp + U + TKE + *L* + (1|ID)	-89.2	14.9	54.29	0.454	0.653
~ log (Mass) + Temp + U + TKE + (1|ID)	-88.6	15.5	52.60	0.461	0.651
~ log (Mass) + Temp + U * $U_{T rms}$ + *T* + (1|ID)	-87.7	16.4	55.06	0.441	0.659
~ log (Mass) + Temp + U + U_{rms} + *T* + (1|ID)	-87.6	16.5	53.51	0.468	0.661
~ log (Mass) + Temp + U^2 + TKE + (1|ID)	-87.5	16.6	52.06	0.447	0.639
~ log (Mass) + Temp + U + k + *T* + (1|ID)	-86.8	17.3	53.11	0.460	0.646
~ log (Mass) + Temp + U + $U_{T rms}$ + *L* + (1|ID)	-85.8	18.3	52.61	0.409	0.627
~ log (Mass) + Temp + U + $U_{T rms}$ + *T* + (1|ID)	-83.6	20.5	51.50	0.421	0.620

Table 3.8 (cont.)

~ 1 + (1|ID)	-82.4	21.7	44.46	0.000	0.443
~ log (Mass) + Temp + U^2 + U + (1|ID)	-82.2	21.9	49.39	0.251	0.561
~ log (Mass) + Temp + *L* + (1|ID)	-82.0	22.1	47.96	0.265	0.506
~ log (Mass) + Temp + U^2 + *T* + (1|ID)	-78.8	25.3	47.71	0.295	0.527
~ log (Mass) + Temp + U + *L* + (1|ID)	-78.6	22.5	47.61	0.238	0.511
~ log (Mass) + Temp + U + (1|ID)	-78.3	25.8	46.09	0.216	0.515
~ log (Mass) + Temp + U^2 + *L* + (1|ID)	-78.3	25.8	47.45	0.237	0.503
~ log (Mass) + Temp + U^2 + (1|ID)	-77.5	26.6	45.71	0.202	0.503

Table 3.9. Model selection process to identify the top bioenergetics model relating oxygen consumption ($\dot{M}O_2$) to the log of fish body mass, water temperature ("temp"), and flow metrics for smallmouth bass participating in flume experiments. Fish were tested with structures in one of three orientations (vertical, horizontal, diagonal) and one of three diameters (2.54-cm, 5.08-cm, 7.62-cm), across three body-length (BL) velocities (1.0, 1.5, and 2.0 BL /s^{-1}). Models are ranked by AIC score from lowest to highest.

Model formula	AIC score	ΔAIC	Log likelihood	Marginal r^2	Conditional r^2
~ log (Mass) + Temp + U * *L* + U_{Trms} + (1|ID)	**-227.7**	**0**	**123.97**	**0.518**	**0.580**
~ log (Mass) + Temp + U^2 * *T* + U_{Trms} + (1|ID)	-226.7	1	123.97	0.534	0.585
~ log (Mass) + Temp + U * *L* + TI_U + (1|ID)	-225.7	2.0	122.98	0.522	0.577
~ log (Mass) + Temp + U * *L* + U_{rms} + (1|ID)	-225.4	2.3	122.83	0.508	0.568
~ log (Mass) + Temp + U * *T* + U_{Trms} + (1|ID)	-221.8	5.9	121.05	0.512	0.563
~ log (Mass) + Temp + U * *L* + TKE + (1|ID)	-221.4	6.3	120.83	0.485	0.536
~ log (Mass) + Temp + U * *T* + TI_U + (1|ID)	-219.2	8.5	119.71	0.511	0.555
~ log (Mass) + Temp + U * *T* + U_{rms} + (1|ID)	-218.8	8.9	119.55	0.498	0.546
~ log (Mass) + Temp + U * U_{Trms} + *L* + (1|ID)	-217.2	10.5	118.73	0.490	0.531
~ log (Mass) + Temp + U * U_{Trms} + (1|ID)	-216.9	10.8	117.36	0.467	0.512
~ log (Mass) + Temp + U * *T* + TKE + (1|ID)	-214.8	12.9	117.51	0.472	0.512
~ log (Mass) + Temp + U * U_{Trms} + *T* + (1|ID)	-213.1	14.6	116.70	0.477	0.517

Table 3.9 (cont.)

~ log (Mass) + Temp + U + U_{Trms} + (1|ID)	-213.0	14.7	123.46	0.429	0.475
~ log (Mass) + Temp + U * U_{rms} + *L* + (1|ID)	-212.7	15.0	116.50	0.465	0.507
~ log (Mass) + Temp + U^2 + U_{Trms} + (1|ID)	-212.4	15.3	114.16	0.424	0.469
~ log (Mass) + Temp + U + U_{rms} + *L* + (1|ID)	-212.3	15.4	115.02	0.448	0.489
~ log (Mass) + Temp + U + U_{Trms} + *L* + (1|ID)	-212.0	15.7	114.87	0.447	0.485
~ log (Mass) + Temp + L * U + (1|ID)	-211.8	15.9	114.80	0.387	0.433
~ log (Mass) + Temp + U + TI_U + *L* + (1|ID)	-211.0	16.7	114.41	0.453	0.489
~ log (Mass) + Temp + U^2 * *T* + (1|ID)	-210.7	17.0	114.25	0.400	0.446
~ log (Mass) + Temp + *L* * U_{Trms} + (1|ID)	-209.4	18.3	113.61	0.356	0.398
~ log (Mass) + Temp + U * TI_U + *L* + (1|ID)	-209.2	18.5	114.75	0.467	0.499
~ log (Mass) + Temp + U * TKE + *L* + (1|ID)	-208.9	18.8	114.57	0.434	0.464
~ log (Mass) + Temp + U * U_{rms} + *T* + (1|ID)	-208.8	18.9	114.53	0.453	0.493
~ log (Mass) + Temp + U + U_{rms} + *T* + (1|ID)	-208.7	19.0	113.24	0.438	0.479
~ log (Mass) + Temp + U + U_{Trms} + *T* + (1|ID)	-208.5	19.2	113.12	0.434	0.476
~ log (Mass) + Temp + U + TKE + *L* + (1|ID)	-208.1	19.6	112.95	0.419	0.451
~ log (Mass) + Temp + U + TI_U + *T* + (1|ID)	-207.3	20.4	112.56	0.442	0.478
~ log (Mass) + Temp + U * TKE + *T* + (1|ID)	-205.4	22.3	112.83	0.423	0.454

Table 3.9 (cont.)

~ log (Mass) + Temp + U * TI_U + *T* + (1|ID)	-205.2	22.5	112.73	0.453	0.486
~ log (Mass) + Temp + U + TKE + *T* + (1|ID)	-205.0	22.7	111.38	0.410	0.444
~ log (Mass) + Temp + U^2 + (1|ID)	-204.3	23.4	108.66	0.326	0.365
~ log (Mass) + Temp + U + (1|ID)	-204.2	23.5	108.60	0.327	0.366
~ log (Mass) + Temp + U^2 + U + (1|ID)	-201.7	26.0	108.53	0.327	0.365
~ log (Mass) + Temp + U^2 + *L* + (1|ID)	-201.6	26.1	108.49	0.328	0.363
~ log (Mass) + Temp + Temp + U + *L* + (1|ID)	-201.4	26.3	108.41	0.328	0.365
~ log (Mass) + Temp + U_{Trms} + (1|ID)	-200.9	26.8	106.96	0.296	0.340
~ log (Mass) + Temp + U^2 + *T* + (1|ID)	-199.8	27.9	107.57	0.325	0.370
~ log (Mass) + Temp + *L* + U_{Trms} + (1|ID)	-199.7	28.0	107.52	0.310	0.349
~ 1 + (1|ID)	-196.9	30.8	101.60	-0.001	0.207
~ log (Mass) + Temp + *L* + (1|ID)	-192.3	35.4	102.64	0.198	0.230

Table 3.10. Summary of the top bioenergetics model relating fish mass, temperature, mean velocity U, TKE, and *T* with oxygen consumption ($\dot{M}O_2$) for rainbow trout participating in flume experiments. The model shown was determined to best fit rainbow trout oxygen consumption data through a model selection process (Table 3.8).

	Estimate	Standard error	df	t value	Pr(>|t|)	Proportion of fixed-effect variance
(Intercept)	7.89	1.57	12.79	5.04	< 0.01	
log (Mass)	-0.49	0.22	4.69	-2.23	0.08	0.512
Temperature	0.03	0.05	43.80	0.58	0.57	0.012
U	-0.79	0.18	40.89	-4.37	<0.01	0.387
L	-14.90	4.66	41.42	-3.20	<0.01	0.237
TKE	0.47	0.20	42.33	2.35	0.02	0.144
U×L	31.18	8.59	41.10	3.63	<0.01	0.290

Table 3.11. Summary of the bioenergetics model relating fish mass, temperature, mean velocity U, U_{Trms}, and *T* with oxygen consumption ($\dot{M}O_{2)}$ for smallmouth bass participating in flume experiments. The model shown was determined to best fit smallmouth bass oxygen consumption data through a model selection process (Table 3.9)

	Estimate	Standard error	df	t value	Pr(>|t|)	Proportion of fixed-effect variance
(Intercept)	3.05	0.53	10.76	5.72	< 0.01	
log (Mass)	0.30	0.07	4.05	4.11	0.01	0.635
Temperature	0.03	0.02	82.83	1.79	0.08	0.068
U	-0.01	0.86	80.18	-0.18	0.86	0
L	-1.78	0.02	80.39	-2.29	0.02	0.105
U_{Trms}	0.28	0.28	81.57	3.96	< 0.01	0.291
U × *L*	5.78	5.78	80.13	3.16	< 0.01	0.192

CHAPTER FOUR: CONTEXT-DEPENDENT DRIVERS OF FISH HABITAT SELECTION FOR AND WITHIN TURBULENT FLOWS

Abstract

Restoration has emerged as a means to reverse habitat degradation and loss and reverse declines in fish populations and biodiversity. In rivers, this commonly involves the installation of physical structures, however these often have no appreciable impacts on fish. This may be due to a lack of understanding regarding how riverine fish select habitat. Energetics are among the primary forces driving how fish choose what habitat to occupy, but one habitat feature with major impacts on energetics is rarely considered relevant for fish habitat selection: turbulence. Physical structure, such as restoration structures, in flow generate turbulence. The lack of knowledge regarding the potential role of turbulence as a driver of fish selection of habitat near restoration structures potentially hinders our ability to implement successful restoration projects. To address this, I aimed to quantify how fish habitat selection for and within turbulent flows generated by physical structures is mediated by flow characteristics. To accomplish this, two species of fish, rainbow trout (*Oncorhynchus mykiss*) and smallmouth bass (*Micropterus dolomieu*), were first implanted with accelerometers, allowing for the estimation of oxygen consumption ($\dot{M}O_2$, mg O_2/kg/hr) and then placed in a large racetrack flume with structures of varying orientation and diameter to generate a range of flow conditions. Flow characteristics downstream of structures were quantified using particle image velocimetry (PIV). Two different aspects of fish habitat selection were quantified: (1) occupancy upstream or downstream of structures and (2) location selection within the zone downstream of structures. Because turbulence can increase the energetic cost of swimming, and because balancing energetic gains and costs are a driving force for fish habitat selection, it was hypothesized that fish would

consistently select habitat in which the level of turbulence was low. Contrary to this hypothesis, I discovered that fish sometimes selected for habitat in which the level of turbulence was low, but that at other times fish selected against habitat in which the level of turbulence was low. Furthermore, the habitat selection of each species was largely driven by a different set of turbulence-related factors. Taken all together, this study provides new insight into how fish may select restored river habitat and provides guidance for future restoration efforts looking to maximize their benefits for fish.

Introduction

Human alterations have proven a major threat to freshwater ecosystems. Due to habitat degradation and loss originating with anthropogenic causes, freshwater fishes have become the second most threatened vertebrate group on the planet following amphibians (Bruton 1995). As the result of actions such as damming, channelization and water withdrawal, rivers are among the most heavily modified and degraded ecosystem types on the planet, which has manifested in severe reductions of fish biodiversity (Vörösmarty et al. 2010; Darwall and Freyhof 2016; Dudgeon 2019). Therefore, though freshwater fishes overall are in decline, riverine fishes are particularly threatened by habitat degradation and loss.

In recent decades, restoration has emerged as a means to reverse habitat loss and degradation within river systems, and reverse declines in fish populations and biodiversity that have occurred due to degradation (Roni et al. 2008; Beechie et al. 2013; Miller and Hobbs 2016). One approach to river restoration involves the installation of physical structures, often with the intention to simulate or replace natural structure in rivers such as large woody debris (Thompson 2006; Nagayama and Nakamura 2010). Structures may be placed to help stabilize banks, reduce erosion, or bolster flood control, but one of the most common purposes for such structures is,

ostensibly, to provide habitat for fish (Thompson 2006; Nagayama and Nakamura 2010; Gilvear et al. 2013). Physical structure is an attractant for fish, offering protection from predators, providing potential new feeding opportunities, and sheltering fish from high velocity flow (McMahon and Hartman 1989; Fausch 1993; Shuler et al. 1994; Boavida 2011). However, although structure continues to be used widely in river restoration, it often has no appreciable impacts on fish, with many projects never seeing a difference between in pre-restoration and post-restoration fish populations and biodiversity (Lepori et al. 2005; Stewart et al. 2009; Palmer et al. 2010; Kail et al. 2015). This may be due, in part, to a lack of understanding of the full suite of factors regarding how riverine fish select habitat.

The term "habitat selection" refers to differential occupancy of available habitat by an organism. If an organism makes use of a particular habitat in a greater proportion than that habitat is available to them in the environment, or if an organism avoids a particular type of habitat, they are considered to be selecting for or selecting against that habitat (Rosenfeld 2003). Habitat selection is driven by a range of biotic (i.e., food availability, predation risk, competition) and abiotic (i.e., temperature, flow regime, substrate) factors (Lobb and Orth 1991; Orth and White 1993; Craig and Crowder 2002). One of the prevailing views regarding fish habitat selection is that energetics are among the primary forces driving how fish choose what habitat to occupy (Mittelbach 2002; Rosenfeld 2003). In order for fish to survive, they must successfully balance their energetic gains (i.e., energy acquired through feeding) with their energetic costs (i.e., energy expended during routine behaviors such as feeding and swimming) (Kitchell et al. 1977). Most research on this topic to date has focused on the energetic gains side of this equation, with considerably less word devoted to quantifying the energetic costs associated with habitat selection (Rosenfeld 2003; Urabe et al. 2010; Naman et al. 2019)).

Improving our understanding of the costs of habitat selection would help better explain habitat selection in fish. However, certain drivers of fish habitat selection and certain aspects of fish habitat have received a disproportionate amount of attention.

Turbulence is among the most highly understudied aspects of fish habitat selection in rivers, despite the fact that rivers are inherently turbulent. Variable definitions of turbulence exist, but turbulence can be broadly characterized by chaotic and irregular fluctuations in velocity imposed onto the mean velocity, which manifests in swirling eddies (Warhaft 2002). In essence, turbulence encompasses all fluctuating aspects of flow that exist outside of mean flow velocity. Investigations regarding fish habitat selection in rivers have frequently examined flow characteristics such as mean velocity, water depth, and flow variability, but not turbulence (Mouton et al. 2007; Smith et al. 2014). This represents a glaring knowledge gap because turbulence has been shown to have major impacts on fish energetics and the energetic cost of habitat selection (Enders et al. 2005; Strailey et al. 2021), swimming performance (Lupandin 2005), and behavior (Pavlov et al. 2000; Smith et al. 2005). Given the links between fish energetics and turbulence, and between fish energetics and habitat selection, it is likely that energetics, habitat selection, and turbulence are all interrelated. Therefore, the interactions between fish and turbulence flow should be of heightened interest for river restoration; this is particularly true for the usage of instream restoration structures, as the placement of structure in flow leads to the generation of variable flow conditions and additional levels of turbulence relative to unaltered habitats (Daniels and Rhoads 2013; Bennett et al. 2015). Unfortunately, the effects of turbulence on fish habitat selection have largely been ignored, and the potential role of turbulence as a driver of fish selection of habitat near restoration structures is essentially unknown, potentially hindering our ability to implement successful restoration projects.

To address this knowledge gap, this study aimed to quantify how fish habitat selection for and within turbulent flows generated by physical structures is mediated by flow characteristics. To accomplish this, two species of fish, rainbow trout (*Oncorhynchus mykiss*) and smallmouth bass (*Micropterus dolomieu*), were first implanted with accelerometers, allowing for the estimation of oxygen consumption ($\dot{M}O_2$, mg O_2/kg/hr) and then placed in a large racetrack flume with structures of varying orientation and diameter to generate a range of flow conditions. Flow characteristics downstream of structures were quantified using particle image velocimetry (PIV). Two different aspects of fish habitat selection were quantified: (1) occupancy upstream or downstream of structures and (2) location selection within the zone downstream of structures. Because turbulence can increase the energetic cost of swimming, and because balancing energetic gains and costs are a driving force for fish habitat selection, it was hypothesized that fish would consistently select habitat in which the level of turbulence was low. Results provide unique insights into how fish choose turbulent habitat, and, more specifically, to what degree energetics and hydraulics influence those decisions.

Methods

Fish care

Experiments were conducted at the Ecohydraulics and Ecomorphodynamics Laboratory (EEL) in Rantoul, IL. Two species were utilized in habitat selection trials- rainbow trout and smallmouth bass. Both are riverine species that are popular sportfish often targeted through restoration (Moerke and Lamberti 2003; Hrodey and Sutton 2008). Rainbow trout were supplied by Keystone Fish Hatchery (Richmond, IL) and smallmouth bass were supplied by Jake Wolf Memorial Fish Hatchery (Topeka, IL). For the duration of habitat selection trials, fish were held within 208 L aquaria, with two individuals placed in each aquarium and separated by a clear

screen. Each aquarium was outfitted with an aerator, and filter, water quality was measured daily, and water changes were performed as needed to maintain quality. All aquaria were maintained at ambient temperature. This was done because temperature control was not available for the flume in which habitat selection trials took place; holding fish at ambient temperature ensured that fish would experience similar temperatures between holding aquaria and the experimental flume. Further description of fish care and water quality parameters are available in Chapter Three; average water quality parameters are summarized in Table 3.9 for both species.

Estimating oxygen consumption

All fish participating in habitat selections were surgically implanted with accelerometers. This allowed for the estimation of fish oxygen consumption (i.e., energy use; $\dot{M}O2$, mg O_2/kg fish/hr) via pre-existing models relating acceleration and $\dot{M}O2$. These models were derived from small-scale lab experiments, in which rainbow trout and smallmouth bass were acclimated to one of two temperatures (12°C and 18°C for rainbow trout; 15 °C and 25 °C for smallmouth bass), surgically implanted with accelerometers, and then swam in an intermittent-flow respirometer to simultaneously quantify acceleration and $\dot{M}O2$. The purpose estimating $\dot{M}O2$ in flume experiments was to develop a bioenergetics model for each species relating estimated $\dot{M}O2$ with various flow metrics (i.e., energetic cost of swimming in different environments). These estimated $\dot{M}O2$ data are incorporated as a predictor in certain analyses for the current study, and comparisons are made between the findings of these bioenergetics models and the findings of the current study. The goal of the current study is to examine drivers of fish habitat selection in turbulent flow, therefore these analyses and findings are not discussed further in this current study. The methodology used for producing acceleration-$\dot{M}O2$ models and turbulence-

bioenergetics models, as well as the associated results and discussion can be found described in detail in Chapter Three.

Experimental setup for habitat selection trials

Trials to relate fish habitat selection with swimming energetics and flow conditions utilized a large racetrack flume. Flow in this flume was driven by a large paddle wheel, while a pre-existing calibration allowed flow velocity to be estimated based on paddle wheel frequency. Three test sections were established within the flume, on the opposite side from the paddle wheel, to allow for three fish to be tested at a time. Test sections were 1.0 m long, and each were preceded by a 25.4-cm long flow straightener constructed from 7.62-cm diameter PVC pipe, and ended by a screen barrier. Flow straighteners ensured consistency in flow conditions between test sections, while screen barriers contained fish and prevented visual contact with other fish during trials. Structure treatments were placed approximately 33 cm downstream of the flow straightener, such that one-third of the test section was upstream of the structure, and two-thirds were downstream. A total of nine structure treatments were used to vary flow conditions. Examinations of the wake systems produced downstream from fish habitat structures have shown that the wake produced by such structures are comparable to those produced by simple geometric shapes (Shamloo et al. 2001). Therefore, each structure was a single PVC cylinder of one of three diameters (2.54 cm, 5.08 cm, 7.62 cm) and one of three orientations (vertical, horizontal, diagonal on the YZ plane). A case in which no structure was present was used as a control.

The reference frame utilized for this study is defined as follows. The longitudinal coordinate in the direction of mean flow is represented by X, the horizontal transverse coordinate perpendicular to the mean flow is represented by Y, and the vertical dimension, or depth, is represented by Z. Vertical structures were placed in the center of the flume and were aligned

with the Z-axis. Horizontal structures were centered at mid-depth and aligned with the Y-axis. Diagonal structures were placed at a 45° angle within the YZ plane, with the high end of the structure placed against the flume's inner wall. For the control case, no structures were present within the flume. Hereafter, structure treatments are referred to by the combination of its orientation (vertical – V; horizontal – HS; diagonal – D) and diameter (2.54 cm – 1; 5.08 cm – 2; 7.62 cm – 3), or simply by its orientation (vertical structure– VS; horizontal structure – HS; diagonal structure – DS); the control case is referred to as NS (no structure).

Habitat selection trials

Trials for each species took places across 5 days; trials took place April 2019 for rainbow trout and October 2019 for smallmouth bass. Six individuals from each species were tested during habitat selection trials. A crossover design was utilized, in which all individuals were tested with all possible combinations of flow velocity and structure treatment. This lead to ten total trials per fish, where the order in which fish swam with each structure treatment was randomized. Three fish, each placed individually within a separate test section, swam per day. To minimize the risk of fish becoming over-exercised, fish were randomly sorted into one of two swim groups, each of which swam on alternating days. Velocities utilized were based on the mean size of fish used across all trials (27.4 ± 0.92 cm) and were set to approximate a velocity of a given body length per second (BL/sec). Hereafter, the tested velocities are referred to as BL velocities. A single trial was 45 minutes long, during which time a single structure (or NS) was placed. Each trial was composed of three 15 minute sub-trials, during each of which fish were tested at a different BL velocity, 1.0 BL/sec, 1.5 BL/s, and 2.0 BL/sec, beginning with the lowest BL velocity and ending with the highest BL velocity. When trials began for the day, flow was set at approximately 0.5 BL/sec before a single fish was introduced to each test section. Structures

were placed as needed, and fish left to acclimate for one hour before habitat selection trials began. After the completion of a 45 minute trial, structures were changed and fish left to rest at 0.5 BL/s for an hour until the next trial began. Fish remained in the same test section for all 45 minute trials and participated in a maximum of four 45 minute trials each day. Fish were then returned to their original aquaria to rest for at least 16 hours before inclusion in further trials, and trials continued until all fish swam with all combination of structures. Fish were fed after the third day of trials and rested for two days to ensure food had been completely digested; for rainbow trout, these were Skretting high protein pellets (Tooele, Utah), and for smallmouth bass, these were live minnows.

Fish locations in the flume were recorded via video camera for the duration of each sub-trial. Two planes were targeted for video capture: the horizontal XY plane, and the vertical XZ plane. For VS and HS, video was recorded on a single plane as structures of these orientations would be expected to have strong impacts on a single plane. For VS, this was the XY plane, thus resulting in overhead footage for fish during these sub-trials, and for HS, this was the YZ plane, resulting in side-view footage for fish during these sub-trials. Video was recorded for DS on both the XY and YZ planes because these structures alter flow characteristics on both of these planes. For the NS condition, video was captured from the side.

Flow characterization

Two-dimensional (2D) particle image velocimetry (PIV) was used to capture the velocity field within the racetrack flume. PIV was conducted for two planes: a vertical plane (XZ plane), and a horizontal plane (XY plane), both of which were oriented with the direction of flow. Measurements for the XZ plane were taken at the flume's centerline, while measurements for the XY plane were taken at mid-depth. A 5W-532nm laser (PIV-01251 DPSS, OptoEngine LLC,

Midvale, UT) equipped with a cylindrical lens was used to generate a light-sheet to illuminate particles traveling within either the XZ or XY plane. A monochromatic camera (JAI GO-5000M-USB; JAI Inc., San Jose, CA) recorded 12-bit images with a 2560 × 2058 pixel resolution. PIV was conducted for all flow conditions and BL velocities tested during fish habitat selection trials. For measurements at BL velocities of 1.0 BL/sec and 1.5 BL/sec, images were recorded at a frequency of 50 frames per second (fps) and a frequency of 60 fps for 2.0 BL/sec.

Analysis of velocity statistics

The open-source, Matlab-based software PIVlab (version 2.5; Thielicke and Stamhuis 2014) was used to analyze the flow field images captured through PIV, yielding 2D fields of instantaneous velocities. Utilizing this study's reference frame, the velocity components analyzed through PIVlab are defined as such: *u* in the longitudinal direction (X), *v* in the transverse direction (Y), and *w* in the vertical direction (Z). Instantaneous velocity values are indicated by lower case symbols (*u, v, w*), while time-averaged velocity values are indicated by upper case symbols (*U, V, W*). 2D fields of the instantaneous velocities *u* and *v* were yielded for PIV conducted on the horizontal XY plane and fields of velocities *u* and *w* were yielded for PIV conducted on the vertical XZ plane; the spatial resolution of PIV data was 5.7 mm.

Instantaneous velocity fluctuations, *u', v',* and *w',* were calculated using Reynolds decomposition as:

$$u' = u - U \tag{4.1}$$

$$v' = v - V \tag{4.2}$$

$$w' = w - W \tag{4.3}$$

This then allowed for the calculation of a suite turbulence metrics known to have the potential to affect fish swimming behavior and habitat selection (Lacey et al. 2012): turbulent kinetic energy (TKE), U_{rms}, V_{rms}, W_{rms}, Reynolds stresses, vorticity, turbulent integral time scale, and turbulent integral length scale. TKE was calculated on the XZ and XY planes, respectively, as:

$$TKE_{xz} = \frac{1}{2}\left(2\overline{u'^2} + \overline{w'^2}\right) \tag{4.4}$$

$$TKE_{xy} = \frac{1}{2}\left(2\overline{u'^2} + \overline{v'^2}\right) \tag{4.5}$$

$U_{rms,}$ V_{rms}, and W_{rms} were calculated as the root mean square (RMS) of the instantaneous velocity fluctuations u', v', and w':

$$u_{rms} = \sqrt{\overline{u'^2}} \tag{4.6}$$

$$v_{rms} = \sqrt{\overline{v'^2}} \tag{4.7}$$

$$w_{rms} = \sqrt{\overline{w'^2}} \tag{4.8}$$

TKE measures the mean kinetic energy per unit mass associated with eddies, therefore broadly reflecting the overall level of turbulence intensity, while $U_{rms,}$ V_{rms}, and W_{rms} are directional, representing turbulence intensity in the longitudinal, lateral, and vertical directions of flow respectively. As V_{rms} and W_{rms} both reflect turbulence intensity occurring in the transverse direction to the longitudinal flow, they can be jointly referred to as $U_{Trms.}$ Time-averaged (indicated by overbars) Reynolds stresses were calculated as $\overline{u'v'}$ and $\overline{u'w'}$.

The curl of the velocity vector, $\vec{\omega} = \nabla \times \vec{v}$, where $\vec{v} = (u, v, w)$, was used to calculate two components of vorticity, ω_y and ω_z. Turbulent integral time scale, $T = \int_0^\infty \rho_{uu}(\tau)d\tau$, was

calculated using the autocorrelation function $\rho_{uu}(\tau) = \langle u'(t)u'(t+\tau)\rangle / \langle u'(t)^2\rangle$, in which τ stands for a lag between measurements. Integral time scale, *T*, reflects how long it takes for the larger, predominant eddies in flow to complete one full revolution (Pope 2000). Turbulent integral length scale, *L*, reflects the size of these predominant eddies. *L* was estimated from *T* following Taylor's frozen-turbulence hypothesis (Taylor 1938). *L* was calculated by multiplying *T* at a given location within the test section by a representative velocity, taken as the time-averaged velocity *U* at that location.

The Reynolds number (Re) based on cylinder diameter (*d*) was calculated for each PIV case as Ud/ν, where ν is the kinematic viscosity of water. Calculated values of Re ranged from approximately 7500 to well over 40,000, indicating that the flow was fully turbulent for all cases (Williamson 1996). The Froude number for each case was calculated as Fr = $U / \sqrt{g \times H}$, where H is the water depth in m and g is the gravitational constant. The Froude number was less than 1 for all cases, indicating subcritical flow (Rhoads 2020).

Fish video processing

Matlab (MathWorks R2021A) was used to process fish swimming videos. Habitat selection sub-trials were each 15 minutes long, therefore fish swimming videos were also 15 minutes long. The location of each fish while downstream of structures, and thus within the view of the camera, was manually tracked every 5 seconds throughout each 15-minute video, yielding a time series of X and Y coordinates that reflected the locations occupied by fish throughout a given sub-trial; this yielded a maximum of 180 locations per fish per sub-trial (i.e., 15 minute sub-trial = 900 sec / 5 seconds = 180 locations). These coordinates were used to calculate two metrics that related to fish location preference: (1) the proportion of each sub-trial that fish spent

upstream of structures, which reflected potential avoidance of structure-generated turbulence by fish, and (2) the selection index, which reflected habitat selection when fish were located downstream of structures.

Proportion of time spent upstream

The propensity of fish to either engage with or avoid the turbulence generated by each structure was quantified by calculating the proportion of each 15-minute sub-trial that fish spent in areas upstream or downstream of structures. Structures generating turbulence tend to have the strongest impact on flow characteristics in the areas immediately downstream. Therefore, a fish spending a low proportion of time upstream can potentially indicate a preference for generated by structures, while a fish spending most or all of its time upstream of structures indicates a desire to avoid such conditions. The proportion of time spent upstream (hereafter designated $Prop_{up}$) was calculated as:

$$Prop_{up} = \frac{Upstream\ positions}{Total\ positions} \tag{4.9}$$

The number of upstream positions refers to the number of timepoints for which a fish assumed a position upstream of structures, closer to the flow straightener, for a given sub-trial, while total positions refers to the overall number of positions, across time, for which fish location could be quantified; this proportion therefore was the number of upstream positions, divided by 180 (15 minute sub-trial = 900 sec / 5 seconds = 180 locations). A location was considered to be upstream was observed to have the entirety of their body upstream of a structure at a given point within the coordinate time series. For the control condition with NS, fish were considered to be upstream when occupying the first 33 cm of the test section and were considered to be downstream when occupying the last ~ 66 cm of the test section; this was

because structures, when present, were centered 33 cm downstream of the flow straightener (Figure 4.1).

Generalized linear mixed models were used to define factors that influenced $Prop_{up}$. All candidate models utilized a beta-binomial distribution, as this distribution is recommended for proportion data (Crowder 1978; Bolker et al. 2008). Potential predictors influencing fish preference for areas upstream or downstream of a structure primarily fell into one of two categories. One category of predictors related to turbulence-generating structures, and incorporated structure orientation (i.e., vertical, horizontal, diagonal), structure diameter (i.e., 2.54-cm, 5.08-cm, 7.62-cm), and structure treatment (i.e., V1, V2, V3, H1, H2, H3, D1, D2, D3) in candidate models, as well as different combinations of orientation and diameter. The other category of predictors related to the hydrodynamic conditions generated downstream of structures, and included longitudinal velocity U, TKE, Reynolds stresses, vorticity, L, T, U_{rms} and U_{Trms}. All flow measurements occurred downstream of structures, and thus it was not possible to directly quantify the flow conditions experienced by fish when spending time upstream of a structure. However, it was possible to broadly characterize flow conditions within the test section by taking the spatial and temporal average of turbulence metrics. This was done because it was assumed that fish spending time upstream were seeking to avoid downstream conditions. Candidate models from both approaches additionally assessed species, fish $\dot{M}O2$, and fish length as possible predictors of $Prop_{up}$, and all models included fish ID as a random effect to account for repeated measures of fish across multiple swim trials (Bolker et al. 2009; Zuur et al. 2009).

Model selection was determined via AIC score, whereby the model with the lowest AIC value was considered the be the best fit for $Prop_{up}$ data (Table 4.1). All models, regardless of the fixed effects included, were tested through the same joint model selection process. Once a group

of top models was identified, they were amended to test if including a zero-inflation formula improved model fit. This was done to account for the large number of zeros within the dataset (Zuur et al. 2009); ultimately, all top models determined through this method did include a zero-inflation formula. The top two models were close in AIC score, with ΔAIC of less than two. Of these two models, the model with the lower AIC included an additional parameter that was not present in the model with the second lowest AIC score. Therefore, of these two models, the simpler model with fewer terms was considered to be the top model (Crawley 2013; Aho et al. 2014). Estimated marginal means were used for *post-hoc* testing to define the specific impacts of individual structures on the proportion of time fish spent upstream. Plots relating $Prop_{up}$ to treatment structure appeared to show high variability in fish preference for upstream or downstream locations for certain structures. Therefore, the Fligner-Killeen test for homogeneity of variances was used to assess if fish $Prop_{up}$ was more variable for certain structures than for others (Fligner and Killeen 1976; Beyene and Bekele 2016).

Downstream habitat selection

To quantify fish habitat selection in the downstream portion of the test section, location coordinates derived from swimming videos were used to calculate the selection index (SI) in areas downstream of each structure (Wilkes et al. 2017; Trinci et al. 2021). With SI, the total spatial area that can potentially be occupied by fish downstream of a structure was divided into a grid of cells. Each time a fish occupied a particular cell of the grid for a moment in time, this was considered one occupancy. The SI relates the total count of occupancies by all fish within an individual cell (CO_{cell}) to that of the total count of occupancies for the cell that experienced the highest number of occupancies (CO_{max}), the cell that was most frequently selected by fish. As SI is related to differential occupancy of different locations, it can be used to reflect what locations

fish selected most heavily and can be related to other properties of that cell, such as the flow conditions present within that cell (Wilkes et al. 2017; Trinci et al. 2021). SI was calculated for each cell as:

$$SI = \frac{CO_{cell}}{CO_{max}} \tag{4.10}$$

The size of the cells utilized for analyzing and mapping PIV data were small relative to the size of fish, with sides less than a cm in length. With cells of such a small size, it was not possible for all cells to be occupied, and therefore, a coarser grid with sides of approximately 3 cm, or about 1/8th the length of the average sized fish, was used for determining SI. This was done to reduce overdispersion and to scale cells to a more appropriate size relative to study fish. For fish locations derived from video capturing the XY plane, this resulted in a 29 × 31 cell grid, and fish locations derived from video capturing the XZ plane, this resulted in a 21 × 9 cell grid. Fish locations were mapped to these grids separately for each species, producing a CO_{cell} for each cell within each grid, for each combination of structure orientation, structure diameter, and BL velocity. Therefore, there was a separate CO_{max} and one cell with an SI of 1 for each of these combinations. For DS, fish locations derived from the XY and YZ planes were mapped separately.

To relate SI to the flow conditions in each cell, the same grids used to determine SI were overlaid onto the 2D time-averaged plots for calculated velocity statistics derived from PIV analyses. The time-averaged values for each statistic were then spatially averaged within each cell of the grid and extracted to link with the SI and CO_{cell} calculated for each cell. In all, longitudinal velocity U, TKE, Reynolds stresses, vorticity, U_{rms}, V_{rms}, and W_{rms} were extracted in this manner.

Generalized linear mixed models (GLMM) were used to define the effects of flow predictors on SI count data, and thus were used to determine possible drivers of habitat selection. The SI metric consists of counts, and therefore should follow a Poisson error distribution (Crawley 2013). However, because it was not possible for fish to occupy all possible locations within the downstream portion of the test section, a large number of zeros were present within the SI dataset. Therefore, a negative binomial distribution was utilized and zero inflation was accounted for in all models (Lindén and Mäntyniemi 2011; Wilkes et al. 2017; Stoklosa et al. 2022). The dimensions of the XY and XZ plane were not the same, as the XY plane includes the longitudinal and lateral directions, while the XZ plane includes the longitudinal and vertical directions. The water depth, Z, was not as great as the width of the flume, Y. This meant that fewer locations were available for fish to occupy on the XZ plane. To account for this, plane was included as a random effect within tested models (Zuur 2009).

To identify which predictors to include in analyses, all turbulence metrics were checked for collinearity. This was done by running an initial model with all possible turbulence metrics included, and then assessing the variance inflation factor (VIF) (Zuur et al. 2010) for each variable. Increasing values of VIF indicated higher correlation between variables, with values between 1 and 5 indicating moderate levels of correlation, and values over 5 indicating high levels of correlation between variables. If a variable was found to have a VIF greater than 5, further models were ran and tested with VIF to determine which specific variables were correlated. Based on this, it was determined that TKE, U_{rms}, and U_{Trms}, and L and T should not be incorporated concurrently into models.

Species consistently emerged as a top predictor of SI in preliminary analyses, and thus the overall dataset was split by species. This was done to allow for a closer evaluation of the

combination of flow characteristics that most strongly affected habitat selection of each species separately. As with the overall dataset, TKE, U_{rms}, and U_{Trms}, and *L* and *T*, were not included simultaneously within a tested model. To determine the best-fitting model for SI for each species, models containing all combinations of non-correlated flow variables, from fully parameterized models to single-predictor models, were generated. All models generated were compared via AIC score, where the best model was considered to be that with the lowest AIC score (Table 4.2; Table 4.3). If one or more models had a ΔAIC of less than 2 from the model with the lowest AIC score, indicating that they were equally well-fit to the data, the simplest model with the fewest number of terms was considered the top model (Crawley et al. 2013; Aho et al. 2014). The results of these models are visualized as scatter plots to show how each factor impacted fish SI.

Results

Proportion of time spent upstream

$Prop_{up}$ data reflected the proportion of time fish spent in the upstream portion of the test section, thus reflecting the proportion of time fish spent upstream of turbulence-generating structures when structures were present. The model that best fit $Prop_{up}$ data included treatment structure (i.e., a combination of orientation and diameter, such as V1) and estimated $\dot{M}O2$ as fixed effects (Table 4.4). Structure had a variable effect on $Prop_{up}$, while $\dot{M}O2$ was negatively related with $Prop_{up}$, where fish that experienced lower levels of $\dot{M}O2$ spent more time upstream. Though a range of models focused on hydraulic conditions were tested, models that included flow metrics as predictors had ΔAIC values of 118 or greater indicating that the spatially-averaged flow conditions in the downstream portion of the test section had minimal support as predictors of the proportion of time fish spent upstream. (Burnham and Anderson 2002).

Similarly, models with species as a predictor of $Prop_{up}$ did not receive strong support, indicating that rainbow trout and smallmouth bass did not differ in the proportion of time spent upstream. The null model, including only fish ID as a random effect, was also minimally supported, with a ΔAIC of 127, indicating that tested predictors provided a better fit for $Prop_{up}$ data (Burnham and Anderson 2002).

Fish primarily selected against habitat in the upstream portion of the test section. Across all structure treatments, fish spent approximately 18% of their time upstream. $Prop_{up}$, however, did vary between structures (i.e., V1, V2, V3, H1, H2, H3, D1, D2, D3, or NS control). When NS was present, fish tended to spend the greatest amount of time upstream, with a median $Prop_{up}$ of 25% and an average $Prop_{up}$ of 33% (Figure 4.2). In contrast, when any structure was present, median $Prop_{up}$ was <less than 10%, and for all structures besides D1, D2, and H1, median $Prop_{up}$ was 0%. However, only when V1 or D2 was present did fish spend significantly less time upstream than when NS was present. With the exception of when D3 was present, fish $Prop_{up}$ was lowest when V1 was present (Figure 4.2).

Fish $Prop_{up}$ was highly variable between structure treatments (Figure 4.2). This was especially true for certain DS and HS, with some fish spending 100% of a 15 minute sub-trial upstream when these structures were present and some spending 0% of a sub-trial upstream when these structures were present. This variability was most evident for H3 and D3. When fish swam with H3 or D3, they either spent all of their time upstream, or all of their time downstream. The Fligner-Killeen test (Median $\chi^2 = 59.63$, df = 9, p-value < 0.001) confirmed the high level of variance in $Prop_{up}$.

Fish $\dot{M}O2$ (in mg O_2/kg fish/hr), estimated via acceleration, also impacted $Prop_{up}$. The majority of the fish that spent all or most of their time in the upstream portion of the test section

tended to have lower levels of $\dot{M}O2$ (Figure 4.3). Mean $\dot{M}O2$ for fish that spent 50% or more of their time upstream was 208 mg O_2/kg fish/hr, while mean $\dot{M}O2$ for fish that spent less than 50% of their time upstream was 220 mg O_2/kg fish/hr. Simultaneously, the highest level of $\dot{M}O2$ experienced by fish that spent 100% of their time upstream was around 240 mg O_2/kg fish/hr, whereas the highest level of $\dot{M}O2$ experienced by fish that spent 0% of their time upstream was around 300 mg O_2/kg fish/hr.

Downstream habitat selection

Habitat selection in the downstream portion of test sections, evaluated through SI count, was heavily driven by flow characteristics for both rainbow trout and smallmouth bass. All parameters included in the top-fitting model for each species had a significant impact on SI ($P < 0.05$). Longitudinal velocity U, Reynolds stresses, and vorticity were found to be the most important drivers of selection for rainbow trout (Table 4.5), while vorticity and U_{rms} were the most important drivers of selection for smallmouth bass (Table 4.6).

Rainbow trout SI was positively related to U. When examining the entire range of velocities available to them over the course of trials, fish preferred to occupy areas of elevated U (Figure 4.4). Specific preferences appeared to fall into three bands, centered approximately on 0.3 m/s, 0.5 m/s, and 0.65 m/s. Relative frequency histograms relating available flow conditions to flow conditions selected by fish showed that rainbow trout often selected values of U at the low and high end of what was available to them for a given trial (Figure 4.5; Figure 4.6). In contrast to U, rainbow trout SI was lower for areas with increased levels of Reynolds stress and vorticity, the two turbulence metrics in the top fitting model for rainbow trout habitat selection. Fish preferentially selected areas of reduced Reynolds stress and vorticity relative to what was available to them; the most selected levels of Reynolds stress were generally between -0.05 and

0.05 m^2/s^2, and the most selected levels of vorticity from -10 to around 2.5 s^{-1}. Interestingly, rainbow trout evenly preferred areas of both positive and negative values of Reynolds stress, but appeared to prefer areas of negative vorticity as compared to areas of positive vorticity of the same magnitude (Figure 4.7; Figure 4.8, panel A).

Smallmouth bass SI was also impacted by vorticity. As compared to rainbow trout, smallmouth bass preferred areas of reduced vorticity relative to the range of available levels of vorticity; they also tended to prefer areas with negative vorticity, but showed a greater preference for positive vorticity than rainbow trout (Figure 4.8, panel B). Smallmouth bass occupied a wider range of vorticities overall as compared to rainbow trout, but selected more heavily for a narrower range of vorticities close to 0, around -1 to 1 s. Habitat selection by smallmouth bass was also driven by U_{rms}, with smallmouth bass exhibiting a preference for lower levels of U_{rms}; most typically, values of U_{rms} selected by smallmouth bass were below 0.5 m/s, with fish tending to more heavily prefer values even closer to 0 (Figure 4.9).

As SI data reflected differential usage of cells and SI was found to be different between species, it was possible to visualize SI to broadly indicate fish occupancy throughout the downstream portion of the test section. When fish were downstream of turbulence-generating structures and interacting with the turbulence that was created, clear preferences for certain locations were identified for both species. More specifically, fish tended to occupy a greater number of cells when BL velocity was low, and then reduced their range as BL velocity increased (Figure 4.10). Overall, however, rainbow trout and smallmouth bass tended to show clear differences in their habitat selection downstream of structures, shown through SI. For a given structure and velocity, rainbow trout tended to select a smaller number of cells and smallmouth bass, in contrast, tended to occupy a larger number of cells, often spread throughout

the test section. This was especially evident when fish swam with the structures that impacted the XZ plane, HS and DS (Figure 4.11). For these cases, rainbow trout tended to occupy a small spatial area close to the bed of the flume, while smallmouth bass occupied a greater number of cells, making use of most of the depth available to them.

Flow characteristics

Due to the large number of cases measured, data are only presented for the flow metrics that were drivers of fish habitat selection, as assessed through SI count. These were time-averaged longitudinal velocity U, U_{rms}, Reynolds stress, and vorticity. Data are presented for NS and all diameters of VS and DS, as measured on the XY plane, and for NS and all diameters of HS and DS, as measured on the XZ plane. Data are aggregated across all BL velocities for each structure, and for DS are aggregated separately for the XY and XZ planes. This was done to allow for more direct comparisons with $Prop_{up}$ data, as these were aggregated across BL velocities as well. An in-depth description of flow conditions can be found in Chapter Three, and heat maps of flow conditions can be found in the supplemental materials (Figures B.25 to B.69). Relatively frequency histograms relating the flow conditions available to fish with the conditions selected by fish of each species are also available within the supplemental materials (Figures C.2 to C.39).

The range of time-averaged longitudinal velocity U levels available to fish across all structures and BL velocities was wide. The lowest velocities generated were approximately 0.2 m/s, but velocities could reach as high as 0.8 m/s. Of the three structure orientations, DS of all diameters most consistently generated the highest longitudinal velocities, between 0.6 to 0.8 m/s, for both the XY (Figure 4.12) and XZ (Figure 4.13) planes. Longitudinal velocities up to 0.6 m/s for V1 and 0.8 m/s for H2 were generated; however, maximum time-averaged velocities for V2,

V3, H1, and H3 were below 0.5 m/s. When NS was present, the lowest time-averaged longitudinal velocity generated was higher than for when structures were present, around 0.3 m/s.

The longitudinal velocities generated by VS and HS followed a bimodal or trimodal distribution; the peaks of these distributions approximately aligned with the longitudinal velocities generated at each BL velocity when each structure, respectively, was present. This likely occurred because VS and HS both generated low-velocity wakes on a single plane that were confined to the area of the test section immediately within the structures' lee; as a result, the velocities occurring immediately downstream of a structure were much lower than surrounding velocities, in turn causing greater separation between the levels of U that occurred at each BL velocity. Such a distribution was not seen for DS, likely because these structures generated wakes on two planes and affected a greater portion of the test section, such that there was not such a strong contrast between the longitudinal velocities generated when DS were present (see Figure 3.6 and 3.7).

Structures of all orientations and diameters generated turbulence in their downstream wake, but structures varied in the level of turbulence generated. U_{rms} was lowest for VS, especially V1, which generated U_{rms} ranging from close to 0 m/s up to approximately 0.2 m/s. HS and DS both generated higher levels of U_{rms} in comparison, with values reaching as high as 1 m/s for a small number of regions downstream of DS when measured on the XZ plane. This pattern, in which the regions downstream of VS had reduced U_{rms} compared to HS and DS, was similarly seen for Reynolds stress and vorticity. Low values of Reynolds stress, between -0.0005 and -0.0005 m^2/s^2, and low values of vorticity, between -2.5 and 2.5 s^{-1}, were produced at the highest frequencies by VS (Figure 4.14). HS and DS, with the exception of H1, produced higher levels

of Reynolds stress and vorticity (Figure 4.15). These structures produced a much wider range of vorticity levels, often ranging well outside of -5 to 5 s^{-1}. The test section was not devoid of turbulence when NS was present, but the levels of turbulence were much lower than when any type of structure was present.

Discussion

Fish selection for habitat in the upstream or downstream portion of the test section was driven by a different set of factors than fish selection for habitat within the downstream portion of the test section. Whether fish preferred to remain downstream, in the area most affected by a structure's wake, or preferred to move upstream, away from the flow conditions generated downstream of structures, was driven by energy use and by what structure was present; flow characteristics did not appear to be important. In contrast, for fish downstream of structures that were interacting with turbulence, selection for specific locations was influenced by flow conditions, with rainbow trout and smallmouth bass selecting habitat based largely on separate characteristics of flow.

Selection for upstream or downstream habitat

Fish in the current study spent time both in areas upstream of turbulence-generating structures and in areas downstream of these structures. Fish preference for habitat in the upstream or downstream portion of the test section was predicted by energy use. Fish that used less energy tended to spend more time upstream of structures, while fish that used more energy tended to spend less time upstream of structures. A central tenet underlying multiple theories of habitat selection is that animals, including fish, select habitats in which they are able to minimize energetic costs and maximize energetic gains (Fretwell and Lucas 1970; Mittelbach 2002). In

essence, fish should prefer habitat in which they can forage efficiently and effectively, using the least amount of energy possible (Kiflawi and Genin 1997; Johansen et al. 2020). If fish are not foraging, they would be expected to instead be refuging, selecting habitat conditions that minimize energetic costs (Mittelbach 2002). In this study, however, fish were found to select habitat downstream of turbulence-generating structures even though it was associated with a higher energetic cost than selection for habitat upstream of structures.

One possible explanation for the selection of upstream versus downstream habitat in this study is that structures generated flow conditions that were ideally suited for feeding in the downstream wake, thereby attracting fish. Riverine fishes will often select "focal positions" downstream of physical structures in rivers (Fausch et al. 1984; Piccolo et al. 2014) to shelter from flow, and then dart out as flow delivers potential prey items downstream. It has been suggested that turbulence can concentrate prey items flowing downstream and increase the number of interactions between fish and prey, and thus causing turbulence to contribute to foraging efficiency (Hill and Grossman 1993; MacKenzie and Kiørboe 1995; Lewis and Pedley 2001; Hayes et al. 2007). As foraging was not a focus of this study, it is not possible to say if structures generated conditions that promote foraging. However, this does not preclude the possibility that fish may have selected habitat downstream of structures, ostensibly, to increase potential feeding efficiency. If fish were indeed motivated by this purpose, this would explain why fish tended to spend a small proportion of time in the upstream portion of the test section, even though it provided energetic benefits.

Preference for habitat in the upstream or downstream portion of the test section was not linked with mean flow characteristics generated downstream structures, but rather was influenced by structure. The presence of structures inherently alters mean flow characteristics,

which should be expected to alter fish swimming behavior and spatial usage in turn (Lacey et al. 2012; Daniels and Rhoads 2013; Wilkes et al. 2017). One possible explanation for why flow characteristics did not affect preference for habitat in the upstream mor downstream portion of the test section is that the spatially- and temporally-averaged turbulent flow characteristics used for these analyses cannot approximate the conditions directly experienced by fish. For example, some fish in this study spent 100% of their time upstream for a given sub-trial. These fish would have never interacted with flow conditions in the downstream portion of the test section and would therefore have not been impacted by the turbulence generated by a structure's presence. This explanation likely still applies for fish that did spend most of their time downstream within a given sub-trial. The turbulence generated downstream of a structure varies over both space and time; a fish swimming in one region will likely experience different conditions than when swimming in another region, and the conditions in each region will likely be variable over time. Therefore, a temporal and spatial average of all downstream conditions would not reflect the flow conditions in the locations that fish actually occupied. This echoes a common theme that has emerged from the literature regarding fish-flow interactions: mean flow characteristics simply do not suffice for predicting fish responses (Lacey and Millar 2004; Lacey et al. 2012; Smith et al. 2014). When turbulence is quantified in the same physical location occupied by a fish, temporal averages can effectively predict fish responses to turbulence, such as habitat selection or energetics (Wilkes et al. 2017). As neither the exact locations of fish within nor measurements of the flow conditions for the upstream portion of the test section were available, it was not possible to take this approach to predict the proportion of time spent upstream by fish. It is likely possible that flow characteristics did affect the proportion of time fish spent upstream,

as structure was a driving force of this, and structure and flow are closely entwined. Mean turbulent flow characteristics, however, did not suggest this.

Downstream habitat selection

Flow characteristics influenced fish habitat selection, assessed through SI, in the downstream portion of the test section when fish were interacting with turbulence generated by structures. Fish showed clear preferences for specific hydraulic conditions, with rainbow trout and smallmouth bass often selecting habitat based upon different aspects of turbulence. Rainbow trout selected for locations with elevated velocity and selected against locations with elevated levels of Reynolds stress and vorticity. Smallmouth bass similarly selected against areas with elevated levels of vorticity, as well as areas with elevated levels of U_{rms}. Previous work has demonstrated that fish often prefer a certain range of turbulence and will select for flow conditions that fall within this range, while selecting against conditions that fall outside this range (Webb 1998). Smith (2003) discovered that rainbow trout would preferentially select areas with reduced levels of turbulence over areas with higher levels of turbulence, even if such areas also had higher flow velocities. Similarly, Cotel et al. (2006) found that brown trout (*Salmo trutta*) selected against locations with elevated turbulence intensity in favor of locations with intermediate levels of turbulence intensity. Guppies (*Poecilia reticulata*) avoid areas with the highest levels of Reynolds stress when swimming near a boulder generating turbulence (Hockley et al. 2014), while Silva et al. (2012) found that Iberian barbels (*Luciobarbarus bocagei*) selected regions of reduced turbulence, and additionally found that Reynolds stress was the most important hydraulic variable driving fish behavior. Interactions between smallmouth bass and turbulent flow are not well-studied, but stream-dwelling smallmouth bass typically prefer occupying locations with reduced flow velocity near log jams and similar large woody debris,

suggesting a preference for lower levels of turbulence (Todd and Rabeni 1989; Orth and Newcomb 2002). In this study, rainbow trout and smallmouth bass were both found to preferentially select against habitat in which turbulence was elevated; however, selection for each species was driven by different aspects of turbulence.

The habitat selection models yielded from SI data provide insight as to why fish preferred to remain downstream more frequently when certain structures were present. Although the turbulence conditions fish experienced upstream of structures were not quantified, the conditions fish experienced and selected for downstream of structures are known. One turbulence metric in particular, vorticity, was an important hydraulic driver of habitat selection for both rainbow trout and smallmouth bass, with fish from both species favoring locations in which vorticity levels were low. Histograms of vorticity levels within the test section revealed that the low levels of vorticity preferred by fish were generated in abundance by V1 (Figure 4.14). Fish may have selected habitat downstream of V1 at a greater frequency because of the low vorticities produced by V1. Conversely, HS and DS generated wider ranges and higher levels of vorticity, and, with the exception of D2, fish spent more time upstream when these structures were present as compared to V1, suggesting possible avoidance of these elevated vorticities. Overall, both rainbow trout and smallmouth bass selected for low levels of vorticity when swimming downstream of structures, which may explain why fish spent less time upstream when structures that generated low levels of vorticity were present and more time upstream when structures that generated elevated levels of vorticity were present

Broader implications

Results from this study provide an abundance of context regarding the factors that drive fish habitat selection within turbulent flow. These results not only have implications for future

laboratory-based studies examining fish habitat selection in turbulent flow, but also, and perhaps more importantly, have two main implications regarding how best river restoration can account for turbulence in its implementation and design.

First, this study demonstrates that while riverine species may share some level of preference for varying degrees of turbulence, this does not necessarily manifest in selection for the same flow conditions or physical locations. The tendency of rainbow trout and smallmouth bass to remain downstream of turbulence-generating structures was approximately equal and both rainbow trout and smallmouth bass preferred areas of reduced vorticity. However, the two species did not have the same spatial usage while downstream of structures, and their respective selection of hydraulic habitat was affected, apart from vorticity, by separate aspects of turbulence. These results highlight that fish of different species are unlikely to respond to restoration in the same way. This may not be a large concern for certain restoration efforts focused on a single species or handful of species, such as in the case of most restoration efforts in salmonid-bearing streams (Lacey and Millar 2004; Whiteway et al. 2010; Louhi et al. 2016; Wheaton et al. 2018). However, if restoration is targeted at improving habitat conditions for the fish community as a whole, then this needs to be needs to be a consideration for restoration practitioners. If practitioners do not take this into consideration, an instream restoration structure may generate flow conditions that benefit certain species, while simultaneously generate flow conditions that are deleterious for other species. In turn, the species benefitted may select for habitat within and around the structure, but the species negatively impacted may select against this habitat entirely.

Second, results indicate that fish habitat selection in turbulent flow is likely context dependent. In this study, fish that spent a greater proportion of their time in the upstream portion

of the test section, upstream of structures when present, expended less energy than fish that spent a smaller proportion of their time upstream. If expending less energy was the primary motivator underlying fish habitat selection, it would therefore be expected that fish would have entirely selected for upstream habitat, and that no time would have been spent downstream. However, this was not the case. At times, fish selected upstream habitat, but fish primarily preferred to remain in the downstream proportion of the test section. This suggests that minimizing energetic costs was not the sole driver of habitat selection, and that fish rely on multiple factors in choosing what habitat to occupy. A refuging fish may seek different turbulent flow conditions from a feeding fish, while a prey fish attempting to avoid predators may seek different turbulent flow conditions from a predatory fish attempting to acquire prey. Therefore, in order for river restoration efforts to fully utilize the altered flow characteristics downstream of instream restoration structures and in order to maximize their benefits for fish, it will likely be necessary to consider how fish will use structures.

Caveats and future directions

Not all aspects of fish habitat selection in turbulent flow were investigated within this study, and, therefore, there are two primary caveats that should be addressed in future studies. First, given that this study focused on the effects of turbulence generated downstream of structures on fish habitat selection, all flow characterization was similarly generated downstream of structures. As a result, the specific habitat preferences of fish upstream of structures were unknown in this study. There is a chance that time spent upstream reflected not avoidance of turbulence generated by structures, but rather preference for a different area affected by structure presence. In addition to generating downstream wakes that can be exploited by fish, structures also generate upstream bow wakes (Bleckmann et al. 2012). The energetic costs of swimming for

fish occupying such wakes may be even less than the costs of swimming for fish occupying downstream wakes (Liao 2003). This could therefore have served as a motivation for fish to occupy the area upstream of structures. Given that fish often spent more time downstream when swimming with structures that generated flow conditions found to drive hydraulic habitat selection in this study, and often spent more time upstream when structures that generated less favorable flow conditions were present, it is likely that fish were at times moving upstream to avoid certain flow conditions. Thus, to expand on understanding of fish usage of hydraulic habitat around structure, future work should seek to fully characterize the flow surrounding structures in each direction and should track fish movement throughout the entire region in which structures affect flow.

The second consideration for future studies relates to testing environment. More specifically, setting this study within an experimental flume limited the scale at which fish were able to select habitat. The focus of this study was to quantify how specific aspects and levels of turbulence drove fish habitat selection by developing clear links between the locations occupied by fish and the flow conditions they directly experienced in those locations. Therefore, in addition to the size of the flume limiting the potential for fish to range broadly, it was necessary to further restrict the size of the area that fish could occupy in to encourage fish to interact with turbulence generating-structures. As such, what was investigated within this study could potentially be termed “microhabitat selection”. Habitat selection occurs over multiple scales, whereby habitat selection at small spatial scales (i.e., a particular aggregation of large woody debris) may be driven by different factors than habitat selection at medium spatial scales (i.e., selection for a pool versus a riffle) which may be driven by different factors than habitat selection at large spatial scales (i.e., selection for a particular river reach) (Mayor et al. 2009).

Findings from this study are highly relevant for understanding habitat selection at small spatial scales but may not be as pertinent for understanding habitat selection at larger spatial scales. Future laboratory-based studies relating fish habitat selection with turbulent flows are likely to face the same limitations experienced.

Conclusion

Turbulent flows have been a highly understudied component of fish habitat selection, despite the fact that turbulence has strong impacts on fish energetics, commonly considered to be one of the primary drivers of fish habitat selection. This lack of emphasis has likely had consequences for the success of river restoration efforts, which do not always succeed in bolstering fish populations and biodiversity. The link between turbulence and river restoration is physical structure. River restoration frequently involves the implementation and installation of instream restoration structures that alter a site's original flow characteristics and generate additional levels of turbulence. These structures are often aimed at providing habitat for fish, but the impact of the turbulence they generate on fish habitat selection is largely unknown. To address this, the current study utilized a laboratory-based approach to quantify how fish habitat selection for and within turbulent flows is mediated by flow characteristics. The habitat selection for two separate species, rainbow trout and smallmouth bass, was characterized into two main categories: the proportion of time spent in the upstream portion of a flume test section, and the selection of specific locations in the downstream portion of a flume test section. The proportion of time spent upstream reflected fish propensity to select for or against habitat within a structure's downstream wake, while the selection for specific locations downstream indicated fish preference for specific components of turbulent flow generated by a structure. Results revealed that spending a greater proportion of time upstream was associated with a lower

energetic cost for fish relative to when fish spent less time upstream, and yet fish most frequently spend their time downstream. The habitat selection of fish downstream of structures was heavily influenced by flow characteristics. However, each species largely selected habitat based on separate flow metrics, with rainbow trout selecting downstream habitat based on longitudinal velocity U, Reynolds stress, and vorticity, and smallmouth bass selecting downstream habitat based on vorticity and U_{rms}. Taken all together, this study provides new insight into how fish may select restored river habitat and provides guidance for future restoration efforts looking to maximize their benefits for fish.

Figures

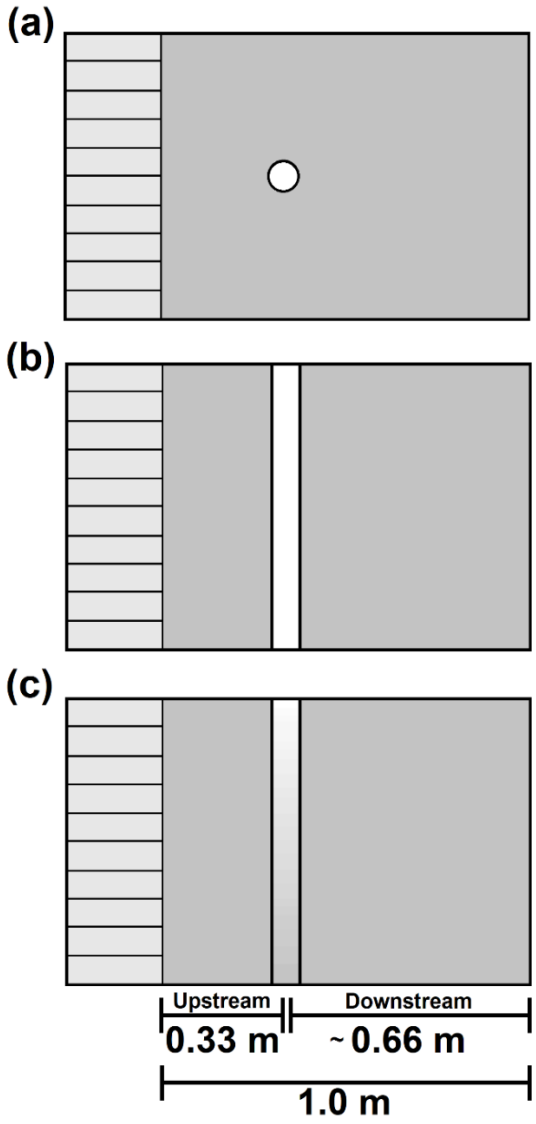

Figure 4.1. Diagram depicting the 1.0-m long test sections utilized for fish habitat selection experiments. Test sections are shown on the horizontal XY plane, from the overhead view, for 7.62-cm diameter structures oriented vertically (*a*), horizontally (*b*), and diagonally (*c*). Each test section was preceded by a flow straightener composed of 7.62-cm diameter PVC pipe. Structures, when present, were placed with their mid-point 33 cm downstream of the flow straightener. These first 33 cm were considered to be "upstream", while the last ~ 66 cm were considered to be "downstream".

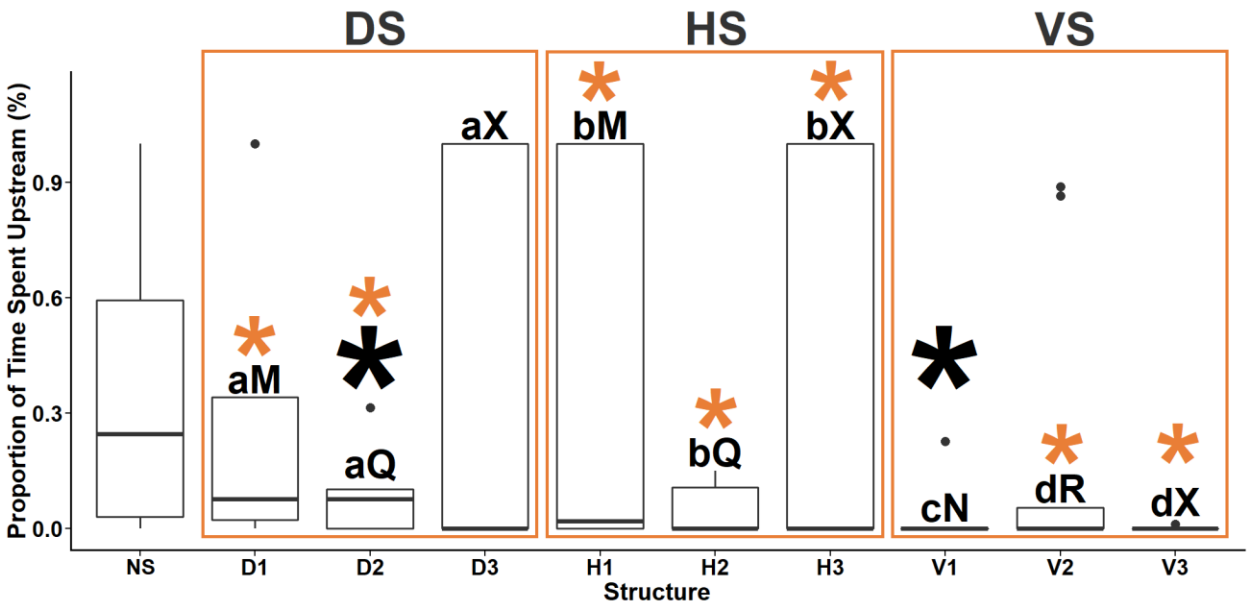

Figure 4.2. The proportion of time spent upstream of turbulence-generating structures for rainbow trout and smallmouth bass participating in flume experiments to examine fish habitat selection in turbulent flow. Fish were tested with structures in three orientations (D- Diagonal; H- Horizontal; V- Vertical) and one of three diameters (1- 2.54 cm; 2- 5.08-cm; 3- 7.62-cm), across a range of velocities. Boxes show groupings of structures (DS- D1, D2, D3; HS – H1, H2, H3; VS – V1, V2, V3) by their orientation. Black asterisks (*) indicate significance between the proportion of time fish spent upstream when a given structure was present relative to the control with no structure (NS) and orange asterisks (*) indicate a significant difference in this proportion relative to when V1 was present. Lower case letters indicate significant differences between structures of the same orientation for diagonal (a), horizontal (b), and vertical (cd) structures. Upper case letters indicate significant differences between structures the same diameter, for 2.54-cm (MN), 5.08-cm (QR), and 7.62-cm (X) diameters. Shared letters indicate that the proportion of time spent upstream by fish was not different between the structures.

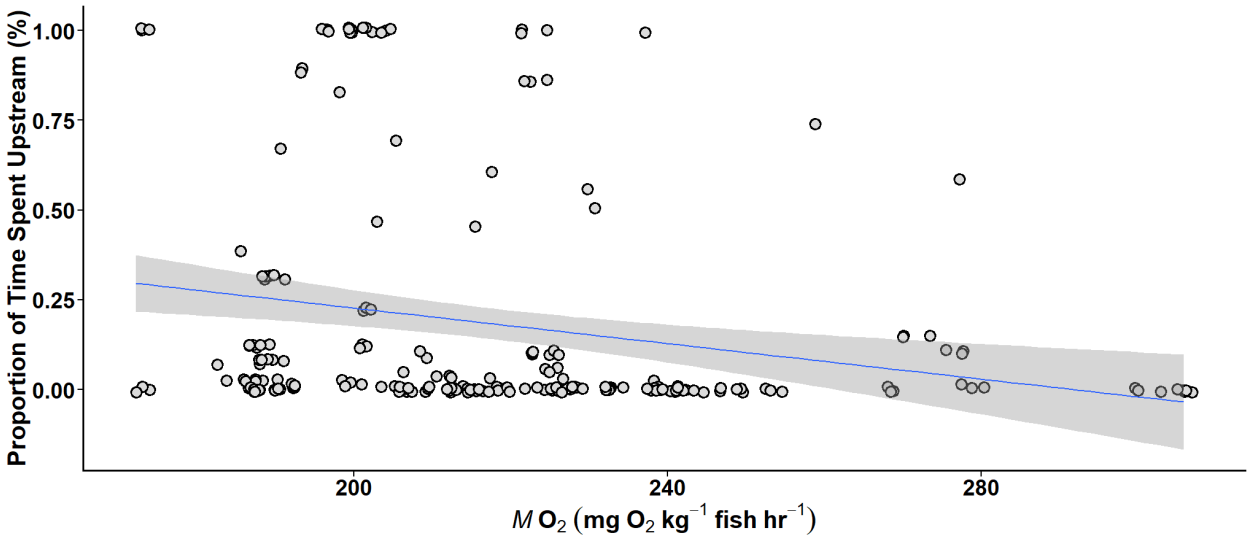

Figure 4.3. The proportion of time spent upstream of turbulence-generating structures as a product of fish oxygen consumption (*$\dot{M}O2$*) for rainbow trout and smallmouth bass (combined) participating in flume experiments to examine fish habitat selection in turbulent flow. All fish were tagged with accelerometers, allowing for the estimation of oxygen consumption from acceleration using a pre-existing model relating the two. The line and confidence band for the linear regression relating the proportion of time spent upstream with *$\dot{M}O2$* are shown to visualize how the proportion of time spent upstream differed with different levels of fish oxygen consumption. Data points are shown with a jitter effect to improve readability and account for overlapping data points.

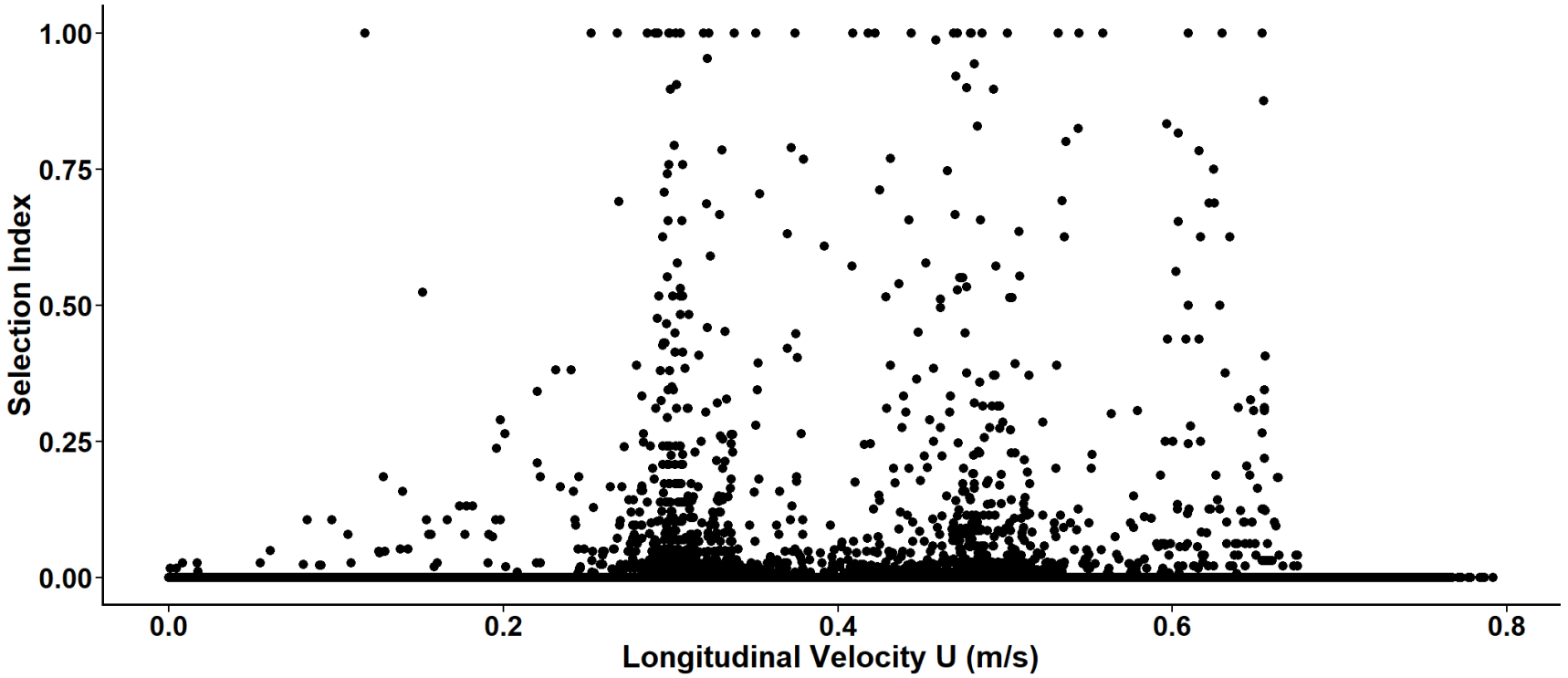

Figure 4.4. The selection index of rainbow trout for varying levels of longitudinal velocity U relative to all available levels of U. Rainbow trout participated in trials to examine fish habitat in turbulent flow. Higher values for selection index, approaching 1, indicate greater selection of and preference for a particular U.

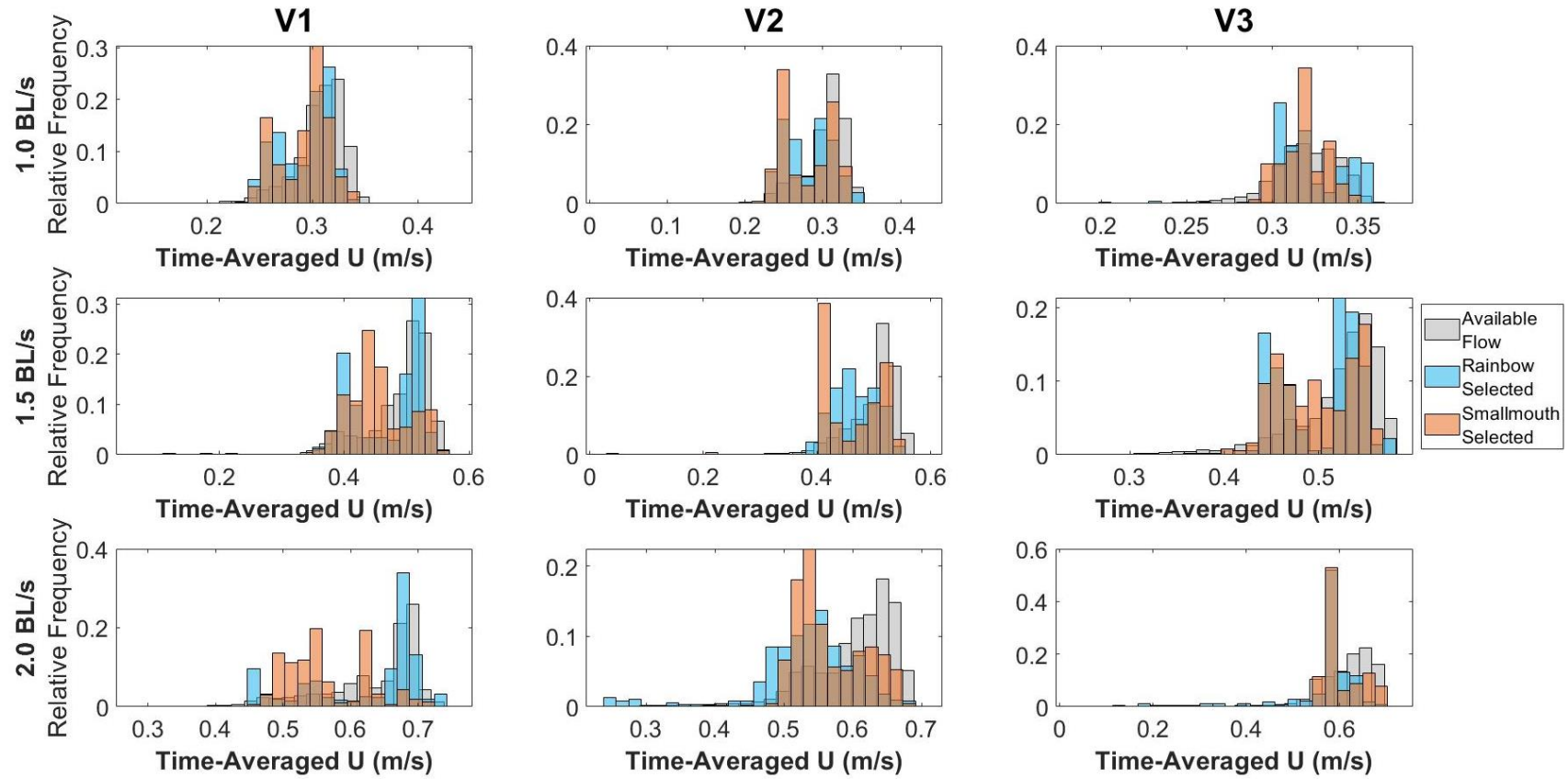

Figure 4.5. Relative frequency histograms relating the distribution of available levels of longitudinal velocity U to the distribution of U selected by rainbow trout and smallmouth bass to swimming downstream of vertical structures in one of three diameters (V1 – 2.54-cm; V2 – 5.08-cm; V3 – 7.62-cm), across three body-length velocities, 1.0, 1.5, and 2.0 BL/s.

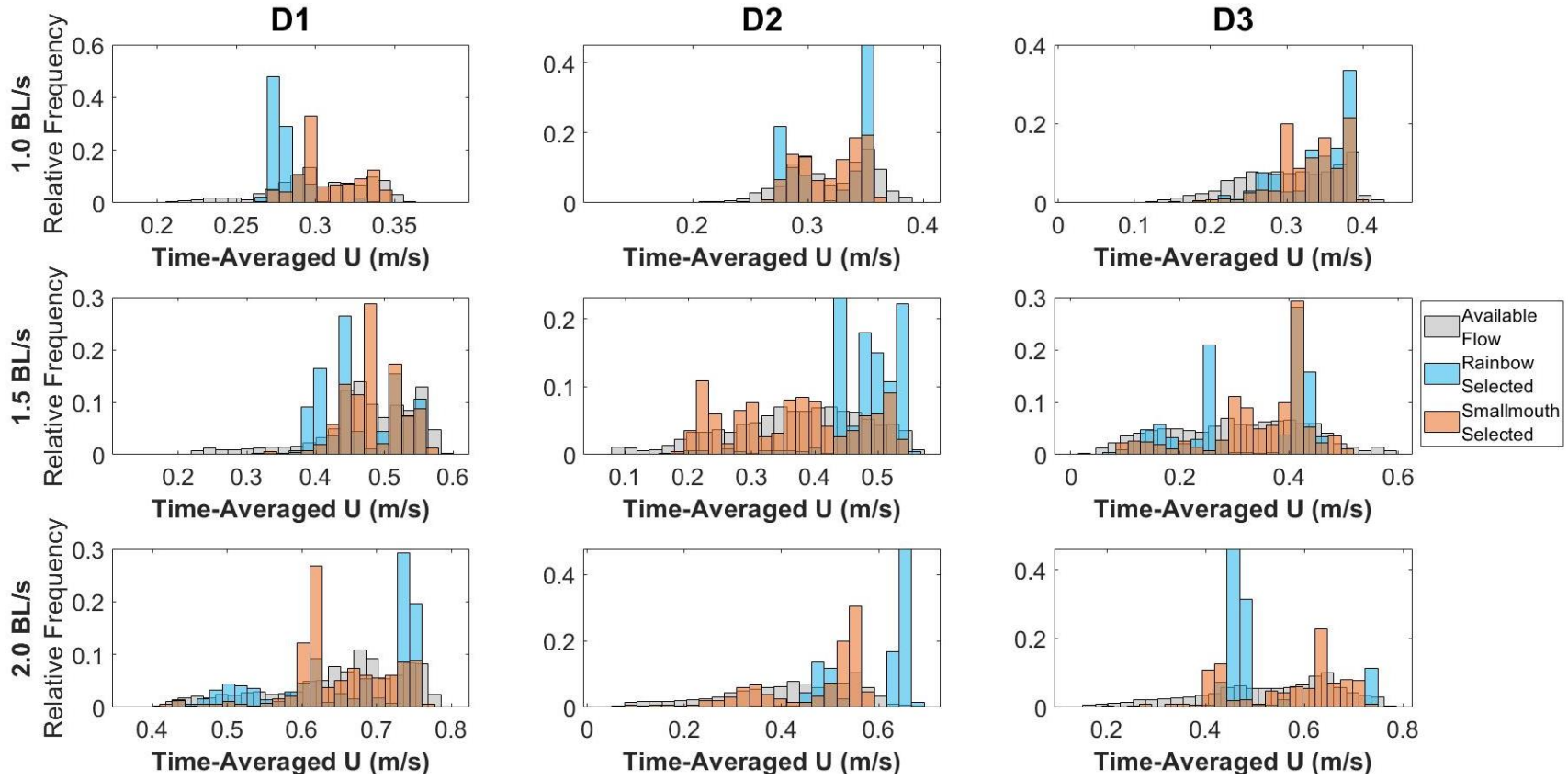

Figure 4.6. Relative frequency histograms relating the distribution of available levels of longitudinal velocity U to the distribution of U selected by rainbow trout and smallmouth bass to swimming downstream of diagonal structures in one of three diameters (D1 – 2.54-cm; D2 – 5.08-cm; D3 – 7.62-cm), across three body-length velocities, 1.0, 1.5, and 2.0 BL/s. Data presented are derived from the XY plane.

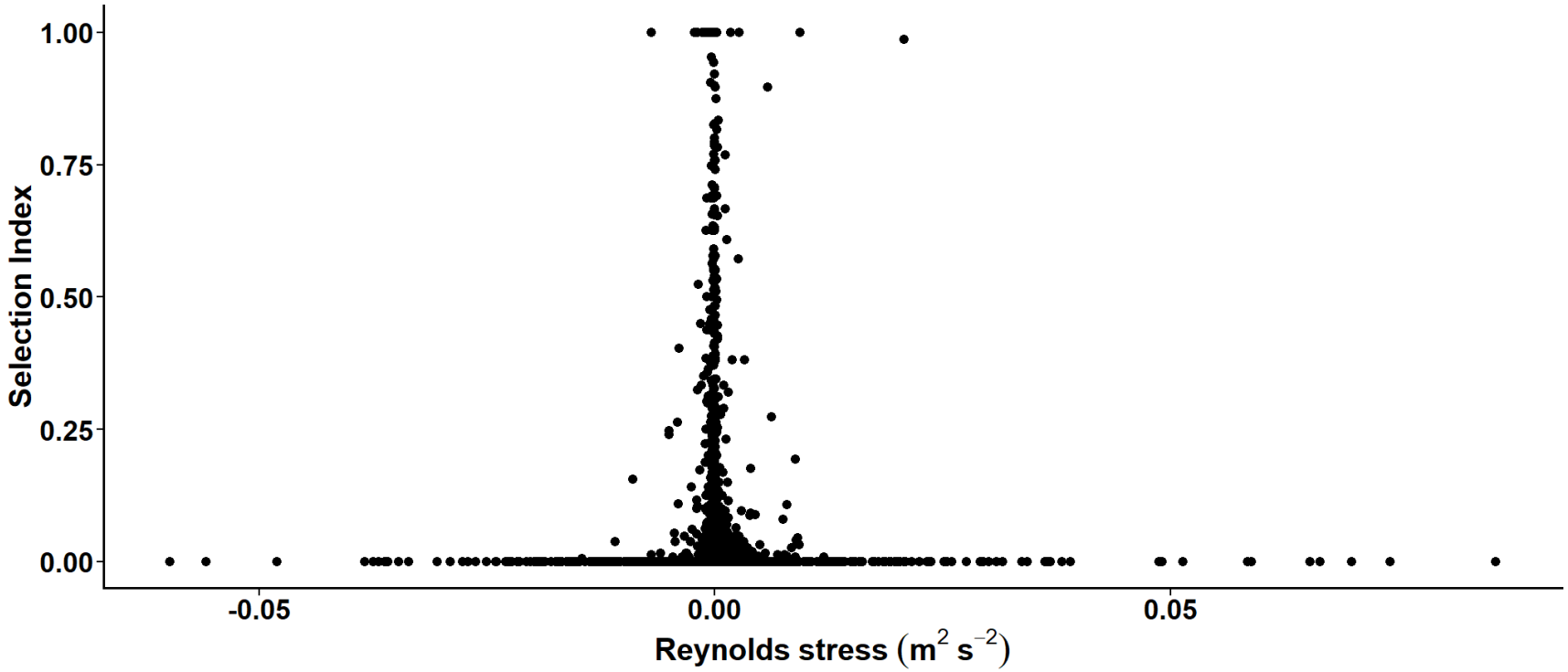

Figure 4.7. The selection index of rainbow trout for varying levels of Reynolds stress relative to all available levels of Reynolds stress. Rainbow trout participated in trials to examine fish habitat in turbulent flow. Higher values for selection index, approaching 1, indicate greater selection of and preference for a particular level of Reynolds stress.

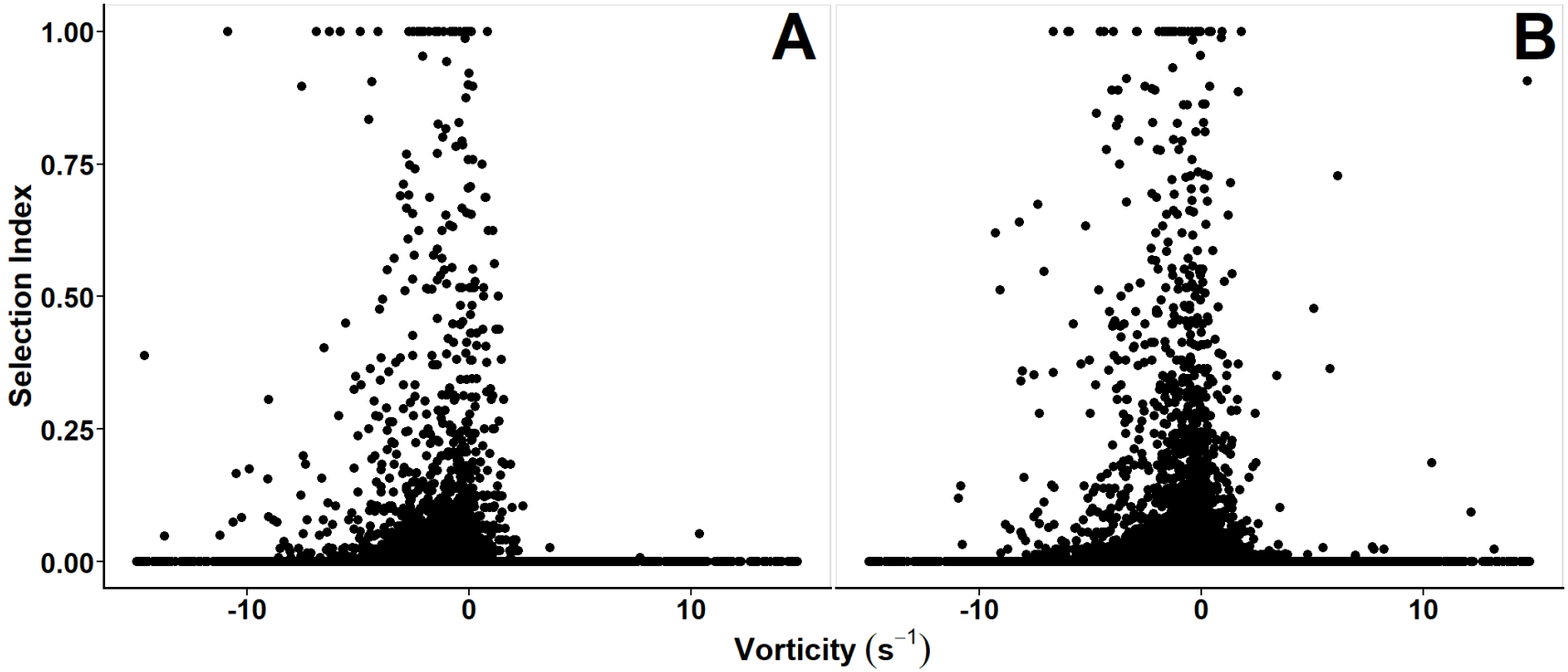

Figure 4.8. The selection index of rainbow trout (panel A) and smallmouth bass (panel B) for varying levels of vorticity relative to all available levels of vorticity. Rainbow trout participated in trials to examine fish habitat in turbulent flow. Higher values for selection index, approaching 1, indicate greater selection of and preference for a particular level of vorticity.

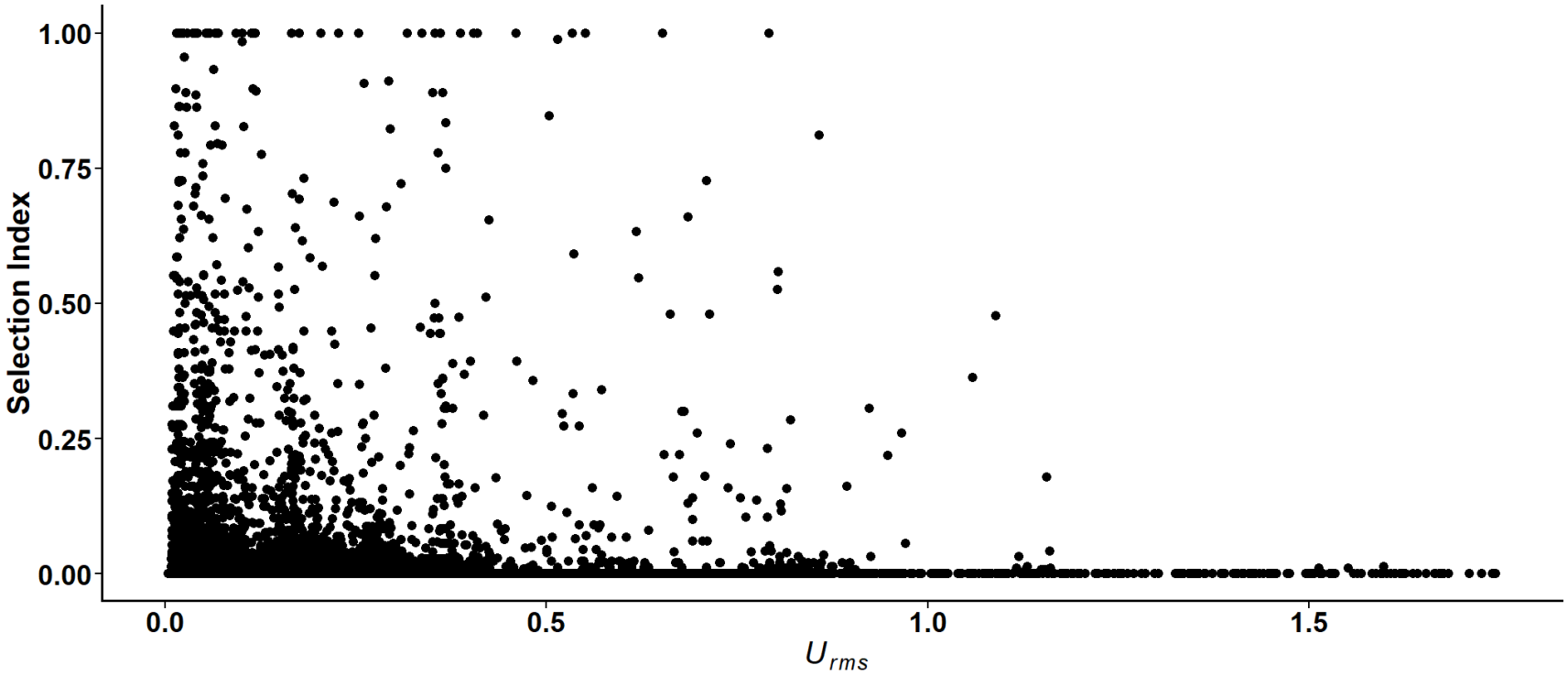

Figure 4.9. The selection index of smallmouth bass for varying levels of U_{rms} relative to all available levels of U_{rms}. Smallmouth bass participated in trials to examine fish habitat in turbulent flow. Higher values for selection index, approaching 1, indicate greater selection of and preference for a particular level of U_{rms}.

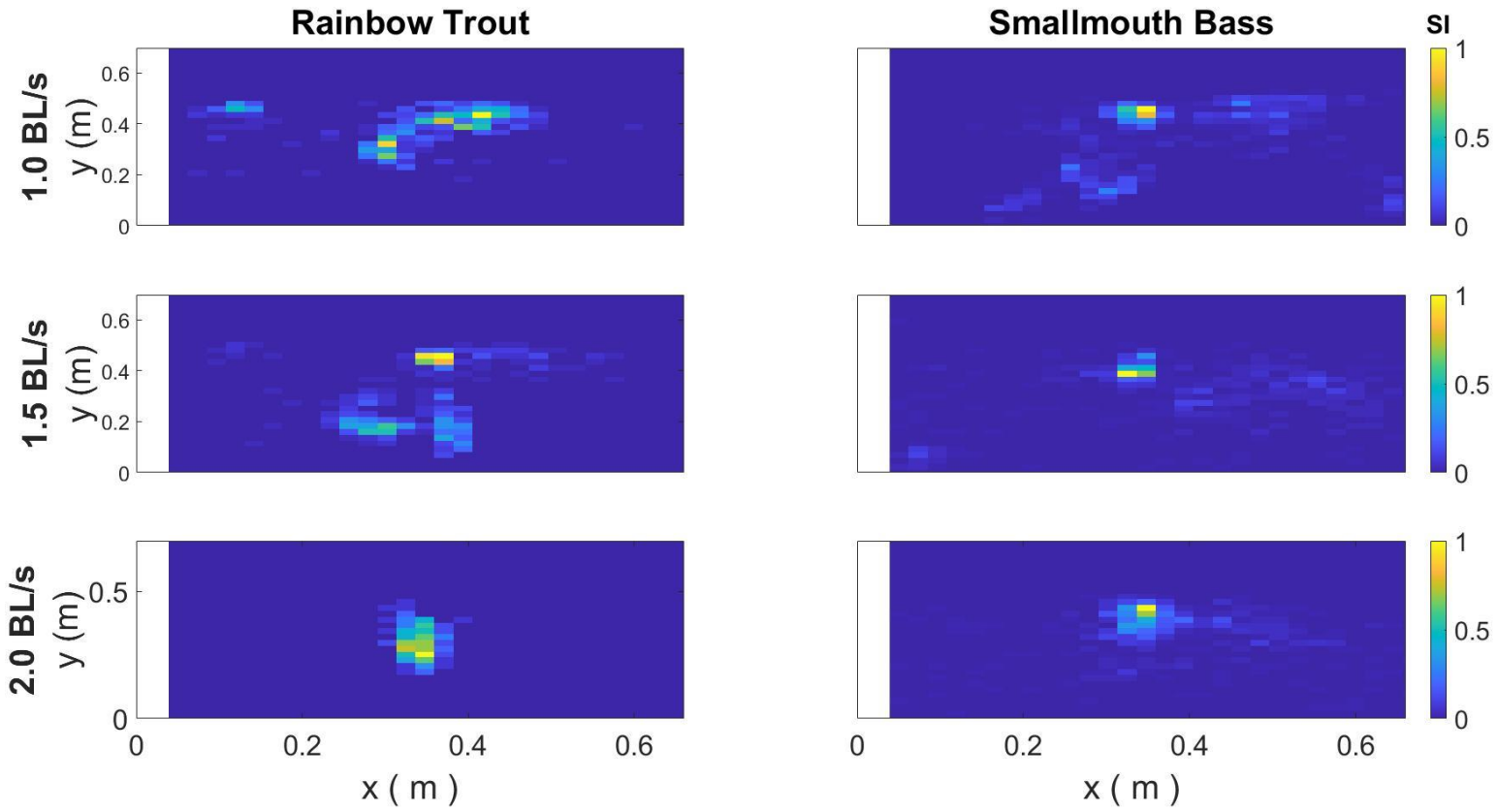

Figure 4.10. The selection indices (SI) for habitat selection of rainbow trout and smallmouth bass swimming downstream of small vertical structures (2.54-cm diameter) in test sections established within large racetrack flume, shown on the horizontal XY plane. Indices are shown separated by species and body-length velocity. Warmer color indicates higher occupancy by fish within a given cell. Vertical structures were centered 0.33 cm downstream of the beginning of the test section (x = 0 m), and centered the midline of the flume (y = 0.38 m).

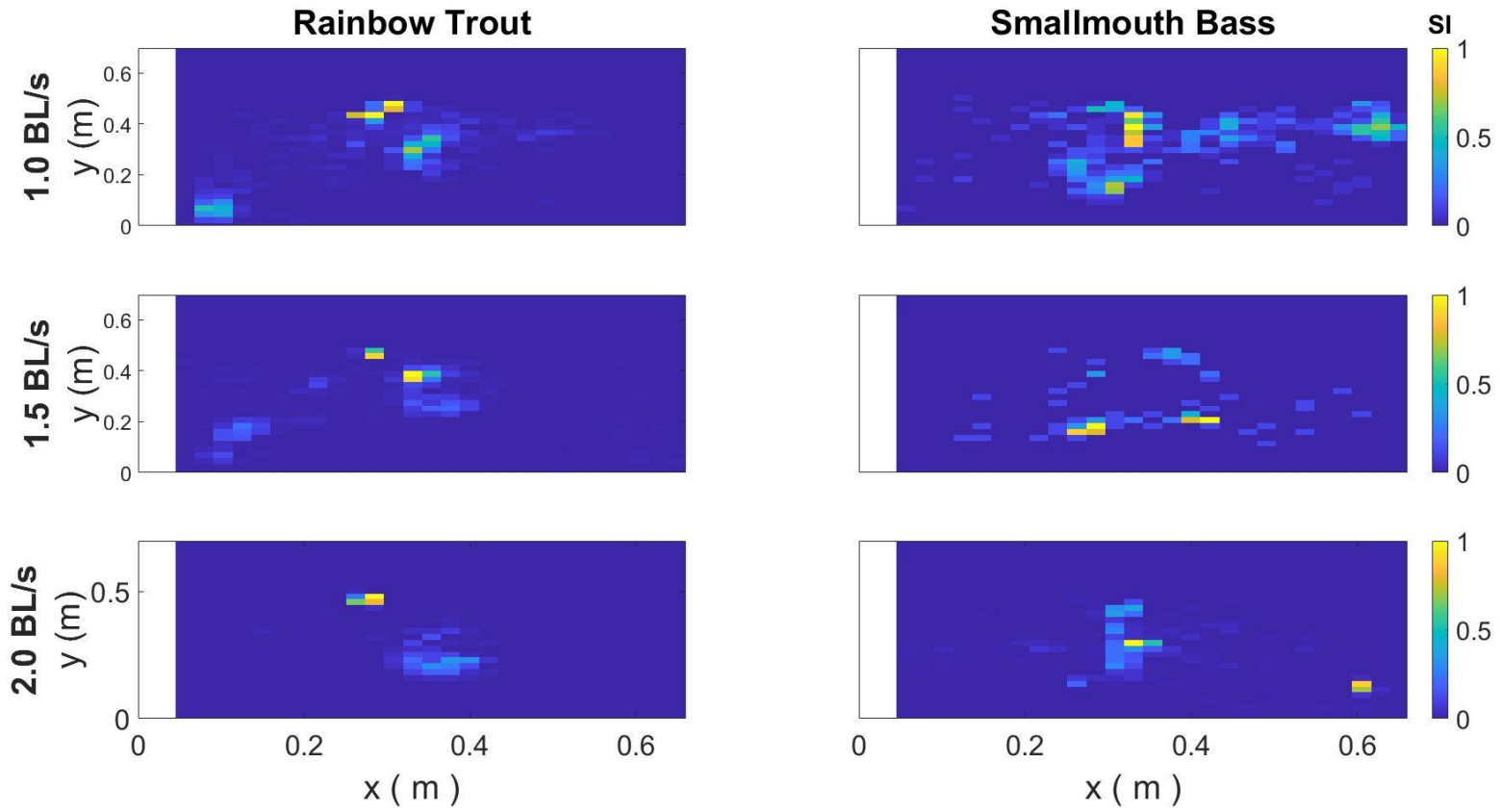

Figure 4.11. The selection indices (SI) for habitat selection of rainbow trout and smallmouth bass swimming downstream of small vertical structures (2.54-cm diameter) in test sections established within large racetrack flume, shown on the horizontal XY plane. Indices are shown separated by species and body-length velocity. Warmer color indicates higher occupancy by fish within a given cell. Vertical structures were centered 0.33 cm downstream of the beginning of the test section (x = 0 m), and centered the midline of the flume (y = 38 cm).

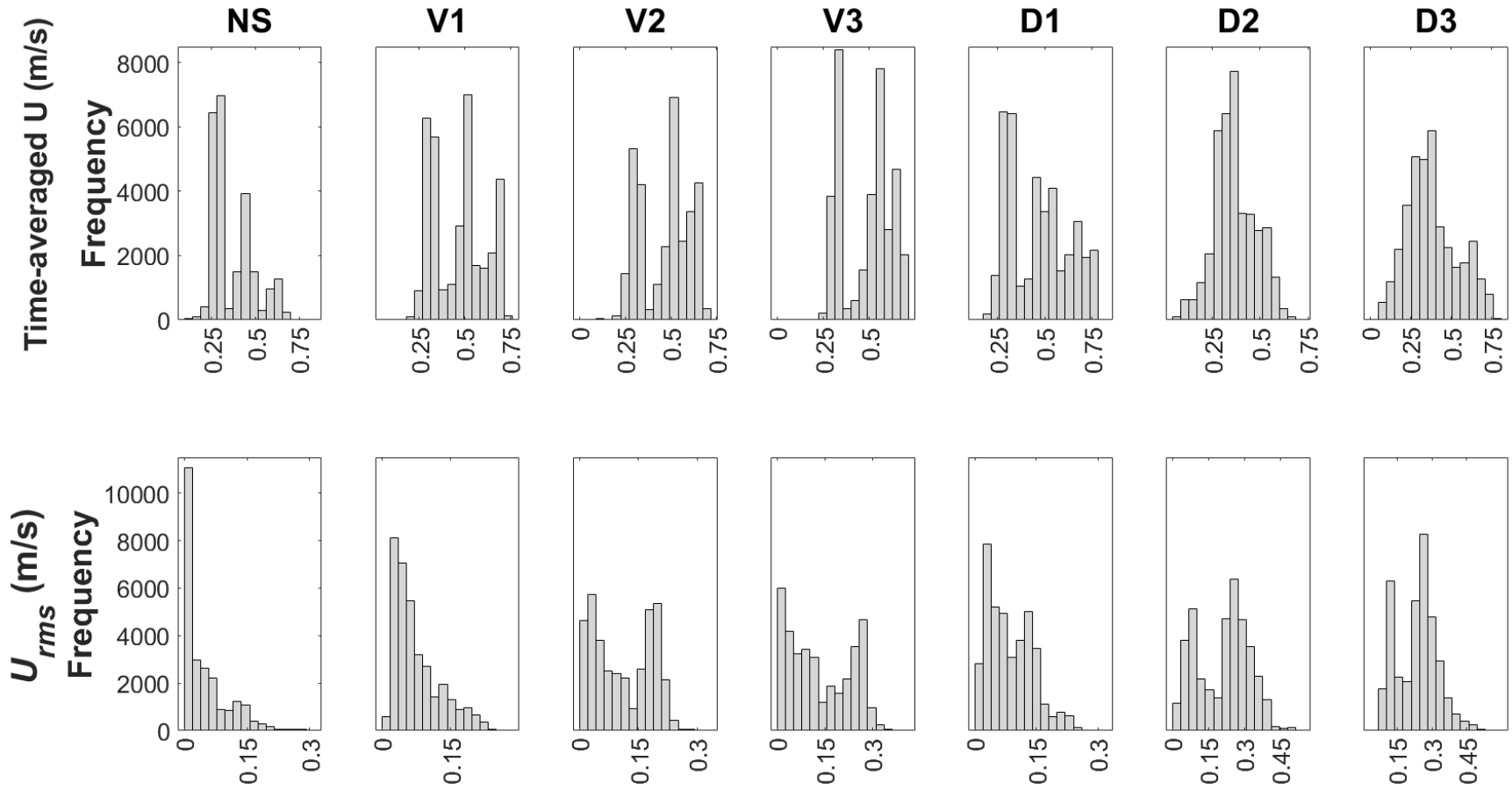

Figure 4.12. Histograms displaying the distribution of longitudinal velocity U values and U_{rms} values generated in a 1.0 m long test section within a racetrack flume. Distributions are presented for a control case with no structure, three diameters of vertical structure (V1, V2, V3), and three diameters of diagonal structure (D1, D2, D3). For cases with structures, distributions shown were measured downstream of each structure, respectively. Data presented are derived from the XY plane.

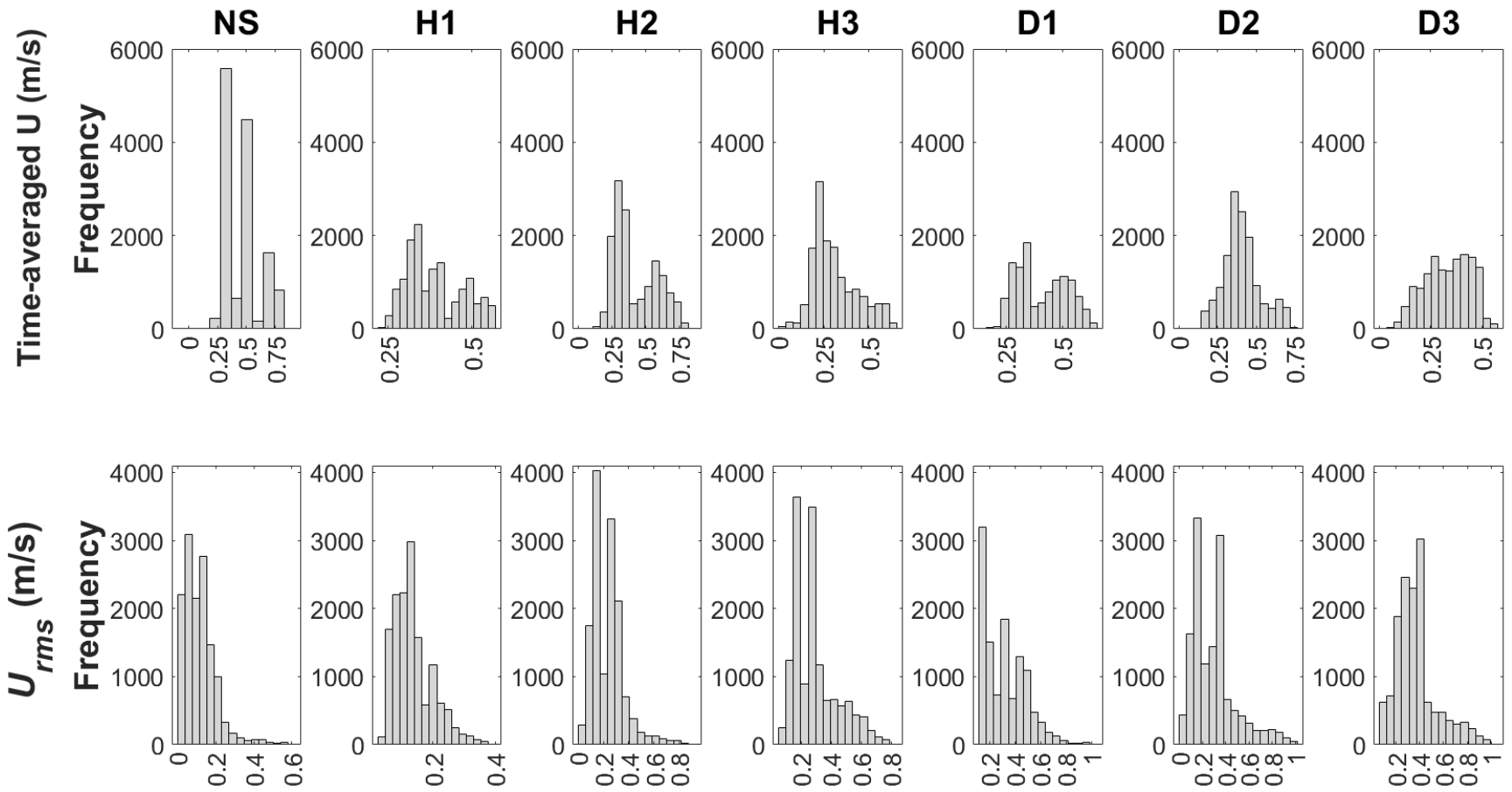

Figure 4.13. Histograms displaying the distribution of longitudinal velocity U values and U_{rms} values generated in a 1.0 m long test section within a racetrack flume. Distributions are presented for a control case with no structure, three diameters of horizontal structure (H1, H2, H3), and three diameters of diagonal structure (D1, D2, D3). For cases with structures, distributions shown were measured downstream of each structure, respectively. Data presented are derived from the XZ plane.

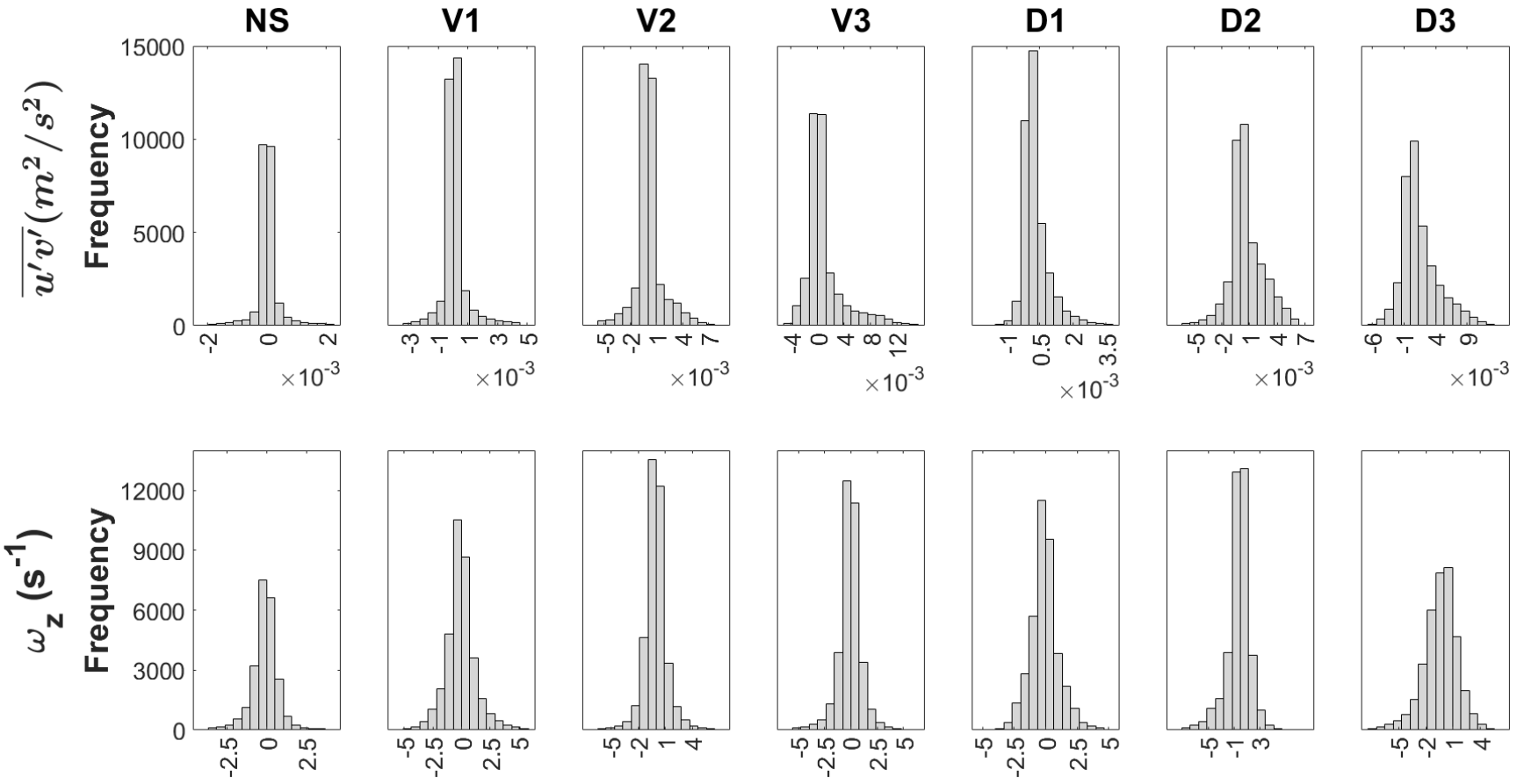

Figure 4.14. Histograms displaying the distribution of Reynolds stress ($\overline{u'v'}$) values and vorticity (ω_z) values generated in a 1.0 m long test section within a racetrack flume. Distributions are presented for a control case with no structure, three diameters of vertical structure (V1, V2, V3), and three diameters of diagonal structure (D1, D2, D3). For cases with structures, distributions shown were measured downstream of each structure, respectively. Data presented are derived from the XY plane.

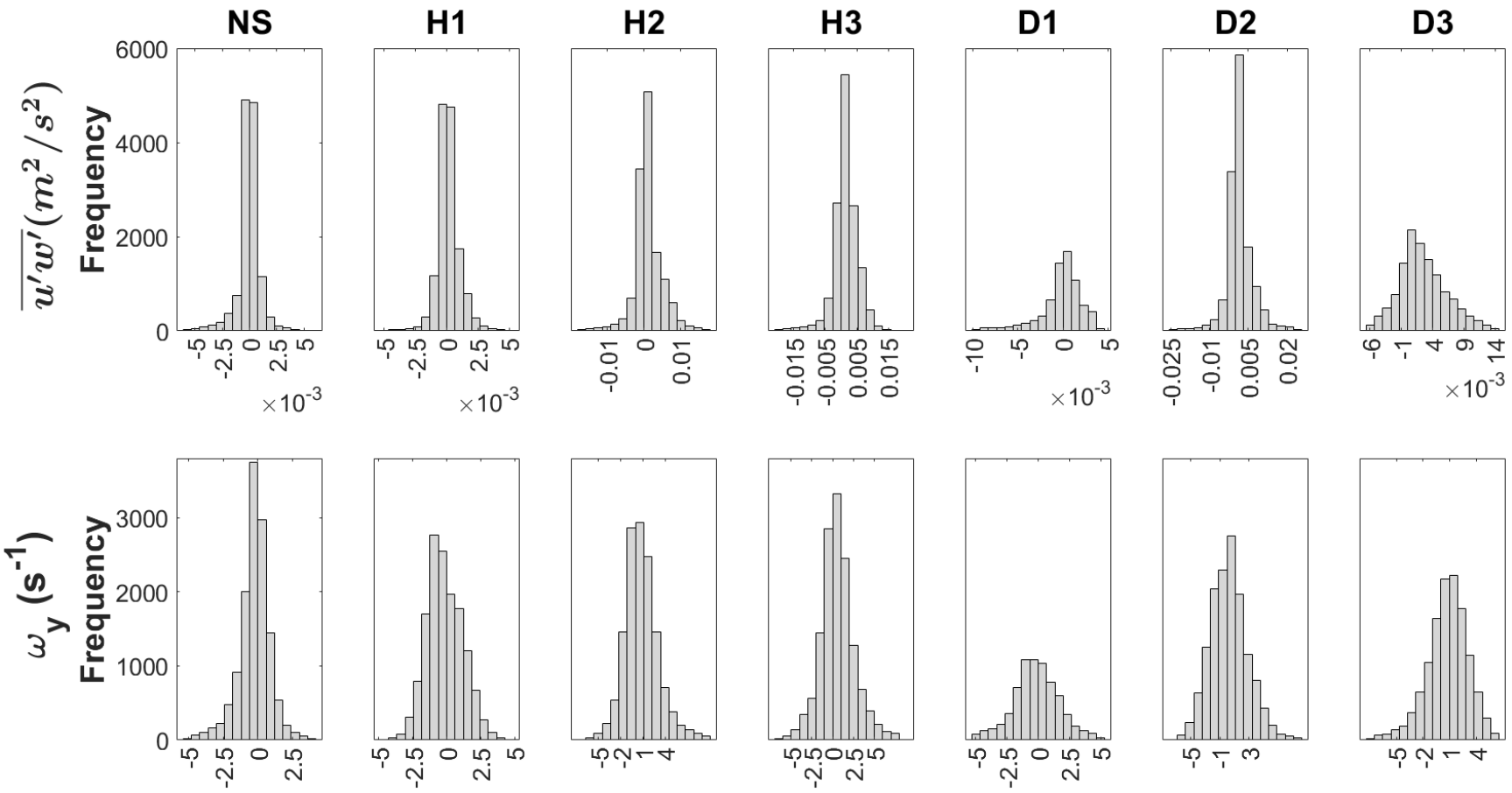

Figure 4.15. Histograms displaying the distribution of Reynolds stress ($\overline{u'w'}$) values and vorticity (ω_y) values generated in a 1.0 m long test section within a racetrack flume. Distributions are presented for a control case with no structure, three diameters of vertical structure (H1, H2, H3), and three diameters of diagonal structure (D1, D2, D3). For cases with structures, distributions shown were measured downstream of each structure, respectively. Data presented are derived from the XZ plane.

Tables

Table 4.1. Model selection process to identify the top model relating the proportion of time rainbow trout and smallmouth bass spent in the upstream portion of the test section ($Prop_{up}$), upstream of turbulence-generating structures, with structure treatment, species, and fish energy use ($\dot{M}O_2$). Fish participated in flume experiments to examine fish habitat selection in turbulent flow. Fish were tested with structures in one of three orientations (vertical, horizontal, and diagonal in the YZ plane) and one of three diameters (2.54-cm, 5.08-cm, and 7.62-cm), across three swimming velocities (1.0, 1.5, and 2.0 BL/s). The top four models with structure-related predictors and the top four models with flow-related predictors, plus the null model, are shown. The selected model is presented in the top row in bold; all models below the top model are ranked by AIC score from highest to lowest.

Model formula	AIC score	ΔAIC	Log likelihood
~ Structure + $\dot{M}O_2$ + (1|ID)	**1060**	**1**	**-512**
~ Structure + $\dot{M}O_2$ + Species + (1|ID)	1059	0	-514
~ Structure + Species + (1|ID)	1063	4	-515
~ Structure + Length + Species + (1|ID)	1065	6	-549
~ U_{Trms} + $\dot{M}O_2$ + (1|ID)	1178	118	-582
~ U_{rms} + $\dot{M}O_2$ + (1|ID)	1178	118	-582
~ TKE + $\dot{M}O_2$ + (1|ID)	1179	119	-582
~ Reynolds stress + $\dot{M}O_2$ + (1|ID)	1179	119	-582
~ 1 + (1|ID)	1187	127	-588

Table 4.2. Model selection process to identify the top model relating fish selection index (SI, CO_{cell}/CO_{max}) to flow conditions for rainbow trout participating in flume experiments to examine fish habitat selection in turbulent flow. Fish were tested with structures in one of three orientations (vertical, horizontal, and diagonal in the YZ plane) and one of three diameters (2.54-cm, 5.08-cm, and 7.62-cm), across three swimming velocities (1.0, 1.5, and 2.0 BL/s). The top four models, plus the null model, are shown. The top model is presented in the top row in bold; all models below the top model are ranked by AIC score from lowest to highest. "Vort" refers to vorticity.

Model formula	AIC score	ΔAIC	Log likelihood
~ U + Reynolds stress + Vort + (1|Plane)	**10033**	**0**	**-5009**
~ U + Reynolds stress + Vort + U_{rms} + (1|Plane)	10035	2	-5008
~ U + Reynolds stress + Vort + *T* + (1|Plane)	10035	2	-5008
~ Reynolds stress + Vort + *T* + (1|Plane)	10036	3	-5009
~ 1 + (1|Plane)	10109	76	-5049

Table 4.3. Model selection process to identify the top model relating fish selection index (SI, CO_{cell}/CO_{max}) to flow conditions for smallmouth bass participating in flume experiments to examine fish habitat selection in turbulent flow. Fish were tested with structures in one of three orientations (vertical, horizontal, and diagonal in the YZ plane) and one of three diameters (2.54-cm, 5.08-cm, and 7.62-cm), across three swimming velocities (1.0, 1.5, and 2.0 BL/s). The top four models, plus the null model, are shown. The top model is presented in the top row in bold; all models below the top model are ranked by AIC score from lowest to highest. "Vort" refers to vorticity.

Model formula	AIC score	ΔAIC	Log likelihood
~ Vort + U_{rms} + (1|Plane)	**17911**	**0**	**-8948**
~ U + Vort + U_{rms} + *T* + (1|Plane)	17913	2	-8947
~ Reynolds stress + Vort + *T* + (1|Plane)	17913	2	-8947
~ U + Reynolds stress + Vort + U_{rms} + (1|Plane)	17914	3	-8948
~ 1 + (1|Plane)	17955	44	-8972

Table 4.4. Summary of the top model relating the proportion of time spent in upstream ($Prop_{up}$) with structure treatment and fish oxygen consumption ($\dot{M}O2$, mg O_2/kg fish), estimated using a pre-existing model between $\dot{M}O2$ and fish acceleration, for rainbow trout and smallmouth bass participating in flume experiments to examine fish habitat selection in turbulent flow. The model shown was determined to best fit fish $Prop_{up}$ data through a model selection process (Table 4.1).

	Estimate	Standard error	z value	Pr(>|z|)
(Intercept)	8.55	3.74	2.29	0.02
D1	-0.87	0.59	-1.49	0.14
D2	-1.53	0.50	-3.09	< 0.01
D3	21.02	1871.72	0.01	0.99
H1	0.49	0.62	0.78	0.44
H2	-0.78	0.52	-1.49	0.14
H3	-1.74	2.36	-0.74	0.46
V1	-8.89	1.94	-4.59	< 0.01
V2	0.11	0.58	0.20	0.84
V3	-0.82	1.02	-0.81	0.42
$\dot{M}O2$	-0.04	0.02	-2.64	< 0.01

Table 4.5. Summary of the top model relating time-averaged longitudinal velocity U, Reynolds stress, and vorticity to selection index count (SI, CO_{cell}/CO_{max}) for rainbow trout participating in flume experiments to examine fish habitat selection in turbulent flow. The model shown was determined to best fit rainbow trout oxygen consumption data through a model selection process (Table 4.2).

	Estimate	Standard error	z value	Pr(>|z|)
(Intercept)	1.87	0.30	6.16	< 0.001
U	0.49	0.23	2.12	0.04
Reynolds stress	-32.0	15.68	-2.04	0.04
Vorticity	0.04	0.01	-3.09	< 0.001

Table 4.6. Summary of the top model relating vorticity and U_{rms} to selection index (SI, CO_{cell} /CO_{max}) for smallmouth bass participating in flume experiments to examine fish habitat selection in turbulent flow. The model shown was determined to best fit smallmouth bass oxygen consumption data through a model selection process (Table 4.3).

	Estimate	Standard error	z value	Pr(>|z|)
(Intercept)	1.62	0.16	10.11	< 0.001
Vorticity	-0.05	0.01	-4.94	< 0.001
U_{rms}	0.51	0.12	4.34	< 0.001

CHAPTER FIVE: GENERAL CONCLUSION AND RECOMMENDATIONS FOR FUTURE WORK

Aquatic ecosystems have been extensively modified by human activity. The resulting degradation of aquatic habitats has led to devastating declines in fish biodiversity, with freshwater-dependent species suffering disproportionately (Gleick 2003; Dudgeon et al. 2006; Vörösmarty et al. 2010). Restoration has become an increasingly popular strategy aimed at remedying the degradation of aquatic systems and reversing declines in fish biodiversity. Many restoration efforts aimed at reversing declines in fish populations in riverine systems involve placement of artificial structures in streams or adoption of management approaches that encourage the development of natural structures in streams to improve physical habitat (Thompson 2006; Palmer et al. 2014). River restoration has yielded inconsistent results, however, likely due in part to a lack of understanding of the mechanisms that guide fish interactions with natural or artificial structures. In particular, fish interactions are likely modulated by turbulence, because physical structures in flow, such as restoration structures, generate turbulence (Daniels and Rhoads 2013; Bennett et al. 2015). Turbulence may destabilize fish and increase the cost of swimming, thus requiring fish to use more energy when swimming in turbulent flows (Enders et al. 2003; Tritico and Cotel 2010; Maia et al. 2015), but some fish may be capable of exploiting turbulence and use it to reduce energy expenditure (Taguchi and Liao 2011; van der Hoop et al. 2018). Whether turbulence yields energetic benefits or costs, it is likely to affect fish habitat selection because energetics are among the primary forces driving how fish choose what habitat to occupy. Our lack of understanding regarding the interplay between fish energetics, habitat selection, and turbulence, therefore, potentially hinders our ability to implement successful restoration projects.

The overall aim of my research was to investigate this interplay between fish energetics, habitat selection, and turbulence generated by structures. I explored this across a range of spatial scales, differing levels of structural size, orientation, and complexity, and environmental contexts to potentially provide new explanatory mechanisms for fish-instream structure interactions. To achieve this aim, I completed research in three parts.

First, in Chapter Two, I conducted small-scale laboratory experiments to provide new insights regarding the close-range, local interactions between fish and turbulent flow generated by simulated instream restoration structures. I swam smallmouth bass (*Micropterus dolomieu*) implanted with rate-of-change accelerometers in an intermittent-flow respirometer with cylindrical, 2.54-cm diameter structures oriented vertically, horizontally, or diagonally to test their energy use and swimming stability. Although horizontally- and diagonally-oriented structures generate turbulence oriented in a plane that is likely to destabilize fish, I found that structures of all orientations conferred energetic and stability-related benefits to fish, relative to a control with no structure. The results from this study suggested that when fish interactions with structures occur at small spatial scales, the orientation of a structure doesn't matter- all orientations can provide fish with benefits.

In Chapter Three, I increased the scale at which I tested fish with structures and increased the complexity and variety of structures with which they were tested to produce bioenergetics models linking specific turbulence metrics with fish energetics. Using accelerometer-tagged rainbow trout (*Oncorhynchus mykiss*) and smallmouth bass, I first linked fish swimming acceleration with energy usage in an intermittent-flow respirometer, allowing me to estimate the energy use of tagged-fish beyond the spatially-limited environment of a respirometer. Large-scale laboratory studies with tagged rainbow trout and smallmouth bass were then conducted

within a racetrack flume, in which I placed structures of the same orientations as in Chapter Two, but with a range of diameters from 2.54-cm up to 7.62-cm. This allowed fish to be exposed to a greater range of turbulent flow conditions, and to have a level of freedom to choose where to swim. While energetic comparisons were not made between structures, fish energetic costs were found to vary with differing levels of turbulence. In particular, I identified that the energy usage of both species was driven by an interaction between mean longitudinal velocity and turbulent eddy size, but that the energy usage of each species was affected by a different measure of turbulence intensity.

Finally, in Chapter Four, I examined how habitat selection by rainbow trout and smallmouth bass differed during large-scale laboratory experiments within the racetrack flume, again looking at the impacts of structures in one of three orientations and one of three diameters. Specifically, I tested how fish habitat selection was driven by energy usage (as estimated in the previous study) and turbulent flow conditions. Two aspects of habitat selection were quantified: fish tendency to select habitat upstream or downstream of structures, and fish tendency to select specific locations and flow conditions when downstream of structures. Through this approach, I discovered that fish energy use was associated with habitat selection some of the time, but that fish often selected habitat that resulted in greater energetic expenses. I also found that each species selected habitat downstream of structures based on different aspects of turbulent flow.

"How does the turbulence generated by structures affect fish energy use and habitat selection?"

Based on my research, my answer to this question, though perhaps frustrating is, "it depends". Across my three studies, I discovered that fish-turbulence interactions appear to play out in markedly different ways depending on the scale at which fish interact with turbulence, on

whether fish are forced to interact with turbulence or are given the flexibility to choose to interact with it, and on whether a fish's response is measured in energetic costs or in habitat selection. In Chapter Two, fish interacting with turbulence-generating structures at close range, approximating the microhabitat range, experienced reduced energetic costs relative to fish that did not swim with structures, regardless of how a structure was oriented. This would suggest that the presence of a structure, rather than the specific aspects of the turbulence it generates, will confer energetic benefits on fish. In contrast, in Chapter Three, when fish were not forced to interact with structures at a close range, it was revealed that specific aspects of turbulence did in fact impact fish energy usage, and that the most influential aspects varied between species. The results of these two chapters, taken together, suggest that the scale of fish-turbulence interactions is an important component in determining how such interactions play out. In Chapter Four, based on these previous findings, I would have expected fish to select habitat that minimized their energetic costs. In particular, when fish swam downstream of structures, I would have expected them to select habitat based on the same aspects of turbulence that were found to influence energy use in Chapter Three. Instead, I found that a separate suite of factors drove fish habitat selection as compared to those that drove fish energy usage, and that they were, again, species-related. Therefore, I suggest that there is one overarching factor that is the most important to consider in fish-turbulence studies: context.

In using the term "context", I refer to the full range of environmental conditions, physical scales, temporal scales, fish responses, and biological settings in which and for which fish-turbulence interactions could potentially be investigated. Differences are likely to be found between studies using differing structures to generate turbulence, and between those that utilize and do not utilize structures to generate turbulence. Differences are likely to be found when fish

are tested within the physically-limited space of a respirometer versus when they are tested *in situ* in actual streams or rivers. Differences are likely to be found when fish energy use is the response of interest, versus behavior, versus kinematics, versus habitat selection.

In particular, differences are likely to be found across different biological settings. We have discovered an abundance of information regarding how turbulence affects fish energetics, how turbulence affects fish behavior, how turbulence affects fish swimming. But we still know relatively little as to how turbulence affects fish across different biological settings. How do schools of fish select habitat in turbulent flow? Are decisions guided by social dynamics, or by the mechanics of swimming within a school? Do hungry fish occupy areas of increased turbulence to increase feeding efficiency, while satiated fish refuge away from turbulent flow? Does this between predatory species and prey species? Will fish select restored habitat that generates destabilizing, energetically-costly flow conditions if such habitat provides other benefits, such as increased feeding opportunities and places to hide? Much of this remains to be seen.

The "real world" applicability of our knowledge of fish-turbulence interactions has often been limited because so much of the research has been focused on basic science, conducted within the laboratory environment. This is not necessarily problematic. Laboratory experiments, though perhaps not capable of fully replicating the conditions that fish experience *in situ*, offer many benefits over experiments conducting field-based experiments or observational studies. Laboratory experiments offer the ability to closely control the conditions in which fish are tested and obtain high-resolution measurements of both flow characteristics and fish responses. This places laboratory experiments in the unique position to be able to investigate fish-turbulence

interactions across a greater range of biological settings. Future investigations should use this ability to its fullest.

Related to this concept, I have developed many recommendations as to how we can improve our approach to investigating fish-turbulence interactions. Specific recommendations have been given within Chapters Two, Three, and Four. To reiterate, these are:

- As much as possible, future studies should set experiments in large flumes, or utilize field deployments of fish. This will allow fish unrestricted choice in position and enable tracking of fish positions, which in turn will allow for the precise evaluation of potential swimming strategies at play. Larger test environments will additionally allow for the investigation of interactions between fish and structure-generated turbulence at a larger scale.
- Future studies should utilize multiple combinations of fish body length to structure diameter ratios to allow detailed characterization of eddy size and eddy orientation and to relate these with fish responses.
- Future studies should investigate the effects of instream structures of increasing size and complexity on turbulent flow conditions and fish energetic responses.
- Future studies, whether their focus be on fish energy use or another response to turbulence, should aim to utilize a broader range of fish species and turbulent flow conditions to maximize the conclusions that can be drawn from them.
- Future work should seek to track fish movement as much as possible in order to identify the specific locations and thus flow conditions selected by fish.
- Future studies should measure a greater range of turbulence metrics from multiple categories of the IPOS framework.

- Future work examining the impact of turbulence generated by structures on fish should seek to fully characterize the flow surrounding structures in each direction and should track fish movement throughout the entire region in which structures affect flow.

I have also developed two primary recommendations not for fish-turbulence studies, but for the practical consideration of fish-turbulence interactions, and their impact on energetics and habitat selection, for river restoration:

- River restoration practitioners must consider that turbulence generated by restoration structures will affect different species of fish in different ways. Riverine species may share some level of preference for varying degrees of turbulence, but this does not necessarily manifest in selection for the same flow conditions or physical locations, and so fish of different species are unlikely to respond to restoration in the same way. If restoration is targeted at improving habitat conditions for the fish community as a whole, then this needs to be needs to be a consideration for restoration practitioners. If practitioners do not take this into consideration, an instream restoration structure may generate flow conditions that benefit certain species, while simultaneously generate flow conditions that are deleterious for other species. In turn, the species benefitted may select for habitat within and around the structure, but the species negatively impacted may select against this habitat entirely.
- River restoration practitioners must consider the multiple contexts in which and reasons for which fish may utilize turbulence generated by restoration structures. Fish rely on multiple factors in choosing what habitat to occupy. A refuging fish may seek different turbulent flow conditions from a feeding fish, while a prey fish attempting to avoid predators may seek different turbulent flow conditions from a predatory fish attempting

to acquire prey. Therefore, in order for river restoration efforts to fully utilize the altered flow characteristics downstream of instream restoration structures and in order to maximize their benefits for fish, it will likely be necessary to consider how fish will use structures.

Whether exploring the effects of turbulence on fish at different spatial scales, for different fish species, or for different fish responses, my research has made one thing abundantly clear. We cannot take a "one size fits all" approach to turbulence. It is my hope that my recommendations, when combined, will lead to future investigation that generate research with greater relevance to the conditions and settings fish experience in the wild, that in turn will have beneficial applications for the conservation, restoration, and management of fish habitats, and, in turn, lead to a brighter future for our fish.

REFERENCES

Abbe, T., and Brooks, A. 2011. Geomorphic, engineering, and ecological considerations when using wood in river restoration. *In* Geophysical Monograph Series. pp. 419–451. doi:10.1029/2010GM001004.

Adams, N.S., Rondorf, D.W., Evans, S.D., Kelly, J.E., and Perry, R.W. 1998. Effects of surgically and gastrically implanted radio transmitters on growth and feeding behavior of juvenile Chinook Salmon. Can. J. Fish. Aquat. Sci. **127**(1): 128–136. doi:10.1577/1548-8659(1998)127<0128:EOSAGI>2.0.CO;2.

Aho, K., Derryberry, D., and Peterson, T. 2014. Model selection for ecologists : the worldviews of AIC and BIC Author (s): Ken Aho , DeWayne Derryberry and Teri Peterson Stable URL : http://www.jstor.org/stable/43495189 Model selection for ecologi. Ecology **95**(3): 631–636. Available from http://www.esajournals.org/doi/full/10.1890/13-1452.1.

Akobeng, A.K. 2016. Understanding type i and type II errors, statistical power and sample size. Acta Paediatr. Int. J. Paediatr. **105**(6): 605–609. doi:10.1111/apa.13384.

Angermeier, P.L., and Karr, J.R. 1984. Relationships between woody debris and fish habitat in a small warmwater stream. Trans. Am. Fish. Soc. **113**: 716–726. doi:10.1577/1548-8659(1984)113<716.

Antón, A., Elosegi, A., García-Arberas, L., Díez, J., and Rallo, A. 2011. Restoration of dead wood in Basque stream channels: Effects on brown trout population. Ecol. Freshw. Fish **20**(3): 461–471. doi:10.1111/j.1600-0633.2010.00482.x.

Baguley, T. 2004. Understanding statistical power in the context of applied research. Appl. Ergon. **35**(2): 73–80. doi:10.1016/j.apergo.2004.01.002.

Bates, D., Mächler, M., Bolker, B.M., and Walker, S. 2015. Fitting Linear Mixed-Effects Models Using {lme4}. J. Stat. Softw. **67**(1): 1–48. doi:10.18637/jss.v067.i01.

Beal, D.N., Hover, F.S., Triantafyllou, M.S., Liao, J.C., and Lauder, G. V. 2006. Passive propulsion in vortex wakes. J. Fluid Mech. **549**: 385–402. doi:10.1017/S0022112005007925.

Beamish, F.W.H. 1970. Oxygen consumption of largemouth bass, *Micropterus salmoides*, in relation to swimming speed and temperature. Can. J. Zool. **48**: 1221–1228.

Beamish, F.W.H. 1978. Swimming capacity. *In* Fish Physiology. ACADEMIC PRESS, INC. doi:10.1016/S1546-5098(08)60164-8.

Beechie, T., Imaki, H., Green, J., Wade, A., Wu, H., Pess, G., Roni, P., Kimball, J., Stanford, J., Kiffney, P., and Mantua, N. 2013. Restoring salmon habitat for a changing climate. River Res. Appl. **29**: 939–960. doi:10.1002/rra.

Beechie, T.J., Sear, D.A., Olden, J.D., Pess, G.R., Buffington, J.M., Moir, H., Roni, P., and Pollock, M.M. 2010. Process-based principles for restoring river ecosystems. Bioscience **60**(3): 209–222. doi:10.1525/bio.2010.60.3.7.

Beitinger, T.L., and Lutterschmidt, W.I. 2011. Temperature | Measures of Thermal Tolerance. *In* Encyclopedia of Fish Physiology. Elsevier Inc. doi:10.1016/B978-0-12-374553-8.00200-8.

Bennett, S.J., Ghaneeizad, S.M., Gallisdorfer, M.S., Cai, D., Atkinson, J.F., Simon, A., and Langendoen, E.J. 2015. Flow, turbulence, and drag associated with engineered log jams in a fixed-bed experimental channel. Geomorphology **248**: 172–184. Elsevier B.V. doi:10.1016/j.geomorph.2015.07.046.

Bernhardt, E., Palmer, M.A., Allan, J.D., Alexander, G., Barnas, K., Brooks, S., Carr, J., Clayton, S., Dahm, C., Galat, D., Gloss, S., Goodwin, P., Hart, D., Hassett, B., Jenkinson, R., Katz, S., Kondolf, G.M., Lake, P.S., Lave, R., Meyer, J.L., Donnell, T.K.O., Pagano, L., Powell, B., and Sudduth, E. 2005. Synthesizing U.S. river restoration efforts. Science (80-.). **308**(April): 636–637. doi:10.1126/science.1104258.

Bernhardt, E.S., and Palmer, M.A. 2007. Restoring streams in an urbanizing world. Freshw. Biol. **52**(4): 738–751. doi:10.1111/j.1365-2427.2006.01718.x.

Bernhardt, E.S., Sudduth, E.B., Palmer, M.A., Allan, J.D., Meyer, J.L., Alexander, G.G., Follastad-Shah, J., Hassett, B., Jenkinson, R., Lave, R., Rumps, J., and Pagano, L. 2007. Restoring rivers one reach at a time: results from a survey of U.S. river restoration practitioners. Restor. Ecol. **15**(3): 482–493. doi:10.1111/j.1526-100X.2007.00244.x.

Beyene, K.M., and Bekele, S.A. 2016. Assessing univariate and multivariate homogeneity of variance: a guide for practitioners. Math. Theory Model. **6**(2): 26–33. Available from www.iiste.org/Journals/index.php/MTM/article/download/28571/29333.

Blake, R.W. 2004. Fish functional design and swimming performance. J. Fish Biol. **65**(5): 1193 1222. doi:10.1111/j.0022-1112.2004.00568.x.

Bleckmann, H., Przybilla, A., Klein, A., Schmitz, A., Kunze, S., and Brucker, C. 2012. Station Holding of Trout: Behavior, Physiology and Hydrodynamics. *In* Nature-Inspired Fluid Mechanics. pp. 161–178.

Boavida, I., Santos, J.M., Cortes, R. V., Pinheiro, A.N., and Ferreira, M.T. 2011. Assessment of instream structures for habitat improvement for two critically endangered fish species. Aquat. Ecol. **45**(1): 113–124. doi:10.1007/s10452-010-9340-x.

Bolker, B.M., Brooks, M.E., Clark, C.J., Geange, S.W., Poulsen, J.R., Stevens, M.H.H., and White, J.-S.S. 2008. Generalized linear mixed models: a practical guide for ecology and evolution. Trends Ecol. Evol. **24**: 127–135.

Bouyoucos, I.A., Montgomery, D.W., Brownscombe, J.W., Cooke, S.J., Suski, C.D., Mandelman, J.W., and Brooks, E.J. 2017. Swimming speeds and metabolic rates of semi-captive juvenile lemon sharks (*Negaprion brevirostris*, Poey) estimated with acceleration biologgers. J. Exp. Mar. Bio. Ecol. **486**: 245–254. Elsevier B.V. doi:10.1016/j.jembe.2016.10.019.

Brandt, S.B., and Hartman, K.J. 1993. Innovative Approaches with Bioenergetics Models : Future Applications to Fish Ecology and Management Innovative Approaches with Bioenergetics Models : Future Applications to Fish Ecology and Management. Trans. Am. Fish. Soc. **122**: 731–735. doi:10.1577/1548-8659(1993)122<0731.

Brooks, M.E., Kristensen, K., van Benthem, K.J., Magnusson, A., Berg, C.W., Nielsen, A., Skaug, H.J., Maechler, M., and Bolker, B.M. 2017. {glmmTMB} balances speed and flexibility among packages for zero-inflated generalized linear mixed modeling. R J. **9**(2): 378–400. Available from https://journal.r-project.org/archive/2017/RJ-2017-066/index.html.

Brown, R.S., Cooke, S.J., Anderson, W.G., and McKinley, R.S. 2004. Evidence to challenge the "2% rule" for biotelemetry. North Am. J. Fish. Manag. **19**(3): 867–871. doi:10.1577/1548-8675(1999)019<0867:etctrf>2.0.co;2.

Brownscombe, J.W., Cooke, S.J., Algera, D.A., Hanson, K.C., Eliason, E.J., Burnett, N.J., Danylchuk, A.J., Hinch, S.G., and Farrell, A.P. 2017. Ecology of exercise in wild fish: Integrating concepts of individual physiological capacity, behavior, and fitness through diverse case studies. Integr. Comp. Biol. **57**(2): 281–292. doi:10.1093/icb/icx012.

Brownscombe, J.W., Lennox, R.J., Danylchuk, A.J., and Cooke, S.J. 2018. Estimating fish swimming metrics and metabolic rates with accelerometers: the influence of sampling frequency. J. Fish Biol. **93**(2): 207–214. doi:10.1111/jfb.13652.

Bureau, D.P., Kaushik, S.J., and Cho, C.Y. 2002. Bioenergetics. *In* Fish Nutrition. pp. 1–59. doi:10.5005/jp/books/11965_2.

Burnham, K.P., and Anderson, D.R. 2002. Model Selection and Inference: A Practical Information-Theoretic Approach. *In* The Journal of Wildlife Management. doi:10.2307/3803117.

Burnham, K.P., Anderson, D.R., and Huyvaert, K.P. 2011. AIC model selection and multimodel inference in behavioral ecology: Some background, observations, and comparisons. Behav. Ecol. Sociobiol. **65**(1): 23–35. doi:10.1007/s00265-010-1029-6.

Chagnaud, B.P., Bleckmann, H., and Hofmann, M.H. 2007. Kármán vortex street detection by the lateral line. J. Comp. Physiol. A Neuroethol. Sensory, Neural, Behav. Physiol. **193**(7): 753–763. doi:10.1007/s00359-007-0230-1.

Clarke, A., and Johnston, N.M. 1999. Scaling of metabolic rate with body mass and in teleost temperature fish. J. Anim. Ecol. **68**(5): 893–905.

Cook, C.L., and Coughlin, D.J. 2010. Rainbow trout *Oncorhynchus mykiss* consume less energy when swimming near obstructions. J. Fish Biol. **77**(7): 1716–1723. doi:10.1111/j.1095-8649.2010.02801.x.

Cooke, S.J., Kassler, T.W., and Philipp, D.P. 2001. Physiological performance of largemouth bass related to local adaptation and interstock hybridization: Implications for conservation and management. J. Fish Biol. **59**(SUPPL. A): 248–268. doi:10.1006/jfbi.2001.1767.

Cooke, S.J., Woodley, C.M., Eppard, M.B., Brown, R.S., and Nielsen, J.L. 2011. Advancing the surgical implantation of electronic tags in fish: a gap analysis and research agenda based on a review of trends in intracoelomic tagging effects studies. Rev. Fish Biol. Fish. **21**: 127–151. doi:10.1007/s11160-010-9193-3.

Cotel, A.J., and Webb, P.W. 2015. Living in a turbulent world - A new conceptual framework for the interactions of fish and eddies. Integr. Comp. Biol. **55**(4): 662–672. doi:10.1093/icb/icv085.

Coughlin, D.J. 2002. Aerobic muscle function during steady swimming in fish. Fish Fish. **3**(2): 63–78. doi:10.1046/j.1467-2979.2002.00069.x.

Craig, J.K., and Crowder, L.. 2002. Factors influencing habitat selection in fishes with a review of marsh. *In* Concepts and Controversies in Tidal Marsh Ecology. Kluwer Academic Publishers. pp. 241–266.

Crawley, M.J. 2013. The R Book. *In* 2nd edition. Wiley Publishing, Chichester. doi:10.1016/0025-5408(96)80018-3.

Crowder, M.J. 1978. Beta-binomial Anova for proportions. J. R. Stat. Soc. Ser. C (Applied Stat. **27**: 34–37.

Cruz-Font, L., Shuter, B.J., and Blanchfield, P.J. 2016. Energetic costs of activity in wild Lake Trout: a calibration study using acceleration transmitters and positional telemetry. Can. J. Fish. Aquat. Sci. **73**(8): 1237–1250.

Currie, R.J., Bennett, W.A., and Beitinger, T.L. 1998. Critical thermal minima and maxima of three freshwater game-fish species acclimated to constant temperatures. Environ. Biol. Fishes **51**(2): 187–200. doi:10.1023/A:1007447417546.

Daniels, M.D., and Rhoads, B.L. 2013. Spatial pattern of turbulence kinetic energy and shear stress in a meander bend with large woody debris. Riparian Veg. Fluv. Geomorphol.: 87–97. doi:10.1029/008WSA07.

Darwall, W.R.T., and Freyhof, J. 2016. Lost fishes, who is counting? The extent of the threat to freshwater fish biodiversity. *In* Conservation of Freshwater Fishes. *Edited by* G.P. Gloss, M. Krkosek, and J.D. Olden. Cambridge University Press, Cambridge.

Deng, Z., Guensch, G.R., McKinstry, C.A., Mueller, R.P., Dauble, D.D., and Richmond, M.C. 2005. Evaluation of fish-injury mechanisms during exposure to turbulent shear flow. Can. J. Fish. Aquat. Sci. **62**(7): 1513–1522. doi:10.1139/f05-091.

Downs, P.W., and Kondolf, G.M. 2002. Post-project appraisals in adaptive management of river channel restoration. Environ. Manage. **29**(4): 477–496. doi:10.1007/s00267-001-0035-X.

Drucker, E.G., and Lauder, G. V. 2000. A hydrodynamic analysis of fish swimming speed: Wake structure and locomotor force in slow and fast labriform swimmers. J. Exp. Biol. **203**(16): 2379–2393. doi:10.1242/jeb.203.16.2379.

Drucker, E.G., and Lauder, G. V. 1999. Measuring the forces. **2412**: 2393–2412.

Dudgeon, D. 2010. Prospects for sustaining freshwater biodiversity in the 21st century: Linking ecosystem structure and function. Curr. Opin. Environ. Sustain. **2**(5–6): 422–430. Elsevier B.V. doi:10.1016/j.cosust.2010.09.001.

Dudgeon, D. 2019. Multiple threats imperil freshwater biodiversity in the Anthropocene. Curr. Biol. **29**(19): R960–R967. Elsevier. doi:10.1016/j.cub.2019.08.002.

Dudgeon, D., Arthington, A.H., Gessner, M.O., Kawabata, Z.-I., Knowler, D.J., Lévêque, C., Naiman, R.J., Prieur-Richard, A., Soto, D., Stiassny, M.L.J., and Sullivan, C.A. 2006. Freshwater biodiversity: importance, threats, status and conservation challenges. Biol. Rev. **81**: 163–182. doi:10.1017/S1464793105006950.

Eaton, J.G., and Scheller, R.M. 1996. Effects of climate warming on fish thermal habitat in streams of the United States. Limnol. Oceanogr. **41**(5): 1109–1115.

Enders, E.C., and Boisclair, D. 2016. Effects of environmental fluctuations on fish metabolism: Atlantic salmon *Salmo salar* as a case study. J. Fish Biol. **88**(1): 344–358. doi:10.1111/jfb.12786.

Enders, E.C., Boisclair, D., and Roy, A.G. 2003. The effect of turbulence on the cost of swimming for juvenile Atlantic salmon (*Salmo salar*). Can. J. Fish. Aquat. Sci. **60**(9): 1149–1160. doi:10.1139/f03-101.

Enders, E.C., Boisclair, D., and Roy, A.G. 2005a. A model of total swimming costs in turbulent flow for juvenile Atlantic salmon (Salmo salar). Can. J. Fish. Aquat. Sci. **62**(5): 1079–1089. doi:10.1139/f05-007.

Enders, E.C., Buffin-Bélanger, T., Boisclair, D., and Roy, A.G. 2005b. The feeding behaviour of juvenile Atlantic salmon in relation to turbulent flow. J. Fish Biol. **66**(1): 242–253. doi:10.1111/j.0022-1112.2005.00599.x.

Ennis, D.M., and Bi, J. 1998. The beta-binomial model: accounting for inter-trial variation in replicated difference and preference tests. J. Sens. Stud. **13**(4): 389–412. doi:10.1111/j.1745-459X.1998.tb00097.x.

Farrell, A.P., Johansen, J.A., and Suarez, R.K. 1991. Effects of exercise-training on cardiac performance and muscle enzymes in rainbow trout, Oncorhynchus mykiss. Fish Physiol. Biochem. **9**(4): 303–312. doi:10.1007/BF02265151.

Fausch, K.D. 1993. Experimental analysis of microhabitat selection by juvenile steelhead (*Oncorhynchus mykiss*) and coho salmon (*O. kisutch*) in a British Columbia stream. Can. J. Fish. Aquat. Sci. **50**: 1198–1207.

Fausch, K.D., Karr, J.R., and Yant, P.R. 1984. Regional application of an index of biotic integrity based on stream fish communities. Trans. Am. Fish. Soc. **113**(1): 39–55. doi:10.1577/1548-8659(1984)113<39:raoaio>2.0.co;2.

Fligner, M.A., and Killeen, T.J. 1976. Distribution-free two-sample tests for scale. J. Am. Stat. Assoc. **71**(353): 210–213. doi:10.1080/01621459.1976.10481517.

Fox, J., and Weisberg, S. 2019. An {R} Companion to Applied Regression. *In* Third. Sage, Thousand Oaks {CA}. Available from https://socialsciences.mcmaster.ca/jfox/Books/Companion/.

Fretwell, S.D., and Lucas, H.. 1970. On territorial behavior and other factors influencing habitat distribution in birds. Acta Biotheor. **19**: 16–36.

Gilvear, D.J., Spray, C.J., and Casas-Mulet, R. 2013. River rehabilitation for the delivery of multiple ecosystem services at the river network scale. J. Environ. Manage. **126**: 30–43. Elsevier Ltd. doi:10.1016/j.jenvman.2013.03.026.

Gleick, P.H. 2003. Global freshwater resources: soft-path solutions for the 21st century. Science (80-.). **302**(5650): 1524–1528. doi:10.1126/science.1089967.

Gosline, W.A. 1971. Functional Morphology and Classification of Teleostean Fishes. University of Hawaii Press, Honolulu.

Hansen, E.S., and Budy, P. 2011. The potential of passive stream restoration to improve stream habitat and minimize the impact of fish disease: A short-term assessment. J. North Am. Benthol. Soc. **30**(2): 573–588. doi:10.1899/10-018.1.

Hansen, M.J., Boisclair, D., Brandt, S.B., Hewett, S.W., Kitchell, J.F., Lucas, M.C., and Ney, J.J. 1993. Applications of Bioenergetics Models to Fish Ecology and Management: Where Do We Go from Here? Trans. Am. Fish. Soc. **122**(5): 1019–1030. doi:10.1577/1548-8659(1993)122<1019:aobmtf>2.3.co;2.

Harms, C.A. 2005. Surgery in fish research: common procedures and postoperative care. Lab Anim. (NY). **34**(1): 28–34. doi:96.

Hartig, F. 2019. DHARMa: Residual Diagnostics for Hierarchical (Multi-Level / Mixed) Regression Models. Available from https://cran.r-project.org/package=DHARMa.

Harvey, S.T., Muhawenimana, V., Müller, S., Wilson, C.A.M.E., and Denissenko, P. 2022. An inertial mechanism behind dynamic station holding by fish swinging in a vortex street. Sci. Rep. **12**(1): 12660. Nature Publishing Group UK. doi:10.1038/s41598-022-16181-8.

Hayes, J.W., Hughes, N.F., and Kelly, L.H. 2007. Process-based modelling of invertebrate drift transport, net energy intake and reach carrying capacity for drift-feeding salmonids. Ecol. Modell. **207**(2–4): 171–188. doi:10.1016/j.ecolmodel.2007.04.032.

Hill, J., and Grossman, G.D. 1993. An energetic model of microhabitat use for rainbow trout and rosyside dace. Ecology **74**(3): 685–698. doi:10.2307/1940796.

Hockley, F.A., Wilson, C.A.M.E., Brew, A., and Cable, J. 2014. Fish responses to flow velocity and turbulence in relation to size, sex and parasite load. J. R. Soc. Interface **11**(91). doi:10.1098/rsif.2013.0814.

Hocutt, C.H. 1973. Swimming performance of three warmwater fishes exposed to a rapid temperature change. Chesap. Sci. **14**(1): 11–16. doi:10.2307/1350698.

Hofmann, G.E., and Todgham, A.E. 2010. Living in the Now: Physiological Mechanisms to Tolerate a Rapidly Changing Environment. Annu. Rev. Physiol. **72**(1): 127–145. doi:10.1146/annurev-physiol-021909-135900.

van der Hoop, J.M., Byron, M.L., Ozolina, K., Miller, D.L., Johansen, J.L., Domenici, P., and Steffensen, J.F. 2018. Turbulent flow reduces oxygen consumption in the labriform swimming shiner perch, *Cymatogaster aggregata*. J. Exp. Biol. **221**(11). doi:10.1242/jeb.168773.

Hrodey, P.J., and Sutton, T.M. 2008. Fish community responses to half-log additions in warmwater streams. North Am. J. Fish. Manag. **28**(1): 70–80. doi:10.1577/m06-168.1.

Jaeger, B. 2017. r2glmm: Computers R Squared for Mixed (Multilevel) Models. Avaiable from https://CRAN.R-project.org/package=r2glmm.

Jähnig, S.C., Lorenz, A.W., Hering, D., Antons, C., Sundermann, A., Jedicke, E., and Haase, P. 2011. River restoration success: A question of perception. Ecol. Appl. **21**(6): 2007–2015. doi:10.1890/10-0618.1.

Jeffrey, J.D., Hasler, C.T., Chapman, J.M., Cooke, S.J., and Suski, C.D. 2015. Linking landscape-scale disturbances to stress and condition of fish: Implications for restoration and conservation. Integr. Comp. Biol. **55**(4): 618–630. doi:10.1093/icb/icv022.

Jelks, H.L., Walsh, S.J., Burkhead, N.M., Contreras-Balderas, S., Diaz-Pardo, E., Hendrickson, D.A., Lyons, J., Mandrak, N.E., McCormick, F., Nelson, J.S., Platania, S.P., Porter, B.A., Renaud, C.B., Schmitter-Soto, J.J., Taylor, E.B., and Warren, M.L. 2008a. Conservation status of imperiled North American freshwater and diadromous fishes. Fisheries **33**(8): 372–407. doi:10.1577/1548-8446-33.8.372.

Johansen, J.L., Akanyeti, O., and Liao, J.C. 2020. Oxygen consumption of drift-feeding rainbow trout: The energetic tradeoff between locomotion and feeding in flow. J. Exp. Biol. **223**(12). doi:10.1242/jeb.220962.

Johnston, I.A., and Dunn, J. 1987. Temperature acclimation and metabolism in ectotherms with particular reference to teleost fish. Symp. Soc. Exp. Biol. **41**: 67–93. Available from http://www.ncbi.nlm.nih.gov/pubmed/3332497.

Kail, J., Brabec, K., Poppe, M., and Januschke, K. 2015. The effect of river restoration on fish, macroinvertebrates and aquatic macrophytes: A meta-analysis. Ecol. Indic. **58**: 311–321. Elsevier Ltd. doi:10.1016/j.ecolind.2015.06.011.

Ke, S., Tu, Z., Goerig, E., Tan, J., Cheng, B., Li, Z., and Shi, X. 2022. Swimming behaviour of silver carp (Hypophthalmichthys molitrix) in response to turbulent flow induced by a D-cylinder. J. Fish Biol. **100**(2): 486–497. doi:10.1111/jfb.14958.

Kendall, J.L., Lucey, K.S., Jones, E.A., Wang, J., and Ellerby, D.J. 2007. Mechanical and energetic factors underlying gait transitions in bluegill sunfish (Lepomis macrochirus). J. Exp. Biol. **210**(24): 4265–4271. doi:10.1242/jeb.009498.

Kern, P., Cramp, R.L., Gordos, M.A., Watson, J.R., and Franklin, C.E. 2018. Measuring U crit and endurance: equipment choice influences estimates of fish swimming performance. J. Fish Biol. **92**(1): 237–247. doi:10.1111/jfb.13514.

Kiflawi, M., and Genin, H.. 1997. Prey flux manipulation and the feeding rates of reef-dwelling planktivorous fish. Ecology **78**(4): 1062–1077. doi:10.1890/0012-9658(1997)078[1062:PFMATF]2.0.CO;2.

Killen, S.S., Marras, S., Steffensen, J.F., and Mckenzie, D.J. 2012. Aerobic capacity influences the spatial position of individuals within fish schools. Proc. R. Soc. B Biol. Sci. **279**(1727): 357–364. doi:10.1098/rspb.2011.1006.

Kitchell, J.F., Stewart, D.J., and Weininger, D. 1977. Applications of a bioenergetics model to yellow perch (Perca flavescens) and walleye (Stizostedion vitreum vitreum). J. Fish. Res. Board Canada **34**: 1922–1935.

Kolok, A.S. 1991. Photoperiod alters the critical swimming speed of juvenile largemouth bass, *Micropterus salmoides*, acclimated to cold water. Copeia **1991**(4): 1085–1090.

Lacey, R.W.J., and Millar, R.G. 2004. Reach scale hydraulic assessment of instream salmonid habitat restoration. J. Am. Water Resour. Assoc. **40**(6): 1631–1644. doi:10.1111/j.1752-1688.2004.tb01611.x.

Lacey, R.W.J., Neary, V.S., Liao, J.C., Enders, E.C., and Tritico, H.M. 2012. The IPOS framework: linking fish swimming performance in altered flows from laboratory experiments to rivers. River Res. Appl. **28**: 429–443. doi:10.1002/rra.

Laird, N.M., and Ware, J.H. 1982. Random-effects models for longitudinal data. Biometrics **38**(4): 963–974.

Lauder, G. V., and Drucker, E.G. 2002. Forces, fishes, and fluids: Hydrodynamic mechanisms of aquatic locomotion. News Physiol. Sci. **17**(6): 235–240. doi:10.1152/nips.01398.2002.

Leman, A., Holland, M., and Tinoco, R.O. 2018. Identifying the dominant physical processes for mixing in full-scale raceway tanks. Renew. Energy **129**: 616–628. Elsevier Ltd. doi:10.1016/j.renene.2018.05.087.

Lenth, R. 2019. emmeans: Estimated Marginal Means, aka Least-Squares Means. Available from https://cran.r-project.org/package=emmeans.

Lepori, F., Palm, D., Brännäs, E., and Malmqvist, B. 2005. Does restoration of structural heterogeneity in streams enahnce fish and macroinvertebrate diversity? Ecol. Appl. **15**(6): 2060–2071.

Lewis, D.M., and Pedley, T.J. 2001. The influence of turbulence on plankton predation strategies. J. Theor. Biol. **210**(3): 347–365. doi:10.1006/jtbi.2001.2310.

Liao, J.C. 2003. The Karman gait: novel body kinematics of rainbow trout swimming in a vortex street. J. Exp. Biol. **206**(6): 1059–1073. doi:10.1242/jeb.00209.

Liao, J.C. 2004. Neuromuscular control of trout swimming in a vortex street: implications for energy economy during the Karman gait. J. Exp. Biol. **207**(20): 3495–3506. doi:10.1242/jeb.01125.

Liao, J.C. 2007. A review of fish swimming mechanics and behaviour in altered flows. Philos. Trans. R. Soc. B Biol. Sci. **362**(1487): 1973–1993. doi:10.1098/rstb.2007.2082.

Liao, J.C., and Akanyeti, O. 2017. Fish swimming in a kármán vortex street: Kinematics, sensory biology and energetics. Mar. Technol. Soc. J. **51**(5): 48–55. doi:10.4031/MTSJ.51.5.8.

Liao, J.C., Beal, D.N., Lauder, G. V, and Triantafyllou, M.S. 2003. Fish exploiting vortices decrease muscle activity. Science (80-.). **302**(2003): 1566–1569. doi:10.1126/science.1088295.

Lindén, A., and Mäntyniemi, S. 2011. Using the negative binomial distribution to model overdispersion in ecological count data. Ecology **92**(7): 1414–1421. doi:10.1890/10-1831.1.

Lindstrom, M.J., and Bates, D.M. 1990. Nonlinear mixed effects models for repeated measures data. Biometrics **46**(3): 673–687.

Lobb, M.D., and Orth, D.J. 1991. Habitat Use by an Assemblage of Fish in a Large Warmwater Stream. Trans. Am. Fish. Soc. **120**(1): 65–78. doi:10.1577/1548-8659(1991)120<0065:hubaao>2.3.co;2.

Louhi, P., Vehanen, T., Huusko, A., Mäki-Petäys, A., and Muotka, T. 2016. Long-term monitoring reveals the success of salmonid habitat restoration. Can. J. Fish. Aquat. Sci. **73**(12): 1733–1741. doi:10.1139/cjfas-2015-0546.

Lüdecke, D. 2019. sjstats: Statistical Functions for Regression Models (Version 0.17.5). doi:10.5281/zenodo.1284472.

Lupandin, A.I. 2005. Effect of flow turbulence on swimming speed of fish. Biol. Bull. **32**(5): 461–466. doi:10.1007/s10525-005-0125-z.

MacKenzie, B.R., and Kiørboe, T. 1995. Encounter rates and swimming behavior of pause-travel and cruise larval fish predators in calm and turbulent laboratory environments. Limnol. Oceanogr. **40**(7): 1278–1289. doi:10.4319/lo.1995.40.7.1278.

Maia, A., Sheltzer, A.P., and Tytell, E.D. 2015. Streamwise vortices destabilize swimming bluegill sunfish (*Lepomis macrochirus*). J. Exp. Biol. **218**(5): 786–792. doi:10.1242/jeb.114363.

Manners, R.B., and Doyle, M.W. 2008. A mechanistic model of woody debris jam evolution and its application to wood-based restoration and management. River Res. Appl. **24**: 1104–1123. doi:10.1002/rra.

Matthews, K.R., and Berg, N.H. 1997. Rainbow trout responsed to water temperature and dissolved oxygen stress in two southern California stream pools. J. Fish Biol. **50**(1): 50–67. doi:10.1006/jfbi.1996.0274.

Mayor, S.J., Schneider, D.C., Schaefer, J.A., and Mahoney, S.P. 2009. Habitat selection at multiple scales. Ecoscience **16**(2): 238–247. doi:10.2980/16-2-3238.

McClendon, D.D., and Rabeni, C.F. 1987. Physical and biological variables useful for predicting population characteristics of smallmouth bass and rock bass in an Ozark stream. North Am. J. Fish. Manag. **7**(1): 46–56. doi:10.1577/1548-8659(1987)7<46:pabvuf>2.0.co;2.

McMahon, T.E., and Hartman, G.F. 1989. Influence of cover complexity and current velocity on winter habitat use by juvenile coho salmon (Oncorhynchus kisutch). Can. J. Fish. Aquat. Sci. **46**: 1551–1557.

Metcalfe, J.D., Wright, S., Tudorache, C., and Wilson, R.P. 2016. Recent advances in telemetry for estimating the energy metabolism of wild fishes. J. Fish Biol. **88**(1): 284–297. doi:10.1111/jfb.12804.

Meuser, A. V., Pyne, C.B., and Mandeville, E.G. 2022. Limited evidence of a genetic basis for sex determination in the common creek chub, Semotilus atromaculatus. J. Evol. Biol. (August 2021): 1–11. doi:10.1111/jeb.14006.

Miller, J.R., and Hobbs, R.J. 2016. Habitat restoration — Do we know what we're doing? Restor. Ecol. **15**(2): 382–390.

Miller, J.R., and Kochel, R.C. 2010. Assessment of channel dynamics, in-stream structures and post-project channel adjustments in North Carolina and its implications to effective stream restoration. Environ. Earth Sci. **59**: 1681–1692. doi:10.1007/s12665-009-0150-1.

Milligan, C.L. 1996. Metabolic recovery from exhaustive exercise in rainbow trout. Comp. Biochem. Physiol. - A Physiol. **113**(1): 51–60. doi:10.1016/0300-9629(95)02060-8.

Minke-Martin, V., Hinch, S.G., Braun, D.C., Burnett, N.J., Casselman, M.T., Eliason, E.J., and Middleton, C.T. 2018. Physiological condition and migratory experience affect fitness-related outcomes in adult female sockeye salmon. Ecol. Freshw. Fish **27**(1): 296–309. doi:10.1111/eff.12347.

Mittelbach, G.G. 2002. Fish Foraging and Habitat Choice: A Theoretical Perspective. *In* Handbook of Fish Biology and Fisheries, Volume 1. doi:10.1002/9780470693803.ch11.

Moerke, A.H., and Lamberti, G.A. 2003. Responses in fish community structure to restoration of two Indiana streams. North Am. J. Fish. Manag. **23**(3): 748–759. doi:10.1577/m02-012.

Morin, K., and Davis, J.L. 2017. Cross-validation: What is it and how is it used in regression? Commun. Stat. - Theory Methods **46**(11): 5238–5251. Taylor & Francis. doi:10.1080/03610926.2015.1099672.

Mouton, A.M., Schneider, M., Depestele, J., Goethals, P.L.M., and De Pauw, N. 2007. Fish habitat modelling as a tool for river management. Ecol. Eng. **29**(3): 305–315. doi:10.1016/j.ecoleng.2006.11.002.

Murchie, K.J., Cooke, S.J., Danylchuk, A.J., and Suski, C.D. 2011. Estimates of field activity and metabolic rates of bonefish (Albula vulpes) in coastal marine habitats using acoustic tri-axial accelerometer transmitters and intermittent-flow respirometry. J. Exp. Mar. Bio. Ecol. **396**(2): 147–155. Elsevier B.V. doi:10.1016/j.jembe.2010.10.019.

Nagayama, S., and Nakamura, F. 2010. Fish habitat rehabilitation using wood in the world. Landsc. Ecol. Eng. **6**(2): 289–305. doi:10.1007/s11355-009-0092-5.

Nakagawa, S., and Schielzeth, H. 2013. A general and simple method for obtaining R2 from generalized linear mixed-effects models. Methods Ecol. Evol. **4**(2): 133–142. doi:10.1111/j.2041-210x.2012.00261.x.

Naman, S.M., Rosenfeld, J.S., Neuswanger, J.R., Enders, E.C., and Eaton, B.C. 2019. Comparing correlative and bioenergetics-based habitat suitability models for drift-feeding fishes. Freshw. Biol. **64**(9): 1613–1626. doi:10.1111/fwb.13358.

Nelson, J.A. 2016. Oxygen consumption rate v. rate of energy utilization of fishes: A comparison and brief history of the two measurements. J. Fish Biol. **88**(1): 10–25. doi:10.1111/jfb.12824.

Ohlberger, J., Staaks, G., and Hölker, F. 2006. Swimming efficiency and the influence of morphology on swimming costs in fishes. J. Comp. Physiol. B Biochem. Syst. Environ. Physiol. **176**(1): 17–25. doi:10.1007/s00360-005-0024-0.

Orth, D.J., and Newcomb, T.J. 2002. Certainties and uncertainties in defining essential habitats for riverine smallmouth bass. Am. Fish. Soc. Symp. **2002**(31): 251–264.

Orth, D.J., and White, R.J. 1993. Stream habitat management. Am. Fish. Soc. BETHESDA, MD (USA). pp. 205-230. 1993. (January 1993): 26–230. Available from https://login.proxy.lib.duke.edu/login?url=https://search.proquest.com/docview/16590087?accountid=10598%0Ahttp://pm6mt7vg3j.search.serialssolutions.com?ctx_ver=Z39.88-2004&ctx_enc=info:ofi/enc:UTF-8&rfr_id=info:sid/Aquatic+Science+%2526+Fisheries+Abstracts+%252.

Palmer, M.A., Hondula, K.L., and Koch, B.J. 2014. Ecological restoration of streams and rivers: shifting strategies and shifting goals. Annu. Rev. Ecol. Evol. Syst. **45**: 247–269. doi:10.1146/annurev-ecolsys-120213-091935.

Palmer, M.A., Menninger, H.L., and Bernhardt, E.S. 2010. River restoration, habitat heterogeneity and biodiversity: A failure of theory or practice? Freshw. Biol. **55**(SUPPL. 1): 205–222. doi:10.1111/j.1365-2427.2009.02372.x.

Pavlov, D.S., Lupandin, A.I., and Skorobogatov, M.A. 2000. The effects of flow turbulence on the behavior and distribution of fish. J. Ichthyol. **40**: 232–261.

Peake, S. 2004. An evaluation of the use of critical swimming speed for determination of culvert water velocity criteria for smallmouth bass. Trans. Am. Fish. Soc. **133**(6): 1472–1479. doi:10.1577/t03-202.1.

Peake, S.J., and Farrell, A.P. 2006. Fatigue is a behavioural response in respirometer- confined smallmouth bass. J. Fish Biol. **68**: 1742–1755. doi:10.1111/j.1095-8649.2006.01052.x.

Peake, S.J., McKinley, R.S., and Barth, C. 1997. Effect of recovery parameters on critical swimming speed of juvenile rainbow trout (*Oncorhynchus mykiss*). Can. J. Zool. **75**(10): 1724–1727. doi:10.1139/z97-800.

Pereira, G.H.A. 2019. On quantile residuals in beta regression. Commun. Stat. Simul. Comput. **48**(1): 302–316. doi:10.1080/03610918.2017.1381740.

Piccolo, J.J., Frank, B.M., and Hayes, J.W. 2014. Food and space revisited: The role of drift feeding theory in predicting the distribution, growth, and abundance of stream salmonids. Environ. Biol. Fishes **97**(5): 475–488. doi:10.1007/s10641-014-0222-2.

Plaut, I. 2001. Critical swimming speed: Its ecological relevance. Comp. Biochem. Physiol. - A Mol. Integr. Physiol. **131**(1): 41–50. doi:10.1016/S1095-6433(01)00462-7.

Przybilla, A., Kunze, S., Rudert, A., Bleckmann, H., and Brücker, C. 2010. Entraining in trout: A behavioural and hydrodynamic analysis. J. Exp. Biol. **213**(17): 2976–2986. doi:10.1242/jeb.041632.

Radspinner, R.R., Diplas, P., Lightbody, A.F., and Sotiropoulos, F. 2010. River training and ecological enhancement potential using in-stream structures. J. Hydraul. Eng. **136**(12): 967–980. doi:10.1061/(ASCE)HY.1943-7900.0000260.

Rhoads, B.L. 2020. Flow Dynamics in Rivers. River Dyn.: 72–96. doi:10.1017/9781108164108.004.

Rhoads, B.L., Engel, F.L., and Abad, J.D. 2011. Pool-riffle design based on geomorphological principles for naturalizing straight channels. *In* Geophysical Monograph Series. pp. 367–384. doi:10.1029/2010GM000979.

Richards, S.A., Whittingham, M.J., and Stephens, P.A. 2011. Model selection and model averaging in behavioural ecology: the utility of the IT-AIC framework. Behav. Ecol. Sociobiol. **65**: 77-89.

Ricklefs, R.E., and Wikelski, M. 2002b. The physiology/life-history nexus. Trends Ecol. Evol. **17**(10): 462–468. doi:10.1016/S0169-5347(02)02578-8.

Robinson, S. 1991. Coherent motions in the turbulent boundary layer. Annu. Rev. Fluid Mech. **23**(1): 601–639. doi:10.1146/annurev.fluid.23.1.601.

Rodgers, G.G., Tenzing, P., and Clark, T.D. 2016. Experimental methods in aquatic respirometry: the importance of mixing devices and accounting for background respiration. J. Fish Biol. **88**(1): 65–80. doi:10.1111/jfb.12848.

Roni, P., Hanson, K., and Beechie, T. 2008. Global Review of the Physical and Biological Effectiveness of Stream Habitat Rehabilitation Techniques. North Am. J. Fish. Manag. **28**(3): 856–890. doi:10.1577/M06-169.1.

Rosenfeld, J. 2003. Assessing the Habitat Requirements of Stream Fishes: An Overview and Evaluation of Different Approaches. Trans. Am. Fish. Soc. **132**(5): 953–968. doi:10.1577/t01-126.

Rosi-Marshall, E.J., Moerke, A.H., and Lamberti, G.A. 2006. Ecological responses to trout habitat rehabilitation in a Northern Michigan stream. Environ. Manage. **38**(1): 99–107. doi:10.1007/s00267-005-0177-3.

Rosner, B. 1975. On the detection of many outliers. Technometrics **17**(2): 221–227. doi:10.1080/00401706.1975.10489305.

Sandblom, E., Gräns, A., Axelsson, M., and Seth, H. 2014. Temperature acclimation rate of aerobic scope and feeding metabolism in fishes: Implications in a thermally extreme future. Proc. R. Soc. B Biol. Sci. **281**(1794). doi:10.1098/rspb.2014.1490.

Schneider, K.N., and Winemiller, K.O. 2008. Structural complexity of woody debris patches influences fish and macroinvertebrate species richness in a temperate floodplain-river system. Hydrobiologia **610**(1): 235–244. doi:10.1007/s10750-008-9438-5.

Shamloo, H., Rajaratnam, N., and Katopodis, C. 2001. Hydraulics of simple habitat structures. J. Hydraul. Res. **39**(4): 351–366. doi:10.1080/00221680109499840.

Shirvell, C.S. 1990. Role of instream rootwads as juvenile coho salmon (*Oncorhynchus kisutch*) and steelhead trout (*O. mykiss*) cover habitat under varying streamflows. Can. J. Fish. Aquat. Sci. **47**(1): 852–861.

Shuler, S.W., Nehring, R.B., and Fausch, K.D. 2004. Diel habitat selection by brown trout in the Rio Grande River, Colorado, after placement of boulder structures. North Am. J. Fish. Manag. **14**(1): 99–111. doi:10.1577/1548-8675(1994)014<0099:dhsbbt>2.3.co;2.

Silva, A.T., Katopodis, C., Santos, J.M., Ferreira, M.T., and Pinheiro, A.N. 2012. Cyprinid swimming behaviour in response to turbulent flow. Ecol. Eng. **44**: 314–328. Elsevier B.V. doi:10.1016/j.ecoleng.2012.04.015.

Smith, D.L., Brannon, E.L., and Odeh, M. 2005. Response of juvenile rainbow trout to turbulence produced by prismatoidal shapes. Trans. Am. Fish. Soc. **134**(3): 741–753. doi:10.1577/T04-069.1.

Smith, D.L., Goodwin, R.A., and Nestler, J.M. 2014. Relating Turbulence and Fish Habitat: A New Approach for Management and Research. Rev. Fish. Sci. Aquac. **22**(2): 123–130. doi:10.1080/10641262.2013.803516.

Start, D., McCauley, S., and Gilbert, B. 2018. Physiology underlies the assembly of ecological communities. Proc. Natl. Acad. Sci. U. S. A. **115**(23): 6016–6021. doi:10.1073/pnas.1802091115.

Steffensen, J.F., Johansen, K., and Bushnell, P.G. 1984. An automated swimming respirometer. Comp. Biochem. Physiol. -- Part A Physiol. **79**(3): 437–440. doi:10.1016/0300-9629(84)90541-3.

Stewart, G.B., Bayliss, H.R., Showler, D.A., Sutherland, W.J., and Pullin, A.S. 2009. Effectiveness of engineered in-stream structure mitigation measures to increase salmonid abundance: A systematic review. Ecol. Appl. **19**(4): 931–941. doi:10.1890/07-1311.1.

Stoklosa, J., Blakey, R. V., and Hui, F.K.C. 2022. An Overview of Modern Applications of Negative Binomial Modelling in Ecology and Biodiversity. Diversity **14**(5): 1–25. doi:10.3390/d14050320.

Strailey, K.K., Osborn, R.T., Tinoco, R.O., Cienciala, P., Rhoads, B.L., and Suski, C.D. 2021. Simulated instream restoration structures offer smallmouth bass (Micropterus dolomieu) swimming and energetic advantages at high flow velocities. Can. J. Fish. Aquat. Sci. **78**(1): 40–56. doi:10.1139/cjfas-2020-0032.

Suski, C.D., and Ridgway, M.S. 2009. Seasonal pattern of depth selection in smallmouth bass. J. Zool. **279**(2): 119–128. doi:10.1111/j.1469-7998.2009.00595.x.

Svendsen, J.C., Skov, J., Bildsoe, M., and Steffensen, J.F. 2003. Intra-school positional preference and reduced tail beat frequency in trailing positions in schooling roach under experimental conditions. J. Fish Biol. **62**(4): 834–846. doi:10.1046/j.1095-8649.2003.00068.x.

Svendsen, M.B., Bushnell, P.G., Christensen, E.A.F., and Steffensen, J.F. 2016a. Sources of variation in oxygen consumption of aquatic animals demonstrated by simulated constant oxygen consumption and respirometers of different sizes. J. Fish Biol. **88**(1): 51–64. doi:10.1111/jfb.12851.

Svendsen, M.B., Bushnell, P.G., and Steffensen, J.F. 2016b. Design and setup of intermittent flow respirometry system for aquatic organisms. J. Fish Biol. **88**(1): 26–50. doi:10.1111/jfb.12797.

Taguchi, M., and Liao, J.C. 2011. Rainbow trout consume less oxygen in turbulence: the energetics of swimming behaviors at different speeds. J. Exp. Biol. **214**(9): 1428–1436. doi:10.1242/jeb.052027.

Taylor, G.I. 1938. The spectrum of turbulence. Proc. R. Soc. London, Ser. A **164**(919): 476–490.

Tews, J., Brose, U., Grimm, V., Tielbörger, K., Wichmann, M., Schwager, M., and Jeltsch, F. 2004. Animal species diversity driven by habitat heterogeneity/diversity: the importance of keystone structures. J. Biogeogr. **31**(1): 79–92. doi:10.1046/j.0305-0270.2003.00994.x.

Thielicke, W., and Stamhuis, E.J. 2014. PIVlab - Towards User-Friendly, Affordable and Accurate Digital Particle Image Velocimetry in MATLAB. J. Open. Res. Softw. **2**(1): e30. doi:10.5334/jors.bl.

Thompson, D.M. 2002. Long-term effect of instream habitat-improvement structures on channel morphology along the Blackledge and Salmon rivers, Connecticut, USA. Environ. Manage. **29**(2): 250–265. doi:10.1007/s00267-001-0069-0.

Thompson, D.M. 2005. The history of the use and effectiveness of instream structures in the United States. Rev. Eng. Geol. **16**: 35–50. doi:10.1130/2005.4016(04).For.

Thompson, D.M. 2006. Did the pre-1980 use of in-stream structures improve streams? A reanalysis of historical data. Ecol. Appl. **16**(2): 784–796.

Todd, B.L., and Rabeni, C.F. 1989. Movement and habitat use by stream-dwelling smallmouth bass. Trans. Am. Fish. Soc. **118**(3): 229–242. doi:10.1097/00006324-197606000-00022.

Trinci, G., Harvey, G.L., Henshaw, A.J., Bertoldi, W., and Hölker, F. 2020. Turbulence, instream wood and fish: Ecohydraulic interactions under field conditions. Ecohydrology **13**(5). doi:10.1002/eco.2211.

Tritico, H.M., and Cotel, A.J. 2010. The effects of turbulent eddies on the stability and critical swimming speed of creek chub (*Semotilus atromaculatus*). J. Exp. Biol. **213**(13): 2284–2293. doi:10.1242/jeb.041806.

Tullos, D., and Walter, C. 2014. Fish use of turbulence around wood in winter: Physical experiments on hydraulic variability and habitat selection by juvenile coho salmon, *Oncorhynchus kisutch*. Environ. Biol. Fishes **98**(5): 1339–1353. doi:10.1007/s10641-014-0362-4.

Tullos, D., Walter, C., and Dunham, J. 2015. Does resolution of flow field observation influence apparent habitat use and energy expenditure in juvenile coho salmon? Water Resour. Res. **52**: 5938–5950. doi:10.1111/j.1752-1688.1969.tb04897.x.

Urabe, H., Nakajima, M., Torao, M., and Aoyama, T. 2010. Evaluation of Habitat Quality for Stream Salmonids Based on a Bioenergetics Model. Trans. Am. Fish. Soc. **139**(6): 1665–1676. doi:10.1577/t09-210.1.

US-Environmental Protection Agency. The Quality of Our Nation's Waters. EPA-841-R 02001 (US EPA, 2000)

Vogel, S. 1994. Life in Moving Fluids: The Physical Biology of Flow. *In* 2nd edition. Princeton University Press, Princeton.

Vörösmarty, C.J., McIntyre, P.B., Gessner, M.O., Dudgeon, D., Prusevich, A., Green, P., Glidden, S., Bunn, S.E., Sullivan, C.A., Leirmann, C.R., and Davis, P.M. 2010. Global threats to human water security and river biodiversity. Nature **467**: 555–561. doi:10.1038/nature09440.

Wade, R.J., Rhoads, B.L., Rodríguez, J., Daniels, M.D., Wilson, D., Herricks, E.E., Bombardelli, F., Garcia, M., and Schwartz, J. 2002. Integrating science and technology to support stream naturalization near Chicago, Illinois. J. Am. Water Resour. Assoc. **38**(4): 931–944.

Wagenmakers, E.J., and Farrell, S. 2004. AIC model selection using Akaike weights. Psychon. Bull. Rev. **11**(1): 192–196. doi:10.3758/BF03206482.

Wagner, G.N., Cooke, S.J., Brown, R.S., and Deters, K.A. 2011. Surgical implantation techniques for electronic tags in fish. Rev. Fish Biol. Fish. **21**(1): 71–81. doi:10.1007/s11160-010-9191-5.

Wang, H., and Chanson, H. 2018. Modelling upstream fish passage in standard box culverts: Interplay between turbulence, fish kinematics, and energetics. River Res. Appl. **34**(3): 244–252. doi:10.1002/rra.3245.

Warhaft, Z. 2002. Turbulence in nature and in the laboratory. Proc. Natl. Acad. Sci. **99**: 2481 2486.

Webb, P.W. 1971. The swimming energetics of trout II. Oxygen consumption and swimming efficiency. J. Exp. Biol. **55**: 521–540.

Webb, P.W. 1984. Form and function in fish swimming. Sci. Am. **251**(1): 72–82. doi:10.1038/scientificamerican0784-72.

Webb, P.W. 1994. The biology of fish swimming. *In* The Mechanics and Physiology of Animal Swimming. pp. 45–62.

Webb, P.W. 1998. Entrainment by river chub *Nocomis micropogon* and smallmouth bass *Micropterus dolomieu* on cylinders. J. Exp. Biol. **201**: 2403–2412. Available from https://jeb.biologists.org/content/jexbio/201/16/2403.full.pdf [accessed 14 June 2019].

Webb, P.W. 2002. Control of posture, depth, and swimming trajectories of fishes. Integr. Comp. Biol. **42**(1): 94–101. doi:10.1093/icb/42.1.94.

Webb, P.W. 2004. Response latencies to postural disturbances in three species of teleostean fishes. J. Exp. Biol. **207**(6): 955–961. doi:10.1242/jeb.00854.

Webb, P.W., and Cotel, A.J. 2010. Turbulence: Does vorticity affect the structure and shape of body and fin propulsors. Integr. Comp. Biol. **50**(6): 1155–1166. doi:10.1093/icb/icq020.

Wehrly, K.E., Wiley, M.J., and Seelbach, P.W. 2003. Classifying regional variation in thermal regime based on stream fish community patterns. Trans. Am. Fish. Soc. **132**(1): 18–38. doi:10.1577/1548-8659(2003)132<0018:crvitr>2.0.co;2.

Weigel, D.E., and Sorensen, P.W. 2001. The influence of habitat characteristics on the longitudinal distribution of brook, brown, and rainbow trout in a small midwestern stream. J. Freshw. Ecol. **16**(4): 599–613. doi:10.1080/02705060.2001.9663852.

West, B.T., Welch, K.B., and Galecki, A.T. 2007. Linear mixed models: A practical guide using statistical software. *In* Statistics in Medicine. Chapman & Hall/CRC, Boca Raton. doi:10.1002/sim.3167.

Wheaton, J.M., Bouwes, N., Mchugh, P., Saunders, C., Bangen, S., Bailey, P., Nahorniak, M., Wall, E., and Jordan, C. 2018. Upscaling site-scale ecohydraulic models to inform salmonid population-level life cycle modeling and restoration actions – Lessons from the Columbia River Basin. Earth Surf. Process. Landforms **43**: 21–44. doi:10.1002/esp.4137.

Whiteway, S.L., Biron, P.M., Zimmermann, A., Venter, O., Whiteway, S., Biron, P., Venter, O., and Grant, J. 2010. Do instream structures enhance salmonid abundance? A meta-analysis. Can. J. Fish. Aquat. Sci. **67**(5): 831–841.

Wickham, H. 2016. ggplot2: Elegant graphics for data analysis. Springer-Verlag New York.

Wilke, C.O. 2019. cowplot: Streamlined Plot Theme and Plot Annotations for "ggplot2." Available from https://cran.r-project.org/package=cowplot.

Wilkes, M.A., Enders, E.C., Silva, A.T., Acreman, M., and Maddock, I. 2017. Position choice and swimming costs of juvenile Atlantic salmon salmo salar in turbulent flow . J. Ecohydraulics **2**(1): 16–27. Taylor & Francis. doi:10.1080/24705357.2017.1287532.

Williamson, C. 1996. Vortex dynamics in the cylinder wake. Annu. Rev. Fluid Mech. **28**(1): 477–539. doi:10.1146/annurev.fluid.28.1.477.

Wilson, S.M., Hinch, S.G., Eliason, E.J., Farrell, A.P., and Cooke, S.J. 2013. Calibrating acoustic acceleration transmitters for estimating energy use by wild adult Pacific salmon. Comp. Biochem. Physiol. - A Mol. Integr. Physiol. **164**(3): 491–498. Elsevier Inc. doi:10.1016/j.cbpa.2012.12.002.

Wohl, E., Angermeier, P.L., Bledsoe, B.P., Kondolf, G.M., MacDonnell, L., Merritt, D.M., Palmer, M.A., Poff, N.L., and Tarboton, D. 2005. River restoration. Water Resour. Res. **41**. doi:10.1029/2005WR003985.

Wohl, E., Lane, S.N., and Wilcox, A.C. 2015. The science and practice of river restoration. Water Resour. Res. **51**: 5974–5997. doi:10.1002/2014WR016874.Received.

Yates, L., Aandahl, Z., Richards, S.A., and Brook, B.W. 2022. Cross validation for model selection: a primer with examples from ecology. : 1–36. Available from http://arxiv.org/abs/2203.04552.

Ydesen, K.S., Wisniewska, D.M., Hansen, J.D., Beedholm, K., Johnson, M., and Madsen, P.T. 2014. What a jerk: prey engulfment revealed by high-rate, super-cranial accelerometry on a harbour seal (*Phoca vitulina*). J. Exp. Biol. **217**(13): 2239–2243. doi:10.1242/jeb.100016.

Young, J.L., Bornik, Z.B., Marcotte, M.L., Charlie, K.N., Wagner, G.N., Hinch, S.G., and Cooke, S.J. 2006. Integrating physiology and life history to improve fisheries management and conservation. Fish Fish. **7**(4): 262–283. doi:10.1111/j.1467-2979.2006.00225.x.

Zhang, D. 2018. rsq: R-Squared and Related Measures. Available from https://cran.r project.org/package=rsq.

Zuur, A.F., Ieno, E.N., and Elphick, C.S. 2010. A protocol for data exploration to avoid common statistical problems. Methods Ecol. Evol. **1**(1): 3–14. doi:10.1111/j.2041-210x.2009.00001.x.

Zuur, A.F., Ieno, E.N., Walker, N.J., Saveliev, A.A., and Smith, G.M. 2009. Mixed effects models and extensions in ecology with R. Springer, New York. doi:10.1016/B978-0-12-387667-6.00013-0.

APPENDIX A: SUPPLEMENTAL MATERIALS CHAPTER TWO

Figure

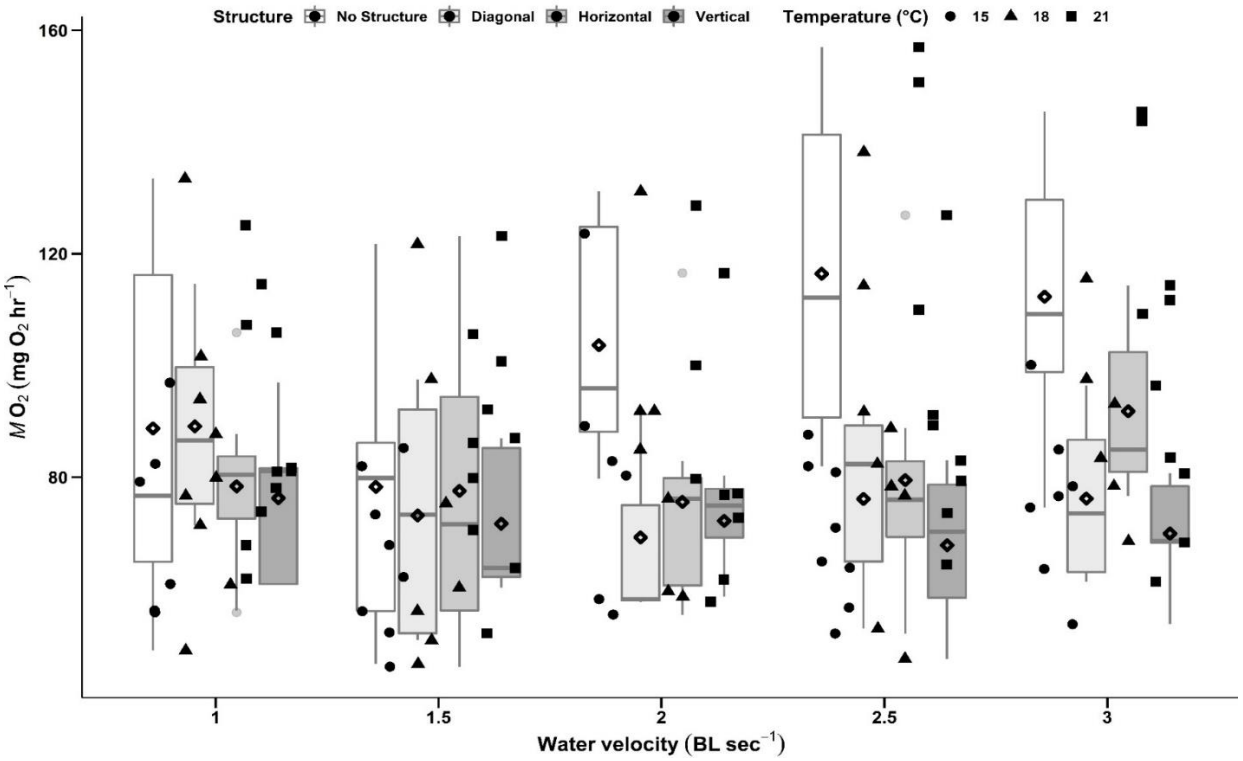

Figure A.1. Oxygen consumption (in mg O_2 hr^{-1}; panel B) by structure treatment and swimming velocity (BL s^{-1}) for smallmouth bass acclimated to one of 3 different temperatures. Temperature data are overlaid on top of Figure 2.1. A simple linear mixed effects model with just temperature and fish ID as predictors of oxygen consumption showed MO_2 values were significantly different between 15 °C and 21 °C fish, but not 18 °C fish.

Table

Table A.1. Summary table of model in which temperature is solely related to the oxygen consumption ($MO_{2)}$ of smallmouth bass swimming at a particular velocity, acclimated to one of three temperatures. In this model acclimation temperature was significant, as opposed to the most parsimonious model, in which acclimation temperature was not significant. MO_2 is log-transformed, and fish ID is treated as a random effect.

	Estimate	Standard Error	df	t value	Pr(>|z|)
(Intercept)	4.27	0.08	25.93	56.51	<0.001
18 °C	0.09	0.10	26.88	0.92	0.36
21 °C	0.20	0.10	25.83	2.06	0.05

APPENDIX B: SUPPLEMENTAL MATERIALS CHAPTER THREE

Figures

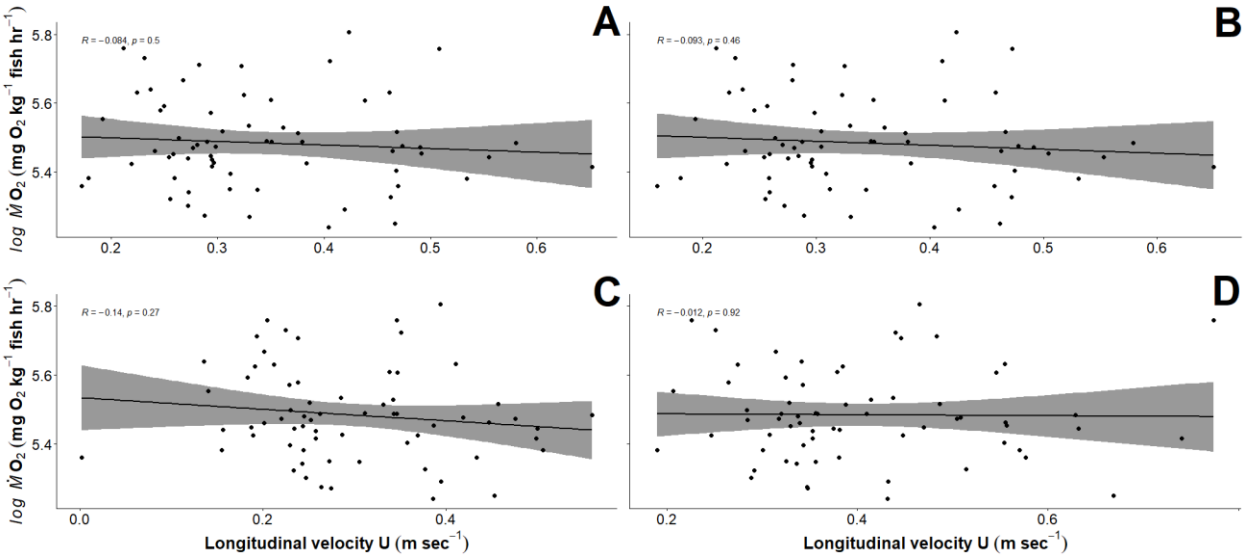

Figure B.1. Scatter plots of the regression relating log-transformed oxygen consumption (MO_2, mg O_2/kg fish/hr) for rainbow trout, estimated via acceleration, participating in flume swim trials with the values of longitudinal velocity U (m/sec) experienced by fish. Regression plots were generated using mean values of U (panel A), median values of U (panel B), minimum values of U (panel C), and maximum values of U (panel D) to evaluate which descriptive statistic to use for bioenergetics model development.

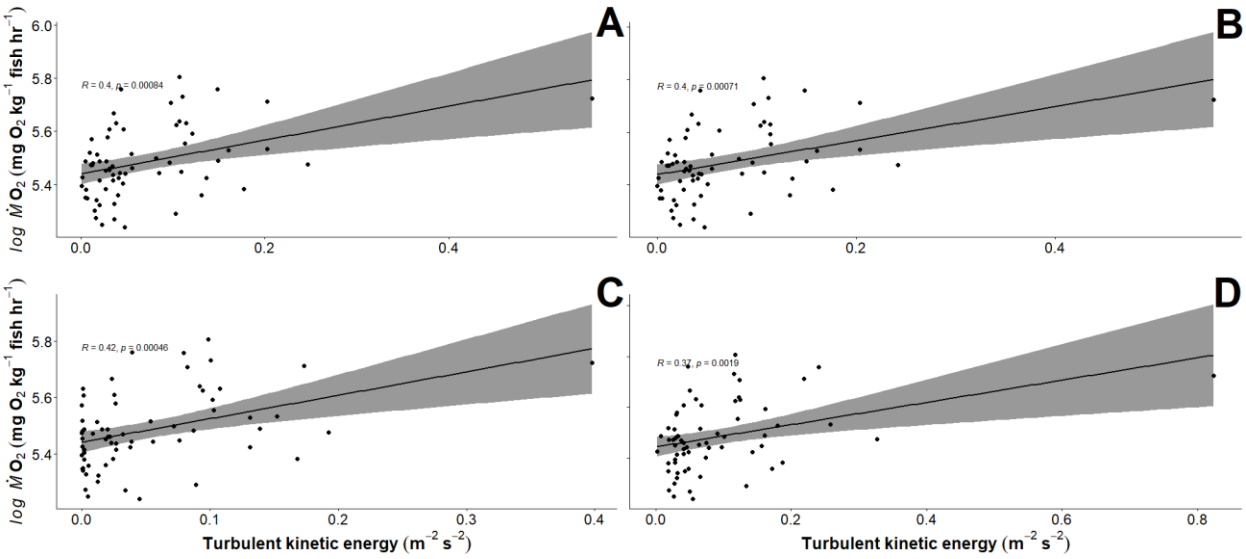

Figure B.2. Scatter plots of the regression relating log-transformed oxygen consumption (MO_2, mg O_2/kg fish/hr) for rainbow trout, estimated via acceleration, participating in flume swim trials with the values of turbulent kinetic energy (TKE; m^2/sec^2) experienced by fish. Regression plots were generated using mean values of TKE (panel A), median values of TKE (panel B), minimum values of TKE (panel C), and maximum values of TKE (panel D) to evaluate which descriptive statistic to use for bioenergetics model development.

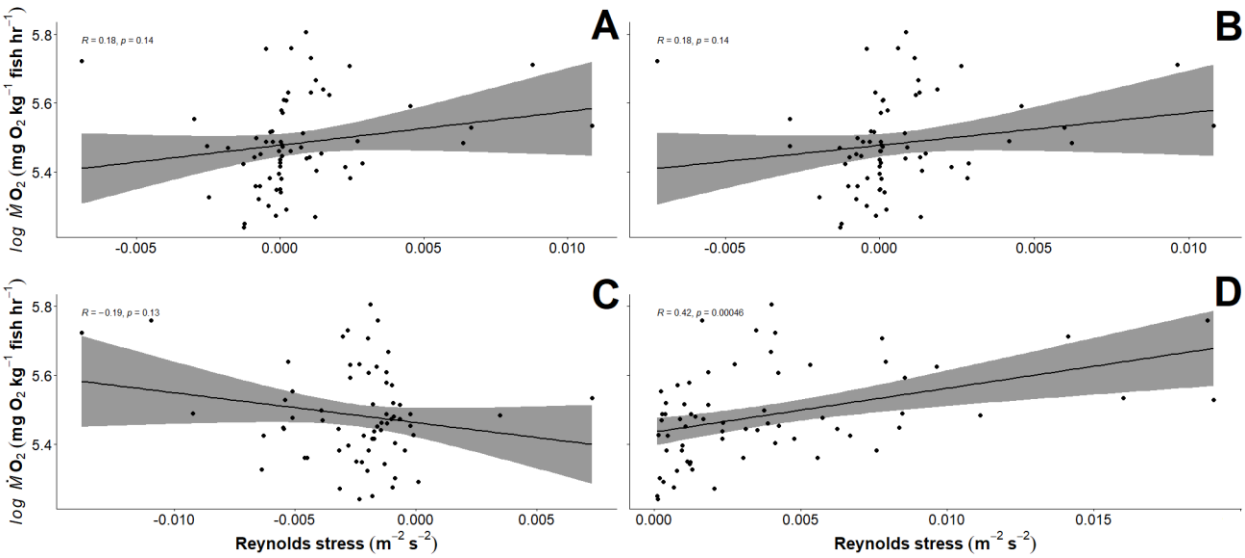

Figure B.3. Scatter plots of the regression relating log-transformed oxygen consumption (MO_2, mg O_2/kg fish/hr) for rainbow trout, estimated via acceleration, participating in flume swim trials with the values of Reynolds stress (m^2/sec^2) experienced by fish. Regression plots were generated using mean values of Reynolds stress (panel A), median values of Reynolds stress (panel B), minimum values of Reynolds stress (panel C), and maximum values of Reynolds stress (panel D) to evaluate which descriptive statistic to use for bioenergetics model development.

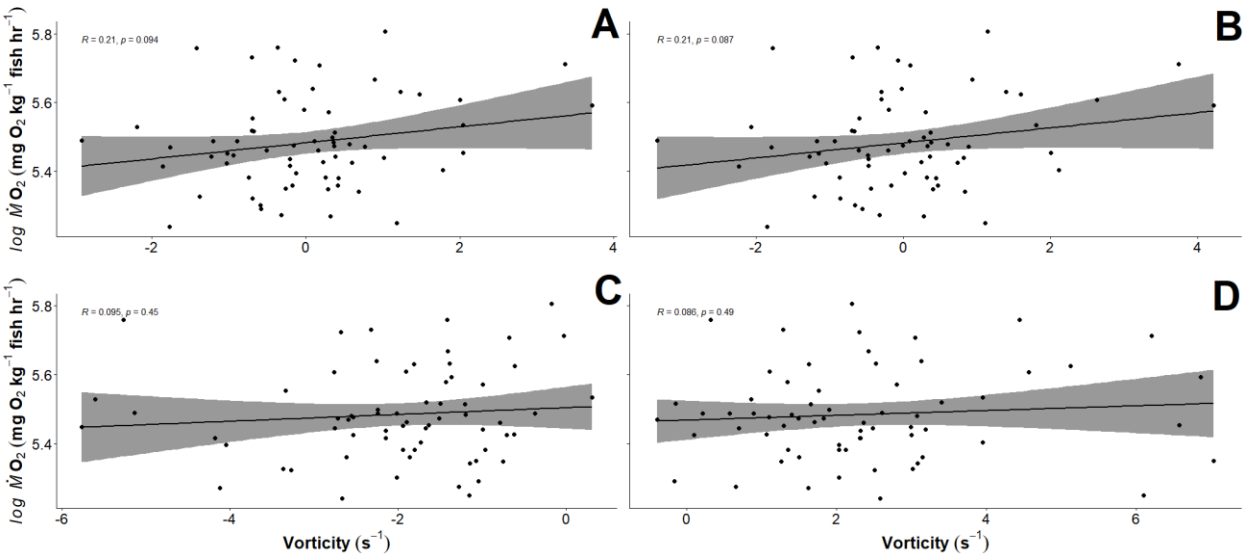

Figure B.4. Scatter plots of the regression relating log-transformed oxygen consumption (MO_2, mg O_2/kg fish/hr) for rainbow trout, estimated via acceleration, participating in flume swim trials with the values of vorticity (s^{-1}) experienced by fish. Regression plots were generated using mean values of vorticity (panel A), median values of vorticity (panel B), minimum values of vorticity (panel C), and maximum values of vorticity (panel D) to evaluate which descriptive statistic to use for bioenergetics model development.

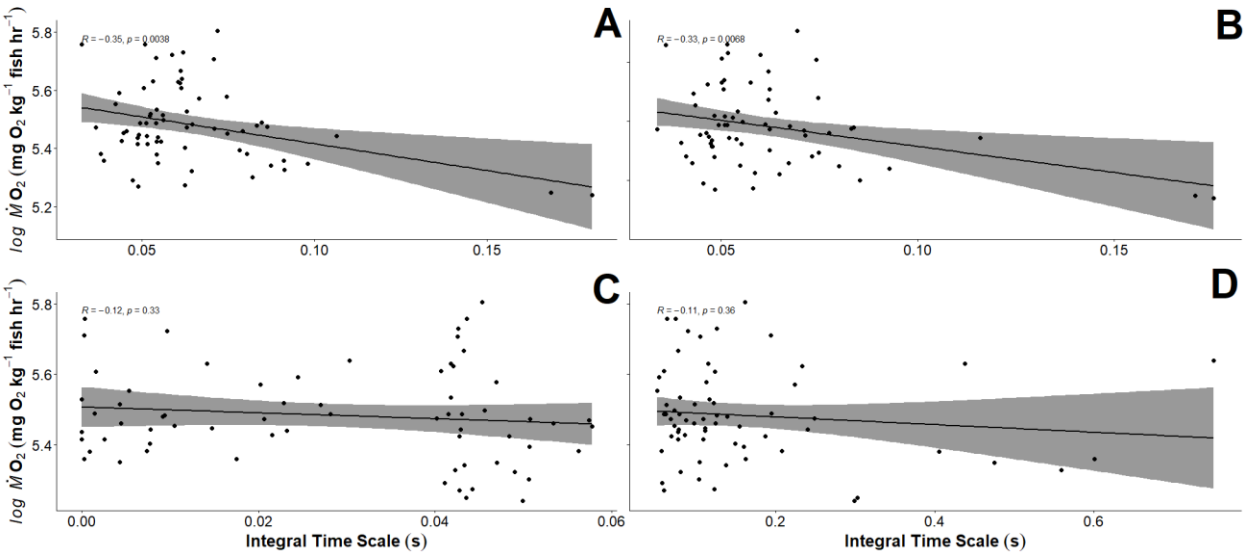

Figure B.5. Scatter plots of the regression relating log-transformed oxygen consumption (MO_2, mg O_2/kg fish/hr) for rainbow trout, estimated via acceleration, participating in flume swim trials with the values of integral time scale (T; sec) experienced by fish. Regression plots were generated using mean values of T (panel A), median values of T (panel B), minimum values of T (panel C), and maximum values of T (panel D) to evaluate which descriptive statistic to use for bioenergetics model development.

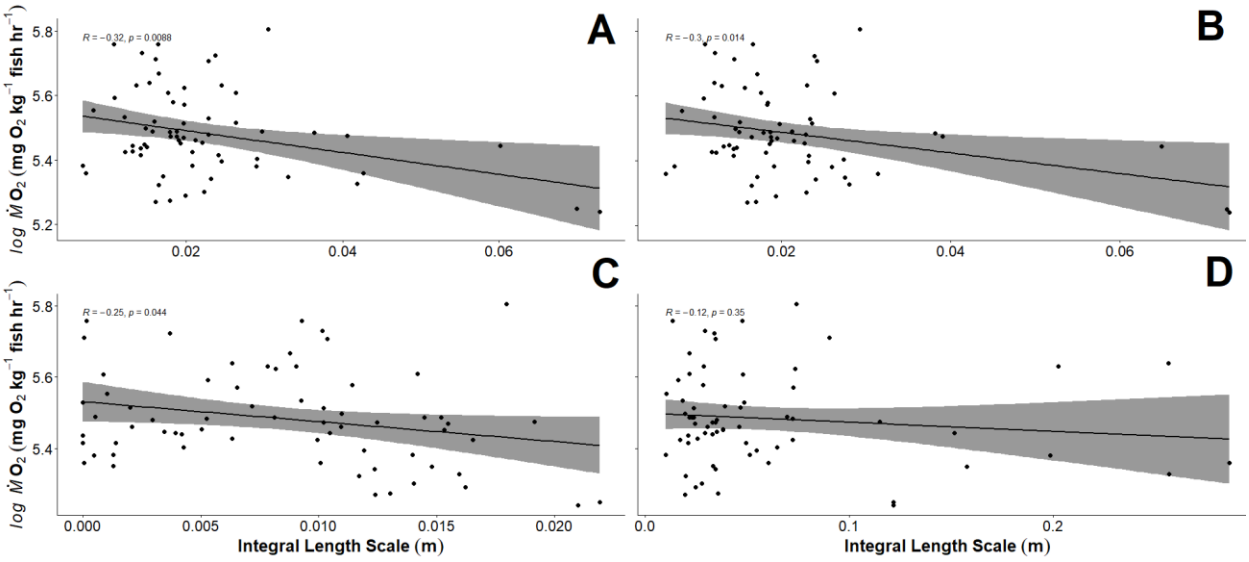

Figure B.6. Scatter plots of the regression relating log-transformed oxygen consumption (MO_2, mg O_2/kg fish/hr) for rainbow trout, estimated via acceleration, participating in flume swim trials with the values of integral time scale (L; m) experienced by fish. Regression plots were generated using mean values of L (panel A), median values of L (panel B), minimum values of L (panel C), and maximum values of L (panel D) to evaluate which descriptive statistic to use for bioenergetics model development.

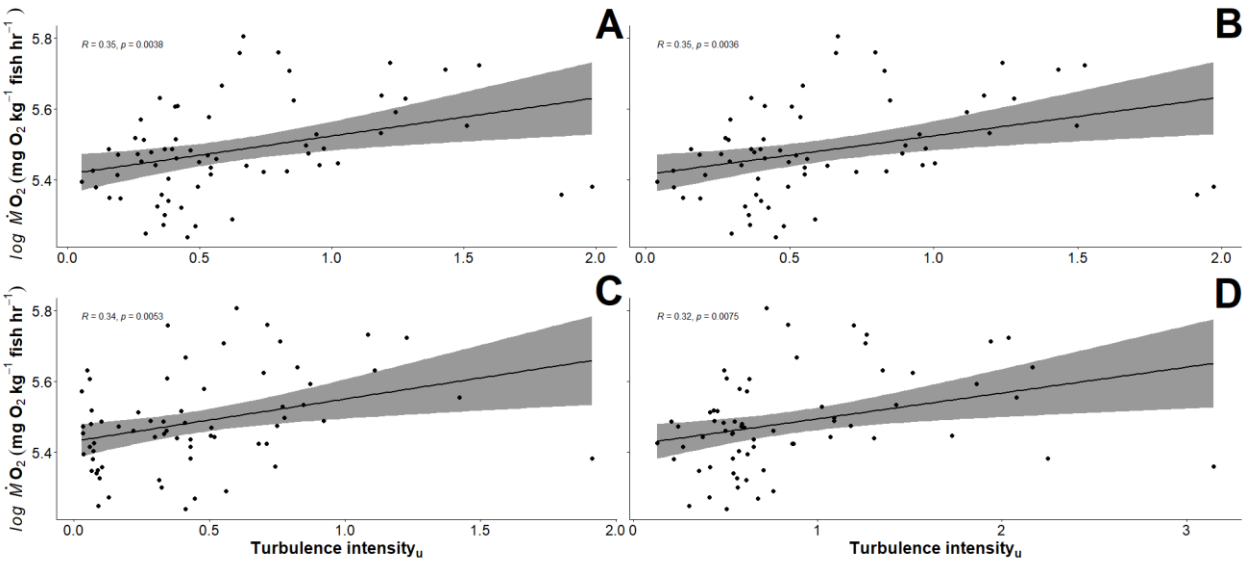

Figure B.7. Scatter plots of the regression relating log-transformed oxygen consumption (MO_2, mg O_2/kg fish/hr) for rainbow trout, estimated via acceleration, participating in flume swim trials with the values of turbulence intensity (TI_u) experienced by fish. Regression plots were generated using mean values of TI_u (panel A), median values of TI_u (panel B), minimum values of TI_u (panel C), and maximum values of TI_u (panel D) to evaluate which descriptive statistic to use for bioenergetics model development.

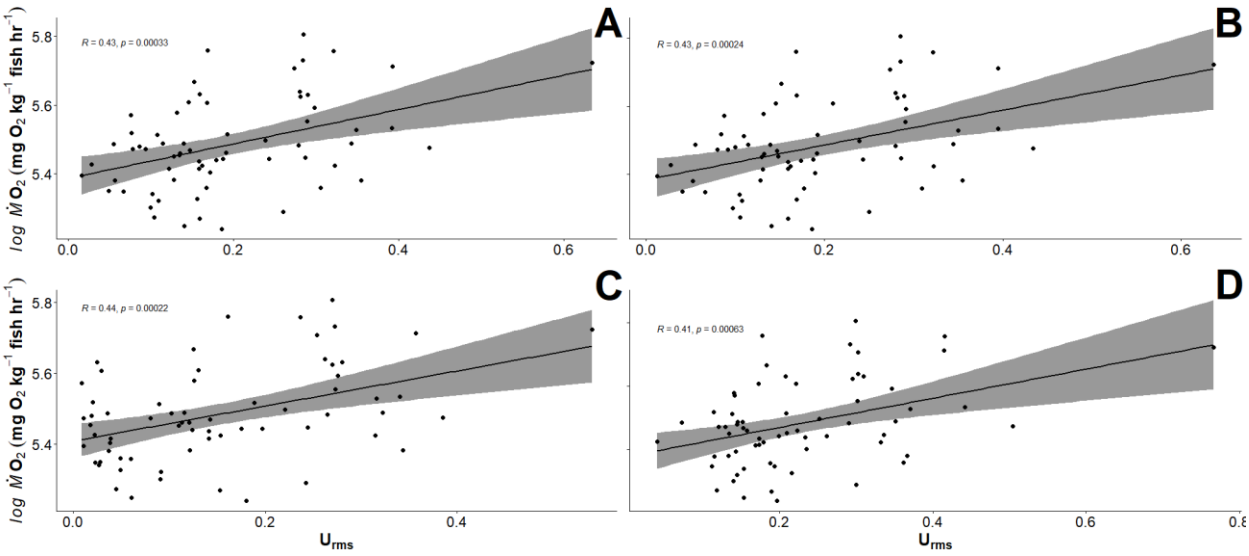

Figure B.8. Scatter plots of the regression relating log-transformed oxygen consumption (MO_2, mg O_2/kg fish/hr) for rainbow trout, estimated via acceleration, participating in flume swim trials with the values of U_{rms} (m/sec) experienced by fish. Regression plots were generated using mean values of U_{rms} (panel A), median values of U_{rms} (panel B), minimum values of U_{rms} (panel C), and maximum values of U_{rms} (panel D) to evaluate which descriptive statistic to use for bioenergetics model development.

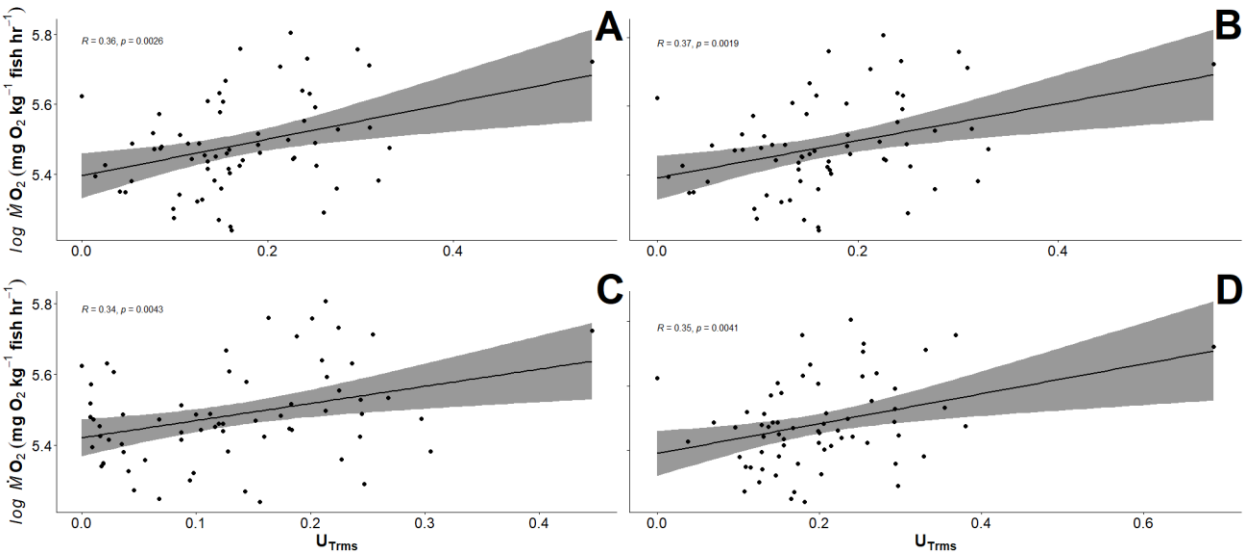

Figure B.9. Scatter plots of the regression relating log-transformed oxygen consumption (MO_2, mg O_2/kg fish/hr) for rainbow trout, estimated via acceleration, participating in flume swim trials with the values of U_{Trms} (m/sec) experienced by fish. Regression plots were generated using mean values of U_{Trms} (panel A), median values of U_{Trms} (panel B), minimum values of U_{Trms} (panel C), and maximum values of U_{Trms} (panel D) to evaluate which descriptive statistic to use for bioenergetics model development.

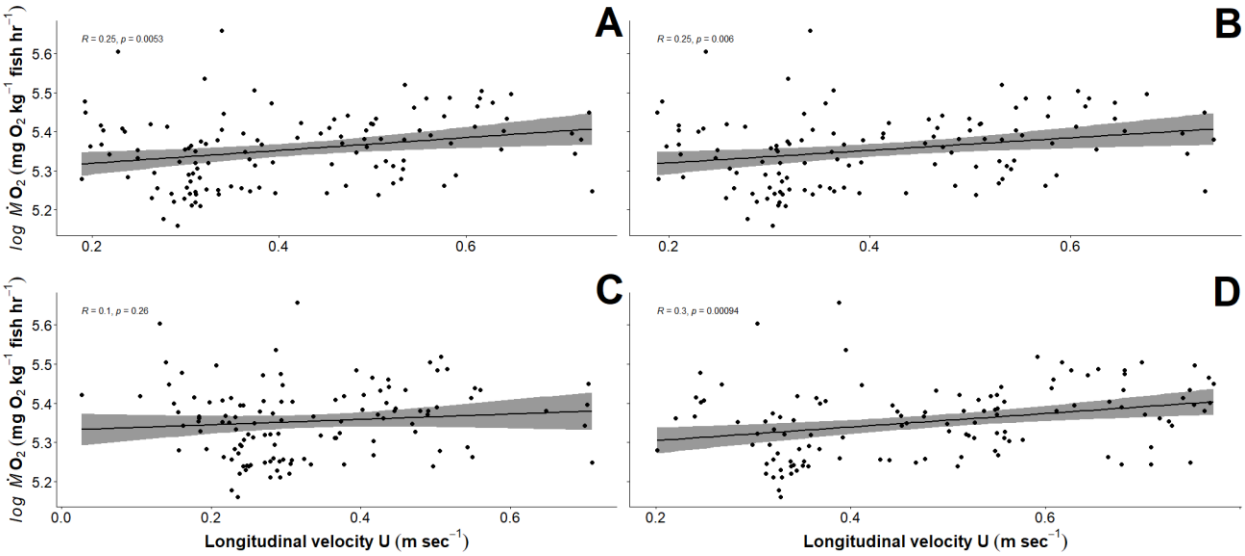

Figure B.10. Scatter plots of the regression relating log-transformed oxygen consumption (MO_2, mg O_2/kg fish/hr) for smallmouth bass, estimated via acceleration, participating in flume swim trials with the values of longitudinal velocity U (m/sec) experienced by fish. Regression plots were generated using mean values of U (panel A), median values of U (panel B), minimum values of U (panel C), and maximum values of U (panel D) to evaluate which descriptive statistic to use for bioenergetics model development.

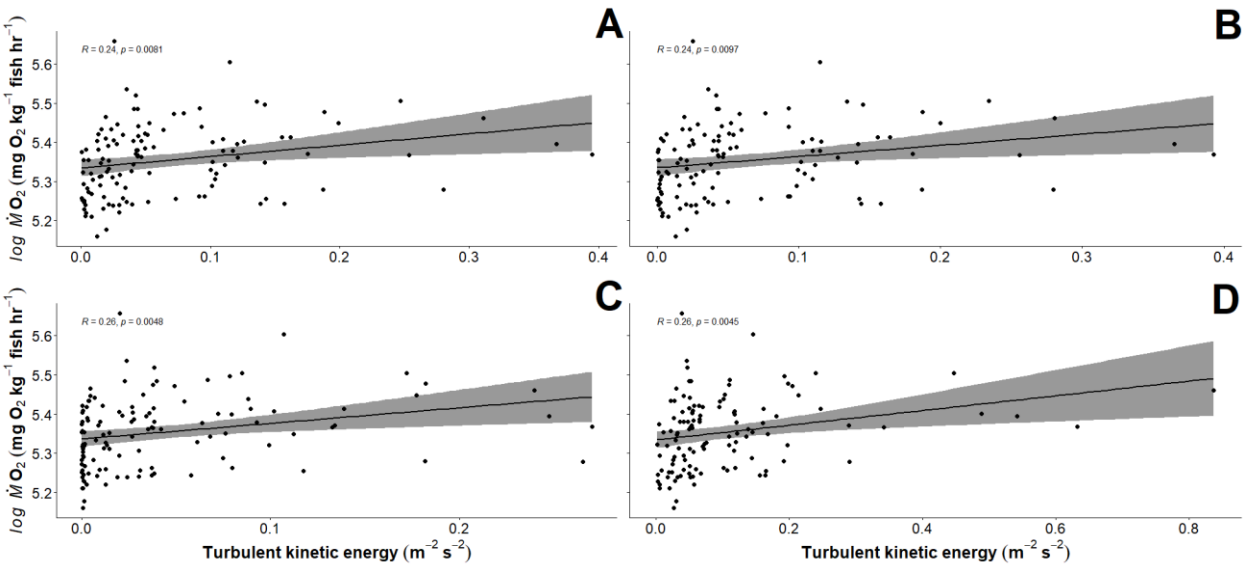

Figure B.11. Scatter plots of the regression relating log-transformed oxygen consumption (MO_2, mg O_2/kg fish/hr) for smallmouth bass, estimated via acceleration, participating in flume swim trials with the values of turbulent kinetic energy (TKE; m^2/sec^2) experienced by fish. Regression plots were generated using mean values of TKE (panel A), median values of TKE (panel B), minimum values of TKE (panel C), and maximum values of TKE (panel D) to evaluate which descriptive statistic to use for bioenergetics model development.

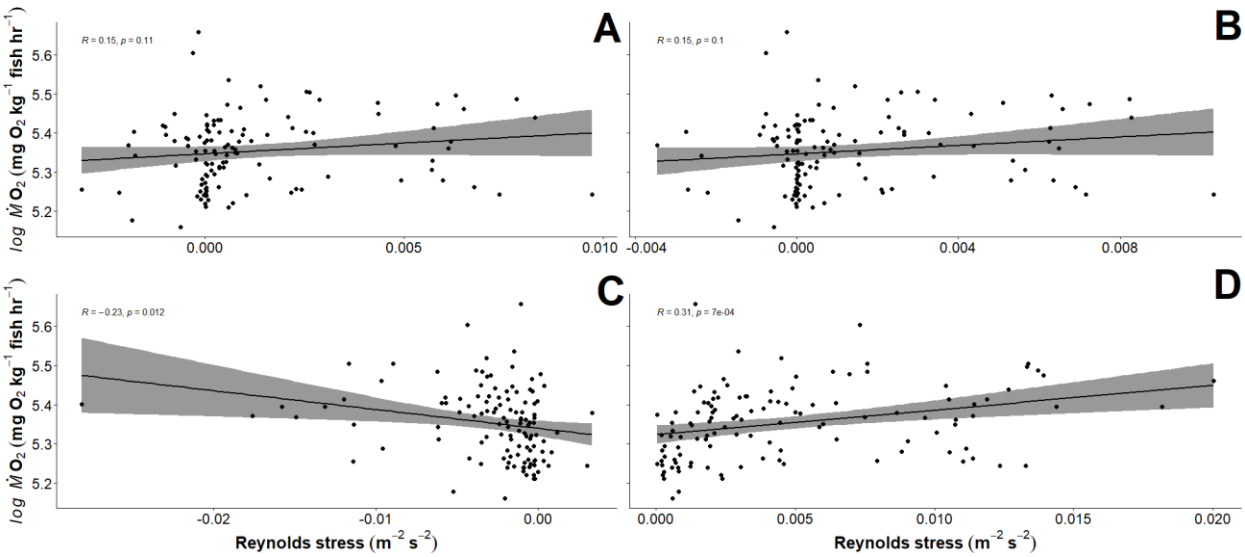

Figure B.12. Scatter plots of the regression relating log-transformed oxygen consumption (MO_2, mg O_2/kg fish/hr) for smallmouth bass, estimated via acceleration, participating in flume swim trials with the values of Reynolds stress (m^2/sec^2) experienced by fish. Regression plots were generated using mean values of Reynolds stress (panel A), median values of Reynolds stress (panel B), minimum values of Reynolds stress (panel C), and maximum values of Reynolds stress (panel D) to evaluate which descriptive statistic to use for bioenergetics model development.

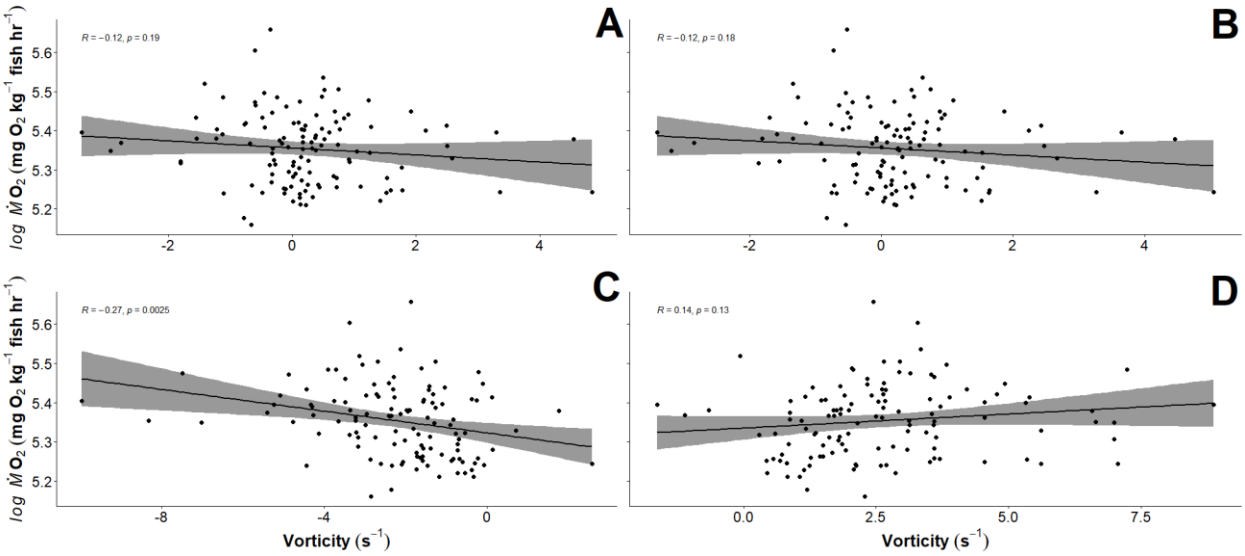

Figure B.13. Scatter plots of the regression relating log-transformed oxygen consumption (MO_2, mg O_2/kg fish/hr) for smallmouth bass, estimated via acceleration, participating in flume swim trials with the values of vorticity (s^{-1}) experienced by fish. Regression plots were generated using mean values of vorticity (panel A), median values of vorticity (panel B), minimum values of vorticity (panel C), and maximum values of vorticity (panel D) to evaluate which descriptive statistic to use for bioenergetics model development.

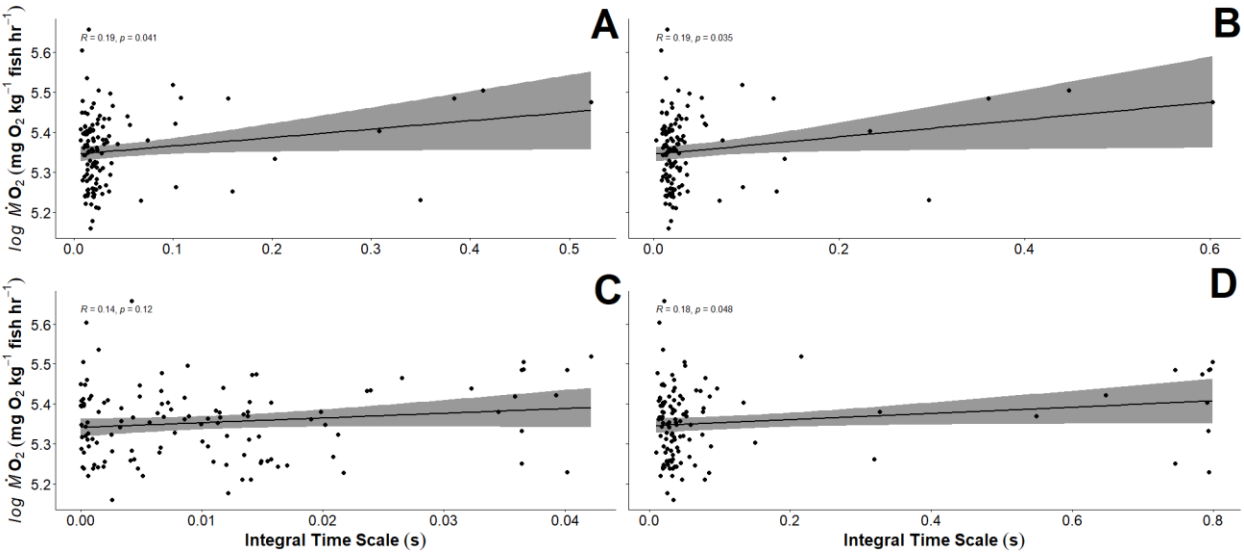

Figure B.14. Scatter plots of the regression relating log-transformed oxygen consumption (MO_2, mg O_2/kg fish/hr) for smallmouth bass, estimated via acceleration, participating in flume swim trials with the values of integral time scale (T; sec) experienced by fish. Regression plots were generated using mean values of T (panel A), median values of T (panel B), minimum values of T (panel C), and maximum values of T (panel D) to evaluate which descriptive statistic to use for bioenergetics model development.

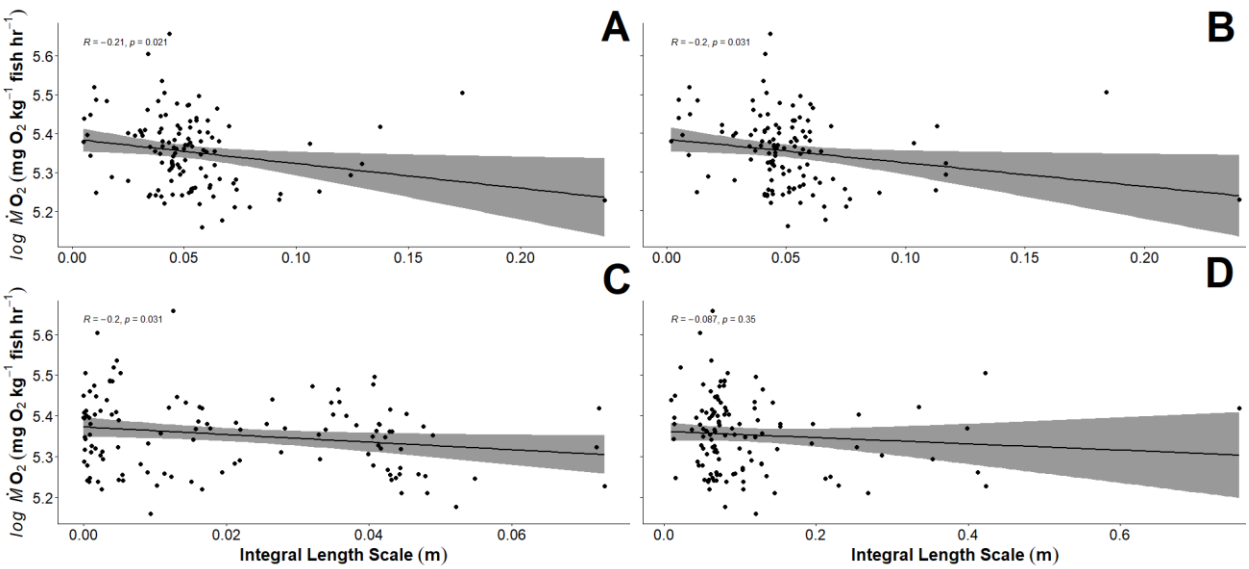

Figure B.15. Scatter plots of the regression relating log-transformed oxygen consumption ($M\dot{O}_2$, mg O_2/kg fish/hr) for smallmouth bass, estimated via acceleration, participating in flume swim trials with the values of integral time scale (L; m) experienced by fish. Regression plots were generated using mean values of L (panel A), median values of L (panel B), minimum values of L (panel C), and maximum values of L (panel D) to evaluate which descriptive statistic to use for bioenergetics model development.

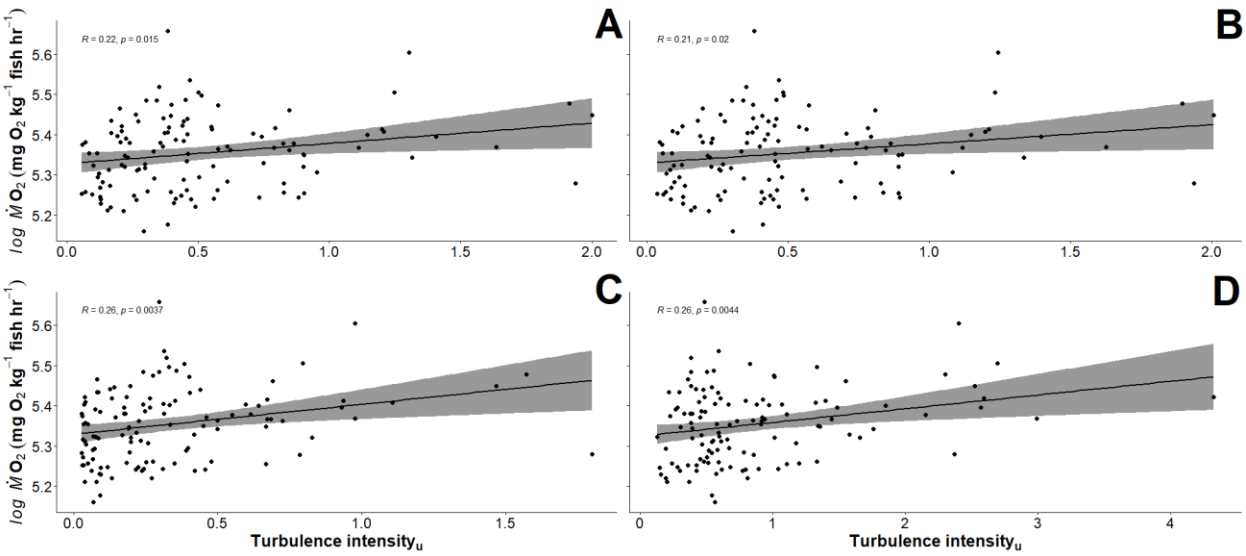

Figure B.16. Scatter plots of the regression relating log-transformed oxygen consumption (MO_2, mg O_2/kg fish/hr) for smallmouth bass, estimated via acceleration, participating in flume swim trials with the values of turbulence intensity (TI_u) experienced by fish. Regression plots were generated using mean values of TI_u (panel A), median values of TI_u (panel B), minimum values of TI_u (panel C), and maximum values of TI_u (panel D) to evaluate which descriptive statistic to use for bioenergetics model development.

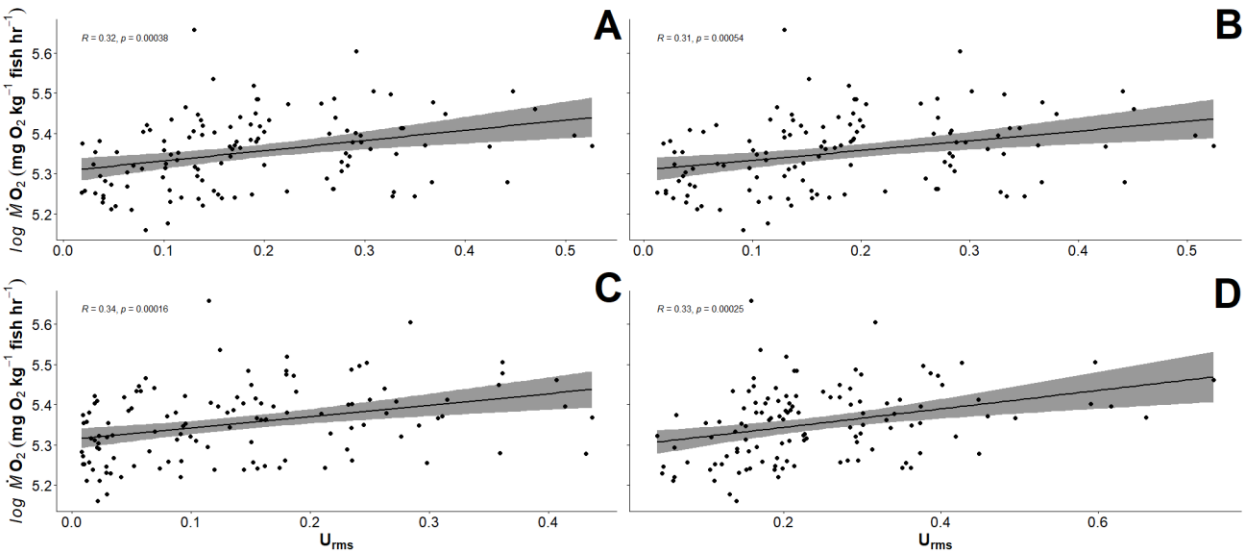

Figure B.17. Scatter plots of the regression relating log-transformed oxygen consumption (MO_2, mg O_2/kg fish/hr) for smallmouth bass, estimated via acceleration, participating in flume swim trials with the values of U_{rms} (m/sec) experienced by fish. Regression plots were generated using mean values of U_{rms} (panel A), median values of U_{rms} (panel B), minimum values of U_{rms} (panel C), and maximum values of U_{rms} (panel D) to evaluate which descriptive statistic to use for bioenergetics model development.

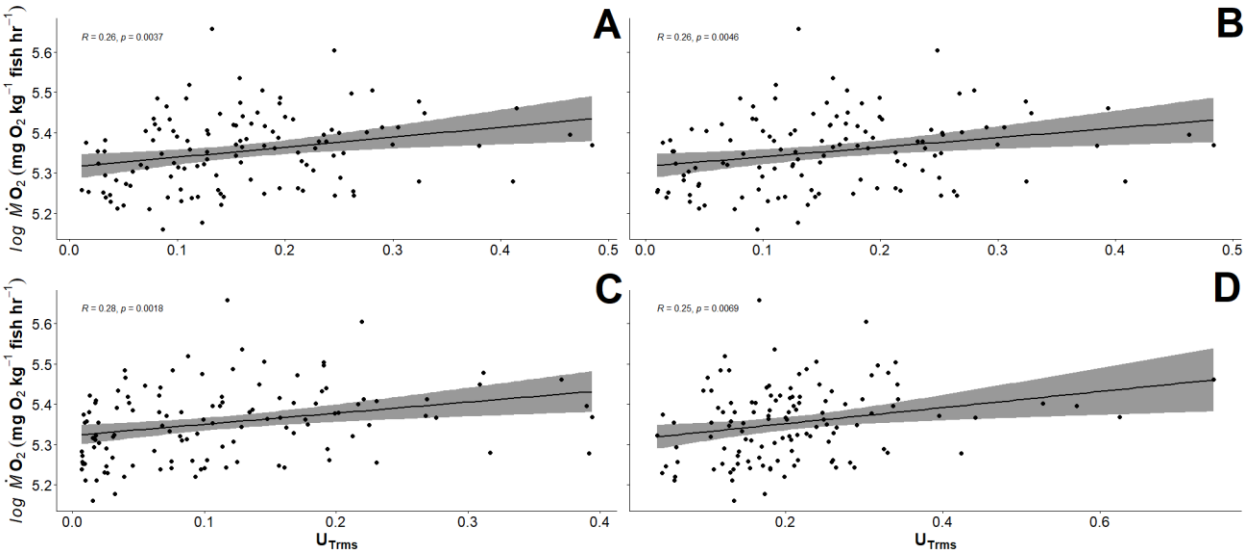

Figure B.18. Scatter plots of the regression relating log-transformed oxygen consumption (MO_2, mg O_2/kg fish/hr) for smallmouth bass, estimated via acceleration, participating in flume swim trials with the values of U_{Trms} (m/sec) experienced by fish. Regression plots were generated using mean values of U_{Trms} (panel A), median values of U_{Trms} (panel B), minimum values of U_{Trms} (panel C), and maximum values of U_{Trms} (panel D) to evaluate which descriptive statistic to use for bioenergetics model development.

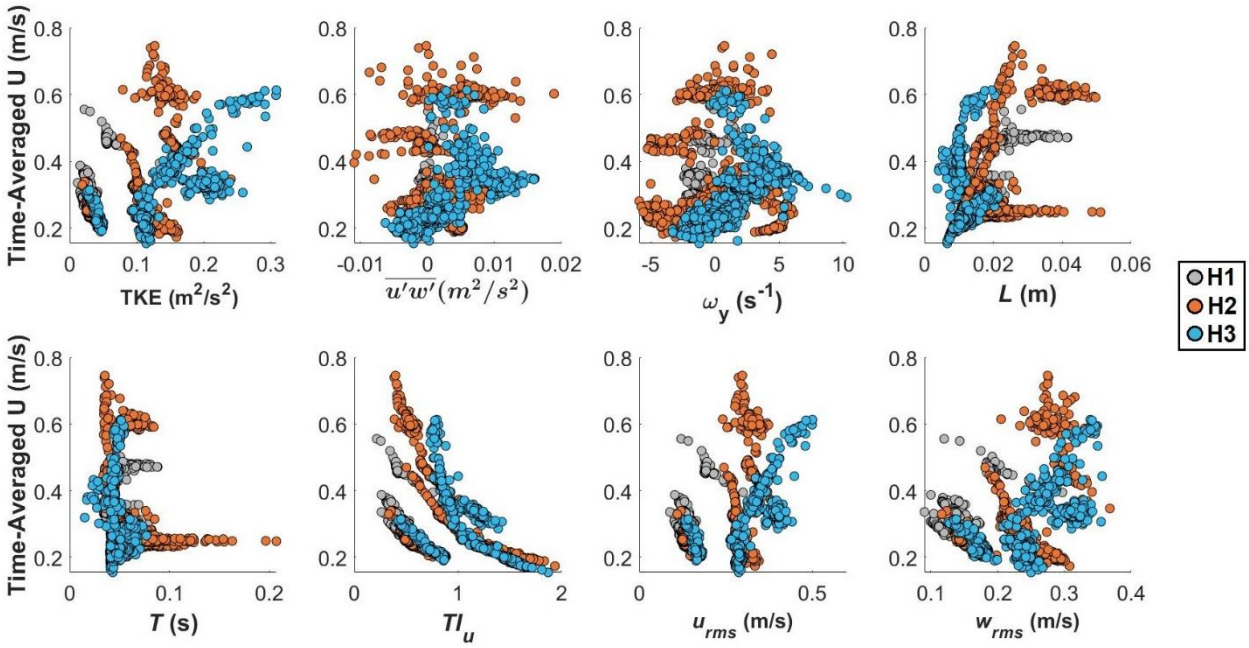

Figure B.19. Time-averaged longitudinal velocity U extracted from locations occupied by rainbow trout swimming with horizontal structures (HS) compared with the turbulent flow conditions for each location. Turbulence metrics depicted include turbulent kinetic energy (TKE), Reynolds stress ($\overline{u'w'}$), vorticity (ω_y), turbulent integral length scale (L), turbulent integral time scale (T), turbulence intensity (TI_U), U_{rms}, and W_{rms}. Scatter plots were generated to identify potential relationship between U and the turbulence metrics examined. Different colors indicate the diameter of the HS, H1 [2.54-cm], H2 [5.08-cm], H3 [7.62-cm].

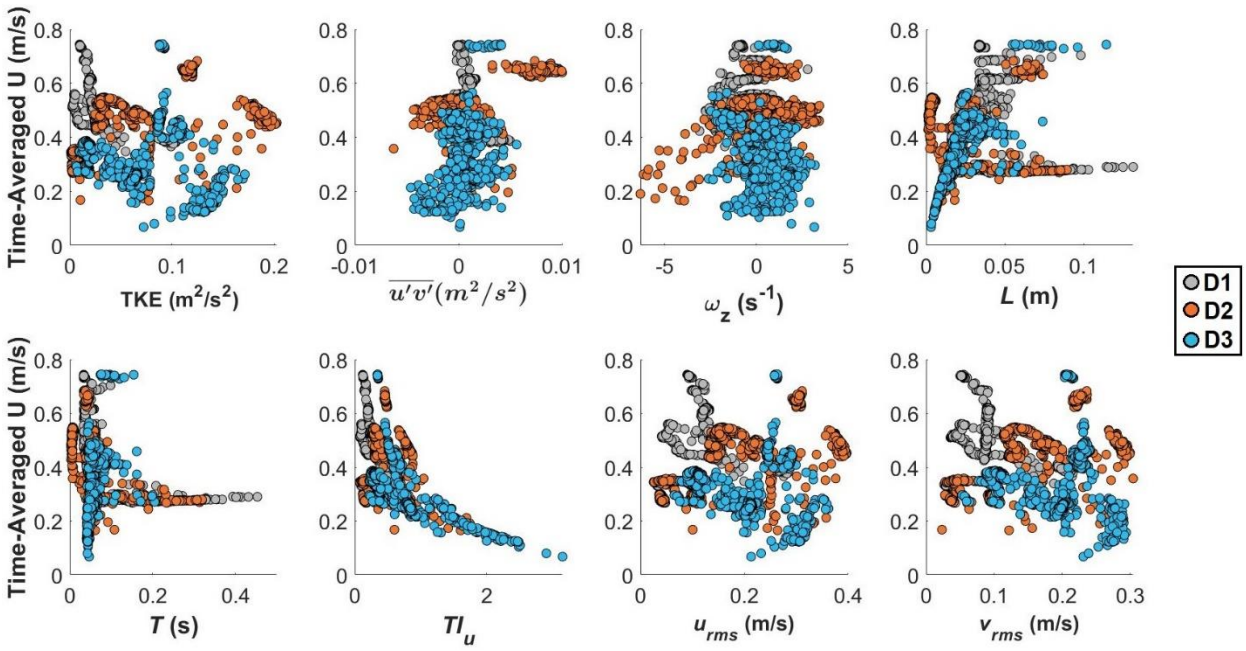

Figure B.20. Time-averaged longitudinal velocity U extracted from locations occupied by rainbow trout swimming with diagonal structures (DS) compared with the turbulent flow conditions for each location. Turbulence metrics depicted include turbulent kinetic energy (TKE), Reynolds stress ($\overline{u'v'}$), vorticity (ω_z), turbulent integral length scale (L), turbulent integral time scale (T), turbulence intensity (TI_U), U_{rms}, and V_{rms}. Scatter plots were generated to identify potential relationship between U and the turbulence metrics examined. Different colors indicate the diameter of the DS, D1 [2.54-cm], D2 [5.08-cm], D3 [7.62-cm]. Data presented are derived from the XY plane.

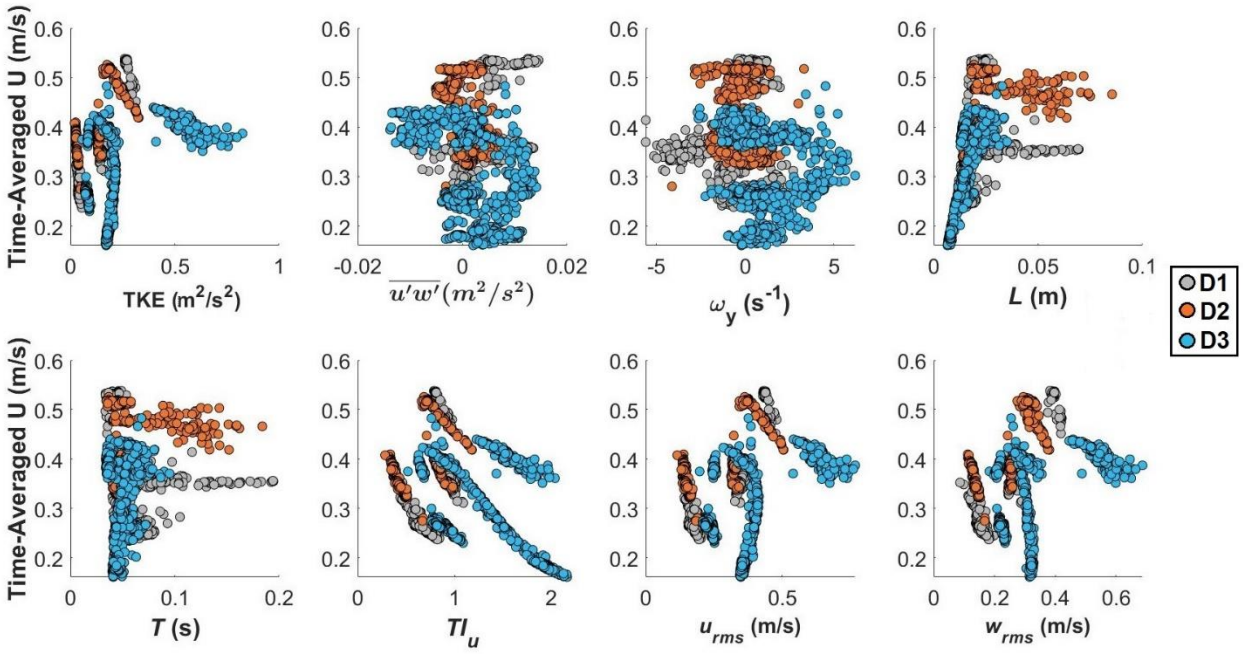

Figure B.21. Time-averaged longitudinal velocity U extracted from locations occupied by rainbow trout swimming with diagonal structures (DS) compared with the turbulent flow conditions for each location. Turbulence metrics depicted include turbulent kinetic energy (TKE), Reynolds stress ($\overline{u'w'}$), vorticity (ω_y), turbulent integral length scale (L), turbulent integral time scale (T), turbulence intensity (TI_U), U_{rms}, and V_{rms}. Scatter plots were generated to identify potential relationship between U and the turbulence metrics examined. Different colors indicate the diameter of the DS, D1 [2.54-cm], D2 [5.08-cm], D3 [7.62-cm]. Data presented are derived from the XZ plane.

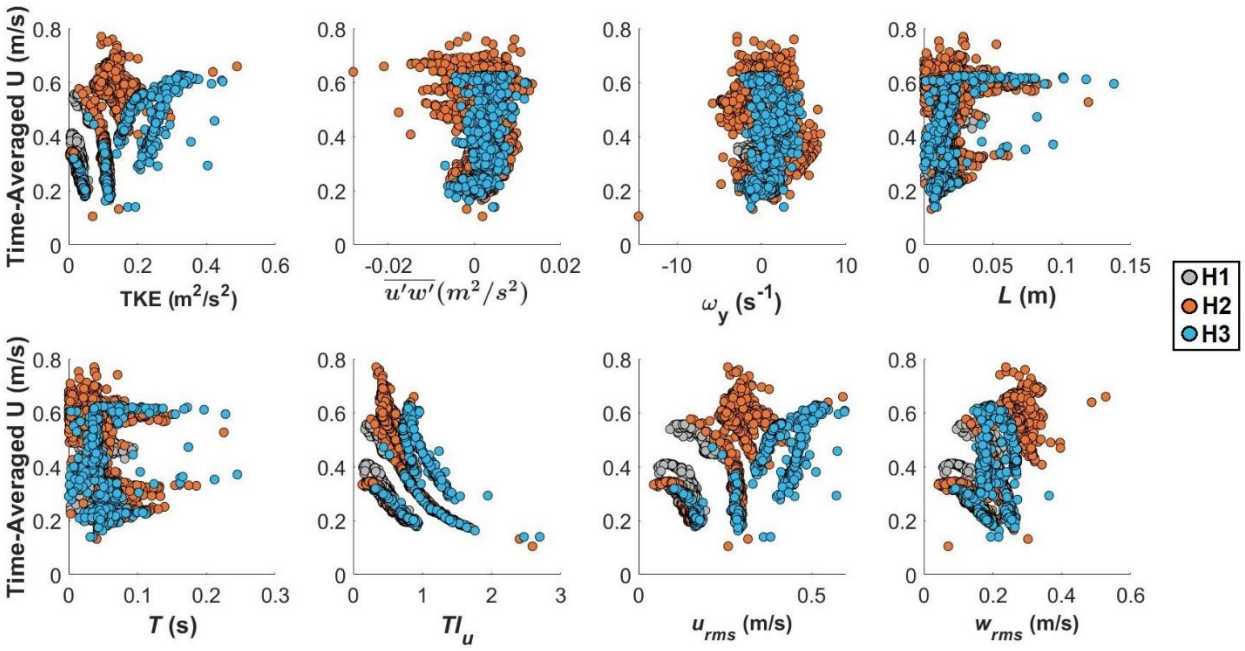

Figure B.22. Time-averaged longitudinal velocity U extracted from locations occupied by smallmouth bass swimming with horizontal structures (HS) compared with the turbulent flow conditions for each location. Turbulence metrics depicted include turbulent kinetic energy (TKE), Reynolds stress ($\overline{u'w'}$), vorticity (ω_y), turbulent integral length scale (L), turbulent integral time scale (T), turbulence intensity (TI_U), U_{rms}, and W_{rms}. Scatter plots were generated to identify potential relationship between U and the turbulence metrics examined. Different colors indicate the diameter of the HS, H1 [2.54-cm], H2 [5.08-cm], H3 [7.62-cm].

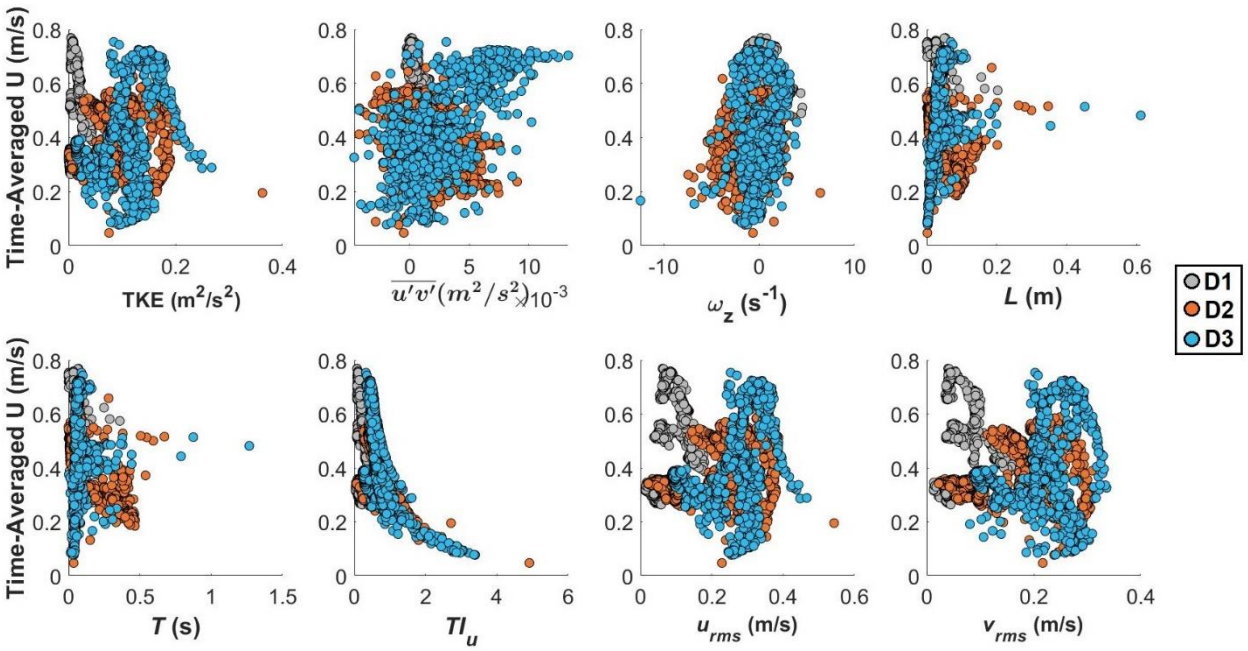

Figure B.23. Time-averaged longitudinal velocity U extracted from locations occupied by smallmouth bass swimming with diagonal structures (DS) compared with the turbulent flow conditions for each location. Turbulence metrics depicted include turbulent kinetic energy (TKE), Reynolds stress ($\overline{u'v'}$), vorticity (ω_z), turbulent integral length scale (L), turbulent integral time scale (T), turbulence intensity (TI_U), U_{rms}, and V_{rms}. Scatter plots were generated to identify potential relationship between U and the turbulence metrics examined. Different colors indicate the diameter of the DS, D1 [2.54-cm], D2 [5.08-cm], D3 [7.62-cm]. Data presented are derived from the XY plane.

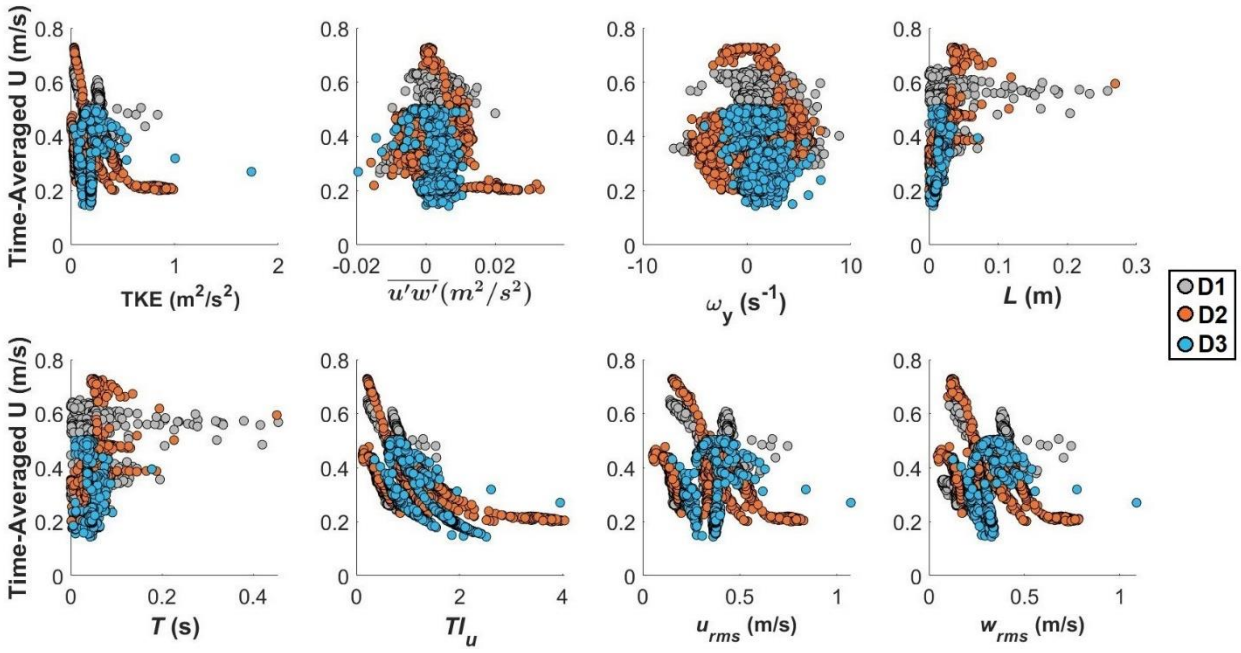

Figure B.24. Time-averaged longitudinal velocity U extracted from locations occupied by smallmouth bass swimming with diagonal structures (DS) compared with the turbulent flow conditions for each location. Turbulence metrics depicted include turbulent kinetic energy (TKE), Reynolds stress ($\overline{u'w'}$), vorticity (ω_y), turbulent integral length scale (L), turbulent integral time scale (T), turbulence intensity (TI_U), U_{rms}, and V_{rms}. Scatter plots were generated to identify potential relationship between U and the turbulence metrics examined. Different colors indicate the diameter of the DS, D1 [2.54-cm], D2 [5.08-cm], D3 [7.62-cm]. Data presented are derived from the XZ plane.

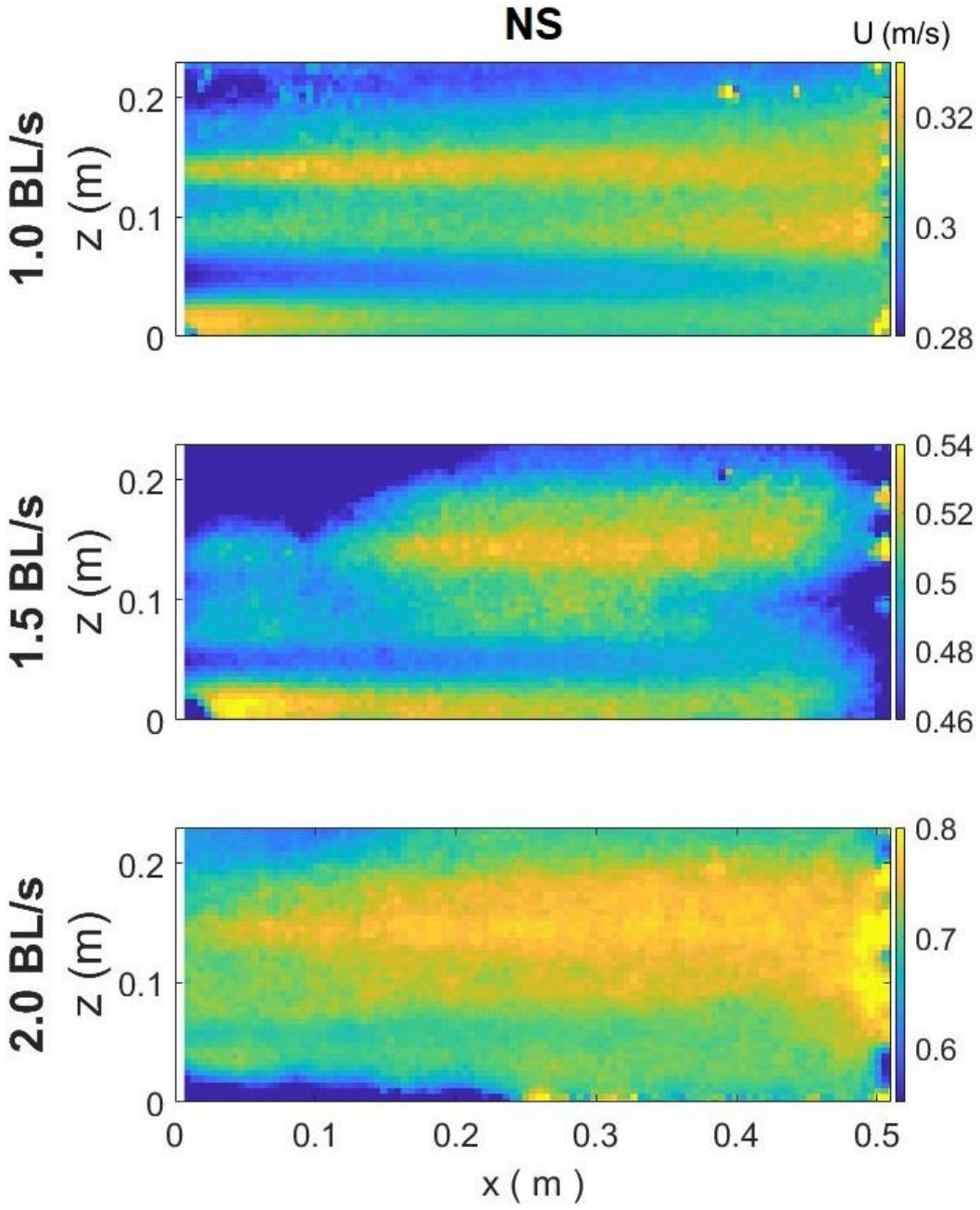

Figure B.25. Time-averaged longitudinal velocity field (*U*; m/s) on the vertical XZ plane tested within a large racetrack flume. Velocity fields are visualized for the control case with no structure (NS) for each of the three body length (BL) velocities in which fish were tested, 1.0 BL/s, 1.5 BL/s, and 2.0 BL/s

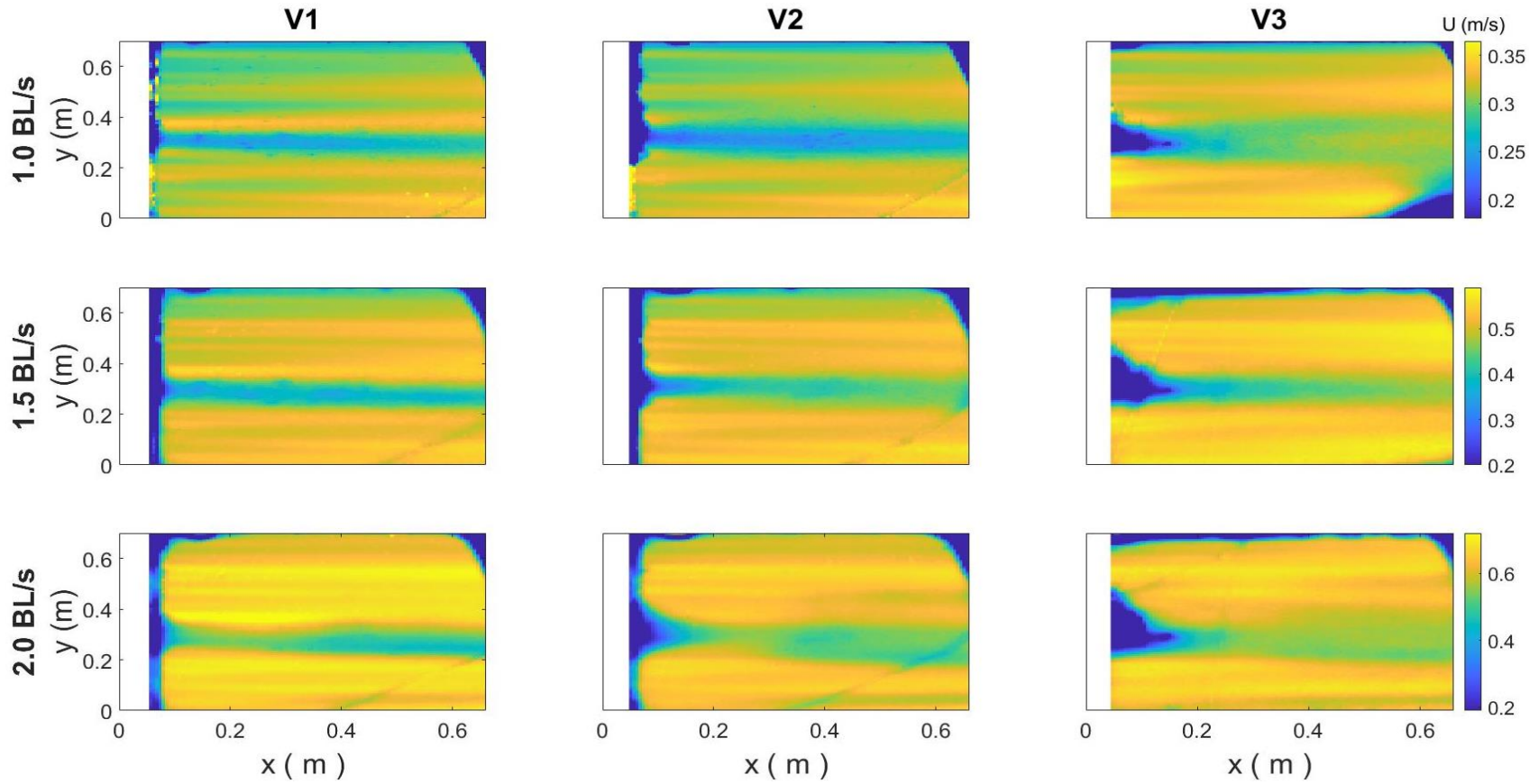

Figure B.26. Time-averaged longitudinal velocity field (*U*; m/s) on the horizontal XY plane tested within a large racetrack flume. Velocity fields are visualized for vertical structures (VS) in all three diameters, 2.54-cm (V1), 5.08-cm (V2), and 7.62-cm (V3), for each of the three body length (BL) velocities in which fish were tested, 1.0 BL/s, 1.5 BL/s, and 2.0 BL/s.

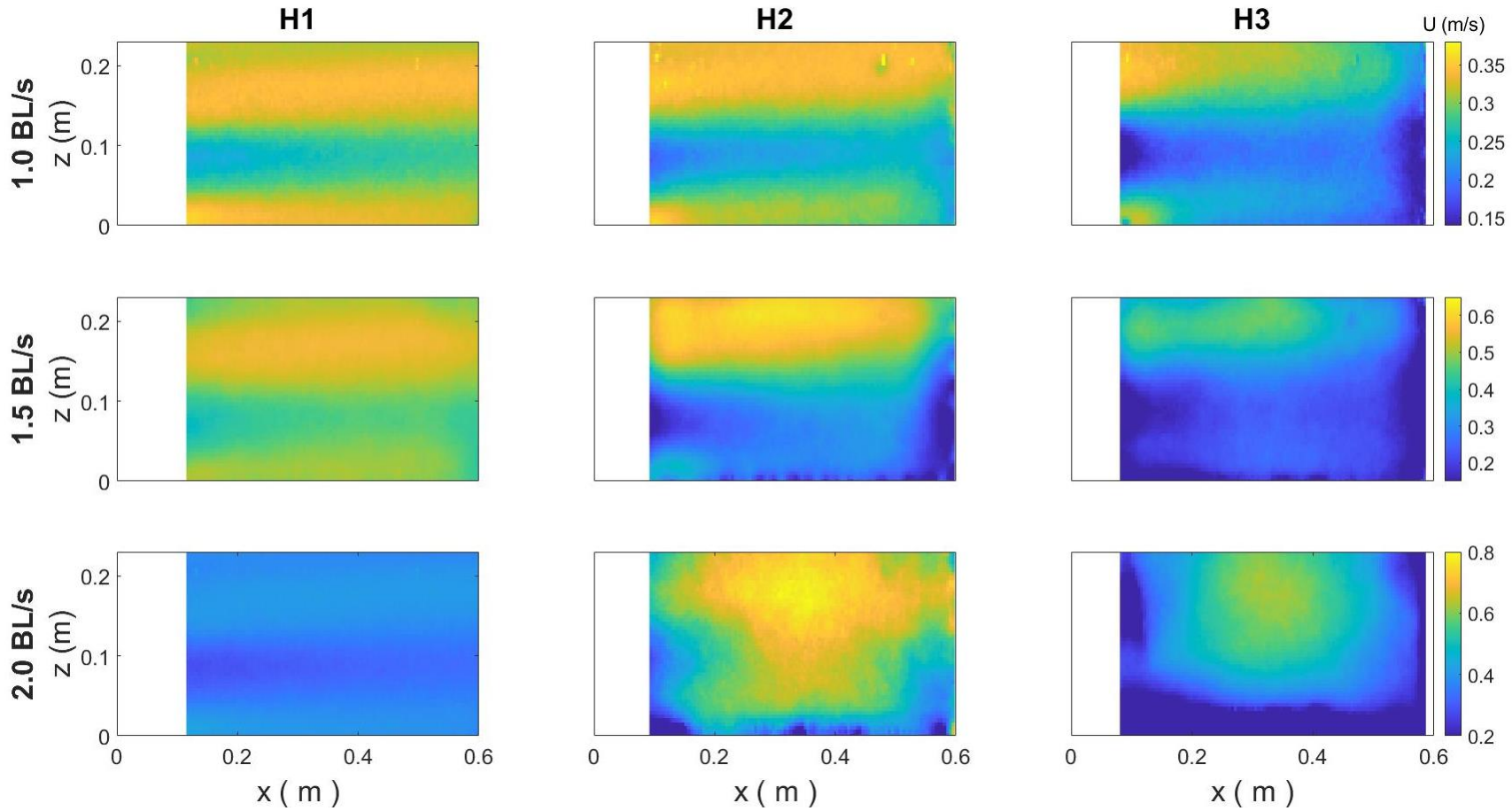

Figure B.27. Time-averaged longitudinal velocity field (*U*; m/s) on the vertical XZ plane tested within a large racetrack flume. Velocity fields are visualized for horizontal sructures in all three diameters, 2.54-cm (H1), 5.08-cm (H2), and 7.62-cm (H3), for each of the three body length (BL) velocities in which fish were tested, 1.0 BL/s, 1.5 BL/s, and 2.0 BL/s.

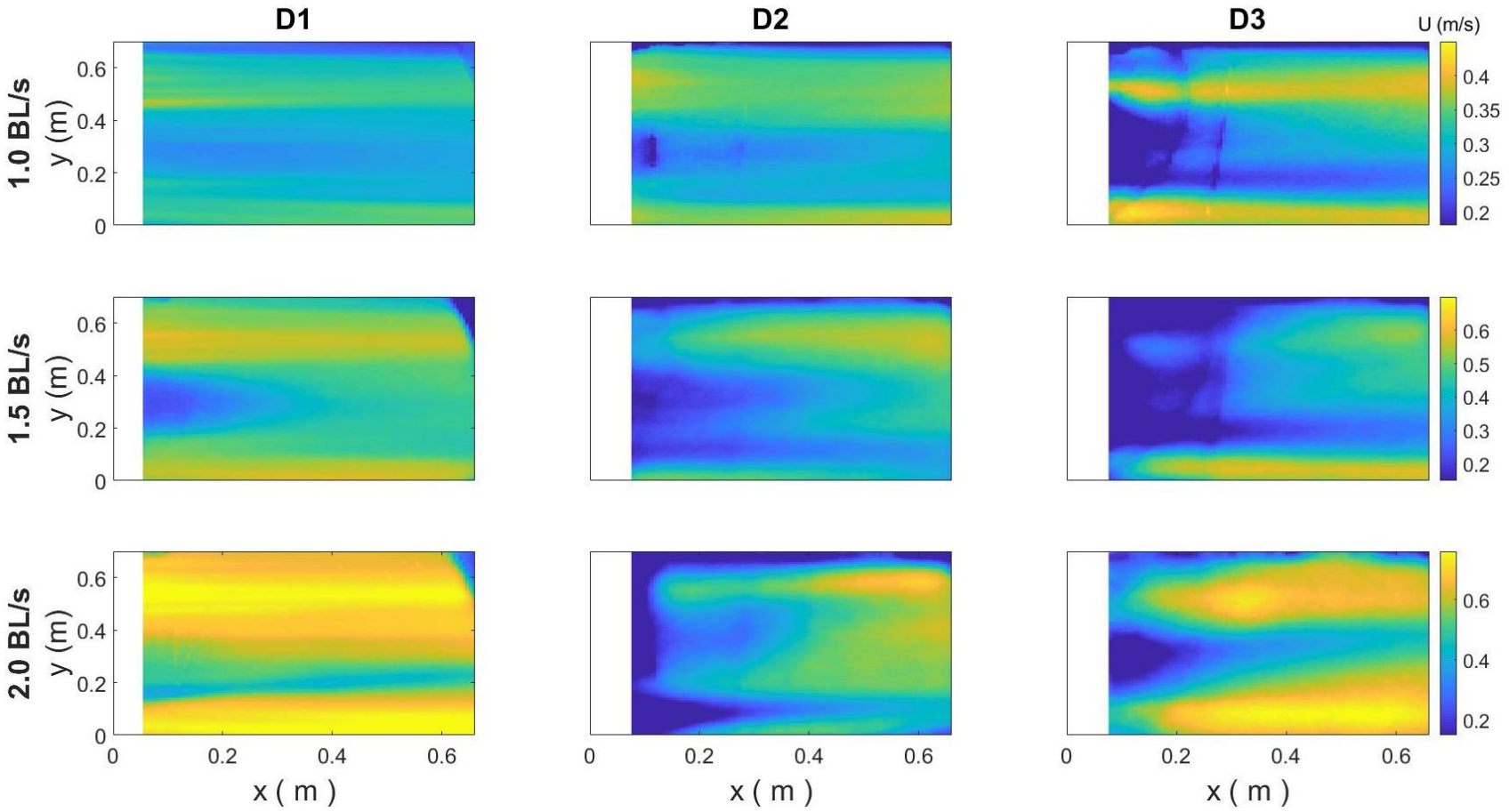

Figure B.28. Time-averaged longitudinal velocity field (*U*; m/s) on the horizontal XY plane tested within a large racetrack flume. Velocity fields are visualized for diagonal structures in all three diameters, 2.54-cm (D1), 5.08-cm (D2), and 7.62-cm (D3), for each of the three body length (BL) velocities in which fish were tested, 1.0 BL/s, 1.5 BL/s, and 2.0 BL/s.

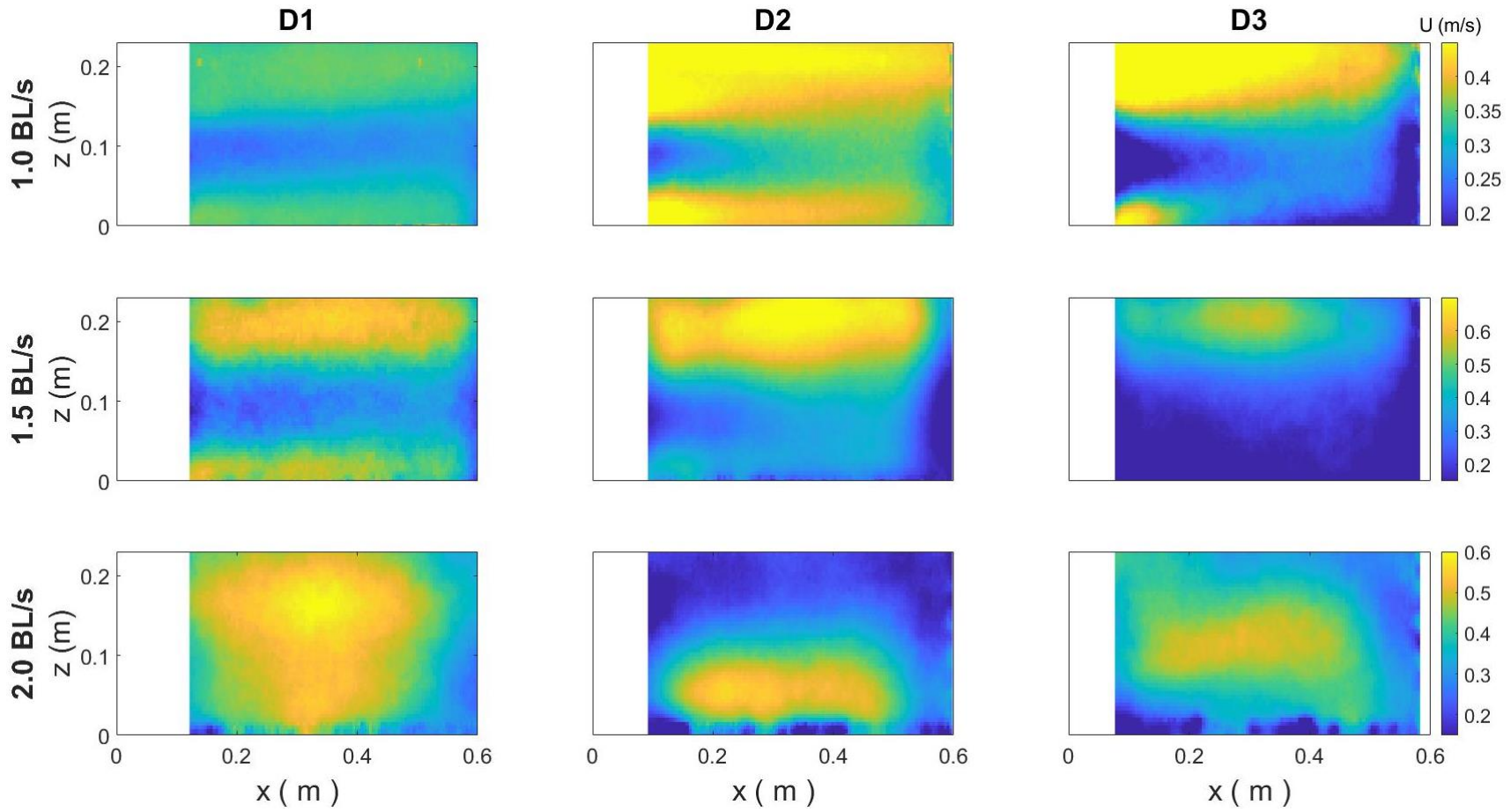

Figure B.29. Time-averaged longitudinal velocity field (*U*; m/s) on the vertical XZ plane tested within a large racetrack flume. Velocity fields are visualized for diagonal sructures in all three diameters, 2.54-cm (D1), 5.08-cm (D2), and 7.62-cm (D3), for each of the three body length (BL) velocities in which fish were tested, 1.0 BL/s, 1.5 BL/s, and 2.0 BL/s.

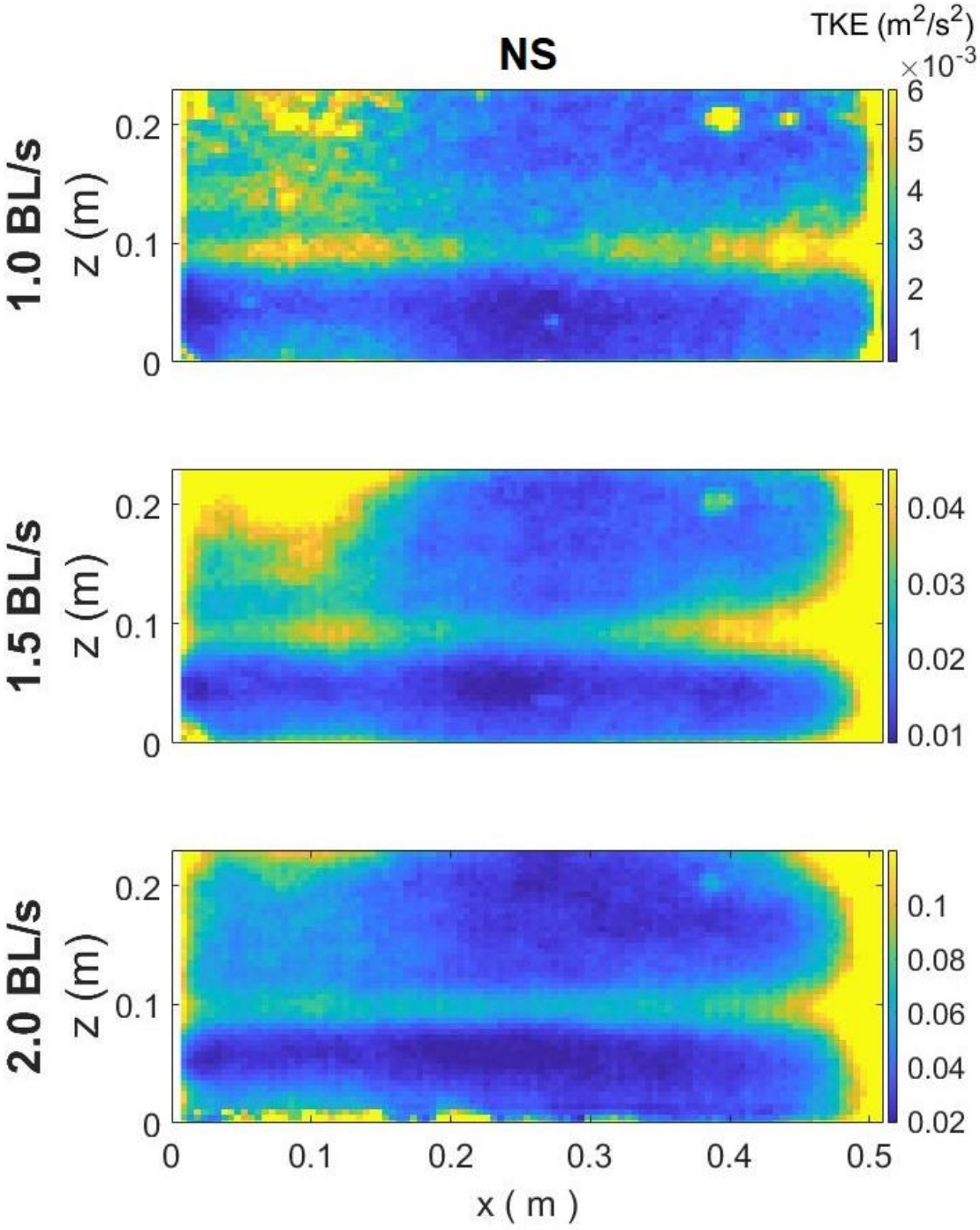

Figure B.30. Time-averaged turbulent kinetic energy field (TKE; m^2/s^2) on the vertical XZ plane tested within a large racetrack flume. Velocity fields are visualized for the control case with no structure (NS) for each of the three body length (BL) velocities in which fish were tested, 1.0 BL/s, 1.5 BL/s, and 2.0 BL/s.

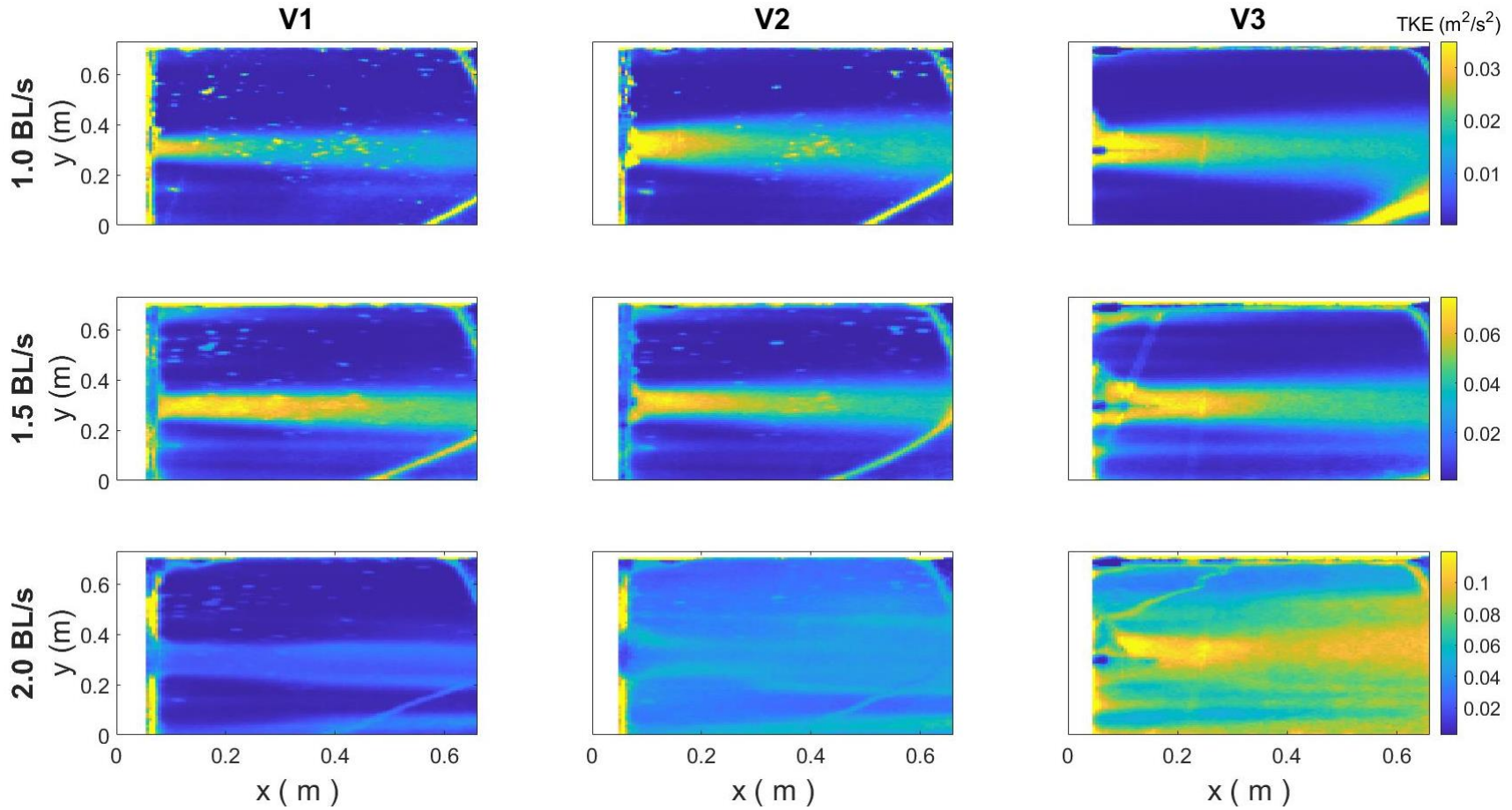

Figure B.31. Time-averaged turbulent kinetic energy field (TKE; m^2/s^2) on the horizontal XY plane tested within a large racetrack flume. Velocity fields are visualized for vertical structures in all three diameters, 2.54-cm (V1), 5.08-cm (V2), and 7.62-cm (V3), for each of the three body length (BL) velocities in which fish were tested, 1.0 BL/s, 1.5 BL/s, and 2.0 BL/s.

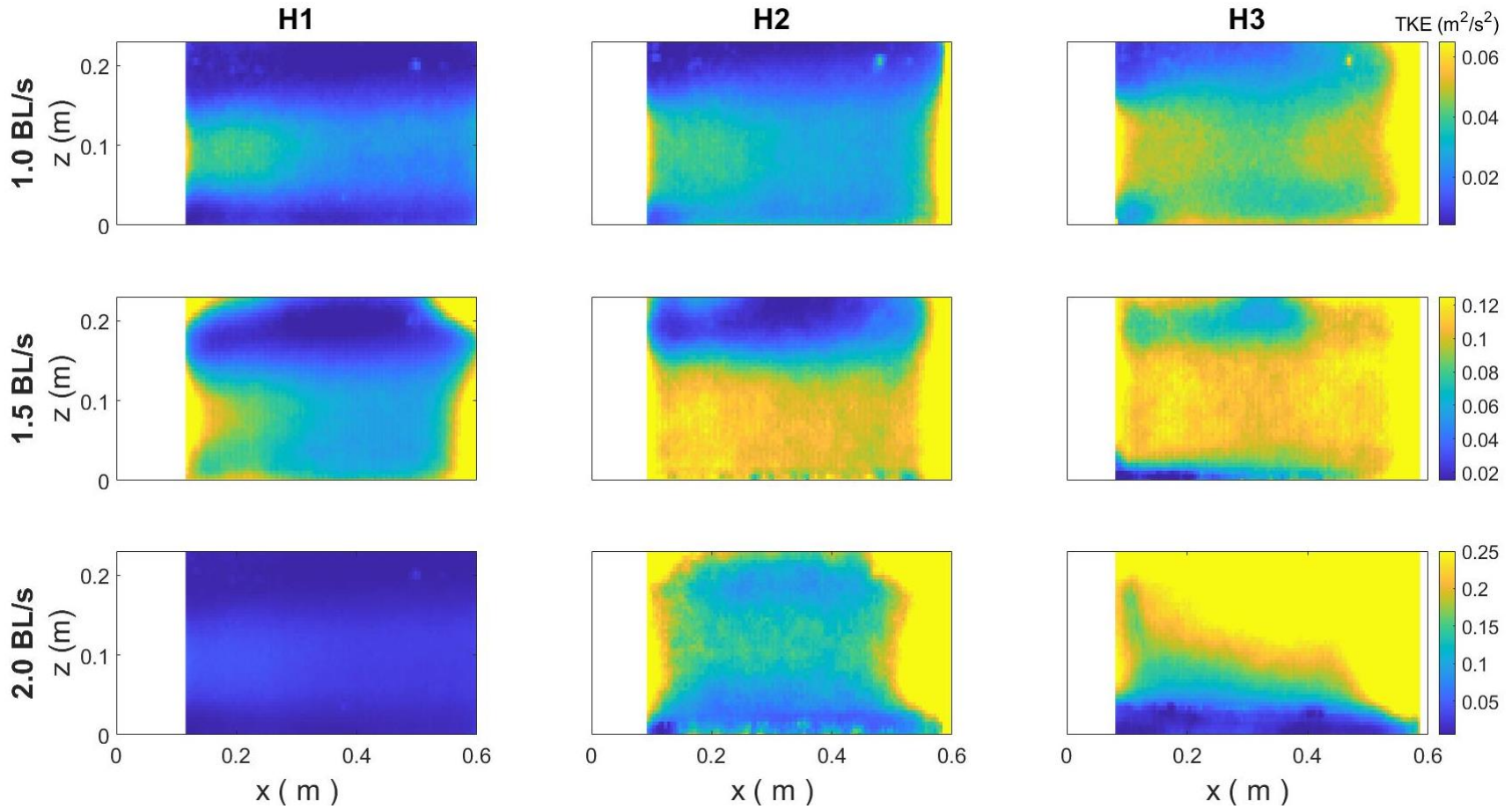

Figure B.32. Time-averaged turbulent kinetic energy field (TKE; m^2/s^2) on the vertical XZ plane tested within a large racetrack flume. Velocity fields are visualized for horizontal sructures in all three diameters, 2.54-cm (H1), 5.08-cm (H2), and 7.62-cm (H3), for each of the three body length (BL) velocities in which fish were tested, 1.0 BL/s, 1.5 BL/s, and 2.0 BL/s.

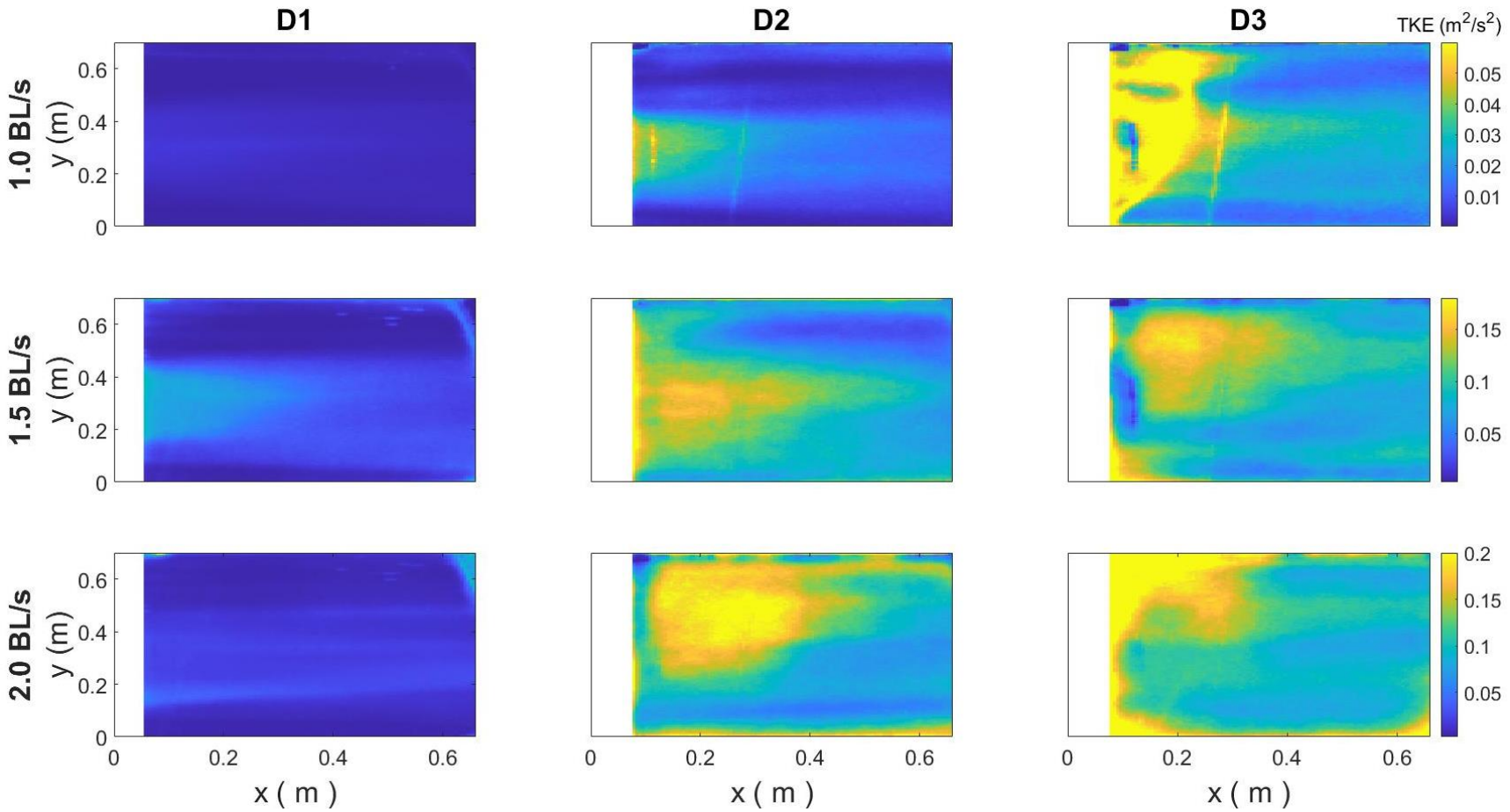

Figure B.33. Time-averaged turbulent kinetic energy field (TKE; m^2/s^2) on the horizontal XY plane tested within a large racetrack flume. Velocity fields are visualized for diagonal sructures in all three diameters, 2.54-cm (D1), 5.08-cm (D2), and 7.62-cm (D3), for each of the three body length (BL) velocities in which fish were tested, 1.0 BL/s, 1.5 BL/s, and 2.0 BL/s.

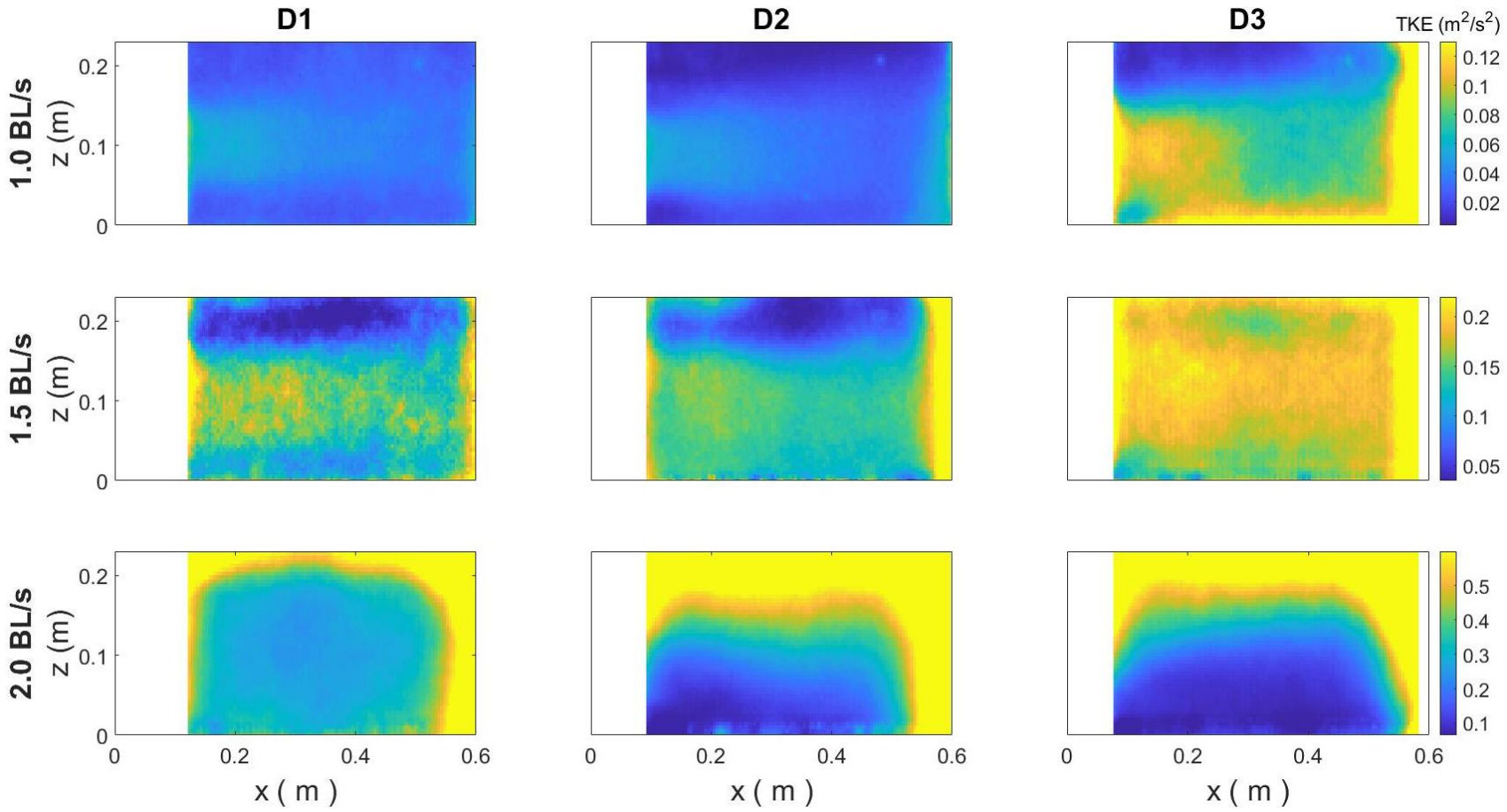

Figure B.34. Time-averaged turbulent kinetic energy field (TKE; m^2/s^2) on the vertical XZ plane tested within a large racetrack flume. Velocity fields are visualized for diagonal sructures in all three diameters, 2.54-cm (D1), 5.08-cm (D2), and 7.62-cm (D3), for each of the three body length (BL) velocities in which fish were tested, 1.0 BL/s, 1.5 BL/s, and 2.0 BL/s.

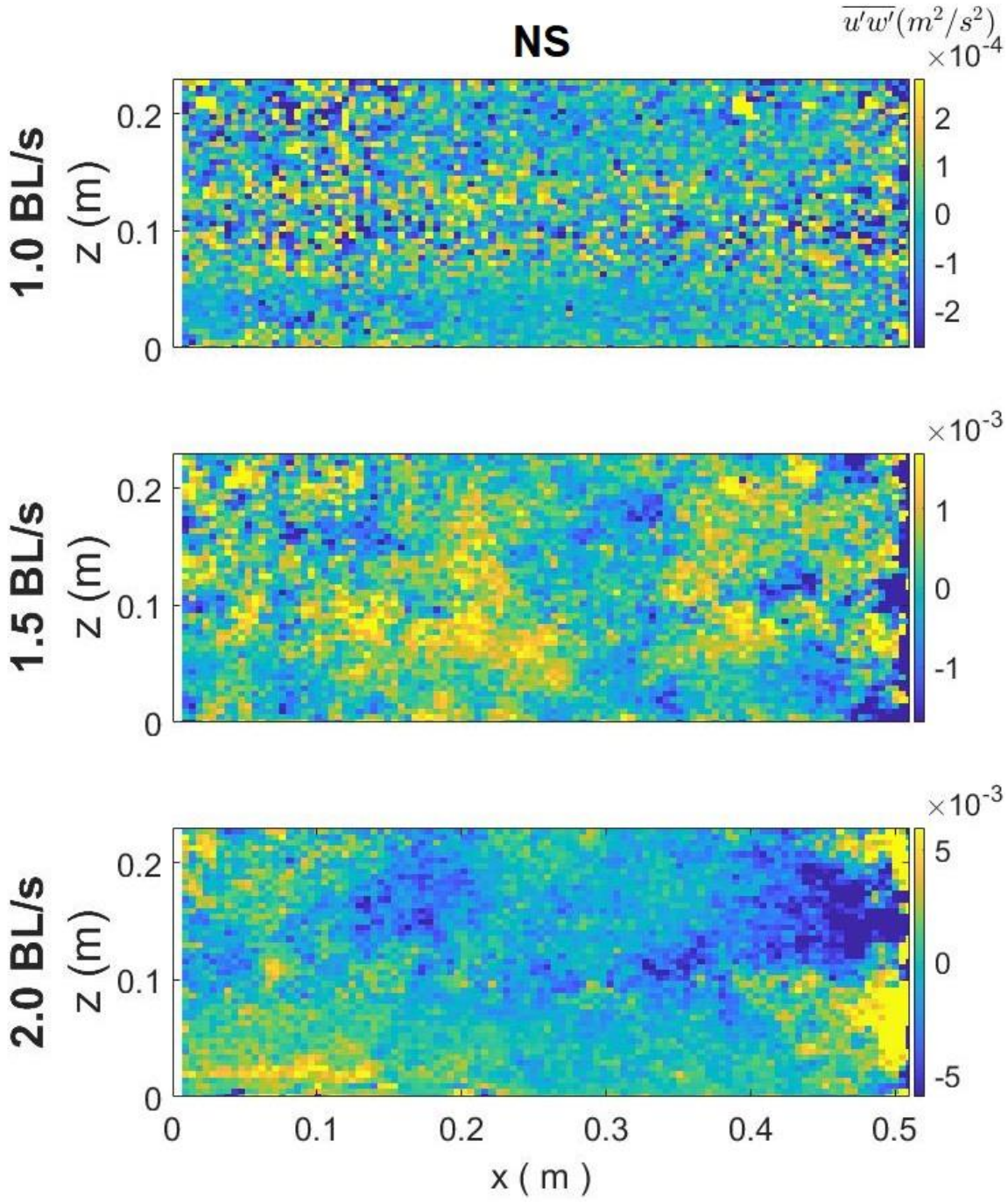

Figure B.35. Time-averaged Reynolds stresses ($\overline{u'w'}$; m^2/s^2) on the vertical XZ plane tested within a large racetrack flume. Velocity fields are visualized for the control case with no structure (NS) for each of the three body length (BL) velocities in which fish were tested, 1.0 BL/s, 1.5 BL/s, and 2.0 BL/s.

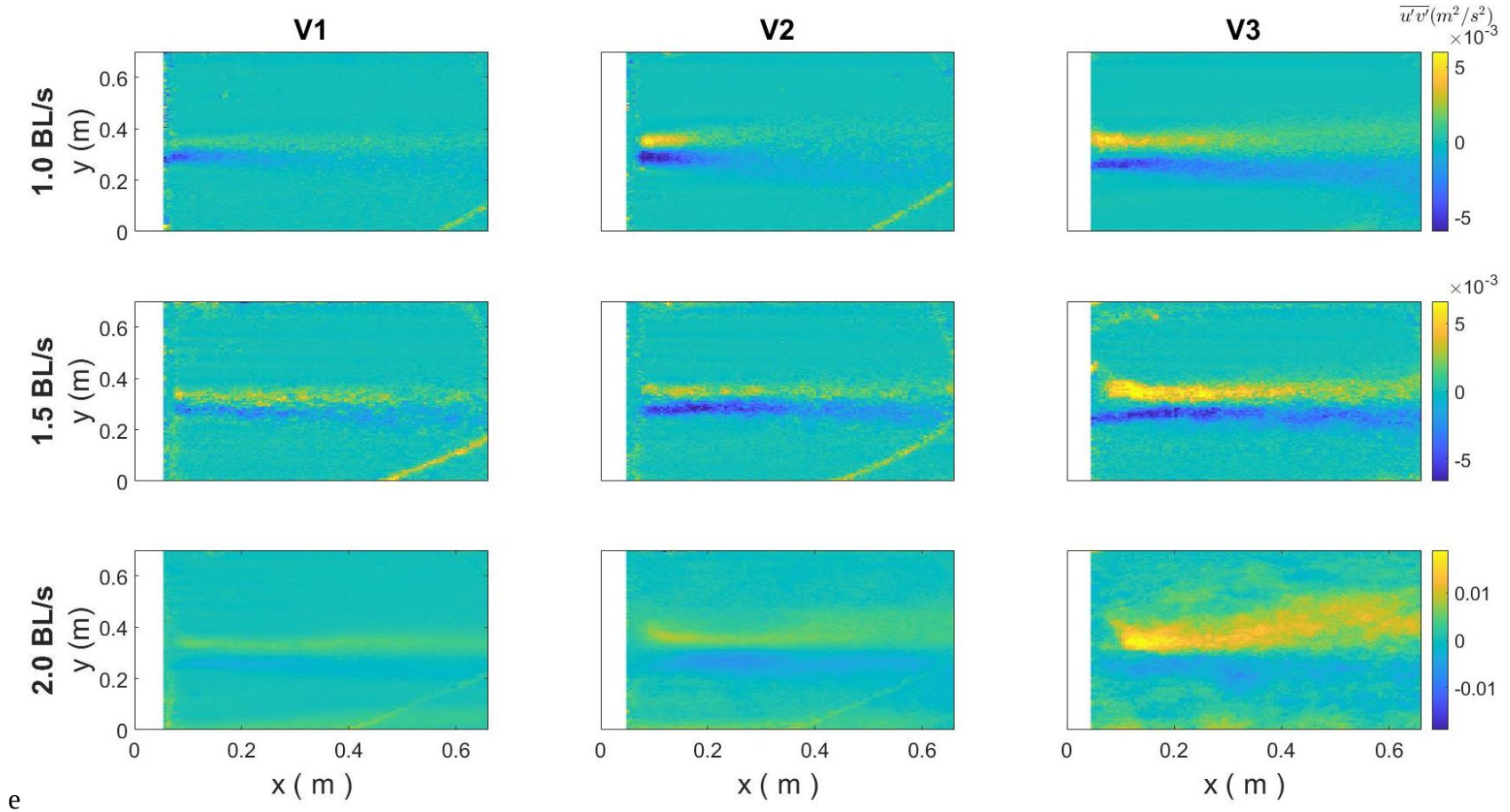

e

Figure B.36. Time-averaged Reynolds stresses ($\overline{u'v'}$; m^2/s^2) on the horizontal XY plane tested within a large racetrack flume. Velocity fields are visualized for vertical structures in all three diameters, 2.54-cm (V1), 5.08-cm (V2), and 7.62-cm (V3), for each of the three body length (BL) velocities in which fish were tested, 1.0 BL/s, 1.5 BL/s, and 2.0 BL/s.

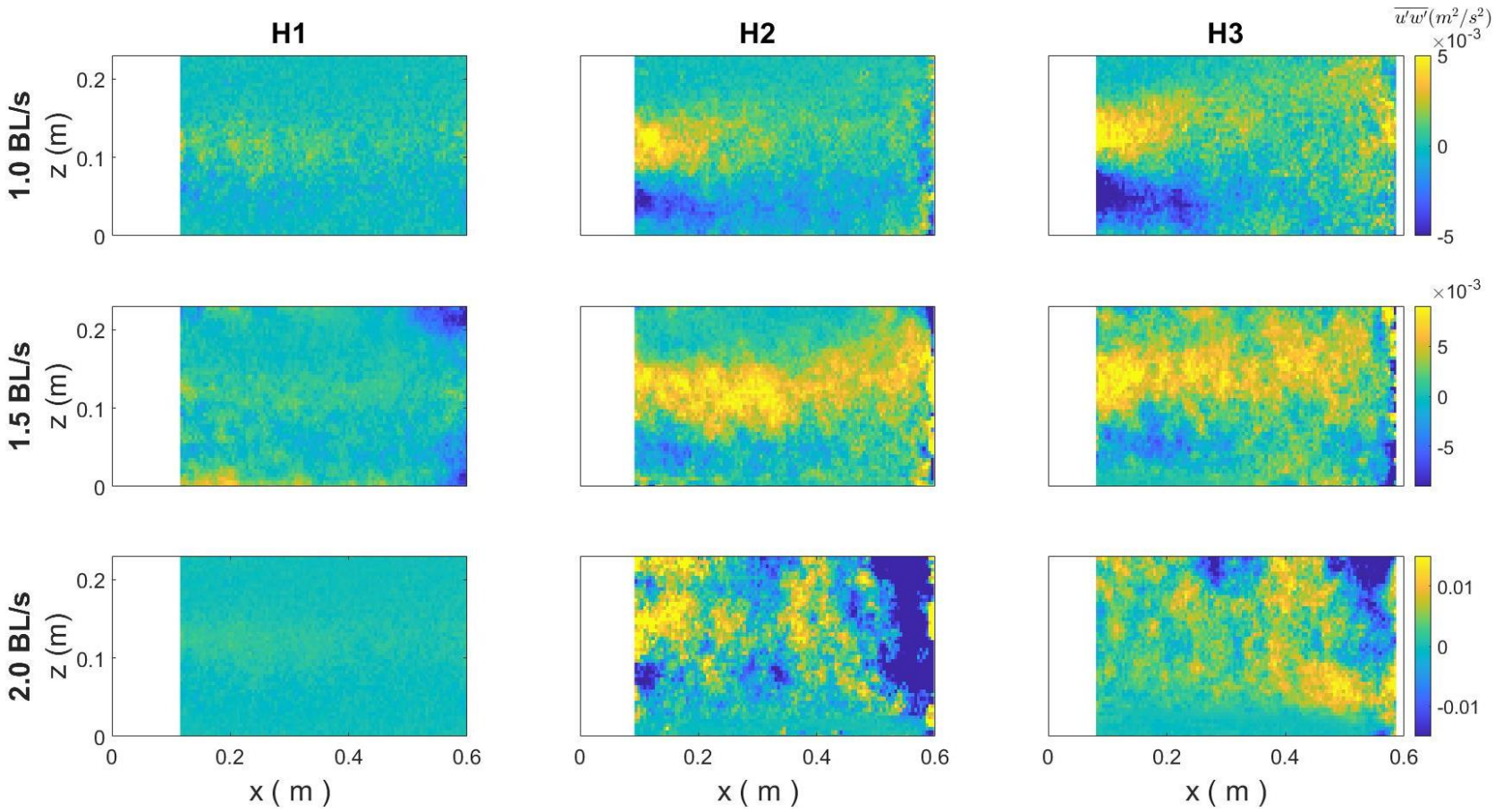

Figure B.37. Time-averaged Reynolds stresses ($\overline{u'w'}$; m^2/s^2) on the vertical XZ plane tested within a large racetrack flume. Velocity fields are visualized for horizontal sructures in all three diameters, 2.54-cm (H1), 5.08-cm (H2), and 7.62-cm (H3), for each of the three body length (BL) velocities in which fish were tested, 1.0 BL/s, 1.5 BL/s, and 2.0 BL/s.

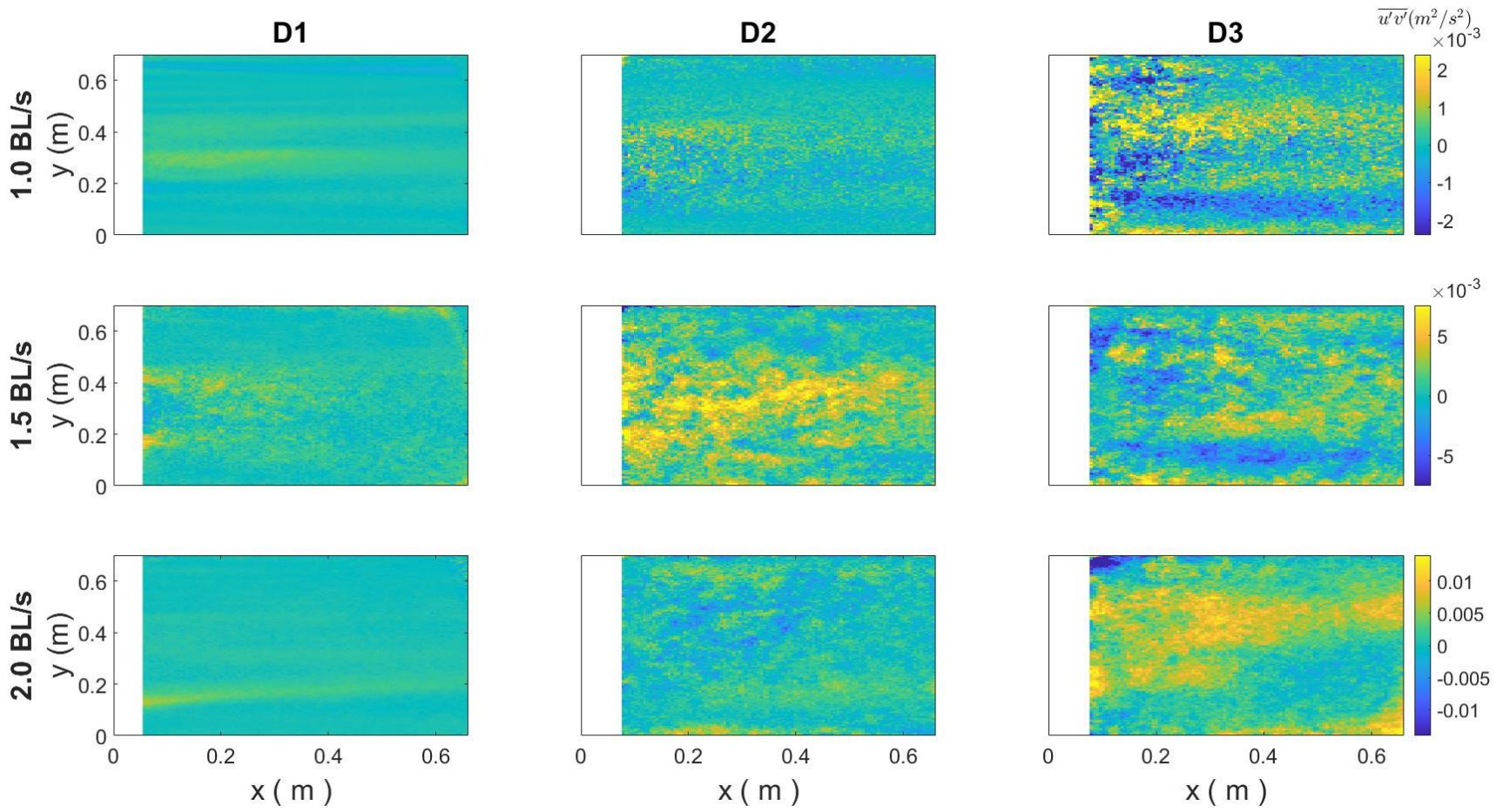

Figure B.38. Time-averaged Reynolds stresses ($\overline{u'v'}$; m^2/s^2) on the horizontal XY plane tested within a large racetrack flume. Velocity fields are visualized for diagonal structures in all three diameters, 2.54-cm (D1), 5.08-cm (D2), and 7.62-cm (D3), for each of the three body length (BL) velocities in which fish were tested, 1.0 BL/s, 1.5 BL/s, and 2.0 BL/s.

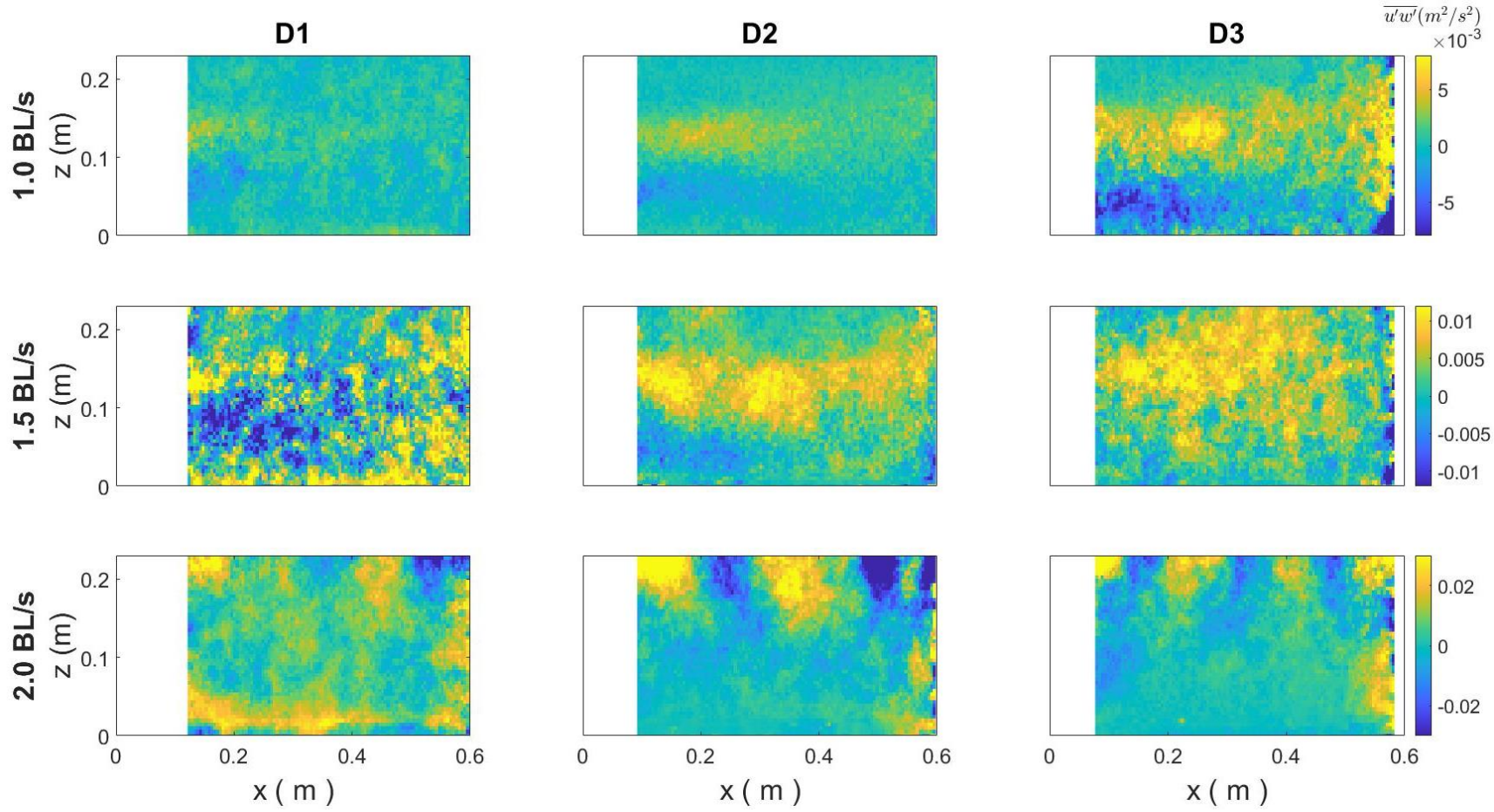

Figure B.39. Time-averaged Reynolds stresses ($\overline{u'w'}$; m^2/s^2) on the vertical XZ plane tested within a large racetrack flume. Velocity fields are visualized for diagonal sructures in all three diameters, 2.54-cm (D1), 5.08-cm (D2), and 7.62-cm (D3), for each of the three body length (BL) velocities in which fish were tested, 1.0 BL/s, 1.5 BL/s, and 2.0 BL/s.

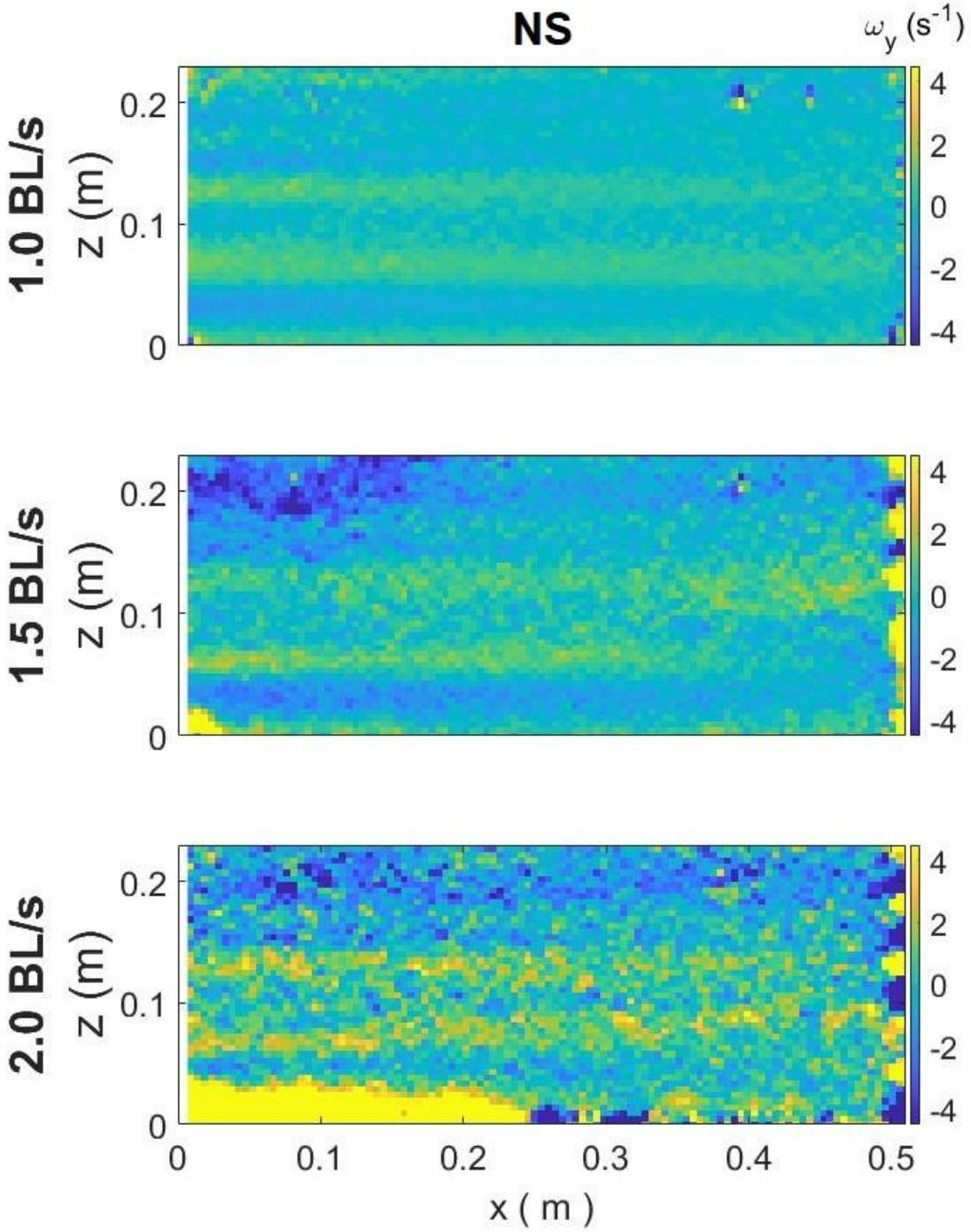

Figure B.40. Time-averaged vorticity (ω_z; s^{-1}) on the vertical XZ plane tested within a large racetrack flume. Velocity fields are visualized for the control case with no structure (NS) for each of the three body length (BL) velocities in which fish were tested, 1.0 BL/s, 1.5 BL/s, and 2.0 BL/s.

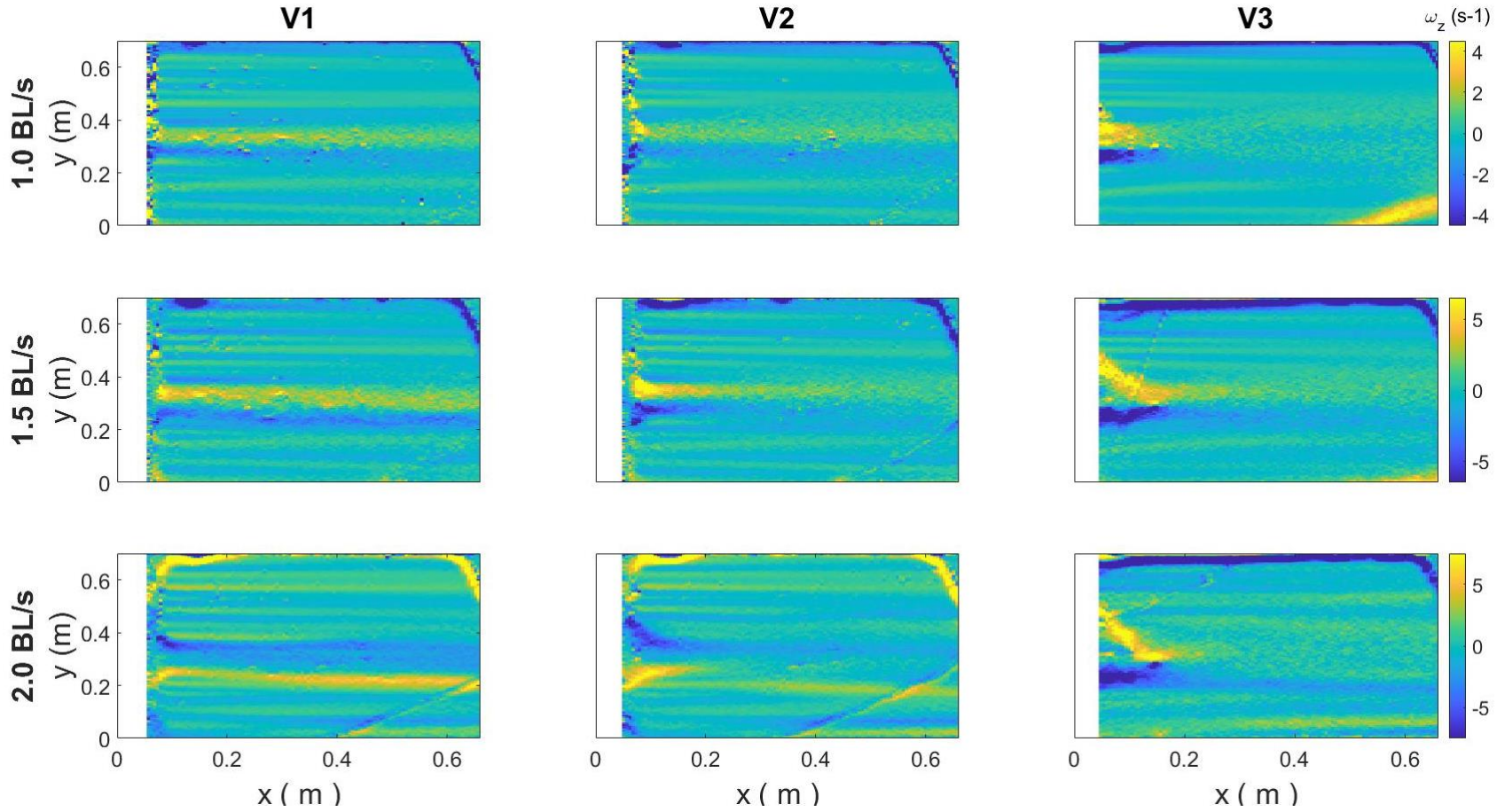

Figure B.41. Time-averaged vorticity (ω_z; s^{-1}) on the horizontal XY plane tested within a large racetrack flume. Velocity fields are visualized for vertical structures in all three diameters, 2.54-cm (V1), 5.08-cm (V2), and 7.62-cm (V3), for each of the three body length (BL) velocities in which fish were tested, 1.0 BL/s, 1.5 BL/s, and 2.0 BL/s.

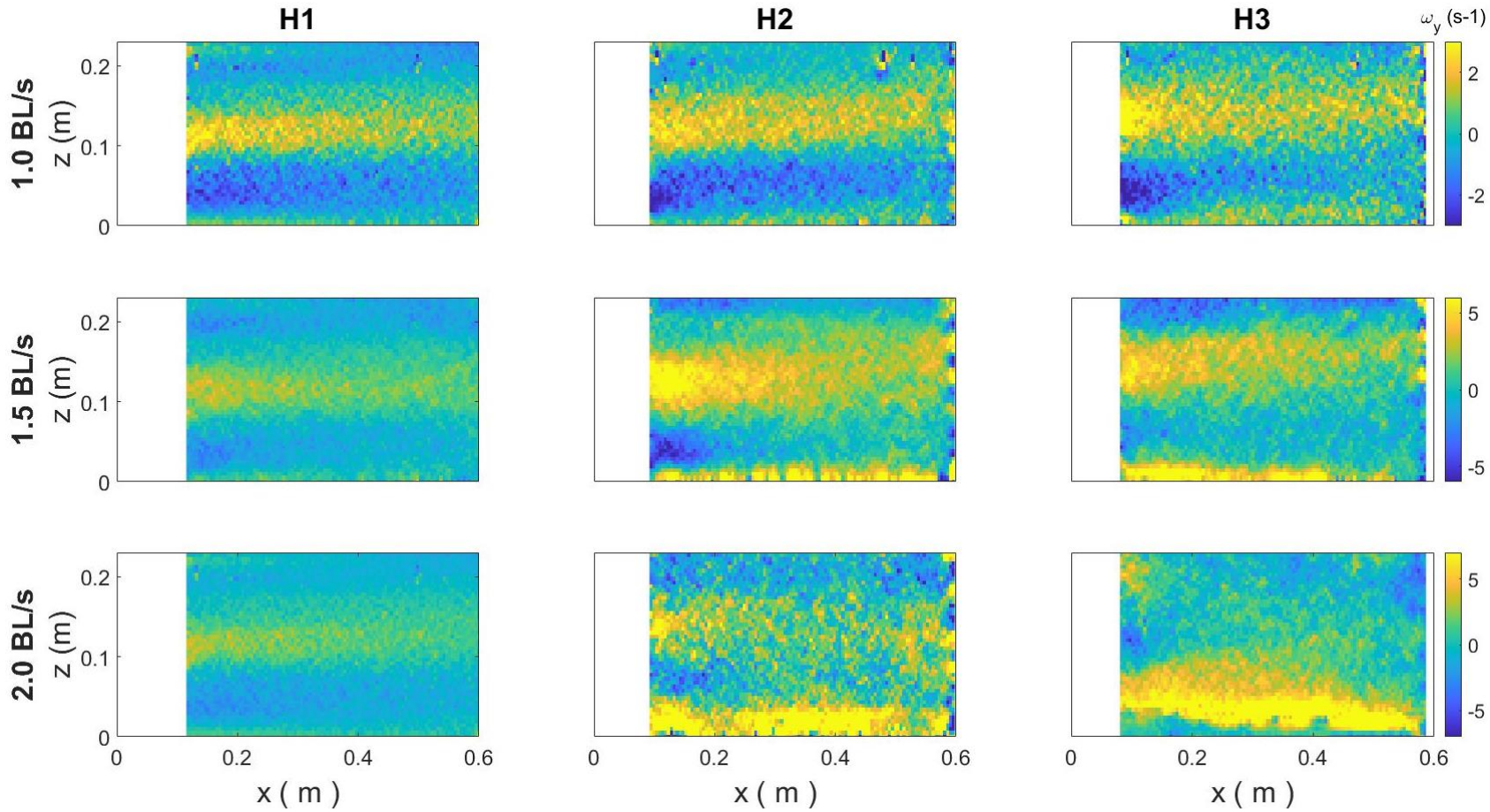

Figure B.42. Time-averaged vorticity (ω_y; s^{-1}) on the vertical XZ plane tested within a large racetrack flume. Velocity fields are visualized for horizontal sructures in all three diameters, 2.54-cm (H1), 5.08-cm (H2), and 7.62-cm (H3), for each of the three body length (BL) velocities in which fish were tested, 1.0 BL/s, 1.5 BL/s, and 2.0 BL/s.

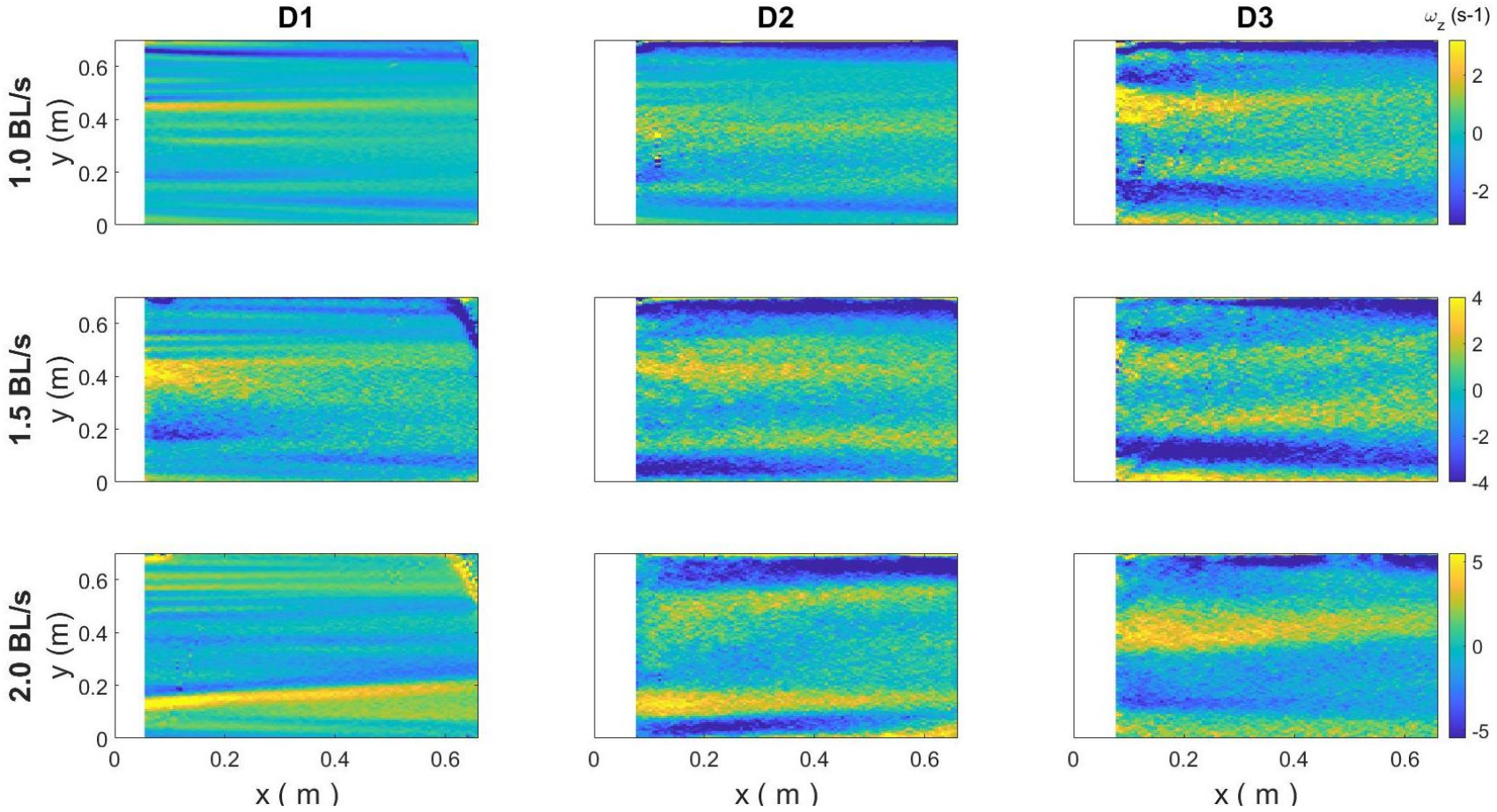

Figure B.43. Time-averaged vorticity (ω_z; s^{-1}) on the horizontal XY plane tested within a large racetrack flume. Velocity fields are visualized for diagonal structures in all three diameters, 2.54-cm (D1), 5.08-cm (D2), and 7.62-cm (D3), for each of the three body length (BL) velocities in which fish were tested, 1.0 BL/s, 1.5 BL/s, and 2.0 BL/s.

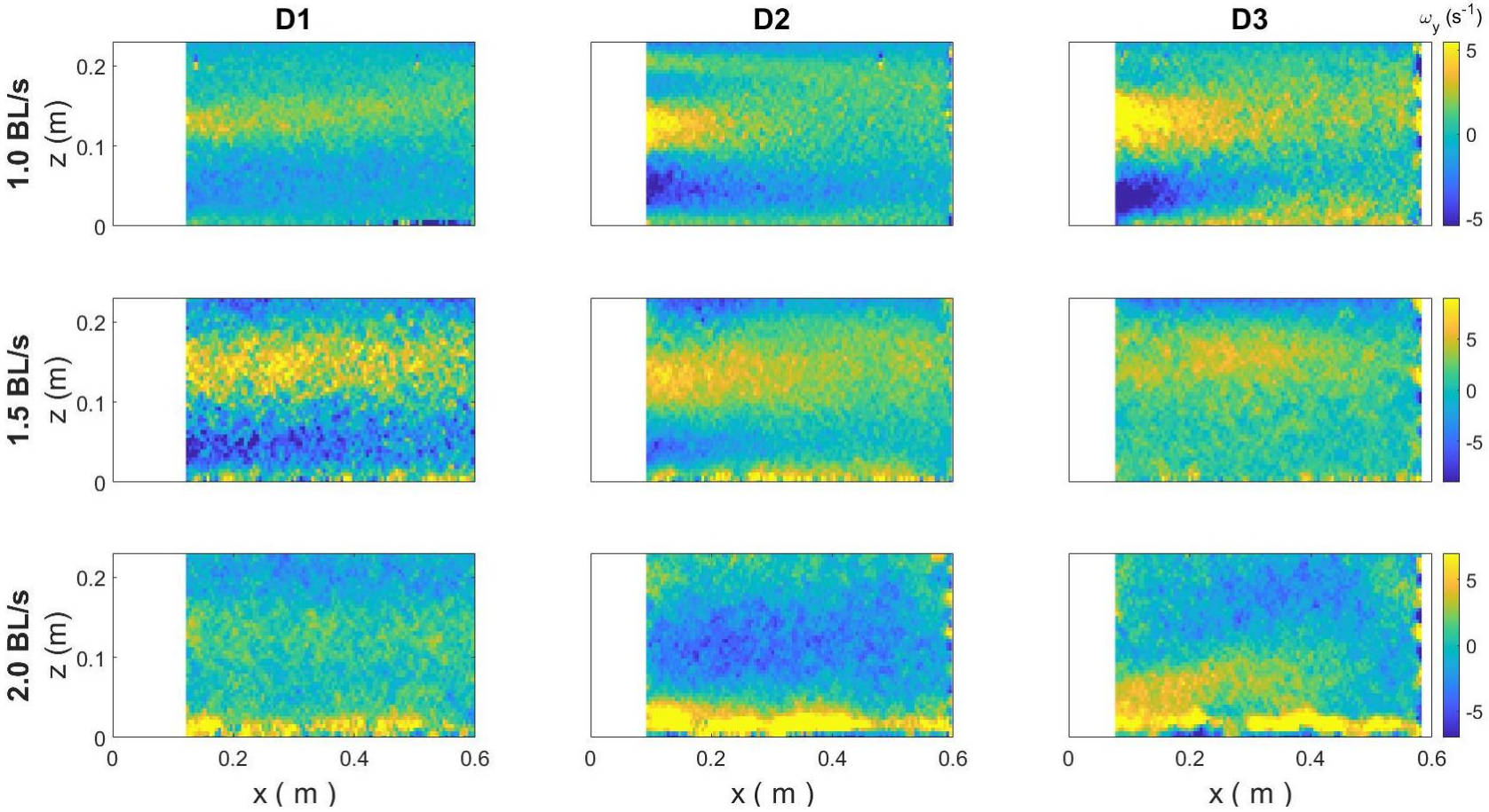

Figure B.44. Time-averaged vorticity (ω_y; s^{-1}) on the vertical XZ plane tested within a large racetrack flume. Velocity fields are visualized for diagonal sructures in all three diameters, 2.54-cm (D1), 5.08-cm (D2), and 7.62-cm (D3), for each of the three body length (BL) velocities in which fish were tested, 1.0 BL/s, 1.5 BL/s, and 2.0 BL/s

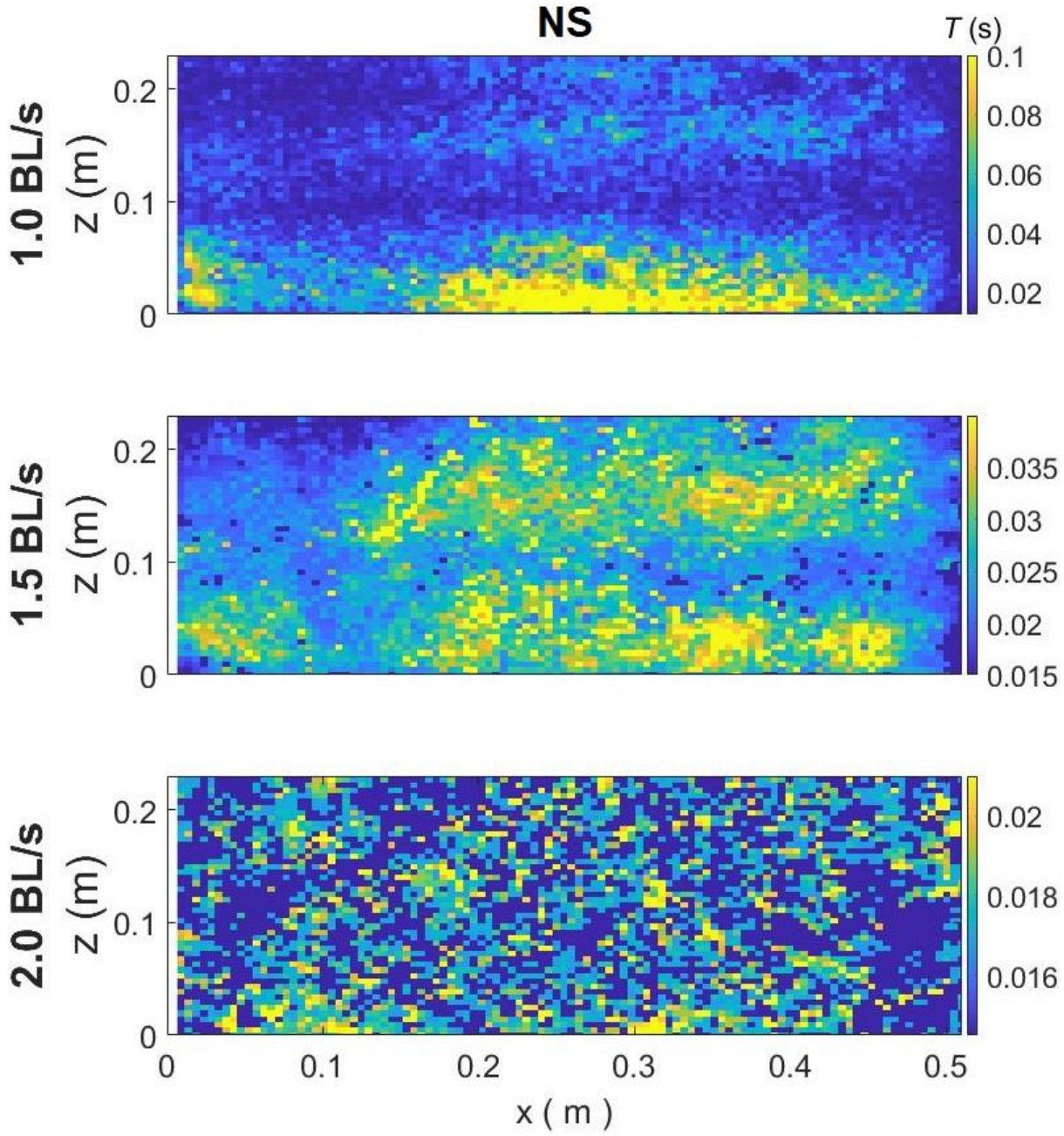

Figure B.45. Time-averaged turbulent integral time scale (*T*; s) on the vertical XZ plane tested within a large racetrack flume. Velocity fields are visualized for the control case with no structure (NS) for each of the three body length (BL) velocities in which fish were tested, 1.0 BL/s, 1.5 BL/s, and 2.0 BL/s.

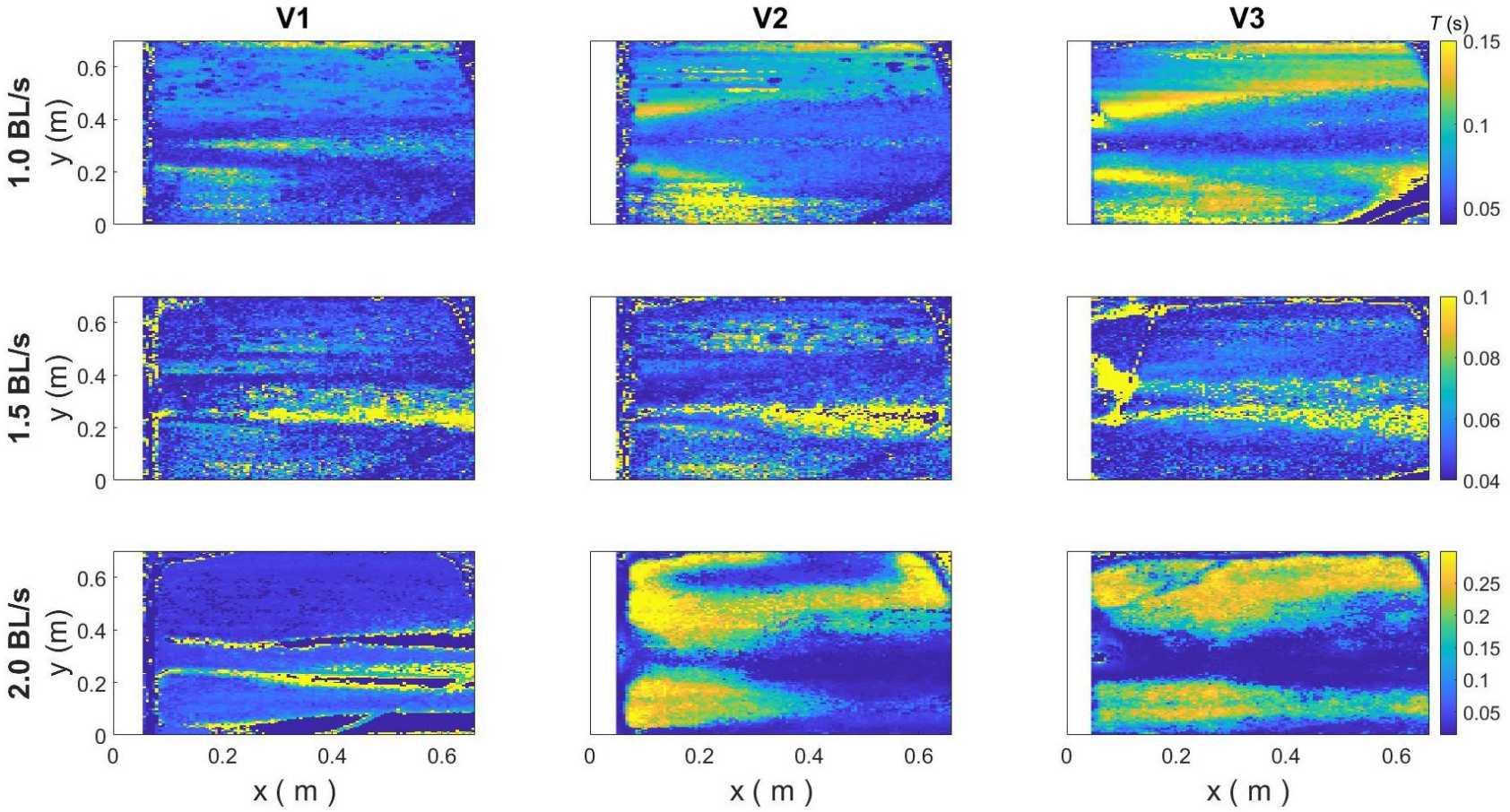

Figure B.46. Time-averaged turbulent integral time scale (*T*; s) on the horizontal XY plane tested within a large racetrack flume. Velocity fields are visualized for vertical structures in all three diameters, 2.54-cm (V1), 5.08-cm (V2), and 7.62-cm (V3), for each of the three body length (BL) velocities in which fish were tested, 1.0 BL/s, 1.5 BL/s, and 2.0 BL/s.

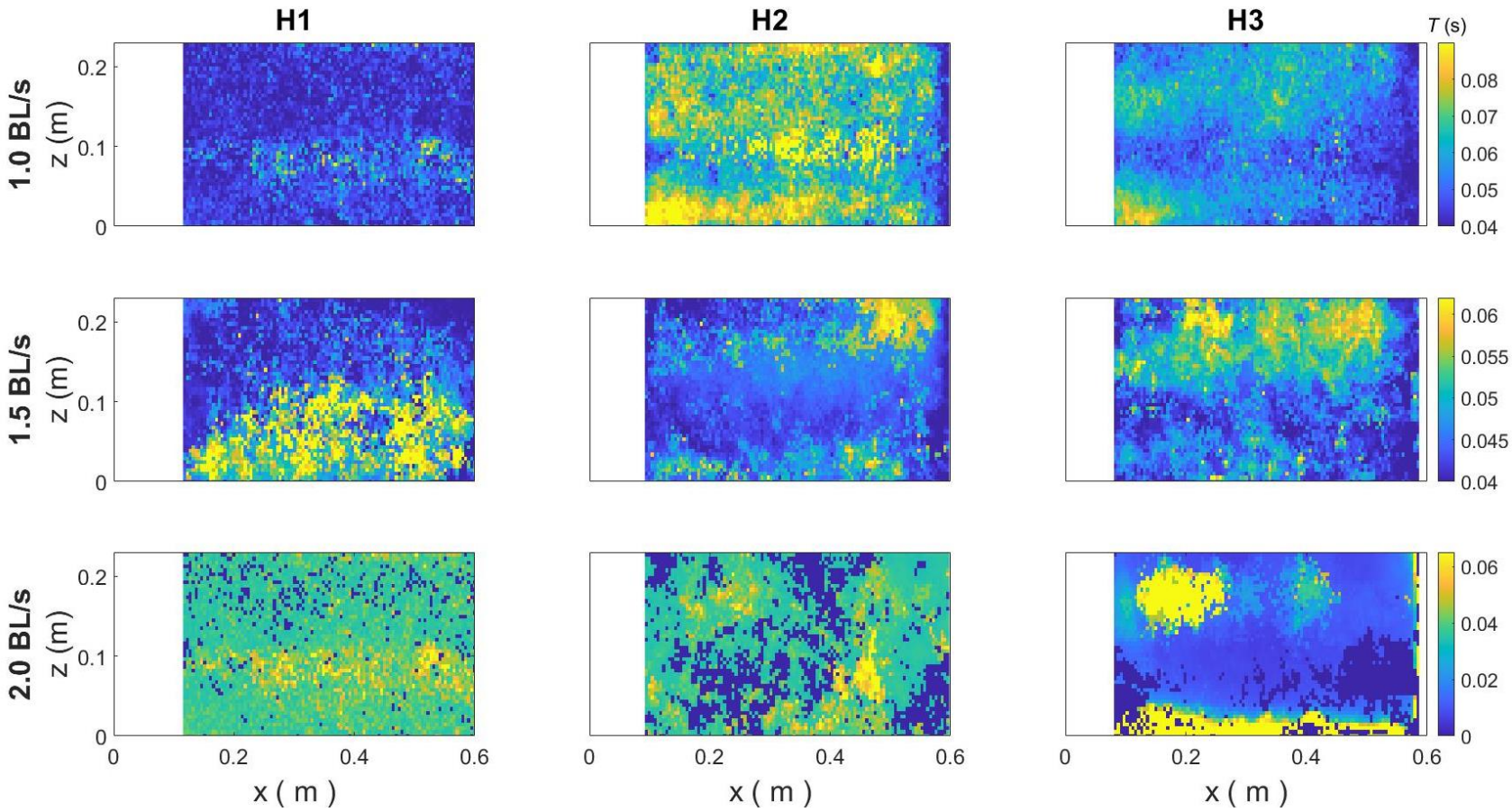

Figure B.47. Time-averaged turbulent integral time scale (*T*; s) on the vertical XZ plane tested within a large racetrack flume. Velocity fields are visualized for horizontal sructures in all three diameters, 2.54-cm (H1), 5.08-cm (H2), and 7.62-cm (H3), for each of the three body length (BL) velocities in which fish were tested, 1.0 BL/s, 1.5 BL/s, and 2.0 BL/s.

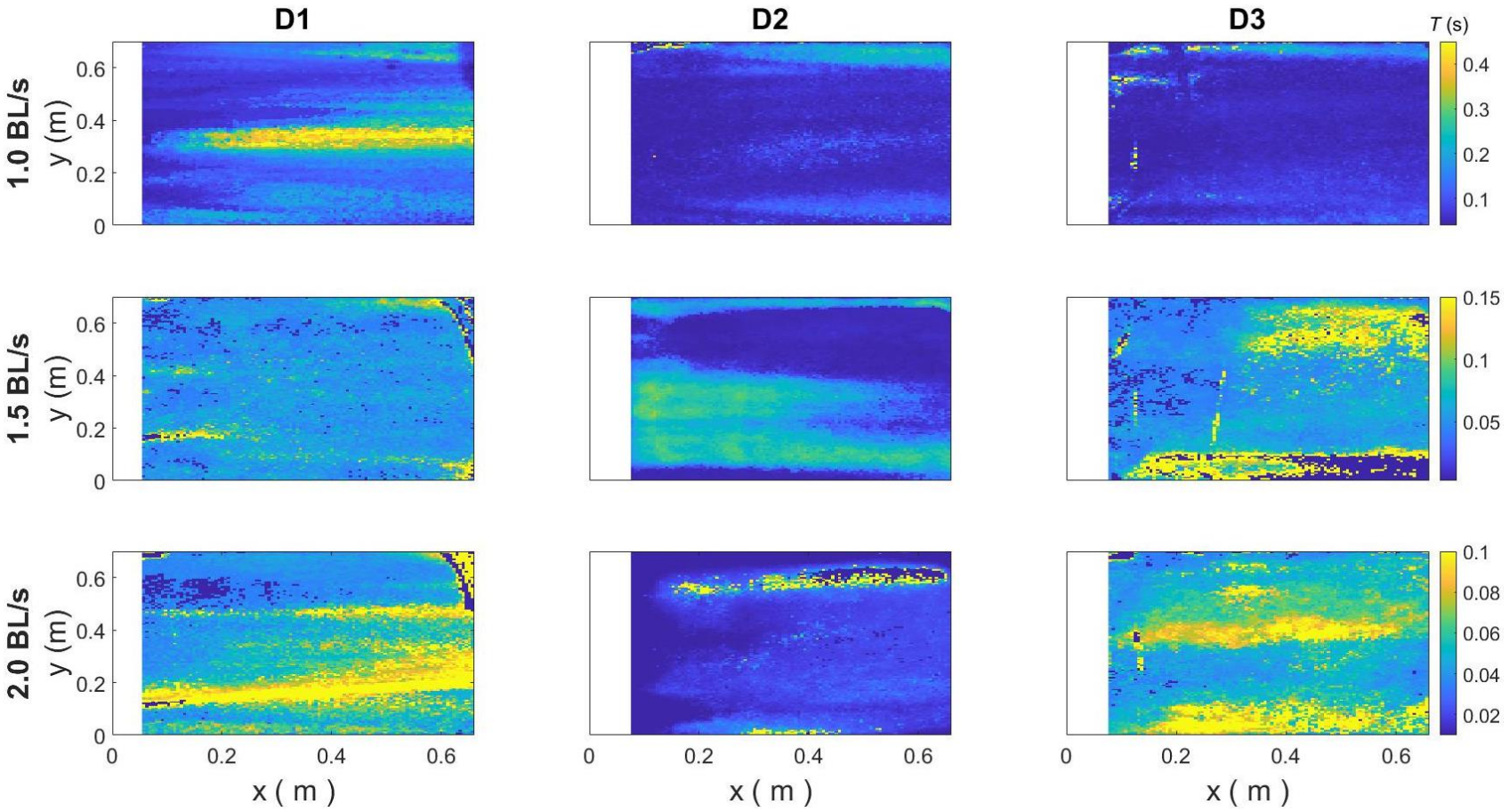

Figure B.48. Time-averaged turbulent integral time scale (*T*; s) on the horizontal XY plane tested within a large racetrack flume. Velocity fields are visualized for diagonal structures in all three diameters, 2.54-cm (D1), 5.08-cm (D2), and 7.62-cm (D3), for each of the three body length (BL) velocities in which fish were tested, 1.0 BL/s, 1.5 BL/s, and 2.0 BL/s.

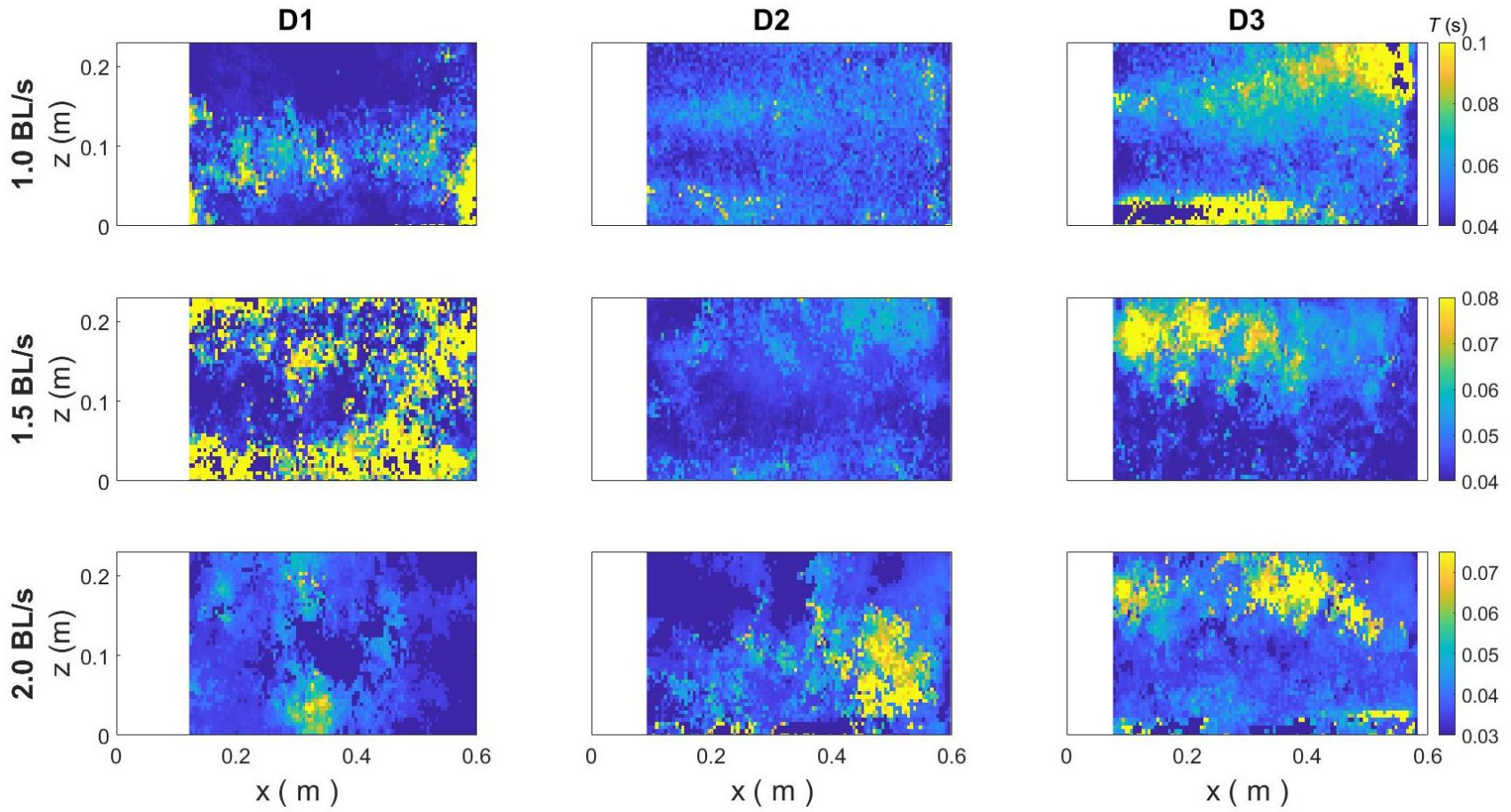

Figure B.49. Time-averaged turbulent integral time scale (*T*; s) on the vertical XZ plane tested within a large racetrack flume. Velocity fields are visualized for diagonal sructures in all three diameters, 2.54-cm (D1), 5.08-cm (D2), and 7.62-cm (D3), for each of the three body length (BL) velocities in which fish were tested, 1.0 BL/s, 1.5 BL/s, and 2.0 BL/s.

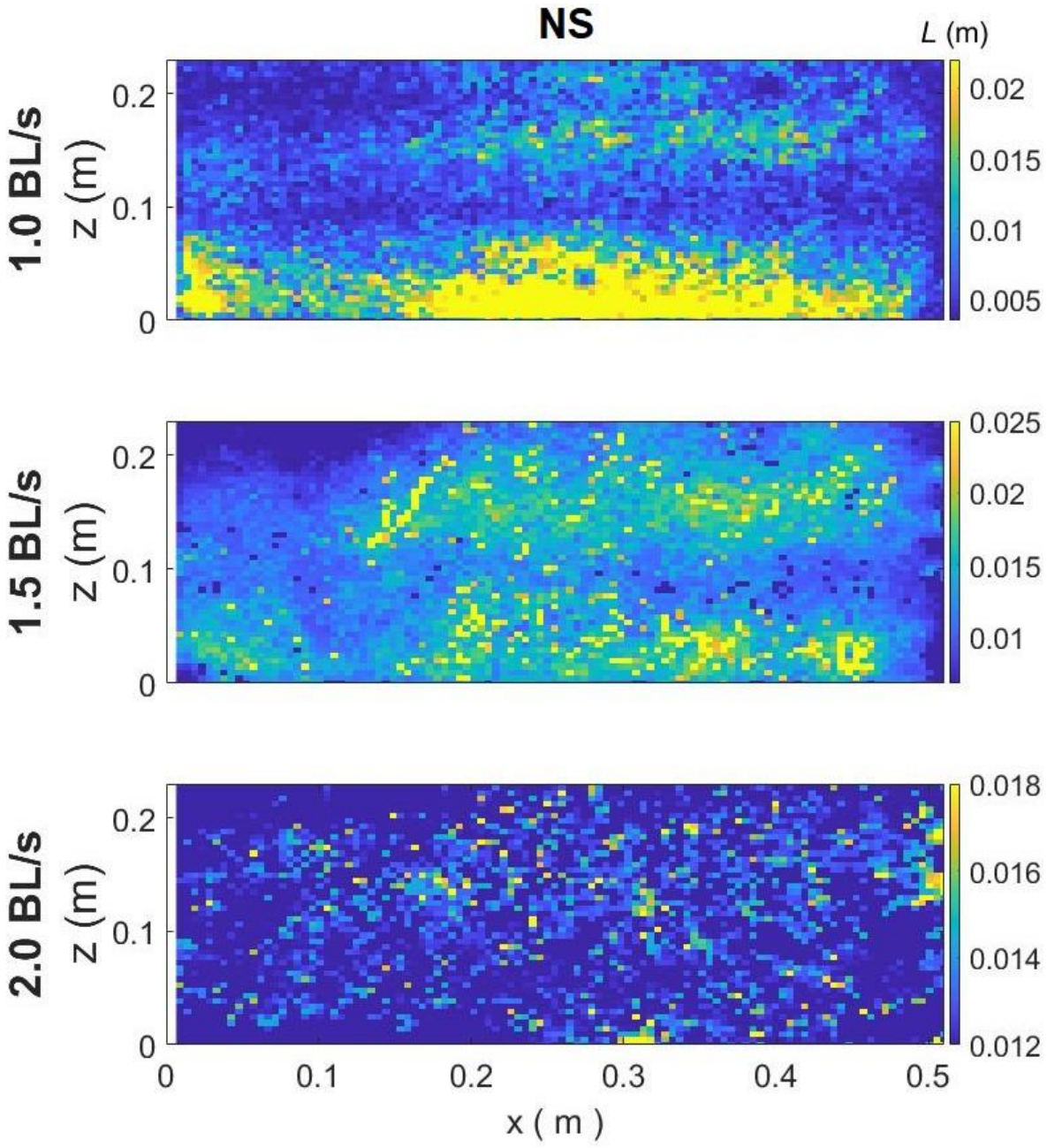

Figure B.50. Time-averaged turbulent integral length scale (*L*; m) on the vertical XZ plane tested within a large racetrack flume. Velocity fields are visualized for the control case with no structure (NS) for each of the three body length (BL) velocities in which fish were tested, 1.0 BL/s, 1.5 BL/s, and 2.0 BL/s.

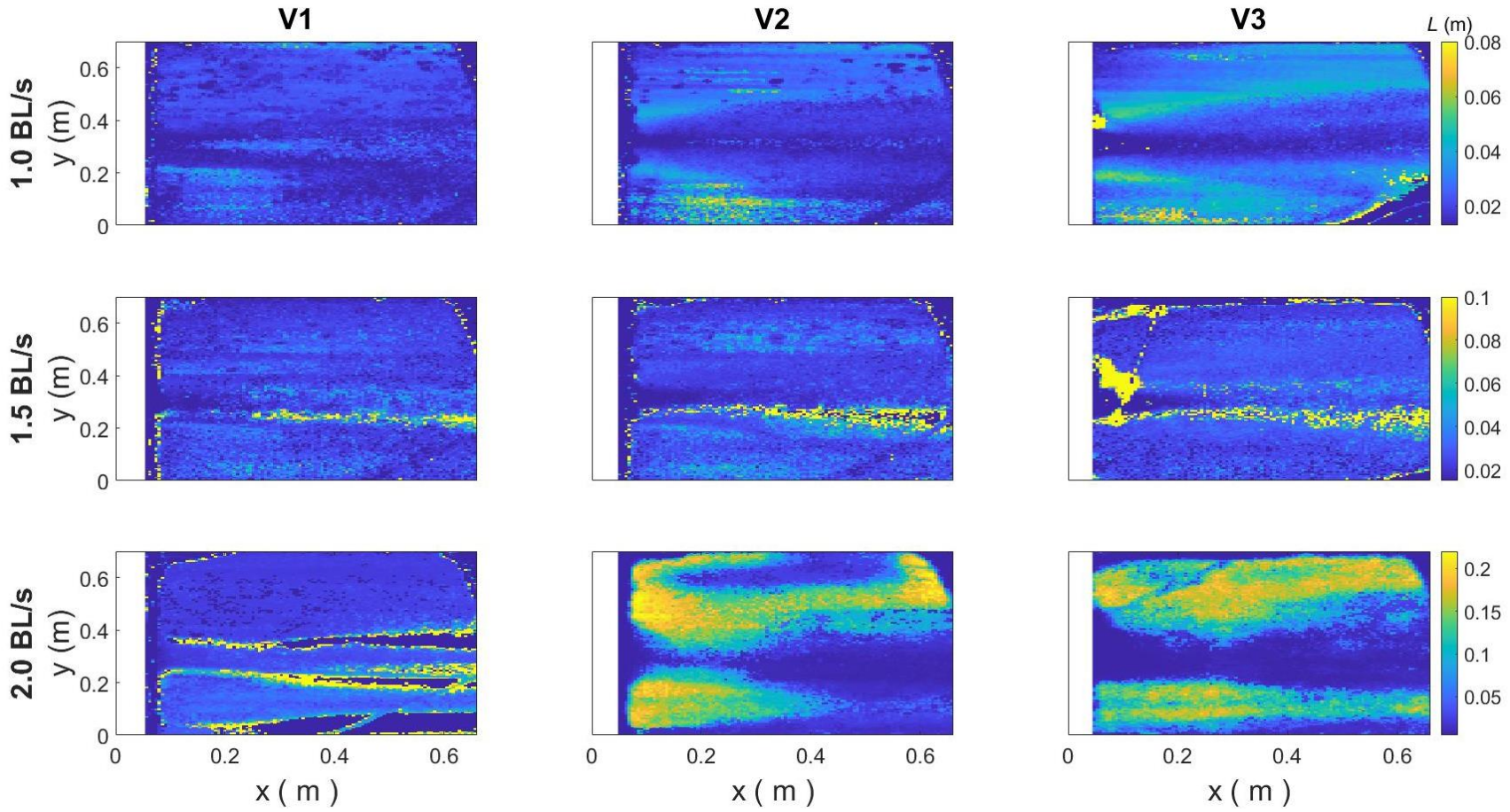

Figure B.51. Time-averaged turbulent integral length scale (*L*; m) on the horizontal XY plane tested within a large racetrack flume. Velocity fields are visualized for vertical structures in all three diameters, 2.54-cm (V1), 5.08-cm (V2), and 7.62-cm (V3), for each of the three body length (BL) velocities in which fish were tested, 1.0 BL/s, 1.5 BL/s, and 2.0 BL/s

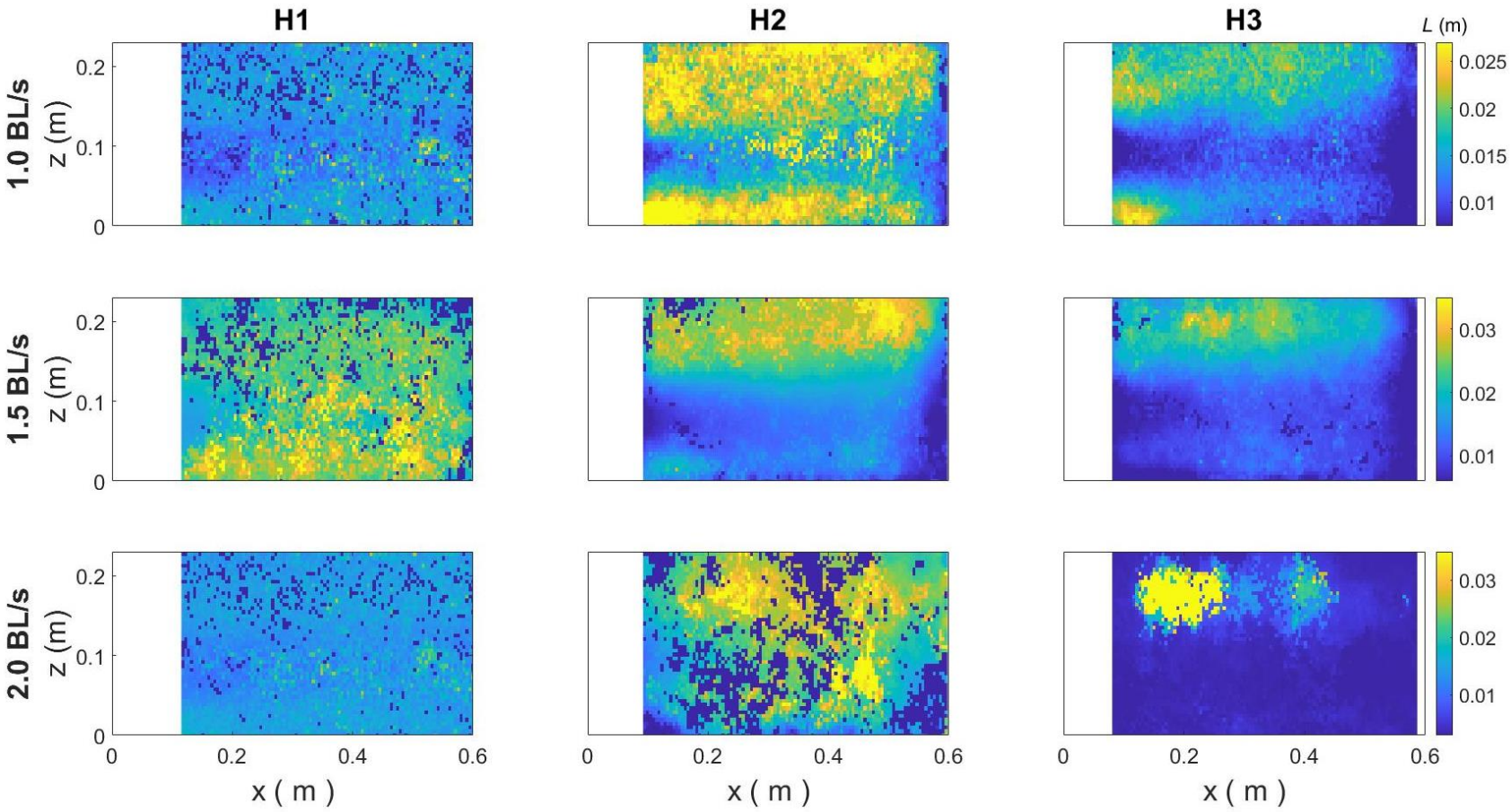

Figure B.52. Time-averaged turbulent integral length scale (*L*; m) on the vertical XZ plane tested within a large racetrack flume. Velocity fields are visualized for horizontal sructures in all three diameters, 2.54-cm (H1), 5.08-cm (H2), and 7.62-cm (H3), for each of the three body length (BL) velocities in which fish were tested, 1.0 BL/s, 1.5 BL/s, and 2.0 BL/s.

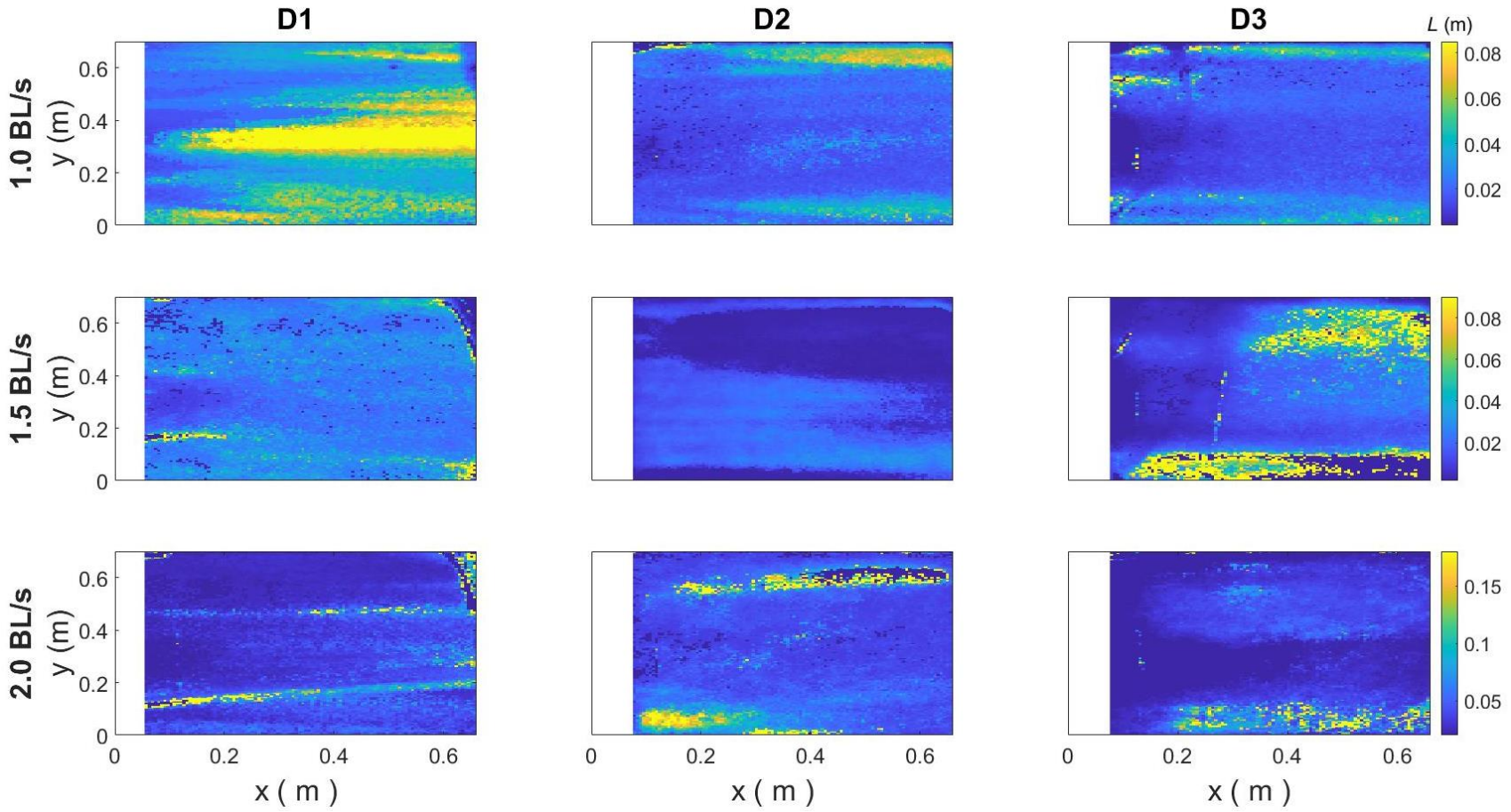

Figure B.53. Time-averaged turbulent integral length scale (*L*; m) on the horizontal XY plane tested within a large racetrack flume. Velocity fields are visualized for diagonal structures in all three diameters, 2.54-cm (D1), 5.08-cm (D2), and 7.62-cm (D3), for each of the three body length (BL) velocities in which fish were tested, 1.0 BL/s, 1.5 BL/s, and 2.0 BL/s.

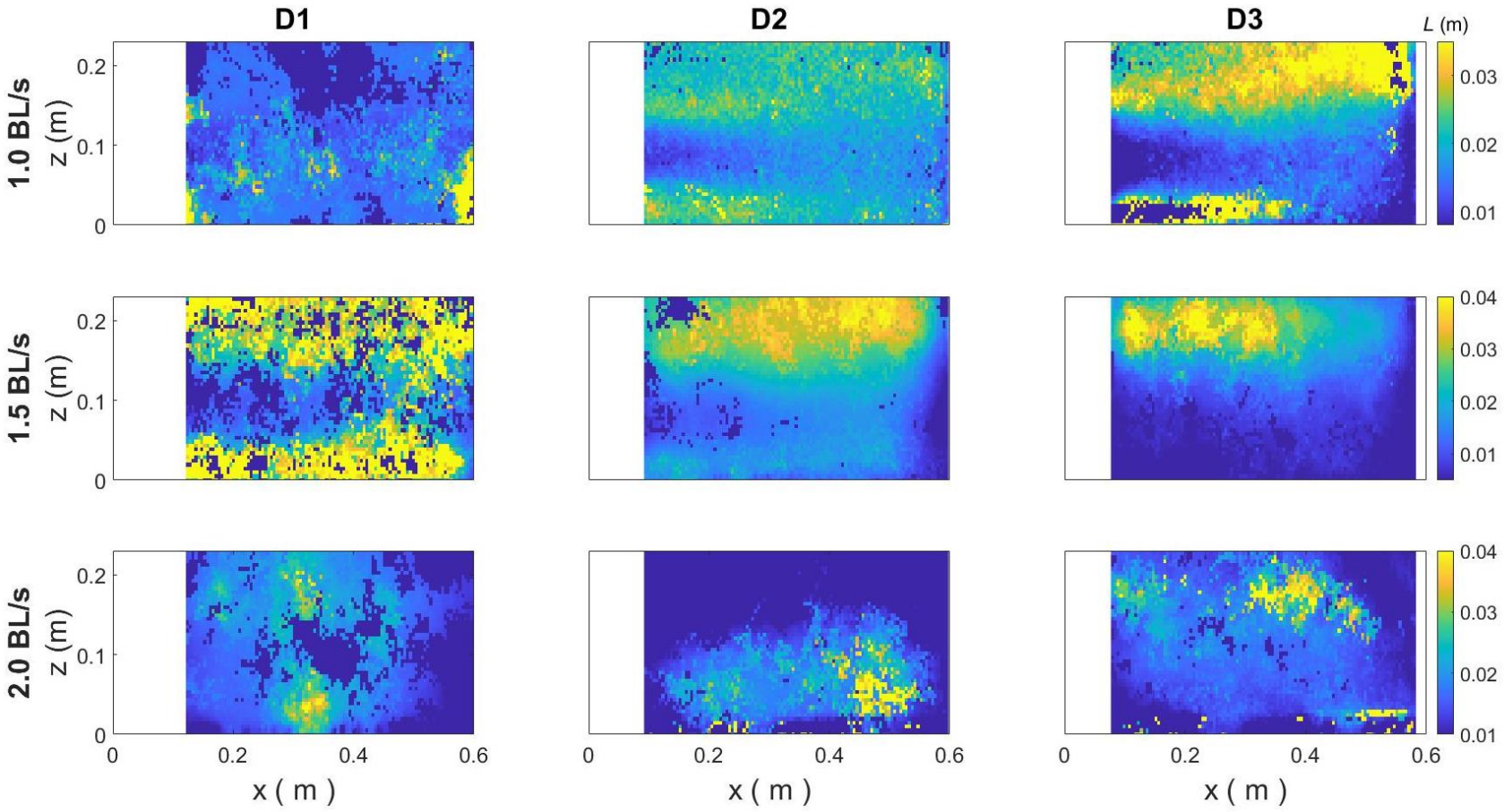

Figure B.54. Time-averaged turbulent integral length scale (*L*; m) on the vertical XZ plane tested within a large racetrack flume. Velocity fields are visualized for diagonal sructures in all three diameters, 2.54-cm (D1), 5.08-cm (D2), and 7.62-cm (D3), for each of the three body length (BL) velocities in which fish were tested, 1.0 BL/s, 1.5 BL/s, and 2.0 BL/s.

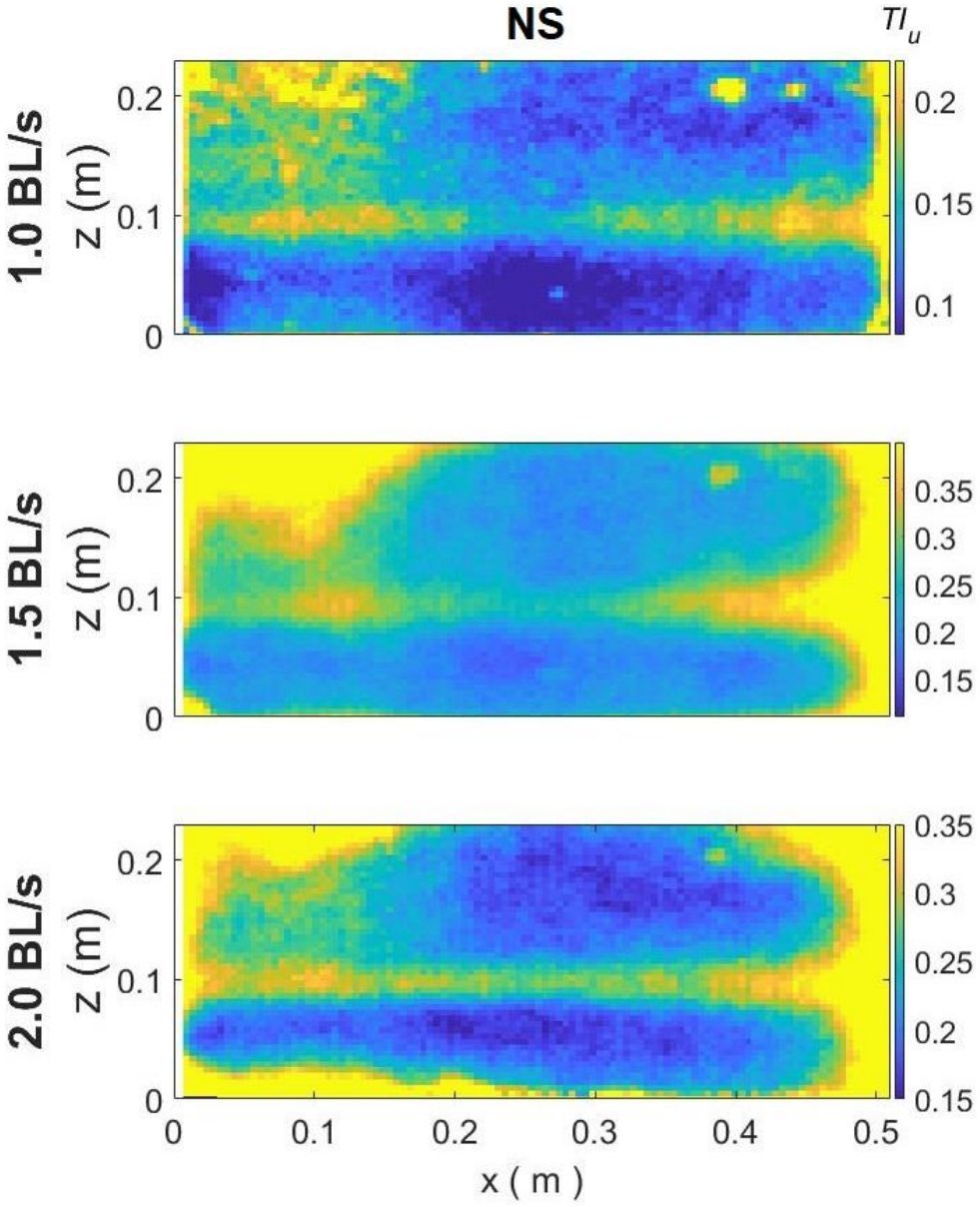

Figure B.55. Time-averaged turbulence intensity, derived from the standard deviation of instaneous velocities *u* and the standard deviation of time-averaged velocity *U* (TI_u), on the vertical XZ plane tested within a large racetrack flume. Velocity fields are visualized for the control case with no structure (NS) for each of the three body length (BL) velocities in which fish were tested, 1.0 BL/s, 1.5 BL/s, and 2.0 BL/s.

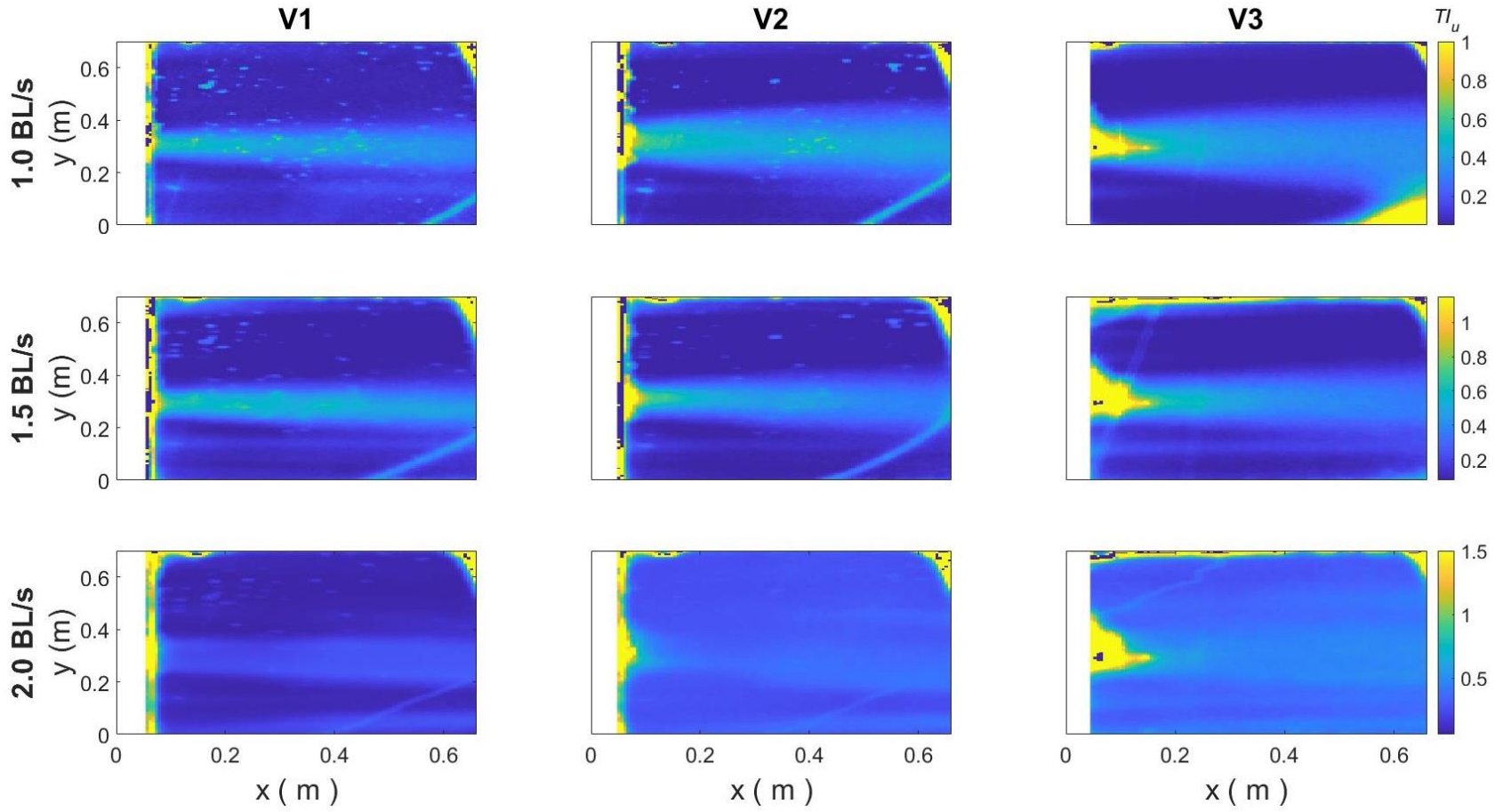

Figure B.56. Time-averaged turbulence intensity, derived from the standard deviation of instaneous velocities *u* and the standard deviation of time-averaged velocity *U* (TI_u), on the horizontal XY plane tested within a large racetrack flume. Velocity fields are visualized for vertical structures in all three diameters, 2.54-cm (V1), 5.08-cm (V2), and 7.62-cm (V3), for each of the three body length (BL) velocities in which fish were tested, 1.0 BL/s, 1.5 BL/s, and 2.0 BL/s.

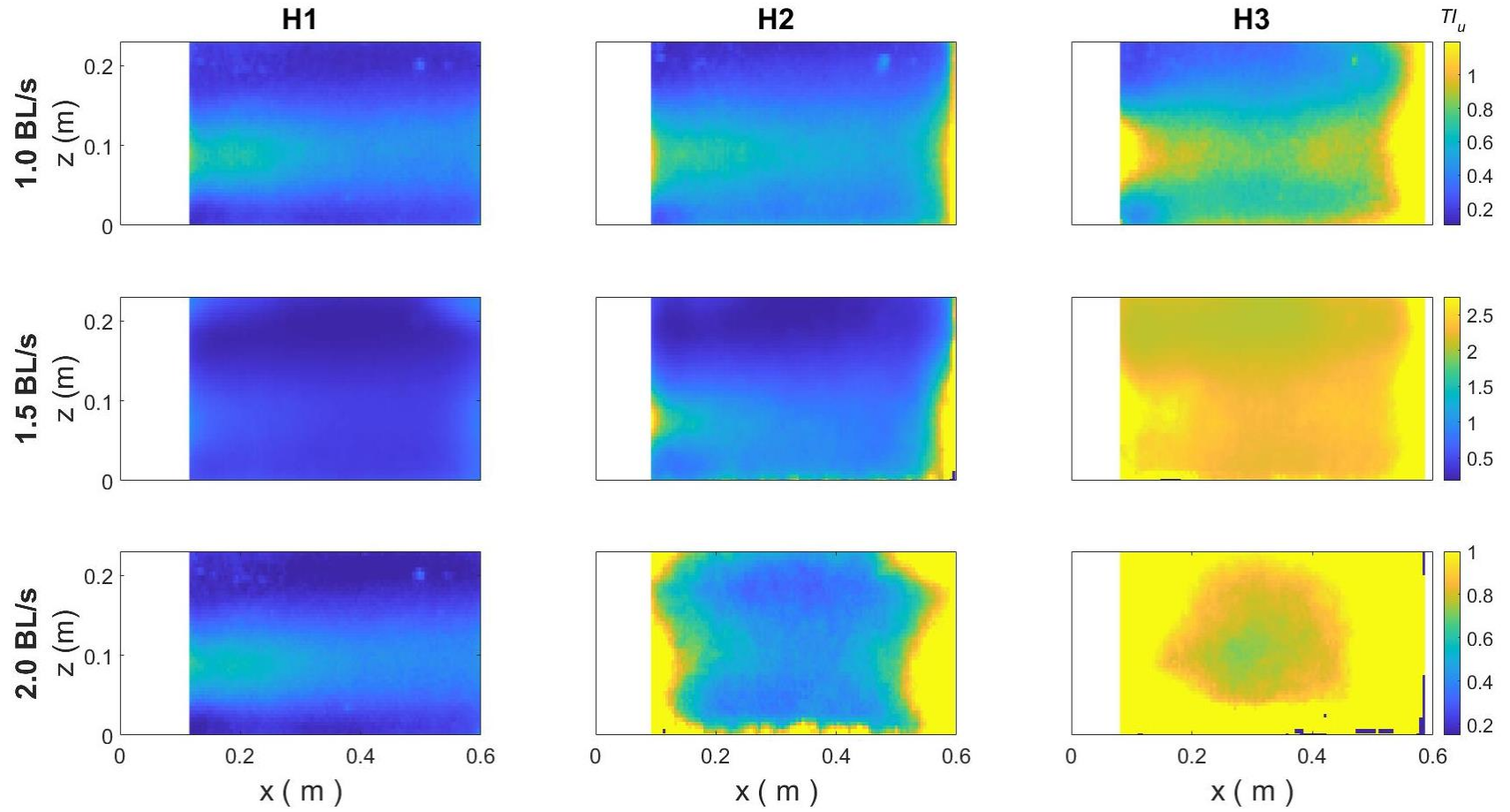

Figure B.57. Time-averaged turbulence intensity, derived from the standard deviation of instaneous velocities *u* and the standard deviation of time-averaged velocity *U* (TI_u), on the vertical XZ plane tested within a large racetrack flume. Velocity fields are visualized for horizontal sructures in all three diameters, 2.54-cm (H1), 5.08-cm (H2), and 7.62-cm (H3), for each of the three body length (BL) velocities in which fish were tested, 1.0 BL/s, 1.5 BL/s, and 2.0 BL/s.

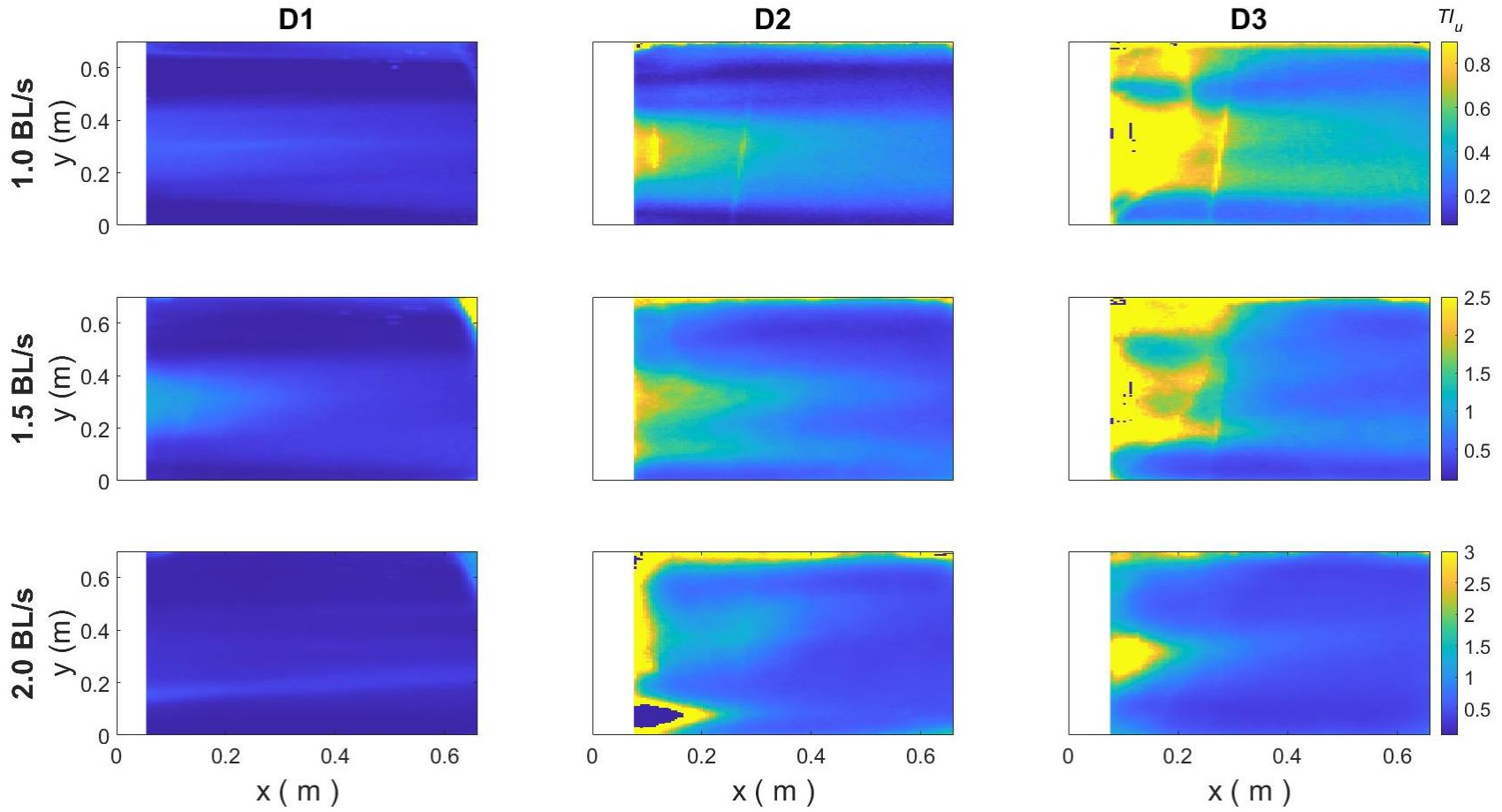

Figure B.58. Time-averaged turbulence intensity, derived from the standard deviation of instaneous velocities *u* and the standard deviation of time-averaged velocity *U* (TI_u), on the horizontal XY plane tested within a large racetrack flume. Velocity fields are visualized for diagonal structures in all three diameters, 2.54-cm (D1), 5.08-cm (D2), and 7.62-cm (D3), for each of the three body length (BL) velocities in which fish were tested, 1.0 BL/s, 1.5 BL/s, and 2.0 BL/s.

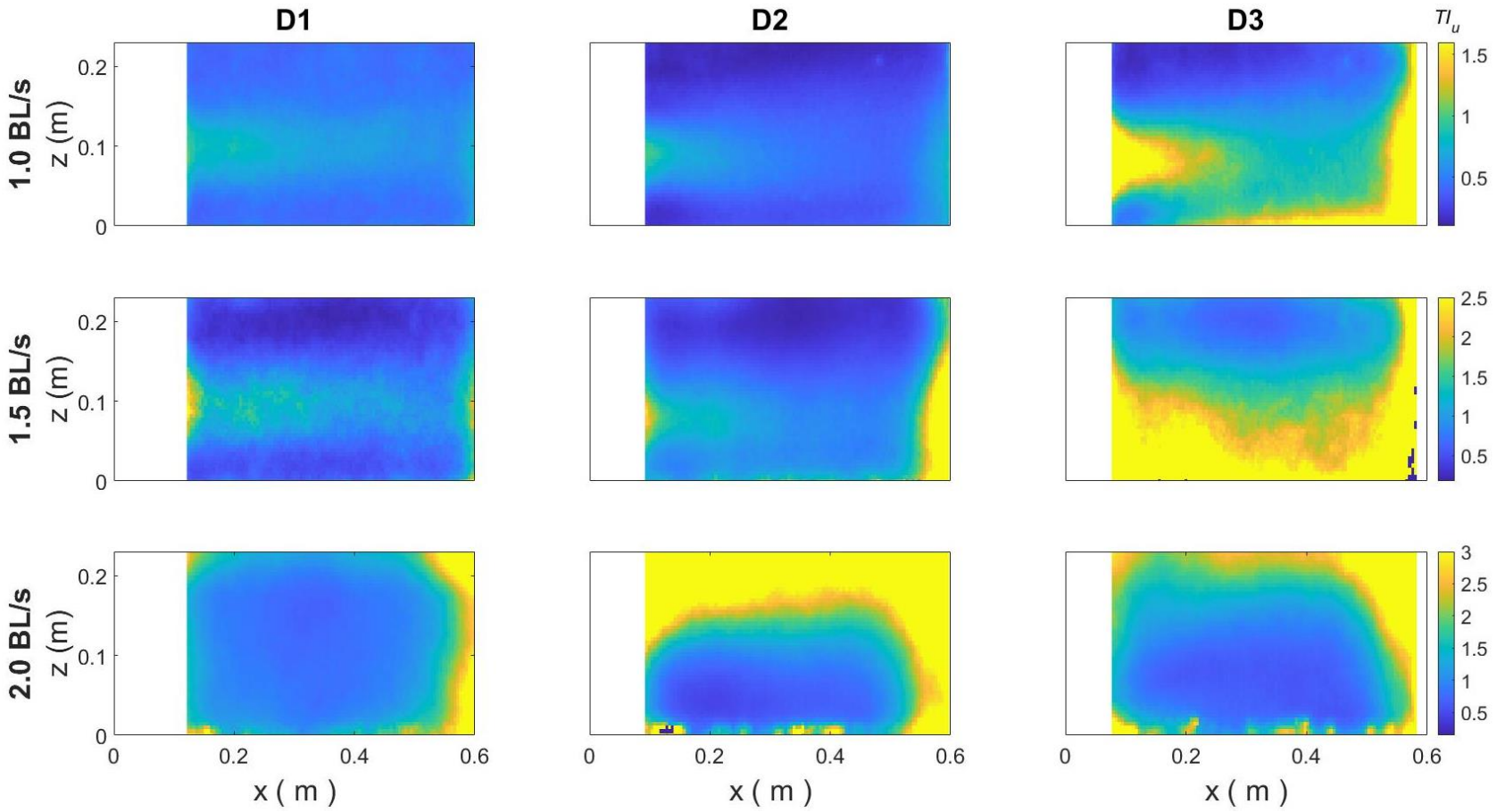

Figure B.59. Time-averaged turbulence intensity, derived from the standard deviation of instaneous velocities *u* and the standard deviation of time-averaged velocity *U* (TI_u), on the vertical XZ plane tested within a large racetrack flume. Velocity fields are visualized for diagonal sructures in all three diameters, 2.54-cm (D1), 5.08-cm (D2), and 7.62-cm (D3), for each of the three body length (BL) velocities in which fish were tested, 1.0 BL/s, 1.5 BL/s, and 2.0 BL/s.

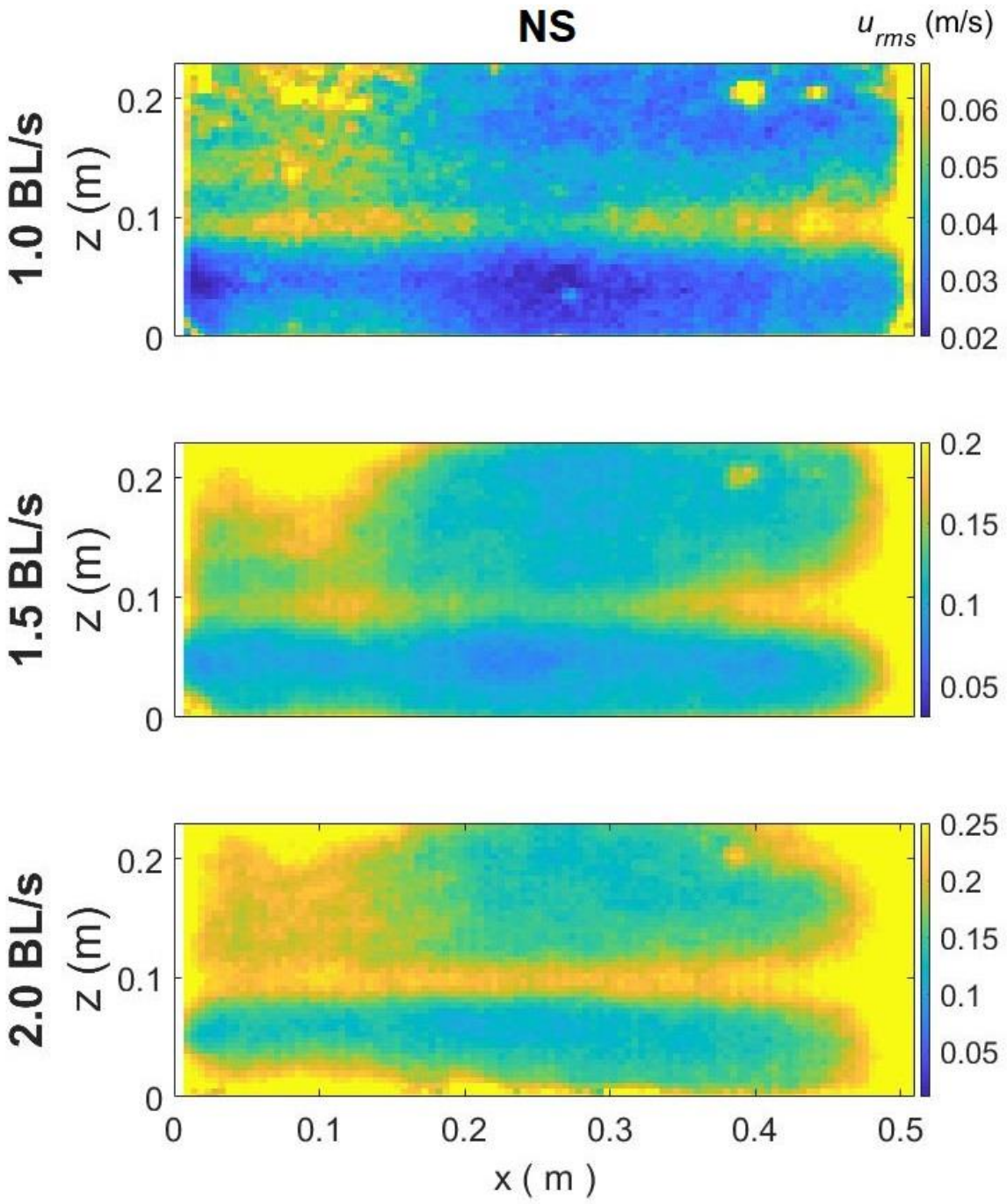

Figure B.60. Time-averaged component of turbulence intensity in the longitudinal direction (u_{rms}; m/s) on the vertical XZ plane tested within a large racetrack flume. Velocity fields are visualized for the control case with no structure (NS) for each of the three body length (BL) velocities in which fish were tested, 1.0 BL/s, 1.5 BL/s, and 2.0 BL/s.

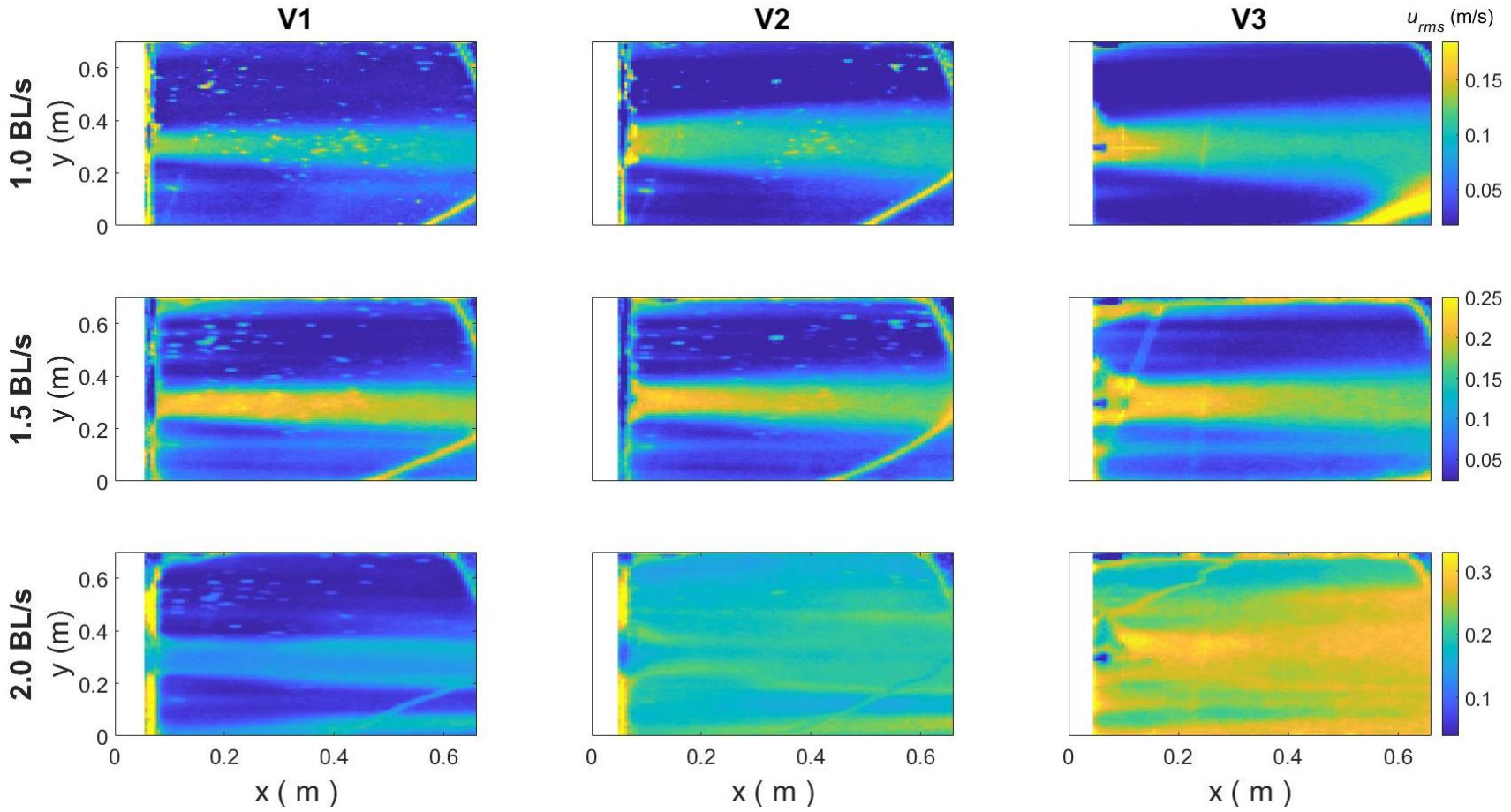

Figure B.61. Time-averaged component of turbulence intensity in the longitudinal direction (u_{rms}; m/s) on the horizontal XY plane tested within a large racetrack flume. Velocity fields are visualized for vertical structures in all three diameters, 2.54-cm (V1), 5.08-cm (V2), and 7.62-cm (V3), for each of the three body length (BL) velocities in which fish were tested, 1.0 BL/s, 1.5 BL/s, and 2.0 BL/s.

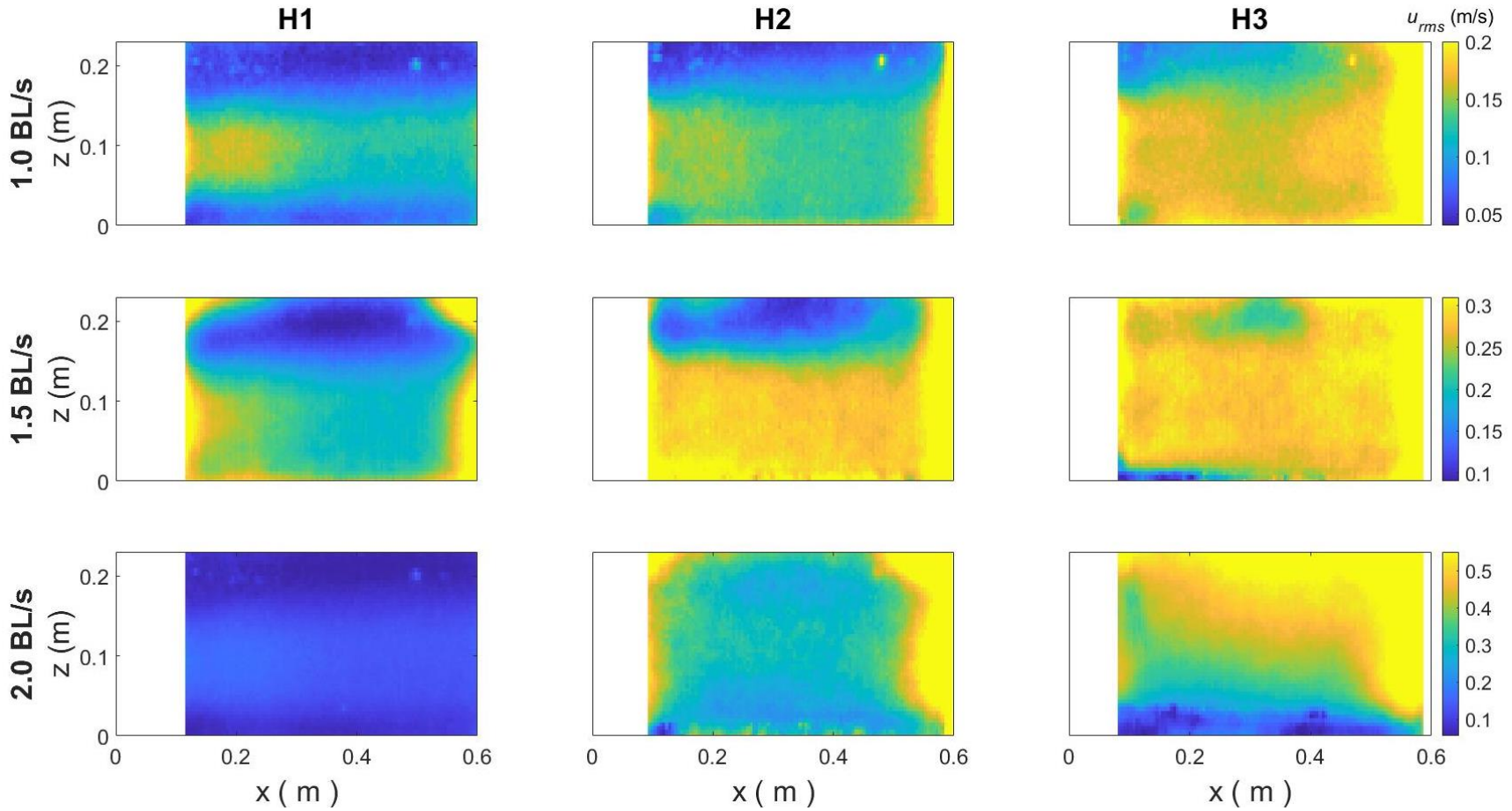

Figure B.62. Time-averaged component of turbulence intensity in the longitudinal direction (u_{rms}; m/s) on the vertical XZ plane tested within a large racetrack flume. Velocity fields are visualized for horizontal sructures in all three diameters, 2.54-cm (H1), 5.08-cm (H2), and 7.62-cm (H3), for each of the three body length (BL) velocities in which fish were tested, 1.0 BL/s, 1.5 BL/s, and 2.0 BL/s.

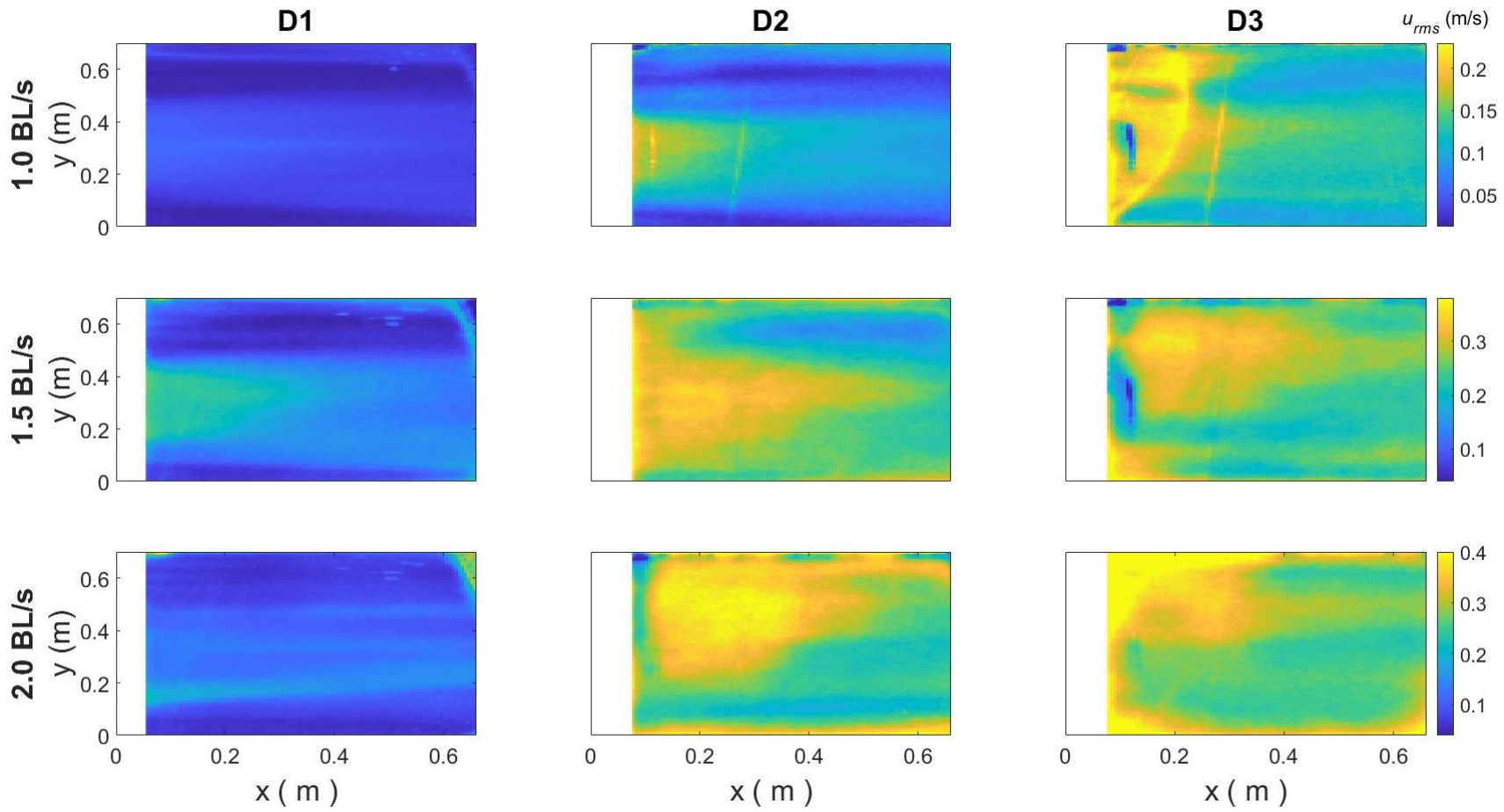

Figure B.63. Time-averaged component of turbulence intensity in the longitudinal direction (u_{rms}; m/s) on the horizontal XY plane tested within a large racetrack flume. Velocity fields are visualized for diagonal structures in all three diameters, 2.54-cm (D1), 5.08-cm (D2), and 7.62-cm (D3), for each of the three body length (BL) velocities in which fish were tested, 1.0 BL/s, 1.5 BL/s, and 2.0 BL/s.

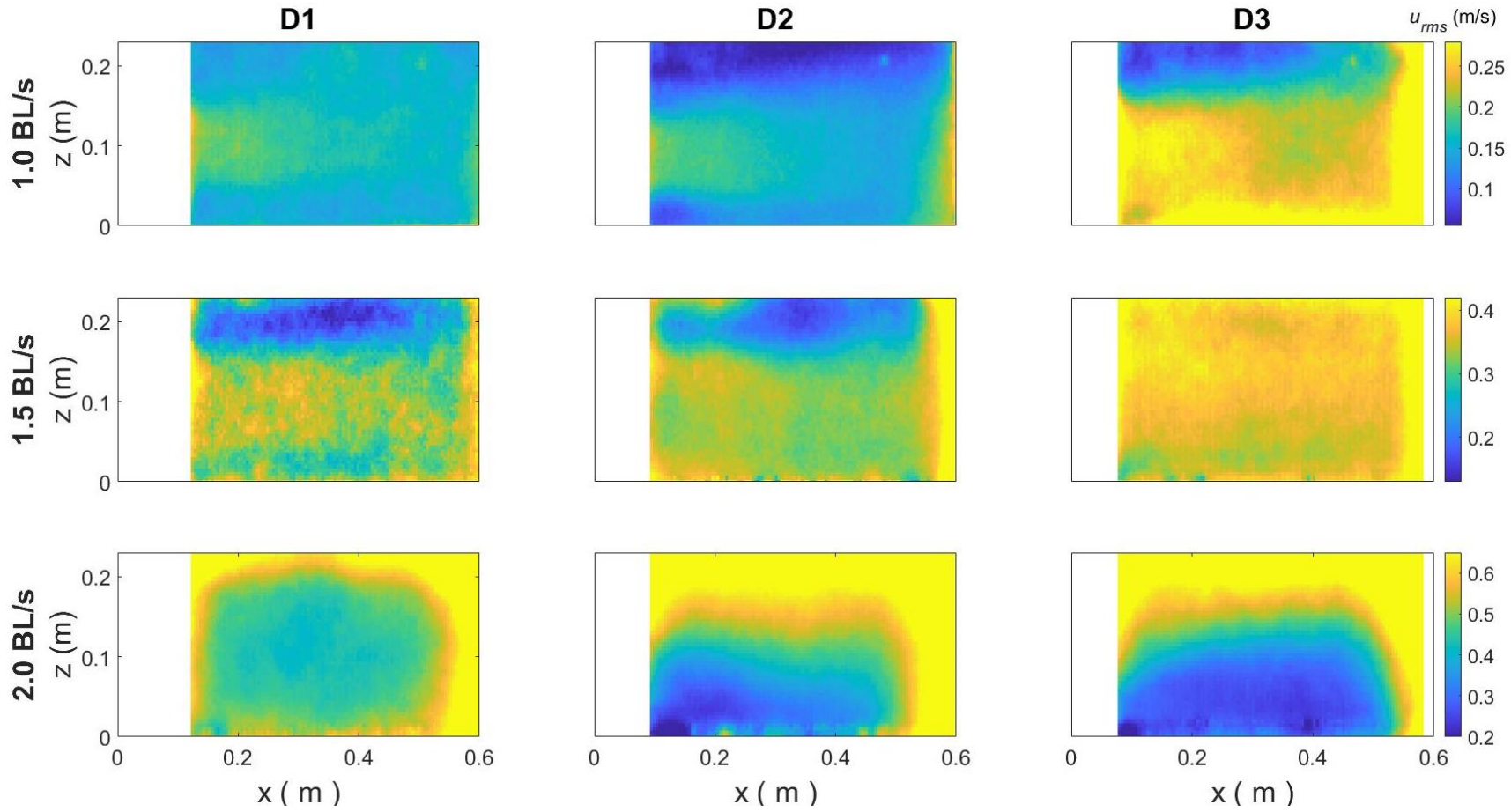

Figure B.64. Time-averaged component of turbulence intensity in the longitudinal direction (u_{rms}; m/s) on the vertical XZ plane tested within a large racetrack flume. Velocity fields are visualized for diagonal sructures in all three diameters, 2.54-cm (D1), 5.08-cm (D2), and 7.62-cm (D3), for each of the three body length (BL) velocities in which fish were tested, 1.0 BL/s, 1.5 BL/s, and 2.0 BL/s.

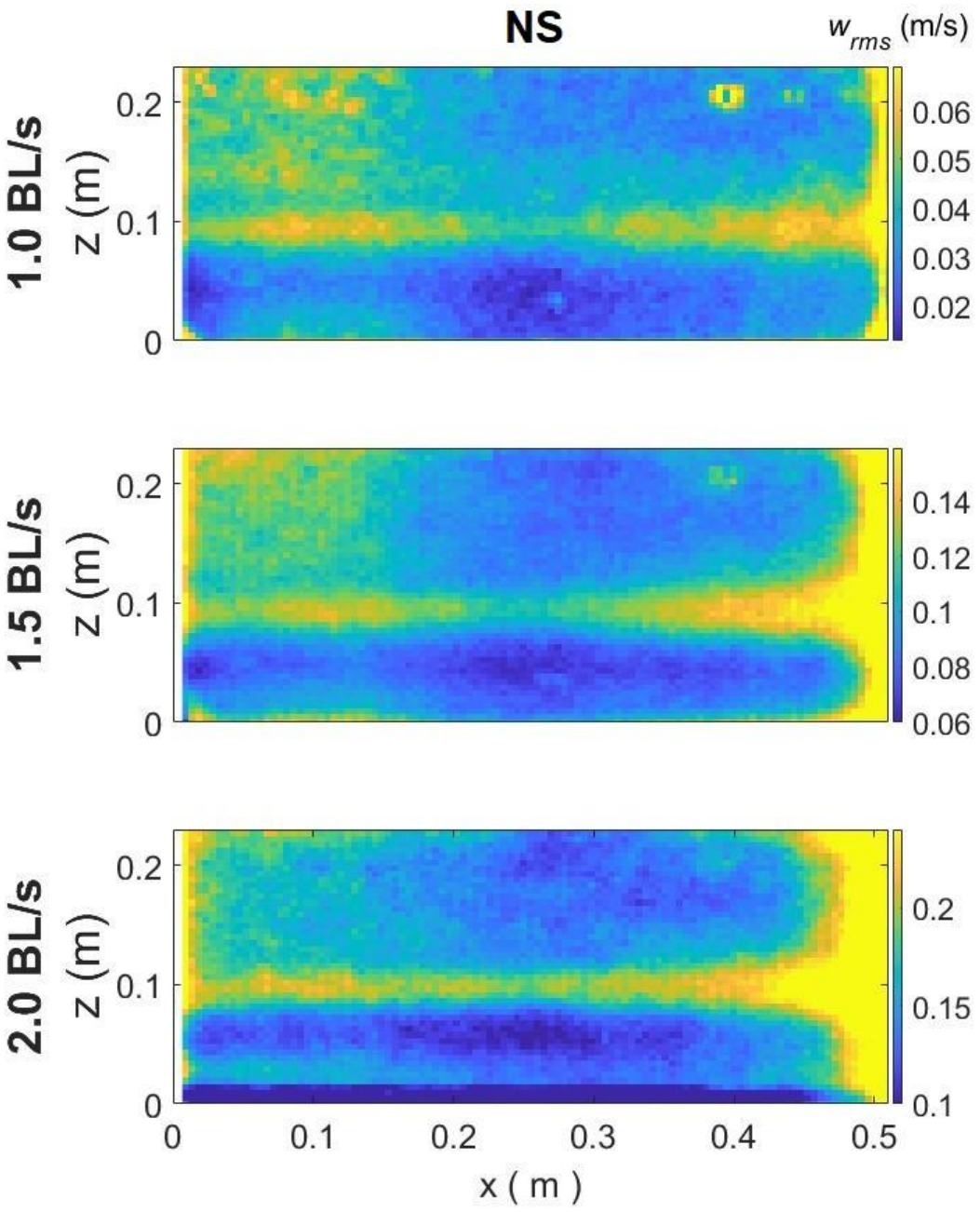

Figure B. 65. Time-averaged component of turbulence intensity in the lateral direction (W_{rms}; m/s) on the vertical XZ plane tested within a large racetrack flume. Velocity fields are visualized for the control case with no structure (NS) for each of the three body length (BL) velocities in which fish were tested, 1.0 BL/s, 1.5 BL/s, and 2.0 BL/s. W_{rms} is generated in a transverse direction to the longitudinal flow, and thus, with V_{rms}, is also referred to as $U_{Trms.}$

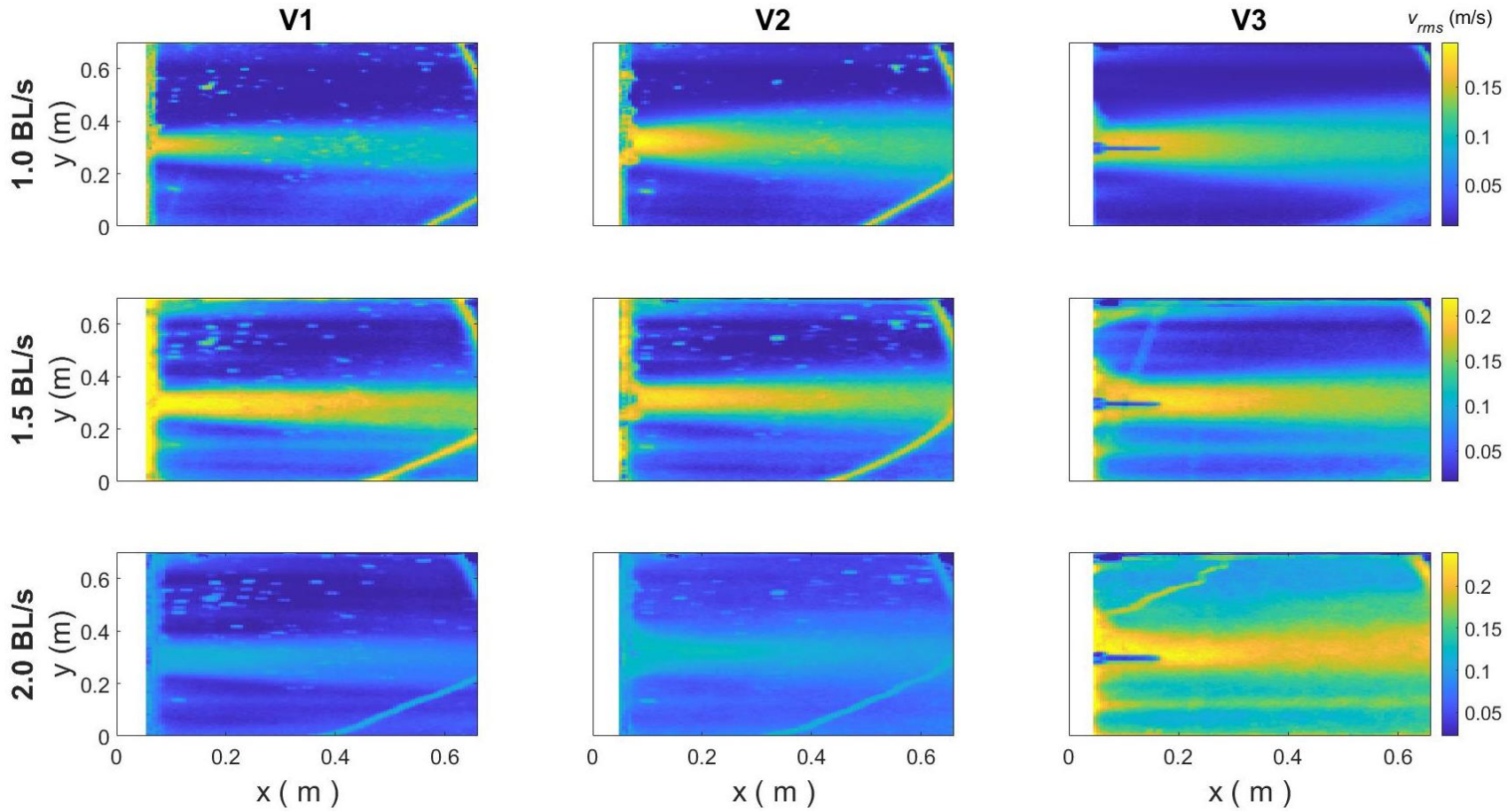

Figure B.66. Time-averaged component of turbulence intensity in the lateral direction (V_{rms}; m/s) on the horizontal XY plane tested within a large racetrack flume. Velocity fields are visualized for vertical structures in all three diameters, 2.54-cm (V1), 5.08-cm (V2), and 7.62-cm (V3), for each of the three body length (BL) velocities in which fish were tested, 1.0 BL/s, 1.5 BL/s, and 2.0 BL/s. V_{rms} is generated in a transverse direction to the longitudinal flow, and thus, with W_{rms}, is also referred to as $U_{Trms.}$

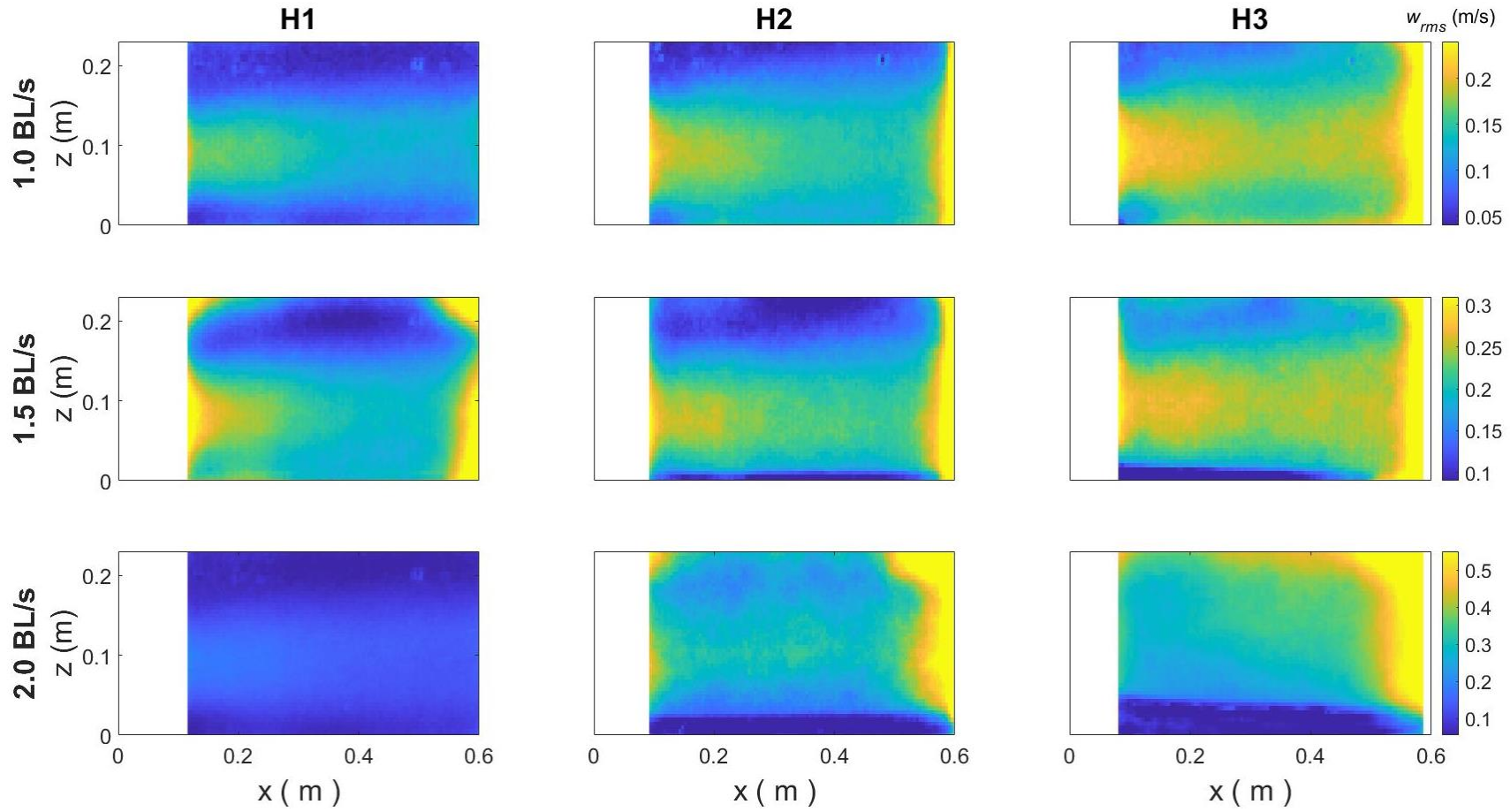

Figure B.67. Time-averaged component of turbulence intensity in the vertical direction (W_{rms}; m/s) on the vertical XZ plane tested within a large racetrack flume. Velocity fields are visualized for horizontal sructures in all three diameters, 2.54-cm (H1), 5.08-cm (H2), and 7.62-cm (H3), for each of the three body length (BL) velocities in which fish were tested, 1.0 BL/s, 1.5 BL/s, and 2.0 BL/s. W_{rms} is generated in a transverse direction to the longitudinal flow, and thus, with V_{rms}, is also referred to as U_{Trms}.

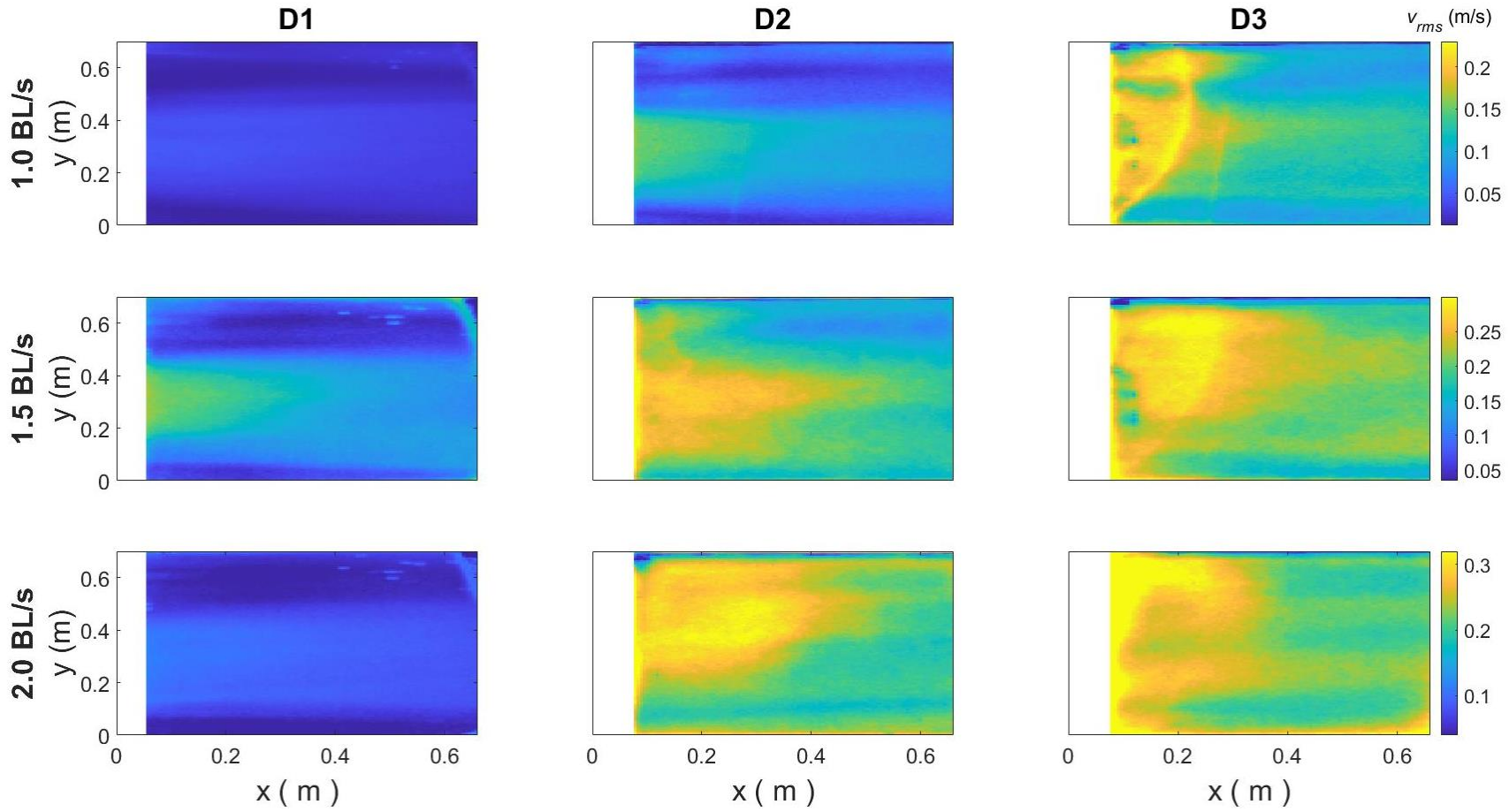

Figure B.68. Time-averaged component of turbulence intensity in the lateral direction (V_{rms}; m/s) on the horizontal XY plane tested within a large racetrack flume. Velocity fields are visualized for diagonal structures in all three diameters, 2.54-cm (D1), 5.08-cm (D2), and 7.62-cm (D3), for each of the three body length (BL) velocities in which fish were tested, 1.0 BL/s, 1.5 BL/s, and 2.0 BL/s. V_{rms} is generated in a transverse direction to the longitudinal flow, and thus, with W_{rms}, is also referred to as U_{Trms}.

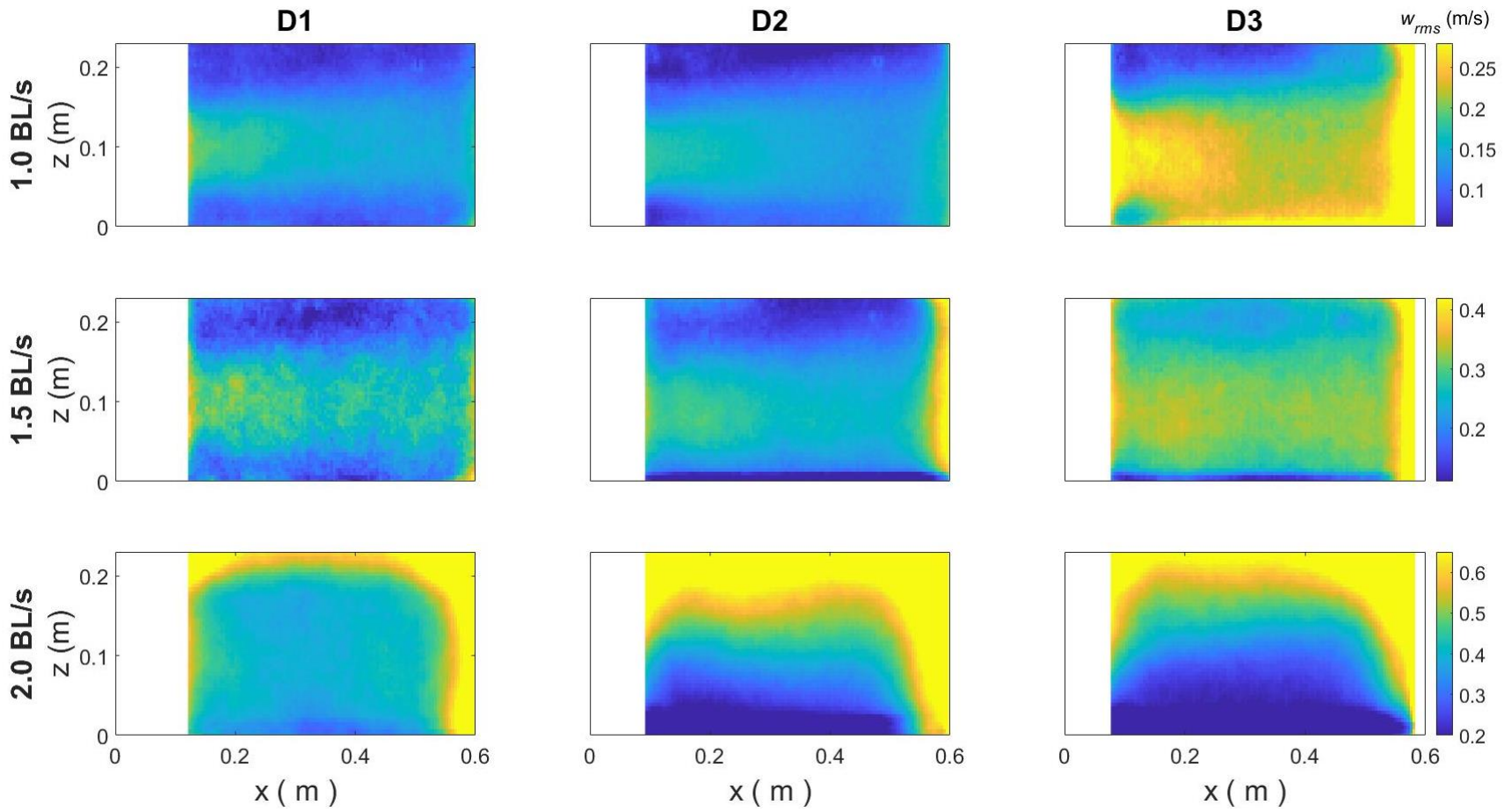

Figure B.69. Time-averaged component of turbulence intensity in the vertical direction (W_{rms}; m/s) on the vertical XZ plane tested within a large racetrack flume. Velocity fields are visualized for diagonal sructures in all three diameters, 2.54-cm (D1), 5.08-cm (D2), and 7.62-cm (D3), for each of the three body length (BL) velocities in which fish were tested, 1.0 BL/s, 1.5 BL/s, and 2.0 BL/s. W_{rms} is generated in a transverse direction to the longitudinal flow, and thus, with V_{rms}, is also referred to as $U_{Trms.}$

Interpreting and Using Bioenergetics Models

① **Examine the model formula.**

$$\log(\dot{M}O_2) \sim \log(\text{Mass}) + \text{Temperature} + U \times L + \text{TKE} + (1|\text{ID})$$

The model formula provides the response variable and arrangement of predictors within the model of interest. This model uses the fixed effects of log-transformed mass, temperature, longitudinal velocity (U), turbulent integral length scale (L) and turbulent kinetic energy (TKE), and the random effect of (1|ID) to predict log-transformed rainbow trout energy use ($\dot{M}O_2$).

The random effect (1|ID) specifies that each individual fish (ID) has a separate intercept. This accounts for the repeated usage of individual fish within the experiment from which the model was produced. Though necessary for the model to be produced, this random effect is not included when utilizing the model to predict $\dot{M}O_2$.

② **Examine the model summary table.** The "Estimate" column provides the coefficients that accompany each variable within the model as well as the global intercept for the model. Models with an interaction term (i.e. U x L) should also include each variable within the interaction separately; in R, this is done automatically. These should also be included when using the model to estimate the response.

	Estimate	Standard error	df	t value	Pr(>|t|)
(Intercept)	7.89	1.57	12.79	5.04	< 0.01
log (Mass)	-0.49	0.22	4.69	-2.23	0.08
Temperature	0.03	0.05	43.80	0.58	0.57
U	-0.79	0.18	40.89	-4.37	<0.01
L	-14.90	4.66	41.42	-3.20	<0.01
TKE	0.47	0.20	42.33	2.35	0.02
U×L	31.18	8.59	41.10	3.63	<0.01

③ **Generate the equation for the model.** The model above would be:

$$\log(\dot{M}O_2) = (-0.49 \times \log(\text{Mass})) + (0.03 \times \text{Temperature}) + (-0.79 \times U) + (-14.90 \times L) + (0.47 \times \text{TKE}) + (31.18 \times (U \times L))$$

④ **Insert available data for each predictor to estimate the value of the response variable.** Each predictor should be scaled to match the units used for production of the original model.

Figure B.70. A guide demonstrating how the bioenergetics models developed for rainbow trout and smallmouth bass swimming in turbulent flows generated by simulated instream restoration structures can be used to estimate the oxygen consumption ($\dot{M}O_2$), or energy use, of other fish from these species swimming in turbulent flows.

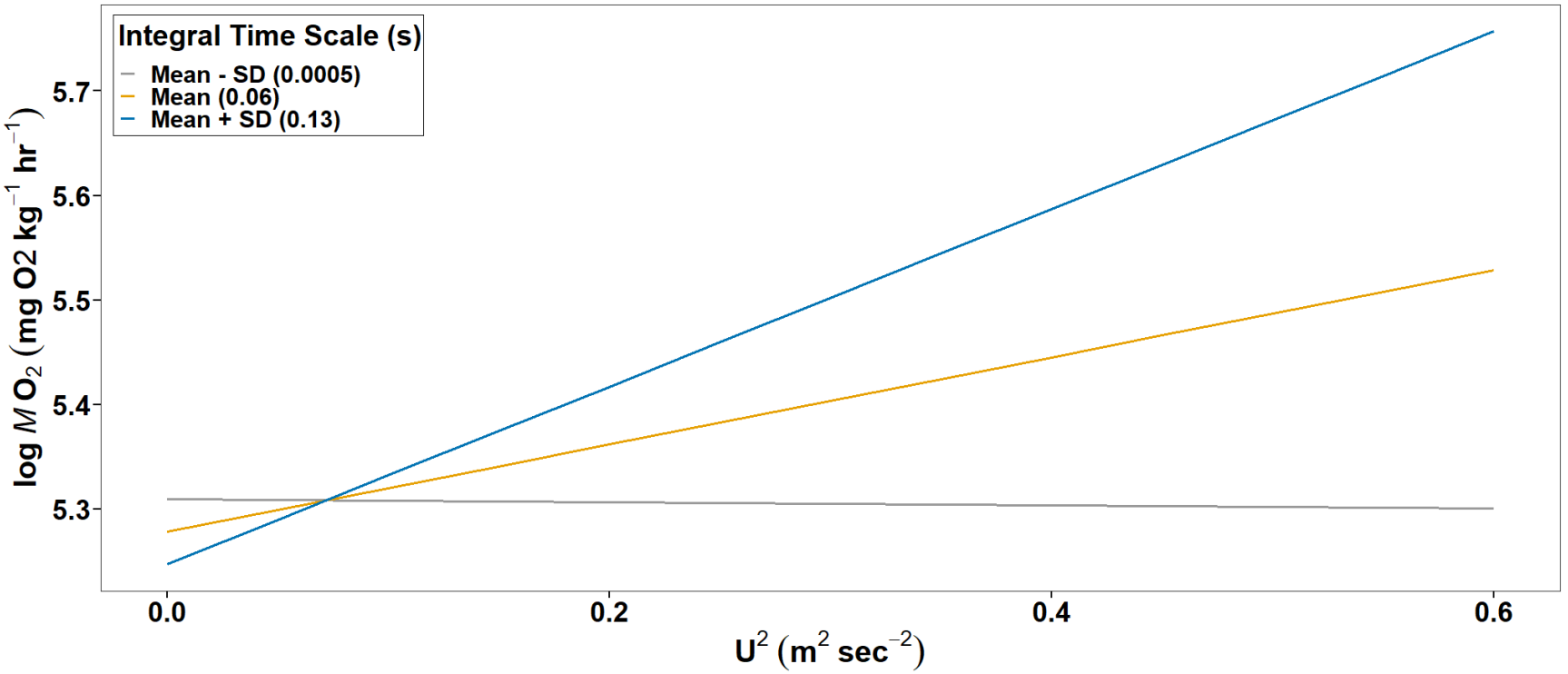

Figure B.71. Plot showing how the influence of U^2 on smallmouth bass oxygen consumption ($\dot{M}O_2$) changes with different integral length scales (T); U^2 relates to drag force. The average values of T selected for each smallmouth bass during each sub-trial were pooled, and the levels of T shown calculated from the overall pool of values for all smallmouth bass. The best-fitting model for smallmouth bass included a U × L interaction, which approximates U^2 × T. A model replacing U × L with U^2 × T performed as well as the top smallmouth bass model, with U × L, indicating that drag may impact smallmouth bass $\dot{M}O_2$.

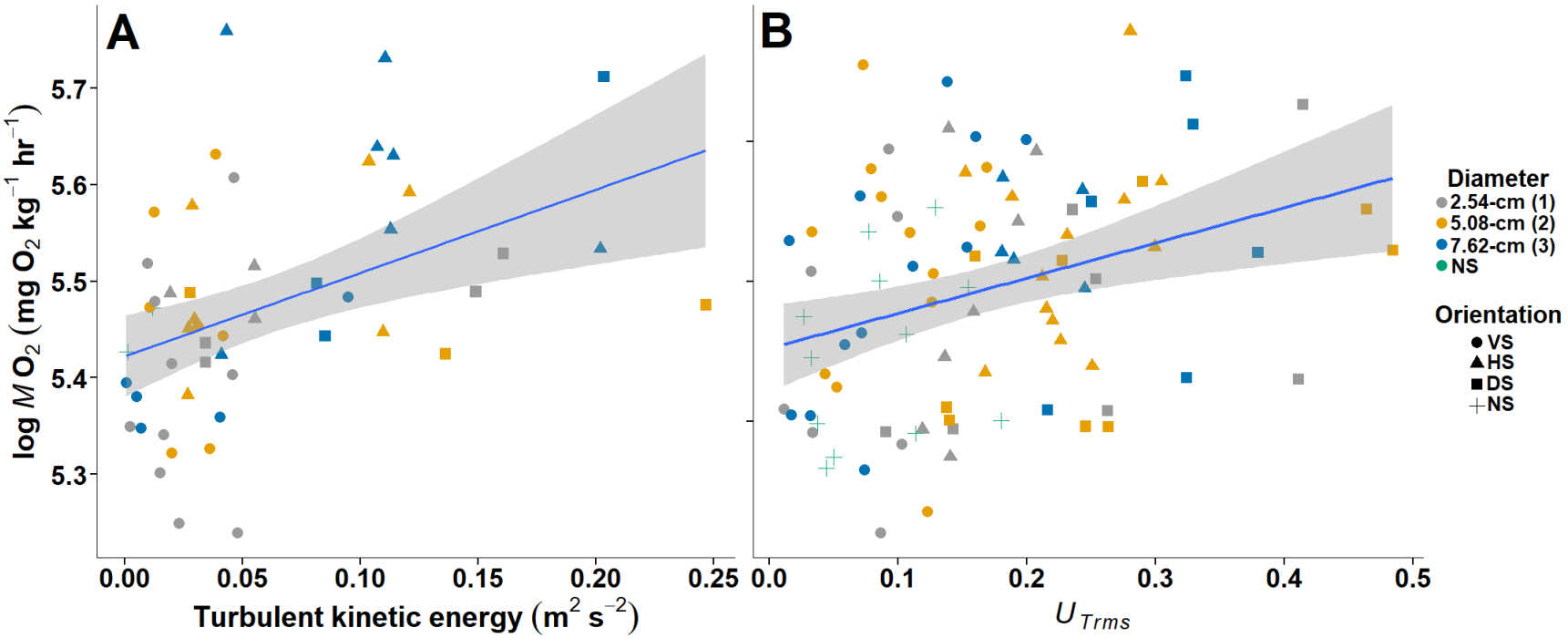

Figure B.72. Relationship between oxygen consumption ($\dot{M}O2$) and the measure of turbulence intensity included in the top bioenergetics model for rainbow trout (Table 10) and smallmouth bass (Table 11). Turbulent kinetic energy was the most impactful measure of turbulence intensity for rainbow trout (panel A), while U_{Trms} was the most impactful measure of turbulence intensity for smallmouth bass (panel B). For both species, fish $\dot{M}O2$ increased as fish experienced higher levels of turbulence intensity. Plots are shown with scatter indicating the diameter (2.54-cm, 5.08-cm, 7.62, none) and orientation (vertical, horizontal, diagonal, none) of the structure from which turbulence intensity values were derived.

Tables

Table B.1. Summary and comparison of linear models relating rainbow trout oxygen consumption to acceleration, derived during respirometry experiments. The acceleration data for each model was processed using one of three separate methods: filtering to remove moments of inactivity (accelerations below the 25th percentile) and moments of burst swimming (accelerations above the 75th percentile), then averaging remaining measurements (Method 1); averaging all acceleration measurements for each fish at each velocity (Method 2); and removing outlier acceleration points identified through inspection of histograms and use of Rosner's outlier test, followed by averaging of remaining points (Method 3). The method that produced the best-fitting model, as determined by having the lowest AIC score, was used to process all acceleration data for analyses derived from respirometry experiments.

	AIC score	ΔAIC	R^2	Estimate	Standard error	t value	Pr(>|t|)
Method 3	675.3	0	0.667				
(Intercept)				84.80	15.43	5.50	<0.01
Acceleration				231.87	20.82	11.14	<0.01
Method 1	679.1	3.8	0.646				
(Intercept)				112.38	13.73	8.19	<0.01
Acceleration				197.27	18.54	10.64	<0.01
Method 2	680.3	5	0.640				
(Intercept)				94.16	15.50	6.08	<0.01
Acceleration				198.77	18.94	10.50	<0.01

Table B.2. Summary and comparison of linear models relating smallmouth bass oxygen consumption to acceleration, derived during respirometry experiments. The acceleration data for each model was processed using one of three separate methods: filtering to remove moments of inactivity (accelerations below the 25th percentile) and moments of burst swimming (accelerations above the 75th percentile), then averaging remaining measurements (Method 1); averaging all acceleration measurements for each fish at each velocity (Method 2); and removing outlier acceleration points identified through inspection of histograms and use of Rosner's outlier test, followed by averaging of remaining points (Method 3). The method that produced the best-fitting model, as determined by having the lowest AIC score, was used to process all acceleration data for analyses derived from respirometry experiments.

	AIC score	ΔAIC	R^2	Estimate	Standard error	t value	Pr(>|t|)
Method 3	700.3	0	0.769				
(Intercept)				124.48	12.90	9.649	5.83e-14
Acceleration				243.20	16.93	14.361	<2e-16
Method 1	706.1	5.8	0.747				
(Intercept)				143.44	12.47	11.50	<2e-16
Acceleration				234.08	17.30	13.53	<2e-16
Method 2	710.5	10.2	0.729				
(Intercept)				129.6	13.9	9.327	2.05e-13
Acceleration				224.7	17.4	12.915	<2e-16

Table B.3. Variance inflation factor (VIF) values for flow metrics tested for inclusion in bioenergetics models for rainbow trout participating in flume experiments.

	U	**TKE**	***T***	***L***	$\mathbf{TI}_{U}$	$\mathbf{U}_{rms}$	$\mathbf{U}_{\mathbf{T}rms}$
U	-	1.01	1.82	1.00	1.30	1.00	1.01
TKE	1.01	-	1.11	1.37	3.09	19.34	3.55
T	1.82	1.11	-	2.08	1.34	1.38	1.38
L	1.00	1.37	2.08	-	1.43	1.09	1.13
$\mathbf{TI}_{U}$	1.30	3.09	1.34	1.43	-	3.84	2.86
$\mathbf{U}_{rms}$	1.00	19.34	1.38	1.09	3.84	-	4.31
$\mathbf{U}_{\mathbf{T}rms}$	1.01	3.55	1.38	1.13	2.86	4.31	-

Table B.4. Variance inflation factor (VIF) values for flow metrics tested for inclusion in bioenergetics models for smallmouth bass participating in flume experiments.

	U	**TKE**	***T***	***L***	$\mathbf{TI}_{U}$	$\mathbf{U}_{rms}$	$\mathbf{U}_{\mathbf{T}rms}$
U	-	1.00	1.07	1.00	1.12	1.01	1.00
TKE	1.00	-	1.11	1.10	2.91	9.81	9.44
T	1.07	1.11	-	6.04	1.07	1.14	1.12
L	1.00	1.10	6.04	-	1.12	1.13	1.12
$\mathbf{TI}_{U}$	1.12	2.91	1.07	1.12	-	3.97	4.46
$\mathbf{U}_{rms}$	1.01	9.81	1.14	1.13	3.97	-	15.63
$\mathbf{U}_{\mathbf{T}rms}$	1.00	9.44	1.12	1.12	4.46	15.63	-

Table B.5. Summary of the top "drag"-based bioenergetics model relating fish mass, temperature, mean velocity U^2, U_{Trms}, and T with oxygen consumption ($\dot{M}O_2$) for smallmouth bass participating in flume experiments. The model shown was an equally good fit for smallmouth bass oxygen consumption data when compared with the top model that did not include U^2. Model fit was assessed through a model selection process (Table 3.9).

	Estimate	Standard error	df	t value	Pr(>|t|)	Proportion of fixed-effect variance
(Intercept)	3.00	0.52	10.28	5.83	< 0.01	
log (Mass)	0.30	0.07	3.87	4.16	0.015	0.610
Temperature	0.03	0.02	82.77	2.03	0.045	0.080
U^2	-0.02	0.07	79.67	-0.25	0.801	0.001
T	–0.49	0.16	80.37	-3.10	< 0.01	0.175
U_{Trms}	0.30	0.06	82.05	5.03	< 0.01	0.403
$U^2 \times T$	6.84	1.50	79.91	4.57	< 0.01	0.334

APPENDIX C: SUPPLEMENTAL MATERIALS CHAPTER FOUR

Figures

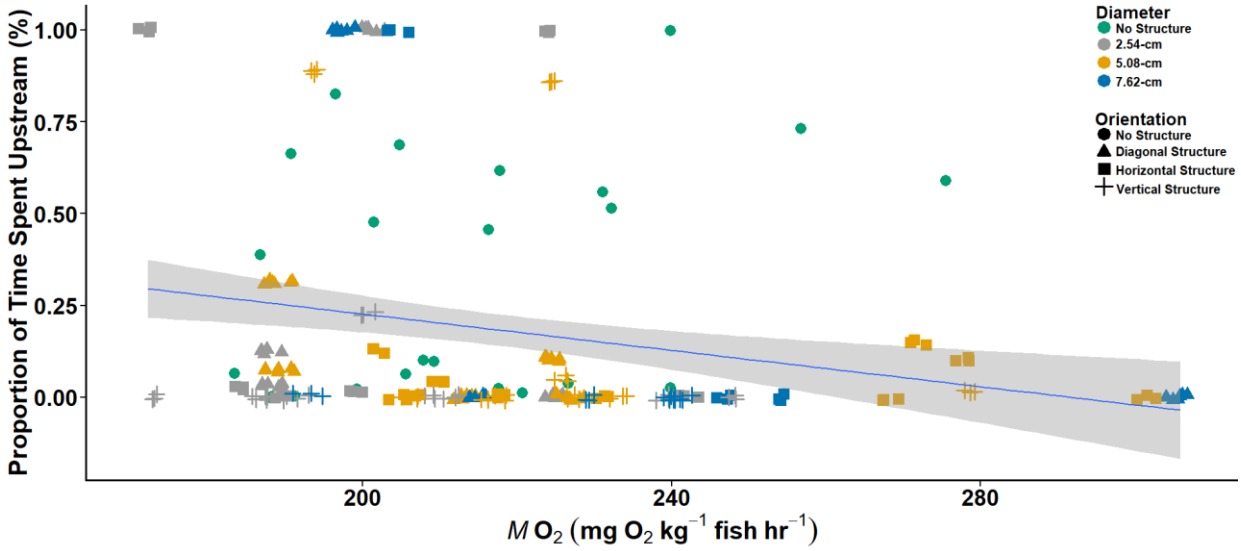

Figure C.1. The proportion of time spent upstream of turbulence-generating structures as a product of fish oxygen consumption ($\dot{M}O_{2\dot{M}O2}$) for rainbow trout and smallmouth bass (combined) participating in flume experiments to examine fish habitat selection in turbulent flow. Fish swam with cylindrical structures of different diameters (2.54-cm, 5.08-cm, 7.62-cm), in one of three orientations (diagonal, horizontal, vertical), or with no structure for a control condition. Data points are shown with a different color and shape to indicate the structure a fish swam with for the trial from which a given data point was derived. All fish were tagged with accelerometers, allowing for the estimation of oxygen consumption from acceleration using a pre-existing model relating the two. The line and confidence band for the linear regression relating the proportion of time spent upstream with $\dot{M}O_{2\dot{M}O2}$ are shown to visualize how the proportion of time spent upstream differed with different levels of fish oxygen consumption. Data points are shown with a jitter effect to improve readability and account for overlapping data points.

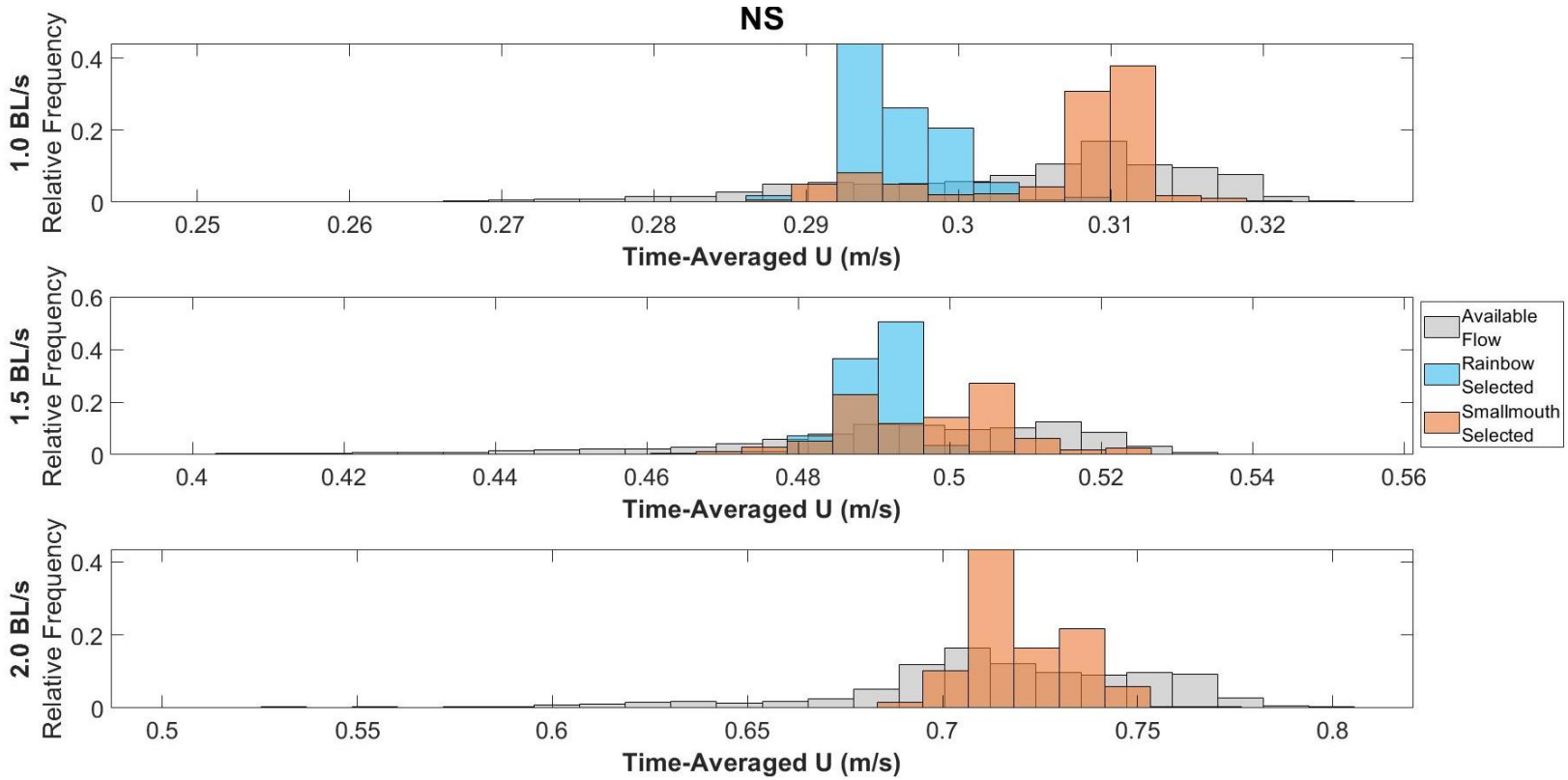

Figure C.2. Relative frequency histograms relating the distribution of available levels of time-averaged longitudinal velocity (*U*; m/s) to the distribution of *U* selected by rainbow trout and smallmouth bass to swimming downstream for the control case with no structure (NS) across three body length velocities, 1.0, 1.5, and 2.0 BL/S. Data presented are derived from the XZ plane.

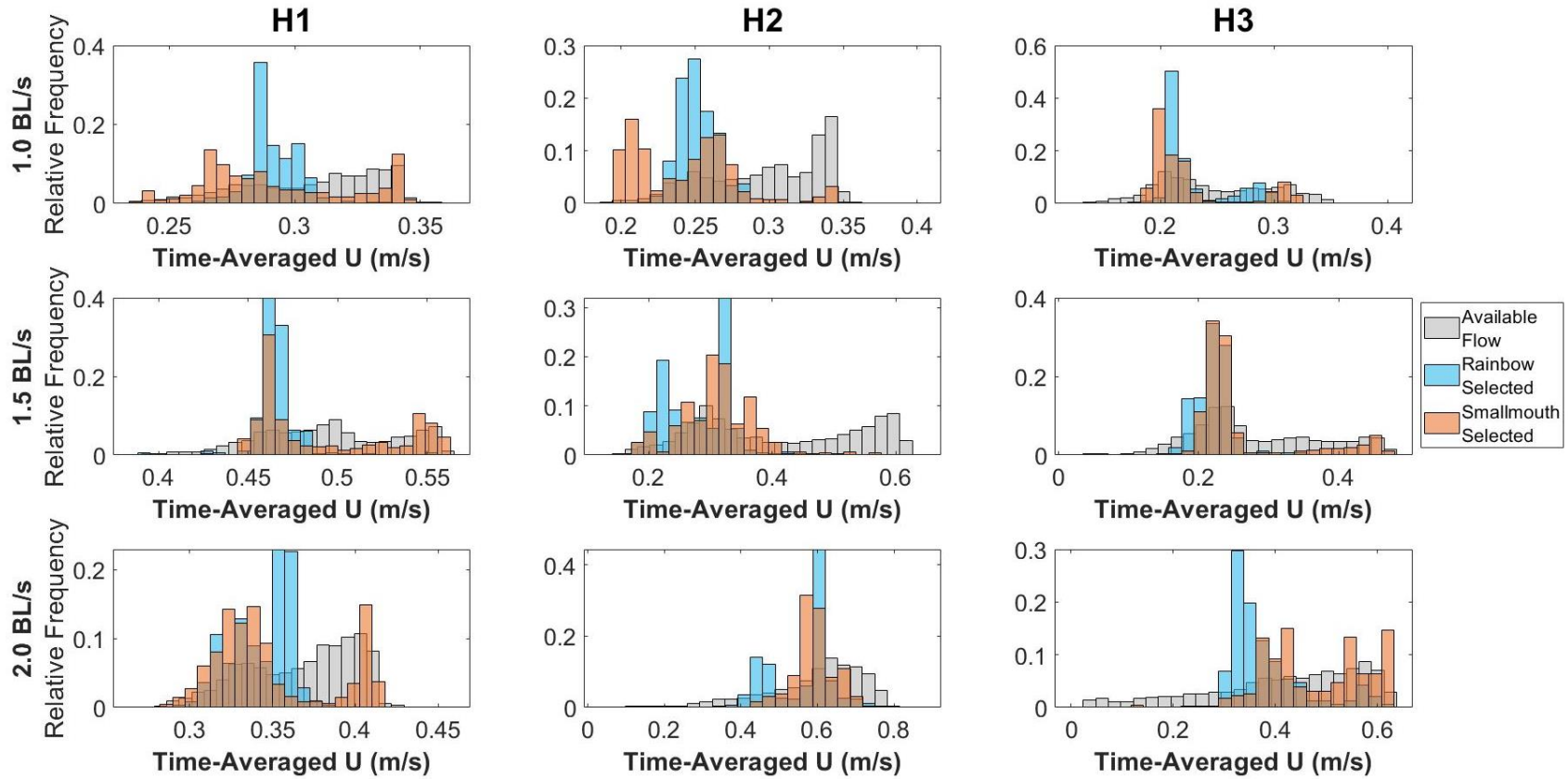

Figure C.3. Relative frequency histograms relating the distribution of available levels of time-averaged longitudinal velocity (*U*; m/s) to the distribution of *U* selected by rainbow trout and smallmouth bass to swimming downstream of horizontal structures (HS) in one of three diameters (H1 – 2.54-cm; H2 – 5.08-cm; H3 – 7.62-cm), across three body length velocities, 1.0, 1.5, and 2.0 BL/S.

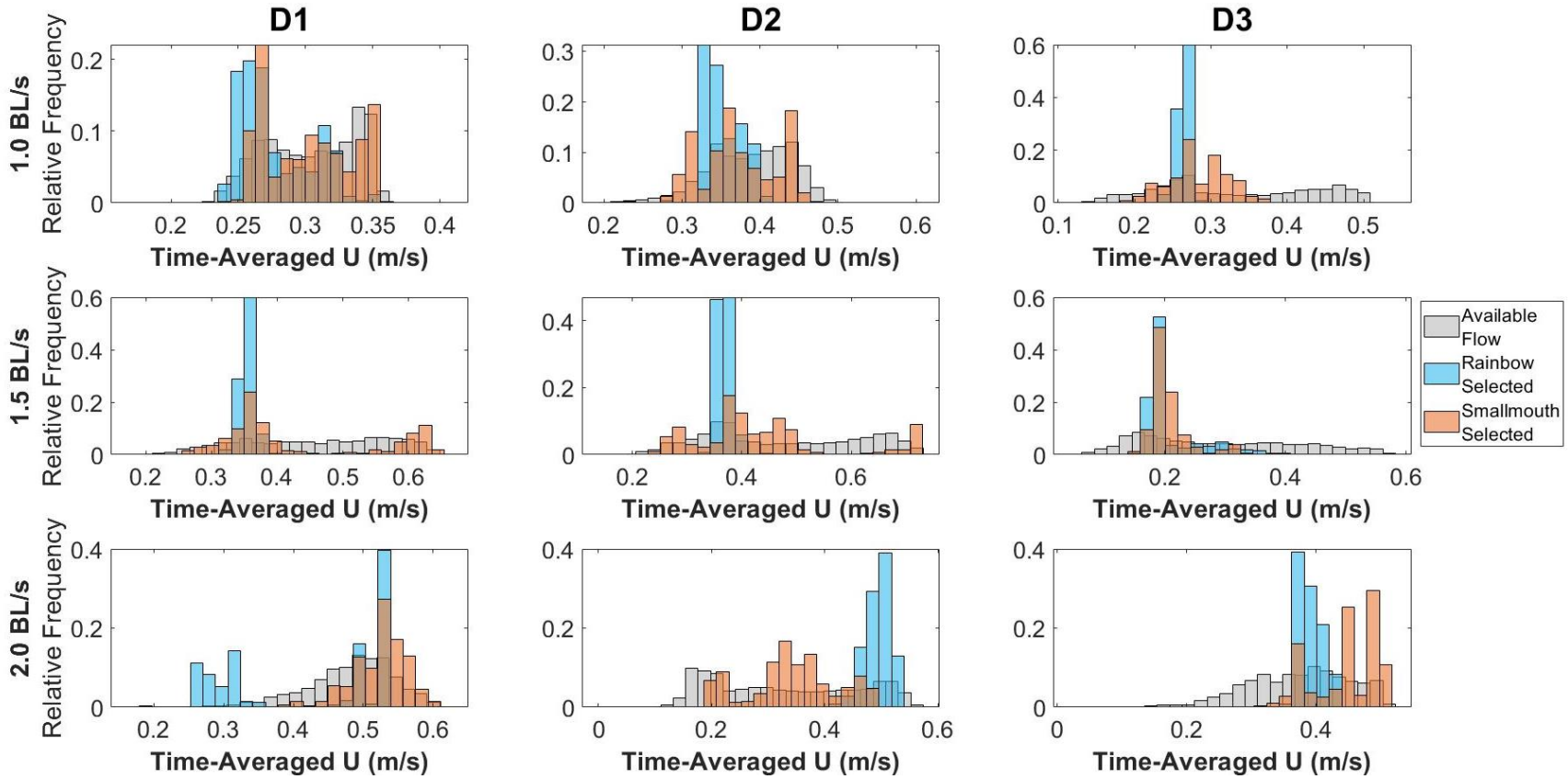

Figure C.4. Relative frequency histograms relating the distribution of available levels of time-averaged longitudinal velocity (*U*; m/s) to the distribution of *U* selected by rainbow trout and smallmouth bass to swimming downstream of diagonal structures (DS) in one of three diameters (D1 – 2.54-cm; D2 – 5.08-cm; D3 – 7.62-cm), across three body length velocities, 1.0, 1.5, and 2.0 BL/S. Data presented are derived from the XZ plane.

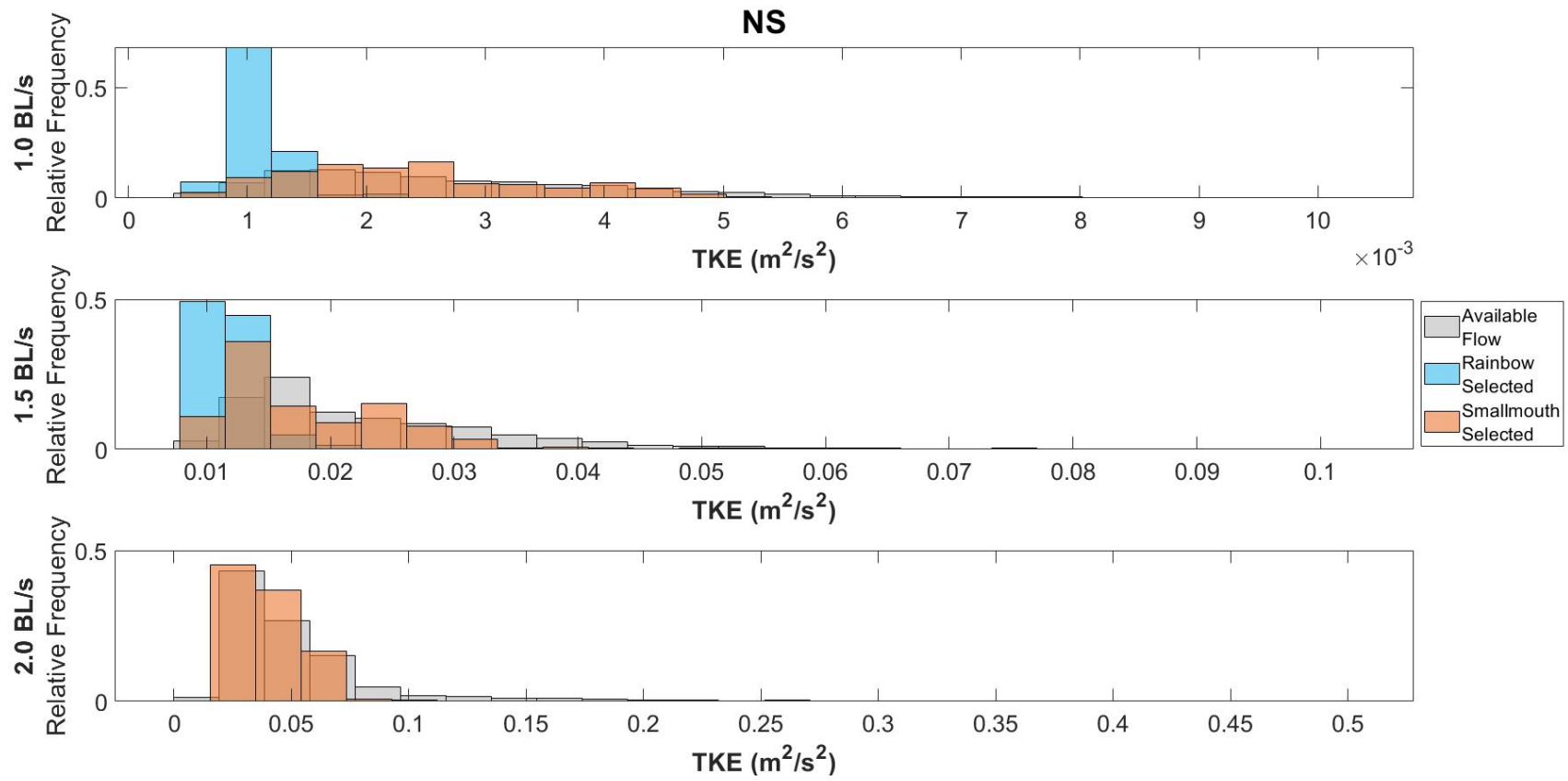

Figure C.5. Relative frequency histograms relating the distribution of available levels of time-averaged turbulent kinetic energy (TKE; m^2/s^2) to the distribution of TKE selected by rainbow trout and smallmouth bass to swimming downstream for the control case with no structure (NS) across three body length velocities, 1.0, 1.5, and 2.0 BL/S. Data presented are derived from the XZ plane.

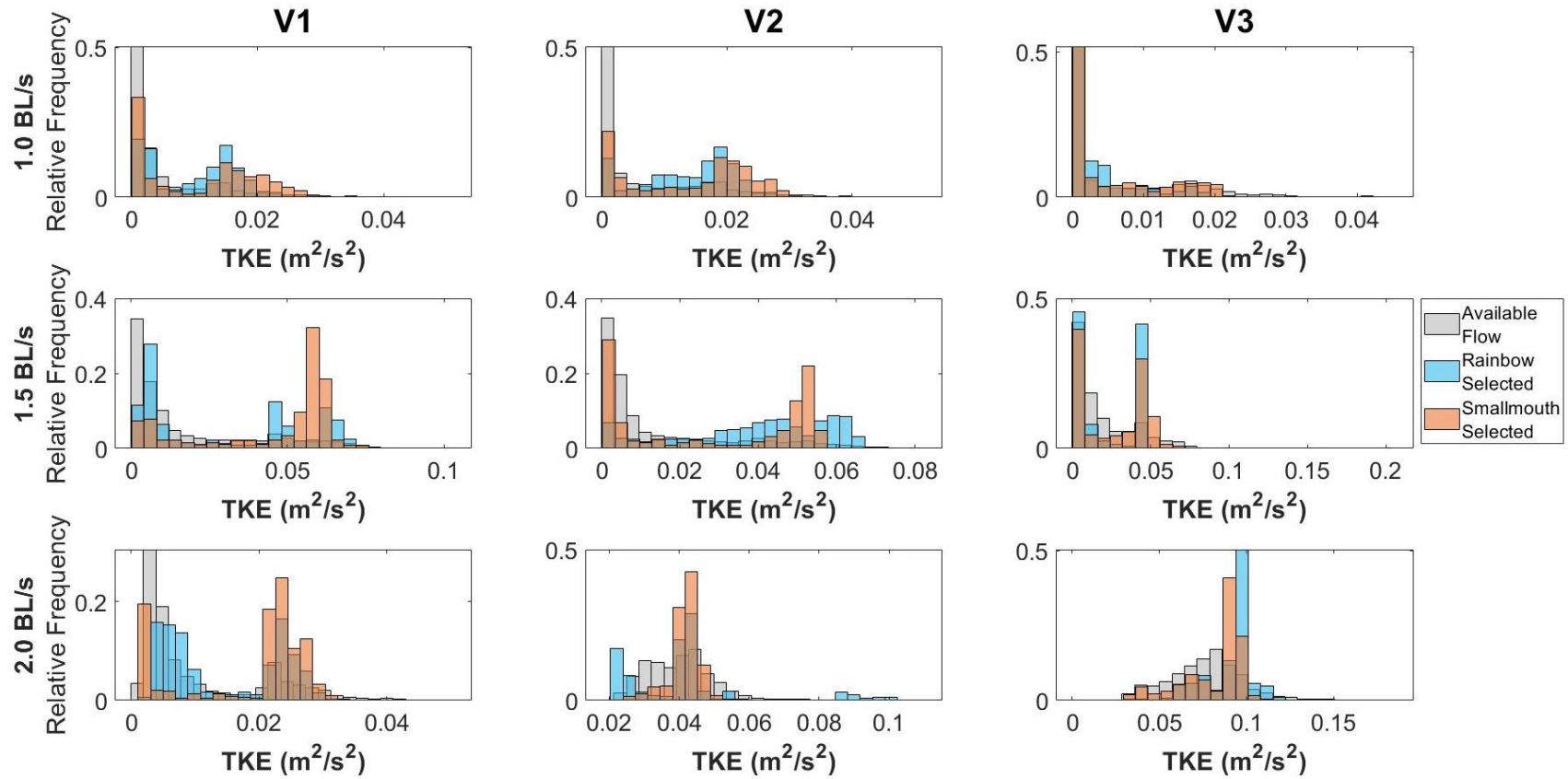

Figure C.6. Relative frequency histograms relating the distribution of available levels of time-averaged turbulent kinetic energy (TKE; m^2/s^2) to the distribution of TKE selected by rainbow trout and smallmouth bass to swimming downstream of vertical structures (VS) in one of three diameters (V1 – 2.54-cm; V2 – 5.08-cm; V3 – 7.62-cm), across three body length velocities, 1.0, 1.5, and 2.0 BL/S.

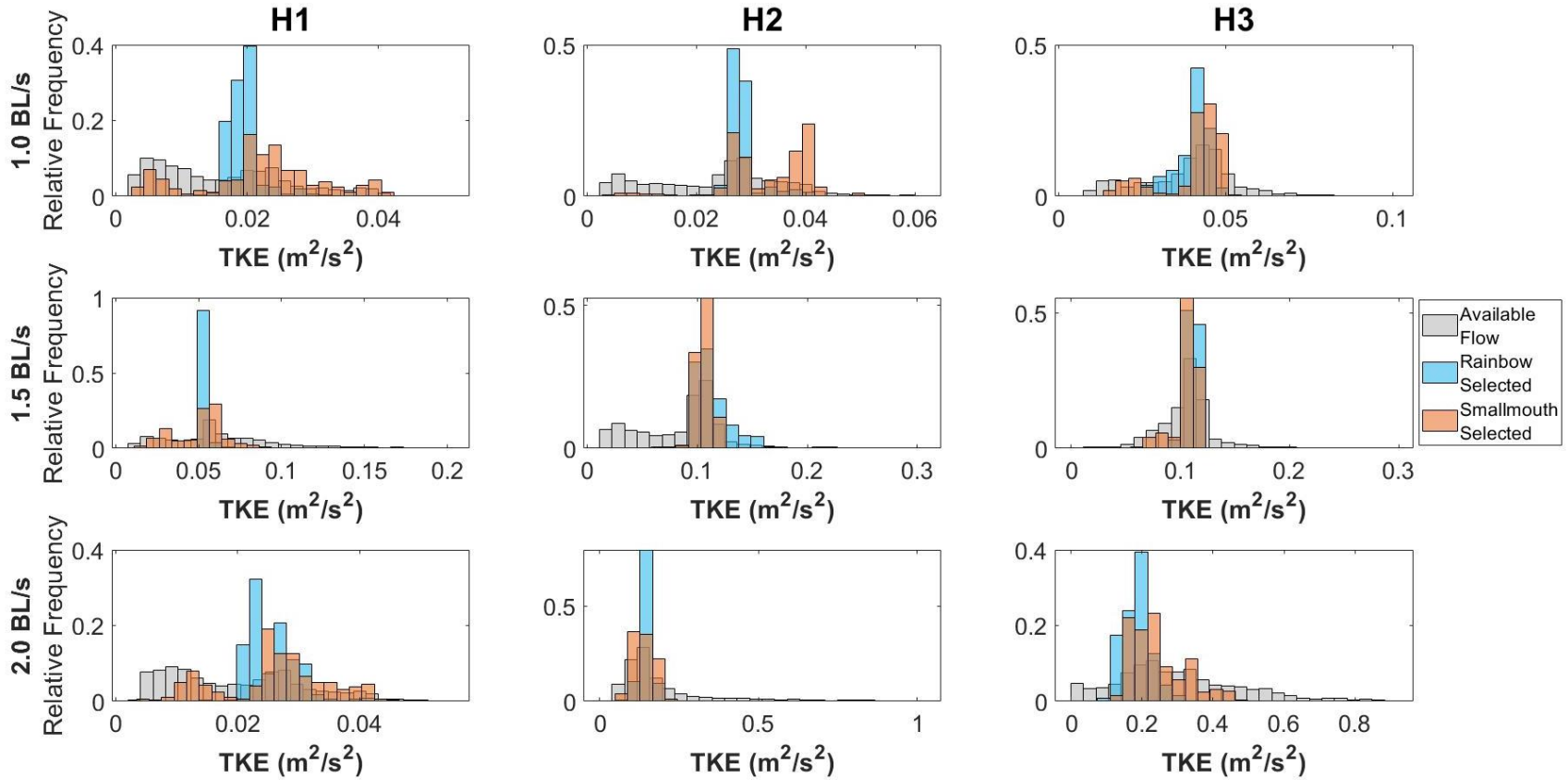

Figure C.7. Relative frequency histograms relating the distribution of available levels of time-averaged turbulent kinetic energy (TKE; m^2/s^2) to the distribution of TKE selected by rainbow trout and smallmouth bass to swimming downstream of horizontal structures (HS) in one of three diameters (H1 – 2.54-cm; H2 – 5.08-cm; H3 – 7.62-cm), across three body length velocities, 1.0, 1.5, and 2.0 BL/S.

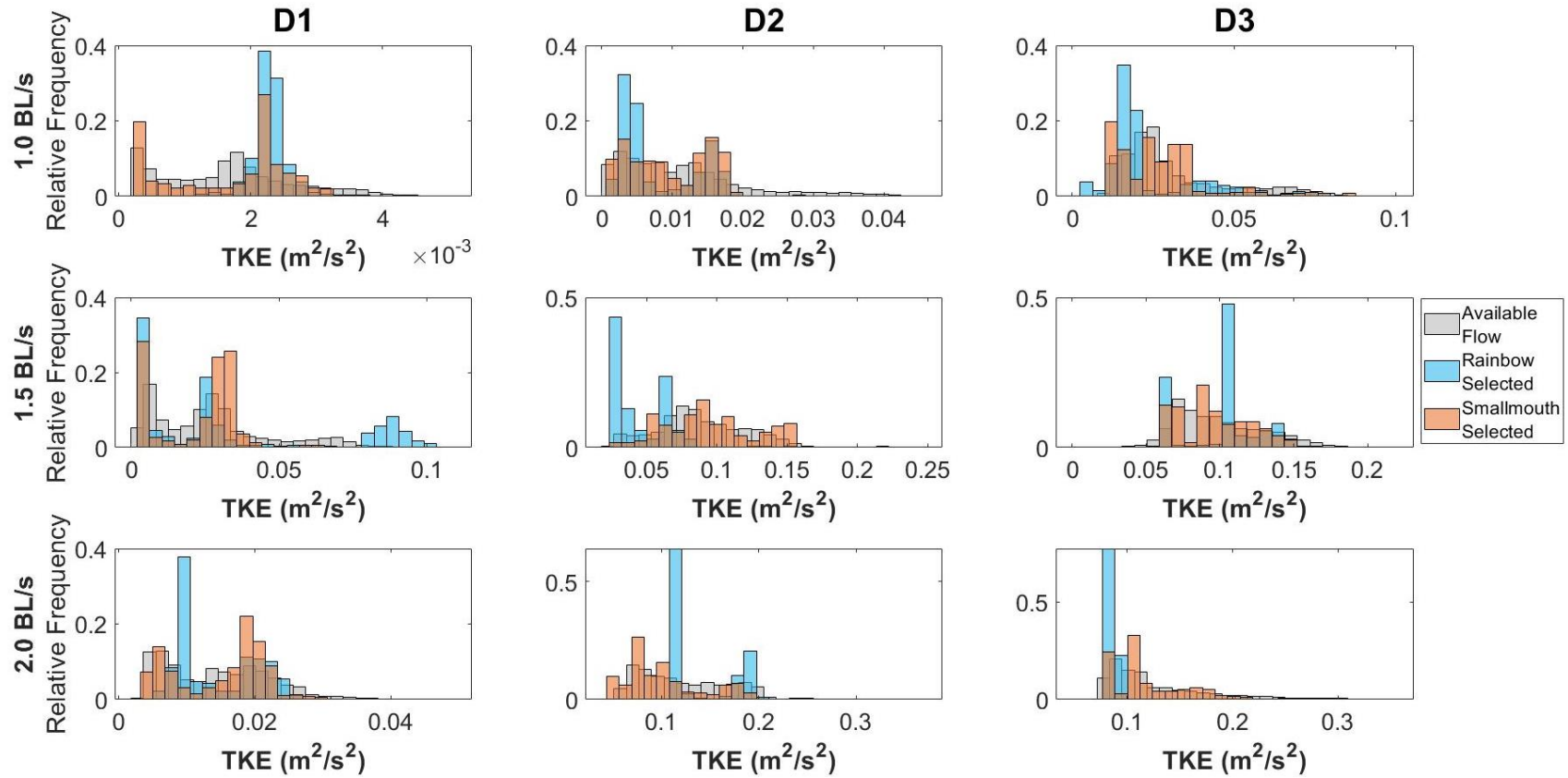

Figure C.8. Relative frequency histograms relating the distribution of available levels of time-averaged turbulent kinetic energy (TKE; m^2/s^2) to the distribution of TKE selected by rainbow trout and smallmouth bass to swimming downstream of diagonal structures (DS) in one of three diameters (D1 – 2.54-cm; D2 – 5.08-cm; D3 – 7.62-cm), across three body length velocities, 1.0, 1.5, and 2.0 BL/S. Data presented are derived from the XY plane.

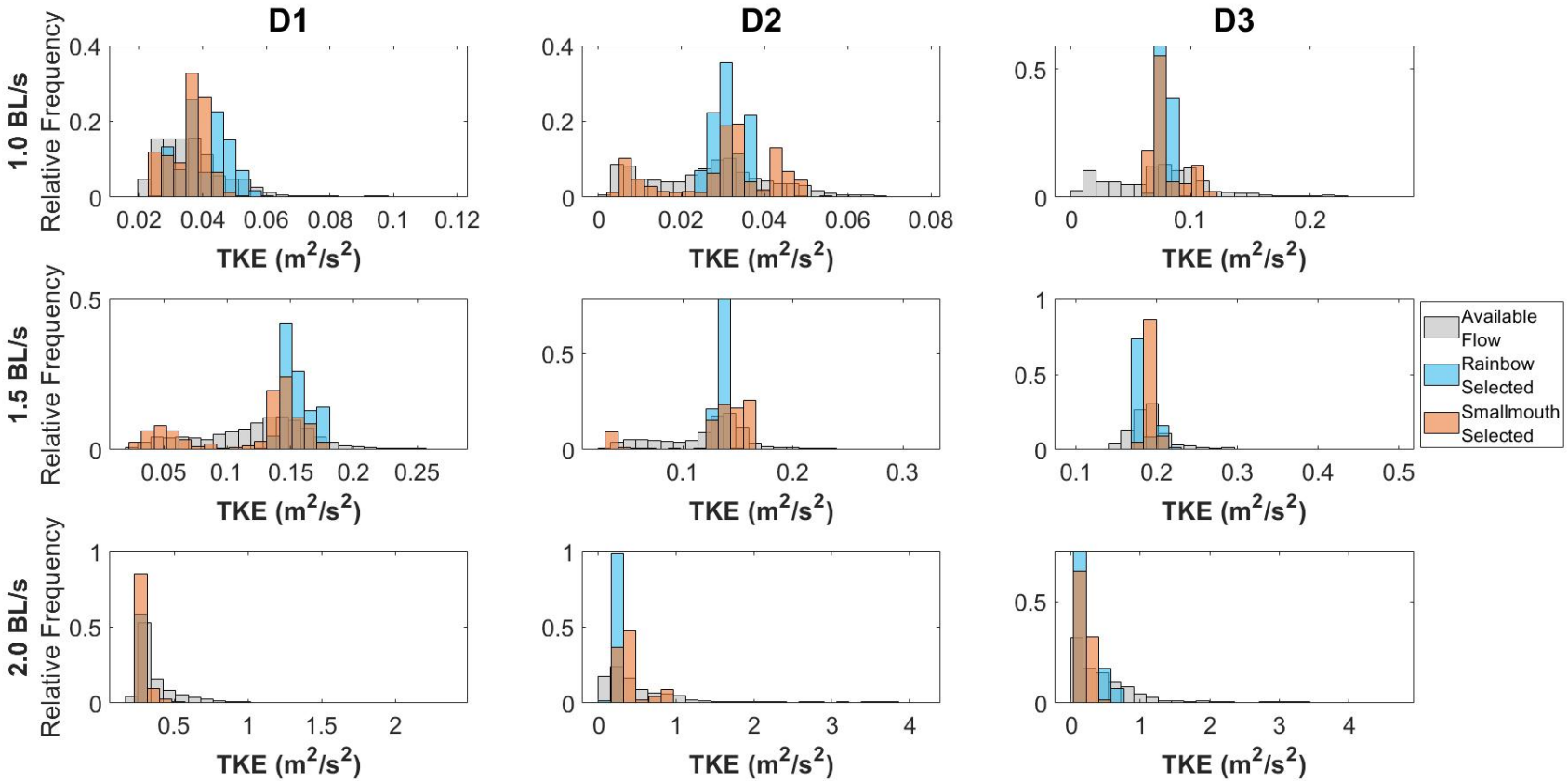

Figure C.9. Relative frequency histograms relating the distribution of available levels of time-averaged turbulent kinetic energy (TKE; m^2/s^2) to the distribution of TKE selected by rainbow trout and smallmouth bass to swimming downstream of diagonal structures (DS) in one of three diameters (D1 – 2.54-cm; D2 – 5.08-cm; D3 – 7.62-cm), across three body length velocities, 1.0, 1.5, and 2.0 BL/S. Data presented are derived from the XZ plane.

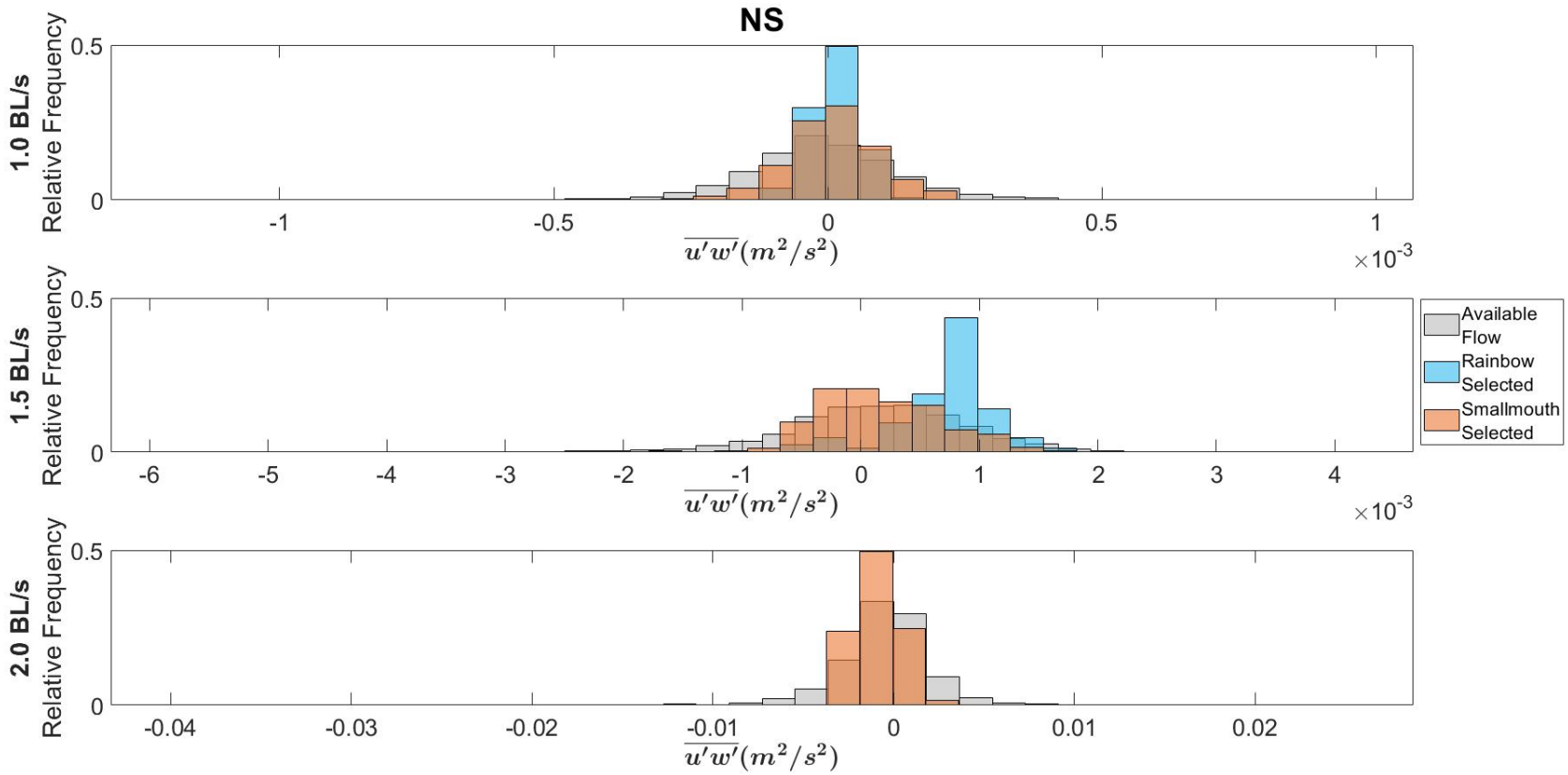

Figure C.10. Relative frequency histograms relating the distribution of available levels of time-averaged Reynolds stress to the distribution of Reynolds stress selected by rainbow trout and smallmouth bass to swimming downstream for the control case with no structure (NS) across three body length velocities, 1.0, 1.5, and 2.0 BL/S. Data presented are derived from the XZ plane.

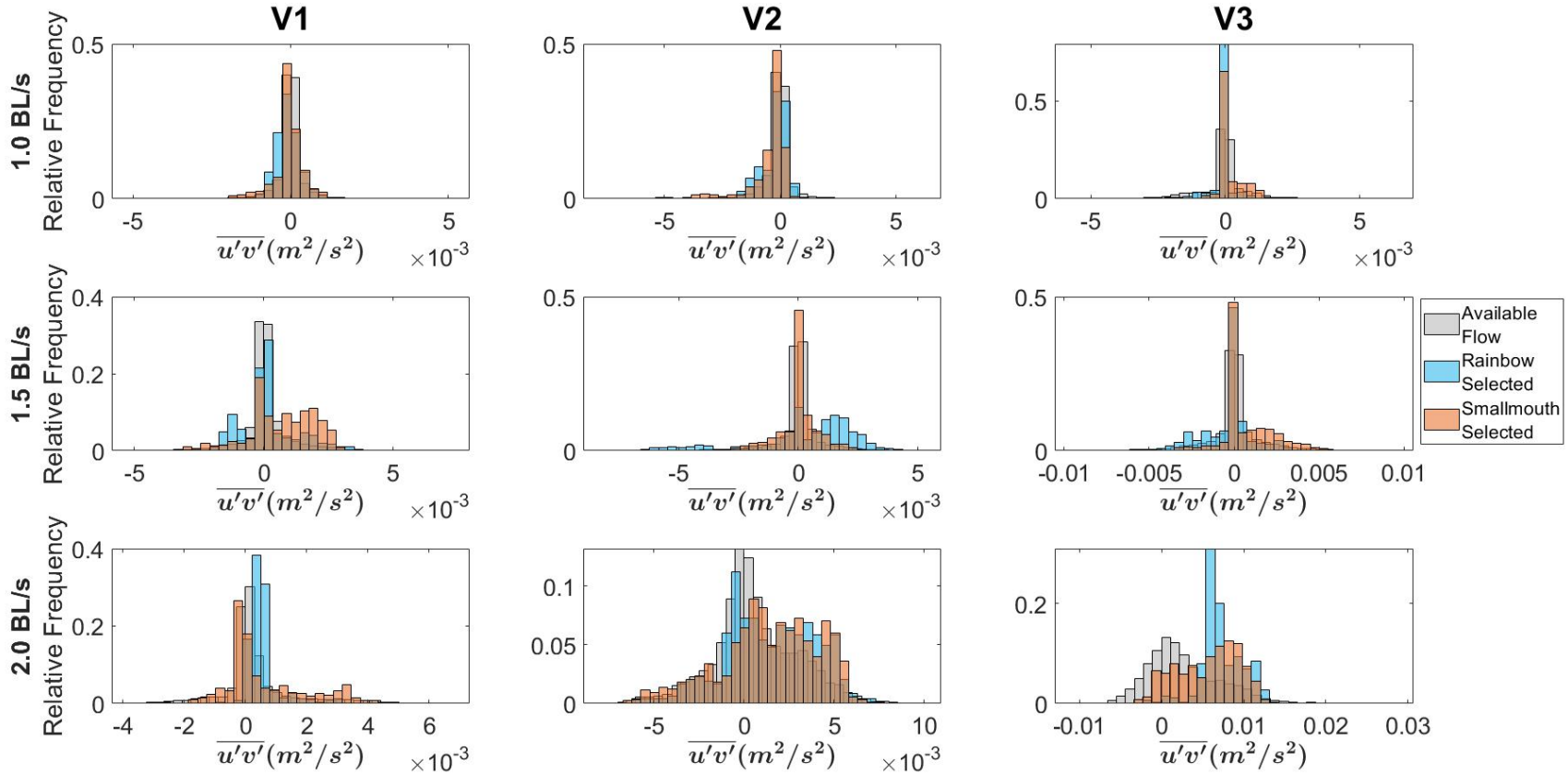

Figure C.11. Relative frequency histograms relating the distribution of available levels of time-averaged Reynolds stress ($\overline{u'v'}$; m^2/s^2) to the distribution of Reynolds stress selected by rainbow trout and smallmouth bass to swimming downstream of vertical structures (VS) in one of three diameters (V1 – 2.54-cm; V2 – 5.08-cm; V3 – 7.62-cm), across three body length velocities, 1.0, 1.5, and 2.0 BL/S.

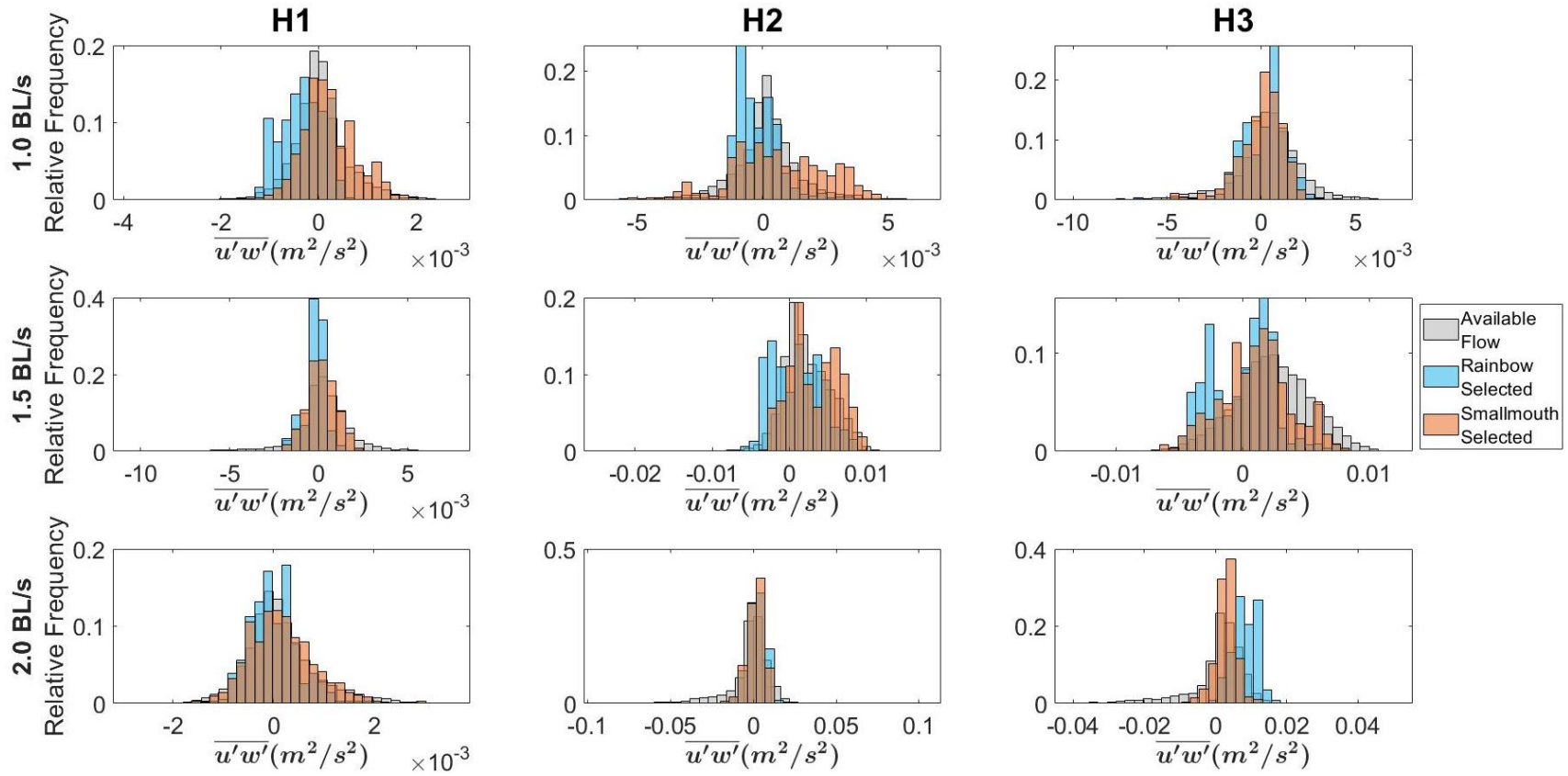

Figure C.12. Relative frequency histograms relating the distribution of available levels of time-averaged Reynolds stress ($\overline{u'w'}$; m^2/s^2) to the distribution of Reynolds stress selected by rainbow trout and smallmouth bass to swimming downstream of horizontal structures (HS) in one of three diameters (H1 – 2.54-cm; H2 – 5.08-cm; H3 – 7.62-cm), across three body length velocities, 1.0, 1.5, and 2.0 BL/S.

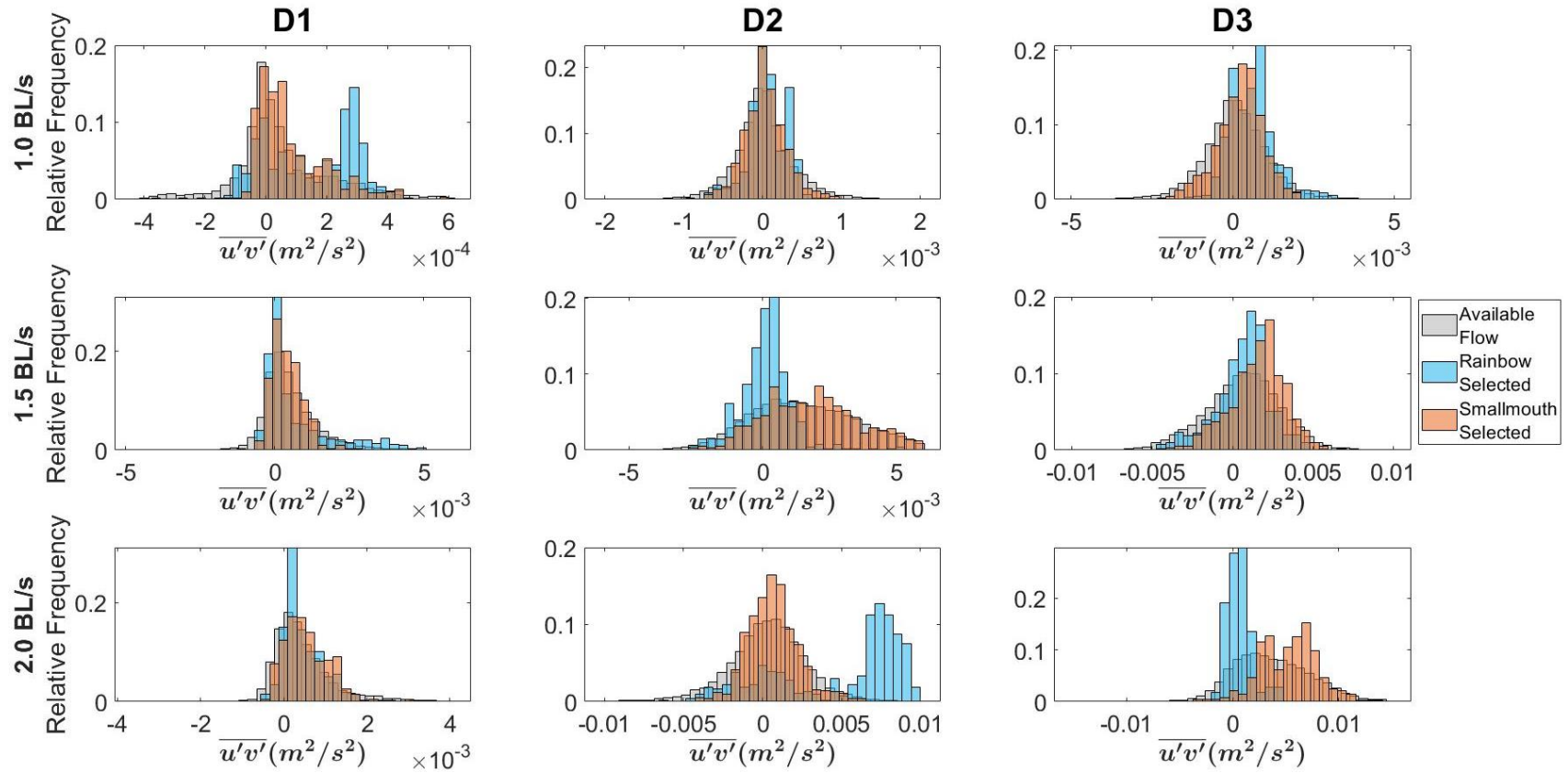

Figure C.13. Relative frequency histograms relating the distribution of available levels of time-averaged Reynolds stress ($\overline{u'v'}$; m^2/s^2) to the distribution of Reynolds stress selected by rainbow trout and smallmouth bass to swimming downstream of diagonal structures (DS) in one of three diameters (D1 – 2.54-cm; D2 – 5.08-cm; D3 – 7.62-cm), across three body length velocities, 1.0, 1.5, and 2.0 BL/S. Data presented are derived from the XY plane.

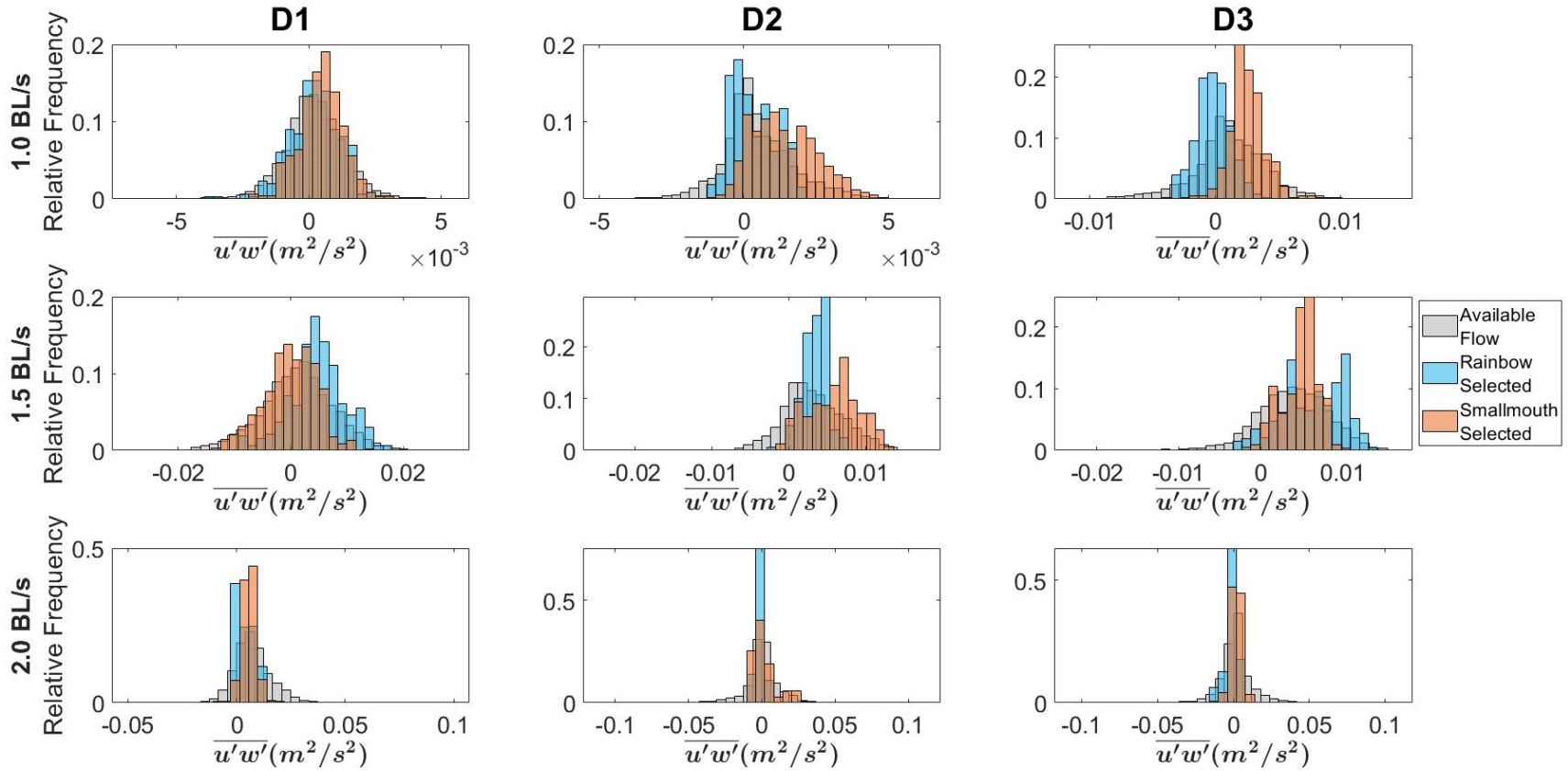

Figure C.14. Relative frequency histograms relating the distribution of available levels of time-averaged Reynolds stress ($\overline{u'w'}$; m^2/s^2) to the distribution of Reynolds stress selected by rainbow trout and smallmouth bass to swimming downstream of diagonal structures (DS) in one of three diameters (D1 – 2.54-cm; D2 – 5.08-cm; D3 – 7.62-cm), across three body length velocities, 1.0, 1.5, and 2.0 BL/S. Data presented are derived from the XZ plane.

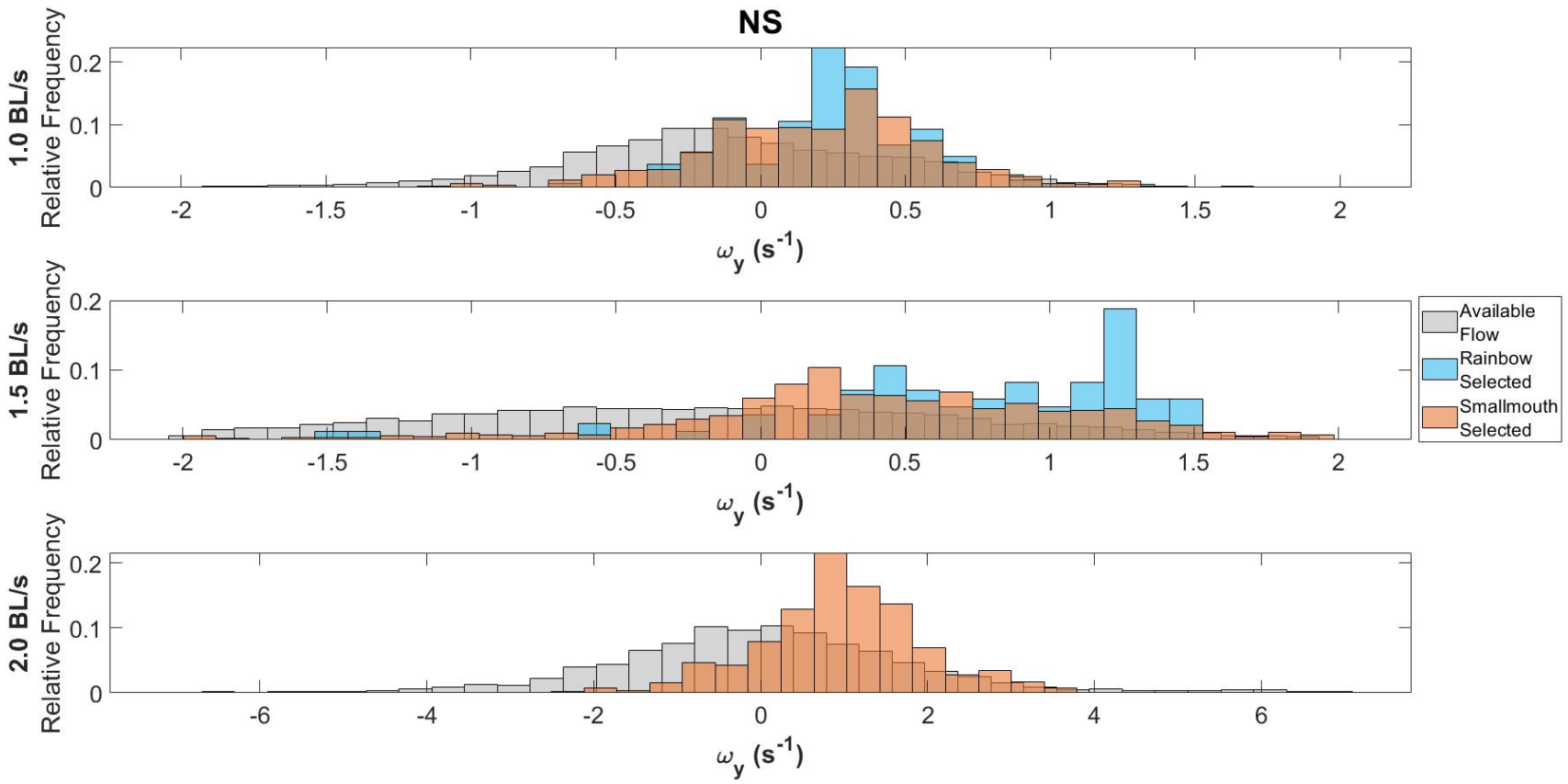

Figure C.15. Relative frequency histograms relating the distribution of available levels of time-averaged vorticity (ω_y; s^{-1}) to the distribution of vorticity selected by rainbow trout and smallmouth bass to swimming downstream for the control case with no structure (NS) across three body length velocities, 1.0, 1.5, and 2.0 BL/S. Data presented are derived from the XZ plane.

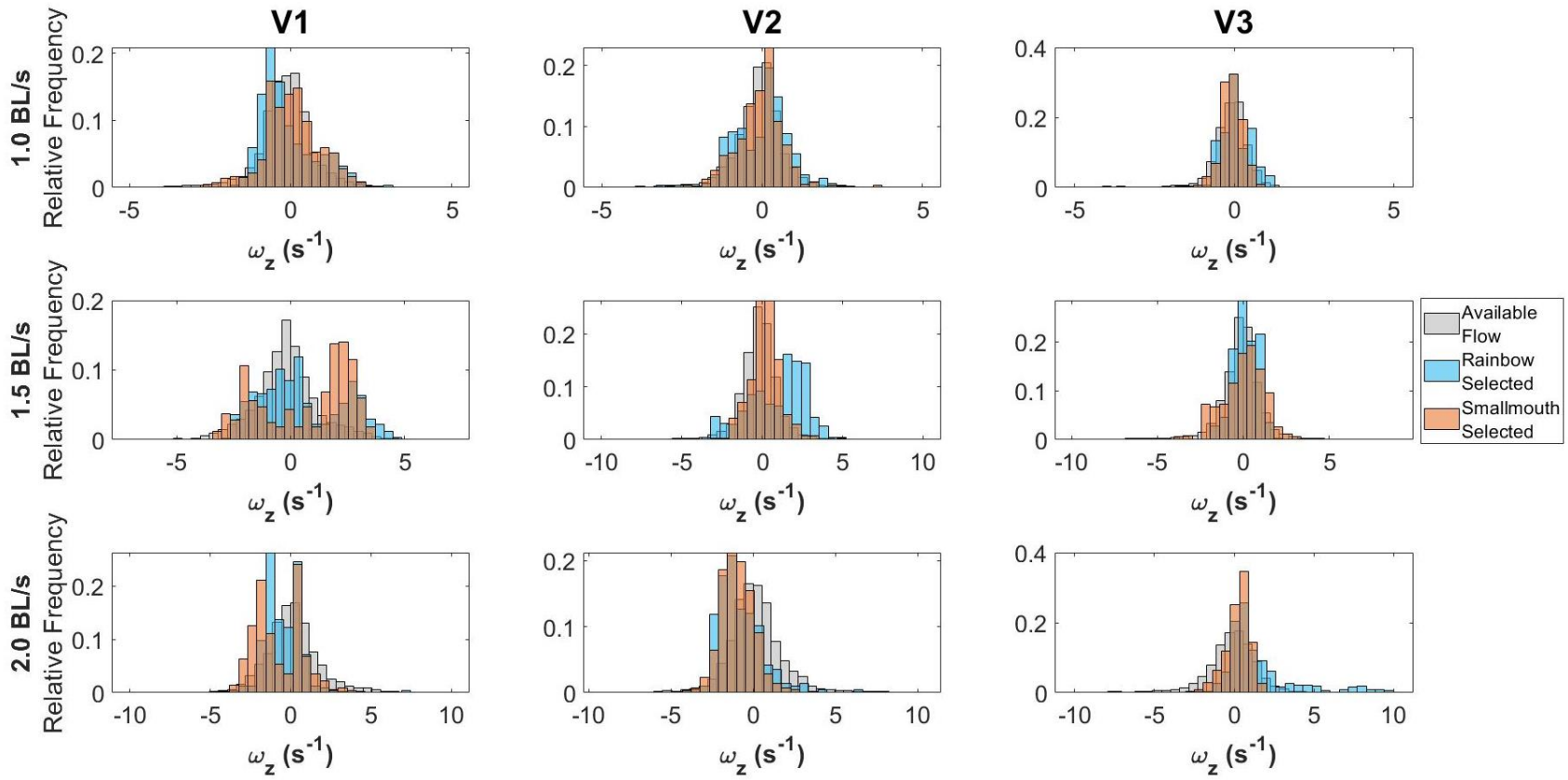

Figure C.16. Relative frequency histograms relating the distribution of available levels of time-averaged vorticity (ω_z; s^{-1}) to the distribution of vorticity selected by rainbow trout and smallmouth bass to swimming downstream of vertical structures (VS) in one of three diameters (V1 – 2.54-cm; V2 – 5.08-cm; V3 – 7.62-cm), across three body length velocities, 1.0, 1.5, and 2.0 BL/S.

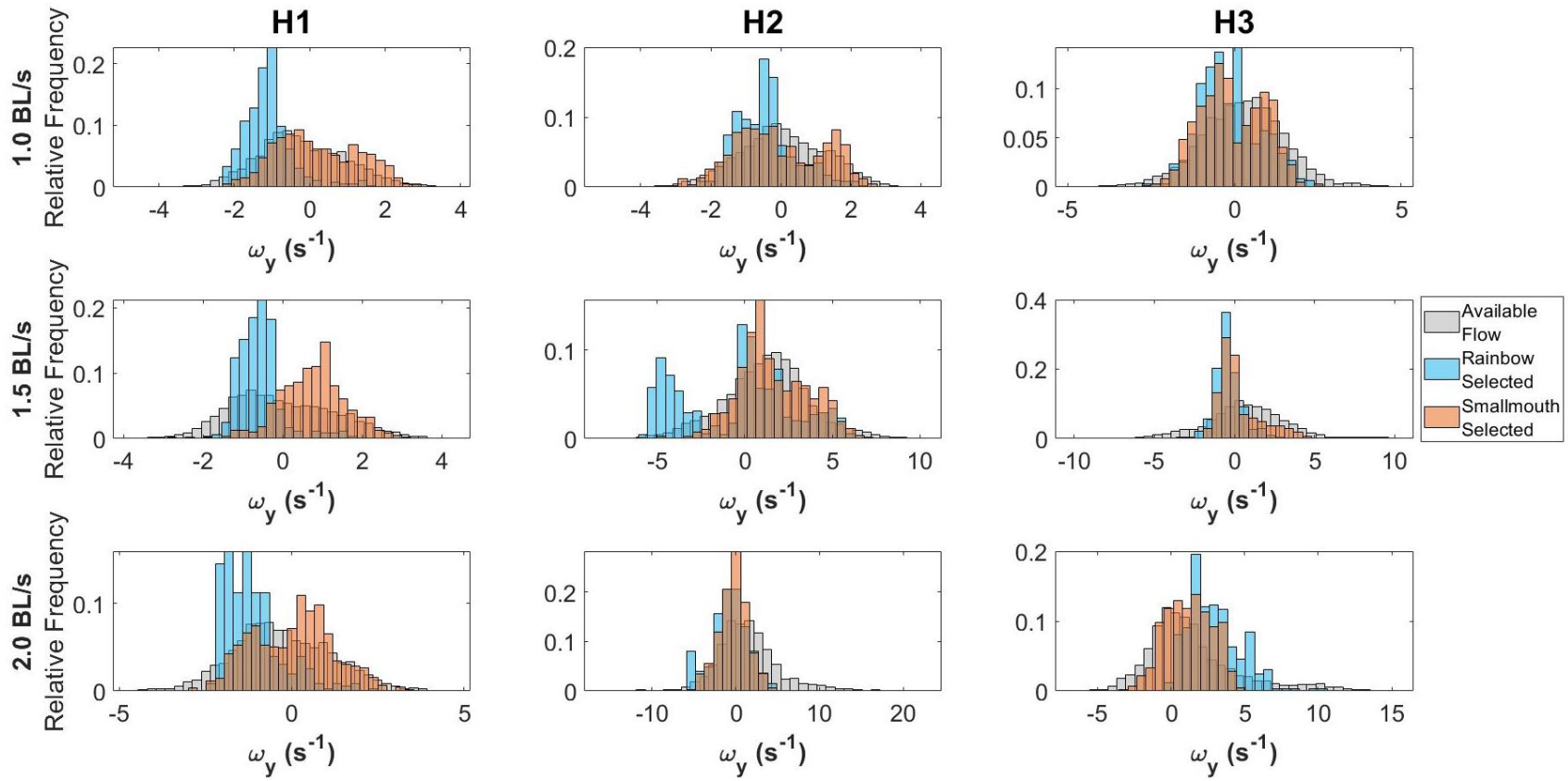

Figure C.17. Relative frequency histograms relating the distribution of available levels of time-averaged vorticity (ω_y; s^{-1}) to the distribution of vorticity selected by rainbow trout and smallmouth bass to swimming downstream of horizontal structures (HS) in one of three diameters (H1 – 2.54-cm; H2 – 5.08-cm; H3 – 7.62-cm), across three body length velocities, 1.0, 1.5, and 2.0 BL/S.

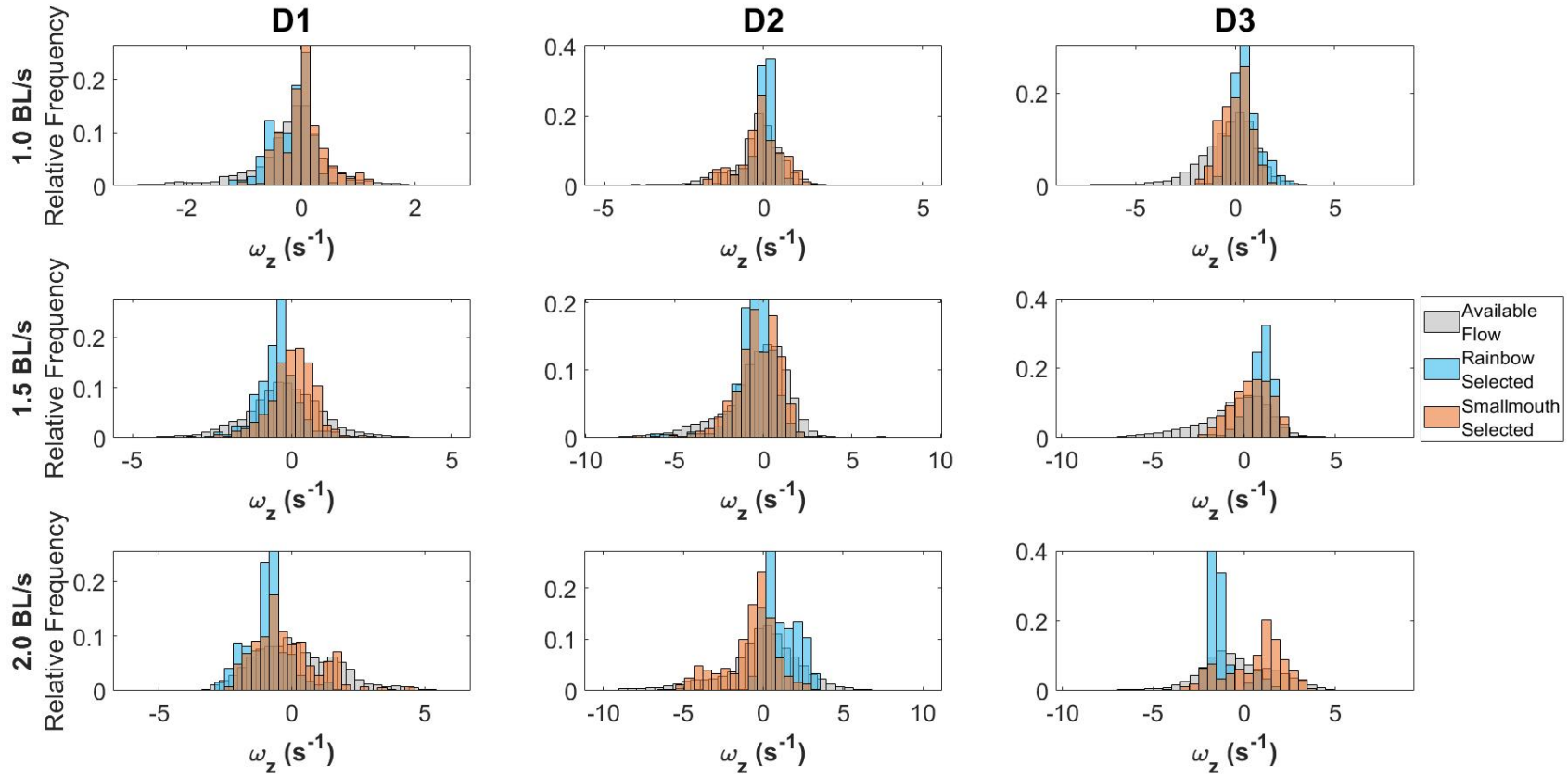

Figure C.18. Relative frequency histograms relating the distribution of available levels of time-averaged vorticity (ω_z; s^{-1}) to the distribution of vorticity selected by rainbow trout and smallmouth bass to swimming downstream of diagonal structures (DS) in one of three diameters (D1 – 2.54-cm; D2 – 5.08-cm; D3 – 7.62-cm), across three body length velocities, 1.0, 1.5, and 2.0 BL/S. Data presented are derived from the XY plane.

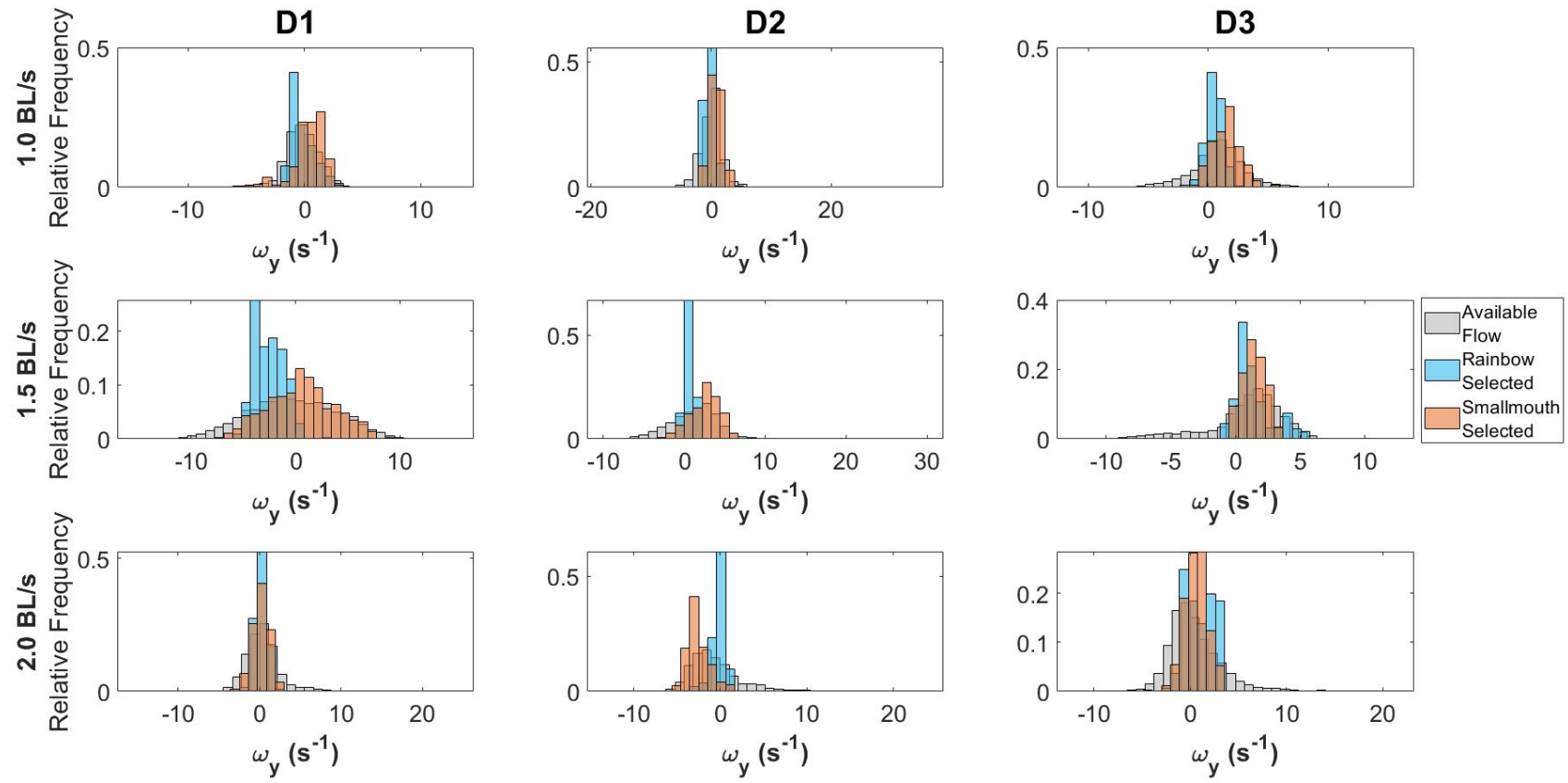

Figure C.19. Relative frequency histograms relating the distribution of available levels of time-averaged vorticity (ω_y; s^{-1}) to the distribution of vorticity selected by rainbow trout and smallmouth bass to swimming downstream of diagonal structures (DS) in one of three diameters (D1 – 2.54-cm; D2 – 5.08-cm; D3 – 7.62-cm), across three body length velocities, 1.0, 1.5, and 2.0 BL/S. Data presented are derived from the XZ plane.

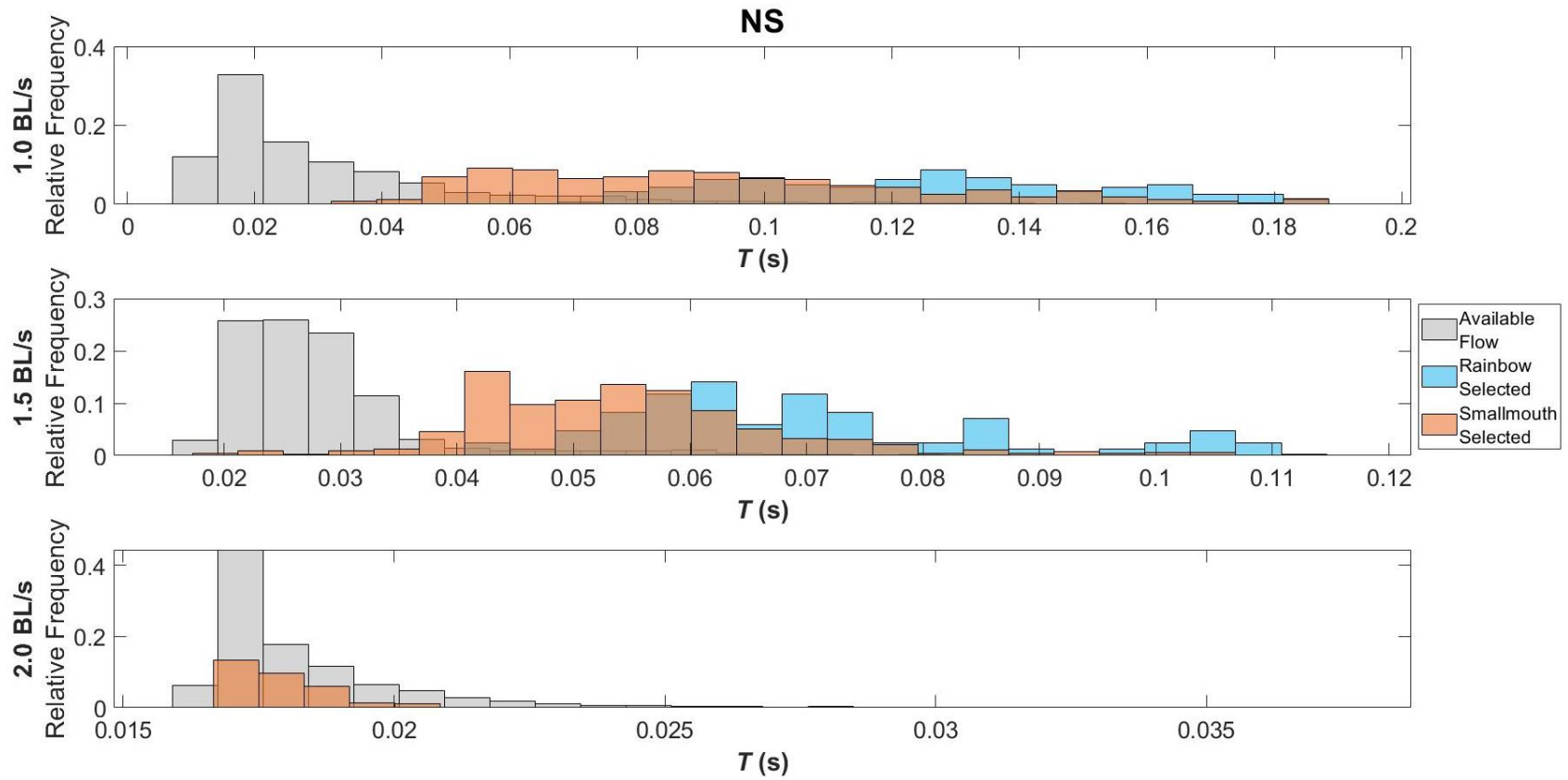

Figure C.20. Relative frequency histograms relating the distribution of available levels of time-averaged turbulent integral time scale (*T*; s) to the distribution of *T* selected by rainbow trout and smallmouth bass to swimming downstream for the control case with no structure (NS) across three body length velocities, 1.0, 1.5, and 2.0 BL/S. Data presented are derived from the XZ plane.

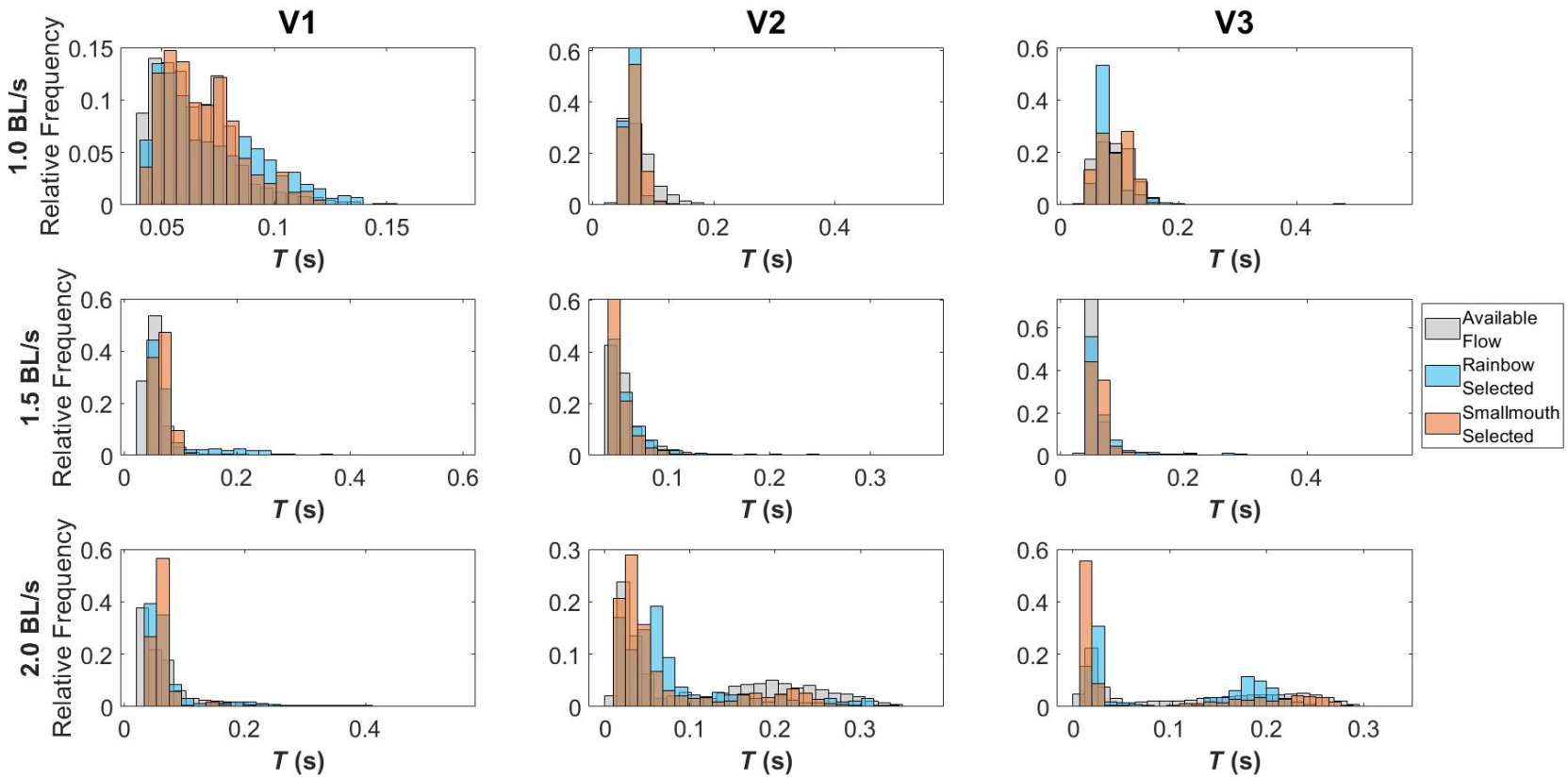

Figure C.21. Relative frequency histograms relating the distribution of available levels of time-averaged turbulent integral time scale (*T*; s) to the distribution of *T* selected by rainbow trout and smallmouth bass to swimming downstream of vertical structures (VS) in one of three diameters (V1 – 2.54-cm; V2 – 5.08-cm; V3 – 7.62-cm), across three body length velocities, 1.0, 1.5, and 2.0 BL/S.

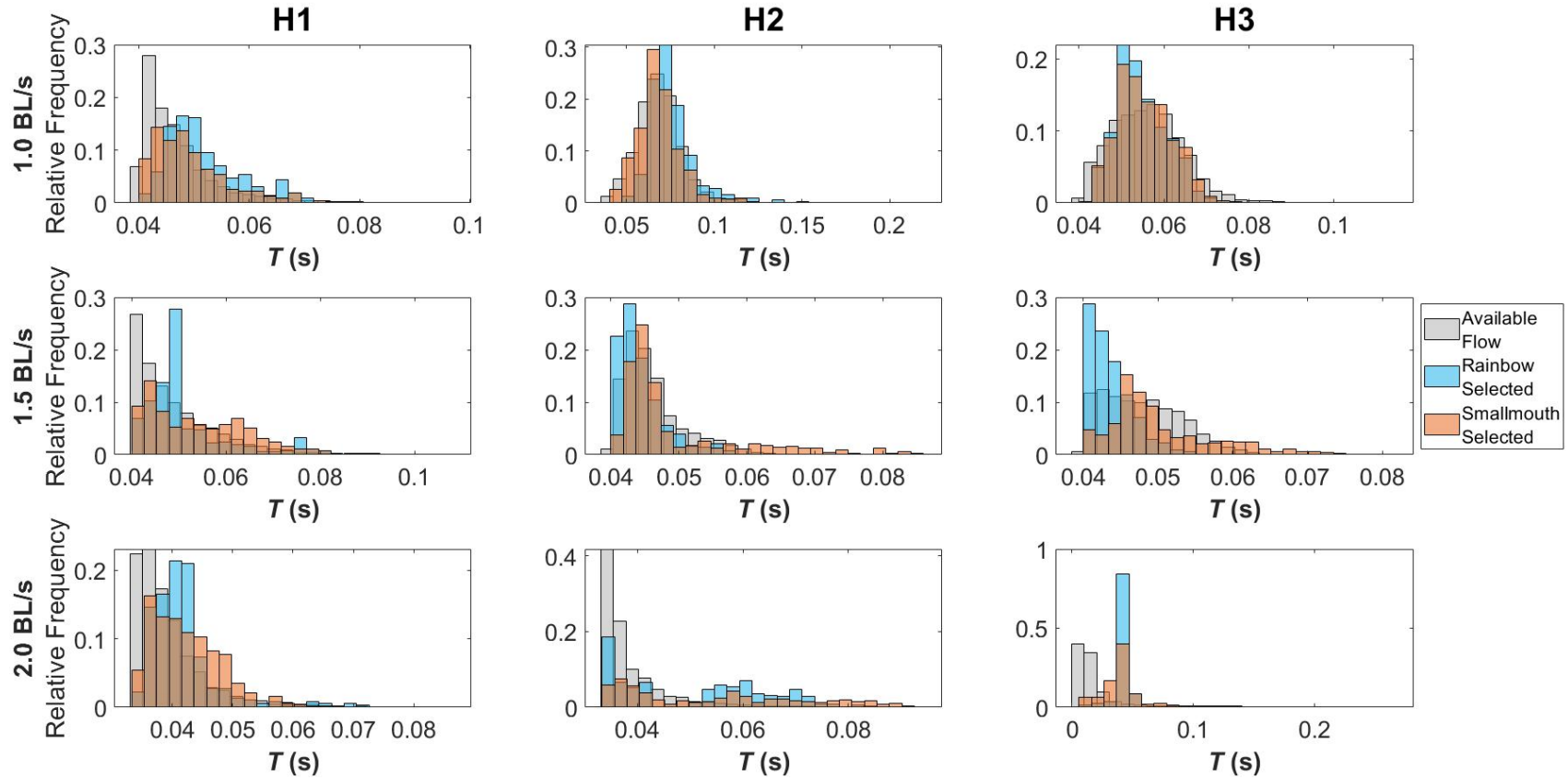

Figure C.22. Relative frequency histograms relating the distribution of available levels of time-averaged turbulent integral time scale (*T*; s) to the distribution of *T* selected by rainbow trout and smallmouth bass to swimming downstream of horizontal structures (HS) in one of three diameters (H1 – 2.54-cm; H2 – 5.08-cm; H3 – 7.62-cm), across three body length velocities, 1.0, 1.5, and 2.0 BL/S.

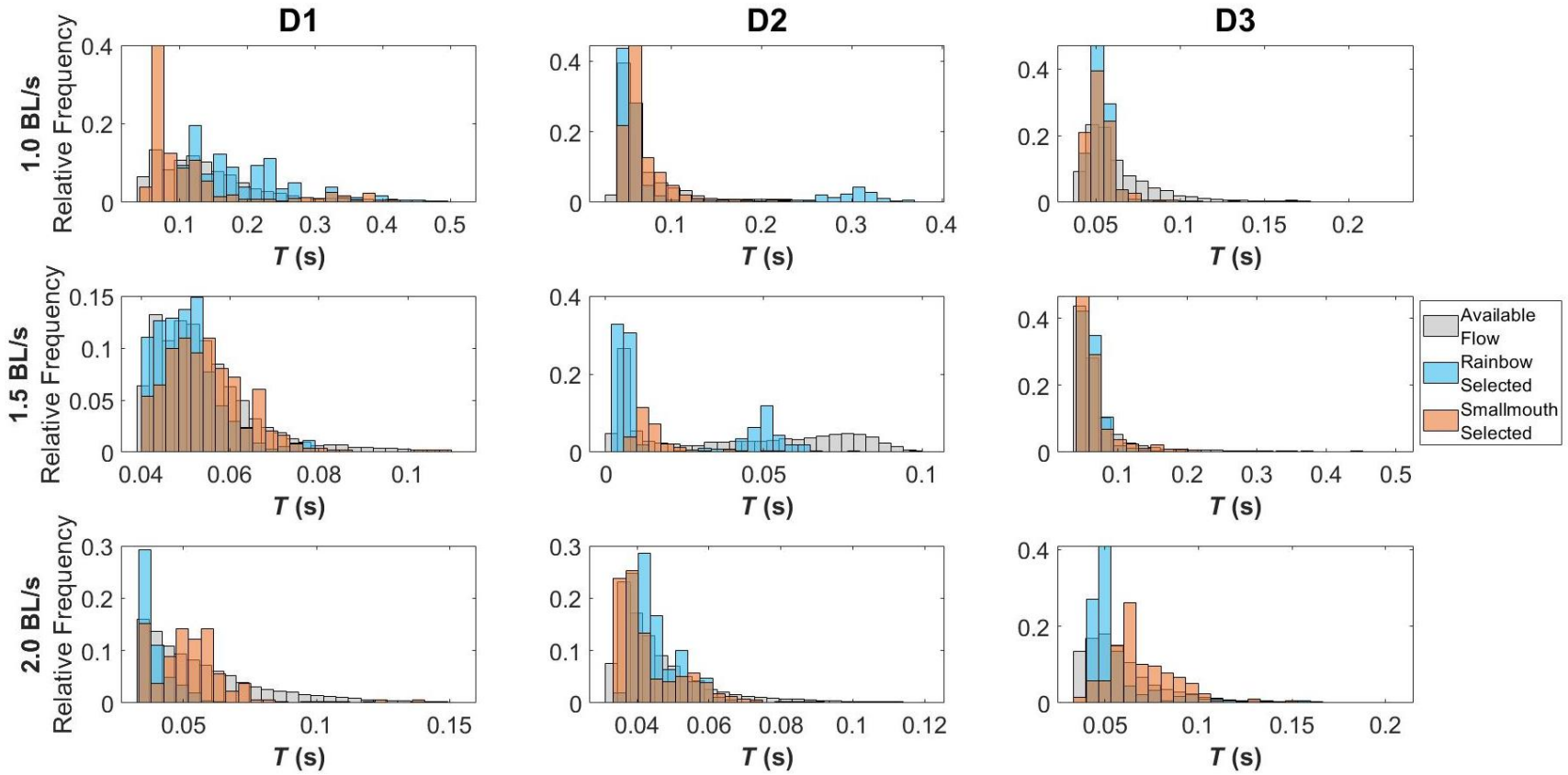

Figure C.23. Relative frequency histograms relating the distribution of available levels of time-averaged turbulent integral time scale (*T*; s) to the distribution of *T* selected by rainbow trout and smallmouth bass to swimming downstream of diagonal structures (DS) in one of three diameters (D1 – 2.54-cm; D2 – 5.08-cm; D3 – 7.62-cm), across three body length velocities, 1.0, 1.5, and 2.0 BL/S. Data presented are derived from the XY plane.

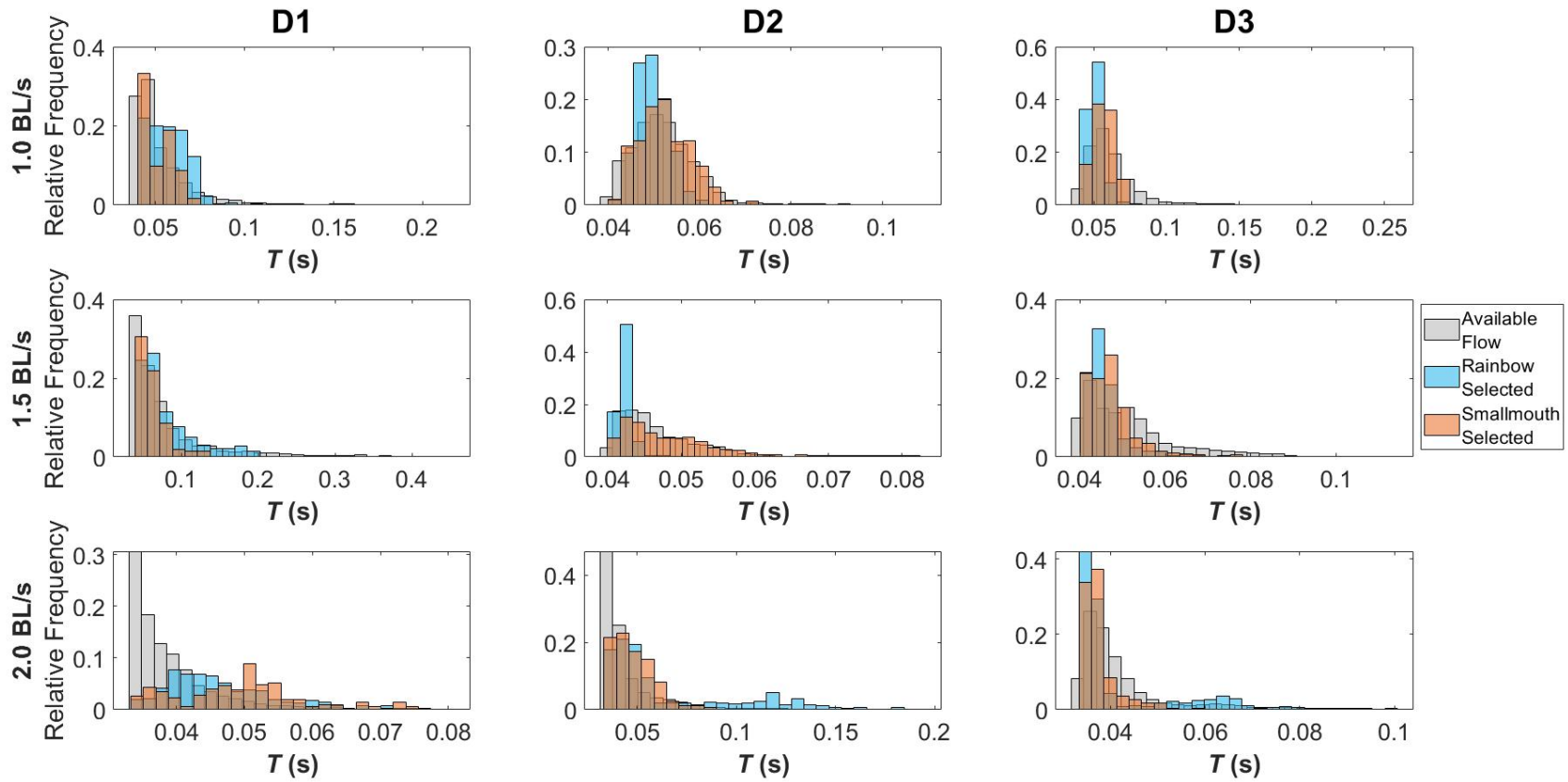

Figure C.24. Relative frequency histograms relating the distribution of available levels of time-averaged turbulent integral time scale (*T*; s) to the distribution of *T* selected by rainbow trout and smallmouth bass to swimming downstream of diagonal structures (DS) in one of three diameters (D1 – 2.54-cm; D2 – 5.08-cm; D3 – 7.62-cm), across three body length velocities, 1.0, 1.5, and 2.0 BL/S. Data presented are derived from the XZ plane.

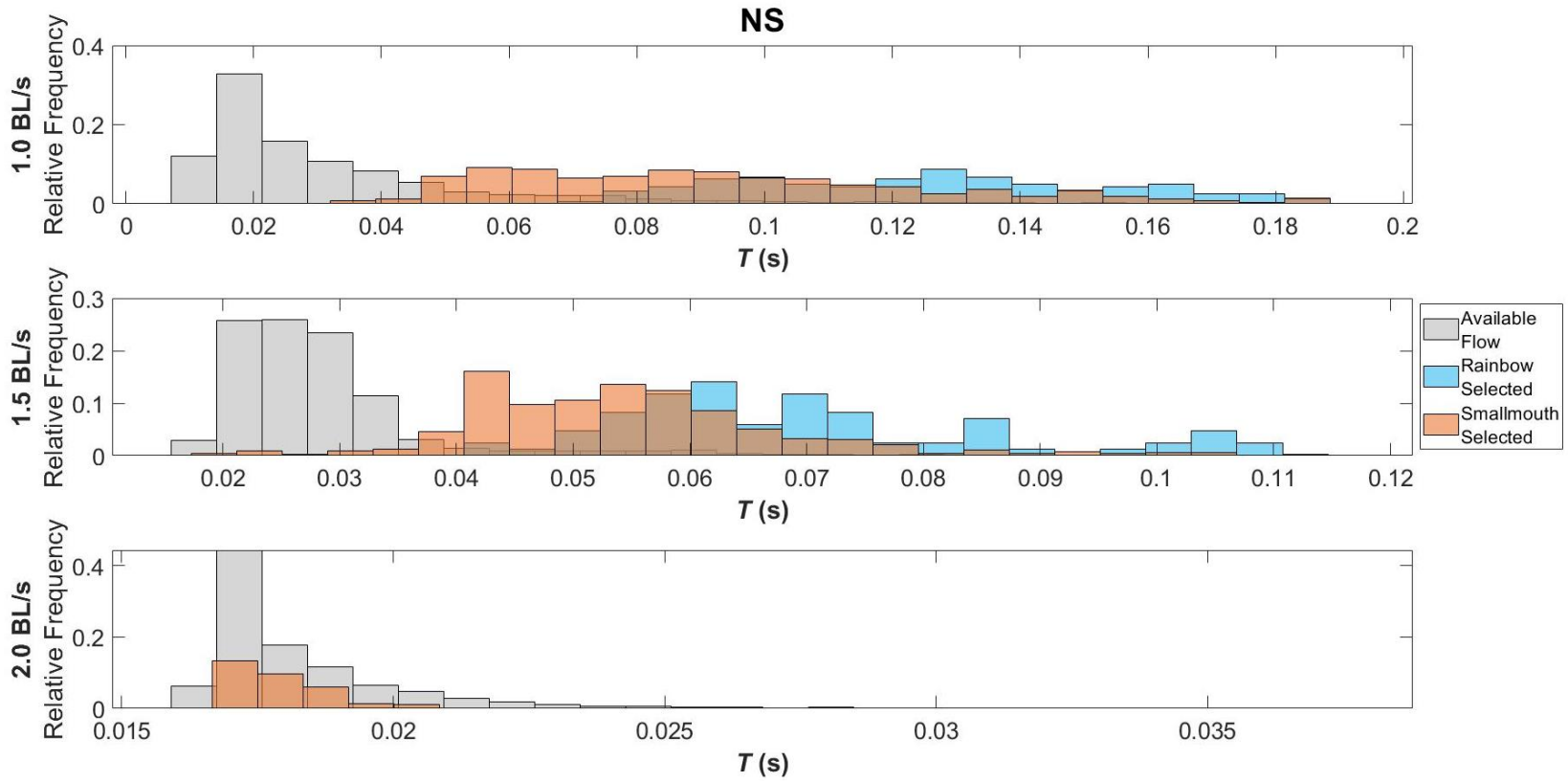

Figure C.25. Relative frequency histograms relating the distribution of available levels of time-averaged turbulent integral length scale (*L*; m) to the distribution of *L* selected by rainbow trout and smallmouth bass to swimming downstream for the control case with no structure (NS) across three body length velocities, 1.0, 1.5, and 2.0 BL/S. Data presented are derived from the XZ plane.

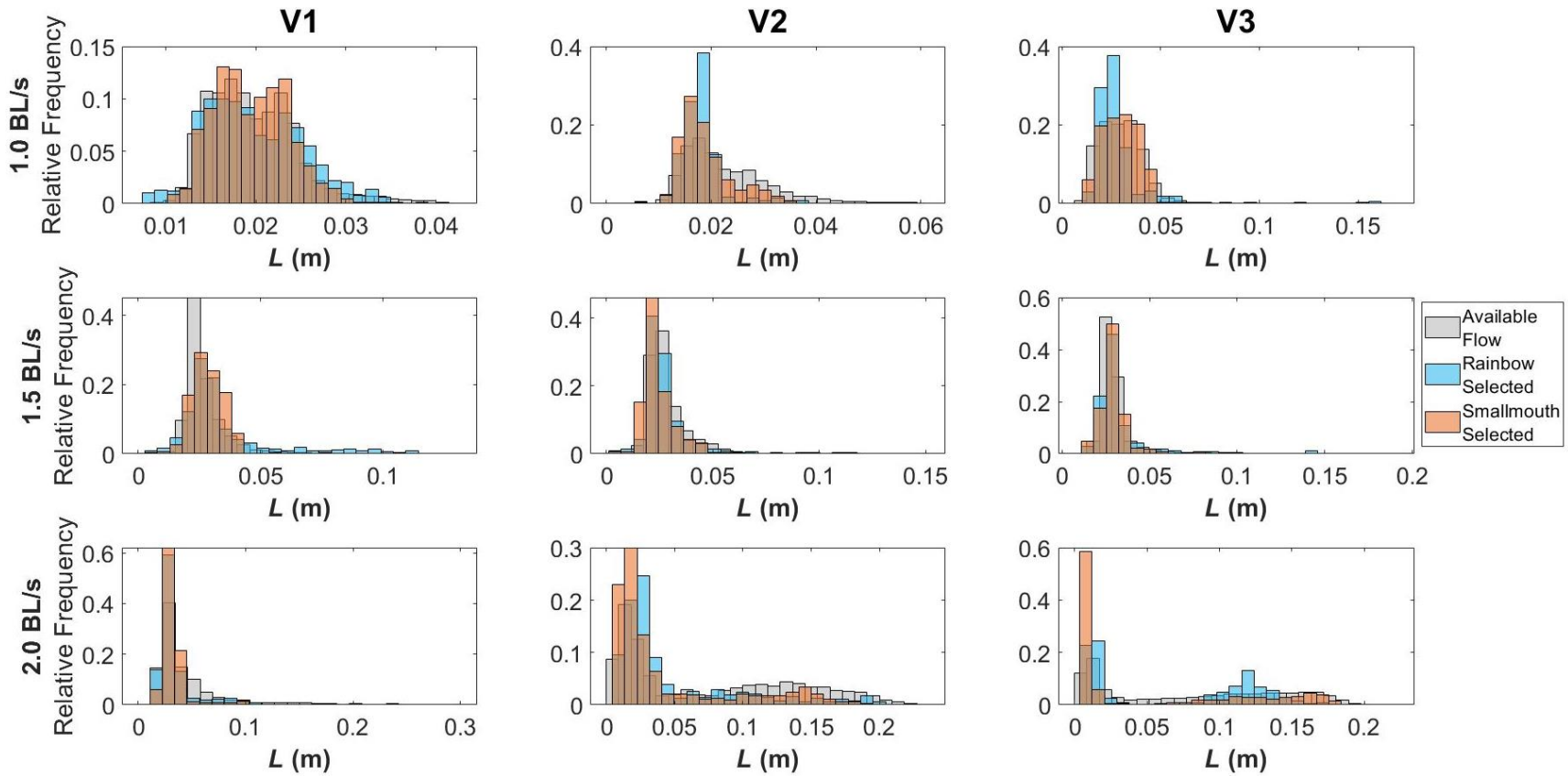

Figure C.26. Relative frequency histograms relating the distribution of available levels of time-averaged turbulent integral length scale (*L*; m) to the distribution of *L* selected by rainbow trout and smallmouth bass to swimming downstream of vertical structures (VS) in one of three diameters (V1 – 2.54-cm; V2 – 5.08-cm; V3 – 7.62-cm), across three body length velocities, 1.0, 1.5, and 2.0 BL/S.

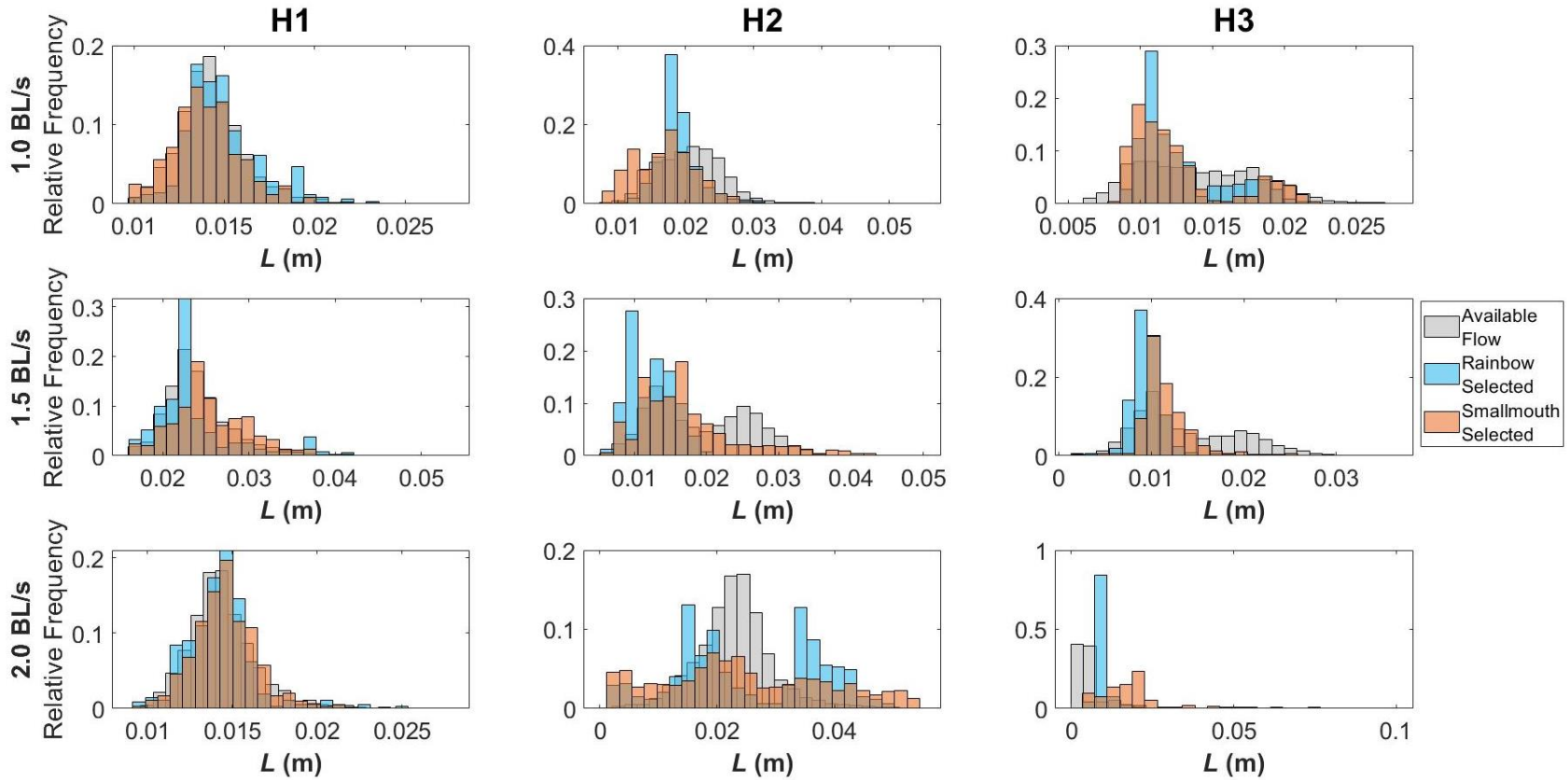

Figure C.27. Relative frequency histograms relating the distribution of available levels of time-averaged turbulent integral length scale (*L*; m) to the distribution of *L* selected by rainbow trout and smallmouth bass to swimming downstream of horizontal structures (HS) in one of three diameters (H1 – 2.54-cm; H2 – 5.08-cm; H3 – 7.62-cm), across three body length velocities, 1.0, 1.5, and 2.0 BL/S.

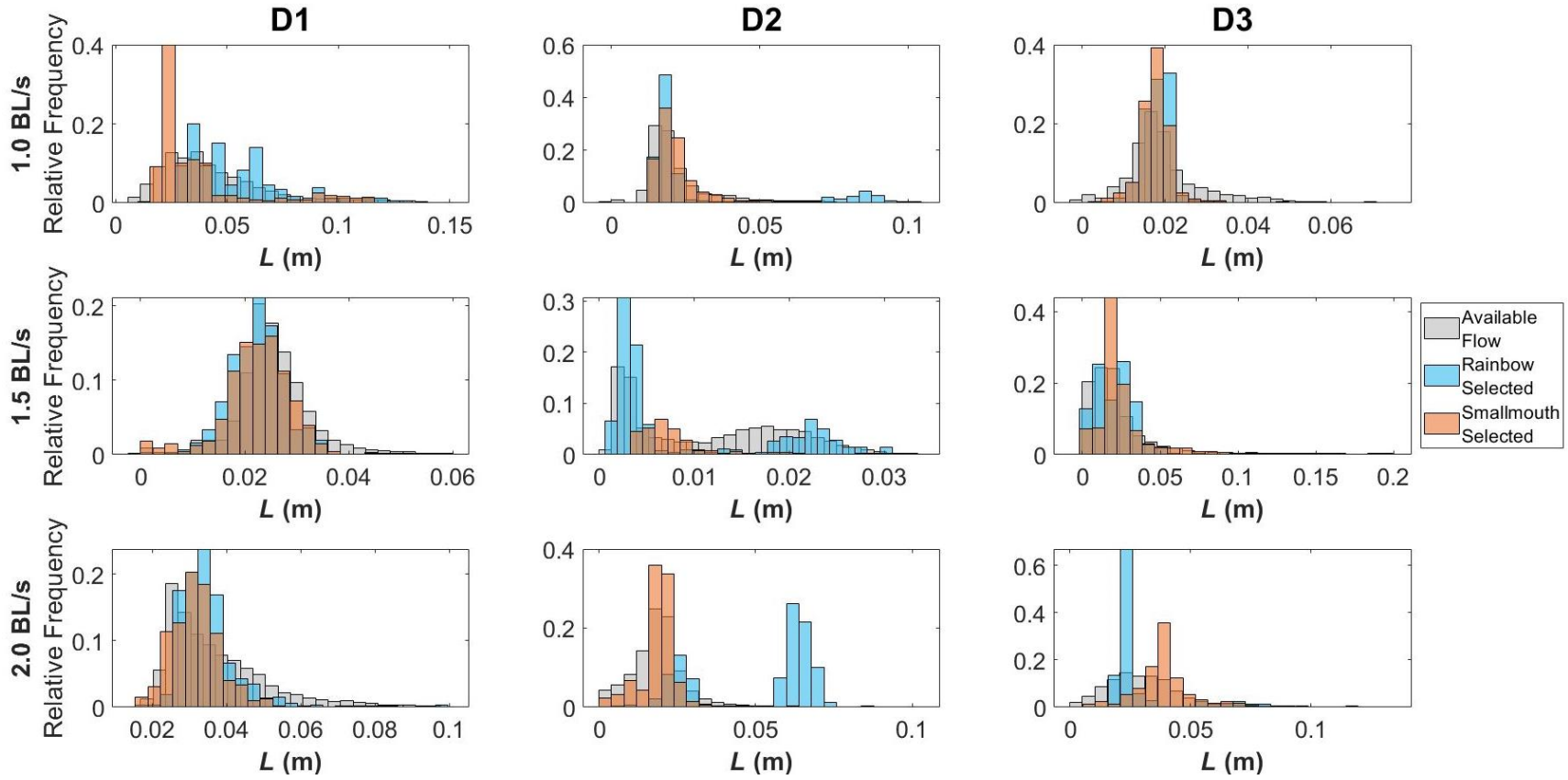

Figure C.28. Relative frequency histograms relating the distribution of available levels of time-averaged turbulent integral length scale (*L*; m) to the distribution of *L* selected by rainbow trout and smallmouth bass to swimming downstream of diagonal structures (DS) in one of three diameters (D1 – 2.54-cm; D2 – 5.08-cm; D3 – 7.62-cm), across three body length velocities, 1.0, 1.5, and 2.0 BL/S. Data presented are derived from the XY plane.

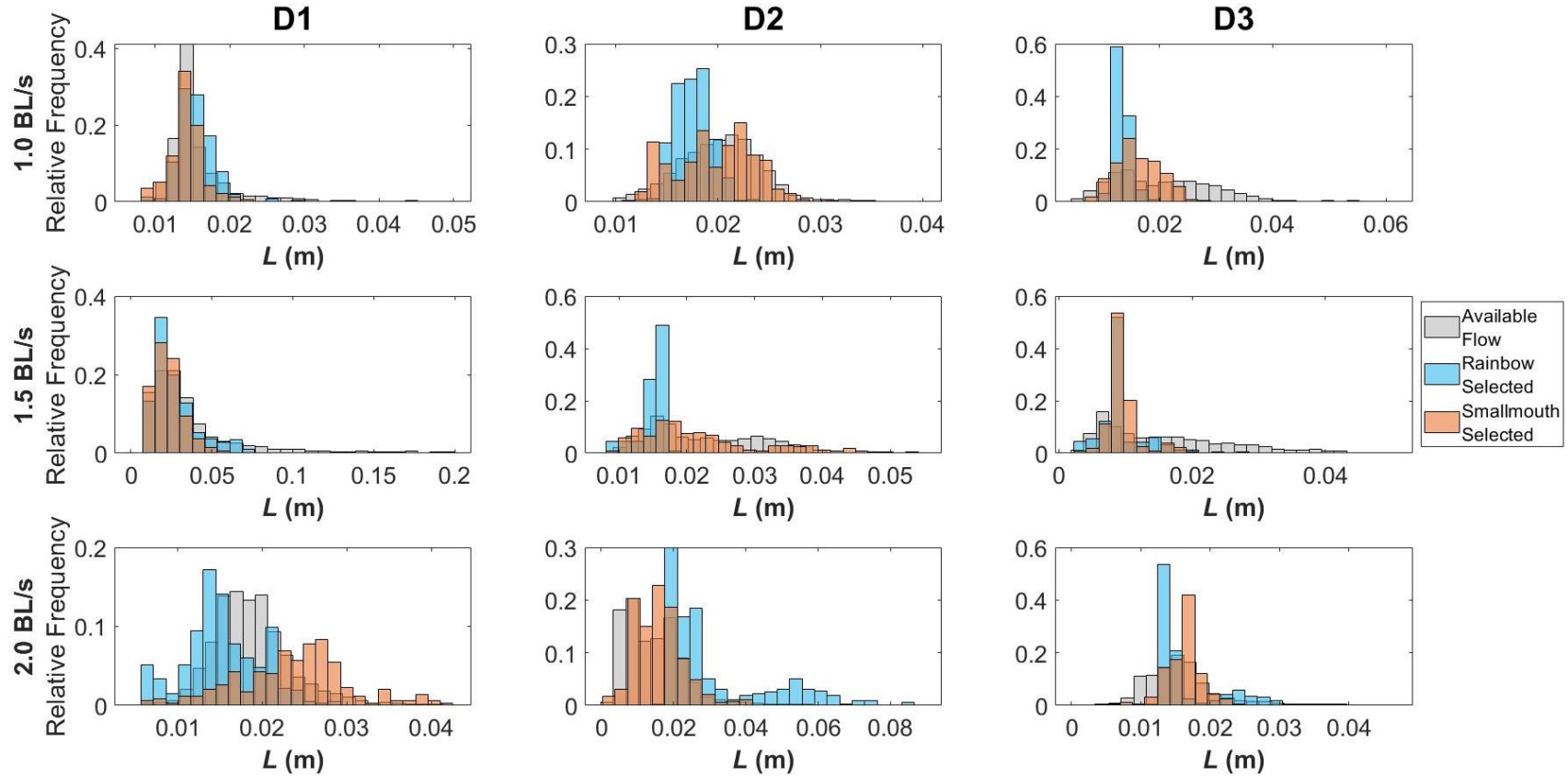

Figure C.29. Relative frequency histograms relating the distribution of available levels of time-averaged turbulent integral length scale (*L*; m) to the distribution of *L* selected by rainbow trout and smallmouth bass to swimming downstream of diagonal structures (DS) in one of three diameters (D1 – 2.54-cm; D2 – 5.08-cm; D3 – 7.62-cm), across three body length velocities, 1.0, 1.5, and 2.0 BL/S. Data presented are derived from the XZ plane.

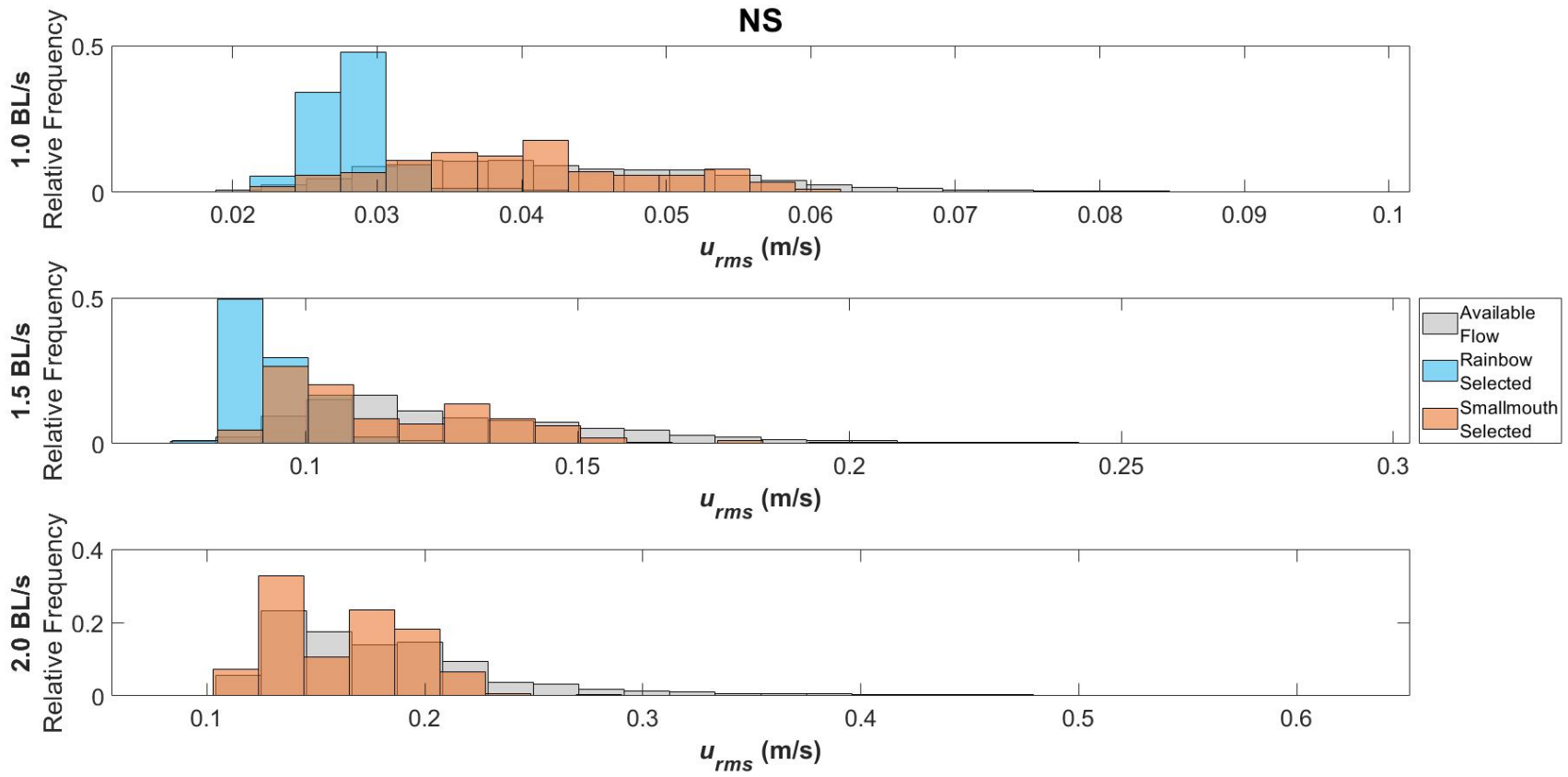

Figure C.30. Relative frequency histograms relating the distribution of available levels of time-averaged U_{rms} (m/s) to the distribution of U_{rms} selected by rainbow trout and smallmouth bass to swimming downstream for the control case with no structure (NS) across three body length velocities, 1.0, 1.5, and 2.0 BL/S. Data presented are derived from the XZ plane.

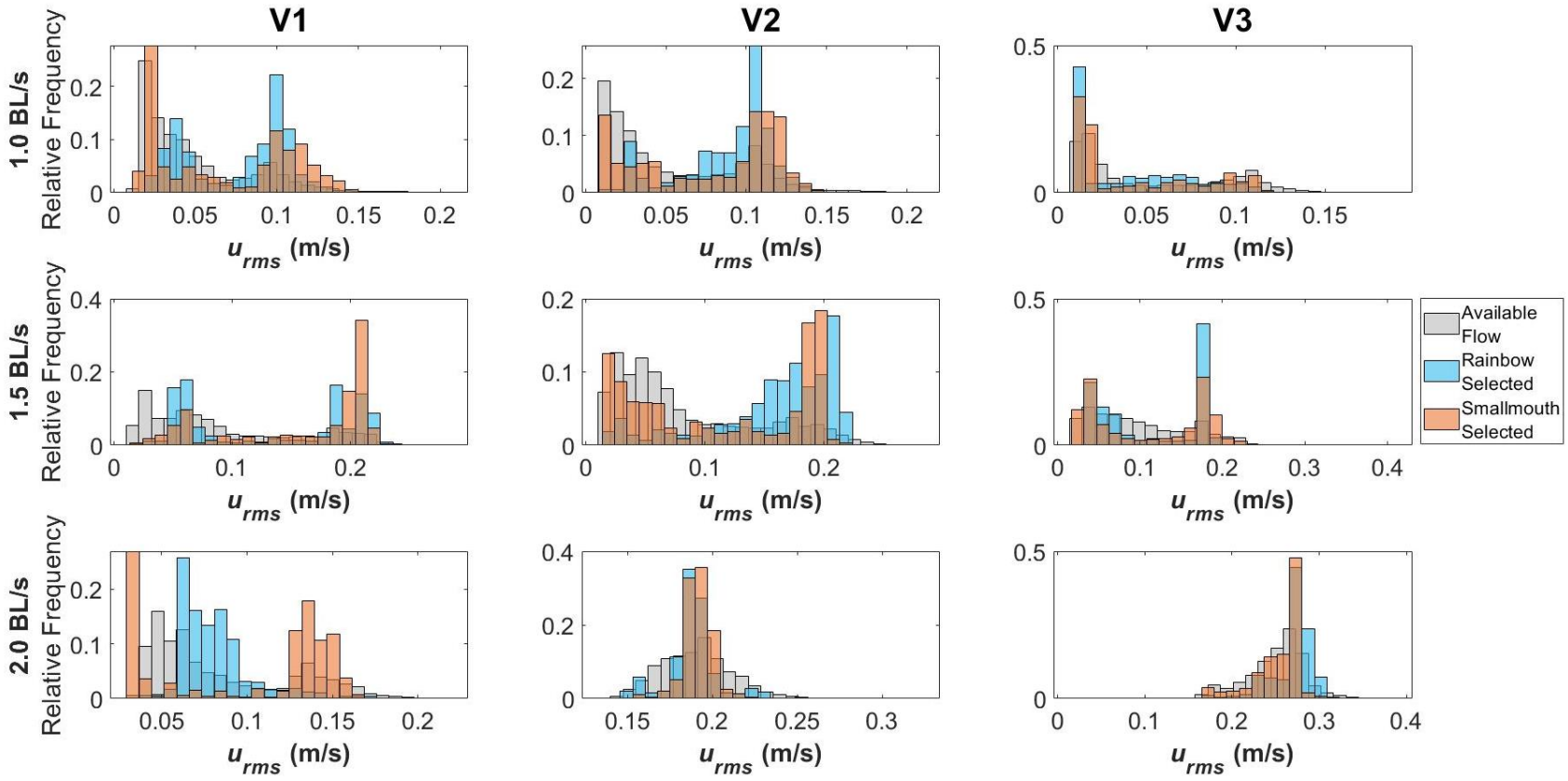

Figure C.31. Relative frequency histograms relating the distribution of available levels of time-averaged U_{rms} (m/s) to the distribution of U_{rms} selected by rainbow trout and smallmouth bass to swimming downstream of vertical structures (VS) in one of three diameters (V1 – 2.54-cm; V2 – 5.08-cm; V3 – 7.62-cm), across three body length velocities, 1.0, 1.5, and 2.0 BL/S.

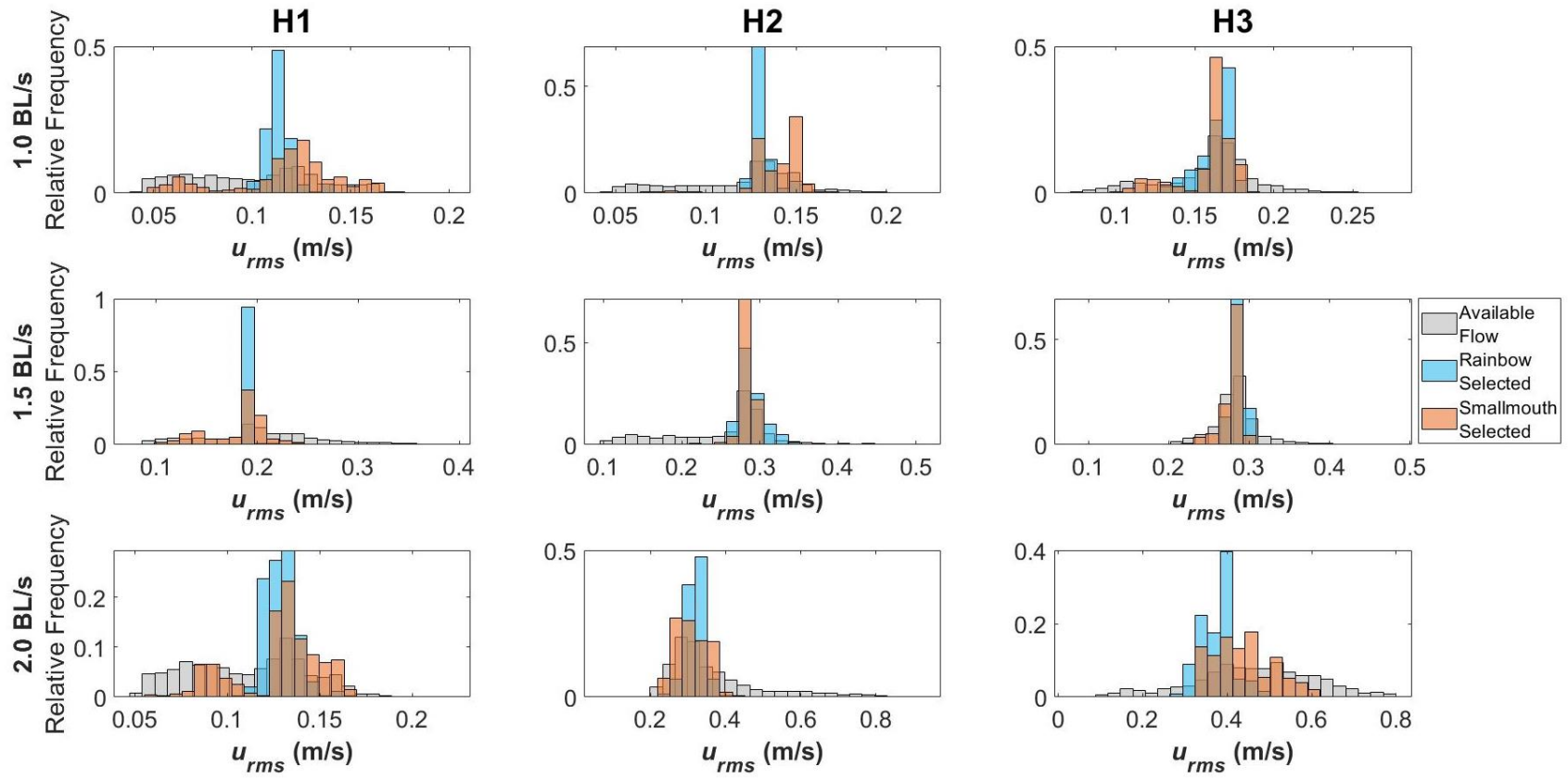

Figure C.32. Relative frequency histograms relating the distribution of available levels of time-averaged U_{rms} (m/s) to the distribution of U_{rms} selected by rainbow trout and smallmouth bass to swimming downstream of horizontal structures (HS) in one of three diameters (H1 – 2.54-cm; H2 – 5.08-cm; H3 – 7.62-cm), across three body length velocities, 1.0, 1.5, and 2.0 BL/S.

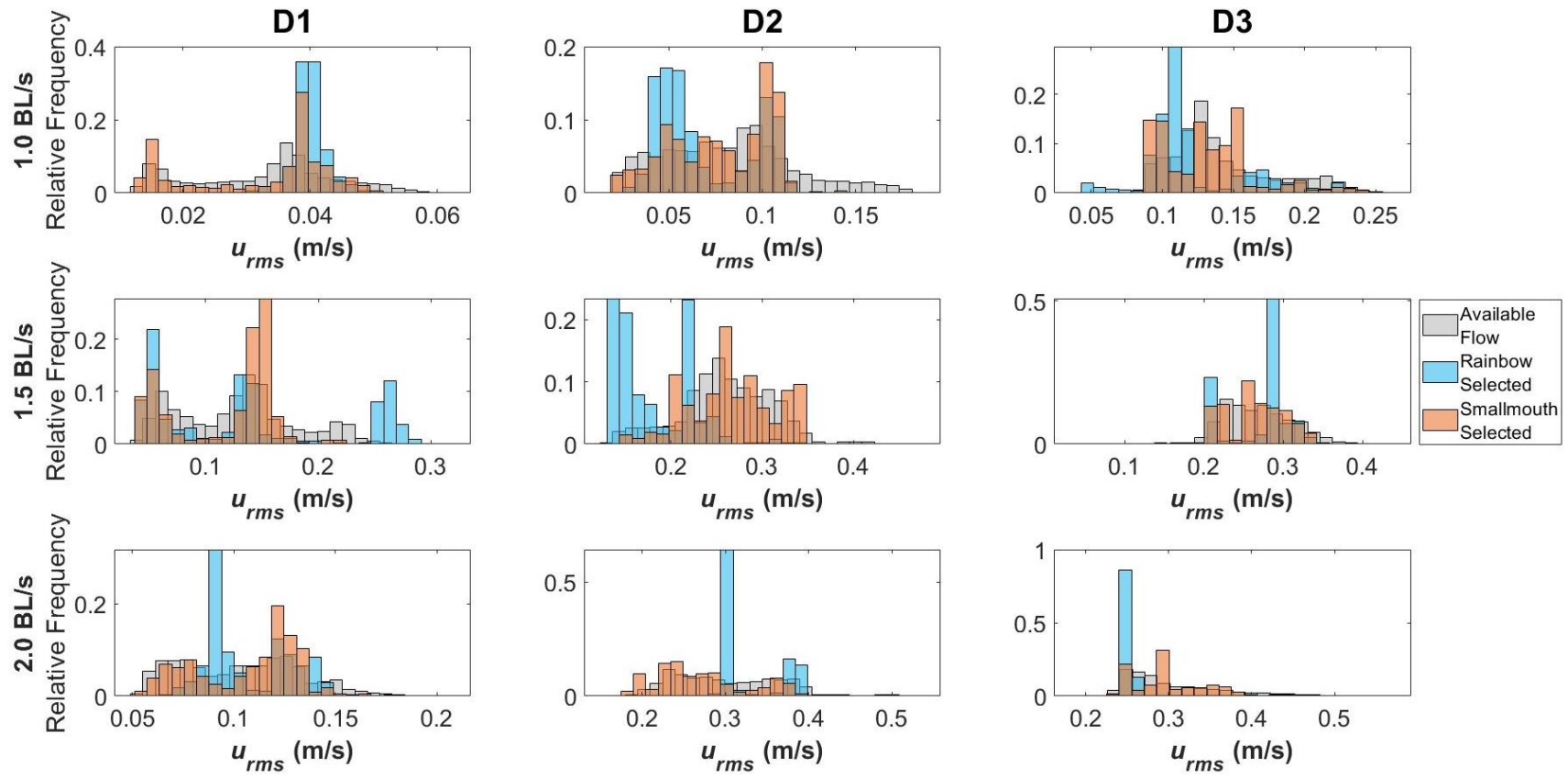

Figure C.33. Relative frequency histograms relating the distribution of available levels of time-averaged U_{rms} (m/s) to the distribution of U_{rms} selected by rainbow trout and smallmouth bass to swimming downstream of diagonal structures (DS) in one of three diameters (D1 – 2.54-cm; D2 – 5.08-cm; D3 – 7.62-cm), across three body length velocities, 1.0, 1.5, and 2.0 BL/S. Data presented are derived from the XY plane.

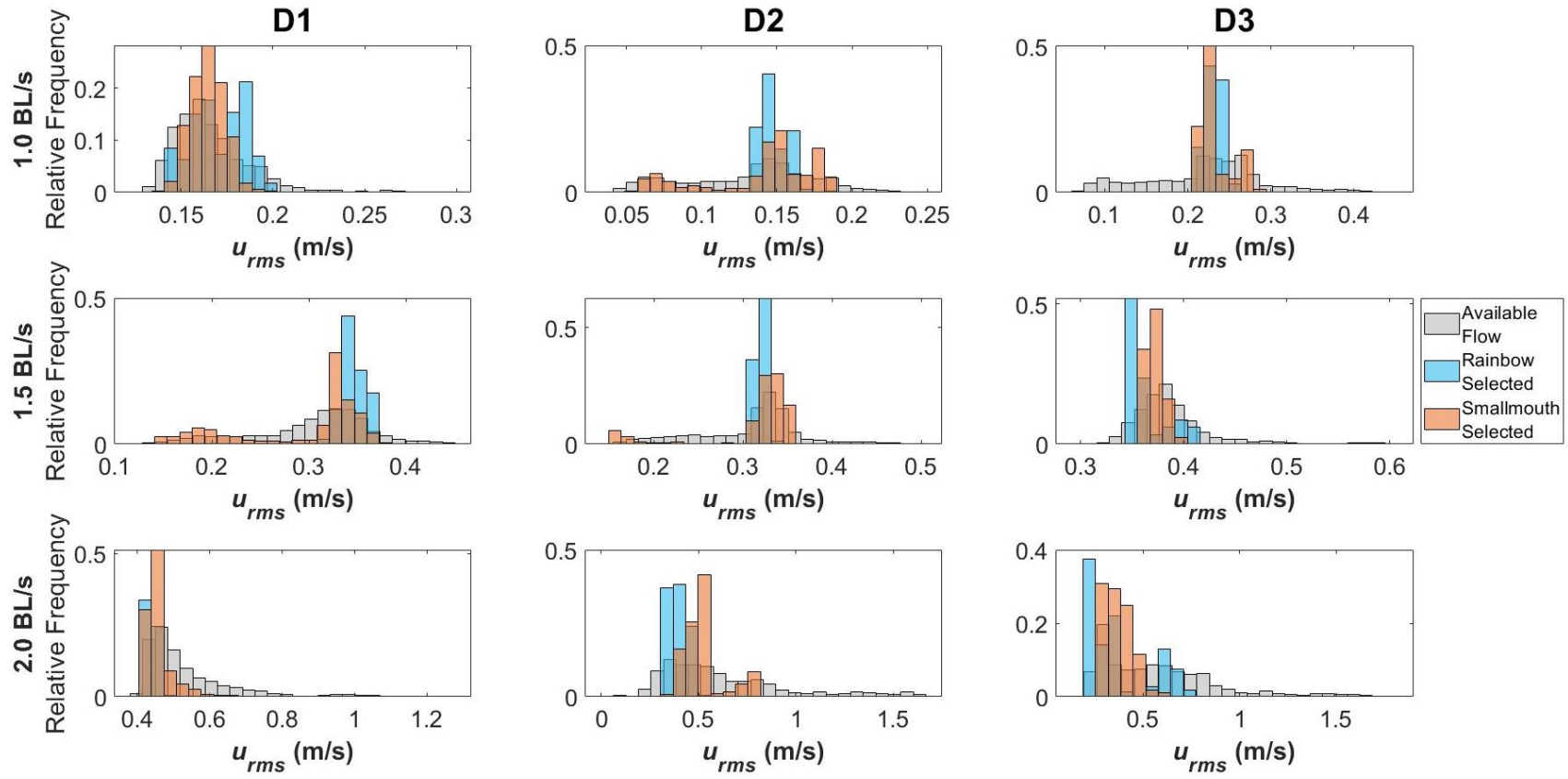

Figure C.34. Relative frequency histograms relating the distribution of available levels of time-averaged U_{rms} (m/s) to the distribution of U_{rms} selected by rainbow trout and smallmouth bass to swimming downstream of diagonal structures (DS) in one of three diameters (D1 – 2.54-cm; D2 – 5.08-cm; D3 – 7.62-cm), across three body length velocities, 1.0, 1.5, and 2.0 BL/S. Data presented are derived from the XZ plane.

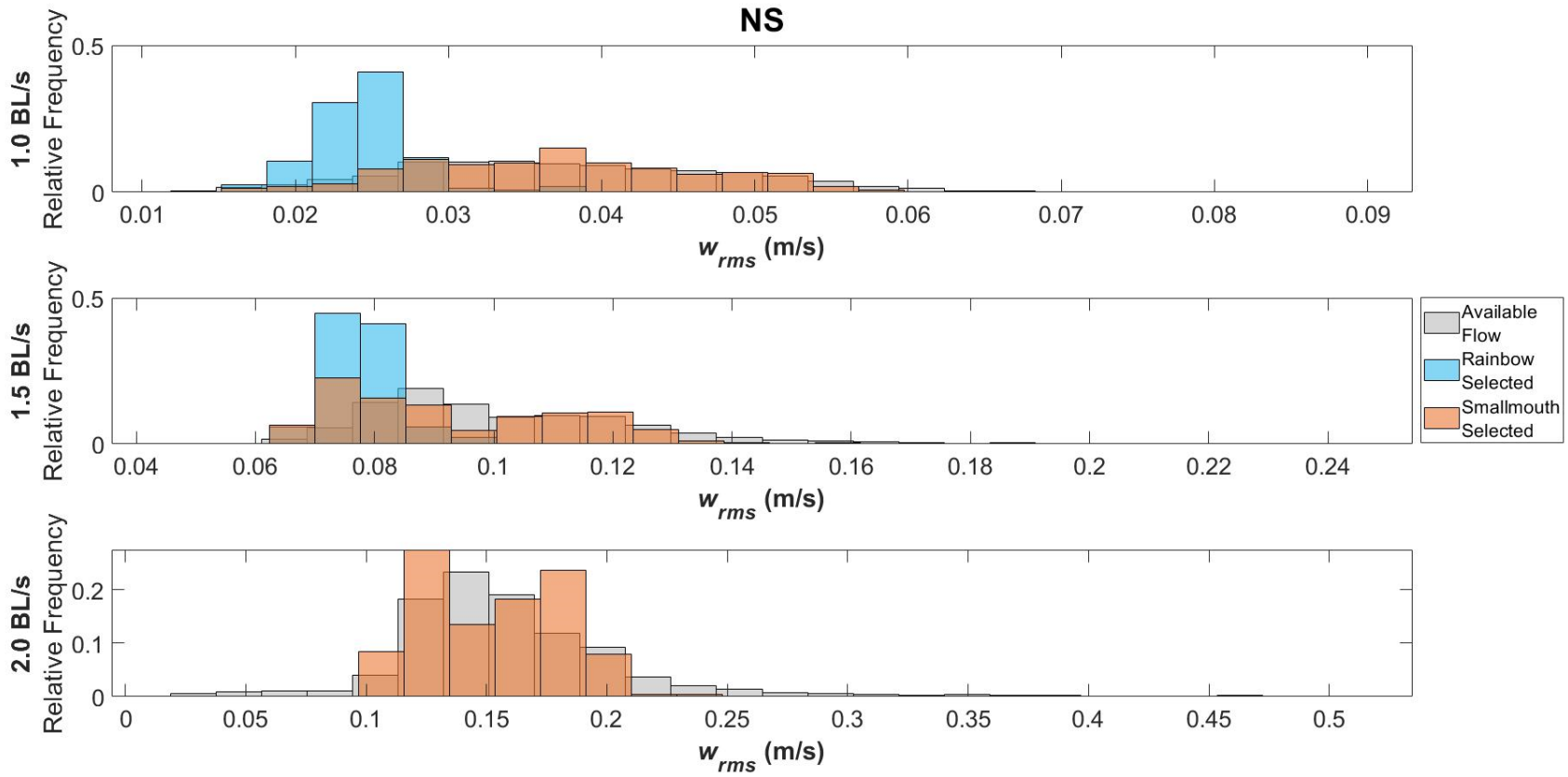

Figure C.35. Relative frequency histograms relating the distribution of available levels of time-averaged W_{rms} (m/s) to the distribution of W_{rms} selected by rainbow trout and smallmouth bass to swimming downstream for the control case with no structure (NS) across three body length velocities, 1.0, 1.5, and 2.0 BL/S. Data presented are derived from the XZ plane. W_{rms} is generated in a transverse direction to the longitudinal flow, and thus, with V_{rms}, is also referred to as $U_{Trms.}$

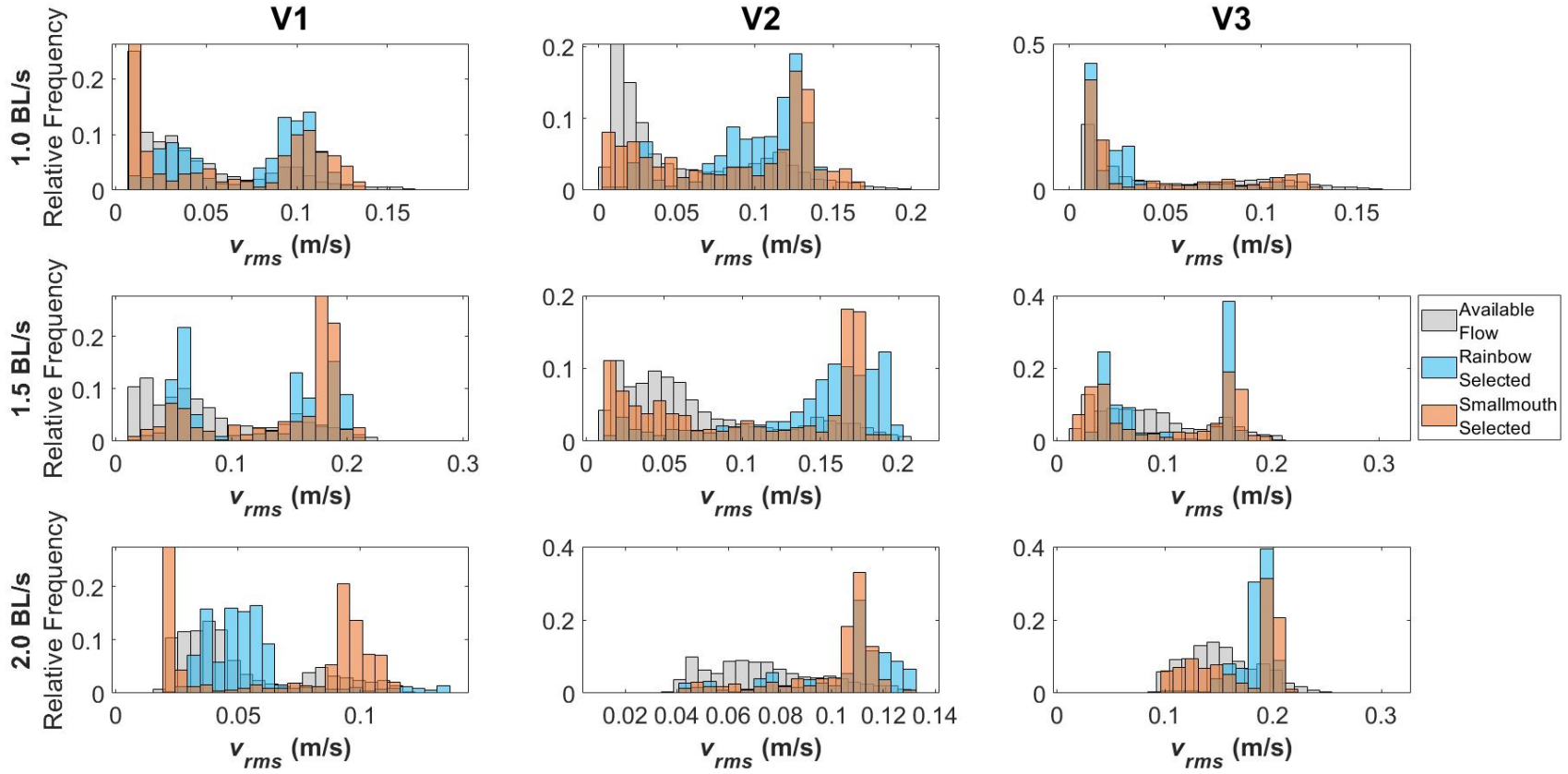

Figure C.36. Relative frequency histograms relating the distribution of available levels of time-averaged V_{rms} (m/s) to the distribution of V_{rms} selected by rainbow trout and smallmouth bass to swimming downstream of vertical structures (VS) in one of three diameters (V1 – 2.54-cm; V2 – 5.08-cm; V3 – 7.62-cm), across three body length velocities, 1.0, 1.5, and 2.0 BL/S. V_{rms} is generated in a transverse direction to the longitudinal flow, and thus, with W_{rms}, is also referred to as U_{Trms}.

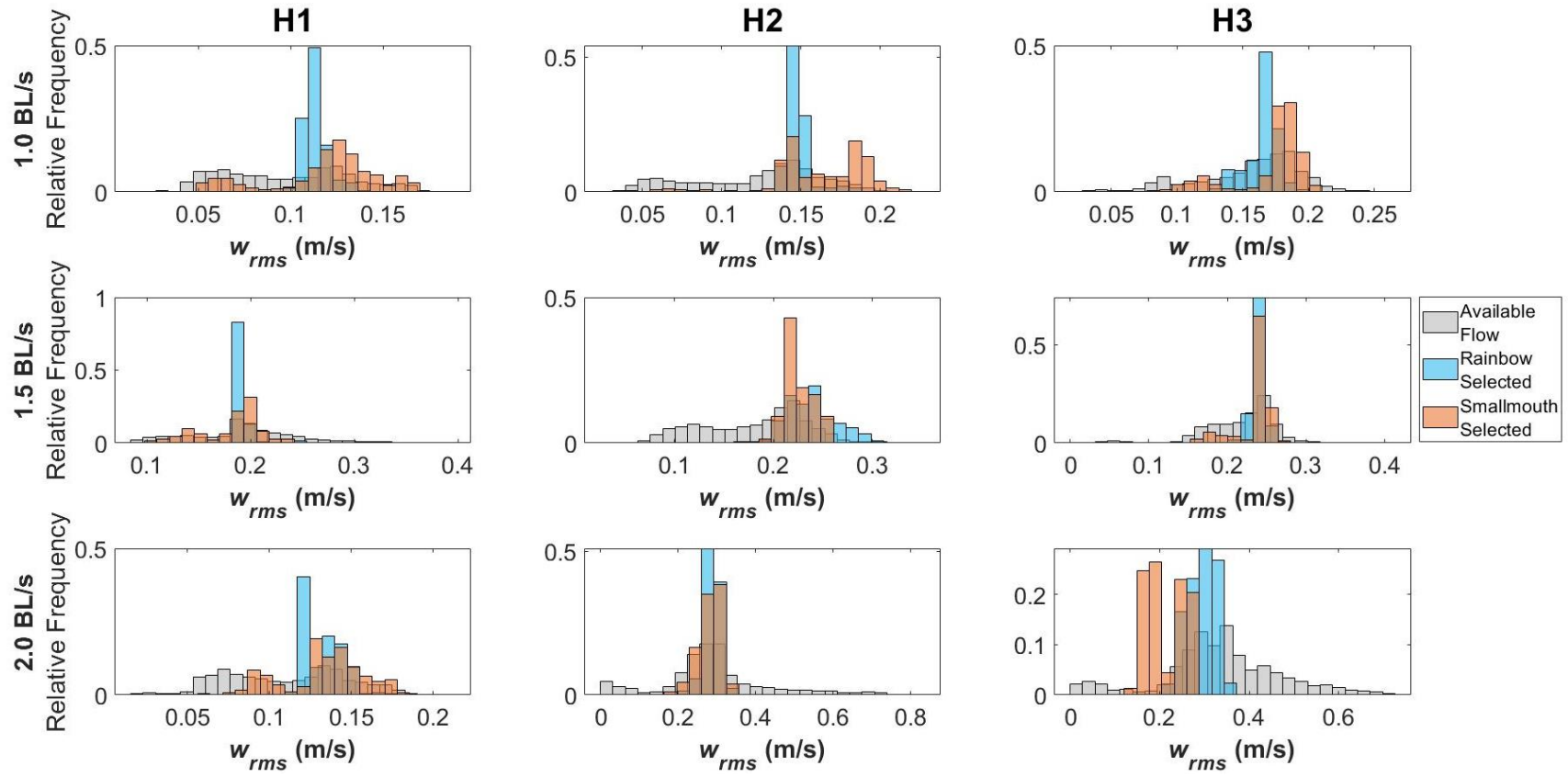

Figure C.37. Relative frequency histograms relating the distribution of available levels of time-averaged W_{rms} (m/s) to the distribution of W_{rms} selected by rainbow trout and smallmouth bass to swimming downstream of horizontal structures (HS) in one of three diameters (H1 – 2.54-cm; H2 – 5.08-cm; H3 – 7.62-cm), across three body length velocities, 1.0, 1.5, and 2.0 BL/S. W_{rms} is generated in a transverse direction to the longitudinal flow, and thus, with V_{rms}, is also referred to as U_{Trms}.

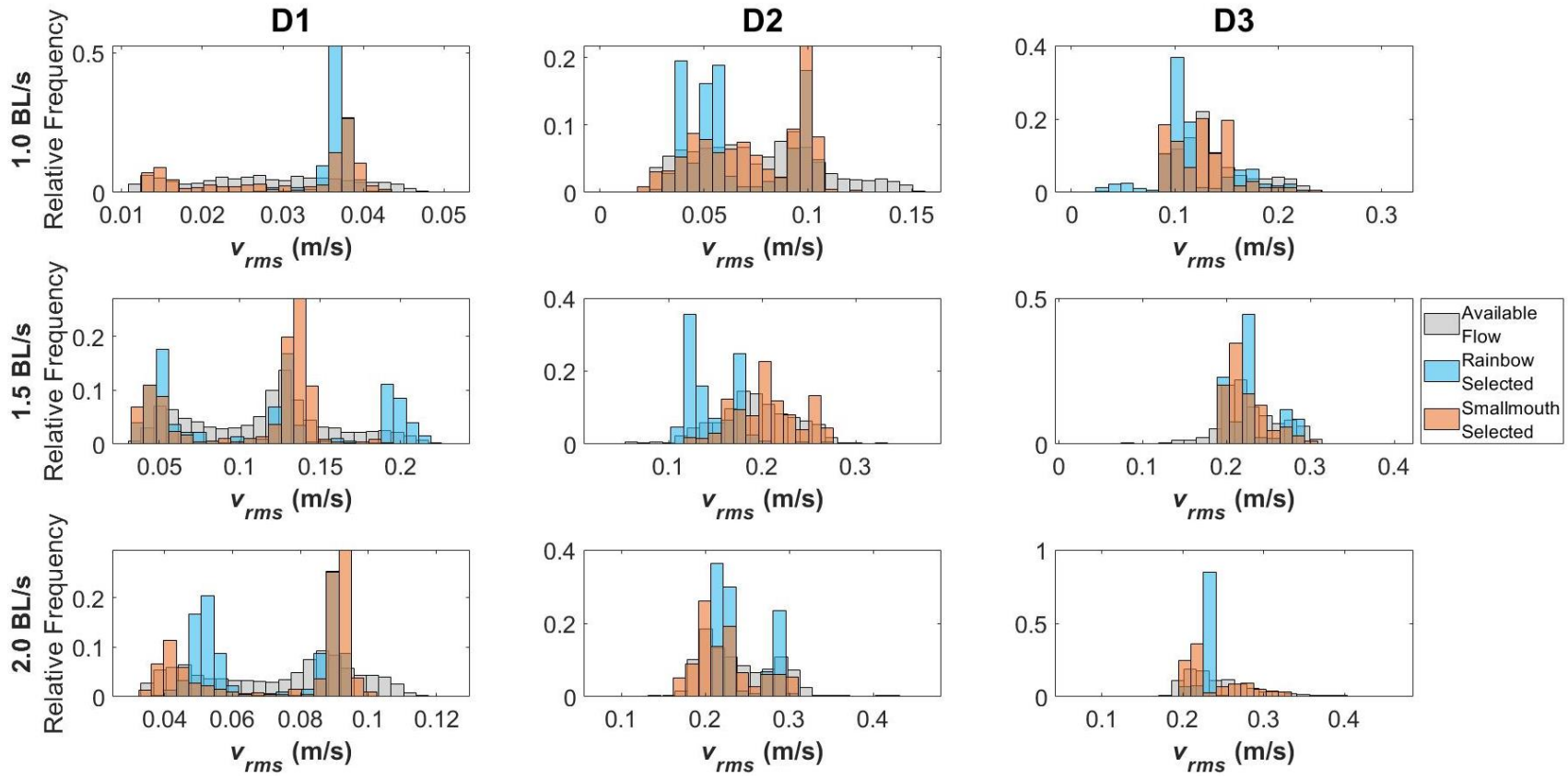

Figure C.38. Relative frequency histograms relating the distribution of available levels of time-averaged V_{rms} (m/s) to the distribution of V_{rms} selected by rainbow trout and smallmouth bass to swimming downstream of diagonal structures (DS) in one of three diameters (D1 – 2.54-cm; D2 – 5.08-cm; D3 – 7.62-cm), across three body length velocities, 1.0, 1.5, and 2.0 BL/S. Data presented are derived from the XY plane. V_{rms} is generated in a transverse direction to the longitudinal flow, and thus, with W_{rms}, is also referred to as $U_{Trms.}$

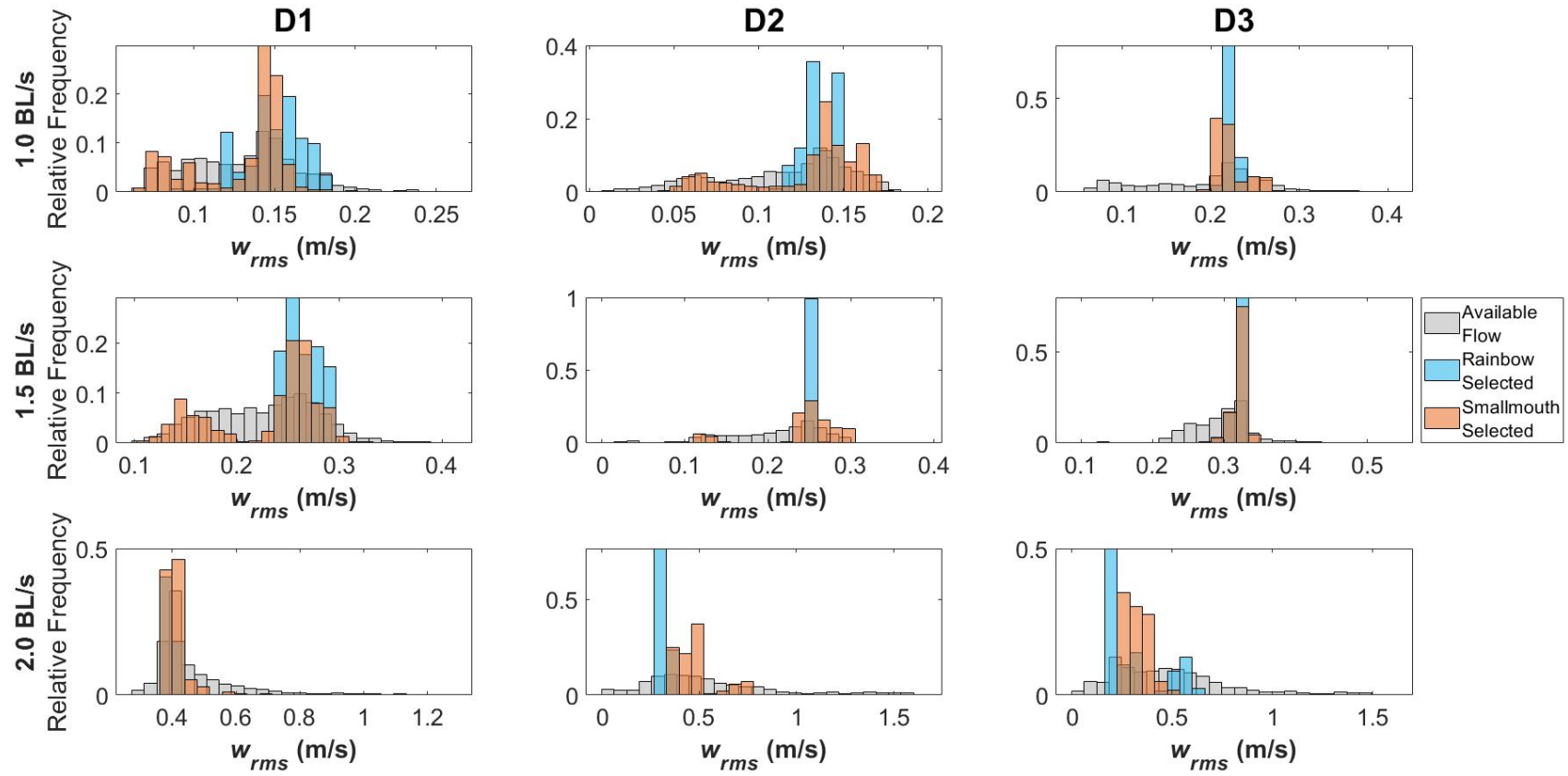

Figure C.39. Relative frequency histograms relating the distribution of available levels of time-averaged W_{rms} (m/s) to the distribution of W_{rms} selected by rainbow trout and smallmouth bass to swimming downstream of diagonal structures (DS) in one of three diameters (D1 – 2.54-cm; D2 – 5.08-cm; D3 – 7.62-cm), across three body length velocities, 1.0, 1.5, and 2.0 BL/S. Data presented are derived from the XZ plane. W_{rms} is generated in a transverse direction to the longitudinal flow, and thus, with V_{rms}, is also referred to as $U_{Trms.}$